Journal of Applied Mathematics

# Mathematical Approaches in Advanced Control Theories

Guest Editors: Baocang Ding, Lihua Xie, Weihai Zhang, Xianxia Zhang, Qiang Ling, and Yugeng Xi

# Mathematical Approaches in Advanced Control Theories

Journal of Applied Mathematics

# Mathematical Approaches in Advanced Control Theories

Guest Editors: Baocang Ding, Lihua Xie, Weihai Zhang, Xianxia Zhang, Qiang Ling, and Yugeng Xi

# Editorial Board

# Contents

Hindawi Publishing Corporation
Journal of Applied Mathematics
Volume 2012, Article ID 984296, 4 pages
doi:10.1155/2012/984296

*Editorial*

# Mathematical Approaches in Advanced Control Theories

**Baocang Ding,[1] Lihua Xie,[2] Weihai Zhang,[3] Xianxia Zhang,[4] Qiang Ling,[5] and Yugeng Xi[6]**

[1] *Ministry of Education Key Lab For Intelligent Networks and Network Security (MOE KLINNS Lab), Department of Automation, School of Electronic and Information Engineering, Xi'an Jiaotong University, Xi'an 710049, China*
[2] *School of Electronic and Electrical Engineering, BLK S2, Nanyang Technological University, Nanyang Avenue, Singapore 639798*
[3] *College of Information and Electrical Engineering, Shandong University of Science and Technology, Qingdao 266590, China*
[4] *Shanghai Key Laboratory of Power Station Automation Technology, School of Mechatronics Engineering and Automation, Shanghai University, Shanghai 200072, China*
[5] *Department of Automation, University of Science and Technology of China, Hefei 230026, China*
[6] *Department of Automation, Shanghai Jiaotong University, Shanghai 200240, China*

Correspondence should be addressed to Baocang Ding, baocang.ding@gmail.com

Received 20 September 2012; Accepted 20 September 2012



Advanced control theory fills a gap between the mathematical control theory and modern control engineering practices. Conceptually, advanced control theories can include any theoretical problems related to the controller design. But in this issue it may include model predictive control, sliding mode control, robust control, real-time optimization, and identification and estimation, which are not limited to controller design. Advanced control technologies have become ubiquitous in various engineering applications (e.g., chemical process control, robot control, air traffic control, vehicle control, multiagent control, networked control). The development of mathematical methods is essential for the applications of advanced control theories. Sometimes, it lacks effective methods to tackle the computational issue (e.g., model predictive control of a fast process). Sometimes, a new application requires a brand-new solver for applying the advanced control theory (e.g., a new production line far exceeding the usual speed). The main focus of this special issue will be on the new research ideas and results for the mathematical problems in advanced control theories.

A total number of 63 papers were submitted for this special issue. Out of the submitted papers, 25 contributions have been included in this special issue. The 25 contributions consider several closely related and interesting topics.

The subjects in controller design and synthesis have occupied 13 contributions. These contributions include, for example, variable structure control, model predictive control (MPC), fuzzy logic control (FLC), robust control, networked and distributed control, optimal control, and adaptive control. For Markovian jump nonlinear systems with unmodeled dynamics and Wiener noise, J. Zhu et al. use backstepping technique and stochastic small-gain theorem, so as to design a switch controller such that stochastic stability is guaranteed. L. Ding et al. consider sliding mode control for mobile manipulators with stochastic jump switching joints. Adaptive parameter techniques are adopted to cope with the effect of Markovian switching and nonlinear dynamics uncertainty and follow the desired trajectory for wheeled mobile manipulators. T. Zou considers the dynamic stability property of the double-layered MPC. The double-layered MPC is a common structure for real applications. X. Zhang et al. develop a three-dimensional FLC design methodology based on clustering and support vector machine regression learning from a spatiotemporal dataset. Y. Wang focuses on the robust stability of Lotka-Volterra predator-prey system with the fuzzy impulsive control. Y. Zhu and L. Fan present the robust force/motion control strategies for mobile manipulators under both holonomic and nonholonomic constraints in the presence of uncertainties and disturbances. Y. H. Yang and C. L. Chen propose a generic spatial domain control scheme for a class of nonlinear rotary systems of variable speeds with spatially periodic disturbances. When the system state is unmeasurable, a nonlinear state observer is established for providing the estimated states. Q. Ling et al. investigate the effects of the network-induced delays, packet dropouts, and the torque disturbance on the speed tracking of a permanent magnet synchronous motors system. The designed controller can robustly guarantee stability and performance. Q. Ling and H. Deng study the second moment stability of a Markov jump linear system with real states. They propose an alternative necessity proof of the stability condition for this system. Y. Guo and T. Pan investigate the problem of robust stability of uncertain linear discrete-time system over network with bounded packet loss. X. Liu et al. consider a containment problem of networked fractional-order system with multiple leaders under a fixed directed interaction graph. The distributed protocol, flocking problem, communication delay, and interconnection topology are studied. Y. Lei et al. establish an optimal control model of distributed parameter systems (DPS) for polymer injection strategies. G. M. Bahaa considers the optimal boundary control problem for an infinite order distributed parabolic systems with multiple time delays given in the integral form both in the state equations and in the Neumann boundary conditions.

Closely related to the controller design and synthesis are the 8 contributions on the estimation problem. These contributions include, for example, Kalman filter, robust state estimator, fusion estimator, target tracking filter, and modeling parameter estimation. X. Lu et al. deal with Kalman smoothing problem for wireless sensor networks with multiplicative noises. Packet loss occurs in the observation equations, and multiplicative noises occur both in the system state equation and the observation equations. L. Zhang et al. revisit the state estimator for polytopic uncertain systems. The notion of quadratic boundedness, which has been useful in specifying stability of the system with uncertain but bounded noise, is utilized. H. Zhao and C. Zhang consider the finite-time $H_\infty$ filter for linear continuous time varying systems with uncertain observations and $\mathcal{L}_2$-norm bounded noise. By using the projection theory in Krein space, the finite-time $H_\infty$ filter is solved. X. Wang and S. Sun present a self-tuning weighted measurement fusion Kalman filter, for the linear discrete stochastic systems with multiple sensors and unknown noise statistics. It is proved that the presented self-tuning weighted measurement fusion Kalman filter converges to the optimal

weighted measurement fusion Kalman filter. F. Lian, C. Han et al. study the convergence of the Gaussian mixture extended-target probability hypothesis density filter and its extended Kalman filtering approximation in mildly nonlinear condition. The problem of extended-target tracking is very valuable for many real applications, such as ground or littoral surveillance, robotics, and autonomous weapons. F. Lian, C. Li et al. study the convergence for the sequential Monte Carlo implementations of the multitarget multi-Bernoulli (MeMBer) filter and cardinality-balanced MeMBer filters. By combining the linear matrix inequalities for the system identification and those to obtain a discrete time controller, K. Hiramoto proposes a framework to integrate two steps for the model-based control system design, that is, the SISO system identification and the controller synthesis. K. Kobayashi and K. Kaito utilize a one-dimensional consolidation model, incorporating inhomogeneous ground subsidence, to generate the sets of sample paths designating ground subsidence processes. The estimation of ground subsidence processes is an important subject for the asset management of civil infrastructures on soft ground, such as airport facilities.

There are also 3 contributions on the image processing and acoustic signal processing. These contributions can be seen as the extensions of the estimation problem, in the context of this special issue. L. Zi and J. Du propose an energy-driven image interpolation algorithm employing Gaussian process regression. Image interpolation, as a method of obtaining a high-resolution image from the corresponding low-resolution image, is a classical problem in image processing. P. Han and J. Du use a nonsubsampled pyramid structure and a nonsubsampled directional filter to achieve multidimensional and translation-invariant image decomposition for spatial images. Spatial images are inevitably mixed with different levels of noise and distortion. C. Wang and P. Zhang present an improved spoken term detection strategy, which integrates a phoneme confusion matrix and an improved word-level minimum classification error training method. Spoken term detection system will degrade significantly if there is mismatch between acoustic model and spontaneous speech.

The last contribution is for the mathematical programming. T. Hasuike et al. consider the risk-control and management approach for a bottleneck spanning tree problem under the situation where edge costs in a given network include randomness and the reliability. Note that several other contributions mentioned above have also considered optimizations (e.g., in the work of G. M. Bahaa, necessary and sufficient optimality conditions for the Neumann problem with the quadratic performance functional are derived; in the work of Y. Lei et al., the necessary conditions for optimality are obtained through application of the calculus of variations and Pontryagin's weak maximum principle; in the work of X. Wang and S. Sun, the global optimality property is considered; some other works utilize optimization to obtain the controller, estimator, or modeling parameters).

From the above contributions, some trends in the advanced control theories seem to become clearer. The studied problems are becoming more and more complex (e.g., considering disturbance/noise, stability/convergence, probability/randomness, distributed parameters, time-delay/networked phenomenon, physical constraints, impulsive system, optimization and control integrated system, fractional-order system, and parametric uncertainties). Usually, several kinds of complexities should be included into a single work in order for it to be publishable as a contribution.

We hope the readers of this special issue will find it interesting and stimulating and expect that the included papers to contribute to further advance the area of advanced control. Finally, we would like to thank all the authors who have submitted papers to the special issue and the reviewers involved in the refereeing of the submissions.

*Baocang Ding*
*Lihua Xie*
*Weihai Zhang*
*Xianxia Zhang*
*Qiang Ling*
*Yugeng Xi*

Hindawi Publishing Corporation
Journal of Applied Mathematics
Volume 2012, Article ID 364086, 17 pages
doi:10.1155/2012/364086

*Research Article*

# Risk-Control Approach for a Bottleneck Spanning Tree Problem with the Total Network Reliability under Uncertainty

**Takashi Hasuike,[1] Hideki Katagiri,[2] and Hiroshi Tsuda[3]**

[1] *Graduate School of Information Science and Technology, Osaka University, 2-1 Yamadaoka, Suita, Osaka 565-0871, Japan*
[2] *Graduate School of Engineering, Hiroshima University, 1-4-1 Kagamiyama, Higashi-Hiroshima, Hiroshima 739-8527, Japan*
[3] *Department of Mathematical Sciences, Faculty of Science and Engineering, Doshisha University, 1-3 Tatara Miyakodani, Kyotanabe, Kyoto 610-0321, Japan*

Correspondence should be addressed to Takashi Hasuike, thasuike@ist.osaka-u.ac.jp

Received 2 April 2012; Accepted 18 August 2012

Academic Editor: Baocang Ding



This paper considers a new risk-control and management approach for a bottleneck spanning tree problem under the situation where edge costs in a given network include randomness and reliability. Particularly, this paper focuses on the case that only mean value and variance of edge costs are calculated without assuming a specific random distribution. In order to develop the risk control approach, a confidence interval-based formulation is introduced. Using this interval, as well as minimizing the maximum value of worse edge costs, maximizing the minimum value of robust parameters to edge costs is introduced as objective functions in the risk-control. Furthermore, in order to maintain the constructing spanning tree network entirely, the reliability for each edge is introduced, and maximizing the total reliability of spanning tree is assumed as the third objective function. The proposed model is a multiobjective programming problem, and hence, it is difficult to solve it directly without setting some optimal criterion. Therefore, satisfaction functions for each object and the integrated function are introduced, and the exact solution algorithm is developed by performing deterministic equivalent transformations. A numerical example is provided by comparing our proposed model with previous standard models.

## 1. Introduction

Minimum spanning tree (MST) problem is one of most important combinatorial optimization nodes. In the real world, MST problems to find a least cost spanning tree in an edge weighted graph connecting all are usually seen in real-world network optimization problems (most recently, Chen [1] and Ferreira et al. [2]). In more detail, when designing a layout for telecommunication and power networks or constructing a large-scale gas pipeline, if

a decision maker wishes to minimize the cost for connection between cities, the situation is formulated as an MST problem. Then, another object is to minimize the working hours for construction or to maximize the reliability to the whole of constructing network. In fact, European Commission [3] today presented its energy infrastructure priorities for the next two decades, aimed at making networks fit for the 21st century. Then, the commission defines EU priority corridors for the transport and networks of electricity, gas, and oil. Thus, it is important to construct several types of networks actually enhancing the importance and the reliability of backbone lines as well as minimizing the cost and constructing time.

In MST problems, there are two main problems whose objects are different from each other. The ordinary object of MST problem is minimizing the total cost of spanning tree, and another is minimizing the maximum value of edge costs in a spanning tree. The latter model is particularly called bottleneck spanning tree (BST) problem, and it is more efficient for the construction of information and communications networks under delivery deadline or capacity constraints of edges. For instance, in the case of constructing new power lines or internet networks among all houses in a town, builders generally construct all lines concurrently, and hence, it is important to construct all lines safely by the delivery deadline. As a mathematical formulation of this case, the BST problem may be appropriate. Therefore, in this paper, we focus on a BST problem.

Previous researches of MST problems including BST problems deal with constant edge costs, and it is possible to apply many exact and polynomial time solution algorithms directly, developed by Cheriton and Tarjan [4], Gabow et al. [5], Geetha and Nair [6], Kruskal [7], and Prim [8]. However, more practically, it is necessary to consider the situation that one makes an optimal decision on the basis of data involving various uncertainties. For instance, the cost to connect between two nodes often depends on the economical environment which varies randomly. In risk-control and management approaches in order to avoid adverse impacts derived from uncertainty, it is recently important to minimize a downside risk which can denote the risk of edge cost going up to some target level set by the decision maker. As a recent study, note the design of a communication network where routing delays on links are not known with certainty due to the time varying nature of the traffic load on the network. In this application, it is desirable to construct a network configuration that hedges against the worst possible contingency in routing delays (Kouvelis and Yu [9]).

If all random distributions to edge costs are certainly determined such as normal distributions, the decision maker may directly use some downside risk measures such as value at risk (VaR) and conditional value at risk (cVaR) (Rockafellar and Uryasev [10]). However, in practice, it is difficult to determine a certain random distribution to each edge cost even if there are a lot of received data. Instead, it is usually possible to calculate mean value and variance derived from received data, and hence, a confidence interval-based approach may be also obtained using only mean value and variance. In general, if the decision maker assumes many practical situations from better to worse cases, this situation mathematically means that the range of confidence interval becomes wide. Therefore, the problem with the confidence interval is regarded as one of robust programming problems. As an extension of the previous confidence interval, Watada et al. [11] recently proposed $d$-confidence interval where parameter $d$ represents an adjustment parameter to the confidence region in robustness. For instance, in a normal distribution with mean value $m$ and variance $\sigma^2$, the $d$-confidence interval is represented as $[m - d\sigma, m + d\sigma]$. In this paper, we propose an MST problem using the $d$-confidence interval.

On the other hand, it is also important to consider how we ensure the reliability of trunk and backbone line in the network. For instance, we consider that the decision maker

constructs a fast Internet network among cities with some important metropolises. In this situation, even if it happens that the only connection between two cites is disrupted by destroying the connection line derived from natural disasters or breakdown of machines, a city loses contact with the other cities and metropolises and this wreaks enormous damages in the whole network. Therefore, it is often important and necessary to construct more reliable lines connecting these metropolises even if the total cost is high. Thus, we need to set the reliability of each edge and to decide the minimum spanning tree maximizing the total reliability to the whole of spanning tree as well as minimizing the total cost.

In mathematical programming under uncertainty, some researchers proposed a stochastic, fuzzy, or uncertain network optimization. As studies of BST problems under uncertainty, Ishii and Nishida [12] and Katagiri et al. [13] investigated BST problems where edge costs are assumed to be random or fuzzy random variables and developed a polynomial-time algorithm. However, risk-control and management models for BST problems with multiobjective functions have not been studied deeply since it is usually formulated as a constrained spanning tree problem which is more difficult to deal with. In this paper, we assume the situation where the decision maker has satisfaction levels for all objects, and hence, we introduce satisfaction functions to objective functions, which are often called fuzzy goals. Furthermore, as an integrated function of multiobjective functions, we focus on the Bellman-Zadeh minimum operator (Bellman and Zadeh [14]) which is one of the standard appropriate aggregation functions and is dealt with in many studies. Using these mathematical formulations, we transform main problems into the deterministic equivalent problems and obtain the exact solution algorithm.

This paper is organized as follows. In Section 2, we introduce a standard BST problem and three objects of our proposed model. Then, we formulate our proposed multiobjective BST problem. In Section 3, in order to solve the proposed BST problem directly in mathematical programming, we introduce satisfaction functions for all objects and Bellman-Zadeh's minimum operator as an integrated function. In Section 4, performing deterministic equivalent transformations of the initial problem, we develop the polynomial-time solution algorithm based on a standard MST problem and the bisection method. Furthermore, in order to represent some features of our proposed BST problem by comparing with the standard BST problem and probability maximization-based BST problem not including the total reliability, Section 5 provides a simple numerical example. Finally, Section 6 concludes this paper.

## 2. Mathematical Formulation of Proposed Multiobjective BST Problem

In this section, we introduce a formulation of standard MST problem and our proposed robust MST problem with the reliability to the whole of spanning tree under uncertainty.

We assume a connected undirected graph $G = (V, E)$ where $V = \{v_1, v_2, \ldots, v_n\}$ is a finite set of $n$ vertices representing terminals or telecommunication stations and so forth. $E = \{e_1, e_2, \ldots, e_m\}$ is a finite set of edges representing connections between these terminals or stations, and $T = \{T_1, T_2, \ldots, T_k\}$ is a finite set of spanning trees in given undirected graph $G = (V, E)$. Let undirected graph $\mathbf{x} = (x_1, x_2, \ldots, x_m)^t$ be a vector defined by

$$x_j = \begin{cases} 1 & (e_j \in T) \\ 0 & (e_j \notin T) \end{cases}, \quad j \in S \triangleq \{1, 2, \ldots, m\}, \tag{2.1}$$

where $S$ is the index set of edges.

### 2.1. Formulation of Standard BST Problem

First, we introduce a standard BST problem. The ordinary MST problem is to find the spanning tree minimizing the total cost. On the other hand, a BST problem is formulated as follows:

$$\begin{aligned} &\text{Minimize} \quad \max_{j\in S}\{c_j x_j\} \\ &\text{subject to} \quad x_j = \begin{cases} 1 & (e_j \in T) \\ 0 & (e_j \notin T) \end{cases}, \quad j \in S. \end{aligned} \tag{2.2}$$

where $c_j (j \in S)$ are edge costs in the given undirected graph. The above problem is easily transformed into a minimum spanning tree problem if all edge costs are constant in this problem. Therefore, the efficient solution algorithms are applied to the problem, and it is not difficult to obtain the optimal spanning tree in a polynomial time.

However, we should consider that all edge costs are uncertain values rather than constant in real-world practical situations. In this paper, we assume the case to calculate the mean value and variance of each edge cost using some data but cannot determine a specific random distribution. From mean value $\overline{c}_j$ and variance $\sigma_j^2$ of each edge cost, we define a $d$-confidence interval of each edge cost based on the study (Watada et al. [11]) using parameter $d_j$ as $[\overline{c}_j - d_j\sigma_j, \overline{c}_j + d_j\sigma_j]$ where mean values $\overline{c}_j$ and robust parameters $d_j$ are positive. If the random distribution occurs according to a general ellipsoidal distribution such as the normal, Student $t$, Pareto's distributions, this formulation denotes the value at risk satisfying with some risk factors. Furthermore, if the random distribution occurs according to the stable distribution such as the normal, Cauchy's, and Levy's distributions, this formulation denotes the conditional value at risk (for instance, Rachev et al. [15]). Therefore, we focus on $\overline{c}_j + d_j\sigma_j$ of $d$-confidence interval and regard parameter $d_j$ as the downside risk in robustness.

### 2.2. Objects for the Proposed Model

(i) Minimizing the maximum value of downside edge cost $\overline{c}_j + d_j\sigma_j$.

In practical network optimization and previous standard BST problem (2.2), it is natural for the decision maker to minimize the maximum value of downside edge costs $\overline{c}_j + d_j\sigma_j$. Therefore, minimizing the maximum value of $\overline{c}_j + d_j\sigma_j$ is also formulated as the following problem:

$$\begin{aligned} &\text{Minimize} \quad \max_{j\in S}\{(\overline{c}_j + d_j\sigma_j)x_j\} \\ &\text{subject to} \quad x_j = \begin{cases} 1 & (e_j \in T) \\ 0 & (e_j \notin T) \end{cases}, \quad j \in S. \end{aligned} \tag{2.3}$$

Introducing parameter $f$ as an acceptable target edge cost, the above problem is equivalently transformed into the following problem:

$$\begin{aligned} &\text{Minimize} \quad f \\ &\text{subject to} \quad \max_{j\in S}\left\{\left(\overline{c}_j + d_j\sigma_j\right)x_j\right\} \geq f \\ &\qquad x_j = \begin{cases} 1 & \left(e_j \in T\right) \\ 0 & \left(e_j \notin T\right) \end{cases}, \quad j \in S. \end{aligned} \tag{2.4}$$

(ii) Maximizing the minimum value of robust parameters $d_j$.

In robustness, if parameter $d_j$ is constant and of larger value, interval $[\overline{c}_j - d_j\sigma_j, \overline{c}_j + d_j\sigma_j]$ is also wide. It urges the decision maker to deal with more robust cases than the small value of $d_j$. In risk control and management, it is also important to maximize the minimum value of parameter $d_j$, and hence, the following robust BST problem is formulated:

$$\begin{aligned} &\text{Maximize} \quad \min_{j\in S}\left\{d_j x_j\right\} \\ &\text{subject to} \quad x_j = \begin{cases} 1 & \left(e_j \in T\right) \\ 0 & \left(e_j \notin T\right) \end{cases}, \quad j \in S. \end{aligned} \tag{2.5}$$

In a way similar to the transformation from problems (2.3) to (2.4), problem (2.5) is also equivalently transformed into the following problem introducing parameter $\overline{d}$ as a target value of robustness:

$$\begin{aligned} &\text{Maximize} \quad \overline{d} \\ &\text{subject to} \quad \min_{j\in S}\left\{d_j x_j\right\} \geq \overline{d} \\ &\qquad x_j = \begin{cases} 1 & \left(e_j \in T\right) \\ 0 & \left(e_j \notin T\right) \end{cases}, \quad j \in S. \end{aligned} \tag{2.6}$$

(iii) Maximizing the total reliability to the whole of spanning tree.

It is also often necessary to construct the network connecting nodes keeping the higher reliability even if the worst value of edge cost is large. This means that we need to set the reliability of each edge and to decide a spanning tree maximizing the total reliability as well as minimizing the maximum value of downside edge costs and maximizing the minimum value of robust parameters. In this paper, we assume that the decision maker gives a constant value of reliability $\beta_j$ to each edge as a constant value from 0 to 1 according to edge costs that is, $\beta_j \in [0, 1]$.

In this paper, we focus on the concept that the whole of spanning tree is nonfunctional as a normal communication network even if only one edge in the spanning tree is broken

down. Therefore, the problem maximizing the total reliability of spanning tree is formulated as the following problem:

$$\begin{aligned} &\text{Maximize} \quad \prod_{e_j \in T} \beta_j x_j \\ &\text{subject to} \quad x_j = \begin{cases} 1 & (e_j \in T) \\ 0 & (e_j \notin T) \end{cases}, \quad j \in S. \end{aligned} \tag{2.7}$$

The objective function of problem is often used in the mathematical formulation maximizing the total reliability in communication networks.

### 2.3. *Main Formulation of Our Proposed BST Model*

By integrating these three objects, our proposed BST model is formulated as the following multiobjective programming problem:

$$\begin{aligned} &\text{Minimize} \quad f \\ &\text{Maximize} \quad \overline{d} \\ &\text{Maximize} \quad \prod_{e_j \in T} \beta_j x_j \\ &\text{subject to} \quad \max_{j \in S} \left\{ \left( \overline{c}_j + d_j \sigma_j \right) x_j \right\} \geq f, \\ &\qquad \min_{j \in S} \left\{ d_j x_j \right\} \geq \overline{d}, \\ &\qquad x_j = \begin{cases} 1 & (e_j \in T) \\ 0 & (e_j \notin T) \end{cases}, \quad j \in S. \end{aligned} \tag{2.8}$$

This problem is a multiobjective programming problem, and hence, it is hard to solve it directly in mathematical programming problem without some optimal criterion. Therefore, in the following sections, we discuss a solution approach to solve problem (2.8) in mathematical programming.

## 3. Introduction of Fuzzy Goals and Bellman-Zadeh's Minimum Operator

In multiobjective programming problem (2.8), it is difficult to deal with a tradeoff between the total cost $f$ and robustness parameter $\overline{d}$ directly, because these attributes are completely opposite. Furthermore, taking account of satisfaction of decision maker and robustness for the execution of network, the decision maker often has satisfaction functions for target values of the total cost $f$, the robust parameter $\overline{d}$, and the total reliability $\beta = \prod_{e_j \in T} \beta_j x_j$, which is often called fuzzy goals.

In this paper, we define the following satisfaction function characterized by linear membership functions:

$$\mu_{f_G}(\omega) = \begin{cases} 1 & (\omega \le f_L), \\ \dfrac{f_U - \omega}{f_U - f_L} & (f_L < \omega \le f_U), \\ 0 & (f_U < \omega), \end{cases}$$

$$\mu_{d_G}(\omega) = \begin{cases} 1 & (d_U \le \omega), \\ \dfrac{\omega - d_L}{d_U - d_L} & (d_L \le \omega < d_U), \\ 0 & (\omega < d_L), \end{cases} \tag{3.1}$$

$$\mu_{\beta_G}(\omega) = \begin{cases} 1 & (\beta_U \le \omega), \\ \dfrac{\omega - \beta_L}{\beta_U - \beta_L} & (\beta_L \le \omega < \beta_U), \\ 0 & (\omega < \beta_U), \end{cases}$$

where $f_L, f_U, d_L, d_U, \beta_L$, and $\beta_U$ are constant positive values determined by the decision maker. Introducing these satisfaction functions into problem (2.8), we reformulate the proposed BST problem as follows:

$$\begin{aligned} &\text{Maximize} \quad \mu_{f_G}(f) \\ &\text{Maximize} \quad \mu_{d_G}\left(\overline{d}\right) \\ &\text{Maximize} \quad \mu_{\beta_G}\left(\prod_{e_j \in T} \beta_j x_j\right) \\ &\text{subject to} \quad \max_{j \in S}\left\{\left(\overline{c}_j + d_j \sigma_j\right) x_j\right\} \ge \mathrm{f}, \\ &\qquad \min_{j \in S}\left\{d_j x_j\right\} \ge \overline{d} \\ &\qquad x_j = \begin{cases} 1 & (e_j \in T) \\ 0 & (e_j \notin T) \end{cases}, \quad j \in S \end{aligned} \tag{3.2}$$

Problem (3.2) is also a multiobjective programming problem, and hence, it remains the difficulty of solving this problem directly since a complete optimal solution that simultaneously optimizes all of the multiobjective functions does not always exist. Therefore, instead of a complete optimal solution, a Pareto optimal solution may be reasonable for a multiobjective case.

As a reasonable solution concept for the fuzzy multiobjective decision-making problem, a Pareto optimal solution is defined as follows in the ordinary multiobjective programming problem proposed by Sakawa et al. (Sakawa [16], Sakawa et al. [17]):

*Definition 3.1.* Let $\mathbf{x}$ and $X$ be a decision variable column vector and a set of feasible solutions, respectively. Then, $\mathbf{x}^* \in X$ is said to be an M-Pareto optimal solution if and only if there does not exist another $\mathbf{x} \in X$ such that $\mu_{f_G}(f) \geq \mu_{f_G}(f^*)$, $\mu_{d_G}(\overline{d}) \geq \mu_{d_G}(\overline{d}^*)$ and $\mu_{\beta_G}(\prod_{e_j \in T} \beta_j x_j) \geq \mu_{\beta_G}(\prod_{e_j \in T} \beta_j x_j^*)$, and either $\mu_{f_G}(f) > \mu_{f_G}(f^*)$, $\mu_{d_G}(\overline{d}) > \mu_{d_G}(\overline{d}^*)$ or $\mu_{\beta_G}(\prod_{e_j \in T} \beta_j x_j) > \mu_{\beta_G}(\prod_{e_j \in T} \beta_j x_j^*)$.

Introducing an aggregation function $\mu_D(x)$ for three membership functions $\mu_{f_G}(f), \mu_{d_G}(\overline{d})$ and $\mu_{\beta_G}(\prod_{e_j \in T} \beta_j x_j)$, the problem can be rewritten as follows:

$$\begin{aligned} &\text{Maximize} \quad \mu_D(\mathbf{x}) \\ &\text{subject to} \quad \max_{j \in S} \left\{ (\overline{c}_j + d_j \sigma_j) x_j \right\} \geq f, \\ &\qquad \min_{j \in S} \left\{ d_j x_j \right\} \geq \overline{d}, \\ &\qquad x_j = \begin{cases} 1 & (e_j \in T) \\ 0 & (e_j \notin T) \end{cases}, \quad j \in S. \end{aligned} \tag{3.3}$$

The aggregation function $\mu_D(\mathbf{x})$ represents the integrated satisfaction or preference degree of the decision maker for the whole of satisfaction functions. Some researchers have proposed aggregation functions: the minimum operator (Bellman and Zadeh [14]), the product operator (Zimmermann [18]), and so forth. Particularly, the following Bellman-Zadeh's minimum operator $Z_G$ is one of the standard appropriate aggregation functions and is dealt with in many studies, and the mathematical formulation is to minimize the aspiration value in all satisfaction functions:

$$Z_G = \min \left\{ \mu_{f_G}(f), \mu_{d_G}\left(\overline{d}\right), \mu_{\beta_G}\left(\prod_{e_j \in T} \beta_j x_j\right) \right\}. \tag{3.4}$$

Therefore, setting satisfaction functions for the multiobjective and introducing the Bellman-Zadeh minimum operator, we transform problem (3.2) into the following single objective programming problem:

$$\begin{aligned} &\text{Maximize} \quad Z_G \\ &\text{subject to} \quad \max_{j \in S} \left\{ (\overline{c}_j + d_j \sigma_j) x_j \right\} \geq f, \\ &\qquad \min_{j \in S} \left\{ d_j x_j \right\} \geq \overline{d}, \\ &\qquad x_j = \begin{cases} 1 & (e_j \in T) \\ 0 & (e_j \notin T) \end{cases}, \quad j \in S. \end{aligned} \tag{3.5}$$

In mathematical programming, the optimal solution of problem (3.5) is also the same as that of the following problem introducing parameter $h$ which means the common target satisfaction level:

$$\begin{aligned}
&\text{Maximize} \quad h \\
&\text{subject to} \quad Z_G \geq h, \\
&\qquad \max_{j\in S}\{(\overline{c}_j + d_j\sigma_j)x_j\} \geq f, \\
&\qquad \min_{j\in S}\{d_j x_j\} \geq \overline{d}, \\
&\qquad x_j = \begin{cases} 1 & (e_j \in T) \\ 0 & (e_j \notin T) \end{cases}, \quad j \in S.
\end{aligned} \tag{3.6}$$

## 4. Development of Polynomial-Time Solution Algorithm for the Proposed BST Problem

In problem (3.6), the first, second, and third constraints are equivalently transformed into the following inequalities without the loss of optimality.

First constraint:

$$\begin{aligned}
&Z_G \geq h \\
&\quad \Longleftrightarrow \mu_{f_G}(f) \geq h, \mu_{d_G}\left(\overline{d}\right) \geq h, \mu_{\beta_G}\left(\prod_{e_j\in T}\beta_j x_j\right) \geq h \\
&\quad \Longleftrightarrow \frac{f_U - f}{f_U - f_L} \geq h, \frac{\overline{d} - d_L}{d_U - d_L} \geq h, \frac{\left(\prod_{e_j\in T}\beta_j x_j\right) - \beta_L}{\beta_U - \beta_L} \geq h \\
&\quad \Longleftrightarrow \begin{cases} f \leq f_U - h(f_U - f_L) \\ \overline{d} \geq d_L + h(d_U - d_L) \\ \prod_{e_j\in T}\beta_j x_j \geq \beta_L + h(\beta_U - \beta_L). \end{cases}
\end{aligned} \tag{4.1}$$

Second constraint:

$$\max\{(\overline{c}_j + d_j\sigma_j)x_j \mid j \in S\} \leq f \Longleftrightarrow (\overline{c}_j + d_j\sigma_j)x_j \leq f. \tag{4.2}$$

Third constraint:

$$\min\{d_j x_j \mid j \in S\} \geq \overline{d} \Longleftrightarrow d_j \geq \overline{d}x_j. \tag{4.3}$$

Furthermore, these constraints (4.1), (4.2), and (4.3) are reduced as follows:

$$\begin{aligned} f \le f_U - h(f_U - f_L) \\ (\overline{c}_j + d_j\sigma_j)x_j \le f \end{aligned} \iff (\overline{c}_j + d_j\sigma_j)x_j \le f_U - h(f_U - f_L),$$
$$\begin{aligned} \overline{d} \ge d_L + h(d_U - d_L) \\ d_j \ge \overline{d}x_j \end{aligned} \iff d_j \ge \{d_L + h(d_U - d_L)\}x_j. \tag{4.4}$$

Consequently, problem (3.6) is equivalently transformed into the following problem:

$$\begin{aligned} &\text{Maximize} && h \\ &\text{subject to} && (\overline{c}_j + d_j\sigma_j)x_j \le f_U - h(f_U - f_L), \\ &&& d_j \ge \{d_L + h(d_U - d_L)\}x_j, \\ &&& \prod_{e_j \in T} \beta_j x_j \ge \beta_L + h(\beta_U - \beta_L), \\ &&& x_j = \begin{cases} 1 & (e_j \in T) \\ 0 & (e_j \notin T) \end{cases}, \quad j \in S. \end{aligned} \tag{4.5}$$

We focus on third constraint $\prod_{e_j \in T} \beta_j x_j \ge \beta_L + h(\beta_U - \beta_L)$ in the above problem. In problem (4.5), decision variables $x_j, (j \in S)$ become only 0 or 1, respectively. Therefore, $\prod_{e_j \in T} \beta_j x_j = \prod_{e_j \in T} \beta_j$ holds. Using this formula, since $\prod_{e_j \in T} \beta_j x_j$ and $\beta_L + h(\beta_U - \beta_L)$ are positive, this constraint is equivalently transformed into the following logarithmic constraint without the loss of optimality:

$$\begin{aligned} &\prod_{e_j \in T} \beta_j x_j \ge \beta_L + h(\beta_U - \beta_L) \\ &\quad \iff \prod_{e_j \in T} \beta_j \ge \beta_L + h(\beta_U - \beta_L) \\ &\quad \iff \log\left(\prod_{e_j \in T} \beta_j\right) \ge \log(\beta_L + h(\beta_U - \beta_L)) \\ &\quad \iff \sum_{e_j \in T} \log \beta_j \ge \log(\beta_L + h(\beta_U - \beta_L)) \\ &\quad \iff \sum_{j \in S} (\log \beta_j) x_j \ge \log(\beta_L + h(\beta_U - \beta_L)). \end{aligned} \tag{4.6}$$

Therefore, the optimal solution of problem (4.5) is the same as that of the following problem:

$$\begin{aligned}
&\text{Maximize} \quad h \\
&\text{subject to} \quad (\overline{c}_j + d_j\sigma_j)x_j \le f_U - h(f_U - f_L), \\
&\qquad\qquad d_j \ge \{d_L + h(d_U - d_L)\}x_j, \\
&\qquad\qquad \sum_{j\in S}(\log\beta_j)x_j \ge \log(\beta_L + h(\beta_U - \beta_L)), \\
&\qquad\qquad x_j = \begin{cases} 1 & (e_j \in T) \\ 0 & (e_j \notin T) \end{cases}, \quad j \in S.
\end{aligned} \tag{4.7}$$

Furthermore, by reducing the first and second constraints in problem (4.7) as follow:

$$\begin{aligned}
&(\overline{c}_j + d_j\sigma_j)x_j \le f_U - h(f_U - f_L) \\
&\quad d_j \ge \{d_L + h(d_U - d_L)\}x_j \\
&\qquad \Longleftrightarrow \begin{cases} d_j x_j \le \dfrac{f(h) - \overline{c}_j x_j}{\sigma_j}, (f(h) = f_U - h(f_U - f_L)) \\ d_j x_j \ge d(h)x_j^2, \qquad (d(h) = d_L + h(d_U - d_L)) \end{cases} \\
&\qquad \Longleftrightarrow d(h)x_j^2 \le \frac{f(h) - \overline{c}_j x_j}{\sigma_j} \\
&\qquad \Longleftrightarrow d(h)x_j \le \frac{f(h) - \overline{c}_j x_j}{\sigma_j} \\
&\qquad \Longleftrightarrow x_j \le \frac{f(h)}{d(h)\sigma_j + \overline{c}_j},
\end{aligned} \tag{4.8}$$

problem (4.7) is also equivalently transformed into the following problem introducing $\beta(h) = \beta_L + h(\beta_U - \beta_L)$:

$$\begin{aligned}
&\text{Maximize} \quad h \\
&\text{subject to} \quad x_j \le \frac{f(h)}{d(h)\sigma_j + \overline{c}_j}, \\
&\qquad\qquad \sum_{j\in S}(\log\beta_j)x_j \ge \log\beta(h), \\
&\qquad\qquad x_j = \begin{cases} 1 & (e_j \in T) \\ 0 & (e_j \notin T) \end{cases}, \quad j \in S.
\end{aligned} \tag{4.9}$$

This problem is a constrained spanning tree problem. In general, it is difficult to solve constrained network optimization problems in the polynomial time. However, since

problem (4.9) fulfills the following theorem, we will show that the solution algorithm of problem (4.9) in the polynomial-time.

**Theorem 4.1.** *Fix parameter $h = \overline{h}$, and set $R_j(\overline{h}) = f(\overline{h})/(d(\overline{h})\sigma_j + \overline{c}_j)$. If $R_j(\overline{h}) < 1$, then $x_j = 0$, that is, edge $e_j$ is not included in the optimal spanning tree.*

*Proof.* Since $R_j(\overline{h}) < 1$ and $x_j \leq R(\overline{h})$, $x_j < 1$ is obtained. Furthermore, since $x_j$ is a 0-1 decision variable, $x_j = 0$ is also obtained. □

From Theorem 4.1, we can narrow feasible spanning trees in the given network. Furthermore, in the case of fixed parameter $\overline{h}$, we introduce an auxiliary problem of problem (4.9) as follows:

$$\begin{aligned} &\text{Maximize} \quad \sum_{j\in S} (\log \beta_j) x_j \\ &\text{subject to} \quad x_j = 0, j = 1, \ldots, i, \\ &\qquad\qquad x_j = \begin{cases} 1 & (e_j \in T) \\ 0 & (e_j \notin T) \end{cases}, \quad j = i+1, \ldots, m, \end{aligned} \tag{4.10}$$

where $i$ is the maximum number of index $j$ satisfying $R_j(\overline{h}) < 1$. Since we assume $0 < \beta_j \leq 1$, $\log \beta_j$ is a negative value. Therefore, the above problem is equivalently transformed into the following minimizing problem:

$$\begin{aligned} &\text{Minimize} \quad \sum_{j=i+1}^{m} (-\log \beta_j) x_j \\ &\text{subject to} \quad x_j = \begin{cases} 1 & (e_j \in T) \\ 0 & (e_j \notin T) \end{cases}, \quad j = i+1, \ldots, m. \end{aligned} \tag{4.11}$$

This auxiliary problem is the same as a standard MST problem, and hence, it is possible to obtain the optimal spanning tree in the polynomial time using the Kruskal algorithm [7] or the Prim algorithm [8]. Furthermore, as an optimality condition between this auxiliary problem and problem (4.9), the following theorem holds.

**Theorem 4.2.** *Let $x_j^*(\overline{h})$, $(j = 1, 2, \ldots, m)$ be the optimal solution of auxiliary problem* (4.11)*, and let $h^*$ be the optimal value of problem* (4.9)*. Then, the following rules hold:*

$$\begin{aligned} &\sum_{j\in S} (\log \beta_j) x_j^*\left(\overline{h}\right) > \log \beta\left(\overline{h}\right) \longrightarrow \overline{h} < h^*, \\ &\sum_{j\in S} (\log \beta_j) x_j^*\left(\overline{h}\right) = \log \beta\left(\overline{h}\right) \longrightarrow \overline{h} = h^*, \\ &\sum_{j\in S} (\log \beta_j) x_j^*\left(\overline{h}\right) < \log \beta\left(\overline{h}\right) \longrightarrow \overline{h} > h^*. \end{aligned} \tag{4.12}$$

*Proof.* $\log\beta(h)$ is an increasing function on $h$ due to setting membership function (3.1). Then, since $R_j(h) = f(h)/(d(h)\sigma_j + \bar{c}_j)$ is a decreasing function on $h$ from decreasing function $f(h)$ and increasing function $d(h)$, the number of indexes satisfying $x_j(h) < 1$ is increasing. Therefore, in the case of $h \leq \overline{h}$, the feasible region of problem (4.11) of $n$ the case of $\overline{h}$ is narrower than $h$, and $\sum_{j\in S}(-\log\beta_j)x_j^*(h) \leq \sum_{j\in S}(-\log\beta_j)x_j^*(\overline{h})$; that is, $\sum_{j\in S}(\log\beta_j)x_j^*(h) \geq \sum_{j\in S}(\log\beta_j)x_j^*(\overline{h})$ holds. Consequently, from increasing function $\log\beta(h)$ and decreasing function $\sum_{j\in S}(\log\beta_j)x_j(h)$, this theorem is obtained.

Consequently, from Theorems 4.1 and 4.2 and auxiliary problem (4.9), we develop the following solution algorithm for our proposed BST problem (3.6). □

### 4.1. Solution Algorithm

*Step 1.* Elicit the satisfaction functions $\mu_{f_G}(\omega)$, $\mu_{d_G}(\omega)$, and $\mu_{\beta_G}(\omega)$ by the decision maker, and go to Step 2.

*Step 2.* Set $h_{\mathrm{L}} \leftarrow 0, h_U \leftarrow 1, k \leftarrow 1$, and go to Step 3.

*Step 3.* In the case $h_1 = 1$, solve problem (4.11). If the optimal spanning tree $x_j^*(1)$ is obtained, then $x_j^*(1)$ is also the optimal spanning tree of our proposed model (3.6), and terminate this algorithm. If not, go to Step 4.

*Step 4.* In the case $h_1 = 0$, solve problem (4.11). If there are no feasible solutions, return to Step 1 and reset parameters of satisfaction functions $\mu_{f_G}(\omega)$, $\mu_{d_G}(\omega)$, and $\mu_{\beta_G}(\omega)$. If not, go to Step 5.

*Step 5.* Set $h_k \leftarrow (h_L + h_U)/2$, and go to Step 6.

*Step 6.* Calculate $R_j(h_k)$ of each edge $e_j$, and check $R_j(h_k) \geq 1$ or not. If $R_j(h_k) < 1$, then $x_j^*(h_k) = 0$, and go to Step 7.

*Step 7.* Solve auxiliary problem (4.11) of the proposed model, and obtain the optimal spanning tree $x_j^*(h_k)$. Then, calculate $\sum_{j\in S}(\log\beta_j)x_j^*(h_k)$, and go to Step 8.

*Step 8.* From Theorem 4.2, if $\sum_{j\in S}(\log\beta_j)x_j^*(h_k) = \log\beta(h_k)$, then $\overline{h}$ is also the optimal solution of our proposed BST problem (3.6), and hence, $x_j^*(h_k)$ is the optimal spanning tree. Therefore, terminate the algorithm. Then, in the case $k \geq 2$, if $x_j^*(h_{k-1}) = x_j^*(h_k), j = 1, 2, \ldots, m$, and the following conditions holds:

$$\sum_{j\in S}(\log\beta_j)x_j^*(h_{k-1}) > \log\beta(h_{k-1}), \sum_{j\in S}(\log\beta_j)x_j^*(h_k) < \log\beta(h_k), \tag{4.13}$$

$x_j^*(h_k)$ is the optimal spanning tree of the proposed problem (3.6), and terminate this algorithm. If not, go to Step 9.

*Step 9.* If $\sum_{j\in S}(\log\beta_j)x_j^*(h_k) > \log\beta(h_k)$, then $h_L \leftarrow h_k, k \leftarrow k+1$ and return to Step 3. If $\sum_{j\in S}(\log\beta_j)x_j^*(\overline{h}) < \log\beta(\overline{h})$, then $h_U \leftarrow h_k, k \leftarrow k+1$ and return to Step 5.

Consequently, solving problem (4.11) on each parameter $h_k$ using this solution algorithm, we obtain an exact bottleneck spanning tree for our proposed BST problem (3.6) according to decision maker's satisfaction. The main steps of this solution algorithm is to solve auxiliary problem (4.11) and to do the bisection method on parameter $h$. The computational complexity to solve auxiliary problem (4.11) are polynomial time due to Kruskal's or Prim's polynomial time algorithm. Then, the computational complexity of bisection method is also polynomial time. Therefore, the total computational complexity of this solution algorithm from Steps 1 to 9 is the polynomial-time.

## 5. Numerical Example

In this section, we provide a simple numerical example. Let $G$ be a graph with 6 vertices that is, $n = 6$. Figure 1 illustrates the given graph $G$, and parameters in this example are given in Table 1. In the real world applications such as construction of telecommunication stations networks between cities, some uncertain factors may intervene in the decision making of the construction cost. Furthermore, in the case to ensure the reliability of trunk and backbone networks, we also need to enhance the reliability of spanning tree as well as robustness of edge costs. Therefore, using the numerical example in this section, we compare our proposed BST problem with the standard BST problem and probability maximization-based BST problem not including the reliability.

First, we solve a standard BST problem using data of constant edge costs not including the reliability. As constant edge costs, we deal with mean values in Table 1. Using the mean values, we solve the standard BST problem, and obtain the optimal spanning tree as Figure 2.

Next, we consider the case where each edge cost is a random variable not including the reliability of spanning tree that is, we solve the following probability maximization-based BST problem:

$$\begin{aligned} &\text{Maximize} \quad \overline{d} \\ &\text{subject to} \quad \max_{j\in S}\left\{\left(\overline{c}_j + d_j\sigma_j\right)x_j\right\} \geq f, \\ &\qquad\qquad \min_{j\in S}\left\{d_j x_j\right\} \geq \overline{d}, \\ &\qquad\qquad x_j = \begin{cases} 1 & \left(e_j \in T\right) \\ 0 & \left(e_j \notin T\right) \end{cases}, \quad j \in S. \end{aligned} \tag{5.1}$$

We use data of parameters in Table 1, and set parameter $f = 5$. We solve problem (5.1) and obtain the optimal spanning tree as Figure 3.

Comparing Figure 3 with Figure 2, edges $e_5$ and $e_{10}$ selected in Figure 2 are changed into edges $e_7$ and $e_{11}$. Numerical data in Table 1 shows that mean values of edges $e_5$ and $e_{10}$ are similar to those of edges $e_7$ and $e_{11}$, respectively. However, variances of edges $e_5$ and $e_{10}$ are much higher than those of edges $e_7$ and $e_{11}$, and hence, probability maximization-based BST problem, which is a subproblem of our proposed BST problem, tends to avoid the uncertain risk derived from variances.

Finally, we solve our proposed BST problem with maximizing the reliability of the whole of spanning tree. We set parameters of satisfaction functions $\mu_{f_G}(\omega), \mu_{d_G}(\omega)$, and

**Table 1:** Parameter values of random edge costs with the reliability.

| Edge | Mean value | Variance | Reliability |
|---|---|---|---|
| $e_1$ | 3.0 | 1.0 | 0.99 |
| $e_2$ | 4.0 | 0.5 | 0.99 |
| $e_3$ | 2.0 | 0.5 | 0.98 |
| $e_4$ | 7.0 | 1.0 | 0.99 |
| $e_5$ | 3.5 | 2.0 | 0.97 |
| $e_6$ | 8.0 | 4.0 | 1.00 |
| $e_7$ | 4.0 | 0.2 | 0.97 |
| $e_8$ | 3.0 | 1.0 | 0.98 |
| $e_9$ | 6.0 | 2.0 | 0.98 |
| $e_{10}$ | 4.0 | 2.5 | 0.99 |
| $e_{11}$ | 4.5 | 0.1 | 0.99 |
| $e_{12}$ | 5.0 | 1.5 | 0.98 |

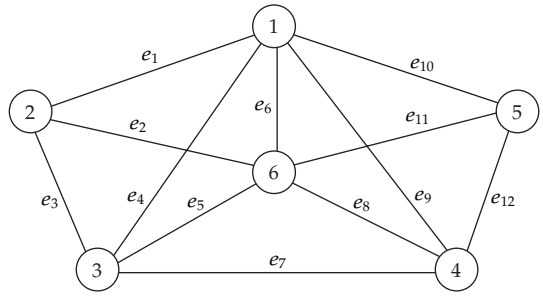


**Figure 1:** Given graph $G$.

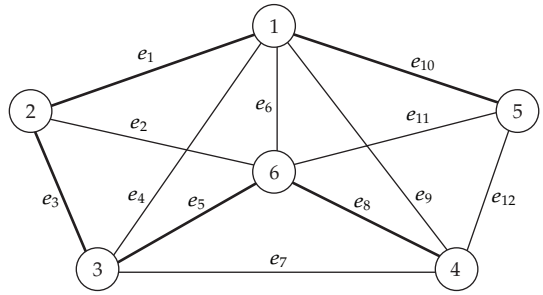


**Figure 2:** Optimal spanning tree of standard BST problem.

$\mu_{\beta_G}(\omega)$ as $f_L = 4, f_U = 6, d_L = 0.5, d_U = 2.0, \beta_L = 0.90, \beta_U = 0.95$, respectively. Using data of random edge costs in Table 1, we solve our proposed BST problem according to the solution algorithm in Section 4 and obtain the optimal spanning tree represented in Figure 4.

Comparing Figure 4 with Figures 2 and 3, edge $e_{11}$ is selected in Figure 4 in the same manner as Figure 3, which is not selected in Figure 2. On the other hand, edge $e_7$ selected in Figure 3 is changed into edge $e_2$. This is why the reliability of $e_7$ is smaller than that of edge $e_2$ from Table 1. In our proposed BST problem, we simultaneously consider the higher total reliability of spanning tree, and hence, our proposed model with randomness and the

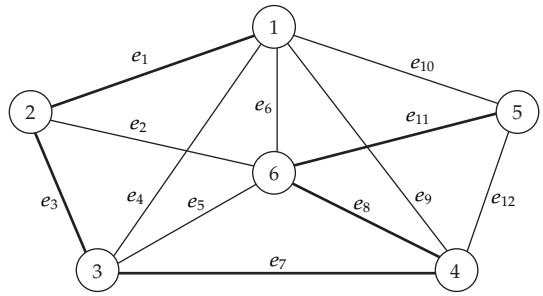


**Figure 3:** Optimal spanning tree of probability maximization-based BST problem.

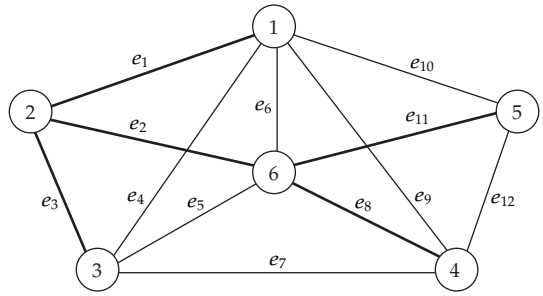


**Figure 4:** Optimal spanning tree of our proposed BST problem with the reliability.

reliability is well balanced between constructing more reliable edges and avoiding uncertain risks.

## 6. Conclusion

In this paper, we have proposed a new bottleneck spanning tree problem that each edge cost includes both uncertainty derived from randomness and the reliability of given spanning tree and have developed the risk control and management approach. Since it is difficult to determine a specific random distribution to each edge cost from received data, we have considered the $d$-confidence interval based on only mean value and variance in risk-control and management to avoid adverse impacts derived from uncertainty. Our proposed model has been formulated as a multiobjective bottleneck spanning tree problem such as (i) minimizing the maximum value of worse edge costs, (ii) maximizing the minimum robustness derived from the $d$-confidence interval of each edge, and (iii) maximizing the reliability to the whole of spanning tree. Furthermore, in order to deal with the satisfaction for the objects of the decision maker and to solve the proposed model in mathematical programming, we have introduced satisfaction functions for all objects and developed the exact solution algorithm using Bellman-Zadeh's minimum operator and deterministic equivalent transformations. By comparing our proposed model with some existing models of bottleneck spanning tree problems using a numerical example, we have obtained the result that our proposed model with randomness and the reliability was well balanced between constructing more reliable edges and avoiding uncertain risks.

Our modeling approach to introduce robustness and reliability in a given network is simple and has usefulness in well-balanced network between robustness and reliability. Furthermore, our proposed model will be naturally applied to the other network optimization problems such as the shortest path problem and the maximum flow problem. Therefore, this study will be based on the other extended studies of network optimization. In this problem, it is also important to determine the value of the reliability to each edge and the relativity between any two edges strictly, and hence, we are now attacking to construct the exact and mathematical method to determine the reliability and relativity of all edges as a future study.

## References


[1] Y. H. Chen, "Polynomial time approximation schemes for the constrained minimum spanning tree problem," *Journal of Applied Mathematics*, vol. 2012, Article ID 394721, 8 pages, 2012.

[2] C. S. Ferreira, L. S. Ochi, V. Parada, and E. Uchoa, "A GRASP-based approach to the generalized minimum spanning tree problem," *Expert Systems with Applications*, vol. 39, no. 3, pp. 3526–3536, 2012.

[3] European Commission, Energy, European Strategy, 2010, http://ec.europa.eu/energy/infrastructure/strategy/2020_en.htm.

[4] D. Cheriton and R. E. Tarjan, "Finding minimum spanning trees," *SIAM Journal on Computing*, vol. 5, no. 4, pp. 724–742, 1976.

[5] H. N. Gabow, Z. Galil, T. Spencer, and R. E. Tarjan, "Efficient algorithms for finding minimum spanning trees in undirected and directed graphs," *Combinatorica*, vol. 6, no. 2, pp. 109–122, 1986.

[6] S. Geetha and K. P. K. Nair, "On stochastic spanning tree problem," *Networks*, vol. 23, no. 8, pp. 675–679, 1993.

[7] J. B. Kruskal, Jr., "On the shortest spanning subtree of a graph and the traveling salesman problem," *Proceedings of the American Mathematical Society*, vol. 7, no. 1, pp. 48–50, 1956.

[8] R. C. Prim, "Shortest connection networks and some generations," *Bell System Technical Journal*, vol. 36, pp. 1389–1401, 1957.

[9] P. Kouvelis and G. Yu, *Robust Discrete Optimization and Its Applications*, Kluwer Academic Publishers, 1997.

[10] R. T. Rockafellar and S. Uryasev, "Optimization of conditional value-at-risk," *Journal of Risk*, vol. 2, no. 3, pp. 1–21, 2000.

[11] J. Watada, S. Wang, and W. Pedrycz, "Building confidence-interval-based fuzzy random regression models," *IEEE Transactions on Fuzzy Systems*, vol. 17, no. 6, pp. 1273–1283, 2009.

[12] H. Ishii and T. Nishida, "Stochastic bottleneck spanning tree problem," *Networks*, vol. 13, no. 3, pp. 443–449, 1983.

[13] H. Katagiri, M. Sakawa, and H. Ishii, "Fuzzy random bottleneck spanning tree problems using possibility and necessity measures," *European Journal of Operational Research*, vol. 152, no. 1, pp. 88–95, 2004.

[14] R. E. Bellman and L. A. Zadeh, "Decision-making in a fuzzy environment," *Management Science*, vol. 17, no. 4, pp. B-141–B-164, 1970.

[15] S. T. Rachev, S. V. Stoyanov, and F. J. Fabozzi, *Advanced Stochastic Models, Risk Assessment, and Portfolio Optimization*, John Wiley & Sons, 2008.

[16] M. Sakawa, *Fuzzy Sets and Interactive Multiobjective Optimization*, Plenum Press, New York, NY, USA, 1993.

[17] M. Sakawa, H. Yano, and T. Yumine, "An interactive fuzzy satisficing method for multiobjective linear-programming problems and its application," *IEEE Transactions on Systems, Man, and Cybernetics*, vol. 17, no. 4, pp. 654–661, 1987.

[18] H. J. Zimmermann, "Fuzzy programming and linear programming with several objective functions," *Fuzzy Sets and Systems*, vol. 1, no. 1, pp. 45–55, 1978.

Hindawi Publishing Corporation
Journal of Applied Mathematics
Volume 2012, Article ID 328186, 18 pages
doi:10.1155/2012/328186

*Research Article*

# Iterative System Identification and Controller Design with an LMI-Based Framework: Windsurfer-Like Approach

**Kazuhiko Hiramoto**

*Department of Mechanical and Production Engineering, Niigata University, 8050 Ikarashi 2-no-cho, Nishi-ku, Niigata 950-2181, Japan*

Correspondence should be addressed to Kazuhiko Hiramoto, hiramoto@eng.niigata-u.ac.jp

Received 1 March 2012; Revised 21 June 2012; Accepted 24 June 2012

Academic Editor: Xianxia Zhang



An LMI-based method for the integrated system identification and controller design is proposed in the paper. We use the fact that a class of a system identification problem results in an LMI optimization problem. By combining LMIs for the system identification and those to obtain a discrete time controller we propose a framework to integrate two steps for the model-based control system design, that is, the system identification and the controller synthesis. The framework enables us to obtain a *good model for control* and a model-based feedback controller simultaneously in the sense of the closed-loop performance. An iterative design algorithm similar to so-called Windsurfer Approach is presented.

## 1. Introduction

In conventional control system design modeling of a control object and a controller synthesis have been dealt with separately, that is, those are divided into two independent steps, although those two processes are inseparably related [1]. Since the early 1990s so-called "iterative system identification and controller design" scheme has been actively studied to achieve the higher closed-loop performance ([2–4], etc.). The iterative manner is required because of the fact that we cannot determine the optimal nominal model (obtained from I/O data of the true plant) and the optimal controller (obtained from the nominal model) simultaneously in the sense of the performance of the closed-loop system with the true plant and the designed controller.

Several methodologies have been proposed on the iterative system identification and controller design and those can be classified as follows.

(1) *Triangular inequality based method* [5, 6]: an iterative frequency weighted system identification and a model-based controller synthesis based on the triangular inequality that shows an upper bound of the closed-loop $\mathcal{H}_2$ norm with the true plant and the model-based controller.

(2) *Windsurfer Approach* [7–10]: expanding the closed-loop bandwidth gradually by the iterative system identification and controller design.

(3) *Frequency weighted LQG control based method* [11]: an iterative update of the frequency weighting used in the quadratic performance index of the frequency weighted LQG control.

In some studies of approaches 1 and 2 the so-called "Hansen scheme" [12] is adopted as a method for the system identification in the closed-loop. With the Hansen scheme the closed-loop identification problem can be transformed into an open-loop one. By combining the Hansen scheme and the controller synthesis methodology based on Youla parameterization we can construct an iterative identification/control algorithm that aims at a (local) convergence of an upper bound of the closed-loop norm. However, in the algorithm the order of the model and the controller tends to be extremely high with the progress of the algorithm.

As another direction in the field of system identification, methodologies based on stochastic gradient have been actively studied for various types of systems, including multivariable systems, the Hammerstein systems, and systems with scarce measurement [13–19].

The objective of above iterative methodologies is essentially to obtain a good plant model that results in the good performance of the closed-loop system with the true plant and the controller. However, in the above methods the system identification and the controller synthesis are still carried out in independent two steps, respectively, that is, the least square method with an appropriate frequency weighting and the model-based controller design. For the model obtained with the above iterative methods we can explain the validity of the obtained plant model with qualitative knowledge about control relevant modeling, for example, the importance of the model accuracy around the closed-loop bandwidth, and so forth [2]. However, we do not have a method to get a quantitatively good model for control, in other words, good parameters of the plant model that directly leads to the improvement of a performance index for evaluating the closed-loop system, for example, closed-loop $\mathcal{H}_2$ or $\mathcal{H}_\infty$ norm although the optimal $\mathcal{H}_2$ or $\mathcal{H}_\infty$ controller design methods have been well established for a given plant model. In general iterative system identification and controller design methods we cannot guarantee the convergence of the closed-loop $\mathcal{H}_2$ or $\mathcal{H}_\infty$ norm. This is because we cannot consider the change of the closed-loop performance coming from the model update in the system identification step (usually conducted in the closed-loop setting) in standard iterative system identification and controller design algorithms. In [9] the amount of the safe controller update for the closed-loop stability and the safe performance improvement in the iterative identification and control are studied with the $\nu$-gap metric [20]. However, the closed-loop performance is measured with the $\nu$-gap only and the control law is confined to the IMC based method.

In this paper a new method for the iterative identification and controller design is proposed aiming to integrate the system identification and the controller design steps under an LMI framework. We assume that the ARX model is the model of the true plant and the $\mathcal{H}_2$ norm of the closed-loop system is the performance index. In the proposed approach the model update is iteratively obtained using the closed-loop I/O data from the closed-loop experiment with a constraint on the norm of the closed-loop system with the updated plant model and the feedback controller. This method is based on the fact that a system

identification problem for ARX models can be formulated as an LMI optimization problem. By combining LMIs to obtain the plant model with the LMI-based method to obtain the discrete time $\mathcal{H}_2$ controller [21] the adjustment existing both in the plant model parameter and the parameters related to the feedback controller can be obtained simultaneously by solving a set of LMIs. The LMI condition is an approximated version of a BMI condition that represents specifications on the closed-loop system identification and the controller update so that the $\mathcal{H}_2$ norm of the closed-loop system with the updated model and controller does not exceed a specified value. In the closed-loop system identification the two-stage method [22] is adopted to minimize the effect of the bias coming from the correlation between the measurement noise and the plant input signal.

In the conventional least square approach for system identification, such simultaneous adjustment of parameters both in the plant model and the feedback controller is not possible. Furthermore there does not occur a problem about the "order explosion" of the plant model and the feedback controller in the proposed method; in contrast to the fact such problem is inevitable in the strategy based on the Hansen scheme. A design algorithm similar to Windsurfer Approach [7, 8], which gradually expands the control authority, while keeping the closed-loop $\mathcal{H}_2$ norm less than a specified value, is presented.

The rest of the paper is organized as follows. In Section 2 the iterative system identification and controller design problem which is addressed in the present study is formulated. An LMI-based system identification method for an SISO ARX model is presented in Section 3. In Section 4 the iterative method for the system identification and the controller design based on the LMI framework is proposed. A design example is presented in Section 5 and the conclusion is given in Section 6.

Notations are as follows: $k$: sample number, $z^{-1}$: the shift operator in discrete time systems, that is, $z^{-1}a(k) = a(k-1)$, $I$, $0$: an identity and zero matrices having the appropriate dimension, respectively, $\mathcal{R}^{m\times n}$: the set of $m \times n$ real matrices, $\mathcal{S}^m$: the set of $m$-dimensional symmetric matrices, trace$(A)$: trace of a square matrix $A$, $\overline{\sigma}(B)$: the maximum singular value of a matrix $B \in \mathcal{R}^{m\times n}$, $C^T$: the transpose of a matrix $C$, $\|D(z)\|_2$: the $\mathcal{H}_2$ norm of a stable transfer function $D(z)$.

## 2. Problem Formulation

Let us consider an SISO linear time invariant discrete time system given as follows:

$$y(k) = y_p(k) + v(k) = P(z)u(k) + v(k), \tag{2.1}$$

where $u(k)$, $y_p(k)$, $y(k)$, and $v(k)$ are the input and output of the plant, the measurement signal, and the noise, respectively. The true plant is defined as the discrete time transfer function $P(z)$.

In the present paper the ARX discrete time system is considered to model the true I/O relationship of the plant in (2.1). The ARX model is parameterized as

$$y_{\mathrm{ARX}}(k) = P_{\mathrm{ARX}}(z)u(k) + v_{\mathrm{ARX}}(k),$$

$$P_{\mathrm{ARX}}(z) = \frac{N_{\mathrm{ARX}}(z)}{D_{\mathrm{ARX}}(z)}, \qquad v_{\mathrm{ARX}}(k) = H_{\mathrm{ARX}}(z)s(k), \qquad H_{\mathrm{ARX}}(z) = \frac{1}{D_{\mathrm{ARX}}(z)},$$

$$N_{\mathrm{ARX}}(z) = b_n z^{-1} + b_{n-1} z^{-2} + \cdots + b_2 z^{-(n+1)} + b_1 z^{-n},$$
$$D_{\mathrm{ARX}}(z) = 1 + a_n z^{-1} + a_{n-1} z^{-2} + \cdots + a_2 z^{-(n+1)} + a_1 z^{-n}, \tag{2.2}$$

where $P_{\mathrm{ARX}}(z)$, $y_{\mathrm{ARX}}(k)$, and $s(k)$ are the ARX model, that is, the $n$th order linear time invariant discrete transfer function, the output of the ARX model, and the zero-mean white noise, respectively. In the ARX model, model parameters to be identified are $a_i, b_i \in \mathcal{R}$, $i = 1, \ldots, n$.

Let $K(z)$ be a linear time invariant feedback controller connected to the plant $P(z)$ as shown in Figure 1. The I/O relationship of the controller $K(z)$ is given as follows:

$$u_k(k) = K(z)y(k). \tag{2.3}$$

The controller $K(z)$ in (2.3) is obtained from the model $P_{\mathrm{ARX}}(z)$ and the order is $n$, that is, the controller $K(z)$ is assumed to be a model-based full-order controller. Note that we cannot get the exact expression of the true plant $P(z)$ in general and the model $P_{\mathrm{ARX}}(z)$ is only available as a model for the controller design.

A state-state realization of the model $P_{\mathrm{ARX}}(z)$ is defined as the following control canonical form:

$$P_{\mathrm{ARX}}(z) : \begin{cases} x_{\mathrm{ARX}}(k+1) = A_{\mathrm{ARX}} x_{\mathrm{ARX}}(k) + B_{\mathrm{ARX}} u(k) \\ y_{\mathrm{ARX}}(k) = C_{\mathrm{ARX}} x_{\mathrm{ARX}}(k) + v_{\mathrm{ARX}}(k), \end{cases}$$
$$A_{\mathrm{ARX}} = \left[\begin{array}{cc} 0_{(n-1)\times 1} & I_{n-1} \\ \hline -a_1 & -a_2 \cdots -a_n \end{array}\right], \quad B_{\mathrm{ARX}} = \begin{bmatrix} 0_{1\times(n-1)} & 1 \end{bmatrix}^T, \quad C_{\mathrm{ARX}} = \begin{bmatrix} b_1 & \cdots b_n \end{bmatrix}. \tag{2.4}$$

By assuming an input disturbance $d(k)$ as shown in Figure 1 we define a generalized plant $G(z)$ as

$$G(z) : \begin{cases} x(k+1) = Ax(k) + B_1 w(k) + B_2 u_k(k) \\ z(k) = C_1 x(k) + D_{12} u(k) \\ y(k) = C_2 x(k) + D_{21} w(k), \end{cases}$$
$$x(k) = x_{\mathrm{ARX}}(k), \quad w(k) := \begin{bmatrix} d(k) \\ v_{\mathrm{ARX}}(k) \end{bmatrix}, \quad z(k) := \begin{bmatrix} z_1(k) \\ z_2(k) \end{bmatrix} := \begin{bmatrix} \rho y_p(k) \\ u(k) \end{bmatrix}, \quad \rho > 0, \tag{2.5}$$
$$A := A_{\mathrm{ARX}}, \quad B_1 := \begin{bmatrix} B_{\mathrm{ARX}} & 0 \end{bmatrix}, \quad B_2 := B_{\mathrm{ARX}}, \quad C_1 := \begin{bmatrix} \rho C_{\mathrm{ARX}} \\ 0 \end{bmatrix},$$
$$C_2 = C_{\mathrm{ARX}}, \quad D_{12} := \begin{bmatrix} 0 \\ 1 \end{bmatrix}, \quad D_{21} := \begin{bmatrix} 0 & 1 \end{bmatrix},$$

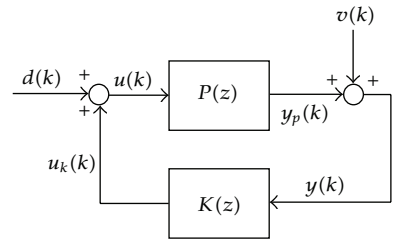


**Figure 1:** Closed-loop system with the true plant $P(z)$ and the model-based controller $K(z)$.

where $\rho > 0$ is a weighting factor that is adjusted by the control designer. We can change the control authority by changing the value of $\rho > 0$;

$$K(z) : \begin{cases} x_K(k+1) = A_K x_K(k) + B_K y(k) \\ u_k(k) = C_K x_K(k). \end{cases} \tag{2.6}$$

Assume that the input disturbance $d(k)$ and the input and the output signals $u(k)$ and $y(k)$ are always available. In this paper a control system design problem is formulated as follows.

*Simultaneous Modeling and Controller Design Problem*

Find the feedback controller $K(z)$ in (2.6) and the ARX model $P_{\mathrm{ARX}}(z)$ in (2.2) so that the closed-loop system with $P(z)$ and $K(z)$ is stable and a performance index given by

$$J_y := \sum_{k=0}^{N_f} y^2(k) \tag{2.7}$$

is minimized for a user-specified disturbance subject to the $\mathscr{H}_2$ norm of the closed-loop system with $G(z)$ and $K(z)$ is less than $\mu > 0$ and

$$|u(k)| \le \overline{u}, \quad \forall k = 0, \ldots, N_f, \tag{2.8}$$

where $\overline{u} > 0$ is the allowed maximum value of $|u(k)|$, $k = 0, \ldots, N_f$.

Note that in the above problem formulation the closed-loop system with the unknown true plant $P(z)$ in (2.1) and the model-based controller $K(z)$ in (2.6), which is obtained with the ARX model $P_{\mathrm{ARX}}(z)$, is not necessarily stable even if the closed-loop system with $P_{\mathrm{ARX}}(z)$ and $K(z)$ is stable. The feature is always true also in general model-based control system design problems.

## 3. LMI-Based System Identification and Controller Design

### 3.1. LMI-Based System Identification

Assume that we have $N+1$ samples of input and output data of the plant $P(z)$ in (2.1), denoted by $u(k)$ and $y(k)$, $k=0,\ldots,N$, from a single identification experiment. In the ARX model in (2.2) the prediction error $e(k,\theta)$ is given by

$$\begin{aligned} e(k,\theta) &:= D_{\mathrm{ARX}}(z)y(k) - N_{\mathrm{ARX}}(z)u(k) = y(k) - D_{IO}(k)\theta, \\ D_{IO}(k) &:= \begin{bmatrix} -D_O(k) & D_I(k) \end{bmatrix}, \\ D_O(k) &:= \begin{bmatrix} y(k-n) & \cdots & y(k-1) \end{bmatrix}, \qquad D_I(k) := \begin{bmatrix} u(k-n) & \cdots & u(k-1) \end{bmatrix}, \\ \theta &:= \begin{bmatrix} a_1 & \cdots & a_n & b_1 & \cdots & b_n \end{bmatrix}^T, \qquad u(k-j) = y(k-j) = 0, \quad \forall k-j<0,\ j=1,\ldots,n. \end{aligned} \tag{3.1}$$

The objective function for the system identification, the sum of the squared prediction error $e(k,\theta)$, is given as

$$J_p := \sum_{k=1}^{N} e^2(k,\theta) = \sum_{k=1}^{N} \left(y(k) - D_{IO}(k)\theta\right)^2. \tag{3.2}$$

Using the Schur complement lemma we can easily see that the square of the prediction error at each $k$th sample is less than $\alpha(k)>0$, $k=1,\ldots,N$, that is, $e^2(k) = \left(y(k)-D_{IO}(k)\theta\right)^2 < \alpha(k)$, $k=1,\ldots,N$ if and only if the following matrix inequalities are satisfied:

$$\begin{bmatrix} \alpha(k) & y(k) - D_{IO}(k)\theta \\ y(k) - D_{IO}(k)\theta & 1 \end{bmatrix} > 0, \quad k=1,\ldots,N. \tag{3.3}$$

Note that conditions in (3.3) are $N$ LMI constraints on the parameter vector $\theta$ and $\alpha(k)$, $k=1,\ldots,N$. With (3.3) the optimal solution to the least square problem can also be obtained as the solution vector $\theta_{\mathrm{opt}}$ that solves the following LMI optimization problem:

$$\text{Minimize } f(\alpha(k)) := \sum_{k=1}^{N} \alpha(k) \text{ subject to (3.3) and } \alpha(k) > 0, \quad \forall k = 1,\ldots,N. \tag{3.4}$$

Note that we can obtain the unique and globally optimal solution vector $\theta_{\mathrm{opt}}$ because of the LMI nature of the optimization problem (3.4).

### 3.2. Controller Design

To solve the control system design problem formulated in Section 2 the feedback controller $K(z)$ in (2.6) is designed so that the $\mathscr{H}_2$ norm of the closed-loop system is less than $\mu > 0$.

We employ the LMI-based discrete time controller design method proposed in [21]. The LMI conditions for the controller design are given as follows:

$$\operatorname{trace}(W) < \mu^2, \tag{3.5}$$

$$\begin{bmatrix} W & C_1X + D_{12}L & C_1 \\ * & X + X^T - P & I + S^T - J \\ * & * & Y + Y^T - H \end{bmatrix} > 0, \tag{3.6}$$

$$\begin{bmatrix} P & J & AX + B_2L & A & B_1 \\ * & H & Q & YA + FC_2 & YB_1 + FD_{21} \\ * & * & X + X^T - P & I + S^T - J & 0 \\ * & * & * & Y + Y^T - H & 0 \\ * & * & * & * & I \end{bmatrix} > 0, \tag{3.7}$$

where $J,\ Q,\ S,\ X,\ Y \in \mathcal{R}^{n\times n}$, $F, L^T \in \mathcal{R}^{n\times 1}$, $H, P \in \mathcal{S}^n$, and $W \in \mathcal{S}^2$. Note that blocks whose descriptions are easily inferred from the symmetric property of LMIs are denoted by "$*$". Coefficient matrices of the controller $K(z)$ in (2.6) can be obtained as follows:

$$A_K = V^{-1}(Q - YAX - YB_2L - FC_2X)U^{-1}, \qquad B_K = V^{-1}F, \qquad C_K = (L - C_2X)U^{-1}, \tag{3.8}$$

where matrices $U, V \in \mathcal{R}^{n\times n}$ are chosen arbitrarily if they satisfy $VU = S - YX$.

## 4. Windsurfer-Like Approach with an LMI-Based Method

### 4.1. Design Algorithm

For the control design problem in Section 2 a method for the iterative system identification and controller design under an LMI framework is proposed by combining the LMI-based system identification and the discrete time controller design [21] in the previous section into a single system of LMIs. With the generalized plant $G(z)$ in (2.5) a following design algorithm, similar to Windsurfer Approach [7, 8], is proposed in the present paper.

#### 4.1.1. Windsurfer-Like Approach with an LMI-Based Method

*Step 1.* Let $i_d = 1$ as the iterative number of the algorithm. If the plant $P(z)$ is stable collect the input and output data of $P(z)$ in the open-loop setting ($K(z) = 0$) and obtain the initial ARX model $P^1_{\mathrm{ARX}}(z)$ in (2.2) by the LMI-based method in Section 3 or the standard least square method so that the objective function $J_p$ (3.2) ($f(\alpha(k))$ in (3.4)) is minimized. If the plant $P(z)$ is unstable, the initial model $P^1_{\mathrm{ARX}}(z)$ is obtained with a method based on the first principle modeling. Set the weighting factor $\rho^{i_d} > 0$ and the closed-loop $\mathcal{H}_2$ norm constraint $\mu > 0$ in (3.5). Note that the weighting factor $\rho^1 > 0$ (the weighting factor in $i_d = 1$) is set to be sufficiently small so that the initial controller $K^1(z)$ that will be obtained in the next step has a *mild* control authority.

*Step 2.* With the LMI-based method shown in the previous section [21], obtain a feedback controller $K^{i_d}(z)$ satisfying the closed-loop $\mathscr{H}_2$ norm constraint. If $i_d = 1$, go to Step 5. Else if such controller $K^{i_d}(z)$ cannot be obtained or the constraint (2.8) is violated, go to Step 7. Otherwise go to Step 3.

*Step 3.* Obtain the performance index $J_y^{i_d}$ in (2.7) for the closed-loop system with the true plant and the controller $K^{i_d}(z)$.

*Step 4.* Let $i_m = 1$ as the iterative number of the minor loop. Inject the disturbance $d(k)$ for the closed-loop identification and collect the input $u(k)$ and the output $y(k)$, $k = 0, \ldots, N_f$ for another system identification in the closed-loop setting.

*Step 5.* Set the weighting factor $\rho^{i_d}$ as $\rho^{i_d+1} = r^{i_m}\rho^{i_d}$ $(r^{i_m} > 1)$ to increase the control authority. Obtain the new model of the plant $P_{\mathrm{ARX}}^{i_d+1}(z)$ and an (approximated) update of the controller corresponding to the plant model $P_{\mathrm{ARX}}^{i_d+1}(z)$ with the closed-loop $\mathscr{H}_2$ norm constraint.

*Step 6.* Obtain $K^{i_d+1}(z)$ satisfying the closed-loop $\mathscr{H}_2$ norm constraint for the newly identified model $P_{\mathrm{ARX}}^{i_d+1}(z)$. Compute $J_y^{i_d+1}$ with the true plant and the controller $K^{i_d+1}(z)$. If $J_y^{i_d} - J_y^{i_d+1} \leq \epsilon$, $0 < \epsilon \ll 1$, set $i_d = i_d + 1$ and go to Step 7. Else if $J_y^{i_d+1} > J_y^{i_d}$, set $r^{i_m+1} < r^{i_m}$, where $r^{i_m+1} \geq 1$. Set $i_m = i_m + 1$ and go to Step 5. Otherwise ($J_y^{i_d+1} < J_y^{i_d}$ and $J_y^{i_d} - J_y^{i_d+1} > \epsilon$) set $i_d = i_d + 1$ and go to Step 2.

*Step 7.* Set the previously obtained controller $K^{i_d-1}(z)$ as the optimal one and stop.

The proposed algorithm can be applied also to unstable plant if the initially designed controller $K^1(z)$ stabilizes the true plant $P(z)$.

Because of checking processes on the value of the performance index $J_y^{i_d}$, $i_d = 1, \ldots$, in Steps 2 and 6 the performance index $J_y^{i_d}$ $(i_d = 1, \ldots)$ that is obtained by the above algorithm is at least nonincreasing for the iteration number $i_d = 1, \ldots$. In other words we can always get at least a locally optimal pair of the ARX model $P_{\mathrm{ARX}}(z)$ and the feedback controller $K(z)$.

On the other hand the result of the proposed algorithm clearly depends on the initially obtained model because of the local convergence property of the algorithm. As a method to avoid the effect of the local optima some models other than the initial model in Step 1, the model obtained with the standard system identification method or the first principle based method, are obtained firstly. Then the algorithm is carried out for those models and the best result is selected. For example such models are able to be obtained by introducing small perturbations into coefficients of the initial model obtained in Step 1.

The simultaneous update of the plant model and the controller in Step 5 of the algorithm is carried out with an LMI-based method, that is, the main idea of the present paper. The detail of the LMI-based method will be described in the next subsection.

### 4.2. Simultaneous Tuning of the Plant Model and the Controller: LMI-Based Method

The LMI-based simultaneous update method of the model and the controller in Step 5 of the algorithm is described. The objective of the present closed-loop identification is to get *adjustments* not only for the model $P_{\mathrm{ARX}}^{i_d}(z)$ but also for *matrices related to the controller* $K^{i_d}(z)$

so that the given closed-loop $\mathcal{H}_2$ norm constraint is not violated even for the increased control authority represented as the increase of the weighting factor $\rho^{i_d+1} = r\rho^{i_d}$ $(r > 1)$. Assume that the plant model derived in the $i_d$th closed-loop identification is given as follows:

$$\begin{aligned} P_{\mathrm{ARX}}^{i_d}(z) &= \frac{N_{\mathrm{ARX}}^{i_d}(z)}{D_{\mathrm{ARX}}^{i_d}(z)}, \\ N_{\mathrm{ARX}}^{i_d}(z) &= b_n^{i_d} z^{-1} + b_{n-1}^{i_d} z^{-2} + \cdots + b_2^{i_d} z^{-(n+1)} + b_1^{i_d} z^{-n}, \\ D_{\mathrm{ARX}}^{i_d}(z) &= 1 + a_n^{i_d} z^{-1} + a_{n-1}^{i_d} z^{-2} + \cdots + a_2^{i_d} z^{-(n+1)} + a_1^{i_d} z^{-n}. \end{aligned} \tag{4.1}$$

Except for the initial system identification ($i_d = 1$) of the proposed design algorithm the system identification is carried out in the closed-loop, that is, the disturbance signal $d(k)$ is injected and the plant input $u^{i_d+1}(k)$ and the output $y^{i_d+1}(k)$, $k = 0, \ldots, N$ are collected in the closed-loop system with $P(z)$ and $K^{i_d}(z)$. To minimize the bias effect coming from the correlation between $u(k)$ and $v(k)$ in (2.1) in the closed-loop identification the two-stage method [22] is adopted. In the two-stage method we firstly obtain the model of the sensitivity function $S_r^{i_d}(z)$ given by

$$S_r^{i_d}(z) = \frac{1}{1 - P(z)K^{i_d}(z)}, \tag{4.2}$$

with the disturbance $d(k)$ and the plant input $u(k)$. Define the model of the sensitivity function $S_r^{i_d}(z)$ in (4.2) as the $N_s$th order FIR model given as

$$S_{\mathrm{FIR}}^{i_d}(z) = s_0^{i_d} + s_1^{i_d} z^{-1} + \cdots + s_{N_s}^{i_d} z^{-N_s}. \tag{4.3}$$

With the model of the sensitivity function $S_{\mathrm{FIR}}^{i_d}(z)$ a filtered plant input $u_f^{i_d}(k)$ is given as

$$u_f^{i_d}(k) = S_{\mathrm{FIR}}^{i_d}(z)d(k), \quad k = 0, \ldots, N. \tag{4.4}$$

The new model $P_{\mathrm{ARX}}^{i_d+1}(z)$ is obtained with the input $u_f^{i_d}(k)$ and the output $y^{i_d}(k)$. Because the synthesized plant input $u_f^{i_d}(k)$ is uncorrelated with the noise $v(k)$, the bias effect caused by the correlation between $v(k)$ and $u(k)$ is suppressed.

The newly identified model $P_{\mathrm{ARX}}^{i_d+1}(z)$ is defined as follows:

$$\begin{aligned} P_{\mathrm{ARX}}^{i_d+1}(z) &= \frac{N_{\mathrm{ARX}}^{i_d+1}(z)}{D_{\mathrm{ARX}}^{i_d+1}(z)} = \frac{N_{\mathrm{ARX}}^{i_d}(z) + \overline{N}_{\mathrm{ARX}}^{i_d}(z)}{D_{\mathrm{ARX}}^{i_d}(z) + \overline{D}_{\mathrm{ARX}}^{i_d}(z)}, \\ \overline{N}_{\mathrm{ARX}}^{i_d}(z) &= \Delta b_n z^{-1} + \cdots + \Delta b_1 z^{-n} := R(z)\Delta N_{\mathrm{ARX}}^{i_d}, \\ \overline{D}_{\mathrm{ARX}}^{i_d}(z) &= \Delta a_n z^{-1} + \cdots + \Delta a_1 z^{-n} := R(z)\Delta D_{\mathrm{ARX}}^{i_d}, \\ \Delta N_{\mathrm{ARX}}^{i_d} &:= \begin{bmatrix} \Delta b_1 & \Delta b_2 & \cdots & \Delta b_{n-1} & \Delta b_n \end{bmatrix}^T, \end{aligned}$$

$$\Delta D_{\mathrm{ARX}}^{i_d} := \left[\Delta a_1 \;\; \Delta a_2 \;\; \cdots \;\; \Delta a_{n-1} \;\; \Delta a_n\right]^T,$$
$$R(z) := \left[z^{-n} \;\; z^{-(n-1)} \;\; \cdots \;\; z^{-2} \;\; z^{-1}\right], \tag{4.5}$$

where vectors $\Delta N_{\mathrm{ARX}}^{i_d}$ and $\Delta D_{\mathrm{ARX}}^{i_d}$ are adjustments for coefficients of the numerator and denominator polynomials of the $i_d$th ARX model $P_{\mathrm{ARX}}^{i_d}(z)$, respectively.

To get the new model $P_{\mathrm{ARX}}^{i_d+1}(z)$ we obtain those adjustment vectors $\Delta N_{\mathrm{ARX}}^{i_d}$ and $\Delta D_{\mathrm{ARX}}^{i_d}$ using the I/O data $u_f^{i_d}(k)$ and $y^{i_d}(k)$ with the fixed $P_{\mathrm{ARX}}^{i_d}(z)$. Similar to the LMI-based system identification in the previous section the problem to obtain adjustment vectors $\Delta N_{\mathrm{ARX}}^{i_d}$ and $\Delta D_{\mathrm{ARX}}^{i_d}$ results in the following LMI optimization problem:

$$\text{Minimize } f^{i_d+1}(\alpha) := \sum_{k=1}^{N} \alpha(k), \qquad \alpha(k) > 0,$$
$$\text{subject to } \begin{bmatrix} \alpha(k) & * \\ y^{i_d+1}(k) - D_{IO}^{i_d+1}\left(\theta^{i_d} + \Delta\theta^{i_d}\right) & 1 \end{bmatrix} > 0, \quad k = 1, \ldots, N, \tag{4.6}$$

where

$$D_{IO}^{i_d+1}(k) := \left[-D_O^{i_d+1}(k) \;\; D_I^{i_d+1}(k)\right],$$
$$D_O^{i_d+1}(k) = \left[y^{i_d+1}(k-n) \;\; \cdots \;\; y^{i_d+1}(k-1)\right], \qquad D_I^{i_d+1}(k) = \left[u_f^{i_d+1}(k-n) \;\; \cdots \;\; u_f^{i_d+1}(k-1)\right],$$
$$\theta^{i_d} := \left[a_1^{i_d} \;\; \cdots \;\; a_n^{i_d} \;\; b_1^{i_d} \;\; \cdots \;\; b_n^{i_d}\right]^T,$$
$$\Delta\theta^{i_d} := \left[\left(\Delta D_{\mathrm{ARX}}^{i_d}\right)^T \;\; \left(\Delta N_{\mathrm{ARX}}^{i_d}\right)^T\right]^T = \left[\Delta a_1 \;\; \cdots \;\; \Delta a_n \;\; \Delta b_1 \;\; \cdots \;\; \Delta b_n\right]^T. \tag{4.7}$$

In the above LMI-based identification problem the unknown parameters are $\alpha(k) > 0$, $i = 1, \ldots, N$ and $\Delta\theta^{i_d}$.

The LMI optimization problem (4.6) to get the new model $P_{\mathrm{ARX}}^{i_d+1}(z)$ is solved jointly with the LMI constraint for the controller synthesis given in (3.5)–(3.7). By the $i_d$-th LMI-based system identification in the above, the transfer function of the ARX model is changed from $P_{\mathrm{ARX}}^{i_d}(z)$ into $P_{\mathrm{ARX}}^{i_d+1}(z)$ shown in (4.5). Considering the state-space realization of $P_{\mathrm{ARX}}^{i_d}(z)$ in (2.4) the state-space realization of the newly identified model

$$P_{\mathrm{ARX}}^{i_d+1}(z) := \left[\begin{array}{cc} A_{\mathrm{ARX}}^{i_d+1} & B_{\mathrm{ARX}}^{i_d+1} \\ \hline C_{\mathrm{ARX}}^{i_d+1} & 0 \end{array}\right] \tag{4.8}$$

is given as

$$A_{\mathrm{ARX}}^{i_d+1} = A_{\mathrm{ARX}}^{i_d} - \Delta A_{\mathrm{ARX}}, \qquad B_{\mathrm{ARX}}^{i_d+1} = B_{\mathrm{ARX}}^{i_d} := B_{\mathrm{ARX}}, \qquad C_{\mathrm{ARX}}^{i_d+1} = C_{\mathrm{ARX}}^{i_d} + \Delta C_{\mathrm{ARX}},$$
$$\Delta A_{\mathrm{ARX}} := \begin{bmatrix} 0_{(n-1)\times n} \\ \hline \left(\Delta D_{\mathrm{ARX}}^{i_d}\right)^T \end{bmatrix}, \qquad \Delta C_{\mathrm{ARX}} := \left(\Delta N_{\mathrm{ARX}}^{i_d}\right)^T. \tag{4.9}$$

The variation of coefficient matrices in the state-state form of $P_{\mathrm{ARX}}^{i_d}(z)$ coming from the $i_d$-th closed-loop system identification and the increase of the weighting factor ($\rho^{i_d+1} = r\rho^{i_d}$, $r > 1$) in Step 5 of the algorithm provides changes of coefficient matrices of the generalized plant $G(z)$ in (2.5). Those changes of parameters are defined as the symbols with "$\Delta$" like $\Delta A_{\mathrm{ARX}}$ and $\Delta C_{\mathrm{ARX}}$ in the above. Reflecting those changes, parameter matrices related to the feedback controller in (3.5)–(3.7), for example, $W$, $P$, and $H$, and so forth, should also be changed because we cannot expect that the constraint on the closed-loop $\mathscr{H}_2$ norm still holds if those controller related parameters are left as they are.

In the present paper not only the changes of the coefficient matrices of the generalized plant, including the changes of the plant model and the weighting factor $\rho > 0$, but also those of parameter matrices related to the feedback controller are simultaneously obtained in the process of the closed-loop identification step.

Define the changes of the matrices related to the feedback controller, for example, $W$, $X$, and $L$, and so forth in (3.5)–(3.7) as $\Delta\bullet$ where $\bullet$ is $W$, $X$, and $L$, and so forth. Then the condition for the controller synthesis in (3.5)–(3.7) so that the closed-loop $\mathscr{H}_2$ norm with the newly obtained plant model $P_{\mathrm{ARX}}^{i_d+1}(z)$ and the feedback controller is less than $\mu > 0$ becomes a system of BMI given as follows:

$$\mathrm{trace}\left(W^{i_d} + \Delta W\right) < \mu^2, \tag{4.10}$$

$$\begin{bmatrix} W^{i_d} + \Delta W & \left(\overline{C_1^{i_d}} + \overline{\Delta C_1}\right)(X^{i_d} + \Delta X) + D_{12}(L^{i_d} + \Delta L) & \overline{C_1^{i_d}} + \overline{\Delta C_1} \\ * & \Theta_{22}^{i_d} & \Theta_{23}^{i_d} \\ * & * & \Theta_{33}^{i_d} \end{bmatrix} > 0, \tag{4.11}$$

$$\begin{bmatrix} P^{i_d} + \Delta P & J^{i_d} + \Delta J & \left(A_{\mathrm{ARX}}^{i_d} - \Delta A_{\mathrm{ARX}}\right)(X^{i_d} + \Delta X) + B_{\mathrm{ARX}}(L^{i_d} + \Delta L) & A_{\mathrm{ARX}}^{i_d} - \Delta A_{\mathrm{ARX}} & B_1 \\ * & H^{i_d} + \Delta H & Q^{i_d} + \Delta Q & \Xi_{24}^{i_d} & \Xi_{25}^{i_d} \\ * & * & X^{i_d} + \Delta X + \left(X^{i_d}\right)^T + \Delta X^T - P^{i_d} - \Delta P & \Xi_{34}^{i_d} & 0 \\ * & * & * & \Xi_{44}^{i_d} & 0 \\ * & * & * & * & I \end{bmatrix}$$
$$> 0,$$

$$\Theta_{22}^{i_d} = X^{i_d} + \Delta X + \left(X^{i_d}\right)^T + \Delta X^T - P^{i_d} - \Delta P, \qquad \Theta_{23}^{i_d} = I + \left(S^{i_d}\right)^T + \Delta S^T - J^{i_d} - \Delta J,$$
$$\Theta_{33}^{i_d} = Y^{i_d} + \Delta Y + \left(Y^{i_d}\right)^T + \Delta Y^T - H^{i_d} - \Delta H,$$
$$\Xi_{24}^{i_d} = \left(Y^{i_d} + \Delta Y\right)\left(A_{\mathrm{ARX}}^{i_d} - \Delta A_{\mathrm{ARX}}\right) + \left(F^{i_d} + \Delta F\right)\left(C_{\mathrm{ARX}}^{i_d} + \Delta C_{\mathrm{ARX}}\right),$$

$$\Xi_{25}^{i_d} = \left(Y^{i_d} + \Delta Y\right)B_1 + \left(F^{i_d} + \Delta F\right)D_{21}, \qquad \Xi_{33}^{i_d} = \Theta_{22}^{i_d}, \qquad \Xi_{34}^{i_d} = \Theta_{23}^{i_d}, \qquad \Xi_{44}^{i_d} = \Theta_{33}^{i_d},$$

$$\overline{C_1^{i_d}} = \begin{bmatrix} \rho^{i_d+1} C_{\mathrm{ARX}}^{i_d} \\ 0 \end{bmatrix}, \qquad \Delta C_1 = \begin{bmatrix} \rho^{i_d+1} \Delta C_{\mathrm{ARX}} \\ 0 \end{bmatrix}, \qquad \Delta C_2 = \Delta C_{\mathrm{ARX}}. \tag{4.12}$$

The update of the plant model $P_{\mathrm{ARX}}^{i_d}(z)$ and the controller $K^{i_d}(z)$ is given as the solution to the LMI optimization problem in (4.6) with BMI constraints in (4.10)–(4.12). However, it is difficult to obtain the global optimal solution to the nonconvex problem. To solve the nonconvex optimization problem in an approximated manner a method that iteratively solves an approximated LMI problem of the original BMI problem. The approximated LMI problem is derived by neglecting the second or higher order products of parameter matrices (symbols with $\Delta$) in the BMI problem. The approximation of the BMIs in (4.10)–(4.12) are given as follows:

$$\mathrm{trace}\left(W^{i_d} + \Delta W\right) < \mu^2, \tag{4.13}$$

$$\begin{bmatrix} W^{i_d} + \Delta W & \overline{C_1^{i_d}} X^{i_d} + \overline{C_1^{i_d}} \Delta X + \overline{\Delta C_1} X^{i_d} + D_{12}\left(L^{i_d} + \Delta L\right) & \overline{C_1^{i_d}} + \overline{\Delta C_1} \\ * & \Phi_{22}^{i_d} & \Phi_{23}^{i_d} \\ * & * & \Phi_{33}^{i_d} \end{bmatrix} > 0, \tag{4.14}$$

$$\begin{bmatrix} P^{i_d} + \Delta P & J^{i_d} + \Delta J & \Psi_{13}^{i_d} & A_{\mathrm{ARX}}^{i_d} - \Delta A_{\mathrm{ARX}} & B_1 \\ * & H^{i_d} + \Delta H & Q^{i_d} + \Delta Q & \Psi_{24}^{i_d} & \Psi_{25}^{i_d} \\ * & * & \Psi_{33}^{i_d} & \Psi_{34}^{i_d} & 0 \\ * & * & * & \Psi_{44}^{i_d} & 0 \\ * & * & * & * & I \end{bmatrix} > 0,$$

$$\Phi_{22}^{i_d} = X^{i_d} + \Delta X + \left(X^{i_d}\right)^T + \Delta X^T - P^{i_d} - \Delta P,$$

$$\Phi_{23}^{i_d} = I + \left(S^{i_d}\right)^T + \Delta S^T - J^{i_d} - \Delta J,$$

$$\Phi_{33}^{i_d} = Y^{i_d} + \Delta Y + \left(Y^{i_d}\right)^T + \Delta Y^T - H^{i_d} - \Delta H,$$

$$\Psi_{13}^{i_d} = A_{\mathrm{ARX}}^{i_d} X^{i_d} + A_{\mathrm{ARX}}^{i_d} \Delta X - \Delta A_{\mathrm{ARX}} X^{i_d} + B_{\mathrm{ARX}}\left(L^{i_d} + \Delta L\right), \tag{4.15}$$

$$\Psi_{24}^{i_d} = Y^{i_d} A_{\mathrm{ARX}}^{i_d} - Y^{i_d} \Delta A_{\mathrm{ARX}} + \Delta Y A_{\mathrm{ARX}}^{i_d} + F^{i_d} C_{\mathrm{ARX}}^{i_d} + F^{i_d} \Delta C_{\mathrm{ARX}} + \Delta F C_{\mathrm{ARX}}^{i_d},$$

$$\Psi_{25}^{i_d} = \left(Y^{i_d} + \Delta Y\right)B_1 + \left(F^{i_d} + \Delta F\right)D_{21}, \qquad \Psi_{33}^{i_d} = \Phi_{22}^{i_d},$$

$$\Psi_{34}^{i_d} = \Phi_{23}^{i_d}, \qquad \Psi_{44}^{i_d} = \Phi_{33}^{i_d}.$$

The above approximation is reasonable only if parameter matrices, symbols with $\Delta$, are small in some sense. In other words, the approximation becomes more accurate if the update of the plant model $P_{\mathrm{ARX}}^{i_d}(z)$ and the model-based controller $K^{i_d}(z)$ are forced to

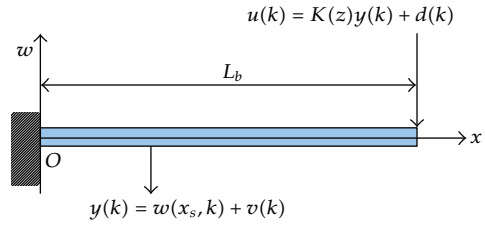


**Figure 2:** Cantilevered beam.

be smaller. To confine the size of parameter matrices to be small enough following LMI constraints on parameter matrices are introduced:

$$(\Delta\bullet)^T(\Delta\bullet) < \left(\beta(\overline{\sigma}(\bullet))\right)^2 I \iff \begin{bmatrix} \beta\overline{\sigma}(\bullet)I & (\Delta\bullet)^T \\ \Delta\bullet & \beta\overline{\sigma}(\bullet)I \end{bmatrix} > 0, \tag{4.16}$$

where $\bullet$ represents the parameter matrix of interest and $\beta > 0$ is a small positive value, say, 0.1. The LMI (4.16) restricts the maximum singular value of the parameter matrix. Then using the plant I/O data we can obtain adjustments of the plant model $P_{\mathrm{ARX}}(z)$ and the feedback controller $K(z)$, represented as the symbols with $\Delta$, by solving the LMI optimization problem (4.6) with LMI constraints (4.13)–(4.15) and (4.16). In other words by solving the above single constrained LMI optimization problem we can get the adjustment not only on the plant model but also on the approximated feedback controller with the closed-loop $\mathscr{H}_2$ norm.

In the proposed algorithm the weighting factor $\rho^{i_d}$ for the output $y_p$ is increased ($z_1 = \rho^{i_d} y_p$) as the iterative number $i_d$ gets larger. Since the controller $K^{i_d}(z)$ is designed so that the closed-loop $\mathscr{H}_2$ norm is less than $\mu > 0$, the controller $K^{i_d}(z)$ tends to be more aggressive according to the increase of the iterative number $i_d$ and the closed-loop response of the $y_p$ is expected to become more desirable until the constraint on the control effort $u(k)$ (2.8) is violated. In this sense the present iterative method is similar to Windsurfer Approach [7, 8] that aims to achieve the wider closed-loop bandwidth with a gradual change of the reference model in the IMC control framework.

## 5. Simulation Example

Let us consider an active vibration control of a cantilevered beam with the length $L_b$ depicted in Figure 2. At $x = x_s = 0.3L_b$ a sensor that measures $y(k) = w(x_s, k) + v(k)$ where $w(x_s, k)$ and $v(k)$ are the deflection of the beam at $x = x_s$ and the measurement noise, respectively. At the free end ($x = L_b$) of the beam an actuator that produces the control force $u(k)$ is installed. The control and disturbance forces are applied as the form of $u(k) = K(z)y(k) + d(k)$ where $K(z)$ is the transfer function of the feedback controller and $d(k)$ is the input disturbance.

The true plant $P(z)$ in (2.1) is defined as follows. Firstly a 30th order finite dimensional continuous time system is analytically derived by approximating the beam system by taking the lower fifteen modes of vibration with a small modal damping for each mode. Secondly the discrete time plant $P(z)$ is obtained by discretizing the 30th order continuous time system with zero-order hold in sampling interval $T_s = 0.05$ [s]. The plant $P(z)$ is stable and non-minimum phase because of noncollocation of the sensor and the actuator. In fact the plant

$P(z)$ has three non-minimum phase zeros at $z = 10.163$, 1.898, and 1.543. It is well known such non-minimum phase zeros of the plant generally constrain the achievable performance of the feedback control system. Moreover the Windsurfer Approach based on IMC method [7] does not work in the case that the model has non-minimum phase zeros within the control bandwidth. In the present simulation study the non-collocation of the sensor and the actuator is assumed to show that the proposed windsurfer-like algorithm works for the plant with non-minimum phase zeros. We assume that we do not have any structural information of the true plant $P(z)$ including the order and the location of poles and zeros in the simulation example. Only the I/O signals of $P(z)$ subject to the disturbance are available throughout the application of the proposed LMI-based algorithm.

As the model of the true plant $P(z)$, the ARX model $P_{\mathrm{ARX}}(z)$ in (2.2) is assumed. In the performance index in (2.7) the disturbance to obtain $J_y$ is the impulse function and $N_f = 10^4$. The allowed maximum absolute value of the control effort in (2.8) is $\overline{u} = 0.1$. The disturbance signal for the system identification is a zero-mean band limited white noise with $1^2$ variance and the sensor measurement is contaminated by a zero-mean band-limited white noise $s(k)$ with $0.01^2$ variance.

In the present example the feedback controller $K(z)$ is obtained so that the closed-loop $\mathscr{H}_2$ norm is less than $\mu = 1$. The model of the sensitivity function $S_r^{i_d}(z)$ in (4.2) in the two-stage approach is defined as 50th order FIR filter in each iteration. The order of the the ARX model $n$ is set to $n = 2, 4, 6, \ldots, 20$ in the present simulation example. Note that we cannot avoid a bias error in the simulation example because the order of all the models considered in the example is lower than that of the true plant. Such undermodeling situation is assumed because the author would like to show that the proposed LMI-based method effectively works even in the undermodeling case that often appears in general control system design problems. Examples that we must accept the undermodeling condition are given as follows.

(i) In general the order of true plant cannot be determined exactly because all existing control objects possibly have nonlinearities to some extent. When we obtain a linear model of the true plant to adopt a linear model-based control law such nonlinearities are ignored or linearized by assuming the order of the linear model (not the true plant).

(ii) Even if we could determine the exact order of the true plant it is often the case that the full order model-based controller cannot be used because the order of the true plant is too high to implement the full-order controller.

The proposed LMI-based iterative algorithm for the system identification and controller design is carried out. The achieved value of the performance index $J_y$ in (2.4) with the LMI-based design algorithm for each order of the model $n$ is summarized in Table 1.

From the result in Table 1 the minimum value of the performance index $J_y$ is achieved in $n = 8$. In other words, the best control performance in the sense of the closed-loop system with the 30th order true plant and the model-based controller is achieved when we take the 8th order ARX model. In $n = 8$ the algorithm is terminated in $i_d = 4$ because the further performance improvement can no longer be achieved in the sense of $J_y$ in (2.7). Bode plots of the obtained models $P_{\mathrm{ARX}}^{i_d}(z)$ for $i_d = 1$ (open-loop identification), ..., 4 with that of the true plant and those of corresponding controllers $K^{i_d}(z)$, $i_d = 1, \ldots, 4$ are shown in Figures 3 and 4. We can see that the gain of the feedback controller is getting larger along with the progress of the algorithm. Closed-loop impulse responses are shown in Figure 5. The closed-loop

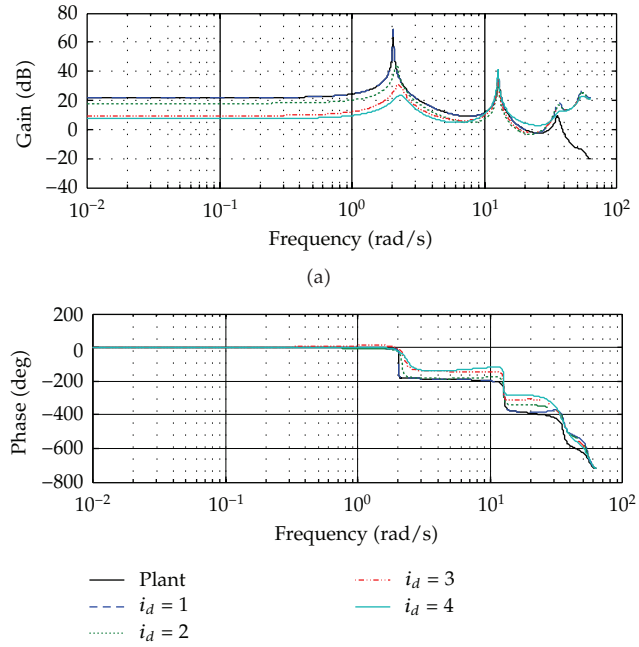


**Figure 3:** Bode plots of the true plant $P(z)$ and its models $P^{i_d}_{\mathrm{ARX}}(z)$'s ($n = 8$).

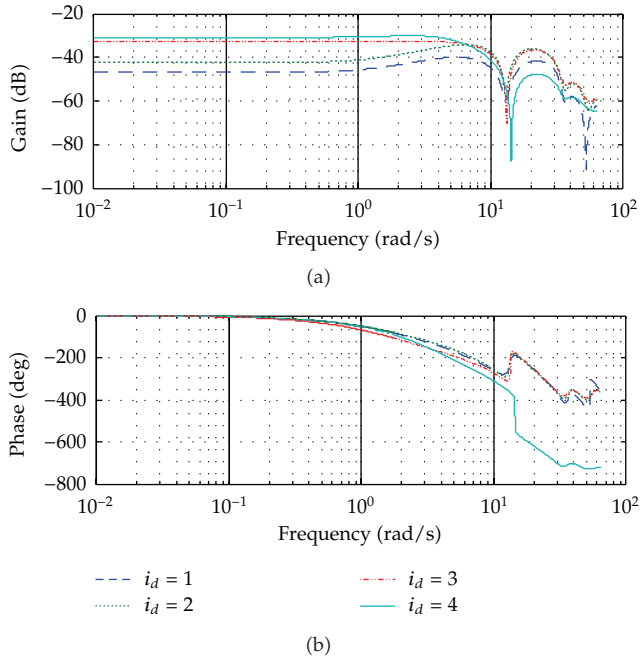


**Figure 4:** Bode plots of the the feedback controllers $K^{i_d}(z)$'s ($n = 8$).

**Table 1:** The achieved value of the performance index $J_y$ for each order of the ARX model. The best control performance is achieved in $n = 8$.

| $n$ | Achieved $J_y$ | $n$ | Achieved $J_y$ |
|---|---|---|---|
| 2 | 1010.7 | 12 | 121.04 |
| 4 | 180.16 | 14 | 152.88 |
| 6 | 102.30 | 16 | 121.79 |
| 8 | **53.071** | 18 | 950.09 |
| 10 | 122.79 | 20 | 564.68 |

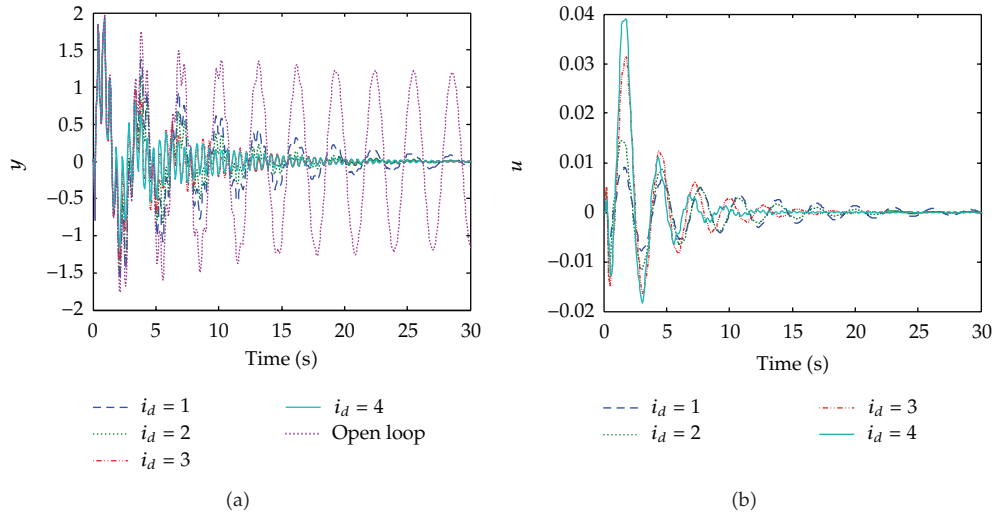


**Figure 5:** Impulse responses of the open and closed-loop systems ($n = 8$).

impulse response $y(k)$ is well controlled and the maximum amplitude of the control effort $u(k)$ becomes larger with the progress of the algorithm.

The result of the present example indicates that the best fit in the sense of some open-loop responses does not necessarily generate a *good model for the controller design*. Furthermore the open-loop accuracy of the plant model does not necessarily promise the *good closed-loop performance*, in other words, there exists the inseparably relationship between the modeling and controller design processes [1, 2].

Furthermore, for a comparison purpose, we obtain a feedback controller minimizing $J_y$ with the constraint on the closed-loop $\mathscr{H}_2$ norm $\mu = 1$ and that on the control effort $\overline{u} = 0.1$ (in (2.8)) when the transfer function of the 30th order true plant is exactly known and is available for the controller design. By applying the $\mathscr{H}_2$ control method in [21] with adjusting the weighting factor $\rho > 0$ the achieved minimum value of $J_y$ with $\mu < 1$ and $\overline{u} = 0.1$ becomes $J_y = 25.404$. The achieved $J_y$ is smaller than the best value ($J_y = 53.071$) in the proposed algorithm. However, the author would like to emphasize that the above ideal situation is possible because the present example is a simulation and such situation can never be realized in general.

As another comparison let us assume that modal parameters up to lower 4th modes of vibration correctly, that is, the 8th-order exact reduced-order model of the 30th order true plant is available. Note that this ideal situation cannot be realized in general. For the 8th

order plant the 8th order controller is obtained so that the performance index $J_y$ is minimized with $\mu < 1$ and $\overline{u} = 0.04$ by increasing the weighting factor $\rho$ gradually with the method in [21]. Notice that 0.04 is the almost same peak value as that of the case where the optimal $J_y = 53.071$ is obtained in $n = 8$ with the proposed algorithm. Then the achieved minimum value of $J_y = 65.733$ and it is larger than $J_y = 53.071$ that is obtained with the proposed design algorithm in $n = 8$.

With the above discussion the obtained 8th order model in the present simulation example is a reasonable solution to the formulated simultaneous modeling and control design problem even if it is a locally optimal solution and the effectiveness of the proposed integrated system identification and controller update methodology with the LMI-based framework is shown.

## 6. Conclusion

An LMI-based methodology for iterative system identification and controller design has been proposed. With the fact that the standard least-square-based system identification results in the LMI optimization problem the plant model and the feedback controller are simultaneously adjusted in a single system of LMI. The iterative design algorithm similar to Windsurfer Approach is proposed.

The relation between the proposed methodology and the other existing methods for iterative identification and control, including IFT [23] and VFRT [24], will be considered in the future study.

## References

[1] R. E. Skelton, "Model error concepts in control design," *International Journal of Control*, vol. 49, no. 5, pp. 1725–1753, 1989.

[2] P. M. J. van den Hof and R. J. P. Schrama, "Identification and control—closed-loop issues," *Automatica*, vol. 31, no. 12, pp. 1751–1770, 1995.

[3] U. Forssell and L. Ljung, "Closed-loop identification revisited," *Automatica*, vol. 35, no. 7, pp. 1215–1241, 1999.

[4] M. Gevers, X. Bombois, B. Codrons, G. Scorletti, and B. D. O. Anderson, "Model validation for control and controller validation in a prediction error identification framework—part I: theory," *Automatica*, vol. 39, no. 3, pp. 403–415, 2003.

[5] M. Okada, H. Fukushima, and T. Sugie, "Joint design of model-subspace based identification and control," in *Proceedings of the 11th IFAC Symposium on System Identification*, vol. 3, pp. 1155–1160, 1997.

[6] H. Ichihara, Y. Matsumoto, N. Abe, and H. Kanoh, "Application of an iterative identification and control design to a vibration system," *JSME International Journal*, vol. 43, no. 1, pp. 18–24, 2000.

[7] W. S. Lee, B. D. O. Anderson, I. M. Y. Mareels, and R. L. Kosut, "On some key issues in the windsurfer approach to adaptive robust control," *Automatica*, vol. 31, no. 11, pp. 1619–1636, 1995.

[8] A. Dehghani, A. Lanzon, and B. D. O. Anderson, "An $\mathscr{H}_\infty$ algorithm for the windsurfer approach to adaptive robust control," *International Journal of Adaptive Control and Signal Processing*, vol. 18, no. 8, pp. 607–628, 2004.

[9] A. Lecchini, A. Lanzon, and B. D. O. Anderson, "A model reference approach to safe controller changes in iterative identification and control," *Automatica*, vol. 42, no. 2, pp. 193–203, 2006.

[10] S. Garatti, M. C. Campi, and S. Bittanti, "Iterative robust control: speeding up improvement through iterations," *Systems & Control Letters*, vol. 59, no. 2, pp. 139–146, 2010.

[11] Z. Zang, R. R. Bitmead, and M. Gevers, "Iterative weighted least-squares identification and weighted LQG control design," *Automatica*, vol. 31, no. 11, pp. 1577–1594, 1995.

[12] F. R. Hansen, G. Franklin, and R. Kosut, "Closed-loop identification via the fractional representation: experiment design," in *Proceedings of the American Control Conference*, pp. 1422–1427, Pittsburgh, Pa, USA, June 1989.

[13] Y. J. Liu, Y. S. Xiao, and X. L. Zhao, "Multi-innovation stochastic gradient algorithm for multiple-input single-output systems using the auxiliary model," *Applied Mathematics and Computation*, vol. 215, no. 4, pp. 1477–1483, 2009.

[14] J. H. Li and F. Ding, "Maximum likelihood stochastic gradient estimation for Hammerstein systems with colored noise based on the key term separation technique," *Computers & Mathematics with Applications*, vol. 62, no. 11, pp. 4170–4177, 2011.

[15] J. Ding, F. Ding, X. P. Liu, and G. Liu, "Hierarchical least squares identification for linear SISO systems with dual-rate sampled-data," *Institute of Electrical and Electronics Engineers*, vol. 56, no. 11, pp. 2677–2683, 2011.

[16] D. Q. Wang, "Least squares-based recursive and iterative estimation for output error moving average systems using data filtering," *IET Control Theory & Applications*, vol. 5, no. 14, pp. 1648–1657, 2011.

[17] Y. J. Liu, J. Sheng, and R. F. Ding, "Convergence of stochastic gradient estimation algorithm for multivariable ARX-like systems," *Computers & Mathematics with Applications*, vol. 59, no. 8, pp. 2615–2627, 2010.

[18] F. Ding, X. P. Liu, and G. Liu, "Identification methods for Hammerstein nonlinear systems," *Digital Signal Processing*, vol. 21, no. 2, pp. 215–238, 2011.

[19] F. Ding, G. Liu, and X. P. Liu, "Partially coupled stochastic gradient identification methods for non-uniformly sampled systems," *Institute of Electrical and Electronics Engineers*, vol. 55, no. 8, pp. 1976–1981, 2010.

[20] G. Vinnicombe, *Uncertainty and Feedback—$\mathscr{H}_\infty$ Loop-Shaping and the $\nu$-Gap Metric*, Imperial College Press, Amsterdam, The Netherlands, 2001.

[21] M. C. de Oliveira, J. C. Geromel, and J. Bernussou, "Extended $H_2$ and $H_\infty$ norm characterizations and controller parametrizations for discrete-time systems," *International Journal of Control*, vol. 75, no. 9, pp. 666–679, 2002.

[22] P. M. J. van den Hof and R. J. P. Schrama, "An indirect method for transfer function estimation from closed loop data," *Automatica*, vol. 29, no. 6, pp. 1523–1527, 1993.

[23] H. Hjalmarsson, "Iterative feedback tuning—an overview," *International Journal of Adaptive Control and Signal Processing*, vol. 16, no. 5, pp. 373–395, 2002.

[24] M. C. Campi, A. Lecchini, and S. M. Savaresi, "Virtual reference feedback tuning: a direct method for the design of feedback controllers," *Automatica*, vol. 38, no. 8, pp. 1337–1346, 2002.

Hindawi Publishing Corporation
Journal of Applied Mathematics
Volume 2012, Article ID 841609, 24 pages
doi:10.1155/2012/841609

*Research Article*

# A Clustering and SVM Regression Learning-Based Spatiotemporal Fuzzy Logic Controller with Interpretable Structure for Spatially Distributed Systems

**Xian-xia Zhang,[1] Jun-da Qi,[1] Bai-li Su,[2] Shi-wei Ma,[1] and Hong-bo Liu[3]**

[1] *Shanghai Key Laboratory of Power Station Automation Technology, School of Mechatronics and Automation, Shanghai University, Shanghai 200072, China*
[2] *School of Electrical Information and Automation, Qufu Normal University, Shandong 276826, China*
[3] *School of Control Science and Engineering, Shandong University, Jinan 250061, China*

Correspondence should be addressed to Xian-xia Zhang, xianxia_zh@shu.edu.cn

Received 8 April 2012; Revised 13 June 2012; Accepted 14 June 2012

Academic Editor: Baocang Ding



Many industrial processes and physical systems are spatially distributed systems. Recently, a novel 3-D FLC was developed for such systems. The previous study on the 3-D FLC was concentrated on an expert knowledge-based approach. However, in most of situations, we may lack the expert knowledge, while input-output data sets hidden with effective control laws are usually available. Under such circumstance, a data-driven approach could be a very effective way to design the 3-D FLC. In this study, we aim at developing a new 3-D FLC design methodology based on clustering and support vector machine (SVM) regression. The design consists of three parts: initial rule generation, rule-base simplification, and parameter learning. Firstly, the initial rules are extracted by a nearest neighborhood clustering algorithm with Frobenius norm as a distance. Secondly, the initial rule-base is simplified by merging similar 3-D fuzzy sets and similar 3-D fuzzy rules based on similarity measure technique. Thirdly, the consequent parameters are learned by a linear SVM regression algorithm. Additionally, the universal approximation capability of the proposed 3-D fuzzy system is discussed. Finally, the control of a catalytic packed-bed reactor is taken as an application to demonstrate the effectiveness of the proposed 3-D FLC design.

## 1. Introduction

Many industrial processes and physical systems such as industrial chemical reactor [1, 2], semiconductor manufacturing [3], and thermal processing [4] are "distributed" in space. They are usually called spatially distributed systems, or distributed parameter systems [1].

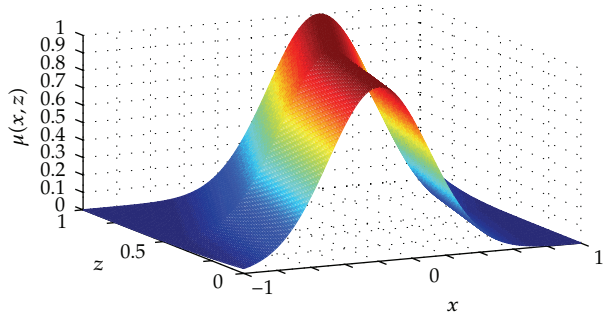


**Figure 1:** A three-dimensional fuzzy set.

The states, controls, and outputs of such systems depend on the space position as well as on the time [2]. Traditionally, model-based methods are used to control such systems, where a good mathematical model is definitely required. However, the process model may not be easily obtained in many complex situations, and then, a model-free control method has to be used. This leads to the recent development of the novel three-dimensional fuzzy-logic control (3-D FLC) [5–8], which has the inherent capability to process spatiotemporal dynamic systems. The 3-D FLC uses one kind of three-dimensional (3-D) fuzzy set (shown in Figure 1), which is composed of the traditional fuzzy set and a third dimension for the spatial information, and executes a 3-D rule inference engine. It is actually a kind of spatiotemporal fuzzy-control system with the traditional model-free advantage.

To date, the 3-D FLC design has been focused on an expert-knowledge-based approach [5], that is, the fuzzy-rule design is from human experts' knowledge. In this approach, human knowledge to the control solution must exist, and be structured. Practically, experts may have problems structuring the knowledge [9]. Sometimes, although experts have the structured knowledge, they may sway between extreme cases: offering too much knowledge in the field of expertise, or tending to hide their knowledge [9]. Thus, we often lack expert knowledge for control that is usually hidden in an input-output data set. Under this circumstance, a data-driven design becomes a good choice for the 3-D FLC, that is, extraction of fuzzy rules from a spatiotemporal input-output data set. Since the research on the 3-D FLC is just at the beginning stage, extracting 3-D fuzzy control rules from a spatiotemporal data set is still a challenging and open problem for spatially distributed systems.

Traditional data-driven FLC design methods have been developed in the past three decades. They are usually composed of three parts: rule generation, structure optimization, and parameter optimization [10]. For instance, grid partitioning of multidimensional space [11] and clustering technique [12] can be used to generate rules automatically; reducing redundancy variable [12], fusing similar clusters [13], and fusing similar fuzzy set [14] can be applied to reduce the rule number and realize the structure optimization; genetic algorithm [15] and gradient decent approach [16] can be adopted for fine tuning of membership function and realize the parameter optimization. For a complete review of data-driven fuzzy system design, one can further refer to [10]. These methods provide useful solutions to a traditional FLC design.

In this study, we aim at developing a new data-driven 3-D FLC design method based on clustering and SVM-regression learning. The initial 3-D rule base is first generated by a nearest-neighborhood-clustering method from a spatiotemporal data set via defining Frobenius norm as a distance. Then, the initial 3-D rule base is simplified based on similarity

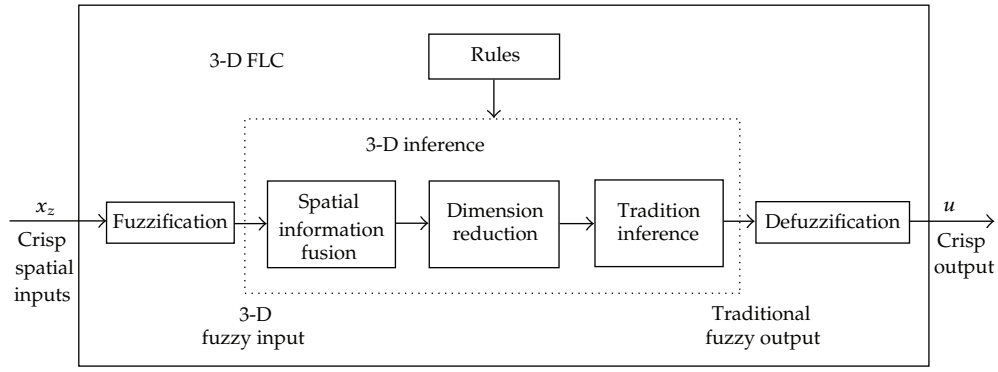


**Figure 2:** Basic structure of a 3-D FLC.

measure technique defined for 3-D fuzzy sets and 3-D fuzzy rules. Subsequently, an SVM-regression learning algorithm is used to learn the parameters of the rule consequent parts. In addition, the universal approximation capability of the proposed 3-D fuzzy system is discussed.

The paper is organized as follows. Preliminaries about 3-D FLC and SVM regression are addressed in Section 2. In Section 3, a clustering and SVM-regression learning-based 3-D fuzzy control design methodology is presented in detail. In Section 4, the universal approximation capability of the proposed 3-D fuzzy system is presented. In Section 5, a catalytic packed-bed reactor is presented as an example to illustrate the proposed design scheme of a 3-D FLC and validate its effectiveness. Finally, conclusions are given in Section 6.

## 2. Preliminaries

### 2.1. 3-D FLC

The 3-D FLC is designed to have the inherent capability to deal with spatial information and its basic structure is shown in Figure 2. It has a similar functional structure similar to the traditional FLC, which consists of three basic blocks: fuzzification, rule inference, and defuzzification. However, it will differ in the detailed operations because of the spatial processing requirement. Generally, the 3-D FLC will be involved with the following basic designs: 3-D membership function (MF), 3-D fuzzification, 3-D rule base, 3-D rule inference, and defuzzification. One can refer to [5] for detailed description. Once each component of a 3-D FLC is set, a precise mathematical formula of the 3-D FLC can be derived.

Assumed that we have 3-D fuzzy rules represented by the following expression:

$$\overline{R}^l : \text{IF } x_1(z) \text{ is } \overline{C}_1^l \text{ and} \cdots \text{and } x_s(z) \text{ is } \overline{C}_s^l, \quad \text{Then } u \text{ is } B^l, \tag{2.1}$$

where $x_i(z) = (x_i(z_1)x_i(z_2)\cdots x_i(z_p))^T$ denotes the $i$th spatial input variable $(1 \le i \le s)$, $x_i(z_j)$ is the input of $x_i(z)$ from the sensing location $z = z_j$ $(1 \le j \le p)$; $z$ denotes one-dimensional space in a discrete space domain $Z = \{z_1, z_2, \ldots, z_p\}$; $\overline{C}_i^l$ denotes a 3-D fuzzy set, $l = 1, \ldots, N$; $u$ denotes output variable (the control action); $B^l$ denotes a traditional fuzzy set.

If Gaussian type 3-D membership functions (MF) are used to describe 3-D fuzzy sets in (2.1), then we have

$$\mu_{Gi}^{l}(x_i(z)) = \exp\left(-\left(\frac{x_i(z) - c_i^l(z)}{\sigma_i^l(z)}\right)^2\right), \tag{2.2}$$

where $\mu_{Gi}^{l}$ denotes the Gaussian type 3-D MF of the $i$th spatial input $x_i(z)$ in the $l$th rule; $c_i^l(z) = (c_i^l(z_1), \ldots, c_i^l(z_p))^T$ and $\sigma_i^l(z) = (\sigma_i^l(z_1), \ldots, \sigma_i^l(z_p))^T$ are the center and width of $\mu_{Gi}^{l}$, respectively; $c_i^l(z_j)$ and $\sigma_i^l(z_j)$ denote center and width of the Gaussian type 2D MF of the $i$th spatial input $x_i(z)$ at the sensing location $z = z_j$. The Gaussian type 3-D MF $\mu_{Gi}^{l}$ can be regarded as an assembly of multiple Gaussian type 2-D MFs over the space domain $Z$. Then, the Gaussian type 2-D MF of the $i$th spatial input $x_i(z)$ at the sensing location $z = z_j$ is given as

$$\mu_{Gij}(x_i(z_j)) = \exp\left(-\left(\frac{x_i(z_j) - c_{ij}^l}{\sigma_{ij}^l}\right)^2\right), \tag{2.3}$$

where $c_{ij}^l = c_i^l(z_j)$ and $\sigma_{ij}^l = \sigma_i^l(z_j)$.

Furthermore, if we employ singleton fuzzification, "product" $t$-norm and "weighted aggregation" dimension reduction [6] in the 3-D rule inference, singleton fuzzy sets for the output variable, and "center of sets" defuzzification [17], the 3-D FLC can be mathematically expressed as

$$\begin{aligned} u(x_z) &= \frac{\sum_{l=1}^{N} \zeta^l \sum_{j=1}^{p} a_j \prod_{i=1}^{s} \mu_{Gij}(x_i(z_j))}{\sum_{l=1}^{N} \sum_{j=1}^{p} a_j \prod_{i=1}^{s} \mu_{Gij}(x_i(z_j))} \\ &= \frac{\sum_{l=1}^{N} \zeta^l \sum_{j=1}^{p} a_j \prod_{i=1}^{s} \exp\left(-\left(\left(x_i(z_j) - c_{ij}^l\right)/\sigma_{ij}^l\right)^2\right)}{\sum_{l=1}^{N} \sum_{j=1}^{p} a_j \prod_{i=1}^{s} \exp\left(-\left(\left(x_i(z_j) - c_{ij}^l\right)/\sigma_{ij}^l\right)^2\right)}, \end{aligned} \tag{2.4}$$

where $x_z = (x_1(z)x_2(z)\cdots x_s(z)) \in \Omega \subset R^{p\times s}$ is a spatial input vector with $\Omega$ as the input domain, $p$ as the number of sensors, and $s$ as the number of spatial inputs; $N$ is the number of rules; $a_j$ is the spatial weight from the $j$th spatial point [6]; $\zeta^l \in U$ is the nonzero value in the singleton fuzzy set of the output variable for the $l$th rule.

In (2.4), let

$$\phi^l(x_z) = \frac{\sum_{j=1}^{p} a_j \prod_{i=1}^{s} \mu_{Gij}(x_i(z_j))}{\sum_{l=1}^{N} \sum_{j=1}^{p} a_j \prod_{i=1}^{s} \mu_{Gij}(x_i(z_j))}, \tag{2.5}$$

then (2.4) can be rewritten as

$$u(x_z) = \sum_{l=1}^{N} \zeta^l \phi^l(x_z). \tag{2.6}$$

Similar to a traditional FLC [16], we define $\phi^l(x_z)$ as a spatial fuzzy basis function (SFBF). Each SFBF corresponds to a 3-D fuzzy rule, and all the SFBFs correspond to a 3-D rule base. Mathematically, a 3-D FLC is a linear combination of all the SFBFs.

Equation (2.6) shows that the 3-D FLC is a nonlinear mapping from the input space $x_z \in \Omega \subset R^{p\times s}$ to the output space $u(x_z) \in U \subset R$. It provides us a way to understand and analyze the 3-D FLC from the point of view of function approximation. In Section 4, we will prove that the 3-D FLC has a universal approximation property based on the nonlinear mapping in (2.6).

## 2.2. Linear SVM Regression

An SVM is a learning algorithm that originated from theoretical foundations of the statistical learning theory [18] and has been widely used in many practical applications, such as bioinformatics, machine vision, text categorization, handwritten character recognition, time series analysis, and so on. The distinct advantage of the SVM over other machine learning algorithms is that it has a good generalization ability and can simultaneously minimize the empirical risk and the expected risk [19]. The SVM algorithms can be categorized into two categories: SVM classification and SVM regression. In this study, we are concerned with the SVM regression with $\varepsilon$-insensitive loss function [20].

Suppose we have a training set $D = \{[x_i, y_i] \in R^s \times R,\ i = 1, \ldots, q\}$ consisting of $q$ pairs $(x_1, y_1), (x_2, y_2), \ldots, (x_q, y_q)$, where the inputs are $s$-dimensional vectors, and the labels are continuous values. In $\varepsilon$-SVM regression, the goal is to find a function $f(x, w)$ so that for all training patterns $x$ has a maximum deviation $\varepsilon$ from the target values $y_i$ and has a maximum margin. The $\varepsilon$-insensitive loss function is defined as follows:

$$\left|y - f(x,w)\right|_\varepsilon = \begin{cases} 0, & \text{if } \left|y - f(x,w)\right| \le \varepsilon, \\ \left|y - f(x,w)\right| - \varepsilon, & \text{otherwise.} \end{cases} \tag{2.7}$$

The $\varepsilon$-insensitive loss function defines an $\varepsilon$ tube [9].

The regression problem can be formulated as a convex optimization problem as follows:

$$\min_{w,b,\xi_i,\xi_i^*} = \frac{1}{2}\|w\|^2 + C\left(\sum_{i=1}^{l}\xi_i + \sum_{i=1}^{l}\xi_i^*\right) \tag{2.8}$$

subject to

$$\begin{aligned} y_i - \langle w \cdot x_i \rangle - b &\le \varepsilon + \xi_i \\ \langle w \cdot x_i \rangle + b - y_i &\le \varepsilon + \xi_i^* \\ \xi_i \ge 0, \quad \xi_i^* \ge 0, \quad i &= 1, \ldots, q, \end{aligned} \tag{2.9}$$

where $\xi_i$ and $\xi_i^*$ are slack variables, and the constant $C$ is a design parameter chosen by the user, which determines the trade off between the complexity of $f(x, w)$ and the approximate error.

The above optimization problem can be solved in a dual space. By introducing the Lagrange multipliers, the primal optimization problem can be formulated in its dual form as follows:

$$\max_{\alpha_i, \alpha_i^*} \left\{ -\frac{1}{2} \sum_{i=1}^{q} \sum_{j=1}^{q} (\alpha_i^* - \alpha_i)\left(\alpha_j^* - \alpha_j\right)\langle x_i \cdot x_j \rangle - \varepsilon \sum_{i=1}^{q} (\alpha_i^* + \alpha_i) + \sum_{i=1}^{q} (\alpha_i^* - \alpha_i) y_i \right\} \tag{2.10}$$

subject to

$$\begin{aligned} \sum_{j=1}^{q} \alpha_i^* &= \sum_{i=1}^{q} \alpha_i, \\ 0 \le \alpha_i^* \le C, \quad 0 \le \alpha_i \le C, \quad i &= 1, \ldots, q. \end{aligned} \tag{2.11}$$

Solving the dual quadratic programming problem, we can find an optimal weight vector $w$ and an optimal bias $b$ of the regression hypersurface given as follows:

$$\begin{aligned} w &= \sum_{i=1}^{q} (\alpha_i^* - \alpha_i) x_i, \\ b &= \frac{1}{q} \left( \sum_{i=1}^{q} (y_i - \langle w \cdot x_i \rangle \right). \end{aligned} \tag{2.12}$$

Then, the best regression hypersurface is given by

$$f(x, w) = \sum_{i=1}^{q} (\alpha_i^* - \alpha_i)\langle x \cdot x_i \rangle + b = \sum_{i \in \mathrm{SV}} (\alpha_i^* - \alpha_i)\langle x \cdot x_i \rangle + b \tag{2.13}$$

The training pattern $x_i$ with nonzero $(\alpha_i^* - \alpha_i)$ is called support vector (SV).

## 3. Clustering and SVM-Regression Learning-Based 3-D FLC Design

Clustering and SVM-regression learning-based 3-D FLC design is a novel design of a 3-D FLC by integrating a nearest-neighborhood-clustering and an SVM-regression. The design

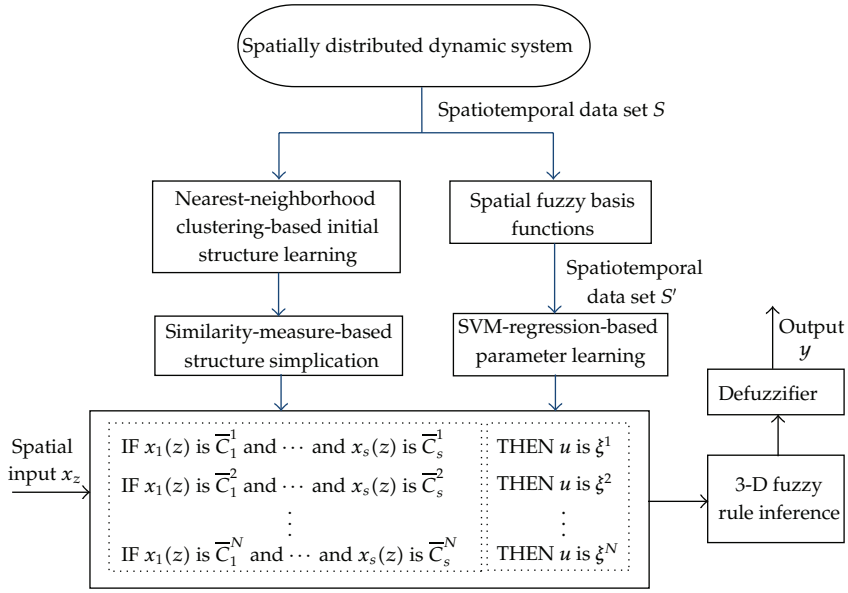


**Figure 3:** Conceptual configuration of a clustering and SVM-regression learning-based 3-D FLC.

methodology can be depicted by Figure 3. Firstly, a nearest-neighborhood-clustering method with Frobenius norm defined as a distance is employed to mine the underlying knowledge of the spatiotemporal data set $S$ and yield the initial structure, that is, antecedent part of 3-D fuzzy rules. Because the obtained input space partition may have redundancy in terms of highly overlapping MFs, it is necessary to optimize the obtained initial fuzzy partition. Then, a similarity measure technique is utilized to merge similar 3-D fuzzy sets and to merge similar 3-D fuzzy rules, and then to simplify the initial rule structure. Finally, a linear SVM-regression algorithm is used to learn the parameters of the consequent parts based on an equivalence relationship between a linear SVM regression and a 3-D FLC.

The spatiotemporal data set $S$ from a spatially distributed system is composed of $n$ spatiotemporal input-output data pairs given as follows:

$$S = \left\{ \left( x_z^k, u^k \right) \mid x_z^k \in R^{p \times s},\ u^k \in R,\ k = 1, \ldots, n \right\}, \tag{3.1}$$

where $x_z^k = (x_1^k(z), \ldots, x_s^k(z))$ denotes the value of $s$ spatial input variables at the $k$th sampling time, $x_i^k(z) = (x_i^k(z_1), \ldots, x_i^k(z_p))^T$ denotes the value of $i$th spatial input variable at the $k$th sampling time ($i = 1, \ldots, s$), $u^k$ denotes the output value at the $k$th sampling time, $n$ denotes the number of sampling time, and $p$ denotes the number of sensors. Since infinite sensors are used, $x_z^k$ is a matrix with $p$ rows and $s$ columns.

## 3.1. Initial Structure Learning

### 3.1.1. Nearest Neighborhood Clustering Method

Clustering method is one of the data-driven learning tools for unlabeled data. It can mine underlying knowledge (or data structure) from a dataset that is difficult for humans to manually identify. One of the simplest clustering algorithms is the nearest-neighborhood clustering algorithm [16]. However, the existing nearest-neighborhood clustering algorithm has not the capability to deal with spatiotemporal data. In this study, we expand its capability to deal with spatiotemporal data set $S$, which is of matrix form. The key point is that the Frobenius norm given in (3.2) is used for defining a distance in a nearest neighborhood clustering algorithm.

$$\|X\|_F = \sqrt{\mathrm{tr}\left(X^T X\right)} \quad \left(X \in R^{p\times s}\right). \tag{3.2}$$

The nearest neighborhood clustering algorithm is summarized as follows.

(i) Step 1: Begin from the first spatiotemporal data $x_z^1$. Let the first cluster center $c_z^1$ be $x_z^1$, the number of data pairs $m_1$ be 1, and the threshold be $\rho_0$ for generating new fuzzy rules.

(ii) Step 2: Suppose that the $k$th spatiotemporal data $x_z^k$ $(k = 2,\ldots,n)$ is considered, when $N$ clusters have been generated and their centers are $c_z^1, c_z^2, \ldots$, and $c_z^N$ respectively. Firstly, compute the distance between $x_z^k$ and each center of $N$ clusters using $\|x_z^k - c_z^l\|_F$ $(l = 1,\ldots,N)$. Then, compute the threshold $\rho$ using

$$\rho = \max_{l=1,\ldots,N}\left(\frac{1}{1+\left\|x_z^k - c_z^l\right\|_F}\right) \tag{3.3}$$

Hence, the corresponding cluster center $c_z^{l_k}$ is taken as the nearest neighborhood cluster of $x_z^k$.

(iii) Step 3: (a) If $\rho < \rho_0$, then $x_z^k$ is taken as a new cluster center, and let $N = N+1$, $m_N = 1$, and $c_z^N = x_z^k$. (b) If $\rho \geq \rho_0$, $x_z^k$ belongs to the cluster with the center $c_z^{l_k}$. The center of $l_k$th cluster is tuned by introducing a learning rate $\eta = \eta_0/(m_{l_k}+1)$ $(\eta_0 \in [0,1])$ as follows:

$$c_z^{l_k} = c_z^{l_k} + \eta\left(x_z^k - c_z^{l_k}\right), \tag{3.4}$$

and let $m_{l_k} = m_{l_k} + 1$.

(iv) Step 4: Let $k = k+1$. If $k \geq n+1$, then quit. Otherwise, back to Step 2.

### 3.1.2. Rule Extraction and 3-D MF Construction

After clustering learning, we obtain an input space partition with $N$ cluster centers $c_z^1, c_z^2, \ldots, c_z^N$. Then, we will produce antecedent part of rule base and construct 3-D MFs in

terms of the partition. Each cluster corresponds to a 3-D fuzzy rule. Assumed that we employ Gaussian type 3-D MF. Then, the cluster center corresponds to the center of Gaussian type 3-D MFs in the antecedent part. Thus, the number of fuzzy rules is equal to the number of clusters $N$. In addition, we determine the width of the Gaussian MFs in terms of the domain of variables. For instance, the width of the Gaussian type 3-D MFs from the same sensing location are defined as

$$\sigma(z_j) = \max_{1\le i\le s}\left(\frac{x_i^{\max}(z_j) - x_i^{\min}(z_j)}{10}\right), \tag{3.5}$$

where $x_i^{\max}(z_j)$ and $x_i^{\min}(z_j)$ are the maximum and the minimum bound values of the $i$th spatial input variable, respectively.

## 3.2. Structure Simplication

After the initial structure learning, the obtained fuzzy partition of the input space and fuzzy rules may have redundancy in terms of highly overlapping MFs. In this step, we will simplify the fuzzy partition and fuzzy rules. The crucial technique for simpification is similarity measure. The previous similarity measure techniques [14, 21, 22] developed for traditional fuzzy sets and traditional fuzzy rules are not suitable to 3-D fuzzy sets and 3-D fuzzy rules. In this study, we will define a new similarity measure technique.

### 3.2.1. Similarity Measure

Firstly, we define the similarity of two 3-D fuzzy sets $\overline{A}$ and $\overline{B}$ as below.

$$\overline{S}\left(\overline{A},\overline{B}\right) = \frac{1}{1 + d\left(\overline{A},\overline{B}\right)}, \quad \overline{S}(\cdot) \in (0,1], \tag{3.6}$$

where $d(\overline{A},\overline{B})$ is a distance between $\overline{A}$ and $\overline{B}$. Since Gaussian type 3-D MFs are chosen, the following simple expression can be used to approximate the distance:

$$d\left(\overline{A},\overline{B}\right) = \left\| \begin{bmatrix} c_{\overline{A}(z_1)} & \sigma_{\overline{A}(z_1)} \\ \vdots & \vdots \\ c_{\overline{A}(z_p)} & \sigma_{\overline{A}(z_p)} \end{bmatrix} - \begin{bmatrix} c_{\overline{B}(z_1)} & \sigma_{\overline{B}(z_1)} \\ \vdots & \vdots \\ c_{\overline{B}(z_p)} & \sigma_{\overline{B}(z_p)} \end{bmatrix} \right\|_F, \tag{3.7}$$

where $c_{\overline{A}(z_j)}(c_{\overline{B}(z_j)})$ and $\sigma_{\overline{A}(z_j)}(\sigma_{\overline{B}(z_j)})$ are center and width of the Gaussian type 3-D MF $\overline{A}(\overline{B})$ at sensing location $z = z_j$ $(j = 1,\ldots,p)$, respectively.

Based on the similarity measure, we can merge similar 3-D fuzzy sets, or merge similar 3-D fuzzy rules.

*(i) Merge of Two Similar 3-D Fuzzy Sets $\overline{A}$ and $\overline{B}$*

Firstly, the similarity between $\overline{A}$ and $\overline{B}$ is computed according to (3.6). If $\overline{S}(\overline{A},\overline{B})$ is higher than a threshold, we can conclude that $\overline{A}$ and $\overline{B}$ are similar, and then merge them into a new 3-D fuzzy set $\overline{C}$. The center and width of $\overline{C}$ are viewed as the average values of $\overline{A}$ and $\overline{B}$, and are given as the following:

$$\begin{aligned} c_{\overline{C}(z_j)} &= \frac{c_{\overline{A}(z_j)} + c_{\overline{B}(z_j)}}{2}, \\ \sigma_{\overline{C}(z_j)} &= \frac{\sigma_{\overline{A}(z_j)} + \sigma_{\overline{B}(z_j)}}{2}. \end{aligned} \tag{3.8}$$

*(ii) Merge of Two Similar 3-D Fuzzy Rules $\overline{R}^{l_1}$ and $\overline{R}^{l_2}$*

The similarity $\overline{R}^{l_1}$ and $\overline{R}^{l_2}$ is inferred by measuring their similarity in the antecedent part. For instance, the similarity computation between $\overline{R}^{l_1}$ and $\overline{R}^{l_2}$ is given by

$$\overline{S}_{\text{rule}}\left(\overline{R}^{l_1},\overline{R}^{l_2}\right) = \min_{1\le i\le s}\left\{\overline{S}\left(\overline{C}_i^{l_1},\overline{C}_i^{l_2}\right)\right\}, \tag{3.9}$$

where $\overline{R}^{l_1}$ and $\overline{R}^{l_2}$ have the same rule form as in (2.1), $\overline{C}_i^{l_1}$ ($\overline{C}_i^{l_2}$) denotes the 3-D fuzzy set for the $i$th spatial input variable $x_i(z)$ in the $l_1$th ($l_2$th) rule. If $\overline{S}_{\text{rule}}(\overline{R}^{l_1},\overline{R}^{l_2})$ is higher than a threshold, we can conclude that $\overline{R}^{l_1}$ and $\overline{R}^{l_2}$ are similar, and then merge them into a new 3-D fuzzy rule $\overline{R}^{l_1 l_2}$. The merging of two 3-D fuzzy rules is realized by merging the two fuzzy sets of each spatial input variable in the two 3-D fuzzy rules, respectively.

### *3.2.2. Similarity Measure-Based Structure Simplification*

Based on the similarity measure, the simplification task includes removing 3-D fuzzy sets similar to the universal set, merging similar 3-D fuzzy sets, and merging similar rules. The detailed procedure of structure simplification is summarized as follows.

(i) Step 1: Given a 3-D fuzzy rule base $\overline{\Re} = \{\overline{R}^l\}_{l=1}^K$. Firstly, set proper thresholds: $\lambda_u \in (0,1]$ for removing 3-D fuzzy sets that are similar to the universal set, $\lambda_{\text{set}} \in (0,1]$ for merging similar 3-D fuzzy sets, and $\lambda_{\text{rule}} \in (0,1]$ for merging 3-D fuzzy rules with similar antecedents.

(ii) Step 2: Calculate $s_{jki} = \overline{S}(\overline{C}_i^j,\overline{C}_i^k)$ with $j \ne k, j = 1,\ldots,K, k = 1,\ldots,K$, and $i = 1,\ldots,s$. Let $s_{rmq} = \max_{j\ne k}\{s_{jki}\}$ and select $\overline{C}_q^r$ and $\overline{C}_q^m$.

(iii) Step 3: If $s_{rmq} \ge \lambda_{\text{set}}$, merge $\overline{C}_q^r$ and $\overline{C}_q^m$ into a new 3-D fuzzy set $\overline{C}_q^{rm}$, set $\overline{C}_q^r = \overline{C}_q^{rm}$ and $\overline{C}_q^m = \overline{C}_q^{rm}$, and back to step 2. If no more two 3-D fuzzy sets have the similarity with $s_{rmq} \ge \lambda_{\text{set}}$ ($j \ne k$), then go to step 4.

(iv) Step 4: Remove the 3-D fuzzy set similar to the universal set and the rule with membership function that is always near zero over the space domain.

(v) Step 5: Calculate the similarity of two rules $s_{l_1 l_2} = \overline{S}_{\text{rule}}(\overline{R}^{l_1}, \overline{R}^{l_2})$ with $l_1 \neq l_2$, $l_1 = 1, \ldots, N, l_2 = 1, \ldots, N$. Let $s_{rm} = \max_{l_1 \neq l_2}\{s_{l_1 l_2}\}$.

(vi) Step 6: If $s_{rm} \geq \lambda_{\text{rule}}$, merge the $r$th and the $m$th rules into a new rule $R_{\text{new}}$ and substitute them. Let $N = N - 1$, and back to step 5. If no more rules have similarity with $s_{rm} \geq \lambda_{\text{rule}}$ $(r \neq m)$, then quit.

Generally speaking, the threshold $\lambda_u$ is higher than the threshold $\lambda_{\text{set}}$, while the choice of a suitable threshold $\lambda_{\text{rule}}$ depends on the application. The lower $\lambda_{\text{set}}$ is set, the less fuzzy sets and less fuzzy rules are yielded in the resulting rule base. In this study, we set $\lambda_u = 0.95$, $\lambda_{\text{set}} = 0.75$, and $\lambda_{\text{rule}} = 1$.

### 3.3. Parameter Learning

After the structure simplification, we obtain a rule base with optimized antecedent parts. For a complete rule base, the rest task is to determine the consequent part parameters. In this study, we employ an SVM regression algorithm to learn the consequent part parameter $\xi^l$ $(l = 1, \ldots, N)$ in the 3-D FLC.

Firstly, the original input samples are transformed into new samples. Utilizing the spatial fuzzy basis functions $\phi^l(x_z^k)$ $(l = 1, \ldots, N)$ in (2.5), we can transform each spatial input sample $x_z^k$ $(k = 1, \ldots, n)$ in $S$ into a new input sample $\phi(x_z^k) = (\phi^1(x_z^k), \phi^2(x_z^k), \ldots, \phi^N(x_z^k))$. Then, the original data set $S$ in (3.1) can be transformed into a new data set $S'$ as follows:

$$S' = \left\{ \left( \phi\left(x_z^k\right), u^k \right) \mid \phi\left(x_z^k\right) \in R^N,\ u^k \in R,\ k = 1, \ldots, n \right\}. \tag{3.10}$$

Secondly, an equivalence relationship of an SVM regression and a 3-D FLC can be derived based on the new data set $S'$. From (2.13), the final decision function $f(\phi(x_z^k))$ of an SVM can be described with the following form:

$$f\left(\phi\left(x_z^k\right)\right) = \sum_{k=1}^{n} (\alpha_k^* - \alpha_k) \left\langle \phi\left(x_z^k\right), \phi(x_z) \right\rangle + b, \tag{3.11}$$

where $\alpha_k^*$ and $\alpha_k$ are associated learning parameters in a SVM, The training pattern $\phi(x_z^k)$ with nonzero $(\alpha_k^* - \alpha_k)$ is called support vector (SV). Furthermore, (3.11) can further be expressed by

$$\begin{aligned} f\left(\phi\left(x_z^k\right)\right) &= \sum_{k=1}^{n} (\alpha_k^* - \alpha_k) \sum_{l=1}^{N} \phi^l\left(x_z^k\right) \phi^l(x_z) + b \\ &= \sum_{l=1}^{N} \left( \sum_{k=1}^{n} (\alpha_k^* - \alpha_k) \phi^l\left(x_z^k\right) \right) \phi^l(x_z) + b \\ &= \sum_{l=1}^{N} \xi^l \phi^l(x_z) + b \\ &= u(x_z) \end{aligned} \tag{3.12}$$

In (3.12), the bias term $b$ in a 3-D FLC can be realized by adding a fuzzy rule as follows:

$$\overline{R}^0 : \text{IF } x_1(z) \text{ is } \overline{C}_1^0 \text{ and} \cdots \text{and } x_s(z) \text{ is } \overline{C}_s^0, \quad \text{THEN } u \text{ is } b, \tag{3.13}$$

where $\overline{C}_i^0$ is a universal 3-D fuzzy set, whose fuzzy degree is 1 over the space domain for any spatial input $x_i(z)$, $i = 1, \ldots, s$. From (3.12), we can see that an SVM will be equivalent to a 3-D FLC if (3.14) holds.

$$\xi^l = \sum_{k=1}^{n} (\alpha_k^* - \alpha_k) \phi^l\left(x_z^k\right). \tag{3.14}$$

Finally, a linear SVM regression is employed to learn the consequent part parameters. Using (3.14), the parameters $\xi^l$ $(l = 1, \ldots, N)$ in consequent parts are obtained in terms of the SVM learning, that is,

$$\xi^l = \sum_{k \in \mathrm{SV}} (\alpha_k^* - \alpha_k) \phi^l\left(x_z^k\right). \tag{3.15}$$

## 4. Universal Approximation of Clustering and SVM-Regression Learning-Based 3-D FLC

In essence, the clustering and SVM-regression learning-based 3-D FLC design is a fuzzy modeling that extracts fuzzy control rules and constructs a 3-D FLC from spatiotemporal data hidden with effective control laws. In other words, the proposed 3-D FLC aims at approximating an unknown nonlinear control function. Thus, in this subsection, we are concerned with its universal approximation capability. The universal approximation capability of the SVM learning-based 3-D FLC can be described by the following theorem.

**Theorem 4.1.** *Suppose that the input universe of discourse $\Omega$ is a compact set in $R^{p \times s}$. Then, for any given real continuous function $g(x_z)$ on $\Omega$ and arbitrary $\varepsilon > 0$, there exists a 3-D FLC $u(x_z)$ as described in* (2.4) *satisfying the following inequality:*

$$\sup_{x_z \in \Omega} \left( \left| u(x_z) - g(x_z) \right| \right) < \varepsilon. \tag{4.1}$$

The proof of the theorem is given in the appendix by using Stone-Weierstrass theorem [23]. Theorem 4.1 indicates that the clustering and SVM-regression learning-based 3-D FLC is a universal approximator, that is, it can approximate continuous control functions to arbitrary accuracy.

## 5. Application

### 5.1. A Catalytic Packed-Bed Reactor

We take a catalytic packed-bed reactor [1, 5] as an example. The reactor is long and thin as shown in Figure 4. It is fed with gaseous reactant $C$ from the right side, and the zero-order

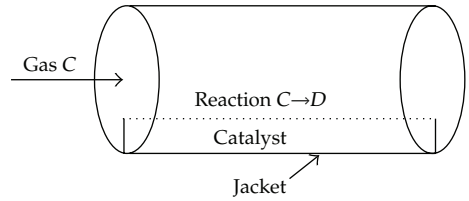


**Figure 4:** Sketch of a catalytic packed-bed reactor.

gas phase reaction $C \rightarrow D$ is carried out on the catalyst. The reaction is endothermic, and a jacket is used to heat the reactor. A dimensionless model that describes this nonlinear tubular chemical reactor is provided as follows:

$$\begin{aligned} \varepsilon_p \frac{\partial T_g}{\partial t} &= -\frac{\partial T_g}{\partial z} + \alpha_c (T_s - T_g) - \alpha_g (T_g - u), \\ \frac{\partial T_s}{\partial t} &= \frac{\partial^2 T_s}{\partial z^2} + B_0 \exp\left(\frac{\gamma T_s}{1 + T_s}\right) - \beta_c (T_s - T_g) - \beta_p (T_s - b(z)u) \end{aligned} \tag{5.1}$$

subject to the boundary conditions

$$z = 0, \quad T_g = 0, \quad \frac{\partial T_s}{\partial z} = 0; \quad z = 1, \quad \frac{\partial T_s}{\partial z} = 0, \tag{5.2}$$

where $T_g, T_s$, and $u$ denote the dimensionless temperature of the gas, the catalyst, and jacket, respectively. The values of the process parameters are given as follows:

$$\varepsilon_p = 0.01, \quad \gamma = 21.14, \quad \beta_c = 1.0, \quad \beta_p = 15.62, \tag{5.3}$$

$$B_0 = -0.003, \quad \alpha_c = 0.5, \quad \alpha_g = 0.5. \tag{5.4}$$

The concerned control problem is to control the catalyst temperature $T_s(z,t)$ throughout the reactor to track a spatial reference profile ($T_{\mathrm{sd}}(z) = 0.42 - 0.2\cos(\pi z)$) in order to maintain a desired degree of reaction rate using the measurements of catalyst temperature from five sensing locations $z' = [0 \ 0.25 \ 0.5 \ 0.75 \ 1]$ and manipulating one spatially distributed heating source ($b(z) = 1 - \cos(\pi z)$). The mathematical model (5.1)-(5.2) is only for the process simulation for evaluation of the control scheme. The method of lines [24] is used to simulate the model.

In this application, we aim at extracting 3-D fuzzy rules from a spatiotemporal data set using clustering and SVM regression learning algorithm and constructing a complete 3-D FLC without any prior knowledge.

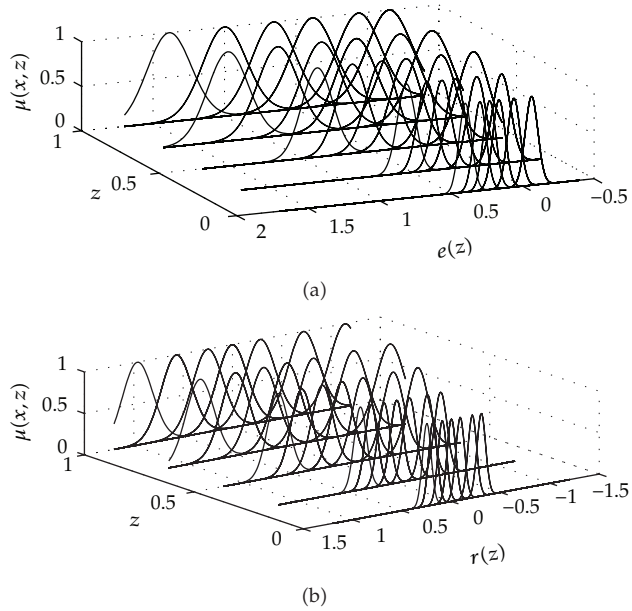


**Figure 5:** Distributions of Gaussian type 3-D fuzzy sets in the simplified fuzzy-rule base.

## *5.2. Design of a Clustering and SVM-Regression Learning-Based 3-D FLC*

### *5.2.1. Spatiotemporal Data Collection*

The spatiotemporal input-output data set is collected from the catalytic packed-bed reactor controlled by expert-knowledge-based 3-D FLC [5], where pseudorandom quinary signal (PRQS) [25] with maximum length of 124 as perturbed signal is added to the control input. Each spatiotemporal input-output data pair consists of a spatial error input $e^*(z) = [e_1^*, \ldots, e_5^*]^T$, a spatial error in change input $r^*(z) = [r_1^*, \ldots, r_5^*]^T$, and an incremental output $\Delta u^*$, where $e_i^* = T_s(z_i, q) - T_{\mathrm{sd}}(z_i)$ $r_i^* = e_i^*(q) - e_i^*(q-1)$; $q$ and $q-1$ denotes the $q$th and $q$-1th sampling time, respectively. The detailed design of the expert-knowledge-based 3-D FLC, including fuzzification, 3-D rule inference, and defuzzification, can refer to [5]. The scaling factors for the spatial error, the spatial error in change, and the incremental output are set as 2.0, 0.001, and 0.8716, respectively. The parameters of PRQS are chosen with the following settings: the number of the levels is 5, the length of the period is 124, the sampling time is 0.2 s, and the minimum switching time (i.e., clock period) is 0.2 s.

Two groups of data sets are obtained by adding PRQS signal with different scaling factor (i.e., 0.447 and 0.1) to the control input. The first group with 150 data pairs is generated for training by adding PRQS perturbation signal with a scaling factor 0.447, and the other group with 150 data pairs is generated for test by adding PRQS perturbation signal with a scaling factor 0.1. To evaluate the performance, we employ the following root-mean-squared error (RMSE) as the criteria:

$$\mathrm{RMSE} = \sqrt{\sum_{k=1}^{n} \frac{\left(\Delta u_k^* - \Delta u_k\right)^2}{n}}, \tag{5.5}$$

**Table 1:** Learning results of an SVM regression with different values of $C$ and $\varepsilon$.

| $C$ | $\varepsilon$ | Number of SV | RMSE training ($\times 10^{-2}$) | RMSE testing ($\times 10^{-2}$) | SSE ($\times 10^{-2}$) | IAE ($\times 10^{-1}$) | ITAE ($\times 10^{-1}$) |
|---|---|---|---|---|---|---|---|
| 1 | 0.00001 | 149 | 4.89 | 3.48 | 1.70 | 2.566 | 8.656 |
| | 0.0001 | 140 | 4.89 | 3.48 | 1.70 | 2.566 | 8.655 |
| | 0.001 | 129 | 4.86 | 3.45 | 1.71 | 2.573 | 8.699 |
| | 0.01 | 105 | 4.75 | 3.13 | 1.84 | 2.699 | 9.389 |
| | 0.1 | 13 | 6.35 | 3.24 | 1.99 | 2.901 | 10.163 |
| | 0.2 | 12 | 12.80 | 6.44 | 3.74 | 4.653 | 19.063 |
| | 0.3 | 10 | 19.29 | 7.76 | 4.77 | 5.715 | 24.248 |
| 10 | 0.00001 | 149 | 4.89 | 3.48 | 1.70 | 2.566 | 8.656 |
| | 0.0001 | 140 | 4.89 | 3.48 | 1.70 | 2.566 | 8.655 |
| | 0.001 | 129 | 4.86 | 3.45 | 1.71 | 2.573 | 8.699 |
| | 0.01 | 105 | 4.75 | 3.13 | 1.84 | 2.699 | 9.389 |
| | 0.1 | 13 | 6.35 | 3.24 | 1.99 | 2.901 | 10.163 |
| | 0.2 | 12 | 12.80 | 6.44 | 3.74 | 4.653 | 19.063 |
| | 0.3 | 10 | 19.29 | 7.76 | 4.77 | 5.715 | 24.248 |
| 100 | 0.00001 | 149 | 4.89 | 3.48 | 170 | 2.566 | 8.656 |
| | 0.0001 | 141 | 4.89 | 3.48 | 1.70 | 2.566 | 8.655 |
| | 0.001 | 129 | 4.86 | 3.45 | 1.71 | 2.573 | 8.699 |
| | 0.01 | 105 | 4.75 | 3.13 | 1.84 | 2.699 | 9.389 |
| | 0.1 | 13 | 6.35 | 3.24 | 1.99 | 2.901 | 10.163 |
| | 0.2 | 12 | 12.80 | 6.44 | 3.74 | 4.653 | 19.063 |
| | 0.3 | 10 | 19.29 | 7.76 | 4.77 | 5.715 | 24.248 |
| 1000 | 0.00001 | 149 | 4.89 | 3.48 | 170 | 2.566 | 8.656 |
| | 0.0001 | 141 | 4.89 | 3.48 | 1.70 | 2.566 | 8.655 |
| | 0.001 | 129 | 4.86 | 3.45 | 1.71 | 2.574 | 8.702 |
| | 0.01 | 106 | 4.75 | 3.13 | 1.84 | 2.700 | 9.395 |
| | 0.1 | 13 | 6.35 | 3.24 | 1.99 | 2.901 | 10.163 |
| | 0.2 | 12 | 12.80 | 6.44 | 3.74 | 4.653 | 19.063 |
| | 0.3 | 10 | 19.29 | 7.76 | 4.77 | 5.715 | 24.248 |

where $n$ denotes the number of samples, $\Delta u_k^*$ denotes actual output, and $\Delta u_k$ denotes expected output.

### 5.2.2. Design of a Clustering and SVM-Regression Learning-Based 3-D FLC

The design procedure of the proposed 3-D FLC is given as follows:

(i) Employ the nearest neighborhood clustering algorithm to deal with the spatiotemporal data set for the input space partition with $\rho_0 = 0.7$ and $\eta_0 = 0$, and then generate 16 3-D fuzzy rules with 32 3-D fuzzy sets, where the width of Gaussian type 3-D fuzzy sets is $\sigma_z = [0.0620, 0.0902, 0.1518, 0.2008, 0.2175]^T$ from (3.5).

(ii) Simplify the 3-D fuzzy sets and 3-D fuzzy rules based on similarity measure (as described in Section 3.2) with $\lambda_u = 0.95$, $\lambda_{\text{set}} = 0.75$, and $\lambda_{\text{rule}} = 1$, and then obtain

**Table 2:** Performance comparisons.

| Performance index | Clustering and SVM-regression learning-based 3-D FLC | Expert-knowledge-based 3-D FLC |
|---|---|---|
| Number of rules | 15 | 49 |
| No disturbance | | |
| ISS ($\times 10^{-2}$) | 1.70 | 1.69 |
| IAE ($\times 10^{-1}$) | 2.566 | 2.557 |
| ITAE ($\times 10^{-1}$) | 8.655 | 8.646 |
| With 50% increase disturbance in velocity of gas | | |
| ISS ($\times 10^{-2}$) | 1.77 | 1.78 |
| IAE ($\times 10^{-1}$) | 2.675 | 2.680 |
| ITAE ($\times 10^{-1}$) | 9.058 | 9.062 |

15 3-D fuzzy rules with 15 3-D fuzzy sets. The distributions of Gaussian type 3-D fuzzy sets are shown in Figure 5.

(iii) SVM algorithm described in Section 3.2 is used to learn the consequent part parameters with $C = \{1, 10, 100, 1000\}$ and $\varepsilon = \{0.00001, 0.0001, 0.001, 0.01, 0.1, 0.2\}$. The RMSE in (5.5) for training and test are listed in Table 1. From Table 1, we can find that: (1) smaller $\varepsilon$ yielded more support vectors and led to reasonable training and test performance; while larger $\varepsilon$ yielded less support vectors and led to worse training and test performance. (2) $C$ almost had no influence on the training and test performance, once $\varepsilon$ was fixed. In this study, we choose $C = 100$ and $\varepsilon = 0.0001$. Finally, a complete 3-D FLC is constructed with 15 3-D fuzzy rules and 15 3-D fuzzy sets as shown in Figure 6. Using the linguistic hedges approach [14, 21], we can interpret these 3-D fuzzy rules using linguistic words. For instance, the first 3 fuzzy rules are interpreted as follows.

(a) $\overline{R}^1$ : IF $e^*(z)$ is less than POSITIVE SMALL and $r^*(z)$ is more than POSITIVE SMALL, THEN $\Delta u^*$ is sort of POSITIVE MEDIUM.

(b) $\overline{R}^2$ : IF $e^*(z)$ is very ZERO and $r^*(z)$ is very NEGATIVE SMALL, THEN $\Delta u^*$ is very ZERO.

(c) $\overline{R}^3$ : IF $e^*(z)$ is sort of POSITIVE SMALL and $r^*(z)$ is more than POSITIVE MEDIUM, THEN $\Delta u^*$ is more than POSITIVE MEDIUM.

### *5.2.3. Control-Performance Validation*

The designed clustering and SVM regression learning-based 3-D FLC is applied to the control of the catalytic packed-bed reactor, where simulation time is 10 s. We select the same quantitative performance criteria as in [5]: steady-state error (SSE), integral of the absolute error (IAE), and integral of time multiplied by absolute error (ITAE). The control performance is given in Table 2, and the control profile is given in Figures 7 and 8, where (a), (b), and (c) represent catalyst temperature evolution profile, manipulated input, and catalyst temperature profiles in steady state, respectively. We can find that the proposed 3-D FLC has

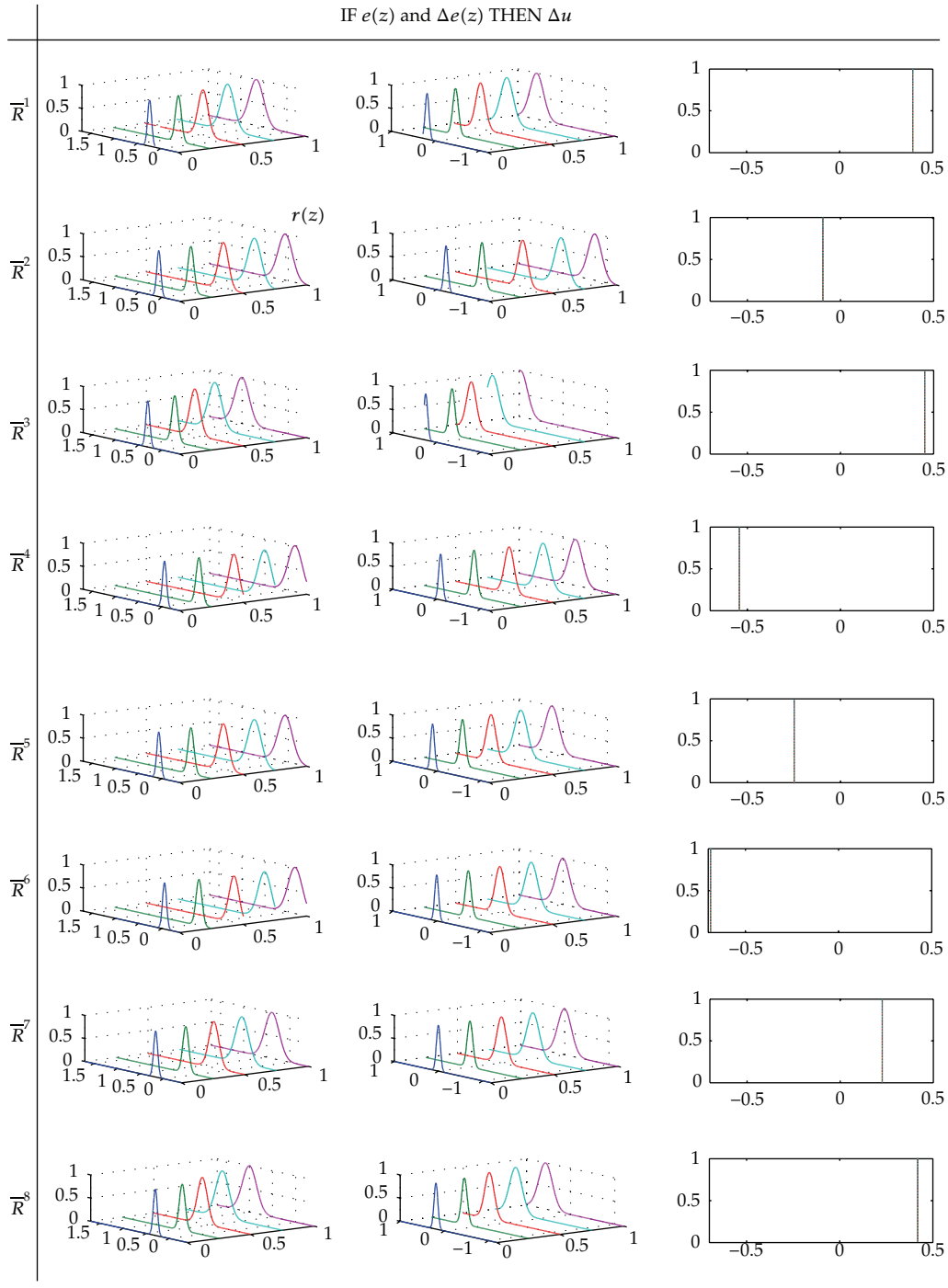


(a)

**Figure 6:** Continued.

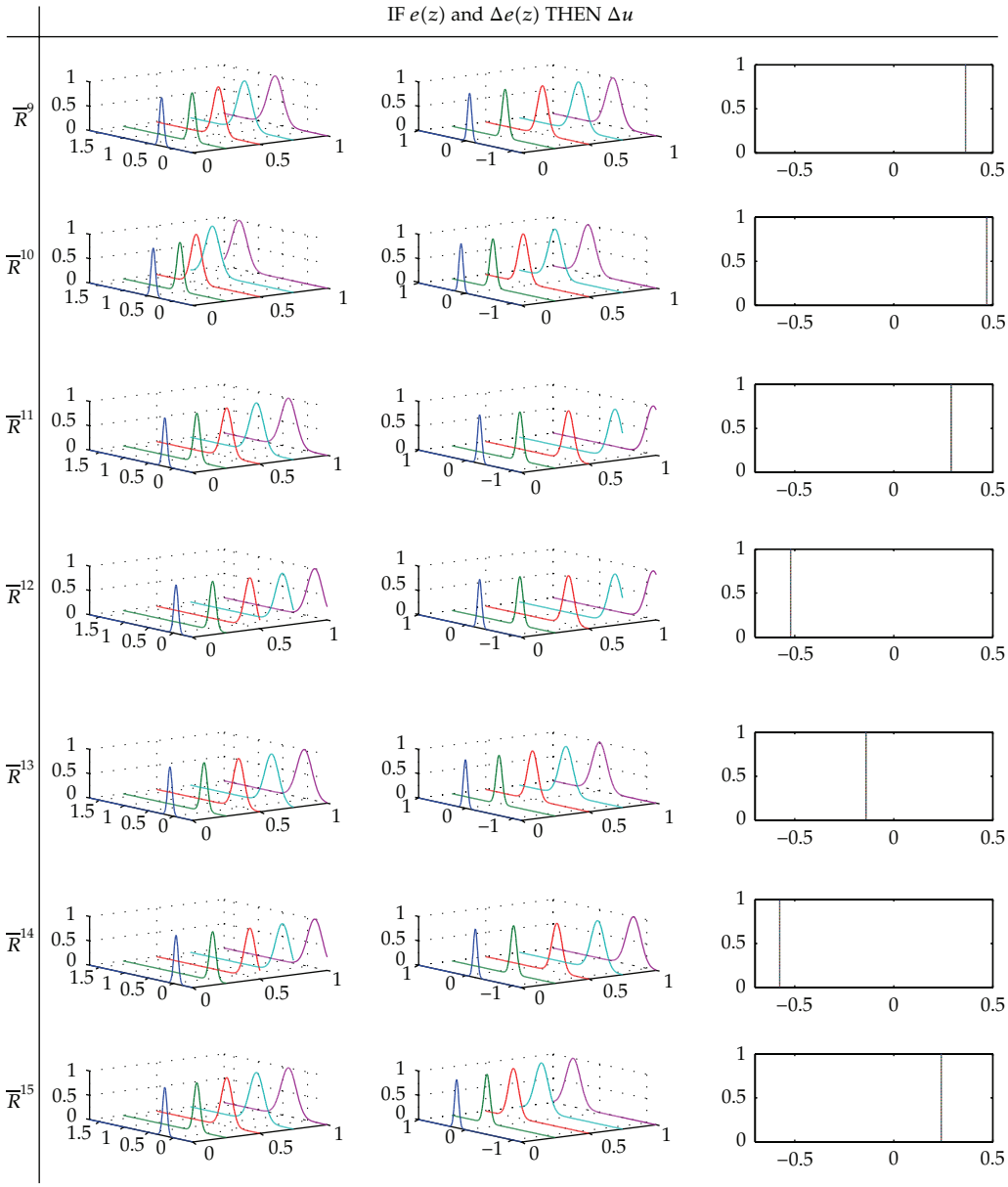


**Figure 6:** 3-D fuzzy rules and their associated 3-D fuzzy sets of a clustering and SVM-regression learning-based 3-D FLC.

comparable control performance to the expert-knowledge-based 3-D FLC in [5] both in ideal condition and in disturbed condition.

In addition, we do more control experiments when the SVM-learning algorithm adopts different $C$ and $\varepsilon$. According to the experimental results (see the last three columns in Table 1), we can find that the proposed 3-D FLC shows good control performance when a smaller $\varepsilon$ is chosen.

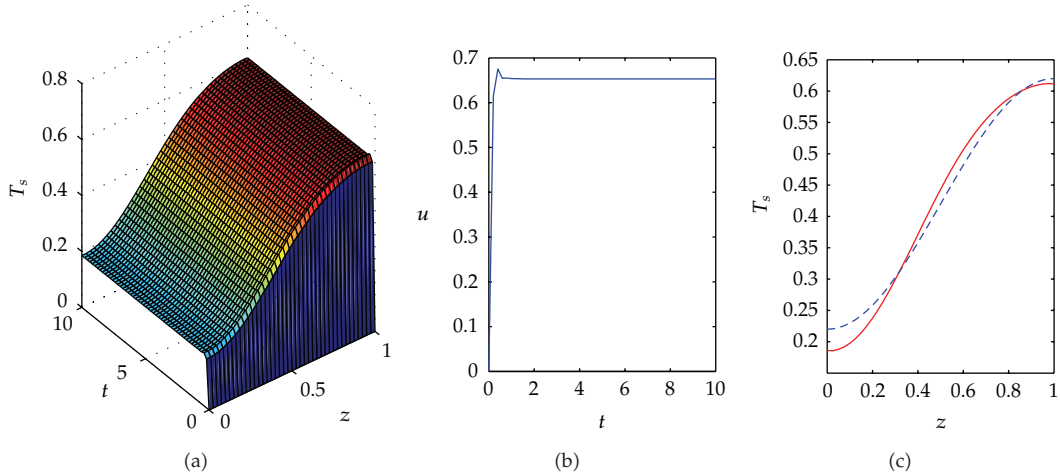


**Figure 7:** Controlled by a clustering and SVM-regression learning-based 3-D FLC under ideal situation (dotted line: reference profile).

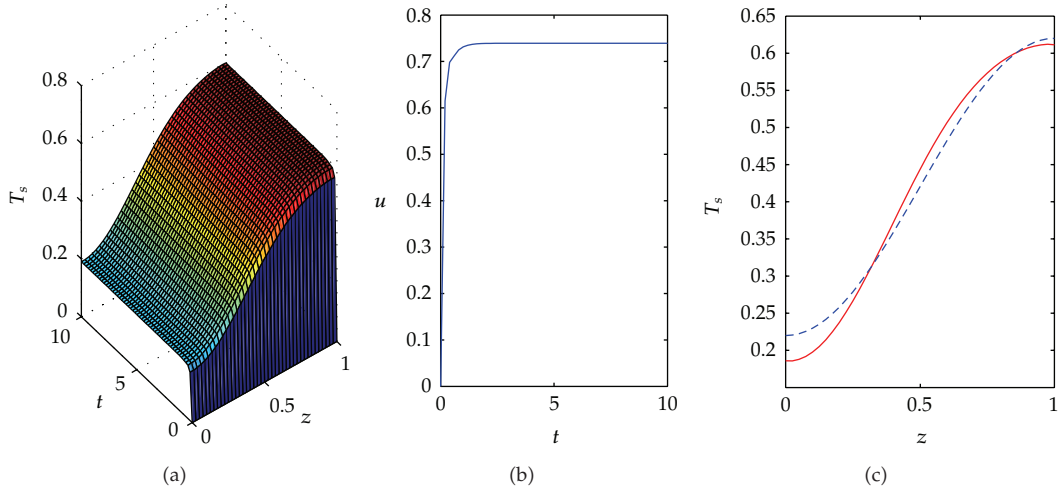


**Figure 8:** Controlled by a clustering and SVM-regression learning-based 3-D FLC under disturbed situation (dotted line: reference profile).

The above simulation results demonstrate that the proposed design method of a clustering and SVM-regression learning-based 3-D FLC is effective. It provides a beneficial complementary design method to 3-D FLCs.

## 6. Conclusions

In this paper, we have proposed a new 3-D FLC design methodology based on clustering and SVM regression learning from a spatiotemporal data set. The 3-D FLC design is divided into three steps. Firstly, an initial rule structure is extracted by a nearest neighborhood clustering method, which is modified to be suitable for spatio-temporal data. Secondly, the initial structure is simplified via using similarity measure technique, which is defined for 3-D fuzzy

sets and 3-D fuzzy rules. Thirdly, the parameters of the rule consequent parts are learned by a spatial fuzzy basis function-based SVM regression learning algorithm. Besides, the universal approximation capability of the proposed 3-D fuzzy system is discussed. Finally, effectiveness of the proposed 3-D FLC design methodology is validated on a catalytic packed-bed reactor.

## Appendix

## A. Proof of the Clustering and SVM-Regression Learning-Based 3-D FLC as a Universal Approximator

Let $\Theta$ be a set of 3-D FLCs defined in $\Omega$, which is a compact set in $R^{p\times s}$. Then, Preliminary 1 is given as follows.

*Preliminary 1*

Let $d_\infty(u,g)$ be a semimetric [26] with the following definition

$$d_\infty(u,g) = \sup_{x_z\in\Omega}\left(\left|u(x_z) - g(x_z)\right|\right) \tag{A.1}$$

Therefore, $(\Theta, d_\infty)$ is a metric space. Since there is at least one fuzzy rule in the rule base of a 3-D FLC, $\Theta$ is non-empty. Thus, $(\Theta, d_\infty)$ is strictly defined.

Subsequently, we will prove that $(\Theta, d_\infty)$ is dense in $(C[\Omega], d_\infty)$ using Stone-Weierstrass theorem, where $C[\Omega]$ is a set of real continuous functions defined in a compact set $\Omega$. The Stone-Weierstrass theorem is first stated here as follows.

*Stone-Weierstrass Theorem (see [16, 23])*

Let $Z$ be a set of real continuous functions on a compact set $U$. If (1) $Z$ is an algebra, that is, the set $Z$ is closed under addition, multiplication, and scalar multiplication; (2) $Z$ separates points on $U$, that is, for every $x, y \in U, x \neq y$, there exists $f \in Z$ such that $f(x) \neq f(y)$; and (3) $Z$ vanishes at no point of $U$, that is, for each $x \in U$ there exists $f \in Z$ such that $f(x) \neq 0$; then, the uniform closure of $Z$ consists of all real continuous functions on $U$, that is, $(Z, d_\infty)$ is dense in $(C[U], d_\infty)$.

*Proof*. (1) Firstly, we prove $(\Theta, d_\infty)$ is an algebra. Let $u_1, u_2 \in \Theta$, then we can write them as

$$\begin{aligned}
u_1(x_z) &= \frac{\sum_{l_1=1}^{N_1} \overrightarrow{u}_1^{l_1} \sum_{j_1=1}^{p_1} \overleftrightarrow{a}_{j_1} \prod_{i=1}^{s} \exp\left(-\left(\left(x_i(z_{j_1}) - \overleftrightarrow{c}_{ij_1}^{l_1}\right)/\overleftrightarrow{\sigma}_{ij_1}^{l_1}\right)^2\right)}{\sum_{l_1=1}^{N_1} \sum_{j_1=1}^{p_1} \overleftrightarrow{a}_{j_1} \prod_{i=1}^{s} \exp\left(-\left(\left(x_i(z_{j_1}) - \overleftrightarrow{c}_{ij_1}^{l_1}\right)/\overleftrightarrow{\sigma}_{ij_1}^{l_1}\right)^2\right)} + b_1,\\
u_2(x_z) &= \frac{\sum_{l_2=1}^{N_2} \overrightarrow{u}_2^{l_2} \sum_{j_2=1}^{p_2} \underset{\leftrightarrow}{a}_{j_2} \prod_{i=1}^{s} \exp\left(-\left(\left(x_i(z_{j_2}) - \underset{\leftrightarrow}{c}_{ij_2}^{l_2}\right)/\underset{\leftrightarrow}{\sigma}_{ij_2}^{l_2}\right)^2\right)}{\sum_{l_2=1}^{N_2} \sum_{j_2=1}^{p_2} \underset{\leftrightarrow}{a}_{j_2} \prod_{i=1}^{s} \exp\left(-\left(\left(x_i(z_{j_2}) - \underset{\leftrightarrow}{c}_{ij_2}^{l_2}\right)/\underset{\leftrightarrow}{\sigma}_{ij_2}^{l_2}\right)^2\right)} + b_2.
\end{aligned} \tag{A.2}$$

Subsequently, we have three derivation procedures. □

*(i) Addition*

$$\begin{aligned} & u_1(x_z) + u_2(x_z) \\ & \quad = \frac{\sum_{l_1=1}^{N_1}\sum_{l_2=1}^{N_2}\left(\overline{u}_1^{l_1} + \overline{u}_2^{l_2}\right)\sum_{j_1=1}^{p_1}\sum_{j_2=1}^{p_2}\overleftrightarrow{a}_{j_1}\underset{\leftrightarrow}{a}_{j_2}\prod_{i=1}^{s}\exp \bigstar}{\sum_{l_1=1}^{N_1}\sum_{l_2=1}^{N_2}\sum_{j_1=1}^{p_1}\sum_{j_2=1}^{p_2}\overleftrightarrow{a}_{j_1}\underset{\leftrightarrow}{a}_{j_2}\prod_{i=1}^{s}\exp \bigstar} \\ & \qquad + (b_1 + b_2), \end{aligned} \tag{A.3}$$

where $\bigstar$ denotes $(-((x_i(z_{j_1}) - \overleftrightarrow{c}_{ij_1}^{l_1})/\overleftrightarrow{\sigma}_{ij_1}^{l_1})^2 - ((x_i(z_{j_2}) - \underset{\leftrightarrow}{c}_{ij_2}^{l_2})/\underset{\leftrightarrow}{\sigma}_{ij_2}^{l_2})^2)$. Equation (A.3) has the same form as (3.12), then $u_1(x_z) + u_2(x_z) \in \Theta$.

*(ii) Multiplication*

$$\begin{aligned} & u_1(x_z)u_2(x_z) \\ & \quad = \frac{\sum_{l_1=1}^{N_1}\sum_{l_2=1}^{N_2}\overline{u}_1^{l_1}\overline{u}_2^{l_2}\sum_{j_1=1}^{p_1}\sum_{j_2=1}^{p_2}\overleftrightarrow{a}_{j_1}\underset{\leftrightarrow}{a}_{j_2}\prod_{i=1}^{s}\exp \bigstar}{\sum_{l_1=1}^{N_1}\sum_{l_2=1}^{N_2}\sum_{j_1=1}^{p_1}\sum_{j_2=1}^{p_2}\overleftrightarrow{a}_{j_1}\underset{\leftrightarrow}{a}_{j_2}\prod_{i=1}^{s}\exp \bigstar} \\ & \qquad + b_2\frac{\sum_{l_1=1}^{N_1}\overline{u}_1^{l_1}\sum_{j_1=1}^{p_1}\overleftrightarrow{a}_{j_1}\prod_{i=1}^{s}\exp\left(-\left(\left(x_i(z_{j_1}) - \overleftrightarrow{c}_{ij_1}^{l_1}\right)/\overleftrightarrow{\sigma}_{ij_1}^{l_1}\right)^2\right)}{\sum_{l_1=1}^{N_1}\sum_{j_1=1}^{p_1}\overleftrightarrow{a}_{j_1}\prod_{i=1}^{s}\exp\left(-\left(\left(x_i(z_{j_1}) - \overleftrightarrow{c}_{ij_1}^{l_1}\right)/\overleftrightarrow{\sigma}_{ij_1}^{l_1}\right)^2\right)} \\ & \qquad + b_1\frac{\sum_{l_2=1}^{N_2}\overline{u}_2^{l_2}\sum_{j_2=1}^{p_2}\underset{\leftrightarrow}{a}_{j_2}\prod_{i=1}^{s}\exp\left(-\left(\left(x_i(z_{j_2}) - \underset{\leftrightarrow}{c}_{ij_2}^{l_2}\right)/\underset{\leftrightarrow}{\sigma}_{ij_2}^{l_2}\right)^2\right)}{\sum_{l_2=1}^{N_2}\sum_{j_2=1}^{p_2}\underset{\leftrightarrow}{a}_{j_2}\prod_{i=1}^{s}\exp\left(-\left(\left(x_i(z_{j_2}) - \underset{\leftrightarrow}{c}_{ij_2}^{l_2}\right)/\underset{\leftrightarrow}{\sigma}_{ij_2}^{l_2}\right)^2\right)} + b_1b_2, \end{aligned} \tag{A.4}$$

where $\bigstar$ denotes $(-((x_i(z_{j_1}) - \overleftrightarrow{c}_{ij_1}^{l_1})/\overleftrightarrow{\sigma}_{ij_1}^{l_1})^2 - ((x_i(z_{j_2}) - \underset{\leftrightarrow}{c}_{ij_2}^{l_2})/\underset{\leftrightarrow}{\sigma}_{ij_2}^{l_2})^2)$. In terms of algebraic operation, the product of functions in Gaussian form is also a function in Gaussian form. Thus, (A.4) has the same form as (3.12), and $u_1(x_z)u_2(x_z) \in \Theta$.

*(iii) Scalar Multiplication*

For arbitrary $c \in R$, we have

$$cu_1(x_z) = c\frac{\sum_{l_1=1}^{N_1}\overline{u}_1^{l_1}\sum_{j_1=1}^{p_1}\overleftrightarrow{a}_{j_1}\prod_{i=1}^{s}\exp\left(-\left(\left(x_i(z_{j_1}) - \overleftrightarrow{c}_{ij_1}^{l_1}\right)/\overleftrightarrow{\sigma}_{ij_1}^{l_1}\right)^2\right)}{\sum_{l_1=1}^{N_1}\sum_{j_1=1}^{p_1}\overleftrightarrow{a}_{j_1}\prod_{i=1}^{s}\exp\left(-\left(\left(x_i(z_{j_1}) - \overleftrightarrow{c}_{ij_1}^{l_1}\right)/\overleftrightarrow{\sigma}_{ij_1}^{l_1}\right)^2\right)} + cb_1. \tag{A.5}$$

Equation (A.5) has the same form as (3.12), and $cu_1(x_z) \in \Theta$.

Finally, by combining (A.3)~(A.5) together, we can conclude that $(\Theta, d_\infty)$ is an algebra.

(2) Secondly, we will prove that $(\Theta, d_\infty)$ separates point on $\Omega$ by constructing a simple 3-D FLC $u(x_z)$ as in (3.12), namely, $u(x_z^0) \neq u(y_z^0)$ holds for arbitrarily given $x_z^0, y_z^0 \in \Omega$ with $x_z^0 \neq y_z^0$.

We choose two fuzzy rules, that is, $N = 2$.

Let

$$\begin{aligned} x_z^0 &= \left( \left(x_1^0(z_1), \ldots, x_1^0(z_p)\right)^T, \ldots, \left(x_s^0(z_1), \ldots, x_s^0(z_p)\right)^T \right) \\ y_z^0 &= \left( \left(y_1^0(z_1), \ldots, y_1^0(z_p)\right)^T, \ldots, \left(y_s^0(z_1), \ldots, y_s^0(z_p)\right)^T \right), \\ a_j &= \frac{1}{p}, \qquad \sigma_{ij}^1 = \sigma_{ij}^2 = 1, \qquad c_{ij}^1 = x_i^0(z_j), \qquad c_{ij}^2 = y_i^0(z_j), \\ & x_z^1 = x_z^0, \qquad x_z^2 = y_z^0 \quad (j = 1, \ldots, p). \end{aligned} \tag{A.6}$$

We have

$$\begin{aligned} u\left(x_z^0\right) &= \frac{\overline{u}^1 + \overline{u}^2 (1/p) \sum_{j=1}^p \prod_{i=1}^s \exp\left(-\left(x_i^0(z_j) - y_i^0(z_j)\right)^2\right)}{1 + (1/p) \sum_{j=1}^p \prod_{i=1}^s \exp\left(-\left(x_i^0(z_j) - y_i^0(z_j)\right)^2\right)} + b \\ &= \zeta \overline{u}^1 + (1 - \zeta)\overline{u}^2 + b, \\ u\left(y_z^0\right) &= \frac{\overline{u}^2 + \overline{u}^1 (1/p) \sum_{j=1}^p \prod_{i=1}^s \exp\left(-\left(x_i^0(z_j) - y_i^0(z_j)\right)^2\right)}{1 + (1/p) \sum_{j=1}^p \prod_{i=1}^s \exp\left(-\left(x_i^0(z_j) - y_i^0(z_j)\right)^2\right)} + \mathrm{b} \\ &= \zeta \overline{u}^2 + (1 - \zeta)\overline{u}^1 + b, \\ \zeta &= \frac{1}{1 + (1/p) \sum_{j=1}^p \prod_{i=1}^s \exp\left(-\left(x_i^0(z_j) - y_i^0(z_j)\right)^2\right)}. \end{aligned} \tag{A.7}$$

Since $x_z^0 \neq y_z^0$, there must be some $i$ and $j$ such that $x_i^0(z_j) \neq y_i^0(z_j)$. Thus, we have $\prod_{i=1}^s \exp(-(x_i^0(z_j) - y_i^0(z_j))^2) \neq 1$. For arbitrary $j$, $\prod_{i=1}^s \exp(-(x_i^0(z_j) - y_i^0(z_j))^2) \leq 1$ holds, therefore, we have $\sum_{j=1}^p \prod_{i=1}^s \exp(-(x_i^0(z_j) - y_i^0(z_j))^2) \neq p$. If we choose $\overline{u}^1 = 0$ and $\overline{u}^2 = 1$, then

$$u\left(x_z^0\right) = 1 - \xi + b \neq \xi + b = u\left(y_z^0\right). \tag{A.8}$$

Therefore, $(\Theta, d_\infty)$ separates point on $\Omega$.

(3) Finally, we prove $(\Theta, d_\infty)$ vanishes at no point of $\Omega$.

For any 3-D FLC $u(x_z)$ expressed as in (3.12), if we choose $\zeta^l \geq 0$ $(l = 1, \ldots, N)$ and $b > 0$, then for any $x_z \in \Omega$, we have $u(x_z) > 0$.

Therefore, $(\Theta, \mathrm{d}_\infty)$ vanishes at no point of $\Omega$.

By combining the results from (1) to (3) together, Theorem 4.1 is proven.

## Acknowledgments

This work was supported partly by the National Specialised Research Fund for the Doctoral Programme of Higher Education under Grant 20113705120003 and by Shandong Natural Science Foundation under Grant ZR2010FM018 and under Grant ZR2010FM022.

## References

[1] W. H. Ray, *Advanced Process Control*, McGraw-Hill, New York, NY, USA, 1981.
[2] P. D. Christofides, *Nonlinear and Robust Control of Partial Differential Equation Systems: Methods and Applications to Transport-Reaction Processes*, Birkhäuser, Boston, Mass, USA, 2001.
[3] C. K. Qi, H.-X. Li, X. C. Zhao, S. Y. Li, and F. Gao, "Hammerstein modeling with structure identification for multi-input multi-output nonlinear industrial processes," *Industrial & Engineering Chemistry Research*, vol. 50, no. 19, pp. 11153–11169, 2011.
[4] C. C. Doumanidis and N. Fourligkas, "Temperature distribution control in scanned thermal processing of thin circular parts," *IEEE Transactions on Control Systems Technology*, vol. 9, no. 5, pp. 708–717, 2001.
[5] H.-X. Li, X.-X. Zhang, and S. Y. Li, "A three-dimensional fuzzy control methodology for a class of distributed parameter systems," *IEEE Transactions on Fuzzy Systems*, vol. 15, no. 3, pp. 470–481, 2007.
[6] X.-X. Zhang, H.-X. Li, and S. Y. Li, "Analytical study and stability design of a 3-D fuzzy logic controller for spatially distributed dynamic systems," *IEEE Transactions on Fuzzy Systems*, vol. 16, no. 6, pp. 1613–1625, 2008.
[7] X.-X. Zhang, S. Li, and H.-X. Li, "Structure and BIBO stability of a three-dimensional fuzzy two-term control system," *Mathematics and Computers in Simulation*, vol. 80, no. 10, pp. 1985–2004, 2010.
[8] X.-X. Zhang, H.-X. Li, and C. K. Qi, "Spatially constrained fuzzy-clustering-based sensor placement for spatiotemporal fuzzy-control system," *IEEE Transactions on Fuzzy Systems*, vol. 18, no. 5, pp. 946–957, 2010.
[9] V. Kecman, *Learning and Soft Computing: Support Vector Machines, Neural Networks, and Fuzzy Logic Models*, MIT Press, London, UK, 2001.
[10] S. Guillaume, "Designing fuzzy inference systems from data: an interpretability-oriented review," *IEEE Transactions on Fuzzy Systems*, vol. 9, no. 3, pp. 426–443, 2001.
[11] I. Rojas, H. Pomares, J. Ortega, and A. Prieto, "Self-organized fuzzy system generation from training examples," *IEEE Transactions on Fuzzy Systems*, vol. 8, no. 1, pp. 23–36, 2000.
[12] M. Sugeno and T. Yasukawa, "A fuzzy-logic-based approach to qualitative modeling," *IEEE Transactions on Fuzzy Systems*, vol. 1, no. 1, pp. 7–31, 1993.
[13] R. Krishnapuram and C. P. Freg, "Fitting an unknown number of lines and planes to image data through compatible cluster merging," *Pattern Recognition*, vol. 25, no. 4, pp. 385–400, 1992.
[14] M. Setnes, R. Babuška, U. Kaymak, and H. R. van Nauta Lemke, "Similarity measures in fuzzy rule base simplification," *IEEE Transactions on Systems, Man, and Cybernetics B*, vol. 28, no. 3, pp. 376–386, 1998.
[15] O. Cordón, F. Herrera, and P. Villar, "Generating the knowledge base of a fuzzy rule-based system by the genetic learning of the data base," *IEEE Transactions on Fuzzy Systems*, vol. 9, no. 4, pp. 667–674, 2001.
[16] L. X. Wang, *A Course in Fuzzy Systems and Control*, Prentice-Hall, Upper Saddle River, NJ, USA, 1997.
[17] J. M. Mendel, *Uncertain Rule-Based Fuzzy Logic Systems: Introduction and New Directions*, Prentice-Hall, Upper Saddle River, NJ, USA, 2001.
[18] V. Vapnik, *Statistical Learning Theory*, John Wiley & Sons, New York, NY, USA, 1998.
[19] J. C. Burges, "A tutorial on support vector machines for pattern recognition," *Data Mining and Knowledge Discovery*, vol. 2, no. 2, pp. 121–167, 1998.
[20] A. J. Smola and B. Schölkopf, "A tutorial on support vector regression," *Statistics and Computing*, vol. 14, no. 3, pp. 199–222, 2004.
[21] M.-Y. Chen and D. A. Linkens, "Rule-base self-generation and simplification for data-driven fuzzy models," *Fuzzy Sets and Systems*, vol. 142, no. 2, pp. 243–265, 2004.
[22] Y. Jin, "Fuzzy modeling of high-dimensional systems: complexity reduction and interpretability improvement," *IEEE Transactions on Fuzzy Systems*, vol. 8, no. 2, pp. 212–221, 2000.
[23] W. Rudin, *Principles of Mathematical Analysis*, McGraw-Hill, New York, NY, USA, 3rd edition, 1976.

[24] W. E. Schiesser, *The Numerical Methods of Lines Integration of Partial Differential Equations*, Academic Press, San Diego, Calif, USA, 1991.
[25] R. Haber and L. Keviczky, *Nonlinear System Identification—Input–Output Modeling Approach*, vol. 1 of *Nonlinear System Parameter Identification*, Kluwer Academic, Dodrecht, The Netherlands, 1999.
[26] J.-J. Chiang and P.-Y. Hao, "Support vector learning mechanism for fuzzy rule-based modeling: a new approach," *IEEE Transactions on Fuzzy Systems*, vol. 12, no. 1, pp. 1–12, 2004.

Hindawi Publishing Corporation
Journal of Applied Mathematics
Volume 2012, Article ID 584140, 25 pages
doi:10.1155/2012/584140

*Research Article*

# Convergence Analysis for the SMC-MeMBer and SMC-CBMeMBer Filters

**Feng Lian,[1] Chen Li,[2] Chongzhao Han,[1] and Hui Chen[1]**

[1] *Ministry of Education Key Laboratory for Intelligent Networks and Network Security (MOE KLINNS), School of Electronics and Information Engineering, Xi'an Jiaotong University, Xi'an 710049, China*
[2] *Software Engineering School, Xi'an Jiaotong University, Xi'an 710049, China*

Correspondence should be addressed to Feng Lian, lianfeng1981@gmail.com

Received 27 February 2012; Revised 15 May 2012; Accepted 22 May 2012

Academic Editor: Qiang Ling



The convergence for the sequential Monte Carlo (SMC) implementations of the multitarget multi-Bernoulli (MeMBer) filter and cardinality-balanced MeMBer (CBMeMBer) filters is studied here. This paper proves that the SMC-MeMBer and SMC-CBMeMBer filters, respectively, converge to the true MeMBer and CBMeMBer filters in the mean-square sense and the corresponding bounds for the mean-square errors are given. The significance of this paper is in theory to present the convergence results of the SMC-MeMBer and SMC-CBMeMBer filters and the conditions under which the two filters satisfy mean-square convergence.

## 1. Introduction

Recently, the random finite-set- (RFS-) based multitarget tracking (MTT) approaches [1] have attracted extensive attention. Although theoretically solid, the RFS-based approaches usually involve intractable computations. By introducing the finite-set statistics (FISSTs) [2], Mahler developed the probability hypothesis density (PHD) [3], and cardinalized PHD (CPHD) [4] filters, which have been shown to be a computationally tractable alternative to full multitarget Bayes filters in the RFS framework. The sequential Monte Carlo (SMC) implementations for the PHD and CPHD filters were devised by Zajic and Mahler [5], Sidenbladh [6], and Vo et al. [7]. Vo et al. [8, 9] devised the Gaussian mixture (GM) implementation for the PHD and CPHD filters under the linear, Gaussian assumption on target dynamics, birth process, and sensor model. However, the SMC-PHD and SMC-CPHD approaches require clustering to extract state estimates from the particle population, which is expensive and unreliable [10, 11].

In 2007, Mahler proposed the multitarget multi-Bernoulli (MeMBer) [2] recursion, which is an approximation to the full multitarget Bayes recursion using multi-Bernoulli

RFSs under low clutter density scenarios. In 2009, Vo et al. showed that the MeMBer filter overestimates the number of targets and proposed a cardinality-balanced MeMBer (CBMeMBer) filter [12] to reduce the cardinality bias. Then, the SMC and GM implementations for the MeMBer and CBMeMBer filters were, respectively, proposed in nonlinear and linear-Gaussian dynamic and measurement models. The key advantage of this approach is that the multi-Bernoulli representation allows reliable and inexpensive extraction of state estimates. The Monte Carlo simulations given by Vo et al. showed that the SMC-CBMeMBer filter outperforms the SMC-CPHD (and hence SMC-PHD) filter despite having smaller complexity under certain range of signal settings.

Although the convergence results for the SMC-PHD and GM-PHD filters were established by Clark and Bell [13] in 2006 and by Clark and Vo [14] in 2007, respectively, there have been no results showing the asymptotic convergence for the SMC-MeMBer and SMC-CBMeMBer filters. This paper demonstrates the mean-square convergence of the errors [15–17] for the two filters. In other words, given simple sufficient conditions, the approximation error of the multi-Bernoulli parameter set comprised of a set of weighted samples is proved to converge to zero as the number of the samples tends to infinity at each stage of the two algorithms. In addition, the corresponding bounds for the mean-square errors are obtained.

## 2. MeMBer and CBMeMBer Filters

A Bernoulli RFS $\Upsilon^{(i)}$ has probability $1 - r^{(i)}$ of being empty, and probability $r^{(i)}$ $(0 \le r^{(i)} \le 1)$ of being a singleton whose only element is distributed according to a probability density $p^{(i)}$. The probability density of $\Upsilon^{(i)}$ is

$$\pi\left(\Upsilon^{(i)}\right) = \begin{cases} 1 - r^{(i)} & \Upsilon^{(i)} = \emptyset, \\ r^{(i)} p^{(i)}(\mathbf{y}_i) & \Upsilon^{(i)} = \{\mathbf{y}_i\}. \end{cases} \tag{2.1}$$

A multi-Bernoulli RFS $\Upsilon$ is a union of a fixed number of independent Bernoulli RFSs $\Upsilon^{(i)}$, $i = 1, \ldots, M$, that is, $\Upsilon = \bigcup_{i=1}^{M} \Upsilon^{(i)}$. $\Upsilon$ is thus completely described by the multi-Bernoulli parameter set $\{(r^{(i)}, p^{(i)})\}_{i=1}^{M}$ with the mean cardinality $\sum_{i=1}^{M} r^{(i)}$ and the probability density [2]:

$$\pi(\Upsilon) = \prod_{j=1}^{M}\left(1 - r^{(j)}\right) \sum_{1 \le i_1 \ne \cdots \ne i_n \le M} \prod_{j=1}^{n} \frac{r^{(i_j)} p^{(i_j)}(\mathbf{y}_j)}{1 - r^{(i_j)}}. \tag{2.2}$$

Throughout this paper, we abbreviate a probability density of the form (2.2) by $\pi = \{(r^{(i)}, p^{(i)})\}_{i=1}^{M}$.

By approximating the multitarget RFS as a multi-Bernoulli RFS at each time step, Mahler proposed the MeMBer recursion, which propagated the multi-Bernoulli parameters of the posterior multitarget density forward in time [2]. The MeMBer filter is summarized as follows.

*MeMBer Prediction*

If at time $k-1$, the posterior multitarget density is a multi-Bernoulli of the form $\pi_{k-1} = \{(r_{k-1}^{(i)}, p_{k-1}^{(i)})\}_{i=1}^{M_{k-1}}$, then the predicted multitarget density is also a multi-Bernoulli and is given by

$$\pi_{k|k-1} = \left\{\left(r_{P,k|k-1}^{(i)}, p_{P,k|k-1}^{(i)}\right)\right\}_{i=1}^{M_{k-1}} \bigcup \left\{\left(r_{\Gamma,k}^{(i)}, p_{\Gamma,k}^{(i)}\right)\right\}_{i=1}^{M_{\Gamma,k}}, \tag{2.3}$$

where $\{(r_{\Gamma,k}^{(i)}, p_{\Gamma,k}^{(i)})\}_{i=1}^{M_{\Gamma,k}}$ are the parameters of the multi-Bernoulli RFS of births at time $k$:

$$r_{P,k|k-1}^{(i)} = r_{k-1}^{(i)} \left\langle p_{k-1}^{(i)}, p_{S,k} \right\rangle, \quad i = 1, \ldots, M_{k-1}, \tag{2.4}$$

$$p_{P,k|k-1}^{(i)}(\mathbf{x}_k) = \frac{\left\langle f_{k|k-1}(\mathbf{x}_k \mid \cdot), p_{k-1}^{(i)} p_{S,k} \right\rangle}{\left\langle p_{k-1}^{(i)}, p_{S,k} \right\rangle}, \quad i = 1, \ldots, M_{k-1}. \tag{2.5}$$

*MeMBer Update*

If at time $k$, the predicted multitarget density is a multi-Bernoulli of the form $\pi_{k|k-1} = \{(r_{k|k-1}^{(i)}, p_{k|k-1}^{(i)})\}_{i=1}^{M_{k|k-1}}$; then the posterior multitarget density can be approximated by a multi-Bernoulli as follows:

$$\pi_k \approx \left\{\left(r_{L,k}^{(i)}, p_{L,k}^{(i)}\right)\right\}_{i=1}^{M_{k|k-1}} \bigcup \left\{\left(r_{U,k}(\mathbf{z}_k), p_{U,k}(\cdot; \mathbf{z}_k)\right)\right\}_{\mathbf{z}_k \in Z_k}, \tag{2.6}$$

where,

$$r_{L,k}^{(i)} = r_{k|k-1}^{(i)} \frac{1 - \left\langle p_{k|k-1}^{(i)}, p_{D,k} \right\rangle}{1 - r_{k|k-1}^{(i)} \left\langle p_{k|k-1}^{(i)}, p_{D,k} \right\rangle}, \quad i = 1, \ldots, M_{k|k-1}, \tag{2.7}$$

$$p_{L,k}^{(i)}(\mathbf{x}_k) = p_{k|k-1}^{(i)}(\mathbf{x}_k) \frac{1 - p_{D,k}(\mathbf{x}_k)}{1 - \left\langle p_{k|k-1}^{(i)}, p_{D,k} \right\rangle}, \quad i = 1, \ldots, M_{k|k-1}, \tag{2.8}$$

$$r_{U,k}(\mathbf{z}_k) = \frac{1}{\kappa_k(\mathbf{z}_k) + \sum_{i=1}^{M_{k|k-1}} r_{\alpha,k}^{(i)}(\mathbf{z}_k)} \sum_{i=1}^{M_{k|k-1}} r_{\alpha,k}^{(i)}(\mathbf{z}_k), \quad \mathbf{z}_k \in Z_k, \tag{2.9}$$

$$p_{U,k}(\mathbf{x}_k; \mathbf{z}_k) = \frac{1}{\sum_{i=1}^{M_{k|k-1}} r_{\alpha,k}^{(i)}(\mathbf{z}_k)} \sum_{i=1}^{M_{k|k-1}} p_{\alpha,k}^{(i)}(\mathbf{x}_k; \mathbf{z}_k), \quad \mathbf{z}_k \in Z_k, \tag{2.10}$$

$$p_{\alpha,k}^{(i)}(\mathbf{x}_k; \mathbf{z}_k) = \frac{r_{k|k-1}^{(i)} p_{k|k-1}^{(i)}(\mathbf{x}_k) \psi_{k,\mathbf{z}_k}(\mathbf{x}_k)}{1 - r_{k|k-1}^{(i)} \left\langle p_{k|k-1}^{(i)}, p_{D,k} \right\rangle}, \quad i = 1, \ldots, M_{k|k-1}, \tag{2.11}$$

$$r_{\alpha,k}^{(i)}(\mathbf{z}_k) = \left\langle p_{\alpha,k}^{(i)}(\mathbf{x}_k; \mathbf{z}_k), 1 \right\rangle = \frac{r_{k|k-1}^{(i)} \left\langle p_{k|k-1}^{(i)}, \psi_{k,\mathbf{z}_k} \right\rangle}{1 - r_{k|k-1}^{(i)} \left\langle p_{k|k-1}^{(i)}, p_{D,k} \right\rangle}, \quad i = 1, \ldots, M_{k|k-1}. \tag{2.12}$$

By correcting the cardinality bias in the $r_{U,k}(\mathbf{z}_k)$ of the MeMBer update step, Vo et al. proposed the CBMeMBer filter [12]. The CBMeMBer recursions are the same as the MeMBer recursions except the update of $r_{U,k}(\mathbf{z}_k)$, which is revised as

$$r^*_{U,k}(\mathbf{z}_k) = \frac{1}{\kappa_k(\mathbf{z}_k) + \sum_{i=1}^{M_{k|k-1}} r^{(i)}_{\alpha,k}(\mathbf{z}_k)} \sum_{i=1}^{M_{k|k-1}} \frac{\left(1 - r^{(i)}_{k|k-1}\right) r^{(i)}_{\alpha,k}(\mathbf{z}_k)}{1 - r^{(i)}_{k|k-1} \left\langle p^{(i)}_{k|k-1}, p_{D,k} \right\rangle}. \tag{2.13}$$

Note that not (38) in [12] but (2.10) in our paper is used in the CBMeMBer update step here. The reasons are (1) the (38) in [12] and the (2.10) in our paper are both the approximations of (36) in [12] under the same assumption $\langle p^{(i)}_{k|k-1}, p_{D,k} \rangle \approx 1$, but the latter is more precise than former; (2) the (38) in [12] is unbounded at $r^{(i)}_{k|k-1} = 1$ while (2.10) in our paper is bounded at $r^{(i)}_{k|k-1} = 1$ as long as $p_{D,k}(\mathbf{x}_k) \neq 1$.

For the multi-Bernoulli representation $\pi_k = \{(r^{(i)}_k, p^{(i)}_k)\}_{i=1}^{M_k}$, the probability $r^{(i)}_k$ indicates how likely the $i$th hypothesized track is a true track, and the posterior density $p^{(i)}_k$ describes the distribution of the estimated current state of the track. Hence, $\sum_{i=1}^{M_k} r^{(i)}_k$ denotes the multitarget number and the multitarget state estimate can be obtained by choosing the means or modes from the posterior densities of the hypothesized tracks with existence probabilities exceeding a given threshold.

## 3. SMC-MeMBer and SMC-CBMeMBer Filters

The SMC implementations of the MeMBer and CBMeMBer recursions are summarized as follows.

*SMC-MeMBer and SMC-CBMeMBer Predictions*

Suppose that at time $k-1$ the (multi-Bernoulli) posterior multitarget density $\tilde{\pi}_{k-1} = \{(r^{(i),L^{(i)}_{k-1}}_{k-1}, p^{(i),L^{(i)}_{k-1}}_{k-1})\}_{i=1}^{M_{k-1}}$ is given and each $p^{(i),L^{(i)}_{k-1}}_{k-1}$, $i = 1, \ldots, M_{k-1}$, is comprised of a set of weighted samples $\{\omega^{(i,j)}_{k-1}, \mathbf{x}^{(i,j)}_{k-1}\}_{j=1}^{L^{(i)}_{k-1}}$:

$$p^{(i),L^{(i)}_{k-1}}_{k-1}(\mathbf{x}_k) = \sum_{j=1}^{L^{(i)}_{k-1}} \omega^{(i,j)}_{k-1} \delta_{\mathbf{x}^{(i,j)}_{k-1}}(\mathbf{x}_k), \quad i = 1, \ldots, M_{k-1}. \tag{3.1}$$

Then, given proposal densities $q^{(i)}_k(\cdot \mid \mathbf{x}^{(i,j)}_{k-1}, Z_k)$ and $b^{(i)}_k(\cdot \mid Z_k)$, the predicted (multi-Bernoulli) multitarget density $\tilde{\pi}_{k|k-1} = \{(r^{(i),L^{(i)}_{k-1}}_{P,k|k-1}, p^{(i),L^{(i)}_{k-1}}_{P,k|k-1})\}_{i=1}^{M_{k-1}} \cup \{(r^{(i),L^{(i)}_{\Gamma,k}}_{\Gamma,k}, p^{(i),L^{(i)}_{\Gamma,k}}_{\Gamma,k})\}_{i=1}^{M_{\Gamma,k}}$ can be computed as follows:

$$r^{(i),L^{(i)}_{k-1}}_{P,k|k-1} = r^{(i),L^{(i)}_{k-1}}_{k-1} \left\langle p^{(i),L^{(i)}_{k-1}}_{k-1}, p_{S,k} \right\rangle, \quad i = 1, \ldots, M_{k-1}, \tag{3.2}$$

$$p_{P,k|k-1}^{(i),L_{k-1}^{(i)}}(\mathbf{x}_k) = \sum_{j=1}^{L_{k-1}^{(i)}} \tilde{\omega}_{P,k|k-1}^{(i,j)} \delta_{\mathbf{x}_{P,k|k-1}^{(i,j)}}(\mathbf{x}_k), \quad i = 1, \ldots, M_{k-1},$$
$$p_{\Gamma,k}^{(i),L_{\Gamma,k}^{(i)}}(\mathbf{x}_k) = \sum_{j=1}^{L_{\Gamma,k}^{(i)}} \tilde{\omega}_{\Gamma,k}^{(i,j)} \delta_{\mathbf{x}_{\Gamma,k}^{(i,j)}}(\mathbf{x}_k), \quad i = 1, \ldots, M_{\Gamma,k}, \tag{3.3}$$

where $r_{\Gamma,k}^{(i),L_{\Gamma,k}^{(i)}}$ $(i = 1, \ldots, M_{\Gamma,k})$ is given by birth model; $\mathbf{x}_{P,k|k-1}^{(i,j)}$, $\tilde{\omega}_{P,k|k-1}^{(i,j)}$ $(i = 1, \ldots, M_{k-1})$ and $\mathbf{x}_{\Gamma,k}^{(i,j)}$, $\tilde{\omega}_{\Gamma,k}^{(i,j)}$ $(i = 1, \ldots, M_{\Gamma,k})$ are, respectively, given by

$$\mathbf{x}_{P,k|k-1}^{(i,j)} \sim q_k^{(i)}\left(\cdot \mid \mathbf{x}_{k-1}^{(i,j)}, Z_k\right), \quad j = 1, \ldots, L_{k-1}^{(i)}, \qquad \mathbf{x}_{\Gamma,k}^{(i,j)} \sim b_k^{(i)}(\cdot \mid Z_k), \quad j = 1, \ldots, L_{\Gamma,k}^{(i)}, \tag{3.4}$$

$$\tilde{\omega}_{P,k|k-1}^{(i,j)} = \frac{1}{\sum_{j=1}^{L_{k-1}^{(i)}} \omega_{P,k|k-1}^{(i,j)}} \omega_{P,k|k-1}^{(i,j)},$$
$$\omega_{P,k|k-1}^{(i,j)} = \frac{\omega_{k-1}^{(i,j)} f_{k|k-1}\left(\mathbf{x}_{P,k|k-1}^{(i,j)} \mid \mathbf{x}_{k-1}^{(i,j)}\right) p_{S,k}\left(\mathbf{x}_{k-1}^{(i,j)}\right)}{q_k^{(i)}\left(\mathbf{x}_{P,k|k-1}^{(i,j)} \mid \mathbf{x}_{k-1}^{(i,j)}, Z_k\right)}, \quad j = 1, \ldots, L_{k-1}^{(i)}, \tag{3.5}$$

$$\tilde{\omega}_{\Gamma,k}^{(i,j)} = \frac{1}{\sum_{j=1}^{L_{\Gamma,k}^{(i)}} \omega_{\Gamma,k}^{(i,j)}} \omega_{\Gamma,k}^{(i,j)}, \qquad \omega_{\Gamma,k}^{(i,j)} = \frac{p_{\Gamma,k}\left(\mathbf{x}_{\Gamma,k}^{(i,j)}\right)}{b_k^{(i)}\left(\mathbf{x}_{\Gamma,k}^{(i,j)} \mid Z_k\right)}, \quad j = 1, \ldots, L_{\Gamma,k}^{(i)}. \tag{3.6}$$

*SMC-MeMBer and SMC-CBMeMBer Updates*

Suppose that at time $k$ the predicted (multi-Bernoulli) multitarget density $\tilde{\pi}_{k|k-1} = \{(r_{k|k-1}^{(i),L_{k|k-1}^{(i)}}, p_{k|k-1}^{(i),L_{k|k-1}^{(i)}})\}_{i=1}^{M_{k|k-1}}$ is given and each $p_{k|k-1}^{(i),L_{k|k-1}^{(i)}}$, $i = 1, \ldots, M_{k|k-1}$, is comprised of a set of weighted samples $\{\omega_{k|k-1}^{(i,j)}, \mathbf{x}_{k|k-1}^{(i,j)}\}_{j=1}^{L_{k|k-1}^{(i)}}$:

$$p_{k|k-1}^{(i),L_{k|k-1}^{(i)}}(\mathbf{x}_k) = \sum_{j=1}^{L_{k|k-1}^{(i)}} \omega_{k|k-1}^{(i,j)} \delta_{\mathbf{x}_{k|k-1}^{(i,j)}}(\mathbf{x}_k), \quad i = 1, \ldots, M_{k|k-1}. \tag{3.7}$$

Then, the multi-Bernoulli approximation of the SMC-MeMBer-updated multitarget density $\tilde{\pi}_k \approx \{(r_{L,k}^{(i),L_{k|k-1}^{(i)}}, p_{L,k}^{(i),L_{k|k-1}^{(i)}})\}_{i=1}^{M_{k|k-1}} \cup \{(r_{U,k}^{L_{k|k-1}^{(i)}}(\mathbf{z}_k), p_{U,k}^{L_{k|k-1}^{(i)}}(\cdot; \mathbf{z}_k))\}_{\mathbf{z}_k \in Z_k}$ and SMC-CBMeMBer-updated multitarget density $\tilde{\pi}_k^* \approx \{(r_{L,k}^{(i),L_{k|k-1}^{(i)}}, p_{L,k}^{(i),L_{k|k-1}^{(i)}})\}_{i=1}^{M_{k|k-1}} \cup \{(r_{U,k}^{*,L_{k|k-1}^{(i)}}(\mathbf{z}_k), p_{U,k}^{L_{k|k-1}^{(i)}}(\cdot; \mathbf{z}_k))\}_{\mathbf{z}_k \in Z_k}$ can be computed as follows:

$$r_{L,k}^{(i),L_{k|k-1}^{(i)}} = r_{k|k-1}^{(i),L_{k|k-1}^{(i)}} \frac{1 - \left\langle p_{k|k-1}^{(i),L_{k|k-1}^{(i)}}, p_{D,k} \right\rangle}{1 - r_{k|k-1}^{(i),L_{k|k-1}^{(i)}} \left\langle p_{k|k-1}^{(i),L_{k|k-1}^{(i)}}, p_{D,k} \right\rangle}, \quad i = 1, \ldots, M_{k|k-1}, \tag{3.8}$$

$$p_{L,k}^{(i),L_{k|k-1}^{(i)}}(\mathbf{x}_k) = \sum_{j=1}^{L_{k|k-1}^{(i)}} \omega_{k|k-1}^{(i,j)} \frac{1 - p_{D,k}\left(\mathbf{x}_{k|k-1}^{(i,j)}\right)}{1 - \left\langle p_{k|k-1}^{(i),L_{k|k-1}^{(i)}}, p_{D,k} \right\rangle} \delta_{\mathbf{x}_{k|k-1}^{(i,j)}}(\mathbf{x}_k), \quad i = 1, \ldots, M_{k|k-1}, \tag{3.9}$$

$$r_{U,k}^{L_{k|k-1}^{(i)}}(\mathbf{z}_k) = \frac{1}{\kappa_k(\mathbf{z}_k) + \sum_{i=1}^{M_{k|k-1}} r_{\alpha,k}^{(i),L_{k|k-1}^{(i)}}(\mathbf{z}_k)} \sum_{i=1}^{M_{k|k-1}} r_{\alpha,k}^{(i),L_{k|k-1}^{(i)}}(\mathbf{z}_k), \quad \mathbf{z}_k \in Z_k, \tag{3.10}$$

$$\begin{aligned} r_{U,k}^{*,L_{k|k-1}^{(i)}}(\mathbf{z}_k) &= \frac{1}{\kappa_k(\mathbf{z}_k) + \sum_{i=1}^{M_{k|k-1}} r_{\alpha,k}^{(i),L_{k|k-1}^{(i)}}(\mathbf{z}_k)} \\ &\quad \times \sum_{i=1}^{M_{k|k-1}} \frac{\left(1 - r_{k|k-1}^{(i),L_{k|k-1}^{(i)}}\right) r_{\alpha,k}^{(i),L_{k|k-1}^{(i)}}(\mathbf{z}_k)}{1 - r_{k|k-1}^{(i),L_{k|k-1}^{(i)}} \left\langle p_{k|k-1}^{(i),L_{k|k-1}^{(i)}}, p_{D,k} \right\rangle}, \quad \mathbf{z}_k \in Z_k, \end{aligned} \tag{3.11}$$

$$p_{U,k}^{L_{k|k-1}^{(i)}}(\mathbf{x}_k; \mathbf{z}_k) = \frac{1}{\sum_{i=1}^{M_{k|k-1}} r_{\alpha,k}^{(i),L_{k|k-1}^{(i)}}(\mathbf{z}_k)} \sum_{i=1}^{M_{k|k-1}} p_{\alpha,k}^{(i),L_{k|k-1}^{(i)}}(\mathbf{x}_k; \mathbf{z}_k), \quad \mathbf{z}_k \in Z_k, \tag{3.12}$$

where,

$$p_{\alpha,k}^{(i),L_{k|k-1}^{(i)}}(\mathbf{x}_k; \mathbf{z}_k) = \sum_{j=1}^{L_{k|k-1}^{(i)}} \frac{\omega_{k|k-1}^{(i,j)} r_{k|k-1}^{(i),L_{k|k-1}^{(i)}} \psi_{k,\mathbf{z}_k}\left(\mathbf{x}_{k|k-1}^{(i,j)}\right)}{1 - r_{k|k-1}^{(i),L_{k|k-1}^{(i)}} \left\langle p_{k|k-1}^{(i),L_{k|k-1}^{(i)}}, p_{D,k} \right\rangle} \delta_{\mathbf{x}_{k|k-1}^{(i,j)}}(\mathbf{x}_k), \quad i = 1, \ldots, M_{k|k-1}, \tag{3.13}$$

$$\begin{aligned} r_{\alpha,k}^{(i),L_{k|k-1}^{(i)}}(\mathbf{z}_k) &= \left\langle p_{\alpha,k}^{(i),L_{k|k-1}^{(i)}}(\mathbf{x}_k; \mathbf{z}_k), 1 \right\rangle \\ &= \frac{r_{k|k-1}^{(i),L_{k|k-1}^{(i)}} \left\langle p_{k|k-1}^{(i),L_{k|k-1}^{(i)}}, \psi_{k,\mathbf{z}_k} \right\rangle}{1 - r_{k|k-1}^{(i),L_{k|k-1}^{(i)}} \left\langle p_{k|k-1}^{(i),L_{k|k-1}^{(i)}}, p_{D,k} \right\rangle}, \quad i = 1, \ldots, M_{k|k-1}. \end{aligned} \tag{3.14}$$

*Resampling*

To reduce the effect of degeneracy, we resample the particles for the multi-Bernoulli parameter set after the update step.

## 4. Convergence of the Mean-Square Errors for the SMC-MeMBer and SMC-CBMeMBer Filters

To show the convergence results for the SMC-MeMBer and SMC-CBMeMBer filters, certain conditions on the functions need to be met:

(1) the transition kernel $f_{k|k-1}(\mathbf{x}_k \mid \mathbf{x}_{k-1})$ satisfies the Feller property [18], that is, for all $\varphi \in C_b(\mathbb{R}^d)$, $\int \varphi(\mathbf{x}_{k-1}) \phi_{k|k-1}(\mathbf{x}_k \mid \mathbf{x}_{k-1}) d\mathbf{x}_{k-1} \in C_b(\mathbb{R}^d)$;

(2) single-sensor/target likelihood density $\psi_{k,\mathbf{z}_k}(\mathbf{x}_k) \in B(\mathbb{R}^d)$;

(3) $Q_k^{(i)}$ are rational-valued random variables such that there exists $p > 1$, some constant $C$, and $\alpha < p - 1$ so that

$$E\left[\left|\sum_{i=1}^{N}\left(Q_k^{(i)} - N\omega_k^{(i)}\right)q^{(i)}\right|^p\right] \le CN^{\alpha}\|q\|^p, \quad \text{with } \sum_{i=1}^{N} Q_k^{(i)} = N \tag{4.1}$$

for all vectors $q = (q^{(1)}, \ldots, q^{(N)})$;

(4) the importance sampling ratios are bounded, that is, there exists constants $B_1$ and $B_2$ such that $\|p_{\Gamma,k}^{(i)}/b_k^{(i)}\| \le B_1$, $i = 1, \ldots, M_{\Gamma,k}$, and $\|f_{k|k-1}/q_k^{(i)}\| \le B_2$, $i = 1, \ldots, M_{k-1}$;

(5) the resampling strategy is multinomial and hence unbiased [19].

First, the convergence of the mean-square errors for the initialization steps of the two filters can easily be established by Lemma 0 in [13]. Assuming that at time $k = 0$, we can sample exactly from the initial distribution $p_0^{(i)}$ $(i = 1, \ldots, M_0)$. Then, for all $\varphi \in B(\mathbb{R}^d)$,

$$\begin{aligned} E\left[\left(r_0^{(i),L_0^{(i)}} - r_0^{(i)}\right)^2\right] &\le \frac{c_0}{L_0^{(i)}}, \quad i = 1, \ldots, M_0, \\ E\left[\left(\left\langle p_0^{(i),L_0^{(i)}}, \varphi\right\rangle - \left\langle p_0^{(i)}, \varphi\right\rangle\right)^2\right] &\le \|\varphi\|^2 \frac{d_0}{L_0^{(i)}}, \quad i = 1, \ldots, M_0 \end{aligned} \tag{4.2}$$

hold for some real numbers $c_0 > 0$ and $d_0 > 0$ which are independent of the number $L_0^{(i)}$ of the sampled particles at time $k = 0$, $i = 1, \ldots, M_0$.

Also, the convergence of the mean-square errors for the resampling steps of the two filters can easily be established by Assumption 5 and Lemma 5 in [19].

The main difficulty and greatest challenge is to prove the mean-square convergence for the prediction steps and update steps of the two filters. They are, respectively, established by Propositions 4.1 and 4.2.

**Proposition 4.1.** *Suppose that, for all $\varphi \in B(\mathbb{R}^d)$,*

$$E\left[\left(r_{k-1}^{(i),L_{k-1}^{(i)}} - r_{k-1}^{(i)}\right)^2\right] \le \frac{c_{k-1}}{L_{k-1}^{(i)}}, \quad i = 1, \ldots, M_{k-1}, \tag{4.3}$$

$$E\left[\left(\left\langle p_{k-1}^{(i),L_{k-1}^{(i)}}, \varphi\right\rangle - \left\langle p_{k-1}^{(i)}, \varphi\right\rangle\right)^2\right] \le \|\varphi\|^2 \frac{d_{k-1}}{L_{k-1}^{(i)}}, \quad i = 1, \ldots, M_{k-1}, \tag{4.4}$$

*hold for some real numbers $c_{k-1} > 0$ and $d_{k-1} > 0$ which are independent of the number $L_{k-1}^{(i)}$ of the resampled particles at time $k - 1$, $i = 1, \ldots, M_{k-1}$.*

Then, after the prediction steps of the SMC-MeMBer and SMC-CBMeMBer filters at time $k$:

$$E\left[\left(r_{P,k|k-1}^{(i),L_{k-1}^{(i)}}-r_{P,k|k-1}^{(i)}\right)^2\right]\leq\frac{c_{P,k|k-1}}{L_{k-1}^{(i)}},\quad i=1,\ldots,M_{k-1}, \tag{4.5}$$

$$E\left[\left(\left\langle p_{P,k|k-1}^{(i),L_{k-1}^{(i)}},\varphi\right\rangle-\left\langle p_{P,k|k-1}^{(i)},\varphi\right\rangle\right)^2\right]\leq\|\varphi\|^2\frac{d_{P,k|k-1}}{L_{k-1}^{(i)}},\quad i=1,\ldots,M_{k-1}, \tag{4.6}$$

$$E\left[\left(\left\langle p_{\Gamma,k|k-1}^{(i),L_{\Gamma,k}^{(i)}},\varphi\right\rangle-\left\langle p_{\Gamma,k|k-1}^{(i)},\varphi\right\rangle\right)^2\right]\leq\|\varphi\|^2\frac{d_{\Gamma,k}}{L_{\Gamma,k}^{(i)}},\quad i=1,\ldots,M_{\Gamma,k}, \tag{4.7}$$

hold for a constant $d_{\Gamma,k}>0$ and some real numbers $c_{P,k|k-1}>0$ and $d_{P,k|k-1}>0$ which are independent of $L_{k-1}^{(i)}$, $i=1,\ldots,M_{k-1}$. $c_{P,k|k-1}$ and $d_{P,k|k-1}$ are defined by (A.8) and (A.18), respectively. The proof of Proposition 4.1 can be found in Appendix A.1.

**Proposition 4.2.** *Suppose that, for all $\varphi\in B(\mathbb{R}^d)$,*

$$E\left[\left(r_{k|k-1}^{(i),L_{k|k-1}^{(i)}}-r_{k|k-1}^{(i)}\right)^2\right]\leq\frac{c_{k|k-1}}{L_{k|k-1}^{(i)}},\quad i=1,\ldots,M_{k|k-1}, \tag{4.8}$$

$$E\left[\left(\left\langle p_{k|k-1}^{(i),L_{k|k-1}^{(i)}},\varphi\right\rangle-\left\langle p_{k|k-1}^{(i)},\varphi\right\rangle\right)^2\right]\leq\|\varphi\|^2\frac{d_{k|k-1}}{L_{k|k-1}^{(i)}},\quad i=1,\ldots,M_{k|k-1} \tag{4.9}$$

*hold for some real numbers $c_{k|k-1}>0$ and $d_{k|k-1}>0$ which are independent of the number $L_{k|k-1}^{(i)}$ of the predicted particles, $i=1,\ldots,M_{k|k-1}$. Then, after the update steps of the SMC-MeMBer and SMC-CBMeMBer filters at time $k$:*

$$E\left[\left(r_{L,k}^{(i),L_{k|k-1}^{(i)}}-r_{L,k}^{(i)}\right)^2\right]\leq\frac{c_{L,k}}{L_{k|k-1}^{(i)}},\quad i=1,\ldots,M_{k|k-1}, \tag{4.10}$$

$$E\left[\left(\left\langle p_{L,k}^{(i),L_{k|k-1}^{(i)}},\varphi\right\rangle-\left\langle p_{L,k}^{(i)},\varphi\right\rangle\right)^2\right]\leq\|\varphi\|^2\frac{d_{L,k}}{L_{k|k-1}^{(i)}},\quad i=1,\ldots,M_{k|k-1}, \tag{4.11}$$

$$E\left[\left(r_{U,k}^{L_{k|k-1}^{(i)}}(\mathbf{z}_k)-r_{U,k}(\mathbf{z}_k)\right)^2\right]\leq\frac{c_{U,k}}{L_{k|k-1}^{\min}},\quad \mathbf{z}_k\in Z_k, \tag{4.12}$$

$$E\left[\left(r_{U,k}^{*,L_{k|k-1}^{(i)}}(\mathbf{z}_k)-r_{U,k}^{*}(\mathbf{z}_k)\right)^2\right]\leq\frac{c_{U,k}^{*}}{L_{k|k-1}^{\min}},\quad \mathbf{z}_k\in Z_k, \tag{4.13}$$

$$E\left[\left(\left\langle p_{U,k}^{L_{k|k-1}^{(i)}}(\cdot;\mathbf{z}_k),\varphi\right\rangle-\left\langle p_{U,k}(\cdot;\mathbf{z}_k),\varphi\right\rangle\right)^2\right]\leq\|\varphi\|^2\frac{d_{U,k}}{L_{k|k-1}^{\min}},\quad \mathbf{z}_k\in Z_k \tag{4.14}$$

*hold for some real numbers* $c_{L,k} > 0$, $d_{L,k} > 0$, $c_{U,k} > 0$, $c^*_{U,k} > 0$, *and* $d_{U,k} > 0$, *which are independent of* $L^{(i)}_{k|k-1}$. $c_{L,k}$, $d_{L,k}$, $c_{U,k}$, $c^*_{U,k}$ *and* $d_{U,k}$ *are defined by* (A.29), (A.35), (A.47), (A.55), *and* (A.61), *respectively.* $L^{\min}_{k|k-1} = \min(L^{(1)}_{k|k-1}, \ldots, L^{(M_{k|k-1})}_{k|k-1})$, $\min(\cdot)$ *denotes the minimum. In addition,* $c_{U,k}$, $c^*_{U,k}$, *and* $d_{U,k}$ *depend on the number of targets and decrease with the increase of the target number. From* (A.47) *and* (A.55), *it can also be seen that* $c^*_{U,k} \geq c_{U,k}$. *It indicates that* $r^{*,L^{(i)}_{k|k-1}}_{U,k}(\mathbf{z}_k)$ *may need more particles than* $r^{L^{(i)}_{k|k-1}}_{U,k}(\mathbf{z}_k)$ *to achieve the same mean-square error bound. The proof of the Proposition 4.2 can be found in Appendix A.2.*

Propositions 4.1 and 4.2 show that the bounds for the mean-square error of the SMC-MeMBer and SMC-CBMeMBer prediction steps and update steps at each stage depend on the number of particles. The mean-square errors tend to zero as the number of particles tends to infinity. The bounds for the mean-square errors of these quantities are inversely proportional to the corresponding particle number.

Moreover, from the proofs of Propositions 4.1 and 4.2, it can be seen that

(1) Assumptions 1, 3, and 4 ensure that (4.6) holds;

(2) Assumption 4 ensures that (4.7) holds;

(3) Assumption 2 ensures that (4.12), (4.13), and (4.14) hold;

(4) Assumption 5 ensures the convergence of the mean-square errors for the resampling steps of the two filters.

Assumptions 3, 4, and 5 are concerned with the SMC method. They can be satisfied as long as the appropriate sampling strategies are chosen. Assumptions 1 and 2 are concerned with the likelihood and target transition kernel. They may be too restrictive or unrealistic for some practical applications. However, these convergence results give justification to the SMC implementations of the MeMBer and CBMeMBer filters and show how the order of the mean-square errors are reduced as the number of particles increases.

## 5. Simulations

Here, we briefly describe the application of the convergence results for the SMC-CBMeMBer filter to the nonlinear MTT example presented in Example 1 of [12]. The experiment settings are the same as those of Example 1 except that the number of the particles $L^{(i)}_k$ used for each hypothesized track at time $k$. For convenience, we assume $L^{(i)}_k = L$. Assumptions 1–5 are satisfied in this example. So, the SMC-CBMeMBer filter converges to the ground truth in the mean-square sense.

For the SMC-CBMeMBer filter, the estimates of the multitarget number and states, which are derived from the particle multi-Bernoulli parameter set, are unbiased. Therefore, via comparing the tracking performance of the algorithm in the various particle number $L$, the convergence results for the SMC-CBMeMBer filter can be verified to a great extent.

The standard deviation of the estimated cardinality distribution and the optimal subpattern assignment (OSPA) multitarget miss-distance [20] of order $p = 2$ with cut-off $c = 100$ m, which jointly captures differences in cardinality and individual elements between two finite sets, are used to evaluate the performance of the method. Table 1 shows the time-averaged standard deviation of the estimated cardinality distribution and the time-averaged OSPA in various $L$ via 200 MC simulation experiments.

**Table 1:** Time-averaged standard deviation of the estimated cardinality distribution and time-averaged OSPA (m) in various $L$.

| Particle number $L$ | 100 | 500 | 1000 | 1500 | 2000 |
|---|---|---|---|---|---|
| Time-averaged standard deviation of the estimated cardinality distribution from the SMC-CBMeMBer filter | 2.69 | 2.03 | 1.48 | 1.23 | 1.04 |
| OSPA (m) from the SMC-CBMeMBer filter | 65.2 | 51.9 | 42.3 | 34.8 | 27.7 |

Table 1 shows that both the standard deviation of the estimated cardinality distribution and OSPA decrease with the increase of the particle number $L$. This phenomenon can be reasonably explained by the convergence results derived in this paper: first, the mean-square error of the particle multi-Bernoulli parameter set decreases as the number of the particles increases; then, the more precise estimates of the cardinality distribution and multitarget states can be derived from the more precise particle multi-Bernoulli parameter set, which eventually leads to the results presented in Table 1.

## 6. Conclusions and Future Work

This paper presents the mathematical proofs of the convergence for the SMC-MeMBer and SMC-CBMeMBer filters and gives the bounds for the mean-square errors. In the linear-Gaussian condition, Vo et al. presented the analytic solutions to the MeMBer and CBMeMBer recursions: GM-MeMBer and GM-CBMeMBer filters [12]. The future work is focused on studying the convergence results and error bounds for the two filters.

## Appendix

## A.

In deriving the proofs, we use the Minkowski inequality, which states that, for any two random variables $X$ and $Y$ in $L^2$,

$$E\left[(X+Y)^2\right]^{1/2} \leq E\left[X^2\right]^{1/2} + E\left[X^2\right]^{1/2}. \tag{A.1}$$

Using Minkowski's inequality, we obtain that, for all $\varphi \in B(\mathbb{R}^d)$,

$$\begin{aligned} &E\left[\left(r^{(i),L^{(i)}}\left\langle p^{(i),L^{(i)}},\varphi\right\rangle - r^{(i)}\left\langle p^{(i)},\varphi\right\rangle\right)^2\right]^{1/2} \\ &= E\left[\left(r^{(i),L^{(i)}}\left\langle p^{(i),L^{(i)}},\varphi\right\rangle - r^{(i)}\left\langle p^{(i),L^{(i)}},\varphi\right\rangle + r^{(i)}\left\langle p^{(i),L^{(i)}},\varphi\right\rangle - r^{(i)}\left\langle p^{(i)},\varphi\right\rangle\right)^2\right]^{1/2} \qquad \text{(A.2)} \\ &\leq E\left[\left\langle p^{(i),L^{(i)}},\varphi\right\rangle^2\left(r^{(i),L^{(i)}} - r^{(i)}\right)^2\right]^{1/2} + r^{(i)}E\left[\left(\left\langle p^{(i),L^{(i)}},\varphi\right\rangle - \left\langle p^{(i)},\varphi\right\rangle\right)^2\right]^{1/2} \qquad \text{(A.3)} \\ &\leq \|\varphi\|E\left[\left(r^{(i),L^{(i)}} - r^{(i)}\right)^2\right]^{1/2} + r^{(i)}E\left[\left(\left\langle p^{(i),L^{(i)}},\varphi\right\rangle - \left\langle p^{(i)},\varphi\right\rangle\right)^2\right]^{1/2} \qquad \text{(A.4)} \end{aligned}$$

holds, $i = 1,\ldots,M$, for the multi-Bernoulli density $\pi = \{(r^{(i)},p^{(i)})\}_{i=1}^{M}$ and its particle approximation $\pi^{L^{(i)}} = \{(r^{(i),L^{(i)}},p^{(i),L^{(i)}})\}_{i=1}^{M}$.

### *A.1. Proof of Proposition 4.1*

We first prove (4.5). From (2.4) and (3.2), we have

$$E\left[\left(r_{P,k|k-1}^{(i),L_{k-1}^{(i)}}-r_{P,k|k-1}^{(i)}\right)^2\right]^{1/2}=E\left[\left(r_{k-1}^{(i),L_{k-1}^{(i)}}\left\langle p_{k-1}^{(i),L_{k-1}^{(i)}},p_{S,k}\right\rangle-r_{k-1}^{(i)}\left\langle p_{k-1}^{(i)},p_{S,k}\right\rangle\right)^2\right]^{1/2} \tag{A.5}$$

(by (A.4))

$$\le \left\|p_{S,k}\right\|E\left[\left(r_{k-1}^{(i),L_{k-1}^{(i)}}-r_{k-1}^{(i)}\right)^2\right]^{1/2}+r_{k-1}^{(i)}E\left[\left(\left\langle p_{k-1}^{(i),L_{k-1}^{(i)}},p_{S,k}\right\rangle-\left\langle p_{k-1}^{(i)},p_{S,k}\right\rangle\right)^2\right]^{1/2} \tag{A.6}$$

(by (4.3), (4.4), and $0\le r_{k-1}^{(i)}\le 1$)

$$\le \left\|p_{S,k}\right\|\frac{\sqrt{c_{k-1}}+\sqrt{d_{k-1}}}{\sqrt{L_{k-1}^{(i)}}}. \tag{A.7}$$

So that (4.5) is proved with

$$c_{P,k|k-1}=\left\|p_{S,k}\right\|^2\left(\sqrt{c_{k-1}}+\sqrt{d_{k-1}}\right)^2. \tag{A.8}$$

Now turn to (4.6). From (2.5), we have

$$\begin{aligned}&E\left[\left(\left\langle p_{P,k|k-1}^{(i),L_{k-1}^{(i)}},\varphi\right\rangle-\left\langle p_{P,k|k-1}^{(i)},\varphi\right\rangle\right)^2\right]^{1/2}\\&\quad=E\left[\left(\left\langle p_{P,k|k-1}^{(i),L_{k-1}^{(i)}},\varphi\right\rangle-\left\langle\frac{\left\langle f_{k|k-1},p_{k-1}^{(i)}p_{S,k}\right\rangle}{\left\langle p_{k-1}^{(i)},p_{S,k}\right\rangle},\varphi\right\rangle\right)^2\right]^{1/2}\end{aligned} \tag{A.9}$$

(adding and subtracting a new term)

$$\begin{aligned}&=E\left[\left(\left\langle p_{P,k|k-1}^{(i),L_{k-1}^{(i)}},\varphi\right\rangle-\left\langle\frac{\left\langle f_{k|k-1},p_{k-1}^{(i),L_{k-1}^{(i)}}p_{S,k}\right\rangle}{\left\langle p_{k-1}^{(i),L_{k-1}^{(i)}},p_{S,k}\right\rangle},\varphi\right\rangle\right.\right.\\&\qquad\left.\left.+\left\langle\frac{\left\langle f_{k|k-1},p_{k-1}^{(i),L_{k-1}^{(i)}}p_{S,k}\right\rangle}{\left\langle p_{k-1}^{(i),L_{k-1}^{(i)}},p_{S,k}\right\rangle},\varphi\right\rangle-\left\langle\frac{\left\langle f_{k|k-1},p_{k-1}^{(i)}p_{S,k}\right\rangle}{\left\langle p_{k-1}^{(i)},p_{S,k}\right\rangle},\varphi\right\rangle\right)^2\right]^{1/2}\end{aligned} \tag{A.10}$$

(using Minkowski's inequality)

$$\leq E\left[\left(\left\langle p_{P,k|k-1}^{(i),L_{k-1}^{(i)}},\varphi\right\rangle-\left\langle\frac{\left\langle f_{k|k-1},p_{k-1}^{(i),L_{k-1}^{(i)}}p_{S,k}\right\rangle}{\left\langle p_{k-1}^{(i),L_{k-1}^{(i)}},p_{S,k}\right\rangle},\varphi\right\rangle\right)^2\right]^{1/2}$$
$$+E\left[\left(\frac{\left\langle p_{k-1}^{(i),L_{k-1}^{(i)}},p_{S,k}\left\langle f_{k|k-1},\varphi\right\rangle\right\rangle}{\left\langle p_{k-1}^{(i),L_{k-1}^{(i)}},p_{S,k}\right\rangle}-\frac{\left\langle p_{k-1}^{(i)},p_{S,k}\left\langle f_{k|k-1},\varphi\right\rangle\right\rangle}{\left\langle p_{k-1}^{(i)},p_{S,k}\right\rangle}\right)^2\right]^{1/2}. \tag{A.11}$$

By Assumption 3 and Lemma 1 in [13], we easily obtain that the first term in (A.11) becomes

$$E\left[\left(\left\langle p_{P,k|k-1}^{(i),L_{k-1}^{(i)}},\varphi\right\rangle-\left\langle\frac{\left\langle f_{k|k-1},p_{k-1}^{(i),L_{k-1}^{(i)}}p_{S,k}\right\rangle}{\left\langle p_{k-1}^{(i),L_{k-1}^{(i)}},p_{S,k}\right\rangle},\varphi\right\rangle\right)^2\right]^{1/2}$$
$$\leq\frac{\|\varphi\|}{\sqrt{L_{k-1}^{(i)}}}\left(\left\|\frac{f_{k|k-1}p_{S,k}}{q_k^{(i)}}\right\|^2+\left\|f_{k|k-1}p_{S,k}\right\|^2\right)^{1/2} \tag{A.12}$$

(since $\|f_{k|k-1}/q_k^{(i)}\|\leq B_2$ by Assumption 4 and $f_{k|k-1}p_{S,k}\in C_b(\mathbb{R}^d)$ by Assumption 1)

$$\leq\frac{\|\varphi\|}{\sqrt{L_{k-1}^{(i)}}}\left(\left\|p_{S,k}\right\|^2B_2^2+\left\|f_{k|k-1}p_{S,k}\right\|^2\right)^{1/2}. \tag{A.13}$$

Adding and subtracting a new term in the second term of (A.11), we have

$$E\left[\left(\frac{\left\langle p_{k-1}^{(i),L_{k-1}^{(i)}},p_{S,k}\left\langle f_{k|k-1},\varphi\right\rangle\right\rangle}{\left\langle p_{k-1}^{(i),L_{k-1}^{(i)}},p_{S,k}\right\rangle}-\frac{\left\langle p_{k-1}^{(i)},p_{S,k}\left\langle f_{k|k-1},\varphi\right\rangle\right\rangle}{\left\langle p_{k-1}^{(i)},p_{S,k}\right\rangle}\right)^2\right]^{1/2}$$

$$= E\left[\left(\frac{\left\langle p_{k-1}^{(i),L_{k-1}^{(i)}}, p_{S,k}\langle f_{k|k-1},\varphi\rangle\right\rangle}{\left\langle p_{k-1}^{(i),L_{k-1}^{(i)}}, p_{S,k}\right\rangle} - \frac{\left\langle p_{k-1}^{(i),L_{k-1}^{(i)}}, p_{S,k}\langle f_{k|k-1},\varphi\rangle\right\rangle}{\left\langle p_{k-1}^{(i)}, p_{S,k}\right\rangle}\right.$$

$$\left. + \frac{\left\langle p_{k-1}^{(i),L_{k-1}^{(i)}}, p_{S,k}\langle f_{k|k-1},\varphi\rangle\right\rangle}{\left\langle p_{k-1}^{(i)}, p_{S,k}\right\rangle} - \frac{\left\langle p_{k-1}^{(i)}, p_{S,k}\langle f_{k|k-1},\varphi\rangle\right\rangle}{\left\langle p_{k-1}^{(i)}, p_{S,k}\right\rangle}\right)^2\Bigg]^{1/2} \tag{A.14}$$

(using Minkowski's inequality)

$$\leq \frac{1}{\left\langle p_{k-1}^{(i)}, p_{S,k}\right\rangle} E\left[\left(\frac{\left\langle p_{k-1}^{(i),L_{k-1}^{(i)}}, p_{S,k}\langle f_{k|k-1},\varphi\rangle\right\rangle}{\left\langle p_{k-1}^{(i),L_{k-1}^{(i)}}, p_{S,k}\right\rangle}\left(\left\langle p_{k-1}^{(i)}, p_{S,k}\right\rangle - \left\langle p_{k-1}^{(i),L_{k-1}^{(i)}}, p_{S,k}\right\rangle\right)\right)^2\right]^{1/2} \tag{A.15}$$

$$+ \frac{1}{\left\langle p_{k-1}^{(i)}, p_{S,k}\right\rangle} E\left[\left(\left\langle p_{k-1}^{(i),L_{k-1}^{(i)}}, p_{S,k}\langle f_{k|k-1},\varphi\rangle\right\rangle - \left\langle p_{k-1}^{(i)}, p_{S,k}\langle f_{k|k-1},\varphi\rangle\right\rangle\right)^2\right]^{1/2}$$

$$\leq 2\frac{\left\|\langle f_{k|k-1},\varphi\rangle\right\|}{\left\langle p_{k-1}^{(i)}, p_{S,k}\right\rangle} E\left[\left(\left(\left\langle p_{k-1}^{(i)}, p_{S,k}\right\rangle - \left\langle p_{k-1}^{(i),L_{k-1}^{(i)}}, p_{S,k}\right\rangle\right)\right)^2\right]^{1/2} \tag{A.16}$$

(by (4.4))

$$\leq 2\frac{\|\varphi\|\cdot\|p_{S,k}\|}{\inf(p_{S,k})}\sqrt{\frac{d_{k-1}}{L_{k-1}^{(i)}}}, \tag{A.17}$$

where $\inf(\cdot)$ denotes the infimum.

Finally, substituting (A.12) and (A.17) into (A.11), (4.6) is proved with

$$d_{P,k|k-1} = \left(\sqrt{\|p_{S,k}\|^2 B_2^2 + \|f_{k|k-1}p_{S,k}\|^2} + \frac{2\|p_{S,k}\|\sqrt{d_{k-1}}}{\inf(p_{S,k})}\right)^2. \tag{A.18}$$

Now, turn to (4.7). By Lemma 0 in [13] and the boundedness of $\|p_{\Gamma,k}^{(i)}/b_k^{(i)}\| \leq B_1$ ($i = 1,\ldots,M_{k-1}$) in Assumption 4, we get that (4.7) holds for a constant $d_{\Gamma,k}$. This completes the proof.

### A.2. Proof of Proposition 4.2

Now turn to (4.10). From (2.7) and (3.8), we have

$$E\left[\left(r_{L,k}^{(i)}-r_{L,k}^{(i),L_{k|k-1}^{(i)}}\right)^2\right]^{1/2}$$

$$=E\left[\left(\mathrm{r}_{k|k-1}^{(i)}\frac{1-\left\langle p_{k|k-1}^{(i)},p_{D,k}\right\rangle}{1-r_{k|k-1}^{(i)}\left\langle p_{k|k-1}^{(i)},p_{D,k}\right\rangle}-r_{k|k-1}^{(i),L_{k|k-1}^{(i)}}\frac{1-\left\langle p_{k|k-1}^{(i),L_{k|k-1}^{(i)}},p_{D,k}\right\rangle}{1-r_{k|k-1}^{(i),L_{k|k-1}^{(i)}}\left\langle p_{k|k-1}^{(i),L_{k|k-1}^{(i)}},p_{D,k}\right\rangle}\right)^2\right]^{1/2} \tag{A.19}$$

(adding and subtracting a new term)

$$=E\left[\left(\begin{array}{c} r_{k|k-1}^{(i)}\dfrac{1-\left\langle p_{k|k-1}^{(i)},p_{D,k}\right\rangle}{1-r_{k|k-1}^{(i)}\left\langle p_{k|k-1}^{(i)},p_{D,k}\right\rangle}-r_{k|k-1}^{(i),L_{k|k-1}^{(i)}}\dfrac{1-\left\langle p_{k|k-1}^{(i),L_{k|k-1}^{(i)}},p_{D,k}\right\rangle}{1-r_{k|k-1}^{(i)}\left\langle p_{k|k-1}^{(i)},p_{D,k}\right\rangle} \\ +r_{k|k-1}^{(i),L_{k|k-1}^{(i)}}\dfrac{1-\left\langle p_{k|k-1}^{(i),L_{k|k-1}^{(i)}},p_{D,k}\right\rangle}{1-r_{k|k-1}^{(i)}\left\langle p_{k|k-1}^{(i)},p_{D,k}\right\rangle}-r_{k|k-1}^{(i),L_{k|k-1}^{(i)}}\dfrac{1-\left\langle p_{k|k-1}^{(i),L_{k|k-1}^{(i)}},p_{D,k}\right\rangle}{1-r_{k|k-1}^{(i),L_{k|k-1}^{(i)}}\left\langle p_{k|k-1}^{(i),L_{k|k-1}^{(i)}},p_{D,k}\right\rangle} \end{array}\right)^2\right]^{1/2} \tag{A.20}$$

(using Minkowski's inequality)

$$\leq\frac{E\left[\left(r_{k|k-1}^{(i)}\left(1-\left\langle p_{k|k-1}^{(i)},p_{D,k}\right\rangle\right)-r_{k|k-1}^{(i),L_{k|k-1}^{(i)}}\left(1-\left\langle p_{k|k-1}^{(i),L_{k|k-1}^{(i)}},p_{D,k}\right\rangle\right)\right)^2\right]^{1/2}}{1-r_{k|k-1}^{(i)}\left\langle p_{k|k-1}^{(i)},p_{D,k}\right\rangle}$$

$$+E\left[\left(r_{k|k-1}^{(i),L_{k|k-1}^{(i)}}\frac{1-\left\langle p_{k|k-1}^{(i),L_{k|k-1}^{(i)}},p_{D,k}\right\rangle}{1-r_{k|k-1}^{(i)}\left\langle p_{k|k-1}^{(i)},p_{D,k}\right\rangle}-r_{k|k-1}^{(i),L_{k|k-1}^{(i)}}\frac{1-\left\langle p_{k|k-1}^{(i),L_{k|k-1}^{(i)}},p_{D,k}\right\rangle}{1-r_{k|k-1}^{(i),L_{k|k-1}^{(i)}}\left\langle p_{k|k-1}^{(i),L_{k|k-1}^{(i)}},p_{D,k}\right\rangle}\right)^2\right]^{1/2}. \tag{A.21}$$

The numerator of the first term in (A.21) is

$$E\left[\left(r_{k|k-1}^{(i)}\left(1-\left\langle p_{k|k-1}^{(i)},p_{D,k}\right\rangle\right)-r_{k|k-1}^{(i),L_{k|k-1}^{(i)}}\left(1-\left\langle p_{k|k-1}^{(i),L_{k|k-1}^{(i)}},p_{D,k}\right\rangle\right)\right)^2\right]^{1/2}$$

$$=E\left[\left(\left(r_{k|k-1}^{(i)}-r_{k|k-1}^{(i),L_{k|k-1}^{(i)}}\right)+\left(r_{k|k-1}^{(i),L_{k|k-1}^{(i)}}\left\langle p_{k|k-1}^{(i),L_{k|k-1}^{(i)}},p_{D,k}\right\rangle-r_{k|k-1}^{(i)}\left\langle p_{k|k-1}^{(i)},p_{D,k}\right\rangle\right)\right)^2\right]^{1/2} \tag{A.22}$$

(using Minkowski's inequality and then (A.4))

$$\begin{aligned}&\leq E\left[\left(r_{k|k-1}^{(i)}-r_{k|k-1}^{(i),L_{k|k-1}^{(i)}}\right)^2\right]^{1/2}+\left\|p_{D,k}\right\|E\left[\left(r_{k|k-1}^{(i)}-r_{k|k-1}^{(i),L_{k|k-1}^{(i)}}\right)^2\right]^{1/2}\\&\quad+r_{k|k-1}^{(i)}E\left[\left(\left\langle p_{k|k-1}^{(i),L_{k|k-1}^{(i)}},p_{D,k}\right\rangle-\left\langle p_{k|k-1}^{(i)},p_{D,k}\right\rangle\right)^2\right]^{1/2}\end{aligned}\tag{A.23}$$

(by (4.8) and (4.9))

$$\leq\frac{\left(1+\left\|p_{D,k}\right\|\right)\sqrt{c_{k|k-1}}+r_{k|k-1}^{(i)}\left\|p_{D,k}\right\|\sqrt{d_{k|k-1}}}{\sqrt{L_{k|k-1}^{(i)}}}.\tag{A.24}$$

The second term in (A.21) is

$$\begin{aligned}&E\left[\left(r_{k|k-1}^{(i),L_{k|k-1}^{(i)}}\frac{1-\left\langle p_{k|k-1}^{(i),L_{k|k-1}^{(i)}},p_{D,k}\right\rangle}{1-r_{k|k-1}^{(i)}\left\langle p_{k|k-1}^{(i)},p_{D,k}\right\rangle}-r_{k|k-1}^{(i),L_{k|k-1}^{(i)}}\frac{1-\left\langle p_{k|k-1}^{(i),L_{k|k-1}^{(i)}},p_{D,k}\right\rangle}{1-r_{k|k-1}^{(i),L_{k|k-1}^{(i)}}\left\langle p_{k|k-1}^{(i),L_{k|k-1}^{(i)}},p_{D,k}\right\rangle}\right)^2\right]^{1/2}\\&=E\left[\left(\frac{r_{k|k-1}^{(i),L_{k|k-1}^{(i)}}-r_{k|k-1}^{(i),L_{k|k-1}^{(i)}}\left\langle p_{k|k-1}^{(i),L_{k|k-1}^{(i)}},p_{D,k}\right\rangle}{1-r_{k|k-1}^{(i),L_{k|k-1}^{(i)}}\left\langle p_{k|k-1}^{(i),L_{k|k-1}^{(i)}},p_{D,k}\right\rangle}\right)^2\right.\\&\qquad\left.\times\left(\frac{r_{k|k-1}^{(i)}\left\langle p_{k|k-1}^{(i)},p_{D,k}\right\rangle-r_{k|k-1}^{(i),L_{k|k-1}^{(i)}}\left\langle p_{k|k-1}^{(i),L_{k|k-1}^{(i)}},p_{D,k}\right\rangle}{1-r_{k|k-1}^{(i)}\left\langle p_{k|k-1}^{(i)},p_{D,k}\right\rangle}\right)^2\right]^{1/2}\end{aligned}\tag{A.25}$$

(by $0\leq r_{k|k-1}^{(i),L_{k|k-1}^{(i)}}\leq 1$)

$$\leq\frac{E\left[\left(r_{k|k-1}^{(i)}\left\langle p_{k|k-1}^{(i)},p_{D,k}\right\rangle-r_{k|k-1}^{(i),L_{k|k-1}^{(i)}}\left\langle p_{k|k-1}^{(i),L_{k|k-1}^{(i)}},p_{D,k}\right\rangle\right)^2\right]^{1/2}}{1-r_{k|k-1}^{(i)}\left\langle p_{k|k-1}^{(i)},p_{D,k}\right\rangle}\tag{A.26}$$

(by (A.4), (4.8) and (4.9))

$$\leq\frac{\left\|p_{D,k}\right\|\sqrt{c_{k|k-1}}+r_{k|k-1}^{(i)}\left\|p_{D,k}\right\|\sqrt{d_{k|k-1}}}{\left(1-r_{k|k-1}^{(i)}\left\langle p_{k|k-1}^{(i)},p_{D,k}\right\rangle\right)\sqrt{L_{k|k-1}^{(i)}}}.\tag{A.27}$$

Substituting (A.24) and (A.27) into (A.21), and then using $0 \le r_{k|k-1}^{(i)} \le 1$, we get

$$\begin{aligned} &E\left[\left(r_{L,k}^{(i)} - r_{L,k}^{(i),L_{k|k-1}^{(i)}}\right)^2\right]^{1/2} \\ &\quad\le \frac{\left(1+2\left\|p_{D,k}\right\|\right)\sqrt{c_{k|k-1}} + 2r_{k|k-1}^{(i)}\left\|p_{D,k}\right\|\sqrt{d_{k|k-1}}}{\left(1 - r_{k|k-1}^{(i)}\left\langle p_{k|k-1}^{(i)}, p_{D,k}\right\rangle\right)\sqrt{L_{k|k-1}^{(i)}}} \\ &\quad\le \frac{\left(1+2\left\|p_{D,k}\right\|\right)\sqrt{c_{k|k-1}} + 2\left\|p_{D,k}\right\|\sqrt{d_{k|k-1}}}{\left(1 - \left\|p_{D,k}\right\|\right)\sqrt{L_{k|k-1}^{(i)}}}. \end{aligned} \tag{A.28}$$

Finally, (4.10) is proved with

$$c_{L,k} = \left(\frac{\left(1+2\left\|p_{D,k}\right\|\right)\sqrt{c_{k|k-1}} + 2\left\|p_{D,k}\right\|\sqrt{d_{k|k-1}}}{1 - \left\|p_{D,k}\right\|}\right)^2. \tag{A.29}$$

Now turn to (4.11). From (2.8) and (3.9), we have

$$\begin{aligned} &E\left[\left(\left\langle p_{L,k}^{(i)}, \varphi\right\rangle - \left\langle p_{L,k}^{(i),L_{k|k-1}^{(i)}}, \varphi\right\rangle\right)^2\right]^{1/2} \\ &\quad= E\left[\left(\frac{\left\langle p_{k|k-1}^{(i)}, \varphi(1-p_{D,k})\right\rangle}{1 - \left\langle p_{k|k-1}^{(i)}, p_{D,k}\right\rangle} - \frac{\left\langle p_{k|k-1}^{(i),L_{k|k-1}^{(i)}}, \varphi(1-p_{D,k})\right\rangle}{1 - \left\langle p_{k|k-1}^{(i),L_{k|k-1}^{(i)}}, p_{D,k}\right\rangle}\right)^2\right]^{1/2} \end{aligned} \tag{A.30}$$

(adding and subtracting a new term)

$$\begin{aligned} &= E\left[\left(\frac{\left\langle p_{k|k-1}^{(i)}, \varphi(1-p_{D,k})\right\rangle}{1 - \left\langle p_{k|k-1}^{(i)}, p_{D,k}\right\rangle} - \frac{\left\langle p_{k|k-1}^{(i),L_{k|k-1}^{(i)}}, \varphi(1-p_{D,k})\right\rangle}{1 - \left\langle p_{k|k-1}^{(i)}, p_{D,k}\right\rangle}\right.\right. \\ &\qquad\left.\left. + \frac{\left\langle p_{k|k-1}^{(i),L_{k|k-1}^{(i)}}, \varphi(1-p_{D,k})\right\rangle}{1 - \left\langle p_{k|k-1}^{(i)}, p_{D,k}\right\rangle} - \frac{\left\langle p_{k|k-1}^{(i),L_{k|k-1}^{(i)}}, \varphi(1-p_{D,k})\right\rangle}{1 - \left\langle p_{k|k-1}^{(i),L_{k|k-1}^{(i)}}, p_{D,k}\right\rangle}\right)^2\right]^{1/2} \end{aligned} \tag{A.31}$$

(using Minkowski's inequality)

$$\leq \frac{E\left[\left(\left\langle p_{k|k-1}^{(i)}, \varphi(1-p_{D,k})\right\rangle - \left\langle p_{k|k-1}^{(i),L_{k|k-1}^{(i)}}, \varphi(1-p_{D,k})\right\rangle\right)^2\right]^{1/2}}{1-\left\langle p_{k|k-1}^{(i)}, p_{D,k}\right\rangle}$$
$$+ E\left[\left(\frac{\left\langle p_{k|k-1}^{(i),L_{k|k-1}^{(i)}}, \varphi(1-p_{D,k})\right\rangle}{1-\left\langle p_{k|k-1}^{(i),L_{k|k-1}^{(i)}}, p_{D,k}\right\rangle}\right)^2 \cdot \left(\frac{\left\langle p_{k|k-1}^{(i)}, p_{D,k}\right\rangle - \left\langle p_{k|k-1}^{(i),L_{k|k-1}^{(i)}}, p_{D,k}\right\rangle}{1-\left\langle p_{k|k-1}^{(i)}, p_{D,k}\right\rangle}\right)^2\right]^{1/2} \tag{A.32}$$

$$\leq \frac{E\left[\left(\left\langle p_{k|k-1}^{(i)}, \varphi(1-p_{D,k})\right\rangle - \left\langle p_{k|k-1}^{(i),L_{k|k-1}^{(i)}}, \varphi(1-p_{D,k})\right\rangle\right)^2\right]^{1/2}}{1-\left\langle p_{k|k-1}^{(i)}, p_{D,k}\right\rangle}$$
$$+ \frac{\|\varphi\| E\left[\left(\left\langle p_{k|k-1}^{(i)}, p_{D,k}\right\rangle - \left\langle p_{k|k-1}^{(i),L_{k|k-1}^{(i)}}, p_{D,k}\right\rangle\right)^2\right]^{1/2}}{1-\left\langle p_{k|k-1}^{(i)}, p_{D,k}\right\rangle} \tag{A.33}$$

(by (4.9))

$$\leq \frac{\|\varphi\|\sqrt{d_{k|k-1}}}{(1-\|p_{D,k}\|)\sqrt{L_{k|k-1}^{(i)}}}. \tag{A.34}$$

Finally, (4.11) is proved with

$$d_{L,k} = \frac{d_{k|k-1}}{(1-\|p_{D,k}\|)^2}. \tag{A.35}$$

Now, turn to (4.12). From (2.9) and (3.10), we have

$$E\left[\left(r_{U,k}^{L_{k|k-1}^{(i)}}(\mathbf{z}_k) - r_{U,k}(\mathbf{z}_k)\right)^2\right]^{1/2}$$
$$= E\left[\left(\frac{\sum_{i=1}^{M_{k|k-1}} r_{\alpha,k}^{(i),L_{k|k-1}^{(i)}}(\mathbf{z}_k)}{\kappa_k(\mathbf{z}_k) + \sum_{i=1}^{M_{k|k-1}} r_{\alpha,k}^{(i),L_{k|k-1}^{(i)}}(\mathbf{z}_k)} - \frac{\sum_{i=1}^{M_{k|k-1}} r_{\alpha,k}^{(i)}(\mathbf{z}_k)}{\kappa_k(\mathbf{z}_k) + \sum_{i=1}^{M_{k|k-1}} r_{\alpha,k}^{(i)}(\mathbf{z}_k)}\right)^2\right]^{1/2} \tag{A.36}$$

(adding and subtracting a new term)

$$= E\left[\left(\frac{\sum_{i=1}^{M_{k|k-1}} r_{\alpha,k}^{(i),L_{k|k-1}^{(i)}}(\mathbf{z}_k)}{\kappa_k(\mathbf{z}_k)+\sum_{i=1}^{M_{k|k-1}} r_{\alpha,k}^{(i),L_{k|k-1}^{(i)}}(\mathbf{z}_k)} - \frac{\sum_{i=1}^{M_{k|k-1}} r_{\alpha,k}^{(i),L_{k|k-1}^{(i)}}(\mathbf{z}_k)}{\kappa_k(\mathbf{z}_k)+\sum_{i=1}^{M_{k|k-1}} r_{\alpha,k}^{(i)}(\mathbf{z}_k)}\right.\right.$$
$$\left.\left. + \frac{\sum_{i=1}^{M_{k|k-1}} r_{\alpha,k}^{(i),L_{k|k-1}^{(i)}}(\mathbf{z}_k)}{\kappa_k(\mathbf{z}_k)+\sum_{i=1}^{M_{k|k-1}} r_{\alpha,k}^{(i)}(\mathbf{z}_k)} - \frac{\sum_{i=1}^{M_{k|k-1}} r_{\alpha,k}^{(i)}(\mathbf{z}_k)}{\kappa_k(\mathbf{z}_k)+\sum_{i=1}^{M_{k|k-1}} r_{\alpha,k}^{(i)}(\mathbf{z}_k)}\right)^2\right]^{1/2} \tag{A.37}$$

(using Minkowski's inequality)

$$\leq E\left[\left(r_{U,k}^{L_{k|k-1}^{(i)}}(\mathbf{z}_k)\frac{\sum_{i=1}^{M_{k|k-1}} r_{\alpha,k}^{(i)}(\mathbf{z}_k) - \sum_{i=1}^{M_{k|k-1}} r_{\alpha,k}^{(i),L_{k|k-1}^{(i)}}(\mathbf{z}_k)}{\kappa_k(\mathbf{z}_k)+\sum_{i=1}^{M_{k|k-1}} r_{\alpha,k}^{(i)}(\mathbf{z}_k)}\right)^2\right]^{1/2}$$
$$+ E\left[\left(\frac{\sum_{i=1}^{M_{k|k-1}} r_{\alpha,k}^{(i),L_{k|k-1}^{(i)}}(\mathbf{z}_k) - \sum_{i=1}^{M_{k|k-1}} r_{\alpha,k}^{(i)}(\mathbf{z}_k)}{\kappa_k(\mathbf{z}_k)+\sum_{i=1}^{M_{k|k-1}} r_{\alpha,k}^{(i)}(\mathbf{z}_k)}\right)^2\right]^{1/2} \tag{A.38}$$

(using $\kappa_k(\mathbf{z}_k) \geq 0$, $0 \leq r_{U,k}^{L_{k|k-1}^{(i)}}(\mathbf{z}_k) \leq 1$)

$$\leq \frac{2\sum_{i=1}^{M_{k|k-1}} E\left[\left(r_{\alpha,k}^{(i),L_{k|k-1}^{(i)}}(\mathbf{z}_k) - r_{\alpha,k}^{(i)}(\mathbf{z}_k)\right)^2\right]^{1/2}}{\sum_{i=1}^{M_{k|k-1}} r_{\alpha,k}^{(i)}(\mathbf{z}_k)}. \tag{A.39}$$

From (2.12) and (3.14), the expectation in the summation of (A.39) is

$$E\left[\left(r_{\alpha,k}^{(i),L_{k|k-1}^{(i)}}(\mathbf{z}_k) - r_{\alpha,k}^{(i)}(\mathbf{z}_k)\right)^2\right]^{1/2}$$
$$= E\left[\left(\frac{r_{k|k-1}^{(i)}\left\langle p_{k|k-1}^{(i)}, \psi_{k,\mathbf{z}_k}\right\rangle}{1-r_{k|k-1}^{(i)}\left\langle p_{k|k-1}^{(i)}, p_{D,k}\right\rangle} - \frac{r_{k|k-1}^{(i),L_{k|k-1}^{(i)}}\left\langle p_{k|k-1}^{(i),L_{k|k-1}^{(i)}}, \psi_{k,\mathbf{z}_k}\right\rangle}{1-r_{k|k-1}^{(i),L_{k|k-1}^{(i)}}\left\langle p_{k|k-1}^{(i),L_{k|k-1}^{(i)}}, p_{D,k}\right\rangle}\right)^2\right]^{1/2} \tag{A.40}$$

(adding and subtracting a new term)

$$= E\left[\left(\frac{r_{k|k-1}^{(i),L_{k|k-1}^{(i)}}\left\langle p_{k|k-1}^{(i),L_{k|k-1}^{(i)}},\psi_{k,\mathbf{z}_k}\right\rangle}{1-r_{k|k-1}^{(i),L_{k|k-1}^{(i)}}\left\langle p_{k|k-1}^{(i),L_{k|k-1}^{(i)}},p_{D,k}\right\rangle}-\frac{r_{k|k-1}^{(i)}\left\langle p_{k|k-1}^{(i)},\psi_{k,\mathbf{z}_k}\right\rangle}{1-r_{k|k-1}^{(i),L_{k|k-1}^{(i)}}\left\langle p_{k|k-1}^{(i),L_{k|k-1}^{(i)}},p_{D,k}\right\rangle}\right.\right.$$
$$\left.\left.+\frac{r_{k|k-1}^{(i)}\left\langle p_{k|k-1}^{(i)},\psi_{k,\mathbf{z}_k}\right\rangle}{1-r_{k|k-1}^{(i),L_{k|k-1}^{(i)}}\left\langle p_{k|k-1}^{(i),L_{k|k-1}^{(i)}},p_{D,k}\right\rangle}-\frac{r_{k|k-1}^{(i)}\left\langle p_{k|k-1}^{(i)},\psi_{k,\mathbf{z}_k}\right\rangle}{1-r_{k|k-1}^{(i)}\left\langle p_{k|k-1}^{(i)},p_{D,k}\right\rangle}\right)^2\right]^{1/2} \tag{A.41}$$

(using Minkowski's inequality)

$$\leq E\left[\left(\frac{r_{k|k-1}^{(i),L_{k|k-1}^{(i)}}\left\langle p_{k|k-1}^{(i),L_{k|k-1}^{(i)}},\psi_{k,\mathbf{z}_k}\right\rangle-r_{k|k-1}^{(i)}\left\langle p_{k|k-1}^{(i)},\psi_{k,\mathbf{z}_k}\right\rangle}{1-r_{k|k-1}^{(i),L_{k|k-1}^{(i)}}\left\langle p_{k|k-1}^{(i),L_{k|k-1}^{(i)}},p_{D,k}\right\rangle}\right)^2\right]^{1/2}$$
$$+\frac{r_{k|k-1}^{(i)}\left\langle p_{k|k-1}^{(i)},\psi_{k,\mathbf{z}_k}\right\rangle}{1-r_{k|k-1}^{(i)}\left\langle p_{k|k-1}^{(i)},p_{D,k}\right\rangle}E\left[\left(\frac{r_{k|k-1}^{(i),L_{k|k-1}^{(i)}}\left\langle p_{k|k-1}^{(i),L_{k|k-1}^{(i)}},p_{D,k}\right\rangle-r_{k|k-1}^{(i)}\left\langle p_{k|k-1}^{(i)},p_{D,k}\right\rangle}{1-r_{k|k-1}^{(i),L_{k|k-1}^{(i)}}\left\langle p_{k|k-1}^{(i),L_{k|k-1}^{(i)}},p_{D,k}\right\rangle}\right)^2\right]^{1/2} \tag{A.42}$$

(by $0 \leq r_{k|k-1}^{(i),L_{k|k-1}^{(i)}} \leq 1$, Assumption 2 and (A.4))

$$\leq \frac{\left\|\psi_{k,\mathbf{z}_k}\right\|E\left[\left(r_{k|k-1}^{(i),L_{k|k-1}^{(i)}}-r_{k|k-1}^{(i)}\right)^2\right]^{1/2}+r_{k|k-1}^{(i)}E\left[\left(\left\langle p_{k|k-1}^{(i),L_{k|k-1}^{(i)}},\psi_{k,\mathbf{z}_k}\right\rangle-\left\langle p_{k|k-1}^{(i)},\psi_{k,\mathbf{z}_k}\right\rangle\right)^2\right]^{1/2}}{1-\left\|p_{D,k}\right\|}$$
$$+\frac{r_{k|k-1}^{(i)}\left\langle p_{k|k-1}^{(i)},\psi_{k,\mathbf{z}_k}\right\rangle}{1-r_{k|k-1}^{(i)}\left\langle p_{k|k-1}^{(i)},p_{D,k}\right\rangle}$$
$$\times\frac{\left\|p_{D,k}\right\|E\left[\left(r_{k|k-1}^{(i),L_{k|k-1}^{(i)}}-r_{k|k-1}^{(i)}\right)^2\right]^{1/2}+r_{k|k-1}^{(i)}E\left[\left(\left\langle p_{k|k-1}^{(i),L_{k|k-1}^{(i)}},p_{D,k}\right\rangle-\left\langle p_{k|k-1}^{(i)},p_{D,k}\right\rangle\right)^2\right]^{1/2}}{1-\left\|p_{D,k}\right\|} \tag{A.43}$$

(by (4.8), (4.9), and $0 \le r_{k|k-1}^{(i)} \le 1$)

$$\le \frac{\|\psi_{k,\mathbf{z}_k}\|\left(\sqrt{c_{k|k-1}}+\sqrt{d_{k|k-1}}\right)}{\left(1-\|p_{D,k}\|\right)^2\sqrt{L_{k|k-1}^{(i)}}}. \tag{A.44}$$

From (2.12), $0 \le r_{k|k-1}^{(i)} \le 1$ and Assumption 2, the denominator of (A.39) is

$$\begin{aligned}\sum_{i=1}^{M_{k|k-1}} r_{\alpha,k}^{(i)}(\mathbf{z}_k) &= \sum_{i=1}^{M_{k|k-1}} \frac{r_{k|k-1}^{(i)}\left\langle p_{k|k-1}^{(i)}, \psi_{k,\mathbf{z}_k}\right\rangle}{1-r_{k|k-1}^{(i)}\left\langle p_{k|k-1}^{(i)}, p_{D,k}\right\rangle} \ge \sum_{i=1}^{M_{k|k-1}} r_{k|k-1}^{(i)}\left\langle p_{k|k-1}^{(i)}, \psi_{k,\mathbf{z}_k}\right\rangle \\ &\ge \inf\left(\psi_{k,\mathbf{z}_k}\right)\sum_{i=1}^{M_{k|k-1}} r_{k|k-1}^{(i)} = \inf\left(\psi_{k,\mathbf{z}_k}\right)n_{k|k-1},\end{aligned} \tag{A.45}$$

where $n_{k|k-1} = \sum_{i=1}^{M_{k|k-1}} r_{k|k-1}^{(i)}$ is the number of the predicted targets at time $k$.

Substituting (A.44) and (A.43) into (A.39), we get

$$\begin{aligned}E\left[\left(r_{U,k}^{L_{k|k-1}^{(i)}}(\mathbf{z}_k) - r_{U,k}(\mathbf{z}_k)\right)^2\right]^{1/2} &\le \frac{2\|\psi_{k,\mathbf{z}_k}\|\left(\sqrt{c_{k|k-1}}+\sqrt{d_{k|k-1}}\right)}{\left(1-\|p_{D,k}\|\right)^2\inf\left(\psi_{k,\mathbf{z}_k}\right)n_{k|k-1}}\sum_{i=1}^{M_{k|k-1}}\left(\frac{1}{\sqrt{L_{k|k-1}^{(i)}}}\right) \\ &\le \frac{2\|\psi_{k,\mathbf{z}_k}\|\left(\sqrt{c_{k|k-1}}+\sqrt{d_{k|k-1}}\right)M_{k|k-1}}{\inf\left(\psi_{k,\mathbf{z}_k}\right)n_{k|k-1}\left(1-\|p_{D,k}\|\right)^2\sqrt{L_{k|k-1}^{\min}}},\end{aligned} \tag{A.46}$$

where $L_{k|k-1}^{\min} = \min\left(L_{k|k-1}^{(1)}, \ldots, L_{k|k-1}^{(M_{k|k-1})}\right)$, $\min(\cdot)$ denotes the minimum.

Finally, (4.12) is proved with

$$c_{U,k} = \left(\frac{2\|\psi_{k,\mathbf{z}_k}\|\left(\sqrt{c_{k|k-1}}+\sqrt{d_{k|k-1}}\right)M_{k|k-1}}{\inf\left(\psi_{k,\mathbf{z}_k}\right)n_{k|k-1}\left(1-\|p_{D,k}\|\right)^2}\right)^2. \tag{A.47}$$

Now, turn to (4.13). First, from (2.12), $0 \le r_{k|k-1}^{(i)} \le 1$ and Assumption 2, we have

$$r_{\alpha,k}^{(i)}(\mathbf{z}_k) = \frac{r_{k|k-1}^{(i)}\left\langle p_{k|k-1}^{(i)}, \psi_{k,\mathbf{z}_k}\right\rangle}{1-r_{k|k-1}^{(i)}\left\langle p_{k|k-1}^{(i)}, p_{D,k}\right\rangle} \le \frac{\|\psi_{k,\mathbf{z}_k}\|}{1-\|p_{D,k}\|}. \tag{A.48}$$

Then, from (2.13), (3.11), and (A.39), we get

$$E\left[\left(r_{U,k}^{*,L_{k|k-1}^{(i)}}(\mathbf{z}_k)-r_{U,k}^{*}(\mathbf{z}_k)\right)^2\right]^{1/2}$$
$$\leq \frac{\sum_{i=1}^{M_{k|k-1}}\left(E\left[\left(\begin{array}{c} r_{\alpha,k}^{(i),L_{k|k-1}^{(i)}}(\mathbf{z}_k) \\ -r_{\alpha,k}^{(i)}(\mathbf{z}_k)\end{array}\right)^2\right]^{1/2}+E\left[\left(\begin{array}{c} \dfrac{r_{\alpha,k}^{(i),L_{k|k-1}^{(i)}}(\mathbf{z}_k)\left(1-r_{k|k-1}^{(i),L_{k|k-1}^{(i)}}\right)}{1-r_{k|k-1}^{(i),L_{k|k-1}^{(i)}}\left\langle p_{k|k-1}^{(i),L_{k|k-1}^{(i)}},p_{D,k}\right\rangle} \\ -\dfrac{r_{\alpha,k}^{(i)}(\mathbf{z}_k)\left(1-r_{k|k-1}^{(i)}\right)}{1-r_{k|k-1}^{(i)}\left\langle p_{k|k-1}^{(i)},p_{D,k}\right\rangle}\end{array}\right)^2\right]^{1/2}\right)}{\sum_{i=1}^{M_{k|k-1}} r_{\alpha,k}^{(i)}(\mathbf{z}_k)} \tag{A.49}$$

(adding and subtracting a new term in the second expectation in the summation)

$$\leq \frac{\sum_{i=1}^{M_{k|k-1}}\left(\begin{array}{l} E\left[\left(r_{\alpha,k}^{(i),L_{k|k-1}^{(i)}}(\mathbf{z}_k)-r_{\alpha,k}^{(i)}(\mathbf{z}_k)\right)^2\right]^{1/2} \\ +E\left[\left(\begin{array}{c} \dfrac{r_{\alpha,k}^{(i),L_{k|k-1}^{(i)}}(\mathbf{z}_k)\left(1-r_{k|k-1}^{(i),L_{k|k-1}^{(i)}}\right)}{1-r_{k|k-1}^{(i),L_{k|k-1}^{(i)}}\left\langle p_{k|k-1}^{(i),L_{k|k-1}^{(i)}},p_{D,k}\right\rangle}-\dfrac{r_{\alpha,k}^{(i)}(\mathbf{z}_k)\left(1-r_{k|k-1}^{(i)}\right)}{1-r_{k|k-1}^{(i)}\left\langle p_{k|k-1}^{(i)},p_{D,k}\right\rangle} \\ +\dfrac{r_{\alpha,k}^{(i)}(\mathbf{z}_k)\left(1-r_{k|k-1}^{(i)}\right)}{1-r_{k|k-1}^{(i),L_{k|k-1}^{(i)}}\left\langle p_{k|k-1}^{(i),L_{k|k-1}^{(i)}},p_{D,k}\right\rangle}-\dfrac{r_{\alpha,k}^{(i)}(\mathbf{z}_k)\left(1-r_{k|k-1}^{(i)}\right)}{1-r_{k|k-1}^{(i)}\left\langle p_{k|k-1}^{(i)},p_{D,k}\right\rangle}\end{array}\right)^2\right]^{1/2}\end{array}\right)}{\sum_{i=1}^{M_{k|k-1}} r_{\alpha,k}^{(i)}(\mathbf{z}_k)} \tag{A.50}$$

It holds that (using Minkowski's inequality for the second term in the summation)

$$\leq \frac{\sum_{i=1}^{M_{k|k-1}}\left(\begin{array}{l} E\left[\left(r_{\alpha,k}^{(i),L_{k|k-1}^{(i)}}(\mathbf{z}_k)-r_{\alpha,k}^{(i)}(\mathbf{z}_k)\right)^2\right]^{1/2} \\ +E\left[\left(\dfrac{r_{\alpha,k}^{(i),L_{k|k-1}^{(i)}}(\mathbf{z}_k)-r_{\alpha,k}^{(i)}(\mathbf{z}_k)+r_{\alpha,k}^{(i)}(\mathbf{z}_k)r_{k|k-1}^{(i)}-r_{\alpha,k}^{(i),L_{k|k-1}^{(i)}}(\mathbf{z}_k)r_{k|k-1}^{(i),L_{k|k-1}^{(i)}}}{1-r_{k|k-1}^{(i),L_{k|k-1}^{(i)}}\left\langle p_{k|k-1}^{(i),L_{k|k-1}^{(i)}},p_{D,k}\right\rangle}\right)^2\right]^{1/2} \\ +\dfrac{r_{\alpha,k}^{(i)}(\mathbf{z}_k)\left(1-r_{k|k-1}^{(i)}\right)}{1-r_{k|k-1}^{(i)}\left\langle p_{k|k-1}^{(i)},p_{D,k}\right\rangle}E\left[\left(\dfrac{r_{k|k-1}^{(i),L_{k|k-1}^{(i)}}\left\langle p_{k|k-1}^{(i),L_{k|k-1}^{(i)}},p_{D,k}\right\rangle-r_{k|k-1}^{(i)}\left\langle p_{k|k-1}^{(i)},p_{D,k}\right\rangle}{1-r_{k|k-1}^{(i),L_{k|k-1}^{(i)}}\left\langle p_{k|k-1}^{(i),L_{k|k-1}^{(i)}},p_{D,k}\right\rangle}\right)^2\right]^{1/2}\end{array}\right)}{\sum_{i=1}^{M_{k|k-1}} r_{\alpha,k}^{(i)}(\mathbf{z}_k)} \tag{A.51}$$

(by $0 \le r_{k|k-1}^{(i),L_{k|k-1}^{(i)}} \le 1$, (A.4), and Minkowski's inequality)

$$\le \frac{\sum_{i=1}^{M_{k|k-1}} \left( \begin{array}{l} (2-\|p_{D,k}\|) E\left[ \left( r_{\alpha,k}^{(i),L_{k|k-1}^{(i)}}(\mathbf{z}_k) - r_{\alpha,k}^{(i)}(\mathbf{z}_k) \right)^2 \right]^{1/2} \\ +E\left[ \left( \begin{array}{l} r_{\alpha,k}^{(i)}(\mathbf{z}_k) r_{k|k-1}^{(i)} - r_{\alpha,k}^{(i)}(\mathbf{z}_k) r_{k|k-1}^{(i),L_{k|k-1}^{(i)}} \\ +r_{\alpha,k}^{(i)}(\mathbf{z}_k) r_{k|k-1}^{(i),L_{k|k-1}^{(i)}} - r_{\alpha,k}^{(i),L_{k|k-1}^{(i)}}(\mathbf{z}_k) r_{k|k-1}^{(i),L_{k|k-1}^{(i)}} \end{array} \right)^2 \right]^{1/2} \\ +\dfrac{r_{\alpha,k}^{(i)}(\mathbf{z}_k)\left(1-r_{k|k-1}^{(i)}\right)}{1-r_{k|k-1}^{(i)}\left\langle p_{k|k-1}^{(i)}, p_{D,k} \right\rangle} \left( \begin{array}{l} \|p_{D,k}\| E\left[ \left( r_{k|k-1}^{(i),L_{k|k-1}^{(i)}} - r_{k|k-1}^{(i)} \right)^2 \right]^{1/2} \\ +r_{k|k-1}^{(i)} E\left[ \left( \left\langle p_{k|k-1}^{(i),L_{k|k-1}^{(i)}}, p_{D,k} \right\rangle - \left\langle p_{k|k-1}^{(i)}, p_{D,k} \right\rangle \right)^2 \right]^{1/2} \end{array} \right) \end{array} \right)}{\left(1-\|p_{D,k}\|\right) \sum_{i=1}^{M_{k|k-1}} r_{\alpha,k}^{(i)}(\mathbf{z}_k)} \tag{A.52}$$

(using $0 \le r_{k|k-1}^{(i),L_{k|k-1}^{(i)}} \le 1$ and Minkowski's inequality again for the second term in the summation)

$$\le \frac{\sum_{i=1}^{M_{k|k-1}} \left( \begin{array}{l} (3-\|p_{D,k}\|) E\left[ \left( r_{\alpha,k}^{(i),L_{k|k-1}^{(i)}}(\mathbf{z}_k) - r_{\alpha,k}^{(i)}(\mathbf{z}_k) \right)^2 \right]^{1/2} + r_{\alpha,k}^{(i)}(\mathbf{z}_k) E\left[ \left( r_{k|k-1}^{(i)} - r_{k|k-1}^{(i),L_{k|k-1}^{(i)}} \right)^2 \right]^{1/2} \\ +\dfrac{r_{\alpha,k}^{(i)}(\mathbf{z}_k)\left(1-r_{k|k-1}^{(i)}\right)}{1-r_{k|k-1}^{(i)}\left\langle p_{k|k-1}^{(i)}, p_{D,k} \right\rangle} \left( \begin{array}{l} \|p_{D,k}\| E\left[ \left( r_{k|k-1}^{(i),L_{k|k-1}^{(i)}} - r_{k|k-1}^{(i)} \right)^2 \right]^{1/2} \\ +r_{k|k-1}^{(i)} E\left[ \left( \left\langle p_{k|k-1}^{(i),L_{k|k-1}^{(i)}}, p_{D,k} \right\rangle - \left\langle p_{k|k-1}^{(i)}, p_{D,k} \right\rangle \right)^2 \right]^{1/2} \end{array} \right) \end{array} \right)}{\left(1-\|p_{D,k}\|\right) \sum_{i=1}^{M_{k|k-1}} r_{\alpha,k}^{(i)}(\mathbf{z}_k)} \tag{A.53}$$

(by $0 \le r_{k|k-1}^{(i)} \le 1$, (4.8), (4.9) (A.44), (A.45), and Assumption 2)

$$\begin{aligned} &\le \frac{\|\psi_{k,\mathbf{z}_k}\| \left( \sqrt{c_{k|k-1}} + \sqrt{d_{k|k-1}} \right)}{\left(1-\|p_{D,k}\|\right)^3 \inf(\psi_{k,\mathbf{z}_k}) n_{k|k-1}} \sum_{i=1}^{M_{k|k-1}} \left( \frac{4 - \left( r_{k|k-1}^{(i)} + 1 \right) \|p_{D,k}\|}{\sqrt{L_{k|k-1}^{(i)}}} \right) \\ &\le \frac{\|\psi_{k,\mathbf{z}_k}\| \left( \sqrt{c_{k|k-1}} + \sqrt{d_{k|k-1}} \right) \left( 4M_{k|k-1} - \left( n_{k|k-1} + M_{k|k-1} \right) \|p_{D,k}\| \right)}{\left(1-\|p_{D,k}\|\right)^3 \inf(\psi_{k,\mathbf{z}_k}) n_{k|k-1} \sqrt{L_{k|k-1}^{\min}}}. \end{aligned} \tag{A.54}$$

Finally, (4.13) is proved with

$$c^*_{U,k} = \left( \frac{\|\psi_{k,\mathbf{z}_k}\| \left( \sqrt{c_{k|k-1}} + \sqrt{d_{k|k-1}} \right)}{\left(1 - \|p_{D,k}\|\right)^3 \inf(\psi_{k,\mathbf{z}_k})} \left( \frac{\left(4 - \|p_{D,k}\|\right) M_{k|k-1}}{n_{k|k-1}} - \|p_{D,k}\| \right) \right)^2. \tag{A.55}$$

Now turn to (4.14). From (2.10) and (3.12), we get

$$\begin{aligned} & E\left[ \left( \langle p_{U,k}(\cdot;\mathbf{z}_k), \varphi \rangle - \left\langle p_{U,k}^{L_{k|k-1}^{(i)}}(\cdot;\mathbf{z}_k), \varphi \right\rangle \right)^2 \right]^{1/2} \\ & \quad = E\left[ \left( \frac{\left\langle \sum_{i=1}^{M_{k|k-1}} p_{\alpha,k}^{(i),L_{k|k-1}^{(i)}}(\mathbf{x}_k;\mathbf{z}_k), \varphi \right\rangle}{\sum_{i=1}^{M_{k|k-1}} r_{\alpha,k}^{(i),L_{k|k-1}^{(i)}}(\mathbf{z}_k)} - \frac{\left\langle \sum_{i=1}^{M_{k|k-1}} p_{\alpha,k}^{(i)}(\mathbf{x}_k;\mathbf{z}_k), \varphi \right\rangle}{\sum_{i=1}^{M_{k|k-1}} r_{\alpha,k}^{(i)}(\mathbf{z}_k)} \right)^2 \right]^{1/2} \end{aligned} \tag{A.56}$$

(adding and subtracting a new term)

$$\begin{aligned} = E\Bigg[ \Bigg( & \frac{\left\langle \sum_{i=1}^{M_{k|k-1}} p_{\alpha,k}^{(i),L_{k|k-1}^{(i)}}(\cdot;\mathbf{z}_k), \varphi \right\rangle}{\sum_{i=1}^{M_{k|k-1}} r_{\alpha,k}^{(i),L_{k|k-1}^{(i)}}(\mathbf{z}_k)} - \frac{\left\langle \sum_{i=1}^{M_{k|k-1}} p_{\alpha,k}^{(i),L_{k|k-1}^{(i)}}(\cdot;\mathbf{z}_k), \varphi \right\rangle}{\sum_{i=1}^{M_{k|k-1}} r_{\alpha,k}^{(i)}(\mathbf{z}_k)} \\ & + \frac{\left\langle \sum_{i=1}^{M_{k|k-1}} p_{\alpha,k}^{(i),L_{k|k-1}^{(i)}}(\cdot;\mathbf{z}_k), \varphi \right\rangle}{\sum_{i=1}^{M_{k|k-1}} r_{\alpha,k}^{(i)}(\mathbf{z}_k)} - \frac{\left\langle \sum_{i=1}^{M_{k|k-1}} p_{\alpha,k}^{(i)}(\cdot;\mathbf{z}_k), \varphi \right\rangle}{\sum_{i=1}^{M_{k|k-1}} r_{\alpha,k}^{(i)}(\mathbf{z}_k)} \Bigg)^2 \Bigg]^{1/2} \end{aligned} \tag{A.57}$$

(using Minkowski's inequality)

$$\begin{aligned} \leq E\Bigg[ & \left( \left\langle \sum_{i=1}^{M_{k|k-1}} p_{\alpha,k}^{(i),L_{k|k-1}^{(i)}}(\cdot;\mathbf{z}_k), \varphi \right\rangle \left( \frac{\sum_{i=1}^{M_{k|k-1}} r_{\alpha,k}^{(i),L_{k|k-1}^{(i)}}(\mathbf{z}_k) - \sum_{i=1}^{M_{k|k-1}} r_{\alpha,k}^{(i)}(\mathbf{z}_k)}{\sum_{i=1}^{M_{k|k-1}} r_{\alpha,k}^{(i)}(\mathbf{z}_k) \sum_{i=1}^{M_{k|k-1}} r_{\alpha,k}^{(i),L_{k|k-1}^{(i)}}(\mathbf{z}_k)} \right) \right)^2 \Bigg]^{1/2} \\ & + \frac{E\left[ \left( \left\langle \sum_{i=1}^{M_{k|k-1}} p_{\alpha,k}^{(i),L_{k|k-1}^{(i)}}(\cdot;\mathbf{z}_k) - \sum_{i=1}^{M_{k|k-1}} p_{\alpha,k}^{(i)}(\cdot;\mathbf{z}_k), \varphi \right\rangle \right)^2 \right]^{1/2}}{\sum_{i=1}^{M_{k|k-1}} r_{\alpha,k}^{(i)}(\mathbf{z}_k)} \end{aligned} \tag{A.58}$$

(by (2.12) and (3.14))

$$\leq \frac{2\|\varphi\|}{\sum_{i=1}^{M_{k|k-1}} r_{\alpha,k}^{(i)}(\mathbf{z}_k)} E\left[ \left( \sum_{i=1}^{M_{k|k-1}} r_{\alpha,k}^{(i),L_{k|k-1}^{(i)}}(\mathbf{z}_k) - \sum_{i=1}^{M_{k|k-1}} r_{\alpha,k}^{(i)}(\mathbf{z}_k) \right)^2 \right]^{1/2} \tag{A.59}$$

(by (A.39) and (A.47))

$$\leq \frac{\|\varphi\|}{\sqrt{L_{k|k-1}^{\min}}} c_{U,k}. \tag{A.60}$$

Finally, (4.14) is proved with

$$d_{U,k} = c_{U,k} = \left( \frac{2\|\psi_{k,\mathbf{z}_k}\| \left( \sqrt{c_{k|k-1}} + \sqrt{d_{k|k-1}} \right) M_{k|k-1.}}{\inf(\psi_{k,\mathbf{z}_k}) n_{k|k-1} (1 - \|p_{D,k}\|)^2} \right)^2. \tag{A.61}$$

This completes the proof.

## Nomenclature

| | |
|---|---|
| $\mathbf{x}_k$: | State vector of a single target at time $k$ |
| $\mathbf{z}_k$: | Single measurement vector at time $k$ |
| $n_k$: | Number of existing targets at time $k$ |
| $m_k$: | Number of measurements collected at time $k$ |
| $X_k = \{\mathbf{x}_{i,k}\}_{i=1}^{n_k}$: | Finite set of multitarget state-vectors at time $k$ |
| $Z_k = \{\mathbf{z}_{i,k}\}_{i=1}^{m_k}$: | Finite set of measurements collected at time $k$ |
| $f_{k\|k-1}(\mathbf{x}_k \mid \mathbf{x}_{k-1})$: | Single-target Markov transition density at time $k$ |
| $p_{S,k}(\mathbf{x}_{k-1})$: | Probability of target survival at time $k$ |
| $p_{D,k}(\mathbf{x}_k)$: | Probability of detection at time $k$ |
| $\kappa_k(\mathbf{z}_k)$: | Intensity of Poisson clutter process at time $k$ |
| $\psi_{k,\mathbf{z}_k}(\mathbf{x}_k) = f_k(\mathbf{z}_k \mid \mathbf{x}_k)$: | Single-sensor/target likelihood density at time $k$ |
| $\delta_{\mathbf{x}}(\cdot)$: | Dirac delta function centered at $\mathbf{x}$ |
| $\mathbb{R}^d$: | $d$-dimensional real space |
| $C_b(\mathbb{R}^d)$: | Set of continuous bounded functions on $\mathbb{R}^d$ |
| $B(\mathbb{R}^d)$: | Set of bounded Borel measurable functions on $\mathbb{R}^d$ |
| $\pi(Y^{(i)})$: | Probability density of a Bernoulli random finite set (RFS) $Y^{(\mathbf{i})}$ |
| $\pi(Y)$: | Probability density of multi-Bernoulli RFS $Y = \bigcup_{i=1}^{M} Y^{(i)}$ |
| $\pi = \{(r^{(i)}, p^{(i)})\}_{i=1}^{M}$: | Abbreviation of $\pi(Y)$. $\{(r^{(i)}, p^{(i)})\}_{i=1}^{M}$ is the multi-Bernoulli parameter set |
| $\tilde{\pi} = \{(r^{(i),L^{(i)}}, p^{(i),L^{(i)}})\}_{i=1}^{M}$: | Particle approximation of $\pi = \{(r^{(i)}, p^{(i)})\}_{i=1}^{M}$. $(r^{(i),L^{(i)}}, p^{(i),L^{(i)}})$ denotes that $(r^{(i)}, p^{(i)})$ is comprised of the number $L^{(i)}$ of the particles |
| $\|\cdot\|$: | Supremum norm. $\|\varphi\| \triangleq \sup(\mid \varphi \mid)$, $\sup(\cdot)$ denotes the supremum |
| $\langle \cdot, \cdot \rangle$: | Inner product. If the measure in $\langle \cdot, \cdot \rangle$ is continuous, it defines the integral inner product; if the measure in $\langle \cdot, \cdot \rangle$ is discrete, it defines the summation inner product. |

## Acknowledgments

This research work was supported by the Natural Science Foundation of China (61004087, 61104051, 61005026), China Postdoctoral Science Foundation (20100481338), and Fundamental Research Funds for the Central University.

## References


[1] I. R. Goodman, R. P. S. Mahler, and H. T. Nguyen, *Mathematics of Data Fusion*, vol. 37 of *Theory and Decision Library B*, Kluwer Academic Publishers, Norwood, Mass, USA, 1997.

[2] R. Mahler, *Statistical Multisource Multitarget Information Fusion*, Artech House, Norwood, Mass, USA, 2007.

[3] R. Mahler, "Multi-target Bayes filtering via first-order multi-target moments," *IEEE Transactions on Aerospace and Electronic Systems*, vol. 39, no. 4, pp. 1152–1178, 2003.

[4] R. Mahler, "PHD filters of higher order in target number," *IEEE Transactions on Aerospace and Electronic Systems*, vol. 43, no. 3, pp. 1523–1543, 2007.

[5] T. Zajic and R. Mahler, "A particle-systems implementation of the PHD multitarget tracking filter," *Proceedings of Spie—the International Society for Optical Engineering*, vol. 5096, pp. 291–299, 2003.

[6] H. Sidenbladh, "Multi-target particle filtering for the probability hypothesis density," in *Proceedings of the 6th International Conference on Information Fusion*, pp. 800–806, Cairns, Australia, 2003.

[7] B. N. Vo, S. Singh, and A. Doucet, "Sequential Monte Carlo methods for multi-target filtering with random finite sets," *IEEE Transactions on Aerospace and Electronic Systems*, vol. 41, no. 4, pp. 1224–1245, 2005.

[8] B.-N. VO and W. K. MA, "The Gaussian mixture probability hypothesis density filter," *IEEE Transactions on Signal Processing*, vol. 54, no. 11, pp. 4091–4104, 2006.

[9] B.-T. Vo, B.-N. Vo, and A. Cantoni, "Analytic implementations of the cardinalized probability hypothesis density filter," *IEEE Transactions on Signal Processing*, vol. 55, no. 7, pp. 3553–3567, 2007.

[10] D. E. Clark and J. Bell, "Multi-target state estimation and track continuity for the particle PHD filter," *IEEE Transactions on Aerospace and Electronic Systems*, vol. 43, no. 4, pp. 1441–1453, 2007.

[11] W. F. Liu, C. Z. Han, F. Lian, and H. Y. Zhu, "Multitarget state extraction for the PHD filter using MCMC approach," *IEEE Transactions on Aerospace and Electronic Systems*, vol. 46, no. 2, pp. 864–883, 2010.

[12] B.-T. Vo, B.-N. Vo, and A. Cantoni, "The cardinality balanced multi-target multi-Bernoulli filter and its implementations," *IEEE Transactions on Signal Processing*, vol. 57, no. 2, pp. 409–423, 2009.

[13] D. E. Clark and J. Bell, "Convergence results for the particles PHD filter," *IEEE Transactions on Signal Processing*, vol. 54, no. 7, pp. 2652–2661, 2006.

[14] D. Clark and B.-N. Vo, "Convergence analysis of the Gaussian mixture PHD filter," *IEEE Transactions on Signal Processing*, vol. 55, no. 4, pp. 1204–1212, 2007.

[15] P. Cholamjiak, S. Suantai, and Y. J. Cho, "Strong convergence to solutions of generalized mixed equilibrium problems with applications," *Journal of Applied Mathematics*, vol. 2012, Article ID 308791, 18 pages, 2012.

[16] V. Colao, "On the convergence of iterative processes for generalized strongly asymptotically $\varphi$-pseudocontractive mappings in Banach spaces," *Journal of Applied Mathematics*, vol. 2012, Article ID 563438, 18 pages, 2012.

[17] G. Gu, S. Wang, and Y. J. Cho, "Strong convergence algorithms for hierarchical fixed points problems and variational inequalities," *Journal of Applied Mathematics*, vol. 2011, Article ID 164978, 17 pages, 2011.

[18] C. Zhu and G. Yin, "Feller continuity, recurrence, and stabilization of regime-switching diffusions," in *Proceedings of the 49th Conference on Decision and Control (CDC '10)*, pp. 667–672, Atlanta, Ga, USA, 2010.

[19] D. Crisan and A. Doucet, "A survey of convergence results on particle filtering methods for practitioners," *IEEE Transactions on Signal Processing*, vol. 50, no. 3, pp. 736–746, 2002.

[20] D. Schuhmacher, B.-T. Vo, and B.-N. Vo, "A consistent metric for performance evaluation of multi-object filters," *IEEE Transactions on Signal Processing*, vol. 56, no. 8, pp. 3447–3457, 2008.

Hindawi Publishing Corporation
Journal of Applied Mathematics
Volume 2012, Article ID 487246, 20 pages
doi:10.1155/2012/487246

*Research Article*

# A Mixed Prediction Model of Ground Subsidence for Civil Infrastructures on Soft Ground

**Kiyoshi Kobayashi[1] and Kiyoyuki Kaito[2]**

[1] *Graduate School of Management, Kyoto University, Yoshida-Honmachi, Sakyo-ku, Kyoto 606-8501, Japan*
[2] *Department of Civil Engineering, Osaka University, 2-1 Yamada-oka, Suita, Osaka 565-0871, Japan*

Correspondence should be addressed to Kiyoshi Kobayashi, kobayashi.kiyoshi.6n@kyoto-u.ac.jp

Received 2 April 2012; Accepted 23 June 2012

Academic Editor: Qiang Ling



The estimation of ground subsidence processes is an important subject for the asset management of civil infrastructures on soft ground, such as airport facilities. In the planning and design stage, there exist many uncertainties in geotechnical conditions, and it is impossible to estimate the ground subsidence process by deterministic methods. In this paper, the sets of sample paths designating ground subsidence processes are generated by use of a one-dimensional consolidation model incorporating inhomogeneous ground subsidence. Given the sample paths, the mixed subsidence model is presented to describe the probabilistic structure behind the sample paths. The mixed model can be updated by the Bayesian methods based upon the newly obtained monitoring data. Concretely speaking, in order to estimate the updating models, Markov Chain Monte Calro method, which is the frontier technique in Bayesian statistics, is applied. Through a case study, this paper discussed the applicability of the proposed method and illustrated its possible application and future works.

## 1. Introduction

In Japan, it is not rare to build airports on man-made islands or reclamation land. In these offshore airports, the airport pavement may be damaged due to the ground's inhomogeneous subsidence. If the performance standard regarding airport pavement gradients is not satisfied, due to the progression of ground subsidence, large-scale repair work on concrete pavement is necessary. Therefore, predicting future ground subsidence is an important issue for asset management strategy of airport pavements.

Ground subsidence estimation models using the consolidation theory have been developed for soft ground [1]. However, there are many uncertainties in the actual ground conditions, and it is extremely difficult to deterministically predict the process of ground subsidence. Therefore, a method of probabilistically predicting the process of

ground subsidence using a one-dimensional consolidation model that takes inhomogeneous subsidence into consideration, and using soil constants that show ground conditions as random variables, was developed [2]. With these probabilistic ground subsidence models, soil constants are generated with Monte Carlo simulation, and sample paths of the process of ground subsidence are simulated in accordance.

In this paper, a statistical ground subsidence model (hereinafter, mixed ground subsidence model) is expressed as the aggregation of sample paths sought by probabilistic ground subsidence models. Then, a mixed ground subsidence model, which employs monitoring information of ground subsidence after the establishment of airports, and sequentially performs Bayesian updating on weight coefficients of sample paths, is proposed. With this method, the accuracy of estimation of ground subsidence using monitoring information can be improved sequentially. The estimation accuracy of the mixed ground subsidence model depends on the method of generation of sample paths and its estimation accuracy.

With the above issues, this paper proposes a mixed ground subsidence model targeted for offshore airports. In the following sections, Section 2 organizes the basic idea of the study, Section 3 formulates a mixed ground subsidence model using the sample paths, Section 4 proposes a Bayesian updating model, and Section 5 introduces a numerical calculation example.

## 2. Basic Approach of This Study

### *2.1. Mixed Ground Subsidence Model*

The target period is divided into two periods: before the airport was in service and after it began services. The former period shall be defined as the planning phase, and the latter the operating phase. For the planning phase, there is no monitoring information regarding ground subsidence process. Therefore, it becomes an issue to predict the amount of ground subsidence over the years for each mesh, using the first model (probabilistic one-dimensional consolidation model). The airport manager performs necessary boring tests during the planning phase and acquires data on ground subsidence. Data acquired by boring tests is partial information regarding ground subsidence, and not complete information. Therefore, the process of ground subsidence cannot be definitely predicted. Consequently, for the planning phase, several scenarios of ground subsidence will be established and sample paths of ground subsidence process for each mesh will be acquired. Then, using the sample information, the statistical regularity of the process of ground subsidence is expressed using the second model. From the second model, it is possible to express the probabilistic distribution of the deterioration process. Next, the operating phase is considered. From the point when the airport begins services, the airport manager continuously monitors ground subsidence amount for each mesh. The airport manager uses the monitoring information of the ground subsidence amount to conduct Bayesian updating on the second model and formulates the third model. The ground subsidence estimation model proposed in this paper is a composite estimation model comprising the following: (1) the probabilistic one-dimensional consolidation model (first model) that generates sample paths of the ground subsidence process, (2) the mixed ground subsidence model (second model) that expresses the statistical regularity of the sample paths generated with the first model, and (3) the third model updated by Bayesian updating on the second model using new monitoring information acquired as time passes.

In this paper, the subsidence process of airport ground is expressed using a probabilistic one-dimensional consolidation model, with consideration to the process of inhomogeneous ground subsidence. Therefore, the targeted airport ground is divided into planar meshes and also uses a three-dimensional model that divides meshes perpendicular to each planar mesh. By using the first model, the change over time in the amount of ground subsidence can be predicted for each planar mesh. However, there are many uncertainties in ground conditions. Therefore, using a one-dimensional consolidation model with randomly sampled ground conditions, multiple ground subsidence scenarios will be generated. The ground condition of each three-dimensional mesh is established by random generation. If the ground condition of each mesh is established in this way, the ground subsidence process over time of each planar mesh can be predicted using the first model. A ground subsidence process obtained in this way is one sample of subsidence process (hereinafter, sample path) for that ground condition scenario by random generation.

By randomly generating ground condition scenarios, multiple sample paths can be obtained for each planar mesh. In order to develop an airport pavement design and maintenance plan, it is necessary to summarize the numerous sample path information created by the first model. The easiest method is to use an expectation path that averages the sample paths generated with the first model. An expectation path is convenient, but it does not adequately utilize the enormous information acquired by the first model. Therefore, in this paper, weight coefficients are assigned to the sample paths acquired by the first model, and a mixed ground subsidence model (second model) that expresses the ground subsidence process by weight average of the sample paths is formulated. As the actual ground subsidence process cannot be observed in the planning phase, it is impossible to statistically predict the second model. Thus, unless there is theoretical or experiential additional information on the certainty of each sample path, the weight of each sample path must be handled equally. In other words, the ground subsidence process is defined as the expectation path that averages all sample paths. However, after the airport begins services, monitoring information on the process of ground subsidence can be acquired. The issue now is to improve the estimation accuracy of the ground subsidence process by using the monitoring information and sequentially performing Bayesian updating on the second model. The model acquired by Bayesian updating using monitoring information will be called the third model.

## 2.2. *Bayesian Updating Scheme*

In airport pavement management, it is required that the ground subsidence process is continuously monitored, the subsidence process predicted in the planning phase is reevaluated, and if necessary the maintenance strategy is reconsidered. As shown in Figure 1, let us say a certain amount of time has passed since the point when airport services began $t_0$ and has reached point $T$. The ground subsidence process is predicted during the planning phase with the probabilistic one-dimensional consolidation model. The dotted lines in the figure are the predicted results of the amount of ground subsidence over time, for a certain planar mesh. The figure shows sample paths of ground subsidence process for 20 calculation scenarios, with altered soil constants. Furthermore, the thick red line in the figure is the expectation path, which is the simple average of these paths. Let us say that after the airport begins services, the ground subsidence process of each mesh is continuously monitored. In the figure, the ground subsidence amount actually observed from point $t_0$ when services began and the current point $T$ is shown with the black dots. In this example, the actual values

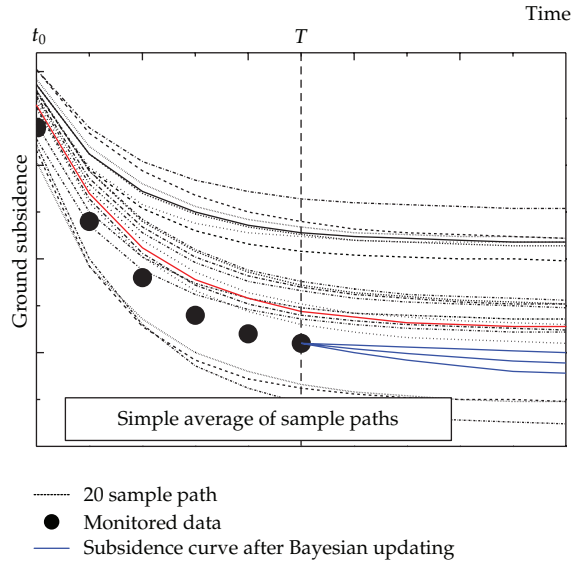


**Figure 1:** Bayesian updating on mixed ground subsidence model.

of the ground subsidence are in a lower position than the expectation path. Therefore, when ground subsidence is predicted using the expectation path, the actual subsidence may be underestimated.

The mixed ground subsidence model can be obtained by assigning weight coefficients to sample paths and seeking the weight average of sample paths. Furthermore, let us say the distribution is according to prior distribution with weight vectors. At the initial point there is no monitoring information regarding ground subsidence. Therefore, equal weight is assigned to all sample paths. However, when monitoring information is acquired, higher weight can be assigned to sample paths closer to the observed values of ground subsidence amount. As a result, it is possible to limit the distribution range of weight coefficients within a narrower range. In Figure 1, the ground subsidence sample paths predicted for after point $T$ are shown in thick blue lines, using the mixed ground subsidence model with Bayesian updating with monitoring information up to point $T$. In comparison to the spread of the sample paths sought with the first model, sample paths with Bayesian updating are collected within a narrower range, and it can be understood that the estimation accuracy of the mixed ground subsidence model is improved.

## 3. Mixed Ground Subsidence Model

### *3.1. Purpose of Second Model*

By using the first model, sample paths regarding multiple ground subsidence processes can be generated for each planar mesh. In other words, each sample path shows the result of ground subsidence process simulation, with randomly generated soil constants as conditions. There are many uncertainties with ground conditions, so there is no guarantee that the actually observed ground subsidence process matches one sample path. In this chapter, the actual ground subsidence process is expressed with a mixed ground subsidence model, which expresses the aggregation of sample paths obtained with the first model. As mentioned

above, the expectation path is the expectation sought from all sample paths and can be said to be a special case of the mixed ground subsidence model with equal weight assigned to all sample paths. Using the mixed ground subsidence model (second model), it is possible to express the probabilistic structure behind the sample paths. Furthermore, merits of the second model include (1) Bayesian updating of the ground subsidence model using monitoring information of ground subsidence amount observed at airports after services begin is made easy and (2) statistical testing on estimation accuracy of the ground subsidence model is possible.

### 3.2. Formalization of Mixed Ground Subsidence Model

The sample path $k = 1, \ldots, K$ calculated with the first model expresses the ground subsidence amount at point $t$ for each mesh. The ground subsidence amount at point $t$ ($t = 0, \ldots, T$) in sample path $k$ of planar mesh $i$ ($i = 1, \ldots, N$) can be expressed as $f_i(t, k)$. The mixed ground subsidence model is defined as an aggregation of sample paths generated with the first model. For weight coefficients assigned to each sample path to be uniquely determined, the sample paths that comprise the mixed ground subsidence model must be independent. Let us say a total of $K$ independent samples are obtained. The mixed ground subsidence model can be expressed as the linear combination of sample paths:

$$y_i^t = \sum_{k=1}^{K} \omega_i(k) f_i(t, k) + \varepsilon_i. \tag{3.1}$$

Here, $\omega_i(k)$ is the weight assigned to the sample path $k$, and the following holds:

$$\sum_{k=1}^{K} \omega_i(k) = 1 \quad (i = 1, \ldots, N). \tag{3.2}$$

Here, the weight vector of planar mesh $i$ shall be expressed as $\boldsymbol{\omega}_i = (\omega_i(1), \ldots, \omega_i(K))$. The weight vector $\boldsymbol{\omega}_i$ is a random variable that satisfies the constrained condition (3.2). Next, let us assume that $\varepsilon_i$ is a random variable that expresses the measurement error and each independently is subject to the one-dimensional normal distribution $N(0, \sigma_i^2)$.

### 3.3. Probabilistic Estimation of Ground Subsidence Amount

The weight matrix $\boldsymbol{\omega}_{\mathrm{i}}$ and probability error $\varepsilon_i$ of the mixed ground subsidence model (3.1) are random variables. If these random variable values can be formalized, specific ground subsidence paths can be acquired. Here, let us say the prior probability density function of $\boldsymbol{\omega}_{\mathbf{i}}$ is subject to the Dirichlet distribution. The probability density function of the Dirichlet distribution is given by

$$D(\omega_i \mid \alpha^{(0)}) = \Psi\left(\alpha^{(0)}\right) \prod_{k=1}^{K} \{\omega_i(k)\}^{\alpha_k^{(0)} - 1}, \tag{3.3a}$$

$$\Psi\left(\alpha^{(0)}\right) = \frac{\Gamma\left(\sum_{k=1}^{K} \alpha_k^{(0)}\right)}{\prod_{k=1}^{K} \Gamma\left(\alpha_k^{(0)}\right)}. \tag{3.3b}$$

Here, Γ(-) is a gamma function, and $\alpha^{(0)} = (\alpha_1^{(0)}, \ldots, \alpha_K^{(0)})$ is a constant parameter vector in the initial data. During the planning phase, the calculation results of the first model (sample paths) are available, as forerunning information [3]. The method of establishing parameters of the Dirichlet distribution using sample paths will be discussed in Section 5.3. Next, we will say $\phi_i = \sigma_i^{-2}$, and the prior probability density function of $\phi_i$ is subject to a gamma distribution. In other words, $\phi_i \backsim G(\beta^{(0)}, \gamma^{(0)})$, and the probability density function of the gamma distribution is given by

$$g\left(\phi_i \mid \beta^{(0)}, \gamma^{(0)}\right) = \frac{\left(\gamma^{(0)}\right)^{\beta^{(0)}}}{\Gamma\left(\beta^{(0)}\right)} \phi_i^{\beta^{(0)}-1} \exp\left(-\gamma^{(0)}\phi_i\right). \tag{3.4}$$

Hence, $\beta^{(0)}$ and $\gamma^{(0)}$ are constant parameters in the initial data. At this time, the prior probability density function $\pi(y_i^t)$ of the ground subsidence amount $y_i^t$ at point $t$ of mesh $i$ can be expressed as

$$\pi(y_i^t) \propto \int \cdots \int \phi_i^{\beta^{(0)}-1/2} \prod_{k=1}^{K} \omega_i(k)^{a_k^{(0)}-1} \exp\left[-\phi_i \left\{\gamma^{(0)} + \frac{1}{2}\left(y_i^t - \sum_{k=1}^{K} \omega_i(k) f_i(t,k)\right)^2\right\}\right] d\phi_i \, d\omega_i(1) \cdots d\omega_i(K-1). \tag{3.5}$$

However, $\omega_i(K) = 1 - \sum_{k=1}^{k-1} \omega_i(k)$. It is difficult to analytically calculate the prior probability density function $\pi(y_i^t)$, so it shall be calculated with Monte Carlo simulation. In other words, by random sampling $\phi_i, \omega_i(1), \ldots, \omega_i(K-1)$ with prior probability density functions (3.3a) and (3.4), and randomly selecting $y_i^t$ with the normal probability density function $N(\sum_{k=1}^{K} \omega_i(k) f_i(t,k), \phi_i^{-1})$, the probability distribution of the ground subsidence amount can be estimated.

## 4. Bayesian Updating Model

### 4.1. Bayesian Updating of the Mixed Ground Subsidence Model

The mixed ground subsidence model is a statistical model that expresses statistical uncertainties in ground subsidence process, using sample paths of ground subsidence process generated by the first model. The mixed ground subsidence model includes random variables $\boldsymbol{\omega}_i$ (weight vector assigned to each sample path) and $\varepsilon_i$ (probabilistic error). At the initial point, measurement values for these random variables do not exist, and the statistical characteristics of the ground subsidence process is expressed with the random variables' prior probability density functions (3.3a) and (3.4). In the operating phase when the airport is in service, monitoring information regarding the ground subsidence amount of each mesh is measured. Now, let us say time has passed from the point when services began (hereinafter, initial point) and has reached point $T$. Furthermore, let us say that from monitoring at point $t$ ($t = 0, \ldots, T$), the data regarding ground subsidence amount $\overline{y}_i^{0,T} = (\overline{y}_i^0, \ldots, \overline{y}_i^T)$ ($i = 1, \ldots, N$) has been acquired. The symbol "—" means the monitoring information (actual value). The overall monitoring results shall be expressed with the vector $\overline{y}^{0,T} = (\overline{y}_1^{0,T}, \ldots, \overline{y}_N^{0,T})$. Here, let us consider for now that the weight vector $\boldsymbol{\omega}_i$ is a given value, and only the probability error is a random variable. Also, the reciprocal $\phi$ of the probability

error variance shall be a given value. Now, the likelihood that the monitoring result $\overline{y}_i^{0,T}$ is observed can be expressed as

$$L\left(\overline{y}_i^{0,T} \mid \omega_i, \phi_i\right) \propto \prod_{t=0}^{T} \phi_i^{1/2} \exp\left[-\frac{\phi_i}{2}\left\{\overline{y}_i^t - \sum_{k=1}^{K} \omega_i(k) f_i(t,k)\right\}^2\right]. \tag{4.1}$$

Next, it shall be assumed that the prior probability density function of $\boldsymbol{\omega}_i$ is subject to the Dirichlet distribution (3.3a), and the reciprocal $\phi_i$ of the variance follows the gamma distribution (3.4).

Here, the conditional posterior probability density function $\pi(\phi_i \mid \omega_i, \overline{y}_i^{0,T})$ of $\phi_i$, with $\boldsymbol{\omega}_i$ and $\overline{y}_i^{0,T}$ as known values, can be expressed as

$$\begin{aligned} \pi\left(\phi_i \mid \omega_i, \overline{y}_i^{0,T}\right) &\propto \phi_i^{\overline{\beta}^{(0)}-1} \exp\left(-\overline{\gamma}^{(0)}\phi_i\right), \\ \overline{\beta}^{(0)} &= \beta^{(0)} + \frac{T+1}{2}, \\ \overline{\gamma}^{(0)} &= \gamma^{(0)} + \frac{1}{2}\sum_{t=0}^{T}\left\{\overline{y}_i^t - \sum_{k=1}^{K}\omega_i(k) f_i(t,k)\right\}^2. \end{aligned} \tag{4.2}$$

In other words, $\pi(\phi_i \mid \omega_i, \overline{y}_i^{0,T})$ is subject to the gamma distribution $G(\overline{\beta}^{(0)}, \overline{\gamma}^{(0)})$, and model samples of $\phi_i$ can be generated from the gamma distribution $G(\overline{\beta}^{(0)}, \overline{\gamma}^{(0)})$.

Next, the conditional posterior probability density function $\pi(\omega_i \mid \phi_i, \overline{y}_i^{0,T})$ of $\boldsymbol{\omega}_i$, with $\phi_i$ and $\overline{y}_i^{0,T}$ as known values, can be expressed as

$$\pi\left(\omega_i \mid \phi_i, \overline{y}_i^{0,T}\right) \propto \exp\left[-\frac{\phi_i}{2}\sum_{t=0}^{T}\left\{\overline{y}_i^t - \sum_{k=1}^{K}\omega_i(k) f_i(t,k)\right\}^2\right] \prod_{k=1}^{K} \omega_i(k)^{a_k^{(0)}-1}. \tag{4.3}$$

### 4.2. MH Algorithm

The conditional posterior probability density function of $\boldsymbol{\omega}_i$, shown in (4.3), is not a generally known distribution. Therefore, it is difficult to conduct direct sampling [4] of model samples of $\boldsymbol{\omega}_i$ from the conditional posterior probability density function $\pi(\omega_i \mid \phi_i, \overline{y}_i^{0,T})$. This paper applies the MH (Metropolis-Hasting) method [5] that does not use a direct sampling method. The MH method samples from a proposed distribution that is similar to $\pi(\omega_i \mid \phi_i, \overline{y}_i^{0,T})$ and according to it obtains samples from the original distribution [6]. Furthermore, to improve the efficiency of sampling, random walk is used. It is not new to use the MH method with random walk, but the algorithm should be explained briefly here, for the convenience of the reader.

First, the initial value of the parameter vector $\boldsymbol{\omega}_i$ can be expressed as $(\omega_i^0(1), \ldots, \omega_i^0(K))$. Here, a new candidate point $\omega_i'$ shall be proposed with

$$\omega_i' = \omega_i^0 + \lambda v. \tag{4.4}$$

Here, $\lambda$ is the constant parameter that establishes the range of step width, and $\nu = (\nu(1), \ldots, \nu(K))$ is the parameter vector that establishes the step width. In order for the candidate point $\omega_i'$ to satisfy the constrained condition $\sum_{k=1}^{K} \omega_i'(k) = 1$, $\sum_{k=1}^{K} \nu(k) = 0$ must hold. Now, from the change of variables $\nu' = \nu + K^{-1}I$, $\nu'$ shall be subject to the Dirichlet distribution. However, $I$ is an identity matrix of $1 \times K$. The range of step width is the same for every $k$ and established at $(-\lambda K^{-1}, \lambda(1 - K^{-1}))$. Also, the proposed distribution shall be defined, using the Dirichlet distribution with the constant parameter vector $x = (x_1, \ldots, x_K)$, as follows:

$$q\left(\omega_i^0, \omega_i' \mid \phi_i, \overline{y}_i^{0,T}\right) = D\left(\frac{\omega_i' - \omega_i^0}{\lambda} + \frac{\mathbf{I}}{\mathbf{K}} \mid \chi\right). \tag{4.5}$$

This proposed distribution satisfies the condition:

$$q\left(\omega_i^0, \omega_i' \mid \phi_i, \overline{y}_i^{0,T}\right) = q\left(\omega_i', \omega_i^0 \mid \phi_i, \overline{y}_i^{0,T}\right). \tag{4.6}$$

Therefore, as the proposed density $q$ is symmetrical to $(\omega_i^0, \omega_i')$, the acceptance probability $\kappa(\omega_i^0, \omega_i' \mid \overline{y}_i^{0,T})$ of the new candidate point can be expressed as

$$\kappa\left(\omega_i^0, \omega_i' \mid \overline{y}_i^{0,T}\right) = \min\left\{\frac{\pi\left(\omega_i' \mid \phi_i^n, \overline{y}_i^{0,T}\right)}{\pi\left(\omega_i^n \mid \phi_i^n, \overline{y}_i^{0,T}\right)}, 1\right\}. \tag{4.7}$$

If accepted, it moves to a new candidate point, and if rejected it remains. The MH algorithm procedure can be organized as follows.

*Step 1* (Initial Establishment). The parameter vectors $\alpha^{(0)} = (\alpha^{(0)}{}_1, \ldots, \alpha^{(0)}{}_k)$, $\beta^{(0)}$, and $\gamma^{(0)}$ of the prior distributions (3.3a) and (3.4) are arbitrarily established. Furthermore, the initial values $\boldsymbol{\omega}_i^0 = (\omega_i^0(1), \ldots, \omega_i^0(K))$ and $\phi_i^0$ of the parameter estimation are arbitrarily established. The constant parameter $\lambda$, constant parameter vector $\chi$, and sample numbers $\underline{n}$ and $\overline{n}$ are established. The influence of these initial values shall decrease gradually, as the number of MCMC simulations increase. The number of simulations has to be $n = 0$.

*Step 2* (Sample Extraction of Parameter Estimation $\boldsymbol{\omega}_i$). The parameter estimation $\omega_i^{n+1} = (\omega_i^{n+1}(1), \ldots, \omega_i^{n+1}(K))$ when the number of simulations is $n + 1$ is generated as follows. $\nu'$ that is subject to the Dirichlet distribution is randomly generated. The parameter vector $\nu$ that establishes the step width is calculated with $\nu = \nu' - K^{-1}I$. The new candidate point $\omega_i'$ is

$$\omega_i' = \omega_i^n + \lambda\nu. \tag{4.8}$$

The acceptance probability is calculated as

$$\kappa\left(\omega_i^n, \omega_i' \mid \phi_i^n, \overline{y}_i^{0,T}\right) = \min\left\{\frac{\pi\left(\omega_i' \mid \phi_i^n, \overline{y}_i^{0,T}\right)}{\pi\left(\omega_i^n \mid \phi_i^n, \overline{y}_i^{0,T}\right)}, 1\right\}. \tag{4.9}$$

Then the uniform distribution $u \sim U(0,1)$ is generated, and if the two following equations are satisfied:

$$\kappa\left(\omega_i^n, \omega_i' \mid \phi_i^n, \overline{y}_i^{0,T}\right) > u,$$
$$\omega_i'(k) \geq 0 \quad (k = 1, \ldots, K), \tag{4.10}$$

then $\omega_i^{n+1} = \omega_i'$, so proceed to Step 3. If not, return to Step 2.

*Step 3* (Sample Extraction of Parameter Estimation $\phi_i$). $\phi_i^{n+1}$ is generated from $\pi(\phi_i \mid \omega_i^{n+1}, \overline{y}_i^{0,T})$. In other words, $\phi_i^{n+1}$ is randomly generated from the gamma distribution $G(\overline{\beta}^{(0)}, \overline{\gamma}^{(0)})$.

*Step 4* (Final Judgment of the Algorithm). The updated values $\omega_i^{n+1} = \omega_i^{n+1}(1), \ldots, \omega_i^{n+1}(K))$, $\phi_i^{n+1}$ of the parameter estimation, obtained from the above steps, are recorded. If $n \leq \overline{n}$, then $n = n + 1$ so return to Step 2. If not, the algorithm is finished.

### 4.3. Bayesian Updating and Bayesian Estimation

It shall be considered that using the monitoring result $\overline{y}_i^{0,T} = (\overline{y}_i^0, \ldots, \overline{y}_i^t)$ of mesh $i$ up to the monitoring at point $t$, the posterior distribution of the unknown parameters of the mixed ground subsidence model is obtained. Then, using the monitoring result $\overline{y}_i^{t+1,t'} = (\overline{y}_i^{t+1}, \ldots, \overline{y}_i^{t'})$ from between point $t + 1$ and $t'$, the problem of updating the posterior distribution of the unknown parameters is supposed. If the posterior probability density function of the unknown parameters of the first Bayesian estimation is $\pi(\omega_i, \phi_i \mid \overline{y}_i^{0,T})$, the posterior probability density function of the unknown parameter after the second Bayesian updating $\pi(\omega_i, \phi_i \mid \overline{y}_i^{0,t'})$ can be expressed as

$$\begin{aligned}\pi\left(\omega_i, \phi_i \mid \overline{y}_i^{0,T}\right) &\propto L\left(\omega_i, \phi_i \mid \overline{y}_i^{t+1,t'}\right)\pi\left(\omega_i, \phi_i \mid \overline{y}_i^{0,T}\right) \\ &\propto L\left(\omega_i, \phi_i \mid \overline{y}_i^{0,T}\right)D\left(\omega_i \mid \alpha^{(0)}\right)\mathrm{g}\left(\phi_i \mid \beta^{(0)}, \gamma\right).\end{aligned} \tag{4.11}$$

Here, $L(\omega_i, \phi_i \mid \overline{y}_i^{0,t'})$ is the likelihood function defined using the database that pools the monitoring results from the initial point to point $t'$. On the other hand, $D(\omega_i \mid \alpha^{(0)})$ and $\mathrm{g}(\phi_i \mid \beta^{(0)}, \gamma^{(0)})$ are each prior distributions of $\boldsymbol{\omega}_i$ and $\phi_i$ used in the first Bayesian estimation. Therefore, the posterior distribution after Bayesian updating is

$$\begin{aligned}\pi\left(\omega_i, \phi_i \mid \overline{y}_i^{0,T}\right) \propto \phi_i^{\beta^{(0)}+(t'-1)/2} \cdot \exp\left[-\phi_i\left\{\gamma^{(0)} + \frac{1}{2}\sum_{t=0}^{t'}\left(\overline{y}_i^t - \sum_{k=1}^{K}\omega_i(k)f_i(t,k)\right)^2\right\}\right] \\ \cdot \prod_{k=1}^{K}\omega_i(k)^{\alpha_k^{(0)}-1}.\end{aligned} \tag{4.12}$$

In other words, in order to update the posterior distribution of unknown parameters, it is necessary to define the likelihood functions with the database that includes new monitoring results and newly estimate the posterior distribution by the MH method.

The monitoring information $\overline{y}_i^{0,T}$ from initial point $t = 0$ to point $t = T$ and the posterior distribution of the parameter of the mixed ground subsidence model $\pi(\omega_i, \phi_i \mid \overline{y}_i^{0,T})$ are assumed to be given values. With this, the ground subsidence amount after point $t = T$ can be estimated. The actual value (monitoring information) of ground subsidence amount of planar mesh $i$ at point $t = T$ shall be expressed as $\overline{y}_i^T$. On the other hand, the predicted value of ground subsidence amount for point $\bar{t}$ $(> T)$, which comes after point $t = T$, predicted at point $t = T$, shall be $\overline{y}_i^{\tilde{t}}(T)$. If it is assumed that with the passing of time ground subsidence always progresses, then the following holds:

$$\overline{y}_i^T \le \widetilde{y}_i^{\tilde{T}+1}(T) \le \cdots \le \widetilde{y}_i^{\tilde{T}+n}(T) \le \cdots . \tag{4.13}$$

Hence, $n$ is a natural number. Here, the parameter $\boldsymbol{\omega}_i$ of the mixed ground subsidence model is a given value. At this time, if ground subsidence amount $\overline{y}_i^T$ is observed at point $t = T$, prediction residual of the mixed ground subsidence model can be expressed as

$$\xi_i^T = \overline{y}_i^T - \sum_{k=1}^{K} \omega_i(k) f_i(t,k). \tag{4.14}$$

Furthermore, if the weight coefficient $\omega_i$ is given, the predicted value of ground subsidence amount at point $\bar{t}$ $(> T)$, which comes after point $t = T$, predicted at point $T$, can be expressed definitely with the mixed ground subsidence model:

$$\widetilde{y}_i^{\tilde{t}}(T) = \sum_{k=1}^{K} \omega_i(k) f_i\left(\widetilde{t}, k\right) + \xi_i^T. \tag{4.15}$$

Next, the posterior distribution $F(\omega_i \mid \overline{y}_i^{0,T})$ of parameter $\boldsymbol{\omega}_i$ updated by Bayesian updating using the monitoring information $\overline{y}^{0,T}$ up to point $t = T$ can be approximated with MCMC method. Furthermore, the weight sample generated with MCMC method can be expressed as $\omega_i^n$ $(n \in M, i = 1, \ldots, N)$. At this point, if ground subsidence amount $\overline{y}_i^T$ is observed at point $T$, the probability distribution function $H_i(\overline{y}_i \mid \bar{t}, \overline{y}_i^T)$ regarding ground subsidence amount $\overline{y}_i^{\tilde{t}}$ $(T)$ at point $\bar{t}$ $(> T)$ can be expressed as

$$H_i\left(\widetilde{y}_i \mid \widetilde{t}, \overline{y}_i^T\right) = \frac{\sharp\left\{\widetilde{y}_i^{\tilde{t},n}(T) \le \widetilde{y}, n \in M\right\}}{\overline{n} - \underline{n}}. \tag{4.16}$$

However, $\overline{y}_i^{\tilde{t},n}(T)$ is the predicted value of ground subsidence for point $\bar{t}$ $(> T)$, predicted at point $T$, using the weight coefficient sample value $\omega_i^n$, and can be defined as

$$\begin{aligned}\tilde{y}_i^{\tilde{t},n}(T) &= \sum_{k=1}^{K}\omega_i^n(k)\,f_i\left(\tilde{t},k\right)+\xi_i^{T,n},\\ \xi_i^{T,n} &= \overline{y}_i^T-\sum_{k=1}^{K}\omega_i^n(k)\,f_i(T,k).\end{aligned}\tag{4.17}$$

Furthermore, the expected value of ground subsidence amount $E[\overline{y}_i^{\tilde{t}}(T)]$ at point $\bar{t}$ can be expressed as

$$E\left[\tilde{y}_i^{\tilde{t}}(T)\right]=\frac{\sum_{n=\underline{n}+1}^{\overline{n}}\omega_i^n(k)\,f_i\left(\tilde{t},k\right)+\xi_i^{T,n}}{\overline{n}-\underline{n}}.\tag{4.18}$$

Also, the 100%$(1-2\delta)$ credible interval of ground subsidence amount $\overline{y}_i^{\tilde{t}}(T)$ of point $\bar{t}$, predicted at point $T$, can be defined as $\underline{y}_i^{\tilde{t}}(\delta,T)<\overline{y}_i^{\tilde{t}}(T)<\overline{y}_i^{\tilde{t}}(\delta,T)$ using sample order statistics $\underline{y}_i^{\tilde{t}}(\delta,T)$ and $\underline{y}_i^{\tilde{t}}(\delta,T)$:

$$\begin{aligned}\underline{y}_i^{\tilde{t}}(\delta,T) &= \arg\max_{y_i^*}\left\{\frac{\sharp\left\{\tilde{y}_i^{\tilde{t},n}(T)\le y_i^*,n\in M\right\}}{\overline{n}-\underline{n}}\le\delta\right\},\\ \underline{y}_i^{\tilde{t}}(\delta,T) &= \arg\min_{y_i^{**}}\left\{\frac{\sharp\left\{\tilde{y}_i^{\tilde{t},n}(T)\ge y_i^{**},n\in M\right\}}{\overline{n}-\underline{n}}\le\delta\right\}.\end{aligned}\tag{4.19}$$

## 5. Empirical Study

### 5.1. Summary of Applied Case

In this paper, the offshore H airport is targeted. At this airport, with approximately 30 thousand commissions of short-range international passenger flights and commissions of international cargo flights during late-night and early-morning hours, PFI is applied from planning and construction to maintenance of basic facilities including aprons, airport safety facilities, supplementary facilities, roads and parking spaces, and green tracts. Among these, aprons are areas where aircraft are parked, and concrete pavement is used because of the necessity of strong resistance of fluidity and oil. These aprons are situated on soft ground, and the fatigue and deterioration of the concrete pavement due to inhomogeneous subsidence of the ground is a problem.

The targeted area was the apron area of H airport, with a range of 825 m × 400 m, and for consolidation subsidence the basic unit was a 25 m × 25 m square mesh. The apron area was divided into planar meshes. Also, the targeted consolidation layers were alluvial clay layer around GL-7 m to GL-25 m and diluvial clay layer around GL-25 m to GL-60 m,

**Table 1:** Soil constants using first model.

| | |
|---|---|
| Compression index: $C_c$ | Normal distribution |
| Initial void ratio $e_0$ | Normal distribution |
| Consolidation yielding stress: $P_c$ | Normal distribution |
| Consolidation coefficient: $c_v$ | Log-normal distribution |

and the one-dimensional consolidation theory was used. With Markov hazard model [7], the correlation between soil constants can be considered. In this applied case, from the boring test results, the horizontal correlation length was set at $b = 100$ m, and the perpendicular correlation length was set at 4-5 m. The perpendicular mesh divisions were divided at every 4 m, even within the same ground. For analysis, from the 17 boring results and consolidation test results conducted on the targeted area, the alluvial clay layer and diluvial clay layer was divided in the depth direction into 10 layers, $A_{c1}$–$A_{c6}$ and $D_{c1}$–$D_{c4}$, respectively, and the soil constants were organized. Table 1 shows the inhomogeneous subsidence simulation soil constant used in the applied case.

### 5.2. Analysis Results by the First Model

The inhomogeneous subsidence shall be simulated with the first model. For each block, the soil constant is randomly generated from the probability distribution. Specifically, the soil constants of each consolidation layer divided perpendicularly were generated from the expected value, standard deviation, and coefficient of variation shown in Table 2, by normal distribution for compression index $C_c$, initial void ratio $e_0$, and consolidation yielding stress $p_c$, and by log-normal distribution for consolidation coefficient $c_v$. Furthermore, these expected values and distributions are established according to boring test results conducted on representative planar meshes. For all three-dimensional blocks, the soil constants were randomly generated by the Monte Carlo simulation. The pairs of soil constants generated for all three-dimensional blocks shall be called calculation scenarios. Furthermore, for each calculation scenario, the ground subsidence process of the targeted calculation scenario is calculated with the first model.

An example of the inhomogeneous subsidence simulation is shown in Figure 2. This figure shows 20 sample paths of ground subsidence amount over time, for the planar mesh $i = 73$, which was chosen as an example. The chosen planar mesh has an existing ground height of AP + 3.0 m, a planned ground height of AP + 6.0 m, and is a part of the area with high embankment. As a result of simulation with the first model, the expected path subsidence amount after 30 years is 35.75 cm as shown in Figure 3 and is predicted to have the largest subsidence among the entire targeted area. In the horizontal axis, the start of services at H airport is set at 0, but it can be seen that ground subsidence had already occurred between roadbed adjustment and the start of services. Also, when comparing the 20 sample paths of Figure 2, it can be understood that the ground subsidence amount changes greatly depending on the soil constant scenario. In fact the average subsidence amount for after 30 years is 35.75 cm and the variance is 30.66 $cm^2$. On the other hand, in any sample path the ground subsidence processes converge with the passing of time.

### 5.3. Creating the Second Model

Using the 20 sample paths obtained with the first model (see Figure 2), the mixed ground subsidence model (second model) is estimated. The sample paths from the first model are

**Table 2:** Soil constants for inhomogeneous subsidence simulation.

| Layer | $C_c$ (kN/m$^2$) | | $e_0$ | | $p_c$ (kN/m$^2$) | | $c_v$ (cm$^2$/day) | | |
|---|---|---|---|---|---|---|---|---|---|
| | EV | SD | EV | SD | EV | CV | EV | log $c_v$ | log $c_v$ SD |
| $A_{c1}$ | 0.45 | 0.07 | 1.34 | 0.17 | 70 | 0.36 | 993 | −4.26 | 0.29 |
| $A_{c2}$ | 0.41 | 0.06 | 1.21 | 0.11 | 59 | 0.33 | 1025 | −4.15 | 0.09 |
| $A_{c3}$ | 0.73 | 0.11 | 1.84 | 0.22 | 95 | 0.49 | 759 | −4.40 | 0.33 |
| $A_{c4}$ | 0.87 | 0.08 | 2.09 | 0.15 | 90 | 0.39 | 787 | −4.32 | 0.23 |
| $A_{c5}$ | 0.74 | 0.21 | 1.91 | 0.39 | 99 | 0.44 | 1103 | −4.20 | 0.26 |
| $A_{c6}$ | 0.31 | 0.12 | 1.17 | 0.22 | 139 | 0.08 | 3435 | −3.63 | 0.09 |
| $D_{c1}$ | 0.44 | 0.13 | 1.32 | 0.30 | 174 | 0.71 | 1680 | −3.95 | 0.14 |
| $D_{c2}$ | 0.57 | 0.16 | 1.54 | 0.27 | 144 | 0.67 | 1945 | −4.01 | 0.34 |
| $D_{c3}$ | 0.66 | 0.12 | 1.58 | 0.19 | 135 | 0.66 | 1000 | −4.27 | 0.29 |
| $D_{c4}$ | 0.70 | 0.25 | 1.64 | 0.67 | 186 | 0.65 | 1002 | −4.23 | 1.66 |

Note—EV: expected value, SD: standard deviation, CV: coefficient of variation. For $A_{c1}$–$A_{c6}$, the alluvial clay ground layer was divided into 6 layers in the depth direction from categorization of soil characteristics, acquired from boring test results and lab consolidation test results, and the layers were numbered from the top layer to the bottom layer. Similarly, for $D_{c1}$–$D_{c4}$ also, according to the categorization of soil characteristics, the diluvial clay ground layers were numbered from the top layer to the bottom layer.

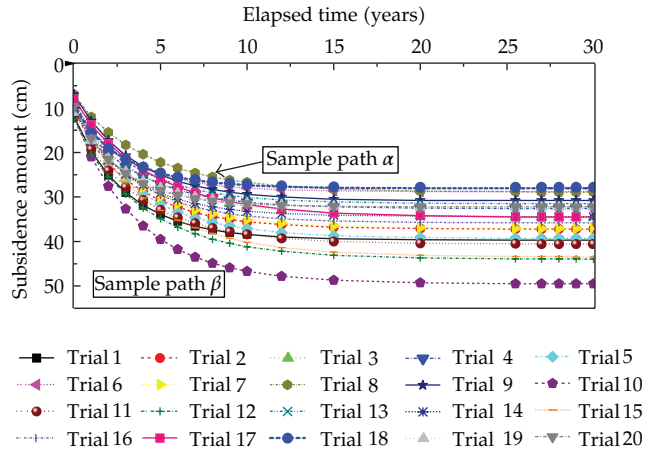


**Figure 2:** Examples of simulation results of inhomogeneous subsidence.

in a strong correlation to each other. For example, the correlation coefficient between the 20 sample paths of Figure 2 was at least 0.976. Therefore, in order to avoid the problem of multicollinearity, out of the 20 sample paths the 2 sample paths that set the upper limit and lower limit of predicted subsidence at the end of the contract were selected for the estimation of the mixed ground subsidence model. Hereinafter, the sample path at the upper limit shall be called $\alpha$ and the sample path at the lower limit shall be called $\beta$. We shall add that with any mesh, the sample path $\alpha$ and $\beta$ set the upper and lower limits of predicted subsidence for the overall contract period. In other words, by selecting sample paths $\alpha$ and $\beta$, it is possible to expand the section between the two sample paths as much as possible and maximize the range created with the second and third models. Figure 3 shows the expected value path by simple average of the 20 sample paths. This figure also shows the averaged results of the 2 sample paths used for the mixed ground subsidence model (sample average). Naturally, this path does not match the expected value path, which is a simple average of the 20 sample

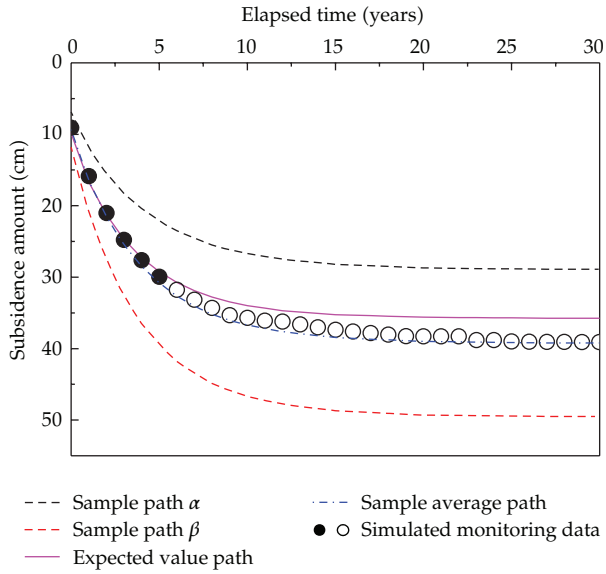


**Figure 3:** Simulated monitoring data and sample paths.

paths. Therefore, in order to predict the ground subsidence amount $y_i^t$ of mesh $i$ at point $t$, the weight coefficient $\boldsymbol{\omega}_i(k)$ $(k = 1, 2)$ of the mixed ground subsidence model must be corrected so that the misfit between the expected path of the mixed ground subsidence model and the sample average is as little as possible. Now, the predicted ground subsidence amount of mesh $i$ at point $t$ of the expected value path from the 20 sample paths shall be expressed as $\overline{y}_i^t$. If $\omega_i(k)$ $(k = 1, 2)$ takes a value that satisfies:

$$\min_{\omega_i(1),\omega_i(2)} \left\{ \tilde{y}_i^t - \sum_{k=1}^{2} \omega_i(k) f_i(t,k) \right\}^2, \tag{5.1}$$

then the misfit between the expected value path and average path is arbitrarily small. However, $f_i(t,k)$ is the sample path (generated with the first model) selected for the mixed ground subsidence model. Now, the weight vector $\omega_i$ at point $t$ established in (5.1) shall be expressed as $\overline{\omega}_i^t$. Furthermore, let us say the prior probability density function of the weight vector $\boldsymbol{\omega}_i$ of the mixed ground subsidence model can be identified as a Dirichlet distribution of (3.3a). The posterior probability density function $\pi(y_i^t)$ of ground subsidence amount $y_i^t$ at point $t$ of mesh $i$ is difficult to analytically estimate as shown in (3.5), so it is necessary to calculate this with Monte Carlo simulation. For this, the weight vector $\boldsymbol{\omega}_i$ is randomly generated from a Dirichlet distribution as shown in (3.3a). Therefore, in order to make the separation between the expected value path and average path arbitrarily small, a Dirichlet distribution and parameter vector is established in which the following equation approximately holds:

$$E[\omega_i(k)] \approx \tilde{\omega}_i^t(k) \quad (k = 1, 2). \tag{5.2}$$

Now, in the Dirichlet distribution, the expected value of $\omega_i(k)$ can be expressed as

$$E[\omega_i(k)] = \frac{\alpha_k^{(0)}}{\sum_{k=1}^{2} \alpha_k^{(0)}} \quad (k = 1, 2). \tag{5.3}$$

Therefore, the initial parameter of the Dirichlet distribution ${\alpha^{(0)}}_k (k = 1, 2)$ is established so that the following holds:

$$\tilde{\omega}_i^t(k) = \frac{\alpha_k^{(0)}}{\sum_{k=1}^{2} \alpha_k^{(0)}} \quad (k = 1, 2). \tag{5.4}$$

Using the mixed ground subsidence model established with the above, the ground subsidence amount after 5 years $y_i^5$ is predicted. The distribution of the predicted subsidence amount can be obtained, as shown in (3.5), by establishing the prior probability density function of $\alpha^{(0)}$ and $\phi_i$. Now, the parameter vector of the Dirichlet distribution $\alpha^{(0)}$ shall be, according to the weight vector $\overline{\omega}_i^5$, established as ${\alpha_1}^{(0)} = 0.593$ and ${\alpha_2}^{(0)} = 0.407$. Figure 4 uses planar mesh $i = 73$ and shows how the predicted subsidence distribution changes after 5 years, due to the values of the parameters $\beta^{(0)}$ and $\gamma^{(0)}$ of the prior probability density function $\phi_i$. As shown in Figure 4, if the values of parameters $\beta^{(0)}$ and $\gamma^{(0)}$ are increased, the predicted subsidence amount is distributed within a narrower range. On the other hand, if the values of $\beta^{(0)}$ and $\gamma^{(0)}$ are decreased, the predicted subsidence amount is distributed within a wider range. Figure 5 shows how the 95% credible interval of the predicted subsidence amount at point $t$ changes according to the values $\beta^{(0)}$ and $\gamma^{(0)}$. The initial parameter of the prior probability density of $\phi_i$ can be arbitrarily established, but for the efficiency of Bayesian learning it is better if the prior distribution is dispersed. In this paper, the initial parameters were established at $\beta^{(0)} = 0.5$ and $\gamma^{(0)} = 0.5$. From the results of Figure 4, the case in which these initial values were used shows greater dispersion of prior distribution of the parameter values, among the 4 calculation cases in the same figure.

### *5.4. Estimating the Third Model*

After services are offered at the airport, information on the ground subsidence amount of each planar mesh can be obtained through continuous monitoring. Using this monitoring information, the mixed ground subsidence model is reconsidered. At the moment, the airport is not in service and there is no monitoring information. So, the monitoring results of ground subsidence amount of each planar mesh are assumed and Bayesian updating is conducted on the mixed ground subsidence model. Now, the period of the airport during operation and management shall be divided into two periods: (1) from the first year to the sixth year and (2) after the sixth year. After services begin, each year periodical monitoring of ground subsidence amount is conducted, and at the fifth year after services begin, Bayesian estimation of the mixed ground subsidence model is considered. Next, after the sixth year, monitoring information of ground subsidence can be obtained each year. Here we shall consider the problem of adding the newly acquired monitoring information to the database and conducting Bayesian updating of the mixed ground subsidence model every year according to the newly updated database.

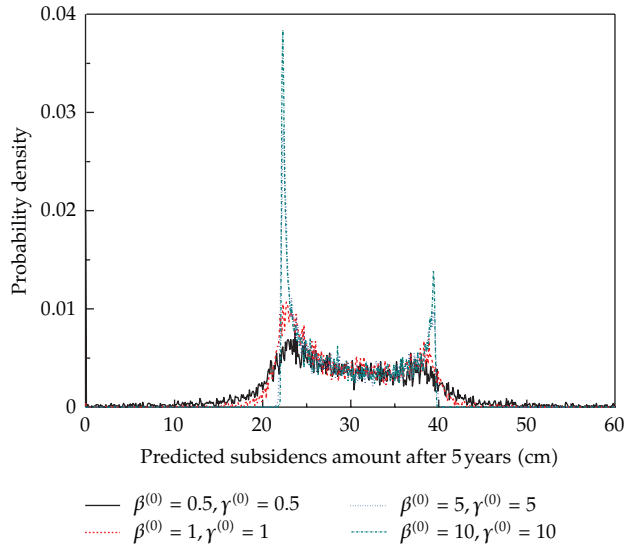


**Figure 4:** Distribution of predicted subsidence after 5 years.

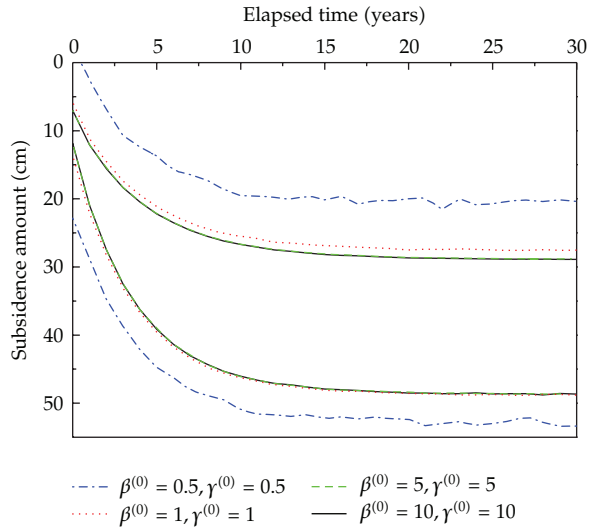


**Figure 5:** 95% credible interval of predicted subsidence amount.

In the targeted airport ground, there are a total of 528 planar meshes. Let us assume the airport apron has been in service for 5 years, and consider the problem of predicting ground subsidence amount after the sixth year, using monitoring information of 5 years to update the mixed ground subsidence model. Figure 3 shows the sample path created with the first model and expected value path calculated with the second model, using an example mesh ($i = 73$) of the 528 planar meshes. Currently, there is no monitoring information so the Bayesian updated third model is created using assumed information. In order to check whether the estimation results of ground subsidence can be appropriately corrected with the Bayesian updated third model, even if the actual ground subsidence amount is larger than

**Table 3:** Estimation results of mixed ground subsidence model.

| Parameter | Expected value | 95% credible interval | | Geweke test statistics |
|---|---|---|---|---|
| $\omega_{73}(1)$ | 0.553 | 0.518 | 0.589 | $-8.63E-02$ |
| $\omega_{73}(2)$ | 0.447 | 0.428 | 0.467 | $-8.63E-02$ |
| $\phi_{73}$ | 2.76 | 0.66 | 7.41 | $-4.49E-02$ |

the expected path of the second model, the hypothesized monitoring information shown with the black dots in Figure 3 was used. The ground subsidence process shown in this example is lower than the expected sample path, and the ground subsidence amount is larger than the expected value path. The mixed ground subsidence model of the targeted mesh can be expressed as

$$y_{73}^{t} = \sum_{k=1}^{2} \omega_{73}(k) f_{73}(t,k) + \varepsilon_{73}. \tag{5.5}$$

Also, $k = 1$ is the sample path $\alpha$ of Figure 3, while $k = 2$ is sample path $\beta$.

Furthermore, for the prior probability density function of weight vector $\boldsymbol{\omega}_i$ of the mixed ground subsidence model, the same distribution was used as the Dirichlet distribution used in the second model. On the other hand, the prior probability density function of the variance parameter $\phi_i$ of the probability error term $\varepsilon_i$ is subject to the gamma distribution of (3.4), and the parameter of the gamma distribution was established as $(\beta^{(0)}, \gamma^{(0)}) = (0.5,0.5)$ according to the consideration of Section 5.3. Also, the number of convergence tests totaled 8,000 samples: $\underline{n} = 2,000$, $\underline{n} = 10,000$.

First, after services, the mixed ground subsidence model is updated with Bayesian updating according to the monitoring information of 5 years. In Table 3, the estimation results of the mixed ground subsidence model are shown with the weights $\omega_{73}(1)$, $\omega_{73}(2)$, expected value of distribution parameter $\phi_{73}$, the 95% credible interval, and the Geweke test statistics [8]. Geweke test statistics are statistics for testing whether the sampling process of MCMC method reaches a steady state and is used to test whether the sample number $\underline{n}$ is appropriate or not. From the estimation results, the total weight is 1 and the constrained condition equation (3.2) is satisfied. Also, the expected value of weight $\omega_{73}(1)$ is high but this is an inevitable result as the simulated monitoring information is at a higher position than the sample average path. The posterior probability density functions of these two parameters are shown in Figures 6 and 7. Also, when conducting the MH method, $\underline{n} = 2,000$ was established as the sample number for the Markov chain to reach a steady state, but the absolute value of the Geweke test statistics are all lower than 1.96 and the hypothesis that it "converges to a steady state" with a significance level of 5% cannot be dismissed. The prior distributions of these parameters are shown in Figures 6 and 7, but the variance of the parameter distributions of the mixed ground subsidence model is smaller with Bayesian updating.

Next, using the mixed ground subsidence model updated with Bayesian updating on the fifth year, the ground subsidence path after the sixth year is estimated and the results are shown in Figure 8. As stated above, the actual path of ground subsidence process is simulated as having greater subsidence than the expected sample path. Therefore, the expected subsidence amount after 30 years has passed is 38.11 cm, 35.75 cm greater than the expected sample path. At year 30, the lower limit of the 95% credible interval is 37.99 cm and the upper limit is 38.22 cm, and it is understood that after Bayesian updating the estimation

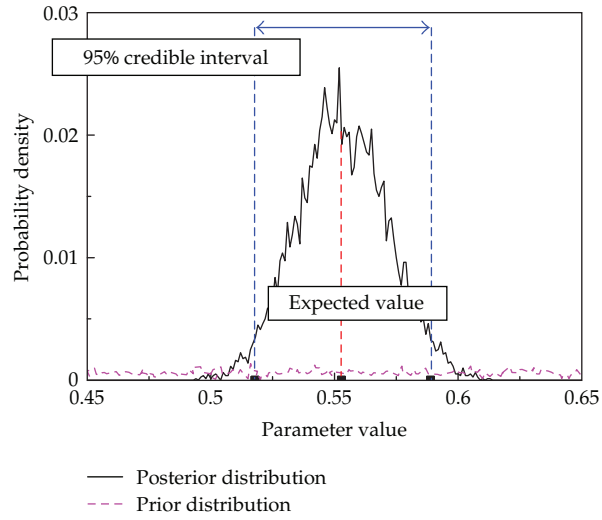


**Figure 6:** Probability distribution of parameter $\omega_{73}(1)$.

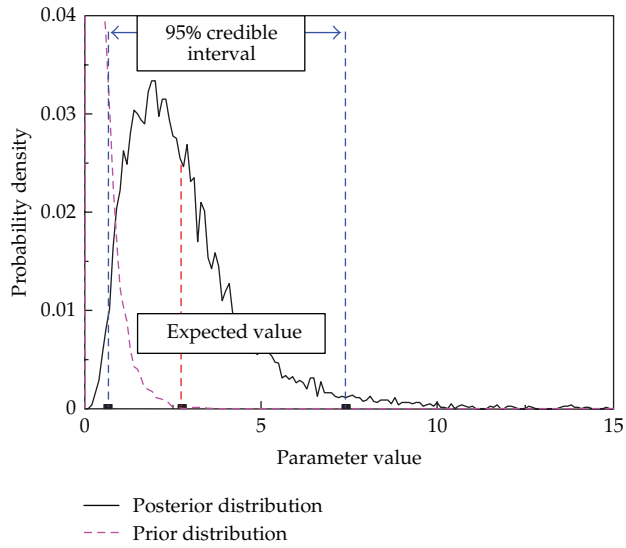


**Figure 7:** Probability distribution of parameter $\phi_{73}$.

accuracy of the mixed ground subsidence model has improved and better risk management of ground subsidence is possible.

Furthermore, we shall consider how after the sixth year monitoring information is continuously accumulated and Bayesian updating is sequentially conducted on the mixed ground subsidence model. Let us look at planar mesh $i = 73$ once more. With this mesh, monitoring information as shown in the white dots in Figure 3 is accumulated after the sixth year. Here, let us say that as new monitoring information is obtained each year, Bayesian updating is conducted on the mixed ground subsidence model. Furthermore, using the updated mixed ground subsidence model, the ground subsidence amount at year 30

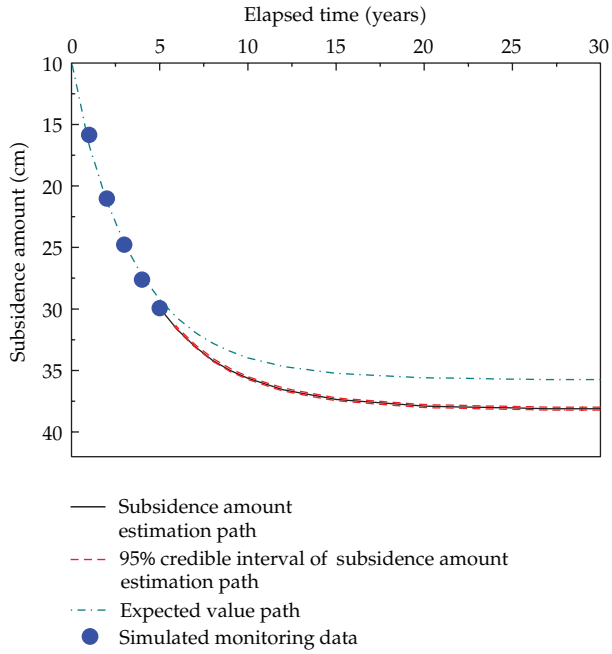


**Figure 8:** Subsidence estimation results at 5th year.

**Table 4:** Estimation results of ground subsidence amount (mesh $i = 73$).

| Year | Subsidence estimation of 30th year | 95% credible interval | | Width of credible interval |
|---|---|---|---|---|
| 5 | 38.109 | 37.990 | 38.224 | 0.234 |
| 6 | 38.209 | 38.139 | 38.279 | 0.140 |
| 7 | 38.218 | 38.174 | 38.263 | 0.089 |
| 8 | 38.226 | 38.199 | 38.254 | 0.055 |
| 9 | 38.439 | 38.419 | 38.457 | 0.038 |
| 10 | 38.151 | 38.140 | 38.163 | 0.023 |
| 15 | 38.115 | 38.114 | 38.116 | 0.002 |
| 20 | 38.477 | 38.477 | 38.477 | 0.000 |
| 25 | 39.046 | 39.046 | 39.046 | 0.000 |

Note: the simulated monitoring data (subsidence amount) at the 30th year is 39.09 cm.

is estimated and the results are shown in Table 4. In this chart, using the mixed ground subsidence model after Bayesian updating with the monitoring information up to that point, the estimation (expected value) of the ground subsidence amount at the 30th year after being in service, as well as the upper and lower limits of the 95% credible interval, is shown. Furthermore, the simulated monitoring information (subsidence amount) at the 30th year is 39.09 cm. Compared to the Bayesian updating result, with the accumulation of information the expected path is slightly corrected and the credible interval range is narrower. From this it can be understood that the estimation accuracy is improved due to Bayesian updating.

## 6. Conclusion

This paper attempts to propose a methodology of conducting Bayesian updating on ground subsidence estimation results using continuous monitoring and monitoring information of ground subsidence, which is an important issue in asset management of airport facilities. Specifically, using a one-dimensional consolidation model that takes inhomogeneous subsidence into consideration, sample paths regarding ground subsidence process and a mixed ground subsidence model that averages the load of the sample paths are calculated. Furthermore, a methodology of conducting Bayesian updating using MCMC method on the mixed ground subsidence model, by continuously monitoring the ground subsidence amount after the airport begins services, is proposed. Furthermore, the applicability of the methodology proposed in this paper is empirically evaluated through an applied case of the ground subsidence estimation management of an airport facility. However, in order to improve the applicability of the Bayesian updating model proposed in this paper, there are several issues to be studied in the future. First, the applied case in this paper is at the state where the airport facilities have just begun services. Therefore, monitoring information is not yet available. Consequently, in the applied case, Bayesian updating of the mixed ground subsidence model was conducted using simulated monitoring information. In the future, it is necessary to continuously monitor the ground subsidence process of airports and use actual monitoring information to evaluate the efficiency of Bayesian updating on the mixed ground subsidence model. Secondly, in airport pavement management, ground subsidence estimation management is an important issue for consideration, but for pavement management, managing deterioration and damage processes of airport pavements is also important. For this, the deterioration and damage progress of airport pavements as well as ground subsidence should be modelized. Thirdly, the Bayesian updating model proposed in this paper is a methodology for conducting Bayesian updating on estimation results based on monitoring information during the designing phase. This type of Bayesian updating model has the potential to be applied to a wider range of problems outside of ground subsidence estimation management. In the future, it is necessary to evaluate the efficiency of the Bayesian updating model on asset management of public facilities other than airport pavements.

## References

[1] W. H. Tang, "Probabilistic evaluation of penetration resistances.," *Journal of the Geotechnical Engineering Division, ASCE*, vol. 105, no. 14902, pp. 1173–1191, 1979.

[2] T. Tsuchida and K. Ono, "Prediction of inhomogeneous subsidence based on numerical simulation and its application to design standard of airport pavement," *The Port and Airport Research Institute Report*, vol. 27, no. 4, pp. 123–200, 1988 (Japanese).

[3] H. Jeffreys, *Theory of Probability*, Clarendon Press, Oxford, UK, 1961.

[4] W. R. Gilks and P. Wild, "Adaptive rejection sampling for Gibbs sampling," *Applied Statistics*, vol. 41, pp. 337–348, 1992.

[5] J. G. Ibrahim, M.-H. Chen, and D. Sinha, *Bayesian Survival Analysis*, Springer Series in Statistics, Springer, New York, NY, USA, 2001.

[6] K. Kobayashi, K. Kaito, and L. T. Nam, "A bayesian estimation method to improve deterioration prediction for infrastructure system with markov chain model," *International Journal of Architecture, Engineering and Construction*, vol. 1, no. 1, pp. 1–13, 2012.

[7] Y. Tsuda, K. Kaito, K. Aoki, and K. Kobayashi, "Estimating Markovian transition probabilities for bridge deterioration forecasting," *Journal of Structural Engineering/Earthquake Engineering*, vol. 23, no. 2, pp. 241s–256s, 2006.

[8] J. Geweke, "Evaluating the accuracy of sampling-based approaches to the calculation of posterior moments," in *Bayesian Statistics*, vol. 4, pp. 169–193, Oxford University Press, 1996.

Hindawi Publishing Corporation
Journal of Applied Mathematics
Volume 2012, Article ID 672947, 25 pages
doi:10.1155/2012/672947

*Research Article*

# Optimality Conditions for Infinite Order Distributed Parabolic Systems with Multiple Time Delays Given in Integral Form

**Bahaa G. M.**[1,2]

[1] *Department of Mathematics, Faculty of Science, Taibah University, Al-Madinah Al-Munawwarah, Saudi Arabia*
[2] *Department of Mathematics, Faculty of Science, Beni-Suef University, Beni-Suef, Egypt*

Correspondence should be addressed to G. M. Bahaa, bahaa_gm@hotmail.com

Received 1 March 2012; Accepted 29 April 2012

Academic Editor: Weihai Zhang



The optimal boundary control problem for $(n \times n)$ infinite order distributed parabolic systems with multiple time delays given in the integral form both in the state equations and in the Neumann boundary conditions is considered. Constraints on controls are imposed. Necessary and suffacient optimality conditions for the Neumann problem with the quadratic performance functional are derived.

## 1. Introduction

Distributed parameters systems with delays can be used to describe many phenomena in the real world. As is well known, heat conduction, properties of elastic-plastic material, fluid dynamics, diffusion-reaction processes, the transmission of the signals at a certain distance by using electric long lines, and so forth, all lie within this area. The object that we are studying (temperature, displacement, concentration, velocity, etc.) is usually referred to as the state.

During the last twenty years, equations with deviating argument have been applied not only in applied mathematics, physics, and automatic control, but also in some problems of economy and biology. Currently, the theory of equations with deviating arguments constitutes a very important subfield of mathematical control theory.

Consequently, equations with deviating arguments are widely applied in optimal control problems of distributed parameter system with time delays [1].

The optimal control problems of distributed parabolic systems with time-delayed boundary conditions have been widely discussed in many papers and monographs. A fundamental study of such problems is given by [2] and was next developed by [3, 4]. It was

also intensively investigated by [1, 5–16] in which linear quadratic problem for parabolic systems with time delays given in the different form (constant, time delays, time-varying delays, time delays given in the integral form, etc.) was presented.

The necessary and sufficient conditions of optimality for systems consist of only one equation and for $(n \times n)$ systems governed by different types of partial differential equations defined on spaces of functions of infinitely many variables and also for infinite order systems are discussed for example in [9, 11, 15–18] in which the argument of [19, 20] was used.

Making use of the Dubovitskii-Milyutin Theorem in [13, 21–28] the necessary and sufficient conditions of optimality for similar systems governed by second order operator with an infinite number of variables and also for infinite order systems were investigated. The interest in the study of this class of operators is stimulated by problems in quantum field theory.

In particular, the papers of [1, 8] present necessary and sufficient optimality conditions for the Neumann problem with quadratic performance functionals, applied to a single one equation of second-order parabolic system with fixed time delay and with multiple time delays given in the integral form both in the state equations and in the Neumann boundary conditions, respectively. Such systems constitute a more complex case of distributed parameter systems with time delays given in the integral form.

Also in [9, 11] time-optimal boundary control for a single one equation distributed infinite order parabolic and hyperbolic systems in which constant time lags appear in the integral form both in the state equation and in the Neumann boundary condition is present. Some specific properties of the optimal control are discussed.

In this paper we recall the problem in a more general formulation. A distributed parameter for infinite order parabolic $(n \times n)$ systems with multiple time delays given in the integral form both in the state equations and in the Neumann boundary conditions is considered. Such an infinite order parabolic system can be treated as a generalization of the mathematical model for a plasma control process. The quadratic performance functionals defined over a fixed time horizon are taken and some constraints are imposed on the initial state and the boundary control. Such a system may be viewed as a linear representation of many diffusion processes, in which time-delayed signals are introduced at a spatial boundary, and there is a freedom in choosing the controlled process initial state. Following a line of the Lions scheme, necessary and sufficient optimality conditions for the Neumann problem applied to the above system were derived. The optimal control is characterized by the adjoint equations.

This paper is organized as follows. In Section 1, we introduce spaces of functions of infinite order. In Section 2, we formulate the mixed Neumann problem for infinite order parabolic operator with multiple time delays given in the integral form. In Section 3, the boundary optimal control problem for this case is formulated, then we give the necessary and sufficient conditions for the control to be an optimal. In Section 4, we generalized the discussion to two cases, the first case: the optimal control for $(2 \times 2)$ coupled infinite order parabolic systems is studied. The second case: the optimal control for $(n \times n)$ coupled infinite order parabolic systems was to be formulated.

## 2. Sobolev Spaces with Infinite Order

The object of this section is to give the definition of some function spaces of infinite order and the chains of the constructed spaces which will be used later.

Let $\Omega$ be a bounded open set of $\mathbb{R}^n$ with a smooth boundary $\Gamma$, which is a $C^\infty$ manifold of dimension $(n-1)$. Locally, $\Omega$ is totally on one side of $\Gamma$. We define the infinite order Sobolev space $W^\infty\{a_\alpha, 2\}(\Omega)$ of infinite order of periodic functions $\phi(x)$ defined on $\Omega$ [29–31] as follows:

$$W^\infty\{a_\alpha, 2\}(\Omega) = \left\{ \phi(x) \in \mathrm{C}^\infty(\Omega) : \sum_{|\alpha|=0}^{\infty} a_\alpha \left\| \mathrm{D}^\alpha \phi \right\|_2^2 < \infty \right\}, \tag{2.1}$$

where $C^\infty(\Omega)$ is the space of infinitely differentiable functions, $a_\alpha \geq 0$ is a numerical sequence, and $\|\cdot\|_2$ is the canonical norm in the space $L^2(\Omega)$, and

$$D^\alpha = \frac{\partial^{|\alpha|}}{(\partial x_1)^{\alpha_1} \cdots (\partial x_n)^{\alpha_n}}, \tag{2.2}$$

$\alpha = (\alpha_1, \ldots, \alpha_n)$ being a multi-index for differentiation, $|\alpha| = \sum_{i=1}^n \alpha_i$.

The space $W^{-\infty}\{a_\alpha, 2\}(\Omega)$ is defined as the formal conjugate space to the space $W^\infty\{a_\alpha, 2\}(\Omega)$, namely:

$$W^{-\infty}\{a_\alpha, 2\}(\Omega) = \left\{ \psi(x) : \psi(x) = \sum_{|\alpha|=0}^{\infty} (-1)^{|\alpha|} a_\alpha D^\alpha \psi_\alpha(x) \right\}, \tag{2.3}$$

where $\psi_\alpha \in L^2(\Omega)$ and $\sum_{|\alpha|=0}^{\infty} a_\alpha \|\psi_\alpha\|_2^2 < \infty$.

The duality pairing of the spaces $W^\infty\{a_\alpha, 2\}$ $(\Omega)$ and $W^{-\infty}\{a_\alpha, 2\}(\Omega)$ is postulated by the formula:

$$(\phi, \psi) = \sum_{|\alpha|=0}^{\infty} a_\alpha \int_\Omega \psi_\alpha(x) D^\alpha \phi(x) dx, \tag{2.4}$$

where

$$\phi \in W^\infty\{a_\alpha, 2\}(\Omega), \qquad \psi \in W^{-\infty}\{a_\alpha, 2\}(\Omega). \tag{2.5}$$

From above, $W^\infty\{a_\alpha, 2\}(\Omega)$ is everywhere dense in $L^2(\Omega)$ with topological inclusions and $W^{-\infty}\{a_\alpha, 2\}(\Omega)$ denotes the topological dual space with respect to $L^2(\Omega)$, so we have the following chain of inclusions:

$$W^\infty\{a_\alpha, 2\}(\Omega) \subseteq L^2(\Omega) \subseteq W^{-\infty}\{a_\alpha, 2\}(\Omega). \tag{2.6}$$

We now introduce $L^2(0,T;L^2(\Omega))$ which we will denoted by $L^2(Q)$, where $Q = \Omega\times]0,T[$ denotes the space of measurable functions $t \to \phi(t)$ such that

$$\|\phi\|_{L^2(Q)} = \left(\int_0^T \|\phi(t)\|_2^2 dt\right)^{1/2} < \infty, \tag{2.7}$$

endowed with the scalar product $(f,g) = \int_0^T (f(t),g(t))_{L^2(\Omega)}dt$, $L^2(Q)$ is a Hilbert space.

In the same manner we define the spaces $L^2(0,T;W^\infty\{a_\alpha,2\}(\Omega))$, and $L^2(0,T;W^{-\infty}\{a_\alpha,2\}(\Omega))$, as its formal conjugate.

Also, we have the following chain of inclusions:

$$L^2(0,T;W^\infty\{a_\alpha,2\}(\Omega)) \subseteq L^2(Q) \subseteq L^2\left(0,T;W^{-\infty}\{a_\alpha,2\}(\Omega)\right). \tag{2.8}$$

The construction of the Cartesian product of $n$-times to the above Hilbert spaces can be constructed, for example

$$\begin{aligned}(W^\infty\{a_\alpha,2\}(\Omega))^n &= \underbrace{W^\infty\{a_\alpha,2\}(\Omega)\times W^\infty\{a_\alpha,2\}(\Omega)\times\cdots\times W^\infty\{a_\alpha,2\}(\Omega)}_{n\text{-times}}\\ &= \prod_{i=1}^n (W^\infty\{a_\alpha,2\}(\Omega))^i,\end{aligned} \tag{2.9}$$

with norm defined by:

$$\|\phi\|_{(W^\infty\{a_\alpha,2\}(\Omega))^n} = \sum_{i=1}^n \|\phi_i\|_{W^\infty\{a_\alpha,2\}(\Omega)}, \tag{2.10}$$

where $\phi = (\phi_1,\phi_2,\ldots,\phi_n) = (\phi_i)_{i=1}^n$ is a vector function and $\phi_i \in W^\infty\{a_\alpha,2\}(\Omega)$.

Finally, we have the following chain of inclusions:

$$\left(L^2(0,T;W^\infty\{a_\alpha,2\}(\Omega))\right)^n \subseteq \left(L^2(Q)\right)^n \subseteq \left(L^2(0,T;W^{-\infty}\{a_\alpha,2\}(\Omega))\right)^n, \tag{2.11}$$

where $(L^2(0,T;W^{-\infty}\{a_\alpha,2\}(\Omega)))^n$ are the dual spaces of $(L^2(0,T;W^\infty\{a_\alpha,2\}(\Omega)))^n$. The spaces considered in this paper are assumed to be real.

## 3. Mixed Neumann Problem for Infinite Order Parabolic System with Multiple Time Lags

The object of this section is to formulate the following mixed initial boundary value Neumann problem for infinite order parabolic system with multiple time delays which defines the state of the system model [1, 5–11, 18, 24, 26].

$$\frac{\partial y}{\partial t} + \mathcal{A}(t)y(x,t) + \sum_{i=1}^{m}\int_{a_i}^{b_i} b_i(x,t)y(x,t-h_i)dh_i = u, \tag{3.1}$$

$$(x,t) \in \Omega \times (0,T), \quad h_i \in (a_i,b_i),$$

$$y(x,t') = \Phi_0(x,t'), \quad (x,t') \in \Omega \times (-\Delta,0), \tag{3.2}$$

$$y(x,0) = y_0(x), \quad x \in \Omega, \tag{3.3}$$

$$\frac{\partial y}{\partial \nu_{\mathcal{A}}}(x,t) = \sum_{s=1}^{l}\int_{c_s}^{d_s} c_s(x,t)y(x,t-k_s)dk_s + v, \quad (x,t) \in \Gamma \times (0,T),\ k_s \in (c_s,d_s), \tag{3.4}$$

$$y(x,t') = \Psi_0(x,t'), \quad (x,t') \in \Gamma \times (-\Delta,0), \tag{3.5}$$

where $\Omega \subset R^n$ has the same properties as in Section 1. We have

$$y \equiv y(x,t;u), \quad y(0) \equiv y(x,0;u), \quad y(T) \equiv y(x,T;u), \quad u \equiv u(x,t), \quad v \equiv v(x,t),$$

$$Q = \Omega \times (0,T), \quad \overline{Q} = \overline{\Omega} \times [0,T], \quad Q_0 = \Omega \times [-\Delta,0), \quad \Sigma = \Gamma \times (0,T), \quad \Sigma_0 = \Gamma \times [-\Delta,0), \tag{3.6}$$

(i) $T$ is a specified positive number representing a finite time horizon,

(ii) $h_i, k_s$ are time delays, such that $h_i \in (a_i,b_i)$ and $k_s \in (c_s,d_s)$ where $0 < a_1 < a_2 < \cdots < a_m$, $0 < b_1 < b_2 < \cdots < b_m$, for $i = 1,2,\ldots,m$ and $0 < c_1 < c_2 < \cdots < c_l$, $0 < d_1 < d_2 < \cdots < d_l$, for $s = 1,2,\ldots,l$,

(iii) $b_i(t), i = 1,2,\ldots,m$ are given real $C^\infty$ functions defined on $\overline{Q}$,

(iv) $c_s(x,t), s = 1,2,\ldots,l$ are given real $C^\infty$ functions defined on $\Sigma$,

(v) $\Delta = \max\{b_m, d_l\}$,

(vi) $y$ is a function defined on $Q$ such that $\Omega \times (0,T) \ni (x,t) \to y(x,t) \in R$,

(vii) $u, v$ are functions defined on $Q$ and $\Sigma$ such that $\Omega \times (0,T) \ni (x,t) \to u(x,t) \in R$ and $\Gamma \times (0,T) \ni (x,t) \to v(x,t) \in R$,

(viii) $\Phi_0, \Psi_0$ are initial functions defined on $Q_0$ and $\Sigma_0$, respectively, such that $\Omega \times [-\Delta,0) \ni (x,t') \to \Phi_0(x,t') \in R$. $\Gamma \times [-\Delta,0) \ni (x,t') \to \Psi_0(x,t') \in R$.

The parabolic operator $(\partial/\partial t) + \mathcal{A}(t)$ in the state equation (3.1) is an infinite order parabolic operator and $\mathcal{A}(t)$ [17, 21, 29–31] is given by:

$$\mathcal{A}y = \sum_{|\alpha|=0}^{\infty} (-1)^{|\alpha|} a_\alpha D^{2\alpha} y(x,t),$$
$$\mathcal{A} = \sum_{|\alpha|=0}^{\infty} (-1)^{|\alpha|} a_\alpha D^{2\alpha} \tag{3.7}$$

is an infinite order self-adjoint elliptic partial differential operator maps $W^{\infty}\{a_\alpha, 2\}(\Omega)$ onto $W^{-\infty}\{a_\alpha, 2\}(\Omega)$.

For this operator we define the bilinear form as follows.

*Definition 3.1.* For each $t \in (0,T)$, we define a family of bilinear forms on $W^{\infty}\{a_\alpha, 2\}(\Omega)$ by:

$$\pi(t; y, \phi) = \left(\mathcal{A}(t)y, \phi\right)_{L^2(\Omega)}, \quad y, \phi \in W^{\infty}\{a_\alpha, 2\}(\Omega), \tag{3.8}$$

where $\mathcal{A}(t)$ maps $W^{\infty}\{a_\alpha, 2\}(\Omega)$ onto $W^{-\infty}\{a_\alpha, 2\}(\Omega)$ and takes the above form. Then

$$\begin{aligned} \pi(t; y, \phi) &= \left(\mathcal{A}(t)y, \phi\right)_{L^2(\Omega)} \\ &= \left( \sum_{|\alpha|=0}^{\infty} (-1)^{|\alpha|} a_\alpha D^{2\alpha} y(x,t), \phi(x) \right)_{L^2(\Omega)} \\ &= \int_\Omega \sum_{|\alpha|=0}^{\infty} a_\alpha D^\alpha y(x) D^\alpha \phi(x) dx. \end{aligned} \tag{3.9}$$

**Lemma 3.2.** *The bilinear form $\pi(t; y, \phi)$ is coercive on $W^{\infty}\{a_\alpha, 2\}(\Omega)$, that is,*

$$\pi(t; y, y) \geq \lambda \, \|y\|^2_{W^{\infty}\{a_\alpha, 2\}(\Omega)}, \quad \lambda > 0. \tag{3.10}$$

*Proof.* It is well known that the ellipticity of $\mathcal{A}(t)$ is sufficient for the coerciveness of $\pi(t; y, \phi)$ on $W^{\infty}\{a_\alpha, 2\}(\Omega)$:

$$\pi(t; \phi, \psi) = \int_\Omega \sum_{|\alpha|=0}^{\infty} a_\alpha D^\alpha \phi D^\alpha \psi \, dx. \tag{3.11}$$

Then

$$\begin{aligned}\pi(t;y,y) &= \int_{\Omega} \sum_{|\alpha|=0}^{\infty} a_{\alpha} D^{\alpha} y D^{\alpha} y \, dx \\ &\geq \sum_{|\alpha|=0}^{\infty} a_{\alpha} \left\| D^{2\alpha} y(x) \right\|^2_{L^2(\Omega)} \\ &\geq \lambda \|y\|^2_{W^{\infty}\{a_{\alpha},2\}(\Omega)}, \quad \lambda > 0.\end{aligned} \tag{3.12}$$

Also we have

$$\begin{aligned}&\forall y, \phi \in W^{\infty}\{a_{\alpha},2\}(\Omega) \text{ the function } t \longrightarrow \pi(t;y,\phi) \\ &\text{is continuously differentiable in } (0,T) \text{ and } \pi(t;y,\phi) = \pi(t;\phi,y).\end{aligned} \tag{3.13}$$

Equations (3.1)–(3.5) constitute a Neumann problem. Then the left-hand side of the boundary condition (3.4) may be written in the following form:

$$\frac{\partial y(x,t)}{\partial \nu_{\mathcal{A}}} = \sum_{|\omega|=0}^{\infty} \left(D^{\omega} y(x,t)\right) \cos(n, x_k) = q(x,t), \quad x \in \Gamma,\ t \in (0,T), \tag{3.14}$$

where $\partial/\partial \nu_{\mathcal{A}}$ is a normal derivative at $\Gamma$, directed towards the exterior of $\Omega$, and $\cos(n, x_k)$ is the $k$th direction cosine of $n$, with $n$ being the normal at $\Gamma$ exterior to $\Omega$.

Then (3.4) can be written as:

$$q(x,t) = \sum_{s=1}^{l} \int_{c_s}^{d_s} c_s(x,t) y(x, t-k_s) dk_s + v(x,t), \quad x \in \Gamma, t \in (0,T). \tag{3.15}$$

□

*Remark 3.3.* We will apply the indication $q(x,t)$ appearing in (3.14) to prove the existence of a unique solution for (3.1)–(3.5).

We will formulate sufficient conditions for the existence of a unique solution of the mixed boundary value problem (3.1)–(3.5) for the cases where the boundary control $v \in L^2(\Sigma)$.

For this purpose, we introduce the Sobolev space $W^{\infty,1}(Q)$ [20, Vol. 2, page 6] defined by:

$$W^{\infty,1}(Q) = L^2(0,T; W^{\infty}\{a_{\alpha},2\}(\Omega)) \cap W^1\Big(0,T; L^2(\Omega)\Big), \tag{3.16}$$

which is a Hilbert space normed by

$$\begin{aligned}\|y\|_{W^{\infty,1}(Q)} &= \left[\int_0^T \int \|y\|^2_{W^\infty\{a_\alpha,2\}(\Omega)} dt + \|y\|^2_{W^1(0,T;L^2(\Omega))}\right]^{1/2} \\ &= \left[\int_Q \left(\sum_{|\alpha|=0}^{\infty} a_\alpha |D^\alpha y|^2 + \left|\frac{\partial y}{\partial t}\right|^2\right) dx\, dt\right]^{1/2} \\ &= \left[\int_Q \left(a_0|y|^2 + \sum_{|\alpha|=1}^{\infty} a_\alpha |D^\alpha y|^2 + \left|\frac{\partial y}{\partial t}\right|^2\right) dx\, dt\right]^{1/2}, \quad a_0 > 0,\end{aligned} \tag{3.17}$$

where the space $W^1(0,T;L^2(\Omega))$ denotes the Sobolev space of order 1 of functions defined on $(0,T)$ and taking values in $L^2(\Omega)$ [20, Vol. 1].

The existence of a unique solution for the mixed initial-boundary value problem (3.1)–(3.5) on the cylinder $Q$ can be proved using a constructive method, that is, solving at first equations (3.1)–(3.5) on the subcylinder $Q_1$ and in turn on $Q_2$ and so forth, until the procedure covers the whole cylinder $Q$. In this way, the solution in the previous step determines the next one.

For simplicity, we introduce the following notation:

$$E_j \widehat{=} \big((j-1)\lambda, j\lambda\big), \quad Q_j = \Omega \times E_j, \quad \Sigma_j = \Gamma \times E_j \quad \text{for } j = 1,\dots,K,\ \lambda = \min\{a_1, c_1\}. \tag{3.18}$$

Making use of the results of [7, 20] we can prove that the following result holds.

**Theorem 3.4.** *Let $y_0$, $\Phi_0$, $\Psi_0$, $v$ and $u$ be given with $y_0 \in W^\infty\{a_\alpha,2\}(\Omega)$, $\Phi_0 \in W^{\infty,1}(Q_0)$, $\Psi_0 \in L^2(\Sigma_0)$, $v \in L^2(\Sigma)$ and $u \in W^{-\infty,-1}(Q)$. Then, there exists a unique solution $y \in W^{\infty,1}(Q)$ for the mixed initial-boundary value problem* (3.1)–(3.5). *Moreover, $y(\cdot, j\lambda) \in W^\infty\{a_\alpha,2\}(\Omega)$ for $j = 1,\dots,K$.*

## 4. Problem Formulation-Optimization Theorems

Now, we formulate the optimal control problem for (3.1)–(3.5) in the context of the Theorem 3.4, that is $v \in L^2(\Sigma)$.

Let us denote by $U = L^2(\Sigma)$ the space of controls. The time horizon $T$ is fixed in our problem.

The performance functional is given by

$$I(v) = \lambda_1 \int_Q \big[y(x,t;v) - z_d\big]^2 dx\, dt + \lambda_2 \int_\Sigma (Nv)v\, d\Gamma dt, \tag{4.1}$$

where $\lambda_i \geq 0$, and $\lambda_1 + \lambda_2 > 0$, $z_d$ is a given element in $L^2(Q)$; $N$ is a positive linear operator on $L^2(\Sigma)$ into $L^2(\Sigma)$.

*Control Contraints*

We define the set of admissible controls $U_{\text{ad}}$ such that

$$U_{\text{ad}} \text{ is closed, convex subset of } U = L^2(\Sigma). \tag{4.2}$$

Let $y(x,t;v)$ denote the solution of the mixed initial-boundary value problem (3.1)–(3.5) at $(x,t)$ corresponding to a given control $v \in U_{\text{ad}}$. We note from Theorem 3.4 that for any $v \in U_{\text{ad}}$ the performance functional (4.1) is well-defined since $(v) \in W^{\infty,1}(Q) \subset L^2(Q)$.

Making use of the Loins's scheme we will derive the necessary and sufficient conditions of optimality for the optimization problem (3.1)–(3.5), (4.1), (4.2). The solving of the formulated optimal control problem is equivalent to seeking a $v^* \in U_{\text{ad}}$ such that

$$I(v^*) \leq I(v), \quad \forall v \in U_{\text{ad}}. \tag{4.3}$$

From the Lion's scheme [19, Theorem 1.3, page 10], it follows that for $\lambda_2 > 0$ a unique optimal control $v^*$ exists. Moreover, $v^*$ is characterized by the following condition:

$$I'(v^*)(v - v^*) \geq 0, \quad \forall v \in U_{\text{ad}}. \tag{4.4}$$

For the performance functional of form (4.1) the relation (4.4) can be expressed as

$$\lambda_1 \int_Q \left(y(v^*) - z_d\right)\left[y(v) - y(v^*)\right] dx\, dt + \lambda_2 \int_\Sigma N v^*(v - v^*) d\Gamma\, dt \geq 0, \quad \forall v \in U_{\text{ad}}. \tag{4.5}$$

In order to simplify (4.5), we introduce the adjoint equation, and for every $v \in U_{\text{ad}}$, we define the adjoint variable $p = p(v) \equiv p(x,t;v)$ as the solution of the equations:

$$\frac{-\partial p(v)}{\partial t} + \mathcal{A}^*(t)p(v) + \sum_{i=1}^{m} \int_{a_i}^{b_i} b_i(x, t + h_i) p(x, t + h_i; v) dh_i = \lambda_1\left(y(v) - z_d\right), \quad (x,t) \in \Omega \times (0, T - \Delta), \quad h_i \in (a_i, b_i), \tag{4.6}$$

$$\frac{-\partial p(v)}{\partial t} + \mathcal{A}^*(t)p(v) = \lambda_1\left(y(v) - z_d\right), \quad (x,t) \in \Omega \times (T - \Delta, T), \tag{4.7}$$

$$p(x,T;v) = 0, \quad x \in \Omega, \tag{4.8}$$

$$p(x,t;v) = 0, \quad (x,t) \in \Omega \times [T - \Delta + \lambda, T), \tag{4.9}$$

$$\frac{\partial p(v)}{\partial v_{\mathcal{A}^*}}(x,t) = \sum_{s=1}^{l} \int_{c_s}^{d_s} c_s(x, t + k_s) p(x, t + k_s; v) dk_s, \quad (x,t) \in \Gamma \times (0, T - \Delta(T)),\ k_s \in (c_s, d_s), \tag{4.10}$$

$$\frac{\partial p(v)}{\partial v_{\mathcal{A}^*}}(x,t) = 0, \quad (x,t) \in \Gamma \times (T - \Delta(T), T), \tag{4.11}$$

where

$$\frac{\partial p(v)}{\partial v_{\mathcal{A}^*}}(x,t) = \sum_{|\omega|=0}^{\infty} \left(D^{\omega} p(v)\right) \cos(n, x_{\omega})(x,t),$$
$$\mathcal{A}^*(t)p(v) = \sum_{|\alpha|=0}^{\infty} (-1)^{|\alpha|} a_{\alpha} D^{2\alpha} p(x,t). \tag{4.12}$$

As in the above section with change of variables, that is, with reversed sense of time. that is, $t' = T - t$, for given $z_d \in L^2(Q)$ and any $v \in L^2(\Sigma)$, there exists a unique solution $p(v) \in W^{\infty,1}(Q)$ for problem (4.6)–(4.11).

The existence of a unique solution for the problem (4.6)–(4.11) on the cylinder $\Omega \times (0,T)$ can be proved using a constructive method. It is easy to notice that for given $z_d$ and $u$, the problem (4.6)–(4.11) can be solved backwards in time starting from $t = T$, that is, first solving (4.6)–(4.11) on the subcylinder $Q_K$ and in turn on $Q_{K-1}$, and so forth until the procedure covers the whole cylinder $\Omega \times (0,T)$. For this purpose, we may apply Theorem 3.4 (with an obvious change of variables).

Hence, using Theorem 3.4, the following result can be proved.

**Lemma 4.1.** *Let the hypothesis of Theorem 3.4 be satisfied. Then for given $z_d \in L^2(\Omega, R^{\infty})$ and any $v \in L^2(\Sigma)$, there exists a unique solution $p(v) \in W^{\infty,1}(Q)$ for the adjoint problem* (4.6)–(4.11).

We simplify (4.5) using the adjoint equation (4.6)–(4.11). For this purpose denoting by $p(0) \equiv p(x,0;v)$ and $p(T) \equiv p(x,T;v)$, respectively, setting $v = v^*$ in (4.6)–(4.11), multiplying both sides of (4.6) and (4.7) by $y(v) - y(v^*)$, then integrating over $\Omega \times (0, T-\Delta)$ and $\Omega \times (T-\Delta, T)$, respectively and then adding both sides of (4.6), (4.11), we get

$$\begin{aligned}
&\lambda_1 \int_Q \left(y(v^*) - z_d\right)\left[y(v) - y(v^*)\right] dx\, dt \\
&\quad = \int_Q \left(-\frac{\partial p(v^*)}{\partial t} + \mathcal{A}^*(t)p(v^*)\right) \times \left[y(v) - y(v^*)\right] dx\, dt \\
&\qquad + \int_0^{T-\Delta} \int_{\Omega} \left(\sum_{i=1}^{m} \int_{a_i}^{b_i} b_i(x, t+h_i) p(x, t+h_i; v^*) dh_i\right) \times \left[y(x,t;v) - y(x,t;v^*)\right] dx\, dt \\
&\quad = \int_0^T \int_{\Omega} p(v^*) \frac{\partial}{\partial t}\left[y(v) - y(v^*)\right] dx\, dt \\
&\qquad + \int_0^T \int_{\Omega} \mathcal{A}^*(t) p(v^*) \left[y(v) - y(v^*)\right] dx\, dt \\
&\qquad + \sum_{i=1}^{m} \int_{a_i}^{b_i} \int_{\Omega} \int_0^{T-\Delta} \left(b_i(x, t+h_i) p(x, t+h_i; v^*)\right) \times \left[y(x,t;v) - y(x,t;v^*)\right] dx\, dt\, dh_i.
\end{aligned} \tag{4.13}$$

Using (3.1), the first integral on the right-hand side of (4.13) can be written as:

$$\begin{aligned}
&\int_0^T \int_\Omega p(v^*)\frac{\partial}{\partial t}\left[y(v)-y(v^*)\right]dx\,dt \\
&\quad= -\int_Q p(v^*)\mathcal{A}(t)\left(y(v)-y(v^*)\right)dx\,dt \\
&\qquad -\sum_{i=1}^m \int_{a_i}^{b_i}\int_\Omega\int_0^T p(x,t;v^*)b_i(x,t)\times\left[y(x,t-h_i;v)-y(x,t-h_i;v^*)\right]dt\,dx\,dh_i \\
&\quad= -\int_Q p(v^*)\mathcal{A}(t)\left(y(v)-y(v^*)\right)dx\,dt \\
&\qquad -\sum_{i=1}^m \int_{a_i}^{b_i}\int_\Omega\int_{-h_i}^{T-h_i} p(x,t'+h_i;v^*)b_i(x,t'+h_i)\times\left[y(x,t';v)-y(x,t';v^*)\right]dt'\,dx\,dh_i \\
&\quad= -\int_\Omega p(v^*)\mathcal{A}(t)\left(y(v)-y(v^*)\right)dx\,dt \\
&\qquad -\sum_{i=1}^m \int_{a_i}^{b_i}\int_\Omega\int_{-h_i}^{0} p(x,t'+h_i;v^*)b_i(x,t'+h_i)\times\left[y(x,t';v)-y(x,t';v^*)\right]dt'\,dx\,dh_i \\
&\qquad -\sum_{i=1}^m \int_{a_i}^{b_i}\int_\Omega\int_{0}^{T-\Delta} p(x,t'+h_i;v^*)b_i(x,t'+h_i)\times\left[y(x,t';v)-y(x,t';v^*)\right]dt'\,dx d\,h_i \\
&\qquad -\sum_{i=1}^m \int_{a_i}^{b_i}\int_\Omega\int_{T-\Delta}^{T-h_i} p(x,t'+h_i;v^*)b_i(x,t'+h_i)\times\left[y(x,t';v)-y(x,t';v^*)\right]dt'\,dx\,dh_i \\
&\quad= -\int_Q p(v^*)\mathcal{A}(t)\left(y(v)-y(v^*)\right)dx\,dt \\
&\qquad -\sum_{i=1}^m \int_{a_i}^{b_i}\int_\Omega\int_{-h_i}^{0} p(x,t'+h_i;v^*)b_i(x,t'+h_i)\times\left[y(x,t';v)-y(x,t';v^*)\right]dt'\,dx\,dh_i \\
&\qquad -\sum_{i=1}^m \int_{a_i}^{b_i}\int_\Omega\int_{0}^{T-\Delta} p(x,t'+h_i;v^*)b_i(x,t'+h_i)\times\left[y(x,t';v)-y(x,t';v^*)\right]dt'\,dx\,dh_i \\
&\qquad -\sum_{i=1}^m \int_{a_i}^{b_i}\int_\Omega\int_{T-\Delta+h_i}^{T} p(x,t;v^*)b_i(x,t)\times\left[y(x,t-h_i;v)-y(x,t-h_i;v^*)\right]dt\,dx\,dh_i.
\end{aligned} \tag{4.14}$$

Using Green's formula, the second integral on the right-hand side of (4.13) can be written as:

$$\begin{aligned}
&\int_0^T \int_\Omega \mathcal{A}^*(t)p(v^*)\left[y(v)-y(v^*)\right]dx\,dt \\
&\qquad= \int_0^T \int_\Omega p(v^*)\mathcal{A}(t)\left[y(v)-y(v^*)\right]dx\,dt
\end{aligned}$$

$$+\int_0^T\int_\Gamma p(v^*)\left(\frac{\partial y(v)}{\partial v_{\mathcal{A}}}-\frac{\partial y(v^*)}{\partial v_{\mathcal{A}}}\right)d\Gamma\,dt$$

$$-\int_0^T\int_\Gamma \frac{\partial p(v^*)}{\partial v_{\mathcal{A}^*}}\left[y(v)-y(v^*)\right]d\Gamma\,dt. \tag{4.15}$$

Using the boundary condition (3.2), one can transform the second integral on the right-hand side of (4.15) into the form:

$$\begin{aligned}
&\int_0^T\int_\Gamma p(v^*)\left(\frac{\partial y(v)}{\partial v_{\mathcal{A}}}-\frac{\partial y(v^*)}{\partial v_{\mathcal{A}}}\right)d\Gamma\,dt\\
&\quad=\sum_{s=1}^{l}\int_{c_s}^{d_s}\int_\Gamma\int_0^T p(x,t;v^*)c_s(x,t)\times\left[y(x,t-k_s;v)-y(x,t-k_s;v^*)\right]d\Gamma\,dt\,dk_s\\
&\qquad+\int_0^T\int_\Gamma p(v^*)(v-v^*)d\Gamma\,dt\\
&\quad=\sum_{s=1}^{l}\int_{c_s}^{d_s}\int_\Gamma\int_{-k_s}^{T-k_s} p(x,t'+k_s;v^*)c_s(x,t'+k_s)\times\left[y(x,t';v)-y(x,t';v^*)\right]dt'\,d\Gamma\,dk_s\\
&\qquad+\int_0^T\int_\Gamma p(v^*)(v-v^*)d\Gamma\,dt\\
&\quad=\sum_{s=1}^{l}\int_{c_s}^{d_s}\int_\Gamma\int_{-k_s}^{0} p(x,t'+k_s;v^*)c_s(x,t'+k_s)\times\left[y(x,t';v)-y(x,t';v^*)\right]dt'\,d\Gamma\,dk_s\\
&\qquad+\sum_{s=1}^{l}\int_{c_s}^{d_s}\int_\Gamma\int_{0}^{T-\Delta} p(x,t'+k_s;v^*)c_s(x,t'+k_s)\times\left[y(x,t';v)-y(x,t';v^*)\right]dt'\,d\Gamma\,dk_s\\
&\qquad+\sum_{s=1}^{l}\int_{c_s}^{d_s}\int_\Gamma\int_{T-\Delta}^{T-k_s} p(x,t'+k_s;v^*)c_s(x,t'+k_s)\times\left[y(x,t';v)-y(x,t';v^*)\right]dt'\,d\Gamma\,dk_s\\
&\qquad+\int_0^T\int_\Gamma p(v^*)(v-v^*)d\Gamma\,dt\\
&\quad=\sum_{s=1}^{l}\int_{c_s}^{d_s}\int_\Gamma\int_{-k_s}^{0} p(x,t'+k_s;v^*)c_s(x,t'+k_s)\times\left[y(x,t';v)-y(x,t';v^*)\right]dt'\,d\Gamma\,dk_s\\
&\qquad+\sum_{s=1}^{l}\int_{c_s}^{d_s}\int_\Gamma\int_{0}^{T-\Delta} p(x,t'+k_s;v^*)c_s(x,t'+k_s)\times\left[y(x,t';v)-y(x,t';v^*)\right]dt'\,d\Gamma\,dk_s
\end{aligned}$$

$$+\sum_{s=1}^{l}\int_{c_s}^{d_s}\int_{\Gamma}\int_{T-\Delta+k_s}^{T} p(x,t;v^*)c_s(x,t)\times\left[y(x,t-k_s;v)-y(x,t-k_s;v^*)\right]dt\,d\Gamma\,dk_s$$
$$+\int_0^T\int_{\Gamma} p(v^*)(v-v^*)d\Gamma\,dt. \tag{4.16}$$

The last component in (4.15) can be rewritten as

$$\int_0^T\int_{\Gamma}\frac{\partial p(v^*)}{\partial v_{\mathcal{A}^*}}\left[y(v)-y(v^*)\right]d\Gamma\,dt$$
$$=\int_0^{T-\Delta}\int_{\Gamma}\frac{\partial p(v^*)}{\partial v_{\mathcal{A}^*}}\left[y(v)-y(v^*)\right]d\Gamma\,dt+\int_{T-\Delta}^{T}\int_{\Gamma}\frac{\partial p(v^*)}{\partial v_{\mathcal{A}^*}}\left[y(v)-y(v^*)\right]d\Gamma\,dt. \tag{4.17}$$

Substituting (4.16) and (4.17) into (4.15) and then the results into (4.13), we obtain

$$\lambda_1\int_Q\left(y(v^*)-z_d\right)\left[y(v)-y(v^*)\right]dx\,dt$$
$$=\int_0^T\int_{\Gamma} p(v^*)(v-v^*)d\Gamma dt-\int_Q p(v^*)\mathcal{A}(t)\left[y(v)-y(v^*)\right]dx\,dt$$
$$-\sum_{i=1}^{m}\int_{a_i}^{b_i}\int_{\Omega}\int_{-h_i}^{0} b_i(x,t+h_i)p(x,t+h_i;v^*)\times\left[y(x,t;v)-y(x,t;v^*)\right]dt\,dx\,dh_i$$
$$-\sum_{i=1}^{m}\int_{a_i}^{b_i}\int_{\Omega}\int_{0}^{T-\Delta} b_i(x,t+h_i)p(x,t+h_i;v^*)\times\left[y(x,t;v)-y(x,t;v^*)\right]dt\,dx\,dh_i$$
$$+\int_Q p(v^*)\mathcal{A}(t)\left[y(v)-y(v^*)\right]dx\,dt$$
$$-\sum_{i=1}^{m}\int_{a_i}^{b_i}\int_{\Omega}\int_{T-\Delta+h_i}^{T} p(x,t;v^*)b_i(x,t)\times\left[y(x,t-h_i;v)-y(x,t-h_i;v^*)\right]dt\,dx\,dh_i$$
$$+\sum_{s=1}^{l}\int_{c_s}^{d_s}\int_{\Gamma}\int_{-k_s}^{0} c_s(x,t+k_s)p(x,t+k_s;v^*)\times\left[y(x,t;v)-y(x,t;v^*)\right]dt\,d\Gamma\,dk_s$$
$$-\sum_{s=1}^{l}\int_{c_s}^{d_s}\int_{\Gamma}\int_{0}^{T-\Delta} c_s(x,t+k_s)p(x,t+k_s;v^*)\times\left[y(x,t;v)-y(x,t;v^*)\right]dt\,d\Gamma\,dk_s$$
$$-\sum_{s=1}^{l}\int_{c_s}^{d_s}\int_{\Gamma}\int_{T-\Delta+k_s}^{T} c_s(x,t)p(x,t;v^*)\times\left[y(x,t-k_s;v)-y(x,t-k_s;v^*)\right]dt\,d\Gamma\,dk_s$$

$$
\begin{aligned}
&-\int_{\Gamma}\int_{0}^{T-\Delta}\frac{\partial p(v^*)}{\partial v_{\mathcal{A}^*}}\times\left[y(x,t;v)-y(x,t;v^*)\right]dt\,d\Gamma\\
&-\int_{\Gamma}\int_{T-\Delta}^{T}\frac{\partial p(v^*)}{\partial v_{\mathcal{A}^*}}\times\left[y(x,t;v)-y(x,t;v^*)\right]dt\,d\Gamma\\
&+\sum_{i=1}^{m}\int_{a_i}^{b_i}\int_{\Omega}\int_{0}^{T-\Delta}b_i(x,t+h_i)p(x,t+h_i;v^*)\times\left[y(x,t;v)-y(x,t;v^*)\right]dt\,dx\,dh_i.
\end{aligned}
\tag{4.18}
$$

Afterwards, using the facts that $y(x,t,v)=y(x,t,v^*)=\Phi_0(x,t)$ for $x\in\Omega$ and $t\in[-\Delta,0)$ and $y(x,t,v)=y(x,t,v^*)=\Psi_0(x,t)$ for $x\in\Gamma$ and $t\in[-\Delta,0)$, $p|_{\Omega}(x,t;v^*)=0$ and consequently $p|_{\Gamma}(x,t;v^*)=0$ for $t\in[T-\Delta+\lambda,T)$, we obtain

$$
\lambda_1\int_{Q}\left[y(v^*)-z_d\right]\times\left(y(v)-y(v^*)\right)dx\,dt=\int_{0}^{T}\int_{\Gamma}p(v^*)(v-v^*)d\Gamma\,dt. \tag{4.19}
$$

Substituting (4.19) into (4.5) gives

$$
\int_{0}^{T}\int_{\Gamma}\left(p(v^*)+\lambda_2 Nv^*\right)(v-v^*)d\Gamma\,dt\geq 0,\quad \forall v\in U_{\mathrm{ad}}. \tag{4.20}
$$

The foregoing result is now summarized.

**Theorem 4.2.** *For the problem* (3.1)–(3.5)*, with the performance functional* (4.1) *with* $z_d\in L^2(Q)$ *and* $\lambda_2>0$ *and with constraints on controls* (4.2)*, there exists a unique optimal control* $v^*$ *which satisfies the maximum condition* (4.20)*.*

### 4.1. Mathematical Examples

*Example 4.3.* Consider now the particular case where $U_{\mathrm{ad}}=U=L^2(\Sigma)$ (no constraints case). Thus the maximum condition (4.20) is satisfied when

$$
v^*=-\lambda_2 N^{-1}p(v^*). \tag{4.21}
$$

If $N$ is the identity operator on $L^2(\Sigma)$, then from Lemma 4.1 it follows that $v^*\in W^{\infty,1}(Q)$.

*Example 4.4.* We can also consider an analogous optimal control problem where the performance functional is given by:

$$
I(v)=\lambda_1\int_{\Sigma}\left[y(x,t;v)|_{\Sigma}-z_d\right]^2 d\Gamma\,dt+\lambda_2\int_{\Sigma}(Nv)v\,d\Gamma\,dt, \tag{4.22}
$$

where $z_d\in L^2(\Sigma)$.

From Theorem 3.4 and the Trace Theorem [20, Vol. 2, page 9], for each $v \in L^2(\Sigma)$, there exists a unique solution $y(v) \in W^{\infty,1}(Q)$ with $y|_\Sigma \in L^2(\Sigma)$. Thus, $I(v)$ is well defined. Then, the optimal control $v^*$ is characterized by:

$$\lambda_1 \int_\Sigma \left(y(v^*)|_\Sigma - z_d\right)\left[y(v)|_\Sigma - y(v^*)|_\Sigma\right] d\Gamma\, dt + \lambda_2 \int_\Sigma N v^*(v - v^*) d\Gamma\, dt \geq 0, \quad \forall v \in U_{\text{ad}}. \tag{4.23}$$

We define the adjoint variable $p = p(v^*) = p(x,t;v^*)$ as the solution of the equations:

$$\begin{aligned}
&-\frac{\partial p(v^*)}{\partial t} + \mathcal{A}^*(t)p(v^*) + \sum_{i=1}^{m} \int_{a_i}^{b_i} b_i(x,t+h_i)p(x,t+h_i;v^*)dh_i = 0,\\
&\qquad (x,t) \in \Omega \times (0, T-\Delta), \quad h_i \in (a_i, b_i),\\
&\frac{-\partial p(v^*)}{\partial t} + \mathcal{A}^*(t)p(v^*) = 0, \quad (x,t) \in \Omega \times (T-\Delta, T),\\
&\qquad p(x,T;v^*) = 0, \quad x \in \Omega,\\
&\qquad p(x,t;v^*) = 0, \quad (x,t) \in \Omega \times [T-\Delta+\lambda, T),\\
&\frac{\partial p(v^*)}{\partial \nu_{\mathcal{A}^*}}(x,t) = \sum_{s=1}^{l} \int_{c_s}^{d_s} c_s(x,t+k_s)p(x,t+k_s;v^*)dk_s + \lambda_1\left(y v^*|_\Sigma - z_{\Sigma d}\right),\\
&\qquad (x,t) \in \Gamma \times (0, T-\Delta(T)), \quad k_s \in (c_s, d_s),\\
&\frac{\partial p(v^*)}{\partial \nu_{\mathcal{A}^*}}(x,t) = \lambda_1\left(y(v^*)|_\Sigma - z_{\Sigma d}\right), \quad (x,t) \in \Gamma \times (T-\Delta(T), T).
\end{aligned} \tag{4.24}$$

As in the above section, we have the following result.

**Lemma 4.5.** *Let the hypothesis of Theorem 3.4 be satisfied. Then, for given $z_{\Sigma d} \in L^2(\Sigma)$ and any $v \in L^2(\Sigma)$, there exists a unique solution $p(v^*) \in W^{\infty,1}(Q)$ to the adjoint problem* (4.24).

Using the adjoint equations (4.24)in this case, the condition (4.23) can also be written in the following form:

$$\int_0^T \int_\Gamma \left(p(v^*) + \lambda_2 N v^*\right)(v - v^*) d\Gamma\, dt \geq 0, \quad \forall v \in U_{\text{ad}}. \tag{4.25}$$

The following result is now summarized.

**Theorem 4.6.** *For the problem* (3.1)–(3.5) *with the performance function* (4.22) *with $z_{\Sigma d} \in L^2(\Sigma)$ and $\lambda_2 > 0$, and with constraint* (4.2), *and with adjoint equations* (4.24), *there exists a unique optimal control $v^*$ which satisfies the maximum condition* (4.25).

*Example 4.7* ($u \in L^2(Q)$). We can also consider an analogous optimal control problem where the performance functional is given by:

$$I(u) = \lambda_1 \int_Q \left[y(x,t;u) - z_d\right]^2 dx\, dt + \lambda_2 \int_Q (Nu)u dx\, dt, \tag{4.26}$$

where $z_d \in L^2(Q)$.

From Theorem 3.4 and the Trace Theorem [20, Vol. 2, page 9], for each $u \in L^2(Q)$, there exists a unique solution $y(u) \in W^{\infty,1}(Q)$. Thus, $I$ is well defined. Then, the optimal control $u^*$ is characterized by:

$$\lambda_1 \int_Q \left(y(u^*) - z_d\right)\left[y(u) - y(u^*)\right] dx\, dt + \lambda_2 \int_Q Nu^*(u - u^*) dx\, dt \geq 0, \quad \forall u \in U_{\text{ad}}. \tag{4.27}$$

We define the adjoint variable $p = p(u^*) = p(x,t;u^*)$ as the solution of the equations:

$$\begin{aligned}
&-\frac{\partial p(u^*)}{\partial t} + \mathcal{A}^*(t)p(u^*) + \sum_{i=1}^{m} \int_{a_i}^{b_i} b_i(x,t+h_i)p(x,t+h_i;u^*)dh_i = \lambda_1\left(y(u^*) - z_d\right), \\
&\qquad\qquad (x,t) \in \Omega \times (0, T-\Delta), \quad h_i \in (a_i, b_i), \\
&-\frac{\partial p(u^*)}{\partial t} + \mathcal{A}^*(t)p(u^*) = \lambda_1\left(y(u^*) - z_d\right), \quad (x,t) \in \Omega \times (T-\Delta, T), \\
&\qquad\qquad p(x,T;u^*) = 0, \quad x \in \Omega, \\
&\qquad p(x,t;u^*) = 0, \quad (x,t) \in \Omega \times [T-\Delta+\lambda, T), \\
&\frac{\partial p(u^*)}{\partial \nu_{\mathcal{A}^*}}(x,t) = \sum_{s=1}^{l} \int_{c_s}^{d_s} c_s(x,t+k_s)p(x,t+k_s;u^*)dk_s, \\
&\qquad\qquad (x,t) \in \Gamma \times (0, T-\Delta(T)), \quad k_s \in (c_s, d_s), \\
&\frac{\partial p(u^*)}{\partial \nu_{\mathcal{A}^*}}(x,t) = 0, \quad (x,t) \in \Gamma \times (T-\Delta(T), T).
\end{aligned} \tag{4.28}$$

As in the above section, we have the following result.

**Lemma 4.8.** *Let the hypothesis of Theorem 3.4 be satisfied. Then, for given $z_d \in L^2(Q)$ and any $u \in L^2(Q)$, there exists a unique solution $p(u^*) \in W^{\infty,1}(Q)$ to the adjoint problem* (4.28).

*Using the adjoint equations* (4.28) *in this case, the condition* (4.27) *can also be written in the following form:*

$$\int_Q \left(p(u^*) + \lambda_2 Nu^*\right)(u - u^*) dx\, dt \geq 0, \quad \forall u \in U_{ad}. \tag{4.29}$$

*The following result is now summarized.*

**Theorem 4.9.** *For the problem* (3.1)–(3.5) *with the performance function* (4.26) *with* $z_d \in L^2(Q)$ *and* $\lambda_2 > 0$, *and with constraint* (4.2), *and with adjoint equations* (4.28), *there exists a unique optimal control* $u^*$ *which satisfies the maximum condition* (4.29).

*Example 4.10.* We can also consider an analogous optimal control problem where the performance functional is given by:

$$I(u) = \lambda_1 \int_\Sigma \left[ y|_\Sigma(x,t;u) - z_{\Sigma d} \right]^2 d\Gamma\, dt + \lambda_2 \int_Q (Nu)u\, dx\, dt, \tag{4.30}$$

where $z_{\Sigma d} \in L^2(\Sigma)$.

From Theorem 3.4 and the Trace Theorem [20, Vol. 2, page 9], for each $u \in L^2(Q)$, there exists a unique solution $y(u) \in W^{\infty,1}(Q)$ with $y|_\Sigma \in L^2(\Sigma)$. Thus, $I$ is well defined. Then, the optimal control $u^*$ is characterized by:

$$\lambda_1 \int_\Sigma \left( y(u^*) - z_{\Sigma d} \right) \left[ y(u) - y(u^*) \right] d\Gamma\, dt + \lambda_2 \int_Q Nu^*(u - u^*) dx\, dt \geq 0, \quad \forall u \in U_{\text{ad}}. \tag{4.31}$$

The above inequality can be simplified by introducing an adjoint equation, the form of which is identical to (4.24). Then using Theorem 3.4 we can establish the existence of a unique solution $p = p(u^*) = p(x,t;u^*) \in W^{\infty,1}(Q)$ for (4.24).

As in the above section, we have the following result.

**Lemma 4.11.** *Let the hypothesis of Theorem 3.4 be satisfied. Then, for given* $z_{\Sigma d} \in L^2(\Sigma)$ *and any* $u \in L^2(Q)$, *there exists a unique solution* $p(u^*) \in W^{\infty,1}(Q)$ *to the adjoint problem* (4.24)–*(37).*

*Using the adjoint equations* (4.24)–*(37) in this case, the condition* (4.31) *can also be written in the following form:*

$$\int_Q \left( p(u^*) + \lambda_2 N u^* \right)(u - u^*) dx\, dt \geq 0, \quad \forall u \in U_{ad}. \tag{4.32}$$

*The following result is now summarized.*

**Theorem 4.12.** *For the problem* (3.1)–(3.5) *with the performance function* (4.30) *with* $z_{\Sigma d} \in L^2(\Sigma)$ *and* $\lambda_2 > 0$, *and with constraint* (4.2), *and with adjoint equations* (4.24), *there exists a unique optimal control* $u^*$ *which satisfies the maximum condition* (4.32).

## 5. Generalization

The optimal control problems presented here can be extended to certain different two cases. Case 1: optimal control for $2 \times 2$ coupled infinite order parabolic systems with multiple time delays. Case 2: optimal control for $n \times n$ coupled infinite order parabolic systems with multiple time delays. Such extension can be applied to solving many control problems in mechanical engineering.

*Case 1* (optimal control for $2 \times 2$ coupled infinite order parabolic systems with multiple time delays). We can extend the discussions to study the optimal control for $2 \times 2$ coupled infinite order parabolic systems with multiple time delays. We consider the case where $v = (v_1, v_2) \in L^2(\Sigma) \times L^2(\Sigma)$, the performance functional is given by [15, 16]:

$$I(v) = I_1(v) + I_2(v) = \sum_{i=1}^{2} \left( \lambda_1 \int_Q \left[ y_i(x,t;v) - z_{id} \right]^2 dx\, dt + \lambda_2 \int_\Sigma (N_i v_i) v_i dx\, dt \right), \tag{5.1}$$

where $z_d = (z_{1d}, z_{2d}) \in (L^2(Q))^2$.

The following results can now be proved.

**Theorem 5.1.** *Let $y_0$, $\Phi_0$,$\Psi_0$, $v$, and $u$ be given with $y_0 = (y_{0,1}, y_{0,2}) \in (W^{\infty}\{\alpha_\alpha, 2\}(\Omega))^2$, $\Psi_0 = (\Psi_{0,1}, \Psi_{0,2}) \in (L^2(\Sigma_0))^2$,$\Phi_0 = (\Phi_{0,1}, \Phi_{0,2}) \in (W^{\infty,1}(Q_0))^2$,$v = (v_1, v_2) \in (L^2(\Sigma))^2$, and $u = (u_1, u_2) \in (W^{-\infty,-1}(Q))^2$. Then, there exists a unique solution $y = (y_1, y_2) \in (W^{-\infty,1}(Q))^2$ for the following mixed initial-boundary value problem:*

$$\begin{aligned}
&\frac{\partial y_1}{\partial t} + \left( \sum_{|\alpha|=0}^{\infty} (-1)^{|\alpha|} a_\alpha D^{2\alpha} + 1 \right) y_1 + \sum_{i=1}^{m} \int_{a_i}^{b_i} b_i(x,t) y_1(x, t-h_i) dh_i - y_2 = u_1, \\
&\qquad\qquad \text{in } Q, h_i \in (a_i, b_i), \\
&\frac{\partial y_2}{\partial t} + \left( \sum_{|\alpha|=0}^{\infty} (-1)^{|\alpha|} a_\alpha D^{2\alpha} + 1 \right) y_2 + \sum_{i=1}^{m} \int_{a_i}^{b_i} b_i(x,t) y_2(x, t-h_i) dh_i + y_1 = u_2, \\
&\qquad\qquad \text{in } Q, h_i \in (a_i, b_i), \\
&y_1(x,t';u) = \Phi_{0,1}(x,t'), \quad (x,t') \in \Omega \times [-\Delta, 0), \\
&y_2(x,t';u) = \Phi_{0,2}(x,t'), \quad (x,t') \in \Omega \times [-\Delta, 0), \\
&y_1(x,0;u) = y_{0,1}, \quad x \in \Omega, \\
&y_2(x,0;u) = y_{0,2}, \quad x \in \Omega, \\
&\frac{\partial y_1}{\partial \nu_{\mathcal{A}}}(x,t) = \sum_{s=1}^{l} \int_{c_s}^{d_s} c_{s1}(x,t) y_1(x, t-k_s) dk_s + v_1, \quad \text{on } \Sigma, k_s \in (c_s, d_s), \\
&\frac{\partial y_2}{\partial \nu_{\mathcal{A}}} = \sum_{s=1}^{l} \int_{c_s}^{d_s} c_{s2}(x,t) y_2(x, t-k_s) dk_s + v_2, \quad \text{on } \Sigma, k_s \in (c_s, d_s), \\
&y_1(x,t';u) = \Psi_{0,1}(x,t'), \quad (x,t') \in \Gamma \times [-\Delta, 0), \\
&y_2(x,t';u) = \Psi_{0,2}(x,t'), \quad (x,t') \in \Gamma \times [-\Delta, 0),
\end{aligned} \tag{5.2}$$

*where*

$$
\begin{aligned}
y \equiv y(x,t;u) &= \left(y_1(x,t;u), y_2(x,t;u)\right) \in \left(W^{\infty,1}(Q)\right)^2,\\
u \equiv u(x,t) &= \left(u_1(x,t), u_2(x,t)\right) \in \left(\left(W^{\infty,1}(Q)\right)'\right)^2,\\
v \equiv v(x,t) &= \left(v_1(x,t), v_2(x,t)\right) \in \left(L^2(\Sigma)\right)^2.
\end{aligned}
\tag{5.3}
$$

**Lemma 5.2.** *Let the hypothesis of Theorem 5.1 be satisfied. Then for given $z_d = (z_{1d}, z_{2d}) \in (L^2(Q))^2$ and any $v = (v_1, v_2) \in (L^2(\Sigma))^2$, there exists a unique solution $p(v) = (p_1(v), p_2(v)) \in (W^{\infty,1}(Q))^2$ for the adjoint problem:*

$$
\begin{aligned}
&-\frac{\partial p_1(v)}{\partial t} + \left(\sum_{|\alpha|=0}^{\infty}(-1)^{|\alpha|}a_\alpha D^{2\alpha} + 1\right)p_1(v) + \sum_{i=1}^{m}\int_{a_i}^{b_i} b_i(x,t+h_i)p_1(x,t+h_i;v)dh_i + p_2(v)\\
&\quad = \lambda_1\left(y_1(v) - z_{1d}\right), \quad (x,t) \in \Omega \times (0, T-\Delta),\ h_i \in (a_i, b_i),\\
&-\frac{\partial p_2(v)}{\partial t} + \left(\sum_{|\alpha|=0}^{\infty}(-1)^{|\alpha|}a_\alpha D^{2\alpha} + 1\right)p_2(v) + \sum_{i=1}^{m}\int_{a_i}^{b_i} b_i(x,t+h_i)p_2(x,t+h_i;v)dh_i - p_1(v)\\
&\quad = \lambda_1\left(y_2(v) - z_{2d}\right), \quad (x,t) \in \Omega \times (0, T-\Delta),\ h_i \in (a_i, b_i),\\
&\frac{\partial p_1(v)}{\partial t} + \left(\sum_{|\alpha|=0}^{\infty}(-1)^{|\alpha|}a_\alpha D^{2\alpha} + 1\right)p_1(v) = \lambda_1\left(y_1(v) - z_{1d}\right), \quad (x,t) \in \Omega \times (T-\Delta, T),\\
&\frac{\partial p_2(v)}{\partial t} + \left(\sum_{|\alpha|=0}^{\infty}(-1)^{|\alpha|}a_\alpha D^{2\alpha} + 1\right)p_2(v) = \lambda_1\left(y_2(v) - z_{2d}\right), \quad (x,t) \in \Omega \times (T-\Delta, T),\\
&p_1(x,T;v) = 0, \quad p_2(x,T;v) = 0, \quad x \in \Omega,\\
&p_1(x,t;v) = 0, \quad p_2(x,t;v) = 0, \quad (x,t) \in \Omega \times [T-\Delta+\lambda, T),\\
&\frac{\partial p_1(x,t;v)}{\partial \nu_{\mathcal{A}^*}} = \sum_{s=1}^{l}\int_{c_s}^{d_s} c_{s1}(x,t+k_s)p_1(x,t+k_s;v)dk_s, \quad (x,t) \in \Gamma \times (0, T-\Delta),\ k_s \in (c_s, d_s),\\
&\frac{\partial p_2(x,t;v)}{\partial \nu_{\mathcal{A}^*}} = \sum_{s=1}^{l}\int_{c_s}^{d_s} c_{s2}(x,t+k_s)p_2(x,t+k_s;v)dk_s, \quad (x,t) \in \Gamma \times (0, T-\Delta),\ k_s \in (c_s, d_s),\\
&\frac{\partial p_1(x,t)}{\partial \nu_{\mathcal{A}^*}} = 0, \quad \frac{\partial p_2(x,t)}{\partial \nu_{\mathcal{A}^*}} = 0, \quad (x,t) \in \Gamma \times (T-\Delta(T), T).
\end{aligned}
\tag{5.4}
$$

**Theorem 5.3.** *The optimal control* $v^* \equiv v^*(x,t) = (v_1^*(x,t), v_2^*(x,t)) \in (L^2(\Sigma))^2$ *is characterized by the following maximum condition:*

$$\int_0^T \int_\Gamma \left( \left[ p_1(v^*) + \lambda_2 N_1 v_1^* \right] (v_1 - v_1^*) + \left[ p_2(v^*) + \lambda_2 N_2 v_2^* \right] (v_2 - v_2^*) \right) d\Gamma \, dt \geq 0, \quad \forall v = (v_1, v_2) \in \left( L^2(\Sigma) \right)^2, \tag{5.5}$$

*where* $p \equiv p(x,t;v) = (p_1(x,t;v), p_2(x,t;v)) \in (W^{\infty,1}(Q))^2$ *is the adjoint state.*

The foregoing result is now summarized.

**Theorem 5.4.** *For the problem* (5.2) *with the performance function* (5.1) *with* $z_d = (z_{1d}, z_{2d}) \in (L^2(Q))^2$ *and* $\lambda_2 > 0$*, and with constraint:* $U_{ad}$ *is closed, convex subset of* $(L^2(\Sigma))^2$*, and with adjoint problem* (5.4)*, then there exists a unique optimal control* $v^* \equiv v^*(x,t) = (v_1^*(x,t), v_2^*(x,t)) \in (L^2(\Sigma))^2$ *which satisfies the maximum condition* (5.5).

*Case 2* (optimal control for $(n \times n)$ coupled infinite order parabolic systems with multiple time delays). We will extend the discussion to $(n \times n)$ coupled infinite order parabolic systems. We consider the case where $v = (v_1, v_2, \ldots, v_n) \in ((L^2(\Sigma))^n$, the performance functional is given by [15, 16]:

$$I(v) = \sum_{j=1}^{n} \left( \lambda_1 \int_Q \left[ y_j(x,t;v) - z_{jd} \right]^2 dx \, dt + \lambda_2 \int_\Sigma (N_j v_j) v_j dx \, dt \right), \tag{5.6}$$

where $z_d = (z_{1d}, z_{2d}, \ldots, z_{nd}) \in (L^2(Q))^n$.

The following results can now be proved.

**Theorem 5.5.** *Let* $y_0, \Phi_0, \Psi_0, v$*, and* $u$ *be given with* $y_p = (y_{p,1}, y_{p,2}, \ldots, y_{p,n}) \in (W^{\infty}\{a_\alpha, 2\}(\Omega))^n$, $\Phi_0 = (\Phi_{0,1}, \Phi_{0,2}, \ldots, \Phi_{0,n}) \in (W^{\infty,1}(Q_0))^n$, $\Psi_0 = (\Psi_{0,1}, \Psi_{0,2}, \ldots, \Psi_{0,n}) \in (L^2(\Sigma_0))^n$, $v = (v_1, v_2, \ldots, v_n) \in (L^2(\Sigma_0))^n$*, and* $u = (u_1, u_2, \ldots, u_n) \in (W^{-\infty,-1}(Q))^n$*. Then, there exists a unique solution* $y = (y_1, y_2, \ldots, y_n) \in (W^{\infty,1}(Q_0))^n$ *for the following mixed initial-boundary value problem: for all* $j, j = 1, 2, \ldots, n$ *one has*

$$\frac{\partial y_j}{\partial t} + \mathcal{S}(t) y_j(x,t) + \sum_{i=1}^{m} \int_{a_i}^{b_i} b_i(x,t) y_j(x, t - h_i) dh_i = u_j, \quad (x,t) \in \Omega \times (0,T), \quad h_i \in (a_i, b_i),$$

$$y_j(x,t') = \Phi_{0,j}(x,t') \quad (x,t') \in \Omega \times [-\Delta, 0),$$

$$y_j(x,0) = y_{0,j}(x), \quad x \in \Omega,$$

$$\begin{aligned}
\frac{\partial y_j}{\partial \nu_{\mathcal{S}}}(x,t) &= \sum_{\mathcal{S}=1}^{l} \int_{c_s}^{d_s} c_s(x,t) y_j(x,t-k_s)\,dk_s + v_j, \\
&\qquad (x,t) \in \Gamma \times (0,T), \quad k_s \in (c_s,d_s), \\
y_j(x,t') &= \Psi_{0,j}(x,t'), \quad (x,t') \in \Gamma \times [-\Delta,0),
\end{aligned} \tag{5.7}$$

*where*

$$\begin{aligned}
y \equiv y(x,t;u) &= \left(y_1(x,t;u), y_2(x,t;u), \ldots, y_n(x,t;u)\right) \in \left(W^{\infty,1}(Q)\right)^n, \\
u \equiv u(x,t) &= \left(u_1(x,t), u_2(x,t), \ldots, u_n(x,t)\right) \in \left(W^{-\infty,-1}(Q)\right)^n, \\
v \equiv v(x,t) &= \left(v_1(x,t), v_2(x,t), \ldots, v_n(x,t)\right) \in \left(L^2(\Sigma)\right)^n.
\end{aligned} \tag{5.8}$$

*The operator $\mathcal{S}(t)$ is an $n \times n$ matrix takes the form [15, 16, 18, 22]:*

$$\begin{aligned}
&\mathcal{S}(t) \\
&= \begin{pmatrix}
\sum\limits_{|\alpha|=0}^{\infty} (-1)^{|\alpha|} a_\alpha D^{2\alpha} + 1 & -1 & \cdots & -1 \\
1 & \sum\limits_{|\alpha|=0}^{\infty} (-1)^{|\alpha|} a_\alpha D^{2\alpha} + 1 & \cdots & -1 \\
\vdots & \vdots & \ddots & \vdots \\
1 & 1 & \cdots & \sum\limits_{|\alpha|=0}^{\infty} (-1)^{|\alpha|} a_\alpha D^{2\alpha} + 1
\end{pmatrix}_{n\times n},
\end{aligned} \tag{5.9}$$

*that is*

$$\mathcal{S}(t) y_j(x) = \sum_{|\alpha|=0}^{\infty} (-1)^{|\alpha|} a_\alpha D^{2\alpha} y_j(x) + \sum_{r=1}^{n} B_{jr} y_j(x), \quad \forall j, j = 1,2,\ldots,n, \tag{5.10}$$

*where*

$$B_{jr} = \begin{cases} 1, & \text{if } j \geq r, \\ -1, & \text{if } j < r. \end{cases} \tag{5.11}$$

**Lemma 5.6.** *Let the hypothesis of Theorem 5.5 be satisfied. Then for given $z_d = (z_{1d}, z_{2d}, \ldots, z_{nd}) \in (L^2(Q))^n$ and any $v(x,t) = (v_1(x,t), v_2(x,t), \ldots, v_n(x,t)) \in (L^2(\Sigma))^n$, there exists a unique solution*

$$p(v) \equiv p(x,t;v) = \left(p_1(x,t;v), p_1(x,t;v), \ldots, p_n(x,t;v)\right) \in \left(W^{\infty,1}(Q)\right)^n, \tag{5.12}$$

*for the adjoint problem: for all* $j, j = 1, 2, \ldots, n$, *one has*

$$\begin{aligned}
&\frac{-\partial p_j(v)}{\partial t} + \mathcal{S}^*(t)p_j(v) + \sum_{i=1}^{m}\int_{a_i}^{b_i} b_i(x,t+h_i)p_j(x,t+h_i;v)dh_i = \lambda_1\left(y_j(v) - z_{jd}\right),\\
&\qquad\qquad (x,t) \in \Omega \times (0, T-\Delta), \quad h_i \in (a_i, b_i),\\
&\frac{\partial p_j(v)}{\partial t} + \mathcal{S}^*(t)p_j(v) = \lambda_j\left(y_j(v) - z_{jd}\right), \quad (x,t) \in \Omega \times (T-\Delta, T),\\
&p_j(x,T,v) = 0, \quad x \in \Omega,\\
&p(x,t;v) = 0, \quad (x,t) \in \Omega \times [T-\Delta+\lambda, T),\\
&\frac{\partial p_j(v)}{\partial v_{\mathcal{S}^*}}(x,t) = \sum_{s=1}^{l}\int_{c_s}^{d_s} c_s(x,t+k_s)p_j(x,t+k_s;v)dk_s, \quad (x,t) \in \Gamma \times (0, T-\Delta),\ k_s \in (c_s, d_s),\\
&\frac{\partial p_j(v)}{\partial v_{\mathcal{S}^*}}(x,t) = 0, \quad (x,t) \in \Gamma \times (T-\Delta, T),
\end{aligned} \tag{5.13}$$

*where*

$$\mathcal{S}^*(t)p_j(x) = \sum_{|\alpha|=0}^{\infty}(-1)^{|\alpha|}a_\alpha D^{2\alpha}p_j(x) + \sum_{r=1}^{n}B_{rj}p_j(x), \quad \forall j, j = 1, 2, \ldots, n, \tag{5.14}$$

$B_{rj}$ *are the transpose of* $B_{jr}$.

**Theorem 5.7.** *The optimal control* $v^* \equiv v^*(x,t) = (v_1^*(x,t), v_2^*(x,t), \ldots, v_n^*(x,t)) \in (L^2(\Sigma))^n$ *is characterized by the following maximum condition:*

$$\sum_{j=1}^{n}\int_{\Sigma}\left[p_j(v^*) + \lambda_2 N_j v_j^*\right]\left(v_j - v_j^*\right)d\Gamma\, dt \geq 0, \quad \forall v = (v_1, v_2, \ldots, v_n) \in (U_{ad})^n, \tag{5.15}$$

*where*

$$p(v^*) \equiv p(x,t;v^*) = \left(p_1(x,t;v^*), p_1(x,t;v^*), \ldots, p_n(x,t;v^*)\right) \in \left(W^{\infty,1}(Q)\right)^n \tag{5.16}$$

*is the adjoint state.*

The foregoing result is now summarized.

**Theorem 5.8.** *For the problem* (5.7) *with the performance function* (5.6) *with* $z_d = (z_{1d}, z_{2d}, \ldots, z_{nd}) \in (L^2(Q))^n$ *and* $\lambda_2 > 0$, *and with constraint:* $U_{ad}$ *is closed, convex subset of* $(L^2(\Sigma))^n$, *and with adjoint equations* (5.13), *then there exists a unique optimal control* $v^* \equiv v^*(x,t) = (v_1^*(x,t), v_2^*(x,t), \ldots, v_n^*(x,t)) \in (L^2(\Sigma))^n$ *which satisfies the maximum condition* (5.15).

In the case of performance functionals (4.1), (4.22), (4.26), (4.30), (5.1), and (5.6) with $\lambda_1 > 0$ and $\lambda_2 = 0$, the optimal control problem reduces to minimization of the functional on a closed and convex subset in a Hilbert space. Then, the optimization problem is equivalent to a quadratic programming one, which can be solved by the use of the well-known Gilbert algorithm.

## 6. Conclusions

The optimization problem presented in the paper constitutes a generalization of the optimal boundary control problem for second-order parabolic systems with Neumann boundary condition involving constant time lag appearing in the state and in the boundary conditions considered in [1, 5–9, 14–16, 18, 21, 32].

Moreover, the results obtained in this paper (Theorems 4.2, 4.6, 5.4, and 5.8) can be treated as a generalization of the optimization theorems proved by [8–10]. Also the main result of the paper contains necessary and sufficient conditions of optimality for $(n \times n)$ infinite order parabolic systems with multiple time delays given in integral form both in the state equation and in the Neumann boundary condition that give characterization of optimal control (Theorem 5.8). But it is easily seen that obtaining analytical formulas for optimal control are very difficult. This results from the fact that state equations (5.7), adjoint equations (5.13), and maximum condition (5.15) are mutually connected that cause that the usage of derived conditions is difficult. Therefore we must resign from the exact determination of the optimal control and therefore we are forced to use approximation methods.

Also it is evident that by modifying:

(i) the boundary conditions, (Dirichlet, Neumann, mixed, etc.),

(ii) the nature of the control (distributed, boundary, etc.),

(iii) the nature of the observation (distributed, boundary, etc.),

(iv) the initial differential system,

(v) the time delays (constant time delays, time-varying delays, multiple time-varying delays, time delays given in the integral form, etc.),

(vi) the number of variables (finite number of variables, infinite number of variables systems, etc.),

(vii) the type of equation (elliptic, parabolic, hyperbolic, etc.),

(viii) the order of equation (second order, Schrödinger, infinite order, etc.),

(ix) the type of control ( optimal control problem, time-optimal control problem, etc.),

an infinity of variations on the above problems are possible to study with the help of [19] and Dubovitskii-Milyutin formalisms [22–27]. Those problems need further investigations and form tasks for future research. These ideas mentioned above will be developed in forthcoming papers.

## Acknowledgments

The research presented here was carried out within the research programme of the Taibah University-Dean of Scientific Research under Project no. 806/1433. The author would like to express his gratitude to the anonymous reviewers for their very valuable remarks.

## References


[1] A. Kowalewski, "Optimization of parabolic systems with deviating arguments," *International Journal of Control*, vol. 72, no. 11, pp. 947–959, 1999.

[2] P. K. C. Wang, "Optimal control of parabolic systems with boundary conditions involving time delays," *SIAM Journal on Control and Optimization*, vol. 13, pp. 274–293, 1975.

[3] G. Knowles, "Time-optimal control of parabolic systems with boundary conditions involving time delays," *Journal of Optimization Theory and Applications*, vol. 25, no. 4, pp. 563–574, 1978.

[4] K. H. Wong, "Optimal control computation for parabolic systems with boundary conditions involving time delays," *Journal of Optimization Theory and Applications*, vol. 53, no. 3, pp. 475–507, 1987.

[5] A. Kowalewski, "Boundary control of distributed parabolic system with boundary condition involving a time-varying lag," *International Journal of Control*, vol. 48, no. 6, pp. 2233–2248, 1988.

[6] A. Kowalewski, "Optimal control of distributed parabolic systems involving time lags," *IMA Journal of Mathematical Control and Information*, vol. 7, no. 4, pp. 375–393, 1990.

[7] A. Kowalewski, "Optimal control of distributed parabolic systems with multiple time-varying lags," *International Journal of Control*, vol. 69, no. 3, pp. 361–381, 1998.

[8] A. Kowalewski, "Optimal control of distributed parabolic systems with multiple time delays given in the integral form," *IMA Journal of Mathematical Control and Information*, vol. 22, no. 2, pp. 149–170, 2005.

[9] A. Kowalewski, "Time-optimal control of infinite order hyperbolic systems with time delays," *International Journal of Applied Mathematics and Computer Science*, vol. 19, no. 4, pp. 597–608, 2009.

[10] A. Kowalewski and J. T. Duda, "An optimization problem for time lag distributed parabolic systems," *IMA Journal of Mathematical Control and Information*, vol. 21, no. 1, pp. 15–31, 2004.

[11] A. Kowalewski and A. Krakowiak, "Time-optimal boundary control of an infinite order parabolic system with time lags," *International Journal of Applied Mathematics and Computer Science*, vol. 18, no. 2, pp. 189–198, 2008.

[12] W. Kotarski, *Some Problems of Optimal and Pareto Optimal Control for Distributed Parameter Systems*, vol. 1668, Silesian University, Katowice, Poland, 1997.

[13] W. Kotarski, H. A. El-Saify, and G. M. Bahaa, "Optimal control of parabolic equation with an infinite number of variables for non-standard functional and time delay," *IMA Journal of Mathematical Control and Information*, vol. 19, no. 4, pp. 461–476, 2002.

[14] W. Kotarski and G. M. Bahaa, "Optimality conditions for infinite order hyperbolic control problem with non-standard functional and time delay," *Journal of Information & Optimization Sciences*, vol. 28, no. 3, pp. 315–334, 2007.

[15] H. A. El-Saify, "Optimal control of $n \times n$ parabolic system involving time lag," *IMA Journal of Mathematical Control and Information*, vol. 22, no. 3, pp. 240–250, 2005.

[16] H. A. El-Saify, "Optimal boundary control problem for $n \times n$ infinite-order parabolic lag system," *IMA Journal of Mathematical Control and Information*, vol. 23, no. 4, pp. 433–445, 2006.

[17] I. M. Gali, H. A. El-Saify, and S. A. El-Zahaby, "Distributed control of a system governed by Dirichlet and Neumann problems for elliptic equations of infinite order," in *Functional-Differential Systems and Related Topics, III*, pp. 83–87, Higher College Engineering, Zielona Góra, Poland, 1983.

[18] H. A. El-Saify and G. M. Bahaa, "Optimal control for $n \times n$ hyperbolic systems involving operators of infinite order," *Mathematica Slovaca*, vol. 52, no. 4, pp. 409–424, 2002.

[19] J.-L. Lions, *Optimal Control of Systems Governed by Partial Differential Equations*, Translated from the French by S. K. Mitter. Die Grundlehren der mathematischen Wissenschaften, Band 170, Springer, New York, NY, USA, 1971.

[20] J. L. Lions and E. Magenes, *Non-Homogeneous Boundary Value Problem and Applications. I*, Springer, New York, NY, USA, 1972.

[21] W. Kotarski, H. A. El-Saify, and G. M. Bahaa, "Optimal control problem for a hyperbolic system with mixed control-state constraints involving operator of infinite order," *International Journal of Pure and Applied Mathematics*, vol. 1, no. 3, pp. 241–254, 2002.

[22] G. M. Bahaa, "Quadratic Pareto optimal control of parabolic equation with state-control constraints and an infinite number of variables," *IMA Journal of Mathematical Control and Information*, vol. 20, no. 2, pp. 167–178, 2003.

[23] G. M. Bahaa, "Time-optimal control problem for parabolic equations with control constraints and infinite number of variables," *IMA Journal of Mathematical Control and Information*, vol. 22, no. 3, pp. 364–375, 2005.

[24] G. M. Bahaa, "Time-optimal control problem for infinite order parabolic equations with control constraints," *Differential Equations and Control Processes*, no. 4, pp. 64–81, 2005.
[25] G. M. Bahaa, "Optimal control for cooperative parabolic systems governed by Schrödinger operator with control constraints," *IMA Journal of Mathematical Control and Information*, vol. 24, no. 1, pp. 1–12, 2007.
[26] G. M. Bahaa, "Quadratic Pareto optimal control for boundary infinite order parabolic equation with state-control constraints," *Advanced Modeling and Optimization*, vol. 9, no. 1, pp. 37–51, 2007.
[27] G. M. Bahaa, "Optimal control problems of parabolic equations with an infinite number of variables and with equality constraints," *IMA Journal of Mathematical Control and Information*, vol. 25, no. 1, pp. 37–48, 2008.
[28] G. M. Bahaa and W. Kotarski, "Optimality conditions for $n \times n$ infinite-order parabolic coupled systems with control constraints and general performance index," *IMA Journal of Mathematical Control and Information*, vol. 25, no. 1, pp. 49–57, 2008.
[29] Ju. A. Dubinskiĭ, "Sobolev spaces of infinite order, and the behavior of the solutions of certain boundary value problems when the order of the equation increases indefinitely," vol. 98, no. 2, pp. 163–184, 1975 (Russian).
[30] Ju. A. Dubinskiĭ, "Nontriviality of Sobolev spaces of infinite order in the case of the whole Euclidean space and the torus," vol. 100, no. 3, pp. 436–446, 1976 (Russian).
[31] J. A. Dubinskii, "Sobolev spaces of infinite order and differential equations. Mathematics and its applications," *East European Series*, vol. 3, p. 164, 1988.
[32] W. Kotarski and G. M. Bahaa, "Optimal control problem for infinite order hyperbolic system with mixed control-state constraints," *European Journal of Control*, vol. 11, no. 2, pp. 150–156, 2005.

Hindawi Publishing Corporation
Journal of Applied Mathematics
Volume 2012, Article ID 141727, 20 pages
doi:10.1155/2012/141727

*Research Article*

# Convergence Results for the Gaussian Mixture Implementation of the Extended-Target PHD Filter and Its Extended Kalman Filtering Approximation

**Feng Lian, Chongzhao Han, Jing Liu, and Hui Chen**

*Ministry of Education Key Laboratory for Intelligent Networks and Network Security (MOE KLINNS), School of Electronics and Information Engineering, Xi'an Jiaotong University, Xi'an 710049, China*

Correspondence should be addressed to Feng Lian, lianfeng1981@gmail.com

Received 23 February 2012; Accepted 31 May 2012

Academic Editor: Qiang Ling



The convergence of the Gaussian mixture extended-target probability hypothesis density (GM-EPHD) filter and its extended Kalman (EK) filtering approximation in mildly nonlinear condition, namely, the EK-GM-EPHD filter, is studied here. This paper proves that both the GM-EPHD filter and the EK-GM-EPHD filter converge uniformly to the true EPHD filter. The significance of this paper is in theory to present the convergence results of the GM-EPHD and EK-GM-EPHD filters and the conditions under which the two filters satisfy uniform convergence.

## 1. Introduction

The problem of extended-target tracking (ETT) [1, 2] arises because of the sensor resolution capacities [3], the high density of targets, the sensor-to-target geometry, and so forth. For targets in near field of a high-resolution sensor, the sensor is able to receive more than one measurement (observation, or detection) at each time from different corner reflectors of a single target. In this case, the target is no longer known as a point object, which at most causes one detection at each time. It is called extended target. ETT is very valuable for many real applications [4, 5], such as ground or littoral surveillance, robotics, and autonomous weapons.

The ETT problem has attracted great interest in recent years. Some approaches [6, 7] have been proposed for tracking a known and fixed number of the extended targets without clutter. Nevertheless, for the problem of tracking an unknown and varying number of the extended targets in clutter, most of the association-based approaches [8], such as nearest neighbor, joint probabilistic data association, and multiple hypothesis tracking, would no longer be applicable straightforwardly owing to their underlying assumption of point objects.

Recently, the random-finite-set- (RFS-) based tracking approaches [9] have attracted extensive attention because of their lots of merits. The probability hypothesis density (PHD) [10] filter, developed by Mahler for tracking multiple point targets in clutter, has been shown to be computationally tractable alternative to full multitarget filter in the RFS framework. The sequential Monte Carlo (SMC) implementation for the PHD filter was devised by Vo et al. [11]. Then, Vo and Ma [12] devised the Gaussian mixture (GM) implementation for the PHD filter under the linear, Gaussian assumption on target dynamics, birth process, and sensor model. Actually the original intention of the PHD filter devised by Clark and Godsill is to address nonconventional tracking problems, that is, tracking in high target density, tracking closely spaced targets, and detecting targets of interest in a dense clutter background [13]. So it is especially suitable for the ETT problem.

Given the Poisson likelihood model for the extended target [14], Mahler developed the theoretically rigorous PHD filter for the ETT problem in 2009 [15]. Under the linear, Gaussian assumption, the GM implementation for the extended-target PHD (EPHD) filter was proposed by Granström et al. [16], in 2010. Similar to the point-target GM-PHD filter, the GM-EPHD filter can also be extended to accommodate mildly nonlinear target dynamics using the extended Kalman (EK) filtering [17] approximation. The extension is called EK-GM-EPHD filter. Experimental results showed the EK-GM-EPHD filter was capable of tracking multiple humans, each of which gave rise to, on average, 10 measurements at each scan and was therefore treated as an extended target, using a SICK LMS laser range sensor [16].

Although the GM-EPHD and EK-GM-EPHD filters have been successfully used for many real-world problems, there have been no results showing the convergence for the two filters. The convergence results on point-target particle-PHD and GM-PHD filters [18, 19] do not apply directly for the GM-EPHD and EK-GM-EPHD filters because of the significant difference between the measurement update steps of the PHD and EPHD filters. Therefore, to ensure the more successful and extensive applications of the EPHD filter to "real-life" problems, it is necessary to answer the following question: do the GM-EPHD and EK-GM-EPHD filters converge asymptotically toward the optimal filter and in what sense?

The answer can actually be derived from Propositions 3.2 and 3.3 in this paper. Proposition 3.2 demonstrates the uniform convergence [20–22] of the errors for the measurement update step of the GM-EPHD filter. In other words, given simple sufficient conditions, the approximation error of the measurement-updated EPHD by a sum of Gaussians is proved to converge to zero as the number of Gaussians in the mixture tends to infinity. In addition, the uniform convergence results for the measurement update step of the EK-GM-EPHD filter are derived from Proposition 3.3.

## 2. EPHD and GM-EPHD Filters

At time $k$, let $\mathbf{x}_k$ be the state vector of a single extended target, and $\mathbf{z}_k$ a single measurement vector received by sensor. Multiple extended-target states and sensor measurements can, respectively, be represented as finite sets $X_k = \{\mathbf{x}_{i,k}\}_{i=1}^{n_k}$ and $Z_k = \{\mathbf{z}_{i,k}\}_{i=1}^{m_k}$, where $n_k$ and $m_k$ denote the number of the extended targets and sensor measurements, respectively. A Poisson model is used to describe the likelihood function for the extended target according to Gilholm et al. [14]:

$$l_{Z_k}(\mathbf{x}_k) = e^{-\gamma(\mathbf{x}_k)} \prod_{\mathbf{z}_k \in Z_k} \gamma(\mathbf{x}_k) \phi_{\mathbf{z}_k}(\mathbf{x}_k), \tag{2.1}$$

where $\phi_{\mathbf{z}_k}(\mathbf{x}_k)$ denotes the single-measurement single-target likelihood density; $\gamma(\mathbf{x}_k)$ denotes the expected number of measurements arising from an extended target.

The clutter is modeled as a Poisson RFS with the intensity $\kappa_k(\mathbf{z}_k) = \lambda_k c_k(\mathbf{z}_k)$, where $\lambda_k$ is the average clutter number per scan and $c_k(\mathbf{z}_k)$ is the density of clutter spatial distribution.

Given the Poisson likelihood model for the extended targets, Mahler derived the EPHD filter using finite-set statistics [15, 23]. The prediction equations of the EPHD filter are identical to those of the point-target PHD filter [10]. The EPHD measurement update equations are

$$\upsilon_k(\mathbf{x}_k) = \left(1 - p_{D,k}(\mathbf{x}_k) + e^{-\gamma(\mathbf{x}_k)} p_{D,k}(\mathbf{x}_k) + \sum_{\wp_k \angle Z_k} \omega_{\wp_k} \sum_{W_k \in \wp_k} \frac{\eta_{W_k}(\mathbf{x}_k)}{d_{W_k}}\right) \upsilon_{k|k-1}(\mathbf{x}_k), \tag{2.2}$$

$$\eta_{W_k}(\mathbf{x}_k) = p_{D,k}(\mathbf{x}_k) e^{-\gamma(\mathbf{x}_k)} \prod_{\mathbf{z}_k \in W_k} \frac{\gamma(\mathbf{x}_k)\phi_{\mathbf{z}_k}(\mathbf{x}_k)}{\lambda_k c_k(\mathbf{z}_k)}, \tag{2.3}$$

$$\omega_{\wp_k} = \frac{\prod_{W_k \in \wp_k} d_{W_k}}{\sum_{\wp'_k \angle Z_k} \prod_{W'_k \in \wp'_k} d_{W'_k}}; \quad d_{W_k} = \delta_{|W_k|,1} + \left\langle \upsilon_{k|k-1}, \eta_{W_k} \right\rangle, \tag{2.4}$$

where $p_{D,k}(\mathbf{x}_k)$ denotes the probability that the set of observations from the extended target will be detected at time $k$; $\wp_k \angle Z_k$ denotes that $\wp_k$ partitions set $Z_k$ [15], for example, let $Z = \{\mathbf{z}_1, \mathbf{z}_2, \mathbf{z}_3\}$, then the partitions of $Z$ are $\wp_1 = \{\{\mathbf{z}_1, \mathbf{z}_2, \mathbf{z}_3\}\}$, $\wp_2 = \{\{\mathbf{z}_1\}, \{\mathbf{z}_2\}, \{\mathbf{z}_3\}\}$, $\wp_3 = \{\{\mathbf{z}_1, \mathbf{z}_2\}, \{\mathbf{z}_3\}\}$, $\wp_4 = \{\{\mathbf{z}_1, \mathbf{z}_3\}, \{\mathbf{z}_2\}\}$, and $\wp_5 = \{\{\mathbf{z}_1\}, \{\mathbf{z}_2, \mathbf{z}_3\}\}$; $|W_k|$ denotes the cardinality of the set $W_k$; $\delta_{|W_k|,1} = 1$ if $|W_k| = 1$, and $\delta_{|W_k|,1} = 0$ otherwise; the notation $\langle \cdot, \cdot \rangle$ is the usual inner product. The measure in $\langle \cdot, \cdot \rangle$ of (2.4) is continuous, it defines the integral inner product

$$\left\langle \upsilon_{k|k-1}, \eta_{W_k} \right\rangle = \int \upsilon_{k|k-1}(\mathbf{x}_k) \eta_{W_k}(\mathbf{x}_k) d\mathbf{x}_k. \tag{2.5}$$

By making the same six assumptions that are made in [12] and the additional assumption that $\gamma(\mathbf{x}_k)$ can be approximated as functions of the mean of the individual Gaussian components, Granström et al. proposed the GM-EPHD filter [16]. At time $k$, let $\upsilon_{k|k-1}^{J_{k|k-1}}$ denote the GM approximation to the predicted EPHD $\upsilon_{k|k-1}$ with $J_{k|k-1}$ Gaussian components, and $\upsilon_k^{J_k}$ the GM approximation to the measurement-updated EPHD $\upsilon_k$ with $J_k$ Gaussian components. The prediction equations of the GM-EPHD filter are identical to those of point-target GM-PHD filter [12]. The GM-EPHD measurement update equations are as follows.

Let the predicted EPHD be a GM of the form

$$\upsilon_{k|k-1}^{J_{k|k-1}}(\mathbf{x}_k) = \sum_{i=1}^{J_{k|k-1}} w_{k|k-1}^{(i)} \mathcal{N}\left(\mathbf{x}_k \mid \mathbf{m}_{k|k-1}^{(i)}, \mathbf{P}_{k|k-1}^{(i)}\right), \tag{2.6}$$

where $\mathcal{N}(\cdot|\mathbf{m}, \mathbf{P})$ denotes the density of Gaussian distribution with the mean $\mathbf{m}$ and covariance $\mathbf{P}$.

Then, the measurement-updated EPHD is a GM given by

$$v_k^{J_k}(\mathbf{x}_k) = v_k^{ND,J_{k|k-1}}(\mathbf{x}_k) + \sum_{\wp_k \angle Z_k} \sum_{W_k \in \wp_k} v_k^{D,J_{k|k-1}}(\mathbf{x}_k, W_k), \tag{2.7}$$

where $v_k^{ND,J_{k|k-1}}(\mathbf{x}_k)$ denotes the Gaussian components handling no detections,

$$\begin{aligned} v_k^{ND,J_{k|k-1}}(\mathbf{x}_k) &= \sum_{j=1}^{J_{k|k-1}} w_k^{(j)} \mathcal{N}\left(\mathbf{x}_k \mid \mathbf{m}_{k|k-1}^{(j)}, \mathbf{P}_{k|k-1}^{(j)}\right), \\ w_k^{(j)} &= \left(1 - \left(1 - e^{-\gamma(\mathbf{m}_{k|k-1}^{(j)})}\right) p_{D,k}\right) w_{k|k-1}^{(j)}, \\ \mathbf{m}_k^{(j)} &= \mathbf{m}_{k|k-1}^{(j)}; \qquad \mathbf{P}_k^{(j)} = \mathbf{P}_{k|k-1}^{(j)}, \end{aligned} \tag{2.8}$$

and $v_k^{D,J_{k|k-1}}(\mathbf{x}_k, W_k)$ denotes the Gaussian components handling detected targets

$$v_k^{D,J_{k|k-1}}(\mathbf{x}_k, W_k) = \sum_{j=1}^{J_{k|k-1}} w_k^{(j)} \mathcal{N}\left(\mathbf{x}_k \mid \mathbf{m}_k^{(j)}, \mathbf{P}_k^{(j)}\right), \tag{2.9}$$

$$w_k^{(j)} = \omega_{\wp_k}^{J_{k|k-1}} \frac{\eta_{W_k}\left(\mathbf{m}_{k|k-1}^{(j)}\right)}{d_{W_k}^{J_{k|k-1}}} w_{k|k-1}^{(j)}, \tag{2.10}$$

$$\omega_{\wp_k}^{J_{k|k-1}} = \frac{\prod_{W_k \in \wp_k} d_{W_k}^{J_{k|k-1}}}{\sum_{\wp_k' \angle Z_k} \prod_{W_k' \in \wp_k'} d_{W_k'}^{J_{k|k-1}}}; \quad d_{W_k}^{J_{k|k-1}} = \delta_{|W_k|,1} + \left\langle v_{k|k-1}^{J_{k|k-1}}, \eta_{W_k} \right\rangle, \tag{2.11}$$

$$\eta_{W_k}\left(\mathbf{m}_{k|k-1}^{(j)}\right) = p_{D,k} e^{-\gamma(\mathbf{m}_{k|k-1}^{(j)})} \prod_{\mathbf{z}_k \in W_k} \frac{\gamma\left(\mathbf{m}_{k|k-1}^{(j)}\right) \phi_{\mathbf{z}_k}\left(\mathbf{m}_{k|k-1}^{(j)}\right)}{\lambda_k c_k(\mathbf{z}_k)}, \tag{2.12}$$

$$\phi_{\mathbf{z}_k}\left(\mathbf{m}_{k|k-1}^{(j)}\right) = \mathcal{N}\left(\mathbf{z}_k \mid \mathbf{H}_k \mathbf{m}_{k|k-1}^{(j)}, \mathbf{R}_k + \mathbf{H}_k \mathbf{P}_{k|k-1}^{(j)} \mathbf{H}_k^T\right), \tag{2.13}$$

$$\mathbf{K}_k^{(j)} = \mathbf{P}_{k|k-1}^{(j)} \overline{\mathbf{H}}_k^T \left(\overline{\mathbf{H}}_k \mathbf{P}_{k|k-1}^{(j)} \overline{\mathbf{H}}_k^T + \overline{\mathbf{R}}_k\right)^{-1}, \tag{2.14}$$

$$\mathbf{m}_k^{(j)} = \mathbf{m}_{k|k-1}^{(j)} + \mathbf{K}_k^{(j)} \left( \begin{bmatrix} \mathbf{z}_1 \\ \vdots \\ \mathbf{z}_{|W_k|} \end{bmatrix} - \overline{\mathbf{H}}_k \mathbf{m}_{k|k-1}^{(j)} \right); \qquad \mathbf{P}_k^{(j)} = \left(\mathbf{I} - \mathbf{K}_k^{(j)} \overline{\mathbf{H}}_k\right) \mathbf{P}_{k|k-1}^{(j)}, \tag{2.15}$$

$$\overline{\mathbf{H}}_k = \left.\begin{bmatrix} \mathbf{H}_k \\ \vdots \\ \mathbf{H}_k \end{bmatrix}\right\} |W_k|; \qquad \overline{\mathbf{R}}_k = \text{blkdiag}\left(\overbrace{\mathbf{R}_k, \ldots, \mathbf{R}_k}^{|W_k|}\right), \tag{2.16}$$

where $\mathbf{I}$ denotes the identity matrix; $p_{D,k}$ has been assumed to be state independent; $\mathbf{H}_k$ and $\mathbf{R}_k$ denote the observation matrix and the observation noise covariance, respectively;

blkdiag(·) denotes block diagonal matrix, the measure in $\langle \cdot, \cdot \rangle$ of (2.11) is discrete, and it defines the summation inner product

$$\left\langle v_{k|k-1}^{J_{k|k-1}}, \eta_{W_k} \right\rangle = \sum_{l=1}^{J_{k|k-1}} \eta_{W_k}\left(\mathbf{m}_{k|k-1}^{(l)}\right) w_{k|k-1}^{(l)}. \tag{2.17}$$

## 3. Convergence of the GM-EPHD and EK-GM-EPHD Filters

The convergence properties and corresponding proof of the initialization step, prediction step, and pruning and merging step for the GM-EPHD filter are identical to those for point-target GM-PHD filter [19]. The main difficulty and greatest challenge is to prove the convergence for the measurement update step of the filter.

In order to derive the convergence results of the measurement update step for the GM-EPHD filter, the following lemma is first presented.

Consider the following assumptions.

B1: After the prediction step at time $k$, $v_{k|k-1}^{J_{k|k-1}}$ converges uniformly to $v_{k|k-1}$. In other words, for any given $\varepsilon_{k|k-1} > 0$ and any bounded measurable function $\varphi \in B(\mathbb{R}^d)$, where $B(\mathbb{R}^d)$ is the set of bounded Borel measurable functions on $\mathbb{R}^d$, there is a positive integer $J$ such that

$$\left| \left\langle v_{k|k-1}^{J_{k|k-1}} - v_{k|k-1}, \varphi \right\rangle \right| \leq \varepsilon_{k|k-1} \|\varphi\|_{\infty}, \tag{3.1}$$

for $J_{k|k-1} \geq J$, where $\|\cdot\|_{\infty}$ denotes $\infty$-norm. $\|\varphi\|_{\infty} \triangleq \sup(|\varphi|)$, $\sup(\cdot)$ denotes the supremum.

B2: The clutter intensity $\kappa_k(\mathbf{z}_k) = \lambda_k c_k(\mathbf{z}_k)$ is known a priori.

B3: $\gamma(\mathbf{x}_k) \in C_b(\mathbb{R}^d)$, where $C_b(\mathbb{R}^d)$ denotes the set of the continuous bounded functions on $\mathbb{R}^d$.

**Lemma 3.1.** *Given a partition $\wp_k = \{W_{1,k}, W_{2,k}, \ldots, W_{n,k}\}$ and suppose that assumptions B1–B3 hold, then*

$$\left| \prod_{i=1,\ldots,n} d_{W_{i,k}}^{J_{k|k-1}} - \prod_{i=1,\ldots,n} d_{W_{i,k}} \right| \leq \varepsilon_{k|k-1} \sum_{j=1,\ldots,n} \left\| \eta_{W_{j,k}} \right\|_{\infty} \prod_{i=1,\ldots,n; i \neq j} \left( d_{W_{i,k}}^{J_{k|k-1}} + d_{W_{i,k}} \right). \tag{3.2}$$

The proof of Lemma 3.1 can be found in Appendix A.

The uniform convergence of the measurement-updated GM-EPHD is now established by Proposition 3.2.

**Proposition 3.2.** *After the measurement update step of the GM-EPHD filter, there exists a real number $a_k$, dependent on the number of measurements such that*

$$\left| \left\langle v_k^{J_k} - v_k, \varphi \right\rangle \right| \leq a_k \varepsilon_{k|k-1} \|\varphi\|_{\infty}, \tag{3.3}$$

*where $a_k$ is defined by* (B.10).

The proof of the Proposition 3.2 can be found in Appendix B.

Proposition 3.2 shows that the error for the GM-EPHD corrector converges uniformly to the true EPHD corrector at each stage of the algorithm and the corresponding error bound is also provided. The error tends to zero as the number of Gaussians in the mixture tends to infinity. However, from (B.10), it can be seen that the error bound for the GM-EPHD corrector depends on the number of all partitions of the measurement set. It is quickly realized that as the size of the measurement set increases, the number of possible partitions grows very large. Therefore, the number of Gaussians in the mixture to ensure the asymptotic convergence of the error to a given bound would grow very quickly with the increase of the measurement number.

Now turn to the convergence for the EK-GM-EPHD filter, which is the nonlinear extension of the GM-EPHD filter. Due to the nonlinearity of the extended-target state and observation processes, the EPHD can no longer be represented as a GM. However, the EK-GM-EPHD filter can be adapted to accommodate models with mild nonlinearities. The convergence property and corresponding proof of the prediction step for the EK-GM-EPHD filter are identical to those for point-target EK-GM-PHD filter [19]. We now establish the conditions for uniform convergence of the measurement update step for the EK-GM-EPHD filter.

**Proposition 3.3.** *Suppose that the predicted EK-EPHD is given by the sum of Gaussians*

$$\upsilon_{k|k-1}^{EK,J_{k|k-1}}(\mathbf{x}_k) = \sum_{i=1}^{J_{k|k-1}} w_{k|k-1}^{(i)} \mathcal{N}\left(\mathbf{x}_k \mid \mathbf{m}_{k|k-1}^{(i)}, \mathbf{P}_{k|k-1}^{(i)}\right), \tag{3.4}$$

*and the $\phi_{\mathbf{z}_k}(\mathbf{x}_k)$ in (2.1) is given by the nonlinear single-measurement single-target equation $\mathbf{z}_k = h_k(\mathbf{x}_k, \mathbf{v}_k)$, where $h_k$ is known nonlinear functions and $\mathbf{v}_k$ is zero-mean Gaussian measurement noise with covariance $\mathbf{R}_k$, then the measurement-updated EK-EPHD approaches the Gaussian sum*

$$\upsilon_k(\mathbf{x}_k) \to \upsilon_k^{EK,J_k}(\mathbf{x}_k) = \upsilon_k^{ND,EK,J_{k|k-1}}(\mathbf{x}_k) + \sum_{\wp_k \angle Z_k} \sum_{W_k \in \wp_k} \upsilon_k^{D,EK,J_{k|k-1}}(\mathbf{x}_k, W_k), \tag{3.5}$$

*uniformly in $\mathbf{x}_k$ and $Z_k$ as $\mathbf{P}_{k|k-1}^{(i)} \to 0$ for $i = 1, \ldots, J_{k|k-1}$, and where*

$$\upsilon_k^{ND,EK,J_{k|k-1}}(\mathbf{x}_k) = \sum_{i=1}^{J_{k|k-1}} \left(1 - p_{D,k} + e^{-\gamma(\mathbf{m}_{k|k-1}^{(i)})} p_{D,k}\right) w_{k|k-1}^{(i)} \mathcal{N}\left(\mathbf{x}_k \mid \mathbf{m}_{k|k-1}^{(i)}, \mathbf{P}_{k|k-1}^{(i)}\right), \tag{3.6}$$

$$\upsilon_k^{D,EK,J_{k|k-1}}(\mathbf{x}_k, W_k) = \sum_{i=1}^{J_{k|k-1}} \omega_{\wp_k}^{EK,J_{k|k-1}} \frac{\eta_{W_k}^{EK}\left(\mathbf{m}_{k|k-1}^{(i)}\right)}{d_{W_k}^{EK,J_{k|k-1}}} w_{k|k-1}^{(i)} \mathcal{N}\left(\mathbf{x}_k \mid \mathbf{m}_k^{(i)}, \mathbf{P}_k^{(i)}\right), \tag{3.7}$$

$$\omega_{\wp_k}^{EK,J_{k|k-1}} = \frac{\prod_{W_k \in \wp_k} d_{W_k}^{EK,J_{k|k-1}}}{\sum_{\wp_k' \angle Z_k} \prod_{W_k' \in \wp_k'} d_{W_k'}^{EK}}; \quad d_{W_k}^{EK,J_{k|k-1}} = \delta_{|W_k|,1} + \sum_{i=1}^{J_{k|k-1}} w_{k|k-1}^{(i)} \eta_{W_k}^{EK}\left(\mathbf{m}_{k|k-1}^{(i)}\right), \tag{3.8}$$

$$\eta_{W_k}^{EK}\left(\mathbf{m}_{k|k-1}^{(i)}\right) = p_{D,k}e^{-\gamma\left(\mathbf{m}_{k|k-1}^{(i)}\right)} \times \prod_{\mathbf{z}_k\in W_k} \frac{\gamma\left(\mathbf{m}_{k|k-1}^{(i)}\right)\mathcal{N}\left(\mathbf{z}_k \mid h_k\left(\mathbf{m}_{k|k-1}^{(i)},\mathbf{0}\right), \mathbf{U}_k^{(i)}\mathbf{R}_k\left(\mathbf{U}_k^{(i)}\right)^T + \mathbf{H}_k^{(i)}\mathbf{P}_{k|k-1}^{(i)}\left(\mathbf{H}_k^{(i)}\right)^T\right)}{\lambda_k c_k(\mathbf{z}_k)}, \tag{3.9}$$

$$\mathbf{H}_k^{(i)} = \left.\frac{\partial h_k(\mathbf{x}_k,\mathbf{0})}{\partial \mathbf{x}_k}\right|_{\mathbf{x}_k=\mathbf{m}_{k|k-1}^{(i)}}; \qquad \mathbf{U}_k^{(i)} = \left.\frac{\partial h_k\left(\mathbf{m}_{k|k-1}^{(i)n},\mathbf{v}_k\right)}{\partial \mathbf{v}_k}\right|_{\mathbf{v}_k=0}, \tag{3.10}$$

$$\mathbf{K}_k^{(i)} = \mathbf{P}_{k|k-1}^{(i)}\left(\overline{\mathbf{H}}_k^{(i)}\right)^T\left(\overline{\mathbf{H}}_k^{(i)}\mathbf{P}_{k|k-1}^{(i)}\left(\overline{\mathbf{H}}_k^{(i)}\right)^T + \overline{\mathbf{U}}_k^{(i)}\mathbf{R}_k\left(\overline{\mathbf{U}}_k^{(i)}\right)^T\right)^{-1}, \tag{3.11}$$

$$\mathbf{m}_k^{(i)} = \mathbf{m}_{k|k-1}^{(i)} + \mathbf{K}_k^{(i)}\left(\begin{bmatrix}\mathbf{z}_1\\ \vdots \\ \mathbf{z}_{|W_k|}\end{bmatrix} - \begin{bmatrix}h\left(\mathbf{m}_{k|k-1}^{(i)},\mathbf{0}\right)\\ \vdots \\ h\left(\mathbf{m}_{k|k-1}^{(i)},\mathbf{0}\right)\end{bmatrix}\right); \mathbf{P}_k^{(i)} = \left(\mathbf{I} - \mathbf{K}_k^{(i)}\overline{\mathbf{H}}_k^{(i)}\right)\mathbf{P}_{k|k-1}^{(i)}, \tag{3.12}$$

$$\left.\begin{matrix}\overline{\mathbf{H}}_k^{(i)} = \begin{bmatrix}\mathbf{H}_k^{(i)}\\ \vdots \\ \mathbf{H}_k^{(i)}\end{bmatrix}\end{matrix}\right\}|W_k|; \quad \left.\begin{matrix}\overline{\mathbf{U}}_k^{(i)} = \begin{bmatrix}\mathbf{U}_k^{(i)}\\ \vdots \\ \mathbf{U}_k^{(i)}\end{bmatrix}\end{matrix}\right\}|W_k|, \tag{3.13}$$

The proof of Proposition 3.3 can be found in Appendix C.

From Propositions 3.2 and 3.3, we can obtain that the EK-GM-EPHD corrector uniformly converges to the true EPHD corrector in $\mathbf{x}_k$ and $Z_k$ under the assumptions that $\mathbf{P}_{k|k-1}^{(i)} \to 0$ for $i = 1,\ldots,J_{k|k-1}$ and the number of Gaussians in the mixture tends to infinity. These assumptions may be too restrictive or be unrealistic for practical problems, although the EK-GM-EPHD filter have demonstrated its potential for real-world applications. However, Propositions 3.2 and 3.3 give further theoretical justification for the use of the GM-EPHD and EK-GM-EPHD filters in ETT problem.

## 4. Simulations

Here we briefly describe the application of the convergence results for the GM-EPHD and EK-GM-EPHD filters to the linear and nonlinear ETT examples.

*Example 4.1* (GM-EPHD filter to linear ETT problem). Consider a two-dimensional scenario with an unknown and time varying number of the extended targets observed over the region $[-1000, 1000] \times [-1000, 1000]$ (in m) for a period of $T = 45$ time steps. The sampling interval is $\Delta t = 1$s. At time $k$, the actual number of the existing extended targets is $n_k$ and the state of the $i$th target is $\mathbf{x}_{i,k} = [x_{i,k}, y_{i,k}, \dot{x}_{i,k}, \dot{y}_{i,k}, \ddot{x}_{i,k}, \ddot{y}_{i,k}]^T$ $(i = 1,\ldots,n_k)$. Assume that the process noise $\boldsymbol{\varpi}_{i,k}$ of the $i$th extended target is independent and identically distributed (IID) zero-mean

Gaussian white noise with the covariance matrix $\mathbf{Q}_{i,k}$. Then the Markovian transition density of $\mathbf{x}_{i,k}$ could be modeled as

$$f_{k|k-1}(\mathbf{x}_{i,k} \mid \mathbf{x}_{i,k-1}) = \mathcal{N}(\mathbf{x}_{i,k} \mid \mathbf{\Phi}_{i,k}\mathbf{x}_{i,k-1}, \mathbf{Q}_{i,k}), \tag{4.1}$$

where $\mathbf{\Phi}_{i,k}$ is discrete-time evolution matrix. Here $\mathbf{\Phi}_{i,k}$ and $\mathbf{Q}_{i,k}$ are given by the constant acceleration model [24], as

$$\mathbf{\Phi}_{i,k} = \begin{bmatrix} 1 & \Delta t & \frac{\Delta t^2}{2} \\ & 1 & \Delta t \\ & & 1 \end{bmatrix} \otimes \mathbf{I}_2; \quad \mathbf{Q}_{i,k} = \sigma_{\varpi}^2 \begin{bmatrix} \frac{\Delta t^4}{4} & \frac{\Delta t^3}{2} & \frac{\Delta t^2}{2} \\ \frac{\Delta t^3}{2} & \frac{\Delta t^2}{2} & \Delta t \\ \frac{\Delta t^2}{2} & \Delta t & 1 \end{bmatrix} \otimes \mathbf{I}_2; \quad \mathbf{I}_2 = \begin{bmatrix} 1 & \\ & 1 \end{bmatrix}, \tag{4.2}$$

where "$\otimes$" denotes the Kronecker product. The parameter $\sigma_{\varpi}$ is the instantaneous standard deviation of the acceleration, given by $\sigma_{\varpi} = 0.05\,\mathrm{m/s^2}$.

Note that the objective of this paper is to focus on the convergence analysis for the GM-EPHD and EK-GM-EPHD filters, rather than the simulation of the extended-target motions. Therefore, although the proposed evolutions for the extended targets seem to be uncritical and oversimplifying, they will have little effect on the intention of the paper. Readers could be referred to [25] for further discussion on the extended-target motion models. The models proposed in [25] can also be accommodated within the EPHD filter straightforwardly.

At time $k$, the $x$-coordinate and $y$-coordinate measurements of the extended targets are generated by a sensor located at $[0, 0]^T$. The measurement noise $\mathbf{v}_k$ is IID zero-mean Gaussian white noise with covariance matrix $\mathbf{R}_k = \mathrm{diag}(\sigma_x^2, \sigma_y^2)$, where $\mathrm{diag}(\cdot)$ denotes the diagonal matrix, $\sigma_x$ and $\sigma_y$ are, respectively, standard deviations of the $x$-coordinate and $y$-coordinate measurements. In this simulation, they are given as $\sigma_x = \sigma_y = 25\,\mathrm{m}$. The single-measurement single-target likelihood density $\phi_{\mathbf{z}_k}(\mathbf{x}_{i,k})$ is

$$\phi_{\mathbf{z}_k}(\mathbf{x}_{i,k}) = \mathcal{N}(\mathbf{z}_k \mid \mathbf{H}_k\mathbf{x}_{i,k}, \mathbf{R}_k), \tag{4.3}$$

where

$$\mathbf{H}_k = \begin{bmatrix} 1 & 0 & 0 & 0 & 0 & 0 \\ 0 & 1 & 0 & 0 & 0 & 0 \end{bmatrix}. \tag{4.4}$$

The detection probability of the sensor is $p_{D,k}(\mathbf{x}_k) = 0.95$.

In this simulation, it is assumed that the effect of the shape for each extended target is much smaller than that of the measurement noise. Hence, the shape estimation is not considered here.

At time $k$, the number of the measurements arising from the $i$th extended target satisfies Poisson distribution with the mean $\gamma(\mathbf{x}_{i,k})$. In this simulation, it is given as $\gamma(\mathbf{x}_{i,k}) = 3$ $(i = 1, \ldots, n_k)$.

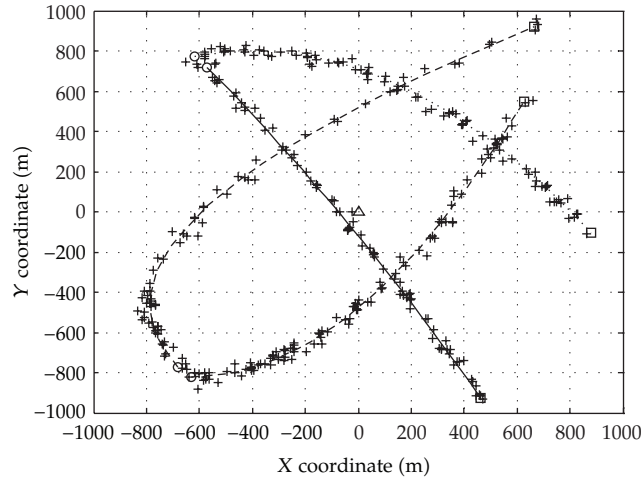


**Figure 1:** The true trajectories for extended targets and sensor location.

The clutter is modeled as a Poisson RFS with the intensity $\kappa_k(\mathbf{z}_k) = \lambda_k c_k(\mathbf{z}_k)$. In this example, the actual clutter density is $c_k(\mathbf{z}_k) = \mathcal{U}(\mathbf{z}_k)$. It means that the clutter is uniformly distributed over the observation region.

Figure 1 shows the true trajectories for extended targets and sensor location.

In Figure 1, "$\Delta$" denotes the sensor location, "$\bigcirc$" denotes the locations at which the extended targets are born, "$\square$" denotes the locations at which the extended targets die, and "+" denotes the measurements generated by the extended targets. Extended target 1 is born at 1 s and dies at 25 s. Extended target 2 is born at 1 s and dies at 30 s. Extended target 3 is born at 10 s and dies at 35 s. Extended target 4 is born at 20s and dies at 45 s.

The intensity of the extended-target birth at time $k$ is modeled as

$$\beta_k(\mathbf{x}_k) = \lambda_\beta f_\beta(\mathbf{x}_k \mid \varphi_\beta), \tag{4.5}$$

where $\lambda_\beta$ is the average number of the extended-target birth per scan, $f_\beta(\mathbf{x}_k|\varphi_\beta)$ is the probability density of the new born extended-target state, and $\varphi_\beta$ is the set of the density parameters. In this example, they are taken as $\lambda_\beta = 0.05$, $f_\beta(\mathbf{x}_k|\varphi_\beta) = \pi_\beta^1 \mathcal{N}(\mathbf{x}_k|\boldsymbol{\mu}_\beta^1, \boldsymbol{\Sigma}_\beta^1) + \pi_\beta^2 \mathcal{N}(\mathbf{x}_k|\boldsymbol{\mu}_\beta^2, \boldsymbol{\Sigma}_\beta^2)$, where $\varphi_\beta = \{\pi_\beta^1, \pi_\beta^2, \boldsymbol{\mu}_\beta^1, \boldsymbol{\mu}_\beta^2, \boldsymbol{\Sigma}_\beta^1, \boldsymbol{\Sigma}_\beta^2\}$, $\pi_\beta^1 = \pi_\beta^2 = 0.5$, $\boldsymbol{\mu}_\beta^1 = [-600, 750, 0, 0, 0, 0]^T$, $\boldsymbol{\mu}_\beta^2 = [-650, -800, 0, 0, 0, 0]^T$, and $\boldsymbol{\Sigma}_\beta^1 = \boldsymbol{\Sigma}_\beta^2 = \mathrm{diag}(400, 400, 100, 100, 9, 9)$.

The GM-EPHD filter is used to estimate the number and states of the extended targets in the linear ETT problem. We now conduct Monte Carlo (MC) simulation experiments on the same clutter intensity and target trajectories but with independently generated clutter and target-generated measurements in each trial. Via comparing the tracking performance of the GM-EPHD filter in the various number $J_k$ of Gaussians in the mixture and in various clutter rate $\lambda_k$, the convergence results for the algorithm can be verified to a great extent. For convenience, we assume $J_k = J$ and $\lambda_k = \lambda$ at each time step. Assumptions B2–B3 are satisfied in this example. So, the GM-EPHD filter uniformly converges to the ground truth.

The standard deviation of the estimated cardinality distribution and the optimal subpattern assignment (OSPA) multitarget miss distance [26] of order $p = 2$ with cutoff

**Table 1:** Time averaged standard deviation of the estimated cardinality distribution and time averaged OSPA (m) from the GM-EPHD filter in various $J$ given $\lambda = 50$.

| Gaussian number $J$ in the mixture | 50 | 100 | 300 | 500 | 700 |
|---|---|---|---|---|---|
| Time averaged standard deviation of the estimated cardinality distribution from the GM-EPHD filter | 2.12 | 1.39 | 0.97 | 0.71 | 0.58 |
| OSPA (m) from the GM-EPHD filter | 83.5 | 58.7 | 49.6 | 43.1 | 39.5 |

**Table 2:** Time averaged standard deviation of the estimated cardinality distribution and time averaged OSPA (m) from the GM-EPHD filter in various $\lambda$ given $J = 700$.

| Clutter rate $\lambda$ | 50 | 100 | 200 | 300 | 400 |
|---|---|---|---|---|---|
| Time averaged standard deviation of the estimated cardinality distribution from the GM-EPHD filter | 0.58 | 0.70 | 0.95 | 1.23 | 1.48 |
| OSPA (m) from the GM-EPHD filter | 39.5 | 42.9 | 49.0 | 56.1 | 61.7 |

$c = 100$ m, which jointly captures differences in cardinality and individual elements between two finite sets, are used to evaluate the performance of the method. Given the clutter rate $\lambda = 50$, Table 1 shows the time averaged standard deviation of the estimated cardinality distribution and the time averaged OSPA from the GM-EPHD filter in various $J$ via 200 MC simulation experiments.

Table 1 shows that both the standard deviation of the estimated cardinality distribution and OSPA decrease with the increase of the Gaussian number $J$ in the mixture. This phenomenon can be reasonably explained by the convergence results derived in this paper. First, according to Proposition 3.2, the error of the GM-EPHD decreases as $J$ increases; then, the more precise estimates of the multitarget number and states can be derived from the more precise GM-EPHD, which eventually leads to the results presented in Table 1.

Given $J = 700$, Table 2 shows the time averaged standard deviation of the estimated cardinality distribution and the time averaged OSPA from the GM-EPHD filter in various clutter rate $\lambda$ via 200 MC simulation experiments. Obviously, the number of the measurements collected at each time step increases with the increase of $\lambda$.

From Table 2, it can be seen that the errors of the multitarget number and state estimates from the GM-EPHD filter grow significantly with the increase of $\lambda$. A reasonable explanation for this is that the partition operation included in (B.10) leads that the error bound of the GM-EPHD corrector grows very quickly with the increase of the measurement number. Therefore, Table 2 consists with the convergence results established by Proposition 3.2, too.

*Example 4.2* (EK-GM-EPHD filter to nonlinear ETT problem). The experiment settings are the same as those of Example 4.1 except the single-measurement single-target likelihood density $\phi_{\mathbf{z}_k}(\mathbf{x}_{i,k})$. The range $r_k$ and bearing $\theta_k$ measurements of the extended targets are generated with the noise covariance matrix $\mathbf{R}_k = \operatorname{diag}(\sigma_r^2, \sigma_\theta^2)$, where $\sigma_r$ and $\sigma_\theta$ are, respectively, standard deviations of the range and bearing measurements. In this simulation, they are given as $\sigma_r = 25$ m and $\sigma_\theta = 0.025$ rad. The $\phi_{\mathbf{z}_k}(\mathbf{x}_{i,k})$ becomes

$$\phi_{\mathbf{z}_k}(\mathbf{x}_{i,k}) = \mathcal{N}(\mathbf{z}_k \mid h_k(\mathbf{x}_{i,k}), \mathbf{R}_k), \tag{4.6}$$

**Table 3:** Time averaged standard deviation of the estimated cardinality distribution and time averaged OSPA (m) from the EK-GM-EPHD filter in various $J$ given $\lambda = 50$.

| Gaussian number $J$ in the mixture | 50 | 100 | 300 | 500 | 700 |
|---|---|---|---|---|---|
| Time averaged standard deviation of the estimated cardinality distribution from the EK-GM-EPHD filter | 3.15 | 2.29 | 1.77 | 1.21 | 0.76 |
| OSPA (m) from the EK-GM-EPHD filter | 93.2 | 86.7 | 75.3 | 54.6 | 43.9 |

**Table 4:** Time averaged standard deviation of the estimated cardinality distribution and time averaged OSPA (m) from the EK-GM-EPHD filter in various $\lambda$ given $J = 700$.

| Clutter rate $\lambda$ | 50 | 100 | 200 | 300 | 400 |
|---|---|---|---|---|---|
| Time averaged standard deviation of the estimated cardinality distribution from the EK-GM-EPHD filter | 0.76 | 0.92 | 1.29 | 1.61 | 1.92 |
| OSPA (m) from the EK-GM-EPHD filter | 43.9 | 48.1 | 55.8 | 67.8 | 79.5 |

where

$$h_k(\mathbf{x}_{i,k}) = \left[\sqrt{x_{i,k}^2 + y_{i,k}^2} \ \arctan \frac{y_{i,k}}{x_{i,k}}\right]^T. \tag{4.7}$$

The EK-GM-EPHD filter is used to estimate the number and states of the extended targets in the nonlinear ETT problem. Given $\lambda = 50$, Table 3 shows the time averaged standard deviation of the estimated cardinality distribution and the time averaged OSPA from the EK-GM-EPHD filter in various $J$ via 200 MC simulation experiments while, given $J = 700$, Table 4 shows the time averaged standard deviation of the estimated cardinality distribution and the time averaged OSPA from the EK-GM-EPHD filter in various $\lambda$ via 200 MC simulation experiments.

As expected, Tables 3 and 4, respectively, show that the errors of the multitarget number and state estimates from the EK-GM-EPHD filter decrease with the increase of $J$ and increase with the increase of $\lambda$. These consist with the convergence results established by Propositions 3.2 and 3.3. In addition, comparing Tables 1 and 2 with Tables 3 and 4, it can be seen that the errors from the EK-GM-EPHD filter are obviously larger than the errors from the GM-EPHD filter given the same $J$ and $\lambda$. The additional errors from the EK-GM-EPHD filter are caused by the reason that the condition $\mathbf{P}_{k|k-1}^{(i)} \to 0$ for $i = 1, \ldots, J_{k|k-1}$ in Proposition 3.3 is very difficult to approach in this example.

## 5. Conclusions and Future Work

This paper shows that the recently proposed GM-EPHD filter converges uniformly to the true EPHD filter as the number of Gaussians in the mixture tends to infinity. Proofs of uniform convergence are also derived for the EK-GM-EPHD filter. Since the GM-EPHD corrector equations involve with the partition operation that grows very quickly with the increase of the measurement number, the future work is focused on studying the computationally

tractable approximation for it and providing the convergence results and error bounds for the approximate GM-EPHD corrector.

# Appendices

## A. Proof of Lemma 3.1

We have known that $\gamma(\mathbf{x}_k) \in C_b(\mathbb{R}^d)$, $\phi_{\mathbf{z}_k}(\mathbf{x}_k) = \mathcal{N}(\mathbf{z}_k|\mathbf{H}_k\mathbf{x}_k, \mathbf{R}_k) \in C_b(\mathbb{R}^d)$, $\lambda_k c_k(\mathbf{z}_k)$ is known a priori and $0 \le p_{D,k} \le 1$ according to assumptions A1–A6 in [12] and assumptions B1–B3. So, from (2.3) we get $\eta_{W_k}(\mathbf{x}_k) \in C_b(\mathbb{R}^d)$. In addition, by (2.4) and (2.11) and the definition of $\infty$-norm, we have $d_{W_k} \ge 0$, $d_{W_k}^{J_{k|k-1}} \ge 0$, and $\|\eta_{W_k}\|_\infty \ge 0$ because of the facts that $\upsilon_{k|k-1}(\mathbf{x}_k) \ge 0$, $\upsilon_{k|k-1}^{J_{k|k-1}}(\mathbf{x}_k) \ge 0$ and $\eta_{W_k}(\mathbf{x}_k) \ge 0$.

For the initial induction step, assume $n = 1$. In this case, from (3.1) we get

$$\left|d_{W_{1,k}}^{J_{k|k-1}} - d_{W_{1,k}}\right| = \left|\left\langle \upsilon_{k|k-1}^{J_{k|k-1}}, \eta_{W_{1,k}}\right\rangle - \left\langle \upsilon_{k|k-1}, \eta_{W_{1,k}}\right\rangle\right| = \left|\left\langle \upsilon_{k|k-1}^{J_{k|k-1}} - \upsilon_{k|k-1}, \eta_{W_{1,k}}\right\rangle\right| \le \varepsilon_{k|k-1}\left\|\eta_{W_{1,k}}\right\|_\infty. \tag{A.1}$$

In the case of $n = 2$, by the triangle inequality and (A.1), we have

$$\begin{aligned}\left|d_{W_{1,k}}^{J_{k|k-1}} d_{W_{2,k}}^{J_{k|k-1}} - d_{W_{1,k}} d_{W_{2,k}}\right| &= \left|\frac{d_{W_{2,k}}^{J_{k|k-1}} + d_{W_{2,k}}}{2}\left(d_{W_{1,k}}^{J_{k|k-1}} - d_{W_{1,k}}\right) + \frac{d_{W_{2,k}}^{J_{k|k-1}} - d_{W_{2,k}}}{2}\left(d_{W_{1,k}}^{J_{k|k-1}} + d_{W_{1,k}}\right)\right| \\ &\le \frac{d_{W_{2,k}}^{J_{k|k-1}} + d_{W_{2,k}}}{2}\left|d_{W_{1,k}}^{J_{k|k-1}} - d_{W_{1,k}}\right| + \left|d_{W_{2,k}}^{J_{k|k-1}} - d_{W_{2,k}}\right|\frac{d_{W_{1,k}}^{J_{k|k-1}} + d_{W_{1,k}}}{2} \\ &\le \varepsilon_{k|k-1}\left\|\eta_{W_{1,k}}\right\|_\infty \frac{d_{W_{2,k}}^{J_{k|k-1}} + d_{W_{2,k}}}{2} + \varepsilon_{k|k-1}\left\|\eta_{W_{2,k}}\right\|_\infty \frac{d_{W_{1,k}}^{J_{k|k-1}} + d_{W_{1,k}}}{2}.\end{aligned} \tag{A.2}$$

Since $\varepsilon_{k|k-1} > 0$, $d_{W_k} \ge 0$, $d_{W_k}^{J_{k|k-1}} \ge 0$ and $\|\eta_{W_k}\|_\infty \ge 0$, (A.2) becomes

$$\left|d_{W_{1,k}}^{J_{k|k-1}} d_{W_{2,k}}^{J_{k|k-1}} - d_{W_{1,k}} d_{W_{2,k}}\right| \le \varepsilon_{k|k-1}\left(\left\|\eta_{W_{1,k}}\right\|_\infty\left(d_{W_{2,k}} + d_{W_{2,k}}^{J_{k|k-1}}\right) + \left\|\eta_{W_{2,k}}\right\|_\infty\left(d_{W_{1,k}} + d_{W_{1,k}}^{J_{k|k-1}}\right)\right). \tag{A.3}$$

Assume that we have established (3.2) for $i = 1, \ldots, n$. We are to establish (3.2) for $i = 1, \ldots, n+1$. Using the triangle inequality and (A.1), we get

$$\begin{aligned}
&\left| \prod_{i=1,\ldots,n+1} d_{W_{i,k}}^{J_{k|k-1}} - \prod_{i=1,\ldots,n+1} d_{W_{i,k}} \right| \\
&= \left| \frac{d_{W_{n+1,k}} + d_{W_{n+1,k}}^{J_{k|k-1}}}{2} \left( \prod_{i=1,\ldots,n} d_{W_{i,k}}^{J_{k|k-1}} - \prod_{i=1,\ldots,n} d_{W_{i,k}} \right) + \frac{d_{W_{n+1,k}}^{J_{k|k-1}} - d_{W_{n+1,k}}}{2} \left( \prod_{i=1,\ldots,n} d_{W_{i,k}}^{J_{k|k-1}} + \prod_{i=1,\ldots,n} d_{W_{i,k}} \right) \right| \\
&\leq \frac{d_{W_{n+1,k}} + d_{W_{n+1,k}}^{J_{k|k-1}}}{2} \left| \prod_{i=1,\ldots,n} d_{W_{i,k}}^{J_{k|k-1}} - \prod_{i=1,\ldots,n} d_{W_{i,k}} \right| + \left| \frac{d_{W_{n+1,k}}^{J_{k|k-1}} - d_{W_{n+1,k}}}{2} \right| \left( \prod_{i=1,\ldots,n} d_{W_{i,k}}^{J_{k|k-1}} + \prod_{i=1,\ldots,n} d_{W_{i,k}} \right) \\
&\leq \varepsilon_{k|k-1} \frac{d_{W_{n+1,k}} + d_{W_{n+1,k}}^{J_{k|k-1}}}{2} \sum_{j=1,\ldots,n} \left\| \eta_{W_{j,k}} \right\|_\infty \prod_{i=1,\ldots,n; i \neq j} \left( d_{W_{i,k}}^{J_{k|k-1}} + d_{W_{i,k}} \right) \\
&\quad + \varepsilon_{k|k-1} \frac{\left\| \eta_{W_{n+1,k}} \right\|_\infty}{2} \left( \prod_{i=1,\ldots,n} d_{W_{i,k}}^{J_{k|k-1}} + \prod_{i=1,\ldots,n} d_{W_{i,k}} \right).
\end{aligned} \tag{A.4}$$

Since $\varepsilon_{k|k-1} > 0$, $d_{W_k} \geq 0$, $d_{W_k}^{J_{k|k-1}} \geq 0$ and $\|\eta_{W_k}\|_\infty \geq 0$, (A.4) becomes

$$\begin{aligned}
&\left| \prod_{i=1,\ldots,n+1} d_{W_{i,k}}^{J_{k|k-1}} - \prod_{i=1,\ldots,n+1} d_{W_{i,k}} \right| \\
&\leq \varepsilon_{k|k-1} \sum_{j=1,\ldots,n} \left\| \eta_{W_{j,k}} \right\|_\infty \prod_{i=1,\ldots,n+1; i \neq j} \left( d_{W_{i,k}}^{J_{k|k-1}} + d_{W_{i,k}} \right) + \varepsilon_{k|k-1} \left\| \eta_{W_{n+1,k}} \right\|_\infty \left( \prod_{i=1,\ldots,n} d_{W_{i,k}}^{J_{k|k-1}} + \prod_{i=1,\ldots,n} d_{W_{i,k}} \right) \\
&\leq \varepsilon_{k|k-1} \sum_{j=1,\ldots,n} \left\| \eta_{W_{j,k}} \right\|_\infty \prod_{i=1,\ldots,n+1; i \neq j} \left( d_{W_{i,k}}^{J_{k|k-1}} + d_{W_{i,k}} \right) + \varepsilon_{k|k-1} \left\| \eta_{W_{n+1,k}} \right\|_\infty \prod_{i=1,\ldots,n} \left( d_{W_{i,k}}^{J_{k|k-1}} + d_{W_{i,k}} \right) \\
&= \varepsilon_{k|k-1} \sum_{j=1,\ldots,n+1} \left\| \eta_{W_{j,k}} \right\|_\infty \prod_{i=1,\ldots,n+1; i \neq j} \left( d_{W_{i,k}}^{J_{k|k-1}} + d_{W_{i,k}} \right),
\end{aligned} \tag{A.5}$$

and this closes the inductive step. This completes the proof.

## B. Proof of Proposition 3.2

By the EPHD corrector equations, (2.2), and the triangle inequality, we get

$$
\begin{aligned}
&\left|\left\langle v_k^{J_k} - v_k, \varphi \right\rangle\right| \\
&\quad = \left| \left\langle \left[ 1 - p_{D,k} + e^{-\gamma} p_{D,k} + \sum_{\wp_k \angle Z_k} \omega_{\wp_k}^{J_{k|k-1}} \sum_{W_k \in \wp_k} \frac{\eta_{W_k}}{d_{W_k}^{J_{k|k-1}}} \right] v_{k|k-1}^{J_{k|k-1}}, \varphi \right\rangle \right. \\
&\qquad \left. - \left\langle \left[ 1 - p_{D,k} + e^{-\gamma} p_{D,k} + \sum_{\wp_k \angle Z_k} \omega_{\wp_k} \sum_{W_k \in \wp_k} \frac{\eta_{W_k}}{d_{W_k}} \right] v_{k|k-1}, \varphi \right\rangle \right| \\
&\quad = \left| \begin{array}{l} \left( \left\langle v_{k|k-1}^{J_{k|k-1}}, \varphi(1 - p_{D,k} + e^{-\gamma} p_{D,k}) \right\rangle - \left\langle v_{k|k-1}, \varphi(1 - p_{D,k} + e^{-\gamma} p_{D,k}) \right\rangle \right) \\ + \sum_{\wp_k \angle Z_k} \sum_{W_k \in \wp_k} \left( \dfrac{\omega_{\wp_k}^{J_{k|k-1}} \left\langle v_{k|k-1}^{J_{k|k-1}}, \varphi \eta_{W_k} \right\rangle}{d_{W_k}^{J_{k|k-1}}} - \dfrac{\omega_{\wp_k} \left\langle v_{k|k-1}, \varphi \eta_{W_k} \right\rangle}{d_{W_k}} \right) \end{array} \right| \qquad \text{(B.1)} \\
&\quad \le \left| \left\langle v_{k|k-1}^{J_{k|k-1}} - v_{k|k-1}, \varphi(1 - p_{D,k} + e^{-\gamma} p_{D,k}) \right\rangle \right| \\
&\qquad + \sum_{\wp_k \angle Z_k} \sum_{W_k \in \wp_k} \left( \left| \frac{\omega_{\wp_k}^{J_{k|k-1}} \left\langle v_{k|k-1}^{J_{k|k-1}}, \varphi \eta_{W_k} \right\rangle}{d_{W_k}^{J_{k|k-1}}} - \frac{\omega_{\wp_k} \left\langle v_{k|k-1}^{J_{k|k-1}}, \varphi \eta_{W_k} \right\rangle}{d_{W_k}} \right| \right. \\
&\qquad\qquad \left. + \left| \frac{\omega_{\wp_k} \left\langle v_{k|k-1}^{J_{k|k-1}}, \varphi \eta_{W_k} \right\rangle}{d_{W_k}} - \frac{\omega_{\wp_k} \left\langle v_{k|k-1}, \varphi \eta_{W_k} \right\rangle}{d_{W_k}} \right| \right).
\end{aligned}
$$

By (3.1), the second term in the summation of (B.1) is

$$
\begin{aligned}
\left| \frac{\omega_{\wp_k} \left\langle v_{k|k-1}^{J_{k|k-1}}, \varphi \eta_{W_k} \right\rangle}{d_{W_k}} - \frac{\omega_{\wp_k} \left\langle v_{k|k-1}, \varphi \eta_{W_k} \right\rangle}{d_{W_k}} \right| &= \frac{\omega_{\wp_k} \left| \left\langle v_{k|k-1}^{J_{k|k-1}} - v_{k|k-1}, \varphi \eta_{W_k} \right\rangle \right|}{d_{W_k}} \\
&\le \frac{\omega_{\wp_k} \varepsilon_{k|k-1} \left\| \varphi \eta_{W_k} \right\|_\infty}{d_{W_k}}.
\end{aligned} \qquad \text{(B.2)}
$$

Using the triangle inequality, the first term in the summation of (B.1) is

$$\begin{aligned}
&\left|\frac{\omega_{\wp_k}^{J_{k|k-1}}\left\langle \upsilon_{k|k-1}^{J_{k|k-1}}, \varphi\eta_{W_k}\right\rangle}{d_{W_k}^{J_{k|k-1}}} - \frac{\omega_{\wp_k}\left\langle \upsilon_{k|k-1}^{J_{k|k-1}}, \varphi\eta_{W_k}\right\rangle}{d_{W_k}}\right| \\
&\quad= \frac{\left\langle \upsilon_{k|k-1}^{J_{k|k-1}}, \varphi\eta_{W_k}\right\rangle \left| d_{W_k}\omega_{\wp_k}^{J_{k|k-1}} - d_{W_k}^{J_{k|k-1}}\omega_{\wp_k}\right|}{d_{W_k}^{J_{k|k-1}} d_{W_k}} \\
&\quad= \frac{\left\langle \upsilon_{k|k-1}^{J_{k|k-1}}, \varphi\eta_{W_k}\right\rangle \left| d_{W_k}\omega_{\wp_k}^{J_{k|k-1}} - d_{W_k}^{J_{k|k-1}}\omega_{\wp_k}^{J_{k|k-1}} + d_{W_k}^{J_{k|k-1}}\omega_{\wp_k}^{J_{k|k-1}} - d_{W_k}^{J_{k|k-1}}\omega_{\wp_k}\right|}{\left(\delta_{|W_k|,1} + \left\langle \upsilon_{k|k-1}^{J_{k|k-1}}, \eta_{W_k}\right\rangle\right) d_{W_k}} \\
&\quad\leq \frac{\left\langle \upsilon_{k|k-1}^{J_{k|k-1}}, \eta_{W_k}\right\rangle \|\varphi\|_\infty \left| \omega_{\wp_k}^{J_{k|k-1}}\left(d_{W_k} - d_{W_k}^{J_{k|k-1}}\right) + d_{W_k}^{J_{k|k-1}}\left(\omega_{\wp_k}^{J_{k|k-1}} - \omega_{\wp_k}\right)\right|}{\left\langle \upsilon_{k|k-1}^{J_{k|k-1}}, \eta_{W_k}\right\rangle d_{W_k}} \\
&\quad\leq \frac{\|\varphi\|_\infty \left(\omega_{\wp_k}^{J_{k|k-1}}\left|d_{W_k} - d_{W_k}^{J_{k|k-1}}\right| + d_{W_k}^{J_{k|k-1}}\left|\omega_{\wp_k}^{J_{k|k-1}} - \omega_{\wp_k}\right|\right)}{d_{W_k}}.
\end{aligned} \tag{B.3}$$

Using the triangle inequality again for the term $|\omega_{\wp_k}^{J_{k|k-1}} - \omega_{\wp_k}|$ in the numerator of (B.3), we get

$$\begin{aligned}
\left|\omega_{\wp_k}^{J_{k|k-1}} - \omega_{\wp_k}\right| &= \left|\frac{\prod_{W_k\in\wp_k} d_{W_k}^{J_{k|k-1}}}{\sum_{\wp_k'\angle Z_k}\prod_{W_k'\in\wp_k'} d_{W_k'}^{J_{k|k-1}}} - \frac{\prod_{W_k\in\wp_k} d_{W_k}}{\sum_{\wp_k'\angle Z_k}\prod_{W_k'\in\wp_k'} d_{W_k'}}\right| \\
&= \left|\frac{\prod_{W_k\in\wp_k} d_{W_k}^{J_{k|k-1}}}{\sum_{\wp_k'\angle Z_k}\prod_{W_k'\in\wp_k'} d_{W_k'}^{J_{k|k-1}}} - \frac{\prod_{W_k\in\wp_k} d_{W_k}}{\sum_{\wp_k'\angle Z_k}\prod_{W_k'\in\wp_k'} d_{W_k'}^{J_{k|k-1}}}\right. \\
&\qquad \left. + \frac{\prod_{W_k\in\wp_k} d_{W_k}}{\sum_{\wp_k'\angle Z_k}\prod_{W_k'\in\wp_k'} d_{W_k'}^{J_{k|k-1}}} - \frac{\prod_{W_k\in\wp_k} d_{W_k}}{\sum_{\wp_k'\angle Z_k}\prod_{W_k'\in\wp_k'} d_{W_k'}}\right| \\
&\leq \frac{\left|\prod_{W_k\in\wp_k} d_{W_k}^{J_{k|k-1}} - \prod_{W_k\in\wp_k} d_{W_k}\right|}{\sum_{\wp_k'\angle Z_k}\prod_{W_k'\in\wp_k'} d_{W_k'}^{J_{k|k-1}}} + \frac{\prod_{W_k\in\wp_k} d_{W_k}}{\sum_{\wp_k'\angle Z_k}\prod_{W_k'\in\wp_k'} d_{W_k'}} \\
&\qquad \cdot \frac{\left|\sum_{\wp_k'\angle Z_k}\left(\prod_{W_k'\in\wp_k'} d_{W_k'} - \prod_{W_k'\in\wp_k'} d_{W_k'}^{J_{k|k-1}}\right)\right|}{\sum_{\wp_k'\angle Z_k}\prod_{W_k'\in\wp_k'} d_{W_k'}^{J_{k|k-1}}} \\
&\leq \frac{\left|\prod_{W_k\in\wp_k} d_{W_k}^{J_{k|k-1}} - \prod_{W_k\in\wp_k} d_{W_k}\right|}{\sum_{\wp_k'\angle Z_k}\prod_{W_k'\in\wp_k'} d_{W_k'}^{J_{k|k-1}}} + \omega_{\wp_k}\frac{\sum_{\wp_k'\angle Z_k}\left|\prod_{W_k'\in\wp_k'} d_{W_k'} - \prod_{W_k'\in\wp_k'} d_{W_k'}^{J_{k|k-1}}\right|}{\sum_{\wp_k'\angle Z_k}\prod_{W_k'\in\wp_k'} d_{W_k'}^{J_{k|k-1}}}.
\end{aligned} \tag{B.4}$$

Using Lemma 3.1, we get

$$\left|\prod_{W_k\in\wp_k} d_{W_k} - \prod_{W_k\in\wp_k} d_{W_k}^{J_{k|k-1}}\right| \le \varepsilon_{k|k-1}\sum_{W_k\in\wp_k}\left\|\eta_{W_k}\right\|_\infty \prod_{V_k\in\wp_k-W_k}\left(d_{V_k}+d_{V_k}^{J_{k|k-1}}\right), \tag{B.5}$$

where $\wp_k - W_k$ denotes the complement of $W_k$ in $\wp_k$.

Then, (B.4) can be rewritten as

$$\left|\omega_{\wp_k}^{J_{k|k-1}} - \omega_{\wp_k}\right| \le \varepsilon_{k|k-1}\rho_k, \tag{B.6}$$

where

$$\begin{aligned}\rho_k = {} & \frac{\sum_{W_k\in\wp_k}\left\|\eta_{W_k}\right\|_\infty \prod_{V_k\in\wp_k-W_k}\left(d_{V_k}+d_{V_k}^{J_{k|k-1}}\right)}{\sum_{\wp_k'\angle Z_k}\prod_{W_k'\in\wp_k'} d_{W'}^{J_{k|k-1}}} \\ & + \frac{\omega_{\wp_k}\sum_{\wp_k'\angle Z_k}\sum_{W_k'\in\wp_k'}\left\|\eta_{W_k'}\right\|_\infty \prod_{V_k'\in\wp_k'-W_k'}\left(d_{V_k'}+d_{V_k'}^{J_{k|k-1}}\right)}{\sum_{\wp_k'\angle Z_k}\prod_{W_k'\in\wp_k'} d_{W'}^{J_{k|k-1}}}.\end{aligned} \tag{B.7}$$

Substitute (A.1) and (B.6) into (B.3),

$$\left|\frac{\omega_{\wp_k}^{J_{k|k-1}}\left\langle \upsilon_{k|k-1}^{J_{k|k-1}}, \varphi\eta_{W_k}\right\rangle}{d_{W_k}^{J_k}} - \frac{\omega_{\wp_k}\left\langle \upsilon_{k|k-1}^{J_{k|k-1}}, \varphi\eta_{W_k}\right\rangle}{d_{W_k}}\right| \le \varepsilon_{k|k-1}\frac{\left\|\varphi\right\|_\infty\left(\omega_{\wp_k}^{J_{k|k-1}}\left\|\eta_{W_k}\right\|_\infty + d_{W_k}^{J_{k|k-1}}\rho_k\right)}{d_{W_k}}. \tag{B.8}$$

Substituting (3.1), (B.2), and (B.8) into (B.1), we have

$$\begin{aligned}\left|\left\langle \upsilon_k^{J_{k|k-1}} - \upsilon_k, \varphi\right\rangle\right| \le \varepsilon_{k|k-1}\left\|\varphi\right\|_\infty \Bigg( & \left\|1 - p_{D,k} + e^{-\gamma}p_{D,k}\right\|_\infty \\ & + \sum_{\wp_k\angle Z_k}\sum_{W_k\in\wp_k}\left(\frac{\omega_{\wp_k}^{J_{k|k-1}}\left\|\eta_{W_k}\right\|_\infty + d_{W_k}^{J_{k|k-1}}\rho_k}{d_{W_k}} + \omega_{\wp_k}\frac{\left\|\eta_{W_k}\right\|_\infty}{d_{W_k}}\right)\Bigg).\end{aligned} \tag{B.9}$$

So that Proposition 3.2 is proved with

$$a_k = \left\|1 - p_{D,k} + e^{-\gamma}p_{D,k}\right\|_\infty + \sum_{\wp_k\angle Z_k}\sum_{W_k\in\wp_k}\frac{\omega_{\wp_k}^{J_{k|k-1}}\left\|\eta_{W_k}\right\|_\infty + d_{W_k}^{J_{k|k-1}}\rho_k + \omega_{\wp_k}\left\|\eta_{W_k}\right\|_\infty}{d_{W_k}}. \tag{B.10}$$

This completes the proof.

## C. Proof of Proposition 3.3

Clearly, by the EPHD corrector equations, (2.2)–(2.4), and the predicted EK-EPHD, (3.4), we obtain that the $v_k^{ND,EK,J_{k|k-1}}(\mathbf{x}_k)$ in (3.5) is a Gaussian sum presented by (3.6). Now turn to the $v_k^{D,EK,J_{k|k-1}}(\mathbf{x}_k, W_k)$ in (3.5). From (2.2), we get

$$v_k^{D,EK,J_{k|k-1}}(\mathbf{x}_k, W_k) = \omega_{\hat{p}_k}^{J_{k|k-1}} \frac{\eta_{W_k}(\mathbf{x}_k)}{d_{W_k}^{J_{k|k-1}}} v_{k|k-1}^{EK,J_{k|k-1}}(\mathbf{x}_k). \tag{C.1}$$

Consider the term $\eta_{W_k}(\mathbf{x}_k) v_{k|k-1}^{EK,J_{k|k-1}}(\mathbf{x}_k)$ in (C.1). Using the predicted EK-EPHD, (3.4),

$$\eta_{W_k}(\mathbf{x}_k) v_{k|k-1}^{EK,J_{k|k-1}}(\mathbf{x}_k) = p_{D,k} e^{-\gamma(\mathbf{x}_k)} \prod_{\mathbf{z}_k \in W_k} \frac{\gamma(\mathbf{x}_k)\phi_{\mathbf{z}_k}(\mathbf{x}_k)}{\lambda_k c_k(\mathbf{z}_k)} \sum_{i=1}^{J_{k|k-1}} w_{k|k-1}^{(i)} \mathcal{N}\left(\mathbf{x}_k \mid \mathbf{m}_{k|k-1}^{(i)}, \mathbf{P}_{k|k-1}^{(i)}\right). \tag{C.2}$$

And by the result for the EK Gaussian sum filter [17], we get

$$\begin{aligned}
&\eta_{W_k}(\mathbf{x}_k) v_{k|k-1}^{EK,J_{k|k-1}}(\mathbf{x}_k) \\
&\quad \longrightarrow \sum_{i=1}^{J_{k|k-1}} w_{k|k-1}^{(i)} p_{D,k} e^{-\gamma(\mathbf{m}_{k|k-1}^{(i)})} \\
&\qquad \times \prod_{\mathbf{z}_k \in W_k} \frac{\gamma\left(\mathbf{m}_{k|k-1}^{(i)}\right) \mathcal{N}\left(\mathbf{z}_k \mid h_k\left(\mathbf{m}_{k|k-1}^{(i)}, \mathbf{0}\right), \mathbf{U}_k^{(i)} \mathbf{R}_k \left(\mathbf{U}_k^{(i)}\right)^T + \mathbf{H}_k^{(i)} \mathbf{P}_{k|k-1}^{(i)} \left(\mathbf{H}_k^{(i)}\right)^T\right)}{\lambda_k c_k(\mathbf{z}_k)} \\
&\qquad \times \mathcal{N}\left(\mathbf{x}_k \mid \mathbf{m}_k^{(i)}, \mathbf{P}_k^{(i)}\right) \\
&\quad = \sum_{i=1}^{J_{k|k-1}} w_{k|k-1}^{(i)} \eta_{W_k}^{EK}\left(\mathbf{m}_{k|k-1}^{(i)}\right) \mathcal{N}\left(\mathbf{x}_k \mid \mathbf{m}_k^{(i)}, \mathbf{P}_k^{(i)}\right),
\end{aligned} \tag{C.3}$$

uniformly as $\mathbf{P}_{k|k-1}^{(i)} \to 0$ for all $i = 1, \ldots, J_{k|k-1}$, and $\eta_{W_k}^{EK}(\mathbf{m}_{k|k-1}^{(i)})$, $\mathbf{H}_k^{(i)}$, $\mathbf{U}_k^{(i)}$, $\mathbf{m}_k^{(i)}$, $\mathbf{P}_k^{(i)}$ are given by (3.9)–(3.13), respectively.

Now consider the terms $\omega_{\hat{p}_k}^{J_{k|k-1}}$ and $d_{W_k}^{J_{k|k-1}}$ in (C.1). First, using the predicted EK-EPHD, (3.4), the inner product $\langle v_{k|k-1}^{EK,J_{k|k-1}}, \eta_{W_k} \rangle$ is given by

$$\begin{aligned}
\left\langle v_{k|k-1}^{EK,J_{k|k-1}}, \eta_{W_k} \right\rangle &= \int \eta_{W_k}(\mathbf{x}_k) v_{k|k-1}^{EK,J_{k|k-1}}(\mathbf{x}_k) d\mathbf{x}_k \\
&= p_{D,k} \int e^{-\gamma(\mathbf{x}_k)} \prod_{\mathbf{z}_k \in W_k} \frac{\gamma(\mathbf{x}_k)\phi_{\mathbf{z}_k}(\mathbf{x}_k)}{\lambda_k c_k(\mathbf{z}_k)} \sum_{i=1}^{J_{k|k-1}} w_{k|k-1}^{(i)} \mathcal{N}\left(\mathbf{x}_k \mid \mathbf{m}_{k|k-1}^{(i)}, \mathbf{P}_{k|k-1}^{(i)}\right) d\mathbf{x}_k.
\end{aligned} \tag{C.4}$$

And by the result for the EK Gaussian sum filter [17], we get

$$\begin{aligned}
&\left\langle \upsilon_{k|k-1}^{EK,J_{k|k-1}}, \eta_{W_k} \right\rangle \\
&\quad \longrightarrow \int \sum_{i=1}^{J_{k|k-1}} w_{k|k-1}^{(i)} p_{D,k} e^{-\gamma(\mathbf{x}_k)} \\
&\qquad \times \prod_{\mathbf{z}_k \in W_k} \frac{\gamma\left(\mathbf{m}_{k|k-1}^{(i)}\right) \mathcal{N}\left(\mathbf{z}_k \mid h_k\left(\mathbf{m}_{k|k-1}^{(i)}, \mathbf{0}\right), \mathbf{U}_k^{(i)} \mathbf{R}_k \left(\mathbf{U}_k^{(i)}\right)^T + \mathbf{H}_k^{(i)} \mathbf{P}_{k|k-1}^{(i)} \left(\mathbf{H}_k^{(i)}\right)^T\right)}{\lambda_k c_k(\mathbf{z}_k)} \\
&\qquad \times \mathcal{N}\left(\mathbf{x}_k \mathbf{m}_k^{(i)}, \mathbf{P}_k^{(i)}\right) d\mathbf{x}_k,
\end{aligned} \tag{C.5}$$

uniformly as $\mathbf{P}_{k|k-1}^{(i)} \to 0$ for all $i = 1, \ldots, J_{k|k-1}$.

Changing the order of the summation and integral, (C.5) is equal to

$$\begin{aligned}
&\left\langle \upsilon_{k|k-1}^{EK,J_{k|k-1}}, \eta_{W_k} \right\rangle \\
&\quad \longrightarrow \sum_{i=1}^{J_{k|k-1}} \int w_{k|k-1}^{(i)} p_{D,k} e^{-\gamma\left(\mathbf{m}_{k|k-1}^{(i)}\right)} \\
&\qquad \times \prod_{\mathbf{z}_k \in W_k} \frac{\gamma\left(\mathbf{m}_{k|k-1}^{(i)}\right) \mathcal{N}\left(\mathbf{z}_k \mid h_k\left(\mathbf{m}_{k|k-1}^{(i)}, \mathbf{0}\right), \mathbf{U}_k^{(i)} \mathbf{R}_k \left(\mathbf{U}_k^{(i)}\right)^T + \mathbf{H}_k^{(i)} \mathbf{P}_{k|k-1}^{(i)} \left(\mathbf{H}_k^{(i)}\right)^T\right)}{\lambda_k c_k(\mathbf{z}_k)} \\
&\qquad \times \mathcal{N}\left(\mathbf{x}_k \mid \mathbf{m}_k^{(i)}, \mathbf{P}_k^{(i)}\right) d\mathbf{x}_k \\
&\quad = \sum_{i=1}^{J_{k|k-1}} w_{k|k-1}^{(i)} \eta_{W_k}^{EK}\left(\mathbf{m}_{k|k-1}^{(i)}\right) \int \mathcal{N}\left(\mathbf{x}_k \mid \mathbf{m}_k^{(i)}, \mathbf{P}_k^{(i)}\right) d\mathbf{x}_k \\
&\quad = \sum_{i=1}^{J_{k|k-1}} w_{k|k-1}^{(i)} \eta_{W_k}^{EK}\left(\mathbf{m}_{k|k-1}^{(i)}\right).
\end{aligned} \tag{C.6}$$

Then, the expressions of $\omega_{W_k}^{EK,J_{k|k-1}}$ and $d_{W_k}^{EK,J_{k|k-1}}$ (see (3.8)) are derived by (2.4) and (C.6).

Finally, (3.7) is obtained by substituting (3.8) and (C.3) into (C.1). This completes the proof.

## Acknowledgments

This research work was supported by Natural Science Foundation of China (61004087, 61104051, 61104214, and 61005026), China Postdoctoral Science Foundation (20100481338 and 2011M501443), and Fundamental Research Funds for the Central University.

## References


[1] M. J. Waxmann and O. E. Drummond, "A bibliography of cluster (group) tracking," in *Signal and Data Processing of Small Targets*, vol. 5428 of *Proceedings of SPIE*, pp. 551–560, Orlando, Fla, USA.

[2] F. Lian, C. Z. Han, W. F. Liu, X. X. Yan, and H. Y. Zhou, "Sequential Monte Carlo implementation and state extraction of the group probability hypothesis density filter for partly unresolvable group targets-tracking problem," *IET Radar, Sonar and Navigation*, vol. 4, no. 5, pp. 685–702, 2010.

[3] F. Daum and R. Fitzgerald, "Importance of resolution in multiple-target tracking," in *Signal and Data Processing of Small Targets*, vol. 2235 of *Proceedings of SPIE*, pp. 329–338, Orlando, Fla, USA, April 1994.

[4] K. Granstrom, C. Lundquist, and U. Orguner, "Tracking rectangular and elliptical extended targets using laser measurements," in *Proceedings of the 14th International Conference on Information Fusion*, pp. 1–8, Chicago, Ill, USA, July 2011.

[5] U. Orguner, C. Lundquist, and K. Granstrom, "Extended target tracking with a cardinalized probability hypothesis density filter," in *Proceedings of the 14th International Conference on Information Fusion*, pp. 1–8, Chicago, Ill, USA, July 2011.

[6] J. W. Koch, "Bayesian approach to extended object and cluster tracking using random matrices," *IEEE Transactions on Aerospace and Electronic Systems*, vol. 44, no. 3, pp. 1042–1059, 2008.

[7] M. Feldmann and D. Fränken, "Tracking of extended objects and group targets using random matrices—a new approach," in *Proceedings of the 11th International Conference on Information Fusion (FUSION '08)*, pp. 1–8, Cologne, Germany, July 2008.

[8] Y. Bar-Shalom and X. R. Li, *Multitarget—Multisensor Tracking: Principles and Techniques*, YBS Publishing, Storrs, Conn, USA, 1995.

[9] I. R. Goodman, R. P. S. Mahler, and H. T. Nguyen, *Mathematics of Data Fusion*, vol. 37 of *Theory and Decision Library. Series B: Mathematical and Statistical Methods*, Kluwer Academic, Norwood, Mass, USA, 1997.

[10] R. P. S. Mahler, "Multitarget Bayes filtering via first-order multitarget moments," *IEEE Transactions on Aerospace and Electronic Systems*, vol. 39, no. 4, pp. 1152–1178, 2003.

[11] B. N. Vo, S. Singh, and A. Doucet, "Sequential Monte Carlo methods for multi-target filtering with random finite sets," *IEEE Transactions on Aerospace and Electronic Systems*, vol. 41, no. 4, pp. 1224–1245, 2005.

[12] B. N. Vo and W. K. Ma, "The Gaussian mixture probability hypothesis density filter," *IEEE Transactions on Signal Processing*, vol. 54, no. 11, pp. 4091–4104, 2006.

[13] D. Clark and S. Godsill, "Group target tracking with the gaussian mixture probability hypothesis density filter," in *Proceedings of the International Conference on Intelligent Sensors, Sensor Networks and Information Processing (ISSNIP '07)*, pp. 149–154, Melbourne, Australia, December 2007.

[14] K. Gilholm, S. Godsill, S. Maskell, and D. Salmond, "Poisson models for extended target and group tracking," in *Signal and Data Processing of Small Targets*, vol. 5913 of *Proceedings of the SPIE*, pp. 1–12, San Diego, Calif, USA, August 2005.

[15] R. Mahler, "PHD filters for nonstandard targets, I: extended targets," in *Proceedings of the 12th International Conference on Information Fusion (FUSION '09)*, pp. 915–921, Seattle, Wash, USA, July 2009.

[16] K. Granström, C. Lundquist, and U. Orguner, "A Gaussian mixture PHD filter for extended target tracking," in *Proceedings of the 13th Conference on Information Fusion (FUSION '10)*, pp. 1–8, Edinburgh, UK, July 2010.

[17] B. D. Anderson and J. B. Moore, *Optimal Filtering*, Prentice-Hall, Englewood Cliffs, NJ, USA, 1979.

[18] D. E. Clark and J. Bell, "Convergence results for the particle PHD filter," *IEEE Transactions on Signal Processing*, vol. 54, no. 7, pp. 2652–2661, 2006.

[19] D. Clark and B.-N. Vo, "Convergence analysis of the Gaussian mixture PHD filter," *IEEE Transactions on Signal Processing*, vol. 55, no. 4, pp. 1204–1212, 2007.

[20] P. Cholamjiak, S. Suantai, and Y. J. Cho, "Strong convergence to solutions of generalized mixed equilibrium problems with applications," *Journal of Applied Mathematics*, vol. 2012, Article ID 308791, 18 pages, 2012.

[21] V. Colao, "On the convergence of iterative processes for generalized strongly asymptotically $\varphi$-pseudocontractive mappings in Banach spaces," *Journal of Applied Mathematics*, vol. 2012, Article ID 563438, 18 pages, 2012.

[22] G. Gu, S. Wang, and Y. J. Cho, "Strong convergence algorithms for hierarchical fixed points problems and variational inequalities," *Journal of Applied Mathematics*, vol. 2011, Article ID 164978, 17 pages, 2011.

[23] R. Mahler, *Statistical Multisource Multitarget Information Fusion*, Artech House, Norwood, Mass, USA, 2007.

[24] X. R. Li and V. P. Jikov, "A survey of maneuvering target tracking: dynamic models," in *Signal and Data Processing of Small Targets*, vol. 4048 of *Proceedings of SPIE*, pp. 212–235, Orlando, Fla, USA, April 2000.

[25] D. J. Salmond and N. J. Gordon, "Group and extended object tracking," *IEE Colloquium on Target Tracking*, vol. 16, pp. 1–4, 1999.

[26] D. Schuhmacher, B.-T. Vo, and B.-N. Vo, "A consistent metric for performance evaluation of multi-object filters," *IEEE Transactions on Signal Processing*, vol. 56, no. 8, pp. 3447–3457, 2008.

Hindawi Publishing Corporation
Journal of Applied Mathematics
Volume 2012, Article ID 808327, 14 pages
doi:10.1155/2012/808327

*Research Article*

# Offset-Free Strategy by Double-Layered Linear Model Predictive Control

**Tao Zou**

*Shenyang Institute of Automation, Chinese Academy of Sciences, Shenyang 110016, China*

Correspondence should be addressed to Tao Zou, zoutao@sia.cn

Received 29 March 2012; Revised 27 May 2012; Accepted 28 May 2012

Academic Editor: Xianxia Zhang



In the real applications, the model predictive control (MPC) technology is separated into two layers, that is, a layer of conventional dynamic controller, based on which is an added layer of steady-state target calculation. In the literature, conditions for offset-free linear model predictive control are given for combined estimator (for both the artificial disturbance and system state), steady-state target calculation, and dynamic controller. Usually, the offset-free property of the double-layered MPC is obtained under the assumption that the system is asymptotically stable. This paper considers the dynamic stability property of the double-layered MPC.

## 1. Introduction

The technique model predictive control (MPC) differs from other control methods mainly in its implementation of the control actions. Usually, MPC solves a finite-horizon optimal control problem at each control interval, so that the control moves for the current time and a period of future time (say, totally $N$ control intervals) are obtained. However, only the current control move is applied to the plant. At the next control interval, the same kind of optimization is repeated with the new measurements [1]. The MPC procedures applied in the industrial processes lack theoretical guarantee of stability. Usually, industrial MPC adopts a finite-horizon optimization, without a special weighting on the output prediction at the end of the prediction horizon.

Theoretically, the regulation problem for the nominal MPC can have guarantee of stability by imposing special weight and constraint on the terminal state prediction [2]. The authors in [2] give a comprehensive framework. However, [2] does not solve everything for the stability of MPC. In the past 10 years, the studies on the robust MPC for regulation problem go far beyond [2]. We could say that, for the case of regulation problem when

the system state is measurable, the research on MPC is becoming mature (see e.g., [3–8]). For the case of regulation problem when the system state is unmeasurable, and there is no model parametric uncertainty, the research on MPC is becoming mature (see e.g. [9–11]). For other cases (output feedback MPC for the systems with parametric uncertainties, tracking MPC, etc.), there are many undergoing researches (see e.g., [12–16]).

A synthesis approach of MPC is that with guaranteed stability. However, the industrial MPC adopts a more complex framework than the existing synthesis approaches of MPC. Its hierarchy is shown in, for example [17]. In other words, the synthesis approaches of MPC have not been sufficiently developed to include the industrial MPC. Today, the separation of the MPC algorithm into steady-state target and dynamic control move calculations is a common part of industrial MPC technology [17]. The use of steady-state target calculation is necessary, since the disturbances entering the systems or new input information from the operator may change the location of the optimal steady-state at any control interval (see e.g., [18]). The goal of the steady-state target calculation is to recalculate the targets from the local optimizer every time the MPC controller executes.

In the linear MPC framework, offset-free control is usually achieved by adding step disturbance to the process model. The most widely used industrial MPC implementations assume a constant output disturbance that can lead to sluggish rejections of disturbances that enter the process elsewhere. In [19, 20], some general disturbance models that accommodate unmeasured disturbances entering through the process input, state, or output, have been proposed. In a more general sense, the disturbance model can incorporate any nonlinearity, uncertainty, and physical disturbance (measured or unmeasured). The disturbance can be estimated by the Kalman filter (or the usual observer). The estimated disturbance is assumed to be step-like, that is unchanging in the future, at each control interval (MPC refreshes its solution at each control interval). The estimated disturbance drives the steady-state target calculation, in order to refresh the new target value for the control move optimization.

This paper visits some preliminary results for the stability of double-layered MPC or output tracking MPC. These results could be useful for incorporating the industrial MPC into the synthesis approaches of MPC. The preliminary results for this paper can be found in [21, 22].

*Notations 1.* For any vector $x$ and positive-definite matrix $M$, $\|x\|_M^2 := x^T M x$. $x(k+i \mid k)$ is the value of vector $x$ at time $k+i$, predicted at time $k$. $I$ is the identity matrix with appropriate dimension. All vector inequalities are interpreted in an element-wise sense. The symbol $\star$ induces a symmetric structure in the matrix inequalities. An optimal solution to the MPC optimization problem is marked with superscript $\star$. The time-dependence of the MPC decision variables is often omitted for brevity.

## 2. System Description and Observer Design

Consider the following discrete-time model:

$$\begin{aligned} x(k+1) &= Ax(k) + Bu(k) + Ed(k), \\ d(k+1) &= d(k) + \Delta d(k), \\ y(k) &= Cx(k) + Dd(k), \end{aligned} \tag{2.1}$$

where $u \in \Re^m$ denotes the control input variables, $x \in \Re^n$ the state variables, $y \in \Re^p$ the output variables, and $d \in \Re^q$ the unmeasured signals including all disturbances and plant-model mismatches.

*Assumption 2.1.* The augmented pair

$$\left( \begin{bmatrix} C & D \end{bmatrix}, \begin{bmatrix} A & E \\ 0 & I \end{bmatrix} \right) \tag{2.2}$$

is detectable, and the following condition holds:

$$\operatorname{rank} \begin{bmatrix} I - A & -E \\ C & D \end{bmatrix} = n + q. \tag{2.3}$$

The augmented observer is

$$\begin{bmatrix} \hat{x}(k+1) \\ \hat{d}(k+1) \end{bmatrix} = \begin{bmatrix} A & E \\ 0 & I \end{bmatrix} \begin{bmatrix} \hat{x}(k) \\ \hat{d}(k) \end{bmatrix} + \begin{bmatrix} B \\ 0 \end{bmatrix} u(k) + \begin{bmatrix} F_s^1 \\ F_s^2 \end{bmatrix} \left( C\hat{x}(k) + D\hat{d}(k) - y(k) \right), \tag{2.4}$$

where $F_s = [(F_s^1)^T, (F_s^2)^T]^T$ is the prespecified observer gain. Define the estimation error $\tilde{x}(k) = x(k) - \hat{x}(k)$ and $\tilde{d}(k) = d(k) - \hat{d}(k)$; then one has the following observer error dynamic equation:

$$\begin{bmatrix} \tilde{x}(k+1) \\ \tilde{d}(k+1) \end{bmatrix} = \left( \begin{bmatrix} A & E \\ 0 & I \end{bmatrix} + \begin{bmatrix} F_s^1 \\ F_s^2 \end{bmatrix} \begin{bmatrix} C & D \end{bmatrix} \right) \begin{bmatrix} \tilde{x}(k) \\ \tilde{d}(k) \end{bmatrix} + \begin{bmatrix} 0 \\ I \end{bmatrix} \Delta d(k). \tag{2.5}$$

*Assumption 2.2.* $\Delta d(k)$ is an asymptotically vanishing item, and the observer error dynamics is asymptotically stable, that is, $\lim_{k \to \infty} \{\Delta d(k), \tilde{x}(k), \tilde{d}(k)\} = \{0, 0, 0\}$.

## 3. Double-Layered MPC with Off-Set Property

For the system (2.1), its steady-state state and input target vectors, $x_t(k)$ and $u_t(k)$, can be determined from the solution of the following quadratic programming (QP) problems (steady-state target calculation, steady-state controller):

$$\min_{x_t, u_t} \| u_t - \overline{u}_r \|_{R_t}^2, \tag{3.1}$$

$$\text{s.t.} \quad \begin{cases} \begin{bmatrix} I - A & -B \\ C & 0 \end{bmatrix} \begin{bmatrix} x_t \\ u_t \end{bmatrix} = \begin{bmatrix} E\hat{d}(k) \\ \overline{y}_r - D\hat{d}(k) \end{bmatrix} \\ u_{\min} \le u_t \le u_{\max} \end{cases} \tag{3.2}$$

$$\min_{x_t,u_t} \left\| y_t - \overline{y}_r \right\|_{Q_t}^2, \tag{3.3}$$

$$\text{s.t.} \quad \begin{cases} \begin{bmatrix} I - A & -B \\ C & 0 \end{bmatrix} \begin{bmatrix} x_t \\ u_t \end{bmatrix} = \begin{bmatrix} E\widehat{d}(k) \\ y_t - D\widehat{d}(k) \end{bmatrix} \\ u_{\min} \le u_t \le u_{\max}, \end{cases} \tag{3.4}$$

where $\overline{y}_r$ is the desired steady-state output (e.g., from the local optimizer), $\overline{u}_r$ is the desired steady-state input, and $(u_{\min}, u_{\max})$ are the input bounds. Problems (3.1) and (3.2) is solved; when (3.1) and (3.2) is feasible, $y_t = \overline{y}_r$ and (3.3) and (3.4) is not solved; when (3.1) and (3.2) is infeasible, (3.3) and (3.4) is solved.

When this target generation problem is feasible, one has

$$\begin{aligned} x_t(k) &= Ax_t(k) + Bu_t(k) + E\widehat{d}(k), \\ y_t(k) &= Cx_t(k) + D\widehat{d}(k). \end{aligned} \tag{3.5}$$

Subtracting (3.5) from (2.1) and utilizing (2.5) yield

$$\widehat{\chi}(k+1,k) = A\widehat{\chi}(k,k) + B\omega(k) - F_s^1\left(C\tilde{x}(k) + D\tilde{d}(k)\right), \tag{3.6}$$

where the shifted variables $\widehat{\chi}(\cdot,k) := \widehat{x}(\cdot) - x_t(k)$, $\omega := u - u_t$. The following nominal model of the transformed system (3.6) is used for prediction

$$\widehat{\chi}(k+i+1 \mid k) = A\widehat{\chi}(k+i \mid k) + B\omega(k+i \mid k). \tag{3.7}$$

Its infinite horizon predictive control performance cost is defined as

$$J_0^\infty(k) = \sum_{i=0}^{\infty} W\left(\widehat{\chi}(k+i \mid k), \omega(k+i \mid k)\right), \tag{3.8}$$

where $W(\widehat{\chi}(k+i \mid k), \omega(k+i \mid k)) = \|\widehat{\chi}(k+i \mid k)\|_Q^2 + \|\omega(k+i \mid k)\|_R^2$.

Defining a quadratic function $V(\widehat{\chi}(k+i \mid k)) = \|\widehat{\chi}(k+i \mid k)\|_P^2$, if one can show that

$$V\left(\widehat{\chi}(k+i+1 \mid k)\right) - V\left(\widehat{\chi}(k+i \mid k)\right) \le -W\left(\widehat{\chi}(k+i \mid k), \omega(k+i \mid k)\right), \tag{3.9}$$

then it can be concluded that $V(\widehat{\chi}(k+i \mid k)) \to 0$ as $i \to \infty$. Furthermore, summing (3.9) from $i = N$ to $\infty$ yields the upper bound of $J_N^\infty$ as

$$\sum_{i=N}^{\infty} W\left(\widehat{\chi}(k+i \mid k), \omega(k+i \mid k)\right) \le V\left(\widehat{\chi}(k+N \mid k)\right). \tag{3.10}$$

By substituting (3.10) into (3.8), one can get

$$J_0^{\infty}(k) \le \sum_{i=0}^{N-1} W\left(\hat{\chi}(k+i \mid k), \omega(k+i \mid k)\right) + V\left(\hat{\chi}(k+N \mid k)\right) =: \overline{J}\left(\hat{\chi}(k), \pi(k)\right). \tag{3.11}$$

Here $\overline{J}(\hat{\chi}(k), \pi(k))$ gives an upper bound of $J_0^{\infty}(k)$; so we can formulate the MPC as an equivalent minimization problem on $\overline{J}(\hat{\chi}, \pi)$ with respect to the optimal control sequence

$$\pi^*(k) = \left[\omega^*(k \mid k)^T, \omega^*(k+1 \mid k)^T, \ldots, \omega^*(k+N-1 \mid k)^T\right]^T. \tag{3.12}$$

When $\hat{x}(k+N \mid k)$ lies in the terminal region, $\omega(k+i \mid k) = K\hat{\chi}(k+i \mid k)$, $i \ge N$. From the definition of $\overline{J}(\hat{\chi}(k), \pi(k))$, at time instant $k+1$, one has

$$\overline{J}\left(\hat{\chi}(k+1), \pi(k+1)\right) = \sum_{i=1}^{N} W\left(\hat{\chi}(k+i \mid k+1), \omega(k+i \mid k+1)\right) + V\left(\hat{\chi}(k+N+1 \mid k+1)\right) \tag{3.13}$$

with the shifted control sequence

$$\begin{aligned} \pi(k+1) = \Big[&\left(\omega^*(k+1 \mid k) + u_t(k) - u_t(k+1)\right)^T, \ldots, \\ &\left(\omega^*(k+N-1k) + u_t(k) - u_t(k+1)\right)^T, \left(K\hat{\chi}(k+Nk) + u_t(k) - u_t(k+1)\right)^T\Big]^T. \end{aligned} \tag{3.14}$$

We can explicitly derive the multi-step-ahead state and output prediction:

$$\hat{\chi}(k+N \mid k) = A^N \hat{\chi}(k) + \tilde{A}_B \pi(k), \tag{3.15}$$

$$\tilde{Y}_{\chi}(k) = \tilde{T}_A \hat{\chi}(k) + \tilde{T}_B \pi(k), \tag{3.16}$$

where

$$\tilde{A}_B = \left[A^{N-1}B, \ldots, AB, B\right], \qquad \tilde{Y}_{\chi}(k) = \begin{bmatrix} \hat{\chi}(k \mid k) \\ \hat{\chi}(k+1 \mid k) \\ \vdots \\ \hat{\chi}(k+N-1 \mid k) \end{bmatrix}, \tag{3.17}$$

$$\tilde{T}_A = \begin{bmatrix} I \\ A \\ \vdots \\ A^{N-1} \end{bmatrix}, \qquad \tilde{T}_B = \begin{bmatrix} 0 & 0 & \cdots & 0 \\ B & 0 & \cdots & 0 \\ \vdots & \ddots & \ddots & \vdots \\ A^{N-2}B & \cdots & B & 0 \end{bmatrix}. \tag{3.18}$$

**Lemma 3.1.** *For a quadratic function $W(x,u) = x^T Q x + u^T R u$, $Q, R > 0$, there exist finite Lipschitz constants $\mathcal{L}_x, \mathcal{L}_u > 0$ such that*

$$\|W(x_1,u_1) - W(x_2,u_2)\| \le \mathcal{L}_x\|x_1 - x_2\| + \mathcal{L}_u\|u_1 - u_2\| \tag{3.19}$$

*for all $x_1, x_2 \in \mathcal{X}$, $u_1, u_2 \in \mathcal{U}$, where $\mathcal{X}$, $\mathcal{U}$ are bounded regions. Similarly, for a quadratic function $V(x) = x^T P x$, $P > 0$, there exists a finite Lipschitz constant $\mathcal{L}_V > 0$ such that*

$$\|V(x_1) - V(x_2)\| \le \mathcal{L}_V\|x_1 - x_2\| \tag{3.20}$$

*for all $x_1, x_2 \in \mathcal{X}$.*

Clearly, $\mathcal{L}_x$, $\mathcal{L}_u$, $\mathcal{L}_V$ depend on $\mathcal{X}$, $\mathcal{U}$. However, it is unnecessary to specify $\mathcal{X}$, $\mathcal{U}$ in the following. Moreover, $\mathcal{L}_V$ depends on $P$, which is time varying; this paper assumes taking $\mathcal{L}_V$ for all possible $P$.

**Lemma 3.2.** *Consider the prediction model* (3.7)*. Then, with the shifted control sequence $\pi(k+1)$,*

$$\begin{aligned}
&\left\|\hat{\chi}(k+i \mid k+1) - \hat{\chi}(k+i \mid k)\right\| \\
&\quad\le \|A\|^{i-1}\left(\left\|F_s^1 C\right\|\|\tilde{x}(k)\| + \left\|F_s^1 D\right\|\left\|\tilde{d}(k)\right\| + \|x_t(k) - x_t(k+1)\|\right) \\
&\qquad + \sum_{j=0}^{i-2}\|A\|^j\|B\|(\|u_t(k) - u_t(k+1)\|).
\end{aligned} \tag{3.21}$$

*Proof .* It is easy to show that

$$\begin{aligned}
\hat{\chi}(k+1,k+1) &= \hat{x}(k+1) - x_t(k+1) \\
&= \hat{\chi}(k+1 \mid k) - F_s^1\left(C\tilde{x}(k) + D\tilde{d}(k)\right) + x_t(k) - x_t(k+1).
\end{aligned} \tag{3.22}$$

Then,

$$\begin{aligned}
&\left\|\hat{\chi}(k+1 \mid k+1) - \hat{\chi}(k+1 \mid k)\right\| \\
&\quad= \left\|\hat{\chi}(k+1) - \hat{\chi}(k+1 \mid k)\right\| \\
&\quad\le \left\|F_s^1 C\right\|\|\tilde{x}(k)\| + \left\|F_s^1 D\right\|\left\|\tilde{d}(k)\right\| + \|x_t(k) - x_t(k+1)\|, \\
&\|\hat{\chi}(k+2 \mid k+1) - \hat{\chi}(k+2 \mid k)\| \\
&\quad= \left\|A\left(\hat{\chi}(k+1 \mid k+1) - \hat{\chi}(k+1 \mid k)\right) + B(\omega(k+1 \mid k+1) - \omega(k+1 \mid k))\right\| \\
&\quad\le \|A\|\left\|\hat{\chi}(k+1 \mid k+1) - \hat{\chi}(k+1 \mid k)\right\| + \|B\|\|u_t(k) - u_t(k+1)\|.
\end{aligned} \tag{3.23}$$

By induction, one can easily show the claimed result, and thus the proof is completed. □

**Theorem 3.3.** *For the system* (2.1) *subject to the input constraints*

$$u_{\min} \le u \le u_{\max}, \tag{3.24}$$

*under Assumptions 2.1-2.2, the closed-loop output feedback model predictive control system, with objective function* $\overline{J}(\widehat{\chi}(k), \pi(k))$, *augmented observer* (2.4), *and target generation procedure* (3.1)–(3.4), *achieves the offset-free reference tracking performance if the following three conditions are satisfied.*

(a) *There exist feasible solutions* $(x_t(k), u_t(k))$ *to the target generation problem* (3.1)–(3.4), *at each time* $k$.

(b) *There exist feasible solutions, including a control sequence* $\pi^*(k)$, *a positive-definite matrix* $\widehat{X}$, *and any matrix* $\widehat{Y}$, *at each time* $k$, *to the dynamic optimization problem* (*dynamic control move calculation problem*)

$$\min_{\gamma_1,\gamma_2,\pi,\widehat{X},\widehat{Y}} (\gamma_1 + \gamma_2), \tag{3.25}$$

*subject to the linear matrix inequalities*

$$\begin{bmatrix} \gamma_1 & \star & \star \\ \widetilde{T}_A\widehat{\chi}(k) + \widetilde{T}_B\pi & \widetilde{Q}^{-1} & \star \\ \pi & 0 & \widetilde{R}^{-1} \end{bmatrix} \ge 0, \tag{3.26}$$

$$\begin{bmatrix} 1 & \star \\ A^N\widehat{\chi}(k) + \widetilde{A}_B\pi & \widehat{X} \end{bmatrix} \ge 0, \tag{3.27}$$

$$\begin{bmatrix} \widehat{X} & \star & \star & \star \\ A\widehat{X} + B\widehat{Y} & \widehat{X} & \star & \star \\ \widehat{X} & 0 & \gamma_2 Q^{-1} & \star \\ \widehat{Y} & 0 & 0 & \gamma_2 R^{-1} \end{bmatrix} \ge 0, \tag{3.28}$$

$$\begin{bmatrix} \overline{u}_j^2 & \star \\ \widehat{Y}^T U_j^T & \widehat{X} \end{bmatrix} \ge 0, \quad j = 1, \ldots, m, \tag{3.29}$$

$$\begin{bmatrix} I_{m\times N} \\ -I_{m\times N} \end{bmatrix} \pi \le \begin{bmatrix} \Pi_m(u_{\max} - u_t(k)) \\ -\Pi_m(u_{\min} - u_t(k)) \end{bmatrix}, \tag{3.30}$$

*where* $U_j$ *is the* $j$*th row of the* $m$*-ordered identity matrix,* $\widetilde{Q} = I_N \otimes Q$, $\widetilde{R} = I_N \otimes R$, $\Pi_m = [I_m, \ldots, I_m]^T$, *and* $\overline{u}_j = \min\{(u_{\max} - u_t(k))_j, (u_t(k) - u_{\min})_j\}$.

(c) *By applying* $u(k) = u_t(k) + \omega^*(k \mid k)$, *where* $\omega^*(k \mid k)$ *is obtained by solving* (3.25)—(3.30), *the closed-loop system is asymptotically stable.*

*Proof.* The matrix inequality (3.28) implies that

$$(A + BK)^T P(A + BK) - P + Q + K^T RK \le 0. \tag{3.31}$$

By referring to [23], it is easy to prove that (3.9) holds for all $i \geq N$. Then, $V(\hat{\chi}(k+N \mid k)) \leq \|\hat{\chi}(k+N \mid k)\|_P^2$. Let $\|\hat{\chi}(k+N \mid k)\|_P^2 \leq \gamma_2(k)$, which is guaranteed by (3.27), where $P = \gamma_2 \widehat{X}^{-1}$. Meanwhile, it is easy to show that, by applying (3.26), the optimal $\gamma_1^*(k)$ is exactly the optimal value of

$$J_0^{N-1*}(k) = \sum_{i=0}^{N-1} W\left(\hat{\chi}(k+i \mid k), \omega^*(k+i \mid k)\right). \tag{3.32}$$

Now we check if each element of the predictive control inputs satisfies the constraints $u_{j,\min} \leq u_j(k+i \mid k) \leq u_{j,\max}$, $i \geq 0$, $j = 1, \ldots, m$. For any $i$ within the finite horizon $N$, the input constraints are satisfied since $\Pi_m(u_{\min} - u_t(k)) \leq \pi \leq \Pi_m(u_{\max} - u_t(k))$, as shown in (3.30). Otherwise, beyond the finite horizon $i \geq N$, $\hat{\chi}(k+i \mid k)$ belongs to the constraint set $\mathcal{E} = \bigcup\{z \in \Re^n \mid z^T \widehat{X}^{-1} z \leq 1\}$, which is guaranteed by (3.27). In this case, by referring to [23], it is easy to show that, (3.27)–(3.29) guarantee that the feedback control law $\omega(k+i \mid k) = K\hat{\chi}(k+i \mid k)$, $i \geq N$, $K = \widehat{Y}\widehat{X}^{-1}$ satisfies the input constraints.

Since point (c) is assumed, the offset-free property can be referred to as in [19, 20, 22]. □

## 4. Improved Procedure for Double-Layered MPC

At each time $k+1 \geq 0$, we consider the following constraints:

$$\begin{bmatrix} I - A & -B \\ C & 0 \end{bmatrix} \begin{bmatrix} x_t \\ u_t \end{bmatrix} = \begin{bmatrix} E\hat{d}(k+1) \\ \overline{y}_r - D\hat{d}(k+1) \end{bmatrix},$$
$$u_{\min} \leq u_t \leq u_{\max}, \tag{4.1}$$

$$\begin{bmatrix} I - A & -B \\ C & 0 \end{bmatrix} \begin{bmatrix} x_t \\ u_t \end{bmatrix} = \begin{bmatrix} E\hat{d}(k+1) \\ y_t - D\hat{d}(k+1) \end{bmatrix},$$
$$u_{\min} \leq u_t \leq u_{\max}, \tag{4.2}$$

$$\begin{bmatrix} \dfrac{1}{\upsilon}(k) & \star \\ A^N[\hat{x}(k+1) - x_t] + \tilde{A}_B \pi(k+1) & \widehat{X}(k) \end{bmatrix} \geq 0, \tag{4.3}$$

$$\left(\upsilon(k) U_j \widehat{Y}(k) \widehat{X}(k)^{-1} \widehat{Y}(k)^T U_j^T\right)^{1/2} \leq (u_{\max} - u_t)_j,$$
$$\left(\upsilon(k) U_j \widehat{Y}(k) \widehat{X}(k)^{-1} \widehat{Y}(k)^T U_j^T\right)^{1/2} \leq (u_t - u_{\min})_j, \tag{4.4}$$
$$j = 1, \ldots, m,$$

where $\upsilon(k) = \gamma_2^*(k)/(\gamma_2^*(k) - W(\hat{\chi}(k+N \mid k), \omega^*(k+N \mid k)) + (1-\varrho)W(\hat{\chi}(k \mid k), \omega^*(k \mid k)))$, with $\varrho \in (0, 1]$ being a given design parameter. Equation (4.1) is utilized for (3.1); (4.2) is utilized for (3.3).

**Theorem 4.1.** *For the system* (2.1) *subject to the input constraints under Assumptions* 2.1-2.2*, the closed-loop output feedback model predictive control system, with objective function* $\overline{J}(\widehat{\chi}(k), \pi(k))$*, augmented observer* (2.4)*, target generation procedure (at* $k = 0$, (3.1)–(3.4)*; at any* $k + 1$, (3.1), (3.3), (4.1)–(4.4)*), and dynamic optimization problem* (3.25)–(3.30)*, is input-to-state (ISS) stable if the following two conditions are satisfied.*

(a) *There exist feasible solutions* $(x_t(k), u_t(k))$ *to the target generation problem, at each control interval.*

(b) *There exist feasible solutions, including a control sequence* $\pi^*(k)$*, a positive-definite matrix* $\widehat{X}$*, and any matrix* $\widehat{Y}$*, at time* $k = 0$*, to the dynamic optimization problem* (3.25)–(3.30)*.*

*Proof.* By applying the shifted control sequence $\pi(k+1)$, at time $k+1$, one has

$$\begin{aligned}\gamma_1(k+1) - \gamma_1^*(k) &= J_0^{N-1}(k+1) - J_0^{N-1*}(k)\\ &= W\left(\widehat{\chi}(k+N \mid k+1), \omega(k+N \mid k+1)\right)\\ &\quad + \sum_{i=1}^{N-1}\left[W\left(\widehat{\chi}(k+i \mid k+1), \omega(k+i \mid k+1)\right)\right.\\ &\qquad \left. - W\left(\widehat{\chi}(k+i \mid k), \omega^*(k+i \mid k)\right)\right] - W\left(\widehat{\chi}(k \mid k), \omega^*(k \mid k)\right).\end{aligned} \tag{4.5}$$

By applying Lemmas 3.1-3.2, it is shown that

$$\begin{aligned}&\gamma_1(k+1) - \gamma_1^*(k)\\ &\quad \le W\left(\widehat{\chi}(k+N \mid k+1), \omega(k+N \mid k+1)\right)\\ &\qquad + \mathcal{L}_x \sum_{i=1}^{N-1}\left[\|A\|^{i-1}\left(\left\|F_s^1 C\right\|\|\widetilde{x}(k)\| + \left\|F_s^1 D\right\|\left\|\widetilde{d}(k)\right\| + \|x_t(k) - x_t(k+1)\|\right)\right.\\ &\qquad\qquad \left. + \sum_{j=0}^{i-2}\|A\|^j\|B\|\left(\|u_t(k) - u_t(k+1)\|\right)\right]\\ &\qquad + (N-1)\mathcal{L}_u\|u_t(k) - u_t(k+1)\| - W\left(\widehat{\chi}(k \mid k), \omega^*(k \mid k)\right).\end{aligned} \tag{4.6}$$

By further applying

$$\begin{aligned}\widehat{\chi}(k+N \mid k+1) &= \widehat{\chi}(k+N \mid k) + A^{N-1}\left[-F_s^1\left(C\widetilde{x}(k) + D\widetilde{d}(k)\right) + x_t(k) - x_t(k+1)\right]\\ &\quad + \sum_{i=0}^{N-2} A^i B[u_t(k) - u_t(k-1)],\end{aligned} \tag{4.7}$$

it is shown that

$$\begin{aligned}\gamma_1(k+1)-\gamma_1^*(k) \le{}& W\left(\hat{\chi}(k+N\mid k),\omega^*(k+N\mid k)\right)\\ &+\widetilde{\mathcal{L}}_x\left(\left\|F_s^1C\right\|\|\tilde{x}(k)\|+\left\|F_s^1D\right\|\left\|\tilde{d}(k)\right\|+\|x_t(k)-x_t(k+1)\|\right)\\ &+\widetilde{\mathcal{L}}_u\|u_t(k)-u_t(k+1)\|-W\left(\hat{\chi}(k\mid k),\omega^*(k\mid k)\right),\end{aligned}\tag{4.8}$$

where $\widetilde{\mathcal{L}}_x,\widetilde{\mathcal{L}}_u>0$ are appropriate scalars.

On the other hand, at time $k+1$, since the target generation problem is feasible, it is feasible to choose $\gamma_2(k+1)=\gamma_2^*(k)-W(\hat{\chi}(k+N\mid k),\omega^*(k+N\mid k)+(1-\varrho)W(\hat{\chi}(k\mid k),\omega^*(k\mid k))$.

Then,

$$\begin{aligned}&\left(\gamma_1(k+1)+\gamma_2(k+1)\right)-\left(\gamma_1^*(k)+\gamma_2^*(k)\right)\\ &\quad\le-\varrho W\left(\hat{\chi}(k\mid k),\omega^*(k\mid k)\right)\\ &\qquad+\widetilde{\mathcal{L}}_x\left(\left\|F_s^1C\right\|\|\tilde{x}(k)\|+\left\|F_s^1D\right\|\left\|\tilde{d}(k)\right\|+\|x_t(k)-x_t(k+1)\|\right)+\widetilde{\mathcal{L}}_u\|u_t(k)-u_t(k+1)\|\\ &\quad\le-\varrho\lambda_{\min}(Q)\left\|\hat{\chi}(k\mid k)\right\|\\ &\qquad+\widetilde{\mathcal{L}}_x\left(\|F_s^1C\|\|\tilde{x}(k)\|+\left\|F_s^1D\right\|\left\|\tilde{d}(k)\right\|+\|x_t(k)-x_t(k+1)\|\right)+\widetilde{\mathcal{L}}_u\|u_t(k)-u_t(k+1)\|.\end{aligned}\tag{4.9}$$

Hence, $\gamma_1^*(k)+\gamma_2^*(k)$ can serve as an ISS (for the definition of this term, see [22]) Lyapunov function, and the closed-loop system is input-to-state stable. □

If we use the terminal equality constraint, rather than the terminal inequality constraint, then (3.27) should be revised as

$$A^N\hat{\chi}(k)+\tilde{A}_B\pi=0\tag{4.10}$$

and (3.28), (3.29) should be removed; moreover, (4.3) should be revised as

$$A^N(\hat{x}(k+1)-x_t)+\tilde{A}_B\pi(k+1)=0\tag{4.11}$$

with the shifted control sequence

$$\begin{aligned}\pi(k+1)=\Big[&\left(\omega^*(k+1\mid k)+u_t(k)-u_t(k+1)\right)^T,\ldots,\\ &\left(\omega^*(k+N-1\mid k)+u_t(k)-u_t(k+1)\right)^T,\left(u_t(k)-u_t(k+1)\right)^T\Big]^T,\end{aligned}\tag{4.12}$$

and (4.4) should be removed.

**Theorem 4.2.** *For the system* (2.1) *subject to the input constraints under Assumptions 2.1–2.2, the closed-loop output feedback model predictive control system, with objective function* $\overline{J}(\widehat{\chi}(k), \pi(k))$, *augmented observer* (2.4), *target generation procedure (at* $k = 0$, (3.1)–(3.4); *at any* $k + 1$, (3.1), (3.3), (4.1), (4.2), (4.11)*), and dynamic optimization problem* (3.25), (3.26), (4.10), (3.30), *is input-to-state stable if the following two conditions are satisfied.*

(a) *There exist feasible solutions* $(x_t(k), u_t(k))$ *to the target generation problem, at each time* $k$.

(b) *There exist feasible solutions* $\pi^*(k)$, *at time* $k = 0$, *to the dynamic optimization problem* (3.25), (3.26), (4.10), (3.30).

*Proof.* By applying the shifted control sequence $\pi(k+1)$, at time $k+1$, one has

$$\begin{aligned}
&\gamma_1(k+1) - \gamma_1^*(k) \\
&\quad = W\big(\widehat{\chi}(k+N \mid k+1), \omega(k+N \mid k+1)\big) \\
&\qquad + \sum_{i=1}^{N-1} \big[W\big(\widehat{\chi}(k+i \mid k+1), \omega(k+i \mid k+1)\big) \\
&\qquad\qquad - W\big(\widehat{\chi}(k+i \mid k), \omega^*(k+i \mid k)\big)\big] - W\big(\widehat{\chi}(k \mid k), \omega^*(k \mid k)\big) \\
&\quad = \big[W\big(\overline{\chi}(k+N \mid k+1), \omega(k+N \mid k+1)\big) \\
&\qquad - W\big(\overline{\chi}(k+N \mid k), \omega(k+N \mid k)\big)\big] \\
&\qquad + \sum_{i=1}^{N-1} \big[W\big(\widehat{\chi}(k+i \mid k+1), \omega(k+i \mid k+1)\big) \\
&\qquad\qquad - W\big(\widehat{\chi}(k+i \mid k), \omega^*(k+i \mid k)\big)\big] - W\big(\widehat{\chi}(k \mid k), \omega^*(k \mid k)\big).
\end{aligned} \tag{4.13}$$

By analogy to Theorem 4.1, it is shown that $\gamma_1^*(k)$ can serve as an ISS Lyapunov function, and the closed-loop system is input-to-state stable. □

Assume that $A$ is nonsingular. Then, applying (4.11) yields

$$x_t = \widehat{x}(k+1) + A^{-N}\widetilde{A}_B\pi(k+1). \tag{4.14}$$

Further applying (4.3) yields $y_t = C\widehat{x}(k+1) + CA^{-N}\widetilde{A}_B\pi(k+1) + D\widehat{d}(k+1)$ and

$$Bu_t = (I - A)\Big[\widehat{x}(k+1) + A^{-N}\widetilde{A}_B\pi(k+1)\Big] - E\widehat{d}(k+1). \tag{4.15}$$

Hence, by applying (4.10)-(4.11), an analytical solution of the steady-state controller may be obtained.

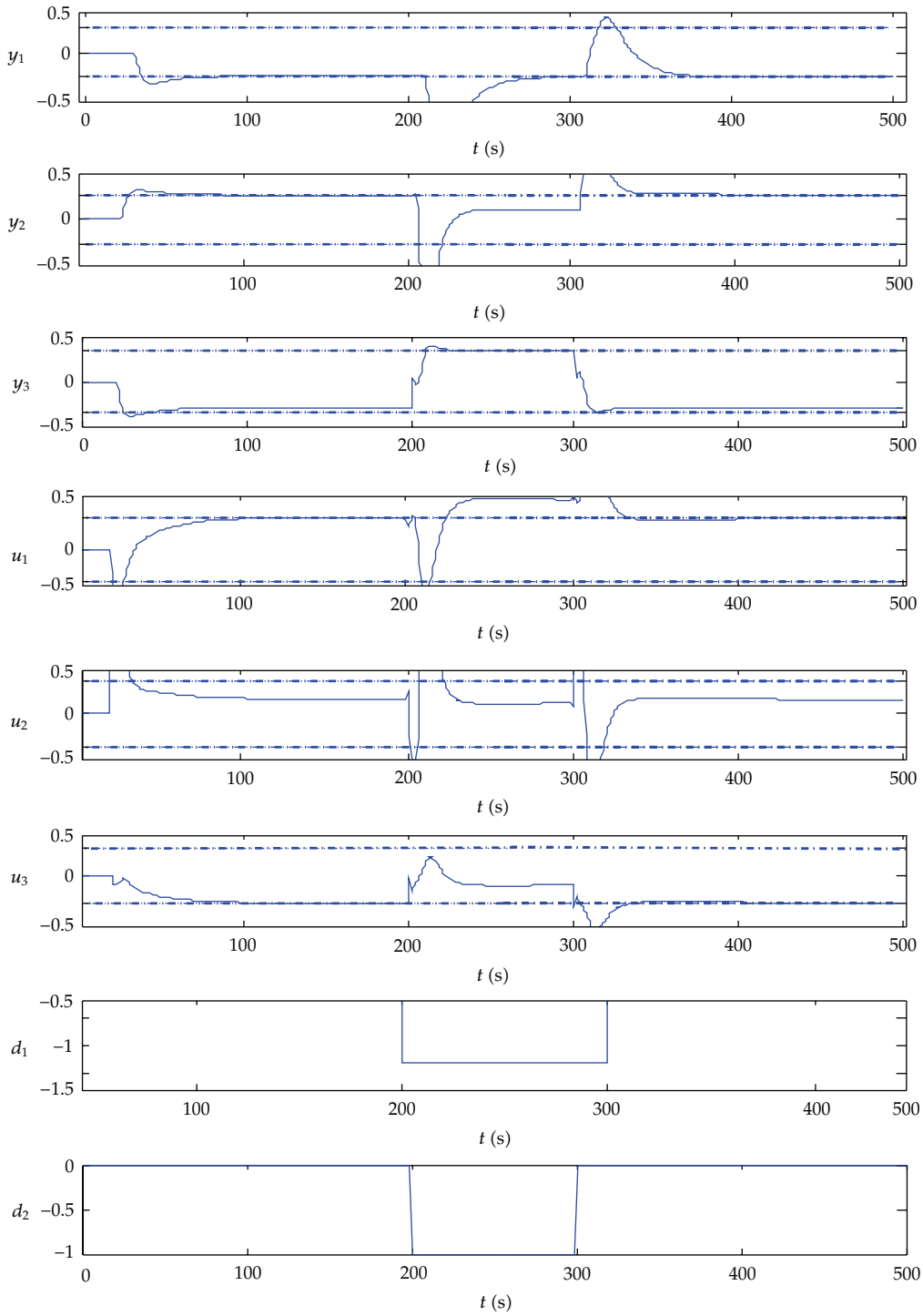


**Figure 1:** The closed-loop output trajectories, the corresponding control input signals, and the disturbances.

## 5. Numerical Example

Let us consider the heavy fractionator, which is a Shell standard problem, with the following model:

$$G_U(s) = \begin{bmatrix} \dfrac{4.05e^{-27s}}{50s+1} & \dfrac{1.77e^{-28s}}{60s+1} & \dfrac{5.88e^{-27s}}{50s+1} \\ \dfrac{5.39e^{-18s}}{50s+1} & \dfrac{5.72e^{-14s}}{60s+1} & \dfrac{6.90e^{-15s}}{40s+1} \\ \dfrac{4.38e^{-20s}}{33s+1} & \dfrac{4.42e^{-22s}}{44s+1} & \dfrac{7.20}{19s+1} \end{bmatrix}, \quad G_F(s) = \begin{bmatrix} \dfrac{1.2e^{-27s}}{45s+1} & \dfrac{1.44e^{-27s}}{60s+1} \\ \dfrac{1.52e^{-18s}}{25s+1} & \dfrac{1.83e^{-15s}}{20s+1} \\ \dfrac{1.14}{27s+1} & \dfrac{1.26}{32s+1} \end{bmatrix}, \tag{5.1}$$

where $G_U(s)$ is the transfer function matrix between inputs and outputs, and $G_F(s)$ between disturbances and outputs. The three inputs of the process are the product draw rates from the top and side of the column $(u_1, u_2)$, and the reflux heat duty for the bottom of the column $(u_3)$. The three outputs of the process represent the draw composition $(y_1)$ from the top of the column, the draw composition $(y_2)$, and the reflux temperature at the bottom of the column $(y_3)$. The two disturbances are the reflux heat duties for the intermediate section and top of the column $(d_1, d_2)$.

The inputs are constrained between −0.5 and 0.5, while the outputs between −0.5 and 0.5. The weighting matrices are identity matrices. $N = 3$. The sampling interval is 3 seconds. With the algorithm as in Theorem 3.3 applied, the simulation results are shown in Figure 1. The steady-state calculation begins running at instant $k = 20$, when the optimizer finds the optimum target $y_t = [-0.5, 0.5, -0.4269]^T$. The objective value is −0.3538, indicating that −0.3538 unit benefits are obtained. During time $k = 200$–$300$, the disturbances $d_1 = -1.3$ and $d_2 = 1$ are added. The simulation verifies our theoretical results.

## 6. Conclusions

We have given some preliminary results for the stability of double-layered MPC. The results cannot be seen as the strict synthesis approaches; rather, they are endeavors towards this kind of approaches. Instead of asymptotic stability, we obtain the input-to-state stability, as in [22]. The results are inspired by [22]; but they are much different, as shown in Remarks 1–11 of [21].

We believe that several works need to be continued. Indeed, assuming feasibility of the target generation problem at each control interval is very restrictive, and overlooking the uncertainties in the prediction model brings difficulties for proving both the asymptotic stability and offset-free property. It may be necessary to develop a whole procedure, where the target generation problem is guaranteed (rather than assumed) to be feasible at each control interval and an augmented system is used for the stability analysis.

## Acknowledgments

This work is supported by the Innovation Key Program (Grant KGCX2-EW-104) of the Chinese Academy of Sciences, by the Nature Science Foundation of China (NSFC Grant no.

61074059), by the Foundation from the State Key Laboratory of Industrial Control Technology (Grant no. ICT1116), by the Public Welfare Project from the Science Technology Department of Zhejiang Province (Grant no. 2011c31040) and by the Nature Science Foundation of Zhejiang Province (Grant no. Y12F030052).

## References

[1] S. J. Qin and T. A. Badgwell, "A survey of industrial model predictive control technology," *Control Engineering Practice*, vol. 11, no. 7, pp. 733–764, 2003.
[2] D. Q. Mayne, J. B. Rawlings, C. V. Rao, and P. O. M. Scokaert, "Constrained model predictive control: stability and optimality," *Automatica*, vol. 36, no. 6, pp. 789–814, 2000.
[3] A. Bemporad, F. Borrelli, and M. Morari, "Min-max control of constrained uncertain discrete-time linear systems," *Institute of Electrical and Electronics Engineers*, vol. 48, no. 9, pp. 1600–1606, 2003.
[4] L. Chisci, J. A. Rossiter, and G. Zappa, "Systems with persistent disturbances: predictive control with restricted constraints," *Automatica*, vol. 37, no. 7, pp. 1019–1028, 2001.
[5] B. Ding, "Properties of parameter-dependent open-loop MPC for uncertain systems with polytopic description," *Asian Journal of Control*, vol. 12, no. 1, pp. 58–70, 2010.
[6] B. Kouvaritakis, J. A. Rossiter, and J. Schuurmans, "Efficient robust predictive control," *Institute of Electrical and Electronics Engineers*, vol. 45, no. 8, pp. 1545–1549, 2000.
[7] D. Li and Y. Xi, "The feedback robust MPC for LPV systems with bounded rates of parameter changes," *Institute of Electrical and Electronics Engineers*, vol. 55, no. 2, pp. 503–507, 2010.
[8] H. Huang, D. Li, Z. Lin, and Y. Xi, "An improved robust model predictive control design in the presence of actuator saturation," *Automatica*, vol. 47, no. 4, pp. 861–864, 2011.
[9] Y. I. Lee and B. Kouvaritakis, "Receding horizon output feedback control for linear systems with input saturation," *IEE Proceedings of Control Theory and Application*, vol. 148, pp. 109–115, 2001.
[10] C. Løvaas, M. M. Seron, and G. C. Goodwin, "Robust output-feedback model predictive control for systems with unstructured uncertainty," *Automatica*, vol. 44, no. 8, pp. 1933–1943, 2008.
[11] D. Q. Mayne, S. V. Raković, R. Findeisen, and F. Allgöwer, "Robust output feedback model predictive control of constrained linear systems: time varying case," *Automatica*, vol. 45, pp. 2082–2087, 2009.
[12] B. Ding, "Constrained robust model predictive control via parameter-dependent dynamic output feedback," *Automatica*, vol. 46, no. 9, pp. 1517–1523, 2010.
[13] B. Ding, Y. Xi, M. T. Cychowski, and T. O'Mahony, "A synthesis approach for output feedback robust constrained model predictive control," *Automatica*, vol. 44, no. 1, pp. 258–264, 2008.
[14] B. Ding, B. Huang, and F. Xu, "Dynamic output feedback robust model predictive control," *International Journal of Systems Science*, vol. 42, no. 10, pp. 1669–1682, 2011.
[15] B. Ding, "Dynamic output feedback predictive control for nonlinear systems represented by a Takagi-Sugeno model," *IEEE Transactions on Fuzzy Systems*, vol. 19, no. 5, pp. 831–843, 2011.
[16] B. C. Ding, "Output feedback robust MPC based-on direct input-output model," in *Proceedings of the Chinese Control and Decision Conference*, Taiyuan, China, 2012.
[17] D. E. Kassmann, T. A. Badgwell, and R. B. Hawkins, "Robust steady-state target calculation for model predictive control," *AIChE Journal*, vol. 46, no. 5, pp. 1007–1024, 2000.
[18] T. Zou, H. Q. Li, X. X. Zhang, Y. Gu, and H. Y. Su, "Feasibility and soft constraint of steady state target calculation layer in LP-MPC and QP-MPC cascade control systems," in *Proceedings of the 4th International Symposium on Advanced Control of Industrial Processes (ADCONIP '11)*, pp. 524–529, Hangzhou, China, 2011.
[19] K. R. Muske and T. A. Badgwell, "Disturbance modeling for offset-free linear model predictive control," *Journal of Process Control*, vol. 12, no. 5, pp. 617–632, 2002.
[20] G. Pannocchia and J. B. Rawlings, "Disturbance models for offset-free model-predictive control," *AIChE Journal*, vol. 49, no. 2, pp. 426–437, 2003.
[21] B. C. Ding, T. Zou, and H. G. Pan, "A discussion on stability of offset-free linear model predictive-control," in *Proceedings of the Chinese Control and Decision Conference*, Taiyuan, China, 2012.
[22] T. Zhang, G. Feng, and X. J. Zeng, "Output tracking of constrained nonlinear processes with offset-free input-to-state stable fuzzy predictive control," *Automatica*, vol. 45, no. 4, pp. 900–909, 2009.
[23] M. V. Kothare, V. Balakrishnan, and M. Morari, "Robust constrained model predictive control using linear matrix inequalities," *Automatica*, vol. 32, no. 10, pp. 1361–1379, 1996.

Hindawi Publishing Corporation
Journal of Applied Mathematics
Volume 2012, Article ID 610971, 20 pages
doi:10.1155/2012/610971

*Research Article*

# Spatial Domain Adaptive Control of Nonlinear Rotary Systems Subject to Spatially Periodic Disturbances

**Yen-Hsiu Yang[1] and Cheng-Lun Chen[2]**

[1] *R&D Division, Inventec Corporation, 66 Hou-Kang Street, Shin-Lin District, Taipei 111, Taiwan*
[2] *Department of Electrical Engineering, National Chung Hsing University, Taichung 40227, Taiwan*

Correspondence should be addressed to Cheng-Lun Chen, chenc@dragon.nchu.edu.tw

Received 22 February 2012; Revised 13 June 2012; Accepted 14 June 2012

Academic Editor: Baocang Ding



We propose a generic spatial domain control scheme for a class of nonlinear rotary systems of variable speeds and subject to spatially periodic disturbances. The nonlinear model of the rotary system in time domain is transformed into one in spatial domain employing a coordinate transformation with respect to angular displacement. Under the circumstances that measurement of the system states is not available, a nonlinear state observer is established for providing the estimated states. A two-degree-of-freedom spatial domain control configuration is then proposed to stabilize the system and improve the tracking performance. The first control module applies adaptive backstepping with projected parametric update and concentrates on robust stabilization of the closed-loop system. The second control module introduces an internal model of the periodic disturbances cascaded with a loop-shaping filter, which not only further reduces the tracking error but also improves parametric adaptation. The overall spatial domain output feedback adaptive control system is robust to model uncertainties and state estimated error and capable of rejecting spatially periodic disturbances under varying system speeds. Stability proof of the overall system is given. A design example with simulation demonstrates the applicability of the proposed design.

## 1. Introduction

Rotary systems play important roles in various industry applications, for example, packaging, printing, assembly, fabrication, semiconductor, robotics, and so forth. Design of control algorithm for a motion system often comes up with nonlinearities and uncertainties. Nonlinearities are either inherent to the system or due to the dynamics of actuators and sensors. Uncertainties are mainly caused by unmodeled dynamics, parametric uncertainty, and disturbances. For dealing with nonlinearities, common techniques, for example, feedback

linearization and backstepping, are to utilize feedback to cancel all or part of the nonlinear terms. On the other hand, design techniques for conducting disturbance rejection or attenuation in control systems mostly originate from the internal model principle [1], for example, those incorporating or estimating the exosystem of the disturbances [2–6]. Conventional controllers are mostly time-based controllers as they are synthesized and operate in temporal or time domain. Several researches [7–9] have started studying spatial domain controllers ever since a repetitive controller design was initiated by Nakano et al. [10]. In the design of Nakano et al., the repetitive control system has its repetitive kernel (i.e., $e^{-Ls}$ with positive feedback) synthesized and operated with respect to a spatial coordinate, for example, angular position or displacement. Hence its capability for rejecting or tracking spatially periodic disturbances or references will not degrade when the controlled system operates at varying speed. All existing studies propose design methods starting with a linear time-invariant (LTI) system. After reformulation, a nonlinear open-loop system is obtained in spatial domain. Subsequently, the open-loop system is either linearized around an operating speed or regarded as a quasi-linear parameter varying (quasi-LPV) system and then adjoined with the spatial domain internal model of the tracking or disturbance signal. Design paradigms based on linear (robust) control theory are then applied to the resulting augmented system. However, presuming the open-loop system to be LTI and resorting to design paradigm of linear control will inevitably restrict the applicability and limit the achievable performance of a design method. Chen and Yang [11] introduced a new spatial domain control scheme based on a second-order LTI system with availability of state measurements. To achieve robust stabilization and high-performance tracking, a two-module control configuration is constructed. One of the modules utilizes adaptive backstepping with projected parametric adaptation to robustly stabilize the system. The other module incorporates a spatial domain internal model of the disturbances cascaded with a loop-shaping filter to improve the tracking performance.

This paper extends the work of Chen and Yang [11, 12]. The control scheme has been generalized such that it is applicable to a class of nonlinear systems (instead of just LTI systems). Moreover, the major shortcoming in Chen and Yang's design [11], that is, which requires full-state feedback, is resolved by incorporation of a nonlinear state observer. Various types of nonlinear state observers have been developed and put into use in the past (e.g., [13, 14]). This paper will study the feasibility of incorporating a $K$-filter-type state observer [13] into the proposed design. The proposed system incorporating the state observer can be proved to be stable under bounded disturbance and system uncertainties. An illustrative example is given for demonstration and derivation of the control algorithm. Simulation is performed to verify the feasibility and effectiveness of the proposed scheme. Compared to the preliminary work in [12] (which is only applicable to second order systems), the results have been generalized to be suited for $n$th order systems. Specifically, the design and stability proof are more comprehensive and rigorous than those presented in [12].

Recently, there have been emerging design techniques based on adaptive fuzzy control (AFC), which may cope with nonlinearities and uncertainties with unknown structures [15–17]. The major differences between those techniques and the proposed one are as follows: (1) design being time based (AFC) versus spatial based (the proposed approach); (2) assuming less information about the nonlinearities/uncertainties (AFC) versus more information about the nonlinearities/uncertainties (the proposed approach). Note that the spatial-based design is not just a change of the independent variable from time to angular displacement. A nonlinear coordinate transformation is actually involved. Therefore, the systems under consideration in AFC and the proposed method are different. Next,

the capability of the design approaches suggested in AFC for tackling systems subject to a more generic class of nonlinearities/uncertainties lies in the usage of a fuzzy system to approximate those nonlinearities/uncertainties. It is actually not clear regarding the complexity of the fuzzy system (i.e., number of membership functions) that should be used to achieve the required control performance. It is also not clear whether or not the control effort is reasonable. In general, when characteristics of the uncertainties or disturbances are known, such information should be incorporated as much as possible into the design to enhance performance, avoid conservativeness, and result in sensible control input. Hence, instead of assuming the disturbances to be generic (probably just being bounded as by AFC), the proposed design is aiming at a type of disturbances specific to rotary systems and utilizes the spatially periodic nature of the disturbances to establish a well-defined control module integrated into the overall control configuration.

This paper is organized as follows. Reformulation of a generic nonlinear rotary system with respect to angular displacement will be presented in Section 2. Design of the state observer is described in Section 3. Section 4 will cover derivation and stability analysis of the proposed spatial domain output feedback control scheme. Simulation verification for the proposed scheme will be presented in Section 5. Conclusion is given in Section 6.

## 2. Problem Formulation

In this section, we show how a generic NTI model can be transformed into an NPI model by choosing an alternate independent variable (angular displacement instead of time) and defining a new set of states (or coordinates) with respect to the angular displacement. Note that the transformation described here is equivalent to a nonlinear coordinate transformation or a diffeomorphism. The NPI model will be used for the subsequent design and discussion,

$$\begin{aligned} \dot{x}(t) &= \left[f_t(x(t),\phi_f) + \Delta f_t(x(t),\phi_f)\right] + \left[g_t(x(t),\phi_g) + \Delta g_t(x(t),\phi_g)\right]u(t), \\ y &= \Psi x(t) + d_y(t) = x_1(t) + d_y(t), \end{aligned} \tag{2.1}$$

where $x(t) = [x_1(t) \ \cdots \ x_n(t)]^T$, $\Psi = [1 \ 0 \ \cdots \ 0]$, and $u(t)$ and $y(t)$ correspond to control input and measured output angular velocity of the system, respectively. $d_y(t)$ represents a class of bounded output disturbances which constitutes (dominant) spatially periodic and band-limited (or nonperiodic) components. Here we refer band-limited disturbances to signals whose Fourier transform or power spectral density is zero above a certain finite frequency. The only available information of the disturbances is the number of distinctive spatial frequencies and the spectrum distribution for band-limited disturbance components. $f_t(x(t),\ \phi_f)$ and $g_t(x(t),\ \phi_g)$ are known vector-valued functions with unknown but bounded system parameters, that is, $\phi_f = [\phi_{f1} \ \cdots \ \phi_{fk}]$ and $\phi_g = [\phi_{g1} \ \cdots \ \phi_{gl}]$; $\Delta f_t(x(t),\ \phi_f)$ and $\Delta g_t(x(t),\ \phi_g)$ represent unstructured modeling inaccuracy, which are also assumed to be bounded. Instead of using time $t$ as the independent variable, consider an alternate independent variable $\theta = \lambda(t)$, that is, the angular displacement. Since by definition

$$\lambda(t) = \int_0^t \omega(\tau)d\tau + \lambda(0), \tag{2.2}$$

where $\omega(t)$ is the angular velocity, the following condition:

$$\omega(t) = \frac{d\theta}{dt} > 0, \quad \forall t > 0, \tag{2.3}$$

will guarantee that $\lambda(t)$ is strictly monotonic such that $t = \lambda^{-1}(\theta)$ exists. Thus all the variables in the time domain can be transformed into their counterparts in the $\theta$-domain, that is,

$$\begin{aligned} \hat{x}(\theta) &= x\left(\lambda^{-1}(\theta)\right), \qquad \hat{y}(\theta) = y\left(\lambda^{-1}(\theta)\right), \\ \hat{u}(\theta) &= u\left(\lambda^{-1}(\theta)\right), \qquad \hat{d}(\theta) = d\left(\lambda^{-1}(\theta)\right), \\ \hat{\omega}(\theta) &= \omega\left(\lambda^{-1}(\theta)\right), \end{aligned} \tag{2.4}$$

where we denote $\hat{\bullet}$ as the $\theta$-domain representation of $\bullet$. Note that, in practice, (2.3) can usually be satisfied for most rotary systems where the rotary component rotates only in one direction. Since

$$\frac{dx(t)}{dt} = \frac{d\theta}{dt}\frac{d\hat{x}(\theta)}{d\theta} = \hat{\omega}(\theta)\frac{d\hat{x}(\theta)}{d\theta}. \tag{2.5}$$

Equation (2.1) can be rewritten as

$$\begin{aligned} \hat{\omega}(\theta)\frac{d\hat{x}(\theta)}{d\theta} &= \left[f_t(\hat{x}(\theta), \phi_f) + \Delta f_t(\hat{x}(\theta), \phi_f)\right] + \left[g_t(\hat{x}(\theta), \phi_g) + \Delta g_t(\hat{x}(\theta), \phi_g)\right]\hat{u}(\theta), \\ \hat{y}(\theta) &= \Psi\hat{x}(\theta) + \hat{d}_y(\theta) = \hat{x}_1(\theta) + \hat{d}_y(\theta). \end{aligned} \tag{2.6}$$

Equation (2.6) can be viewed as a nonlinear position-invariant (as opposed to the definition of time-invariant) system with the angular displacement $\theta$ as the independent variable. Note that the concept of transfer function is still valid for linear position-invariant systems if we define the Laplace transform of a signal $\hat{g}(\theta)$ in the angular displacement domain as

$$\hat{G}(\tilde{s}) = \int_0^\infty \hat{g}(\theta)e^{-\tilde{s}\theta}d\theta. \tag{2.7}$$

This definition will be useful for describing the linear portion of the overall control system.

## 3. Nonlinear State Observer

Drop the $\theta$ notation and note that (2.6) can be expressed as a standard nonlinear system:

$$\dot{\hat{x}} = f\left(\hat{x}, \phi_f\right) + g\left(\hat{x}, \phi_g\right)\hat{u} + \hat{d}_s, \qquad \hat{y} = h(\hat{x}) + \hat{d}_y = \hat{\omega} + \hat{d}_y, \tag{3.1}$$

where terms involving unstructured uncertainty are merged into $\hat{d}_s = \Delta f(\hat{x},\ \phi_f) + \Delta g(\hat{x},\ \phi_g)\hat{u}$ with

$$\Delta f(\hat{x},\phi_f) = \frac{\Delta f_t(\hat{x},\ \phi_f)}{\hat{x}_1}, \qquad \Delta g(\hat{x},\phi_g) = \frac{\Delta g_t(\hat{x},\ \phi_g)}{\hat{x}_1}. \tag{3.2}$$

In addition, we have

$$f(\hat{x},\phi_f) = \frac{f_t(\hat{x},\ \phi_f)}{\hat{x}_1}, \qquad g(\hat{x},\phi_g) = \frac{g_t(\hat{x},\ \phi_g)}{\hat{x}_1}, \qquad h(\hat{x}) = \hat{\omega} = \hat{x}_1. \tag{3.3}$$

The state variables have been specified such that the angular velocity $\hat{\omega}$ is equal to $\hat{x}_1$, that is, the undisturbed output $h(\hat{x})$. It is not difficult to verify that (3.1) has the same relative degree in $D_0 = \{\hat{x} \in \mathbb{R}^n \mid \hat{x}_1 \neq 0\}$ as the NTI model in (2.1). If (3.1) has relative degree $r$, we can define the following nonlinear coordinate transformation:

$$\hat{z} = T(\hat{x}) = \begin{bmatrix} \psi_1(\hat{x}) \\ \vdots \\ \psi_{n-r}(\hat{x}) \\ \hline h(\hat{x}) \\ \vdots \\ L_f^{r-1}h(\hat{x}) \end{bmatrix} \triangleq \begin{bmatrix} \hat{z}_2 \\ \hline \hat{z}_1 \end{bmatrix}, \tag{3.4}$$

where $\psi_1$ to $\psi_{n-r}$ are chosen such that $T(\hat{x})$ is a diffeomorphism on $D_0 \subset D$ and

$$L_g\psi_i(\hat{x}) = 0, \quad 1 \leq i \leq n-r, \quad \forall \hat{x} \in D_0. \tag{3.5}$$

With respect to the new coordinates, that is, $\hat{z}_1$ and $\hat{z}_2$, (3.1) can be transformed into the so-called normal form, that is,

$$\begin{aligned} \dot{\hat{z}}_2 &= L_f\psi(\hat{x})\big|_{\hat{x}=T^{-1}(\hat{z})} + \hat{d}_{so} \triangleq \Psi(\hat{z}_1,\hat{z}_2), \\ \dot{\hat{z}}_1 &= A_c\hat{z}_1 + B_c\left[L_gL_f^{r-1}h(\hat{x})\Big|_{\hat{x}=T^{-1}(\hat{z})}\right]\left[\hat{u} + \frac{L_f^r h(\hat{x})}{L_gL_f^{r-1}h(\hat{x})}\bigg|_{\hat{x}=T^{-1}(\hat{z})}\right] + \hat{d}_{si}, \\ \hat{y} &= C_c\hat{z}_1 + \hat{d}_y, \end{aligned} \tag{3.6}$$

where $\hat{d}_{so}$ and $\hat{d}_{si} = [\hat{d}_{si_1} \ \cdots \ \hat{d}_{si_r}]^T$ come from $\hat{d}_s$ going through the indicated coordinate transformation. $\hat{z}_1 = [\hat{z}_{11} \ \cdots \ \hat{z}_{1r}] \in \mathbb{R}^r$, $\hat{z}_2 \in \mathbb{R}^{n-r}$, and $(A_c, B_c, C_c)$ is a canonical form representation of a chain of $r$ integrators. The first equation is called internal dynamics and the second is called external dynamics. Internal dynamics which is not affected by the control $u$. By setting $\hat{z}_1 = 0$ in that equation, we obtain

$$\dot{\hat{z}}_2 = \Psi(0,\hat{z}_2), \tag{3.7}$$

which is the zero dynamics of (3.1) or (3.6). The system is called minimum phase if (3.7) has an asymptotically stable equilibrium point in the domain of interest. To allow us to present the proposed algorithm and stability analysis in a simpler context, we will make the following assumptions for the subsequent derivation:

(1) $f(\hat{x}(\theta),\ \phi_f)$ and $g(\hat{x}(\theta),\ \phi_g)$ are linearly related to those unknown system parameters, that is,

$$\begin{aligned} f(\hat{x}(\theta),\phi_f) &= \phi_1 f_1(\hat{x}(\theta)) + \cdots + \phi_{fk} f_k(\hat{x}(\theta)), \\ g(\hat{x}(\theta),\phi_g) &= \phi_{g1} g_1(\hat{x}(\theta)) + \cdots + \phi_{gl} g_l(\hat{x}(\theta)). \end{aligned} \tag{3.8}$$

(2) Equation (3.1) is minimum phase, and the internal dynamics in (3.6) is ISS (input-to-state stable).

(3) The output disturbance is sufficiently smooth, that is, $\dot{\hat{d}}_y, \ldots, \hat{d}_y^{(r)}$ exist,

(4) $\hat{d}_{si_1}^{(r-1)}$, $\hat{d}_{si_2}^{(r-2)}, \ldots,$ $\dot{\hat{d}}_{si_{r-1}}$ exist, that is, the transformed unstructured uncertainty is sufficiently smooth.

(5) The reference command $\hat{y}_m$ and its first $r$ derivates are known and bounded. Moreover, the signal $\hat{y}_m^{(r)}$ is piecewise continuous.

With assumption (2), we focus on designing a nonlinear state observer for external dynamics of (3.6),

$$\dot{\hat{z}}_1 = A_c \hat{z}_1 + B_c \left[ L_g L_f^{r-1} h(\hat{x}) \Big|_{\hat{x}=T^{-1}(\hat{z})} \right] \left[ \hat{u} + \frac{L_f^r h(\hat{x})}{L_g L_f^{r-1} h(\hat{x})} \Bigg|_{\hat{x}=T^{-1}(\hat{z})} \right] + \hat{d}_{si}. \tag{3.9}$$

Since $f(\hat{x})$ and $g(\hat{x})$ are linearly related to system parameters, $L_g L_f^{r-1} h(\hat{x})$ and $L_g L_f^{r-1} h(\hat{x})$ can be written as $L_f^r h(\hat{x}) = \Theta^T W_f(\hat{x})$ and $L_g L_f^{r-1} h(\hat{x}) = \Theta^T W_g(\hat{x})$, where $W_f(\hat{x})$ and $W_g(\hat{x})$ are two nonlinear functions, and $\Theta = [\phi_{f1} \ \cdots \ \phi_{fk} \ \phi_{g1} \ \cdots \ \phi_{gl} \ \cdots]^T = [\phi_1 \ \cdots \ \phi_\ell]^T \in \mathbb{R}^\ell$, where $\ell$ is the number of unknown parameters. Next, we adopt the following observer structure: $\dot{\bar{z}}_1 = A_0 \bar{z}_1 + \bar{k} y + F(y,u)^T \Theta$, where $\bar{z}_1 = [\bar{z}_{11} \ \cdots \ \bar{z}_{1r}]^T$ is the estimate of $z_1$, and $\overline{W}_f(y)$ and $\overline{W}_g(y)$ are nonlinear functions with the same structure as $W_f(x)$ and $W_g(x)$ except that each entry of $x$ is replaced by $y$. Furthermore,

$$A_0 = \begin{bmatrix} -k_1 & \\ \vdots & I_{(r-1)\times(r-1)} \\ -k_r & 0_{1\times(r-1)} \end{bmatrix}, \qquad \bar{k} = [k_1 \ \cdots \ k_r]^T, \qquad F(y,u)^T = \begin{bmatrix} 0_{(r-1)\times\ell} \\ \overline{W}_f^T(y) + \overline{W}_g^T(y) u \end{bmatrix} \in \mathbb{R}^{r\times\ell}. \tag{3.10}$$

By properly choosing $\bar{k}$, the matrix $A_0$ can be made Hurwitz. Define the state estimated error as $\varepsilon \triangleq [\varepsilon_{z_{11}} \ \cdots \ \varepsilon_{z_{1r}}]^T \triangleq z_1 - \bar{z}_1$. The dynamics of the estimated error can be obtained as $\dot{\varepsilon} = A_0 \varepsilon + \Delta$, where $\Delta = -\bar{k} d_y + B_c \Theta^T [W_g(x) - \overline{W}_g(y)]\ u + B_c \Theta^T [W_f(x) - \overline{W}_f(y)] + d_{si}$. To

proceed, the role of the state observer is replaced by $\overline{z}_1 \triangleq \xi + \Omega^T\Theta$ and the following two $K$-filters:

$$\dot{\xi} = A_0\xi + \overline{k}y, \qquad \dot{\Omega}^T = A_0\Omega^T + F(y,u)^T, \tag{3.11}$$

such that $\xi = [\xi_{11} \ \cdots \ \xi_{1r}]^T \in \mathbb{R}^r$ and $\Omega^T \triangleq [v_1 \ \cdots \ v_\ell] \in \mathbb{R}^{r\times\ell}$. Decompose the second equation of (3.11) into $\dot{v}_j = A_0 v_j + e_r\sigma_j$, $j = 1,2,\ldots,\ell$, where $e_r = [0 \ \cdots \ 0 \ 1] \in \mathbb{R}^r$ and $\sigma_j = w_{1j} + w_{2j}u$ with $w_{1j}$ and $w_{2j}$ are the $j$th columns of $\overline{W}_f^T(y)$ and $\overline{W}_g^T(y)$, respectively. With the definition of the state estimated error $\varepsilon$, the state estimate $\overline{z}_1$, and (3.11), we acquire the following set of equations which will be used in the subsequent design:

$$z_{1k} = \overline{z}_{1k} + \varepsilon_{z_{1k}} = \xi_{1k} + \sum_{j=1}^{\ell} v_{j,k}\phi_j + \varepsilon_{z_{1k}}, \quad k = 1,\ldots,r, \tag{3.12}$$

where $\bullet_{j,i}$ denotes the $i$th row of $\bullet_j$.

## 4. Spatial Domain Output Feedback Adaptive Control System

To apply adaptive backstepping method, we firstly rewrite the derivative of output $\widehat{y}$ as

$$\dot{\widehat{y}} = \dot{\widehat{z}}_{11} + \dot{\widehat{d}}_y = \widehat{z}_{12} + \widehat{d}_{si_1} + \dot{\widehat{d}}_y = \overline{z}_{12} + \varepsilon_{\widehat{z}_{12}} + \widehat{d}_{si_1} + \dot{\widehat{d}}_y. \tag{4.1}$$

With the second equation in (3.12), (4.1) can be written as

$$\dot{\widehat{y}} = \overline{z}_{12} + \varepsilon_{\widehat{z}_{12}} + \widehat{d}_{si_1} + \dot{\widehat{d}}_y = \xi_{12} + v_{\ell,2}\phi_\ell + \overline{\omega}^T\Theta + \varepsilon_{\widehat{z}_{12}} + \widehat{d}_{si_1} + \dot{\widehat{d}}_y, \tag{4.2}$$

where $\overline{\omega}^T = [v_{1,2} \ \cdots \ v_{\ell-1,2} \ 0]$.

In view of designing output feedback backstepping with $K$-filters, we need to find a set of $K$-filter parameters, that is, $v_{\ell,2},\ldots,v_{1,2}$, separated from $\widehat{u}$ by the same number of integrators between $\widehat{z}_{12}$ and $\widehat{u}$. From (3.11), we can see that $v_{\ell,2},\ldots,v_{1,2}$ are all candidates if $w_{2j}$ are not zero. In the following derivation, we assume that $v_{\ell,2}$ is selected. Hence, the system incorporating the $K$-filters can be expressed as

$$\begin{gathered}\dot{\widehat{y}} = \xi_{12} + v_{\ell,2}\phi_\ell + \overline{\omega}^T\Theta + \varepsilon_{\widehat{z}_{12}} + \widehat{d}_{si_1} + \dot{\widehat{d}}_y, \qquad \dot{v}_{\ell,i} = v_{\ell,i+1} - k_i v_{\ell,1}, \quad i = 2,\ldots,r-1, \\ \dot{v}_{\ell,r} = -k_r v_{\ell,1} + w_{1\ell} + w_{2\ell}\widehat{u}.\end{gathered} \tag{4.3}$$

To apply adaptive backstepping to (4.3), a new set of coordinates will be introduced

$$z_1 = \widehat{y} - \widehat{y}_m, \qquad z_i = v_{\ell,i} - \alpha_{i-1}, \quad i = 2,\ldots,r, \tag{4.4}$$

where $\widehat{y}_m$ is the prespecified reference command and $\alpha_{i-1}$ is the virtual input which will be used to stabilize each state equation. For simplicity, we define $\partial\alpha_0/\partial\widehat{y} \triangleq -1$ for subsequent derivations.

*Step 1* ($i = 1$). With (4.4), the first state equation of (4.3) can be expressed as

$$\dot{z}_1 = \xi_{12} + z_2\phi_\ell + \alpha_1\phi_\ell + \overline{\omega}^T\Theta + \varepsilon_{\widehat{z}_{12}} + \dot{\widehat{d}}_{si_1} + \dot{\widehat{d}}_y - \dot{\widehat{y}}_m. \tag{4.5}$$

Consider a Lyapunov function $V_1 = (1/2)z_1^2$ and calculate its derivative

$$\dot{V}_1 = z_1\dot{z}_1 = z_1\left(\xi_{12} + z_2\phi_\ell + \alpha_1\phi_\ell + \overline{\omega}^T\Theta + \varepsilon_{\widehat{z}_{12}} + \dot{\widehat{d}}_{si_1} + \dot{\widehat{d}}_y - \dot{\widehat{y}}_m\right). \tag{4.6}$$

Define the estimates of $\phi_i$ as $\widetilde{\phi}_i$ and $\Phi = [\Phi_1 \ \cdots \ \Phi_\ell] = \Theta - \widetilde{\Theta}$, where $\widetilde{\Theta} = [\widetilde{\phi}_{f1} \ \cdots \ \widetilde{\phi}_{fk} \ \widetilde{\phi}_{g1} \ \cdots \ \widetilde{\phi}_{gl} \ \cdots]^T = [\widetilde{\phi}_1 \ \cdots \ \widetilde{\phi}_\ell]^T \in \mathbb{R}^\ell$. Note that $\Theta$ is the "true" parameter vector while $\widetilde{\Theta}$ is the estimated parameter vector. Design the virtual input $\alpha_1$ as $\alpha_1 = \overline{\alpha}_1/\widetilde{\phi}_\ell$ and specify

$$\begin{aligned}\overline{\alpha}_1 &= \frac{1}{z_1}\left(-z_1\xi_{12} - z_1z_2\widetilde{\phi}_\ell - z_1\overline{\omega}\widetilde{\Theta} + z_1\dot{\widehat{y}}_m - c_1z_1^2 - d_1z_1^2 - g_1z_1^2\right)\\ &= -\xi_{12} - z_2\widetilde{\phi}_\ell - \overline{\omega}^T\widetilde{\Theta} + \dot{\widehat{y}}_m - c_1z_1 - d_1z_1 - g_1z_1,\end{aligned} \tag{4.7}$$

where $c_i,\ d_i,\ g_i$ are variables. Therefore, (4.6) becomes

$$\dot{V}_1 = -c_1z_1^2 - d_1z_1^2 - g_1z_1^2 + \tau_1\Phi + z_1\left(\varepsilon_{\widehat{z}_{12}} + \dot{\widehat{d}}_{si_1} + \dot{\widehat{d}}_y\right), \tag{4.8}$$

where $\tau_1\Phi = z_1z_2\Phi_\ell + \alpha_1\Phi_\ell + z_1\overline{\omega}^T\Phi$.

*Step 2* ($i = 2, \ldots, r-1$). With respect to the new set of coordinates (4.4), the second equation of (4.3) can be rewritten as

$$\begin{aligned}\dot{z}_i = z_{i+1} + \alpha_i - k_iv_{\ell,1} - \Bigg[&\frac{\partial\alpha_{i-1}}{\partial\widehat{y}}\left(\xi_{12} + v_{\ell,2}\phi_\ell + \overline{\omega}^T\Theta + \varepsilon_{\widehat{z}_{12}} + \dot{\widehat{d}}_{si_1} + \dot{\widehat{d}}_y\right) + \frac{\partial\alpha_{i-1}}{\partial\xi}\left(A_0\xi + \overline{k}\widehat{y}\right)\\ &+\frac{\partial\alpha_{i-1}}{\partial\widetilde{\Theta}}\dot{\widetilde{\Theta}}\sum_{j=1}^{\ell}\frac{\partial\alpha_{i-1}}{\partial v_j}\left(A_0v_j + e_r\sigma_j\right) + \sum_{j=1}^{i-1}\frac{\partial\alpha_{i-1}}{\partial\widehat{y}_m^{(j-1)}}\widehat{y}_m^{(j)}\Bigg].\end{aligned} \tag{4.9}$$

Consider a Lyapunov function $V_i = \sum_{j=1}^{i-1} V_j + (1/2)z_i^2$ and its derivative

$$\dot{V}_i = \sum_{j=1}^{i-1}\dot{V}_j + z_i\left\{ z_{i+1} + \alpha_i - k_i v_{\ell,1} - \left[ \frac{\partial \alpha_{i-1}}{\partial \widehat{y}}\left(\xi_{12} + v_{\ell,2}\phi_\ell + \overline{\omega}^T\Theta + \varepsilon_{\widehat{z}_{12}} + \widehat{d}_{si_1} + \dot{\widehat{d}}_y\right)\right.\right.$$
$$+ \frac{\partial \alpha_{i-1}}{\partial \xi}\left(A_0\xi + \overline{k}\widehat{y}\right) + \frac{\partial \alpha_{i-1}}{\partial \widetilde{\Theta}}\dot{\widetilde{\Theta}}\sum_{j=1}^{\ell}\frac{\partial \alpha_{i-1}}{\partial v_j}\left(A_0 v_j + e_r\sigma_j\right)$$
$$\left.\left. + \sum_{j=1}^{i-1}\frac{\partial \alpha_{i-1}}{\partial \widehat{y}_m^{(j-1)}}\widehat{y}_m^{(j)}\right]\right\}. \tag{4.10}$$

Specify

$$\alpha_i = \frac{1}{z_i}\left\{ -z_i z_{i+1} + z_i k_i v_{\ell,1} + z_i\left[ \frac{\partial \alpha_{i-1}}{\partial \widehat{y}}\left(\xi_{12} + v_{\ell,2}\widetilde{\phi}_\ell + \overline{\omega}^T\widetilde{\Theta}\right) + \frac{\partial \alpha_{i-1}}{\partial \xi}\left(A_0\xi + \overline{k}\widehat{y}\right)\right.\right.$$
$$\left. + \frac{\partial \alpha_{i-1}}{\partial \widetilde{\Theta}}\dot{\widetilde{\Theta}}\sum_{j=1}^{\ell}\frac{\partial \alpha_{i-1}}{\partial v_j}\left(A_0 v_j + e_r\sigma_j\right) + \sum_{j=1}^{i-1}\frac{\partial \alpha_{i-1}}{\partial \widehat{y}_m^{(j-1)}}\widehat{y}_m^{(j)}\right] \tag{4.11}$$
$$\left. - c_i z_i^2 - d_i\left(\frac{\partial \alpha_{i-1}}{\partial \widehat{y}}\right)^2 z_i^2 - g_i\left(\frac{\partial \alpha_{i-1}}{\partial \widehat{y}}\right)^2 z_i^2\right\}.$$

The derivative of $V_i$ becomes

$$\dot{V}_i = -\sum_{j=1}^{i-1}\left( c_j z_j^2 + d_j\left(\frac{\partial \alpha_{j-1}}{\partial \widehat{y}}\right)^2 z_j^2 + g_j\left(\frac{\partial \alpha_{j-1}}{\partial \widehat{y}}\right)^2 z_j^2\right) + \tau_i\Phi - \sum_{j=1}^{i-1} z_j\frac{\partial \alpha_{j-1}}{\partial \widehat{y}}\left(\varepsilon_{\widehat{z}_{12}} + \widehat{d}_{si_1} + \dot{\widehat{d}}_y\right), \tag{4.12}$$

where $\tau_i\Phi = \tau_1\Phi - \sum_{j=2}^{i-1}(\partial \alpha_{j-1}/\partial \widehat{y})(z_j v_{\ell,1}\Phi_\ell + z_j\overline{\omega}^T\Phi)$.

*Step 3.* With respect to the new set of coordinates (4.4), the third equation of (4.3) can be written as

$$\dot{z}_r = -k_r v_{\ell,1} + w_{1\ell} + w_{2\ell}\widehat{u} - \left[ \frac{\partial \alpha_{r-1}}{\partial \widehat{y}}\left(\xi_{12} + v_{\ell,2}\phi_\ell + \overline{\omega}^T\Theta + \varepsilon_{\widehat{z}_{12}} + \widehat{d}_{si_1} + \dot{\widehat{d}}_y\right) + \frac{\partial \alpha_{r-1}}{\partial \xi}\left(A_0\xi + \overline{k}\widehat{y}\right)\right.$$
$$\left. + \frac{\partial \alpha_{r-1}}{\partial \widetilde{\Theta}}\dot{\widetilde{\Theta}}\sum_{j=1}^{\ell}\frac{\partial \alpha_{r-1}}{\partial v_j}\left(A_0 v_j + e_r\sigma_j\right) + \sum_{j=1}^{r-1}\frac{\partial \alpha_{r-1}}{\partial \widehat{y}_m^{(j-1)}}\widehat{y}_m^{(j)}\right]. \tag{4.13}$$

The overall Lyapunov function may now be chosen as

$$V_r = \sum_{j=1}^{r-1} V_j + \frac{1}{2} z_r^2 + \frac{1}{2} \Phi^T \Gamma^{-1} \Phi + \sum_{j=1}^{r} \frac{1}{4d_j} \varepsilon^T P \varepsilon, \tag{4.14}$$

where $\Gamma$ is a symmetric positive definite matrix, that is, $\Gamma = \Gamma^T > 0$. With the definition of state estimated error $\varepsilon$, we can obtain that

$$\begin{aligned} \dot{V}_r = \sum_{j=1}^{r-1} \dot{V}_j + z_r \Bigg\{ & -k_r v_{\ell,1} + w_{1\ell} + w_{2\ell} \widehat{u} - \Bigg[ \frac{\partial \alpha_{r-1}}{\partial \widehat{y}} \left( \xi_{12} + v_{\ell,2} \phi_\ell + \overline{\omega}^T \Theta + \varepsilon_{\widehat{z}_{12}} + \widehat{d}_{si_1} + \dot{\widehat{d}}_y \right) \\ & + \frac{\partial \alpha_{r-1}}{\partial \xi} \left( A_0 \xi + \overline{k} \widehat{y} \right) + \frac{\partial \alpha_{r-1}}{\partial \widetilde{\Theta}} \dot{\widetilde{\Theta}} \sum_{j=1}^{\ell} \frac{\partial \alpha_{r-1}}{\partial v_j} \left( A_0 v_j + e_r \sigma_j \right) \\ & + \sum_{j=1}^{r-1} \frac{\partial \alpha_{r-1}}{\partial \widehat{y}_m^{(j-1)}} \widehat{y}_m^{(j)} \Bigg] \Bigg\} \\ & + \dot{\Phi}^T \Gamma^{-1} \Phi - \sum_{j=1}^{r} \frac{1}{4d_j} \varepsilon^T \varepsilon + \sum_{j=1}^{r} \frac{1}{4d_j} \left( \varepsilon^T P \Delta + \Delta^T P \varepsilon \right). \end{aligned} \tag{4.15}$$

Specify the control input as

$$\begin{aligned} \widehat{u} = \frac{1}{z_r w_{2\ell}} \Bigg\{ & z_r k_r v_{\ell,1} - z_r w_{1\ell} + z_r \Bigg[ \frac{\partial \alpha_{r-1}}{\partial \widehat{y}} \left( \xi_{12} + v_{\ell,2} \widetilde{\phi}_\ell + \overline{\omega}^T \widetilde{\Theta} \right) + \frac{\partial \alpha_{r-1}}{\partial \xi} \left( A_0 \xi + \overline{k} \widehat{y} \right) \\ & + \frac{\partial \alpha_{r-1}}{\partial \widetilde{\Theta}} \dot{\widetilde{\Theta}} \sum_{j=1}^{\ell} \frac{\partial \alpha_{r-1}}{\partial v_j} \left( A_0 v_j + e_r \sigma_j \right) + \sum_{j=1}^{r-1} \frac{\partial \alpha_{r-1}}{\partial \widehat{y}_m^{(j-1)}} \widehat{y}_m^{(j)} \Bigg] \\ & - c_r z_r^2 - d_r \left( \frac{\partial \alpha_{r-1}}{\partial \widehat{y}} \right)^2 z_r^2 - g_r \left( \frac{\partial \alpha_{r-1}}{\partial \widehat{y}} \right)^2 z_r^2 + z_r \widehat{u}_{\widehat{R}} \Bigg\}, \end{aligned} \tag{4.16}$$

where $\widehat{u}_{\widehat{R}}$ is an addition input which will be used to target on rejection of uncertainties.

Substituting (4.16) into $\dot{V}_r$, we have

$$\begin{aligned} \dot{V}_r = & -\sum_{j=1}^{r} \left( c_j z_j^2 + d_j \left( \frac{\partial \alpha_{j-1}}{\partial \widehat{y}} \right)^2 z_j^2 + g_j \left( \frac{\partial \alpha_{j-1}}{\partial \widehat{y}} \right)^2 z_j^2 \right) + \tau_{r-1} \Phi - \frac{\partial \alpha_{r-1}}{\partial \widehat{y}} \left( z_r v_{\ell,1} \Phi_\ell + z_r \overline{\omega}^T \Phi \right) + z_r \widehat{u}_{\widehat{R}} \\ & - \sum_{j=1}^{r} z_j \frac{\partial \alpha_{j-1}}{\partial \widehat{y}} \left( \varepsilon_{\widehat{z}_{12}} + \widehat{d}_{si_1} + \dot{\widehat{d}}_y \right) + \dot{\Phi}^T \Gamma^{-1} \Phi - \sum_{j=1}^{r} \frac{1}{4d_j} \varepsilon^T \varepsilon + \sum_{j=1}^{r} \frac{1}{4d_j} \left( \varepsilon^T P \Delta + \Delta^T P \varepsilon \right). \end{aligned} \tag{4.17}$$

Write $\tau_r\Phi = \tau_{r-1}\Phi - (\partial\alpha_{r-1}/\partial\widehat{y})(z_r v_{\ell,1}\Phi_\ell + z_r\overline{\omega}^T\Phi)$ and we arrive at

$$\begin{aligned}\dot{V}_r = & -\sum_{j=1}^{r}\left(c_j z_j^2 + d_j\left(\frac{\partial\alpha_{j-1}}{\partial\widehat{y}}\right)^2 z_j^2 + g_j\left(\frac{\partial\alpha_{j-1}}{\partial\widehat{y}}\right)^2 z_j^2\right) + \left(\tau_r + \dot{\Phi}^T\Gamma^{-1}\right)\Phi + z_r\widehat{u}_{\widehat{R}} \\ & - \sum_{j=1}^{r} z_j\frac{\partial\alpha_{j-1}}{\partial\widehat{y}}\left(\varepsilon_{\widehat{z}_{12}} + \widehat{d}_{si_1} + \dot{\widehat{d}}_y\right) - \sum_{j=1}^{r}\frac{1}{4d_j}\varepsilon^T\varepsilon + \sum_{j=1}^{r}\frac{1}{4d_j}\left(\varepsilon^T P\Delta + \Delta^T P\varepsilon\right).\end{aligned} \tag{4.18}$$

From (4.18), we may specify the parameter update law in order to cancel the term $(\tau_r + \dot{\Phi}^T\Gamma^{-1})\Phi$. To guarantee the estimated parameters will always lie within allowable region $w$, a projected parametric update law will be specified as

$$\dot{\widetilde{\Theta}} = \begin{cases}\Gamma\tau_r^T & \text{if } \widetilde{\Theta} \in w^0, \\ P_R\left(\Gamma\tau_r^T\right) & \text{if } \widehat{\Theta} \in \partial w,\ \tau_r\Gamma\widetilde{\Theta}_{\text{perp}} > 0,\end{cases} \tag{4.19}$$

where $w$ is the allowable parameter variation set (compact and convex) with its interior and boundary denoted by $w^0$ and $\partial w$, respectively. If the current estimated parameter vector lies within the allowable parameter variation set, normal update law is employed. If the current estimated parameter vector lies on the boundary of the allowable parameter variation set, projected update law denoted by $P_R(\cdot)$ is employed to prevent the parameter vector from leaving the variation set. With (4.19), (4.18) can be written as

$$\begin{aligned}\dot{V}_r = & -\sum_{j=1}^{r}\left(c_j z_j^2 + g_j\left(\frac{\partial\alpha_{j-1}}{\partial\widehat{y}}\right)^2 z_j^2\right) - \sum_{j=1}^{r} d_j\left(\frac{\partial\alpha_{j-1}}{\partial\widehat{y}} z_i + \frac{1}{2d_j}\varepsilon_{\widehat{z}_{12}}\right)^2 + z_r\widehat{u}_{\widehat{R}} \\ & - \sum_{j=1}^{r} z_j\frac{\partial\alpha_{j-1}}{\partial\widehat{y}}\left(\widehat{d}_{si_1} + \dot{\widehat{d}}_y\right) - \sum_{j=1}^{r}\frac{1}{4d_j}\left(\varepsilon^2_{\widehat{z}_{11}} + \varepsilon^2_{\widehat{z}_{13}} + \cdots + \varepsilon^2_{\widehat{z}_{1r}}\right) + \sum_{j=1}^{r}\frac{1}{4d_j}\left(\varepsilon^T P\Delta + \Delta^T P\varepsilon\right) \\ \leq & -\sum_{j=1}^{r}\left(c_j z_j^2 + g_j\left(\frac{\partial\alpha_{j-1}}{\partial\widehat{y}}\right)^2 z_j^2\right) - \sum_{j=1}^{r} d_j\left(\frac{\partial\alpha_{j-1}}{\partial\widehat{y}} z_j + \frac{1}{2d_j}\varepsilon_{\widehat{z}_{12}}\right)^2 + z_r\widehat{u}_{\widehat{R}} \\ & - \sum_{j=1}^{r} z_j\frac{\partial\alpha_{j-1}}{\partial\widehat{y}}\left|\widehat{d}_{si_1} + \dot{\widehat{d}}_y\right| - \sum_{j=1}^{r}\frac{1}{4d_j}\left(\varepsilon^2_{\widehat{z}_{11}} + \varepsilon^2_{\widehat{z}_{13}} + \cdots + \varepsilon^2_{\widehat{z}_{1r}}\right) + \sum_{j=1}^{r}\frac{1}{4d_j}\left(\varepsilon^T P\Delta + \Delta^T P\varepsilon\right).\end{aligned} \tag{4.20}$$

Add and subtract terms $\sum_{j=1}^{r}(1/4g_j)|\hat{d}_{si_1}+\dot{\hat{d}}_y|^2$; we have

$$\begin{aligned}\dot{V}_r \le & -\sum_{j=1}^{r}c_j z_j^2-\sum_{j=1}^{r}d_j\left(\frac{\partial\alpha_{j-1}}{\partial\hat{y}}z_j+\frac{1}{2d_j}\varepsilon_{\hat{z}_{12}}\right)^2+z_r\hat{u}_{\hat{R}}\\ & -\sum_{j=1}^{r}g_j\left(\frac{\partial\alpha_{j-1}}{\partial\hat{y}}\right)^2z_j^2-\sum_{j=1}^{r}z_j\frac{\partial\alpha_{j-1}}{\partial\hat{y}}\left|\hat{d}_{si_1}+\dot{\hat{d}}_y\right|-\sum_{j=1}^{r}\frac{1}{4g_j}\left|\hat{d}_{si_1}+\dot{\hat{d}}_y\right|^2\\ & +\sum_{j=1}^{r}\frac{1}{4g_j}\left|\hat{d}_{si_1}+\dot{\hat{d}}_y\right|^2+\sum_{j=1}^{r}\frac{1}{4d_j}\left(\varepsilon^T P\Delta+\Delta^T P\varepsilon\right)-\sum_{j=1}^{r}\frac{1}{4d_j}\left(\varepsilon^2_{\hat{z}_{11}}+\varepsilon^2_{\hat{z}_{13}}+\cdots+\varepsilon^2_{\hat{z}_{1r}}\right).\end{aligned}\tag{4.21}$$

Moreover, we obtain

$$\begin{aligned}\dot{V}_i \le & -\sum_{j=1}^{r}c_j z_j^2-\sum_{j=1}^{r}d_j\left(\frac{\partial\alpha_{j-1}}{\partial\hat{y}}z_j+\frac{1}{2d_j}\varepsilon_{\hat{z}_{12}}\right)^2-\sum_{j=1}^{r}g_j\left(\frac{\partial\alpha_{j-1}}{\partial\hat{y}}z_j+\frac{1}{2g_j}\left|\hat{d}_{si_1}+\dot{\hat{d}}_y\right|\right)^2\\ & +\sum_{j=1}^{r}\frac{1}{4g_j}\left|\hat{d}_{si_1}+\dot{\hat{d}}_y\right|^2+\sum_{j=1}^{r}\frac{1}{4d_i}\left(\varepsilon^T P\Delta+\Delta^T P\varepsilon\right)-\sum_{j=1}^{r}\frac{1}{4d_j}\left(\varepsilon^2_{\hat{z}_{11}}+\varepsilon^2_{\hat{z}_{13}}+\cdots+\varepsilon^2_{\hat{z}_{1r}}\right)+z_r\hat{u}_{\hat{R}}.\end{aligned}\tag{4.22}$$

As shown in Figure 1, the tracking error $Z_1(\tilde{s})$ and the control input $\hat{U}_{\hat{R}}(\tilde{s})$ are related by

$$\hat{U}_{\hat{R}}(\tilde{s})=-\hat{R}(\tilde{s})\hat{C}(\tilde{s})Z_1(\tilde{s}),\tag{4.23}$$

where we have chosen $\hat{R}(\tilde{s})$ as a low-order and attenuated-type internal model filter, that is,

$$\hat{R}(\tilde{s})=\prod_{i=1}^{k}\frac{\tilde{s}^2+2\zeta_i\omega_{ni}\tilde{s}+\omega_{ni}^2}{\tilde{s}^2+2\xi_i\omega_{ni}\tilde{s}+\omega_{ni}^2},\tag{4.24}$$

where $k$ is the number of periodic frequencies to be rejected, $\omega_{ni}$ is determined based on the $i$th disturbance frequency in rad/rev, and $\xi_i$ and $\zeta_i$ are two damping ratios that satisfy $0<\xi_i<\zeta_i<1$. We can adjust the gain of $\hat{R}(\tilde{s})$ at those periodic frequencies by varying the values of $\xi_i$ and $\zeta_i$.

**Theorem 4.1.** *Consider the control law of* (4.16) *and* (4.23) *applied to a nonlinear system with unmodeled dynamics, parameter uncertainty and subject to output disturbance as given by* (3.1). *Assume that* $\hat{y}_m, \dot{\hat{y}}_m, \ldots, \hat{y}_m^{(r)}$ *(where* $r$ *is the relative degree) and* $\hat{d}_y, \dot{\hat{d}}_y, \ldots, \hat{d}_y^{(r)}$ *are known and bounded,* $\hat{d}_{si_1}^{(r-1)}$, $\hat{d}_{si_2}^{(r-2)}, \ldots,$ $\dot{\hat{d}}_{si_{r-1}}$ *are sufficiently smooth,* $f$, $g$, $h$, $L_f^r h$, $L_g L_f^{r-1}h$ *are Lipschitz continuous functions, at least one column of* $\overline{W}(\hat{y})$ *is bounded away from zero. Furthermore, suppose that a loop-shaping filter* $\hat{C}(\tilde{s})$ *is designed such that the feedback system is stable. Then the modified parameter update law as given by* (4.19) *yields the bounded tracking error.*

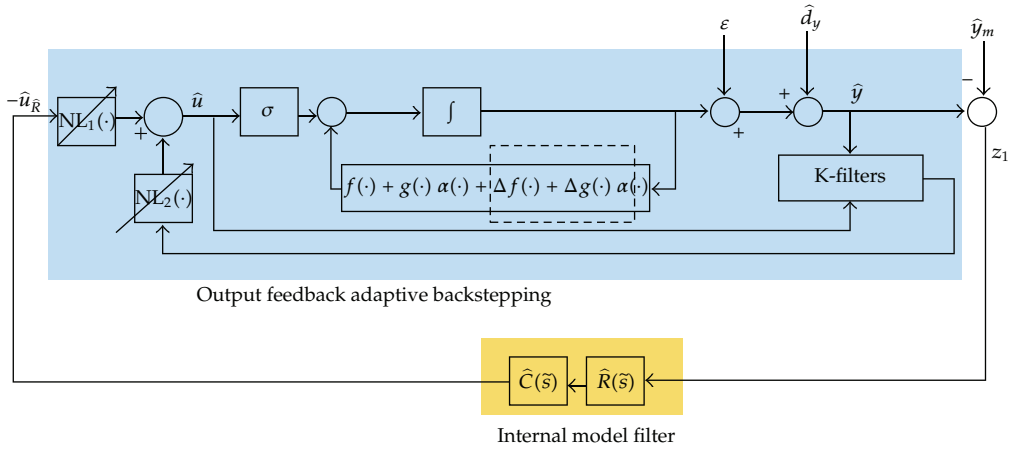


**Figure 1:** The control configuration for the proposed spatial domain adaptive control system.

*Proof. Step 1* (show that only $\tilde{\Theta} \in w^0$ needs to be considered).

Denote by $\dot{\tilde{\Theta}}_{\text{perp}}$ the component of $\dot{\tilde{\Theta}}$ perpendicular to the tangent plane at $\tilde{\Theta}$ so that $\dot{\tilde{\Theta}} = P_R(\dot{\tilde{\Theta}}) + \dot{\tilde{\Theta}}_{\text{perp}}$. Since $\Theta \in w$ and $w$ is convex, we have $(\tilde{\Theta} - \Theta)^T \dot{\tilde{\Theta}}_{\text{perp}} \geq 0$. Choose Lyapunov function $V(\Phi) = \Phi^T\Phi$ and use the parameter update law as defined in (4.19). When $\tilde{\Theta} \in w^0$, we have $\dot{V} = -\Phi^T\dot{\tilde{\Theta}}$. When $\tilde{\Theta} \in \partial w$, we have

$$\dot{V} = -\Phi^T P_R\left(\dot{\tilde{\Theta}}\right) = -\Phi^T\left(\dot{\tilde{\Theta}} - \dot{\tilde{\Theta}}_{\text{perp}}\right) = -\Phi^T\dot{\tilde{\Theta}} + \Phi^T\dot{\tilde{\Theta}}_{\text{perp}} \leq -\Phi^T\dot{\tilde{\Theta}}, \tag{4.25}$$

where we use the fact that

$$\Phi^T\dot{\tilde{\Theta}}_{\text{perp}} = \left(\Theta - \tilde{\Theta}\right)^T\dot{\tilde{\Theta}}_{\text{perp}} = -\left(\tilde{\Theta} - \Theta\right)^T\dot{\tilde{\Theta}}_{\text{perp}} \leq 0. \tag{4.26}$$

Thus, we only have to consider the scenario corresponding to $\tilde{\Theta} \in w^0$ in the sequel.

*Step 2*. Substituting (4.23) back into (4.22), we have

$$\begin{aligned}\dot{V}_r \leq & -\sum_{j=1}^{r} c_j z_j^2 - \sum_{j=1}^{r} d_j\left(\frac{\partial \alpha_{j-1}}{\partial \hat{y}} z_j + \frac{1}{2d_j}\varepsilon_{\hat{z}_{12}}\right)^2 - \sum_{j=1}^{r} g_j\left(\frac{\partial \alpha_{j-1}}{\partial \hat{y}} z_j + \frac{1}{2g_j}\left|\hat{d}_{si_1} + \dot{\hat{d}}_y\right|\right)^2 \\ & + \sum_{j=1}^{r}\frac{1}{4g_j}\left|\hat{d}_{si_1} + \dot{\hat{d}}_y\right|^2 + \sum_{j=1}^{r}\frac{1}{4d_j}\left(\varepsilon^T P\Delta + \Delta^T P\varepsilon\right) \\ & - \sum_{j=1}^{r}\frac{1}{4d_j}\left(\varepsilon^2_{\hat{z}_{11}} + \varepsilon^2_{\hat{z}_{13}} + \cdots + \varepsilon^2_{\hat{z}_{1r}}\right) - z_r\hat{R}(\tilde{s})\hat{C}(\tilde{s})z_1.\end{aligned} \tag{4.27}$$

Using the definition of tracking error $z_1 = \hat{y} - \hat{y}_m = (\overline{z}_{11} - \hat{y}_m) + \varepsilon_{\hat{z}_{11}} - \hat{d}_y$, (4.27) can be

written as

$$\begin{aligned}\dot{V}_r \leq & -\sum_{j=1}^{r} c_j z_j^2 - \sum_{j=1}^{r} d_j \left( \frac{\partial \alpha_{j-1}}{\partial \widehat{y}} z_j + \frac{1}{2d_j} \varepsilon_{\hat{z}_{12}} \right)^2 - \sum_{j=1}^{r} g_j \left( \frac{\partial \alpha_{j-1}}{\partial \widehat{y}} z_j + \frac{1}{2g_j} \left| \widehat{d}_{si_1} + \dot{\widehat{d}}_y \right| \right)^2 \\ & - \sum_{j=1}^{r} \frac{1}{4d_j} \left( \varepsilon^2_{\hat{z}_{11}} + \varepsilon^2_{\hat{z}_{13}} + \cdots + \varepsilon^2_{\hat{z}_{1r}} \right) + \sum_{j=1}^{r} \frac{1}{4g_j} \left| \widehat{d}_{si_1} + \dot{\widehat{d}}_y \right|^2 + \sum_{j=1}^{r} \frac{1}{4d_j} \left( \varepsilon^T P \Delta + \Delta^T P \varepsilon \right) \\ & + \left| z_r \widehat{R}(\widetilde{s}) \widehat{C}(\widetilde{s}) \left( \overline{z}_{11} - \widehat{y}_m \right) \right| + \left| z_r \widehat{R}(\widetilde{s}) \widehat{C}(\widetilde{s}) \left( \varepsilon_{\hat{z}_{11}} - \widehat{d}_y \right) \right|. \end{aligned} \tag{4.28}$$

Use the following equality:

$$\widehat{z}_r \widehat{R}(\widetilde{s}) \widehat{C}(\widetilde{s}) \left( \varepsilon_{\hat{z}_{11}} - \widehat{d}_y \right) \leq \gamma^2 \widehat{z}_r^2 + \left( \frac{1}{2\gamma} \widehat{R}(\widetilde{s}) \widehat{C}(\widetilde{s}) \left( \varepsilon_{\hat{z}_{11}} - \widehat{d}_y \right) \right)^2, \quad \gamma > 0 \text{ is designable.} \tag{4.29}$$

Equation (4.28) becomes

$$\begin{aligned}\dot{V}_r \leq & -\sum_{j=1}^{r-1} c_j z_j^2 - c_r' z_r^2 - \sum_{j=1}^{r} d_j \left( \frac{\partial \alpha_{j-1}}{\partial \widehat{y}} z_j + \frac{1}{2d_j} \varepsilon_{\hat{z}_{12}} \right)^2 - \sum_{j=1}^{r} g_j \left( \frac{\partial \alpha_{j-1}}{\partial \widehat{y}} z_j + \frac{1}{2g_j} \left| \widehat{d}_{si_1} + \dot{\widehat{d}}_y \right| \right)^2 \\ & + \sum_{j=1}^{r} \frac{1}{4g_j} \left| \widehat{d}_{si_1} + \dot{\widehat{d}}_y \right|^2 + \sum_{j=1}^{r} \frac{1}{4d_j} \left( \varepsilon^T P \Delta + \Delta^T P \varepsilon \right) + \left| z_r \widehat{R}(\widetilde{s}) \widehat{C}(\widetilde{s}) \left( \overline{z}_{11} - \widehat{y}_m \right) \right| \\ & + \left( \frac{1}{2\gamma} \widehat{R}(\widetilde{s}) \widehat{C}(\widetilde{s}) \left( \varepsilon_{\hat{z}_{11}} - \widehat{d}_y \right) \right)^2 - \sum_{j=1}^{r} \frac{1}{4d_j} \left( \varepsilon^2_{\hat{z}_{11}} + \varepsilon^2_{\hat{z}_{13}} + \cdots + \varepsilon^2_{\hat{z}_{1r}} \right), \end{aligned} \tag{4.30}$$

where $c_r' = c_r - \gamma^2 > 0$. Moreover, the positive designable parameters $c_i$ can be written as

$$\begin{aligned} c_j &= C_j + h_j, \quad j = 1, \ldots, r-1, \\ c_r' &= C_r + h_r, \end{aligned} \tag{4.31}$$

where $C_j$, $C_r$ and $h_j$, $h_r > 0$. Thus, (4.30) can be written as

$$\begin{aligned}\dot{V}_r \leq & -\sum_{j=1}^{r-1} (C_j + h_j) z_j^2 - (C_r + h_r) z_r^2 - \sum_{j=1}^{r} d_j \left( \frac{\partial \alpha_{j-1}}{\partial \widehat{y}} z_j + \frac{1}{2d_j} \varepsilon_{\hat{z}_{12}} \right)^2 \\ & - \sum_{j=1}^{r} g_j \left( \frac{\partial \alpha_{j-1}}{\partial \widehat{y}} z_j + \frac{1}{2g_j} \left| \widehat{d}_{si_1} + \dot{\widehat{d}}_y \right| \right)^2 - \sum_{j=1}^{r} \frac{1}{4d_j} \left( \varepsilon^2_{\hat{z}_{11}} + \varepsilon^2_{\hat{z}_{13}} + \cdots + \varepsilon^2_{\hat{z}_{1r}} \right) \\ & + \sum_{j=1}^{r} \frac{1}{4g_j} \left| \widehat{d}_{si_1} + \dot{\widehat{d}}_y \right|^2 + \sum_{j=1}^{r} \frac{1}{4d_j} \left( \varepsilon^T P \Delta + \Delta^T P \varepsilon \right) + \left| z_r \widehat{R}(\widetilde{s}) \widehat{C}(\widetilde{s}) \left( \overline{z}_{11} - \widehat{y}_m \right) \right| \\ & + \left( \frac{1}{2\gamma} \widehat{R}(\widetilde{s}) \widehat{C}(\widetilde{s}) \left( \varepsilon_{\hat{z}_{11}} - \widehat{d}_y \right) \right)^2. \end{aligned} \tag{4.32}$$

Utilizing the fact that

$$\left(\sqrt{h_1}|z_1| - \sqrt{h_r}|z_r|\right)^2 = z_1^2 + h_r z_r^2 - \sqrt{h_1 h_r}\left|z_r(\overline{z}_{11} - \widehat{y}_m) + z_r\left(\varepsilon_{\hat{z}_{11}} - \widehat{d}_y\right)\right|, \tag{4.33}$$

we have

$$\begin{aligned}
\dot{V}_r \le & -\sum_{j=2}^{r-1}(C_j + h_j)z_j^2 - C_1 z_1^2 - C_r z_r^2 \\
& - \left(\sqrt{h_1}|z_1| - \sqrt{h_r}|z_r|\right)^2 - \sqrt{h_1 h_r}\left|z_r(\overline{z}_{11} - \widehat{y}_m) + z_r\left(\varepsilon_{\hat{z}_{11}} - \widehat{d}_y\right)\right| \\
& - \sum_{j=1}^{r} d_j\left(\frac{\partial \alpha_{j-1}}{\partial \widehat{y}} z_j + \frac{1}{2d_j}\varepsilon_{\hat{z}_{12}}\right)^2 - \sum_{j=1}^{r} g_j\left(\frac{\partial \alpha_{j-1}}{\partial \widehat{y}} z_j + \frac{1}{2g_j}\left|\widehat{d}_{si_1} + \dot{\widehat{d}}_y\right|\right)^2 \\
& - \sum_{j=1}^{r}\frac{1}{4d_j}\left(\varepsilon_{\hat{z}_{11}}^2 + \varepsilon_{\hat{z}_{13}}^2 + \cdots + \varepsilon_{\hat{z}_{1r}}^2\right) + \sum_{j=1}^{r}\frac{1}{4g_j}\left|\widehat{d}_{si_1} + \dot{\widehat{d}}_y\right|^2 + \sum_{j=1}^{r}\frac{1}{4d_j}\left(\varepsilon^T P\Delta + \Delta^T P\varepsilon\right) \\
& + \left|z_r \widehat{R}(\widetilde{s})\widehat{C}(\widetilde{s})(\overline{z}_{11} - \widehat{y}_m)\right| + \left(\frac{1}{2\gamma}\widehat{R}(\widetilde{s})\widehat{C}(\widetilde{s})\left(\varepsilon_{\hat{z}_{11}} - \widehat{d}_y\right)\right)^2.
\end{aligned} \tag{4.34}$$

To design $h_1, \ldots, h_r$ (or $c_1, \ldots, c_r$), $d_j$ and $g_j$ such that

$$\begin{aligned}
& -\sum_{j=1}^{r} h_j z_j^2 - \sum_{j=1}^{r} d_j\left(\frac{\partial \alpha_{j-1}}{\partial \widehat{y}} z_j + \frac{1}{2d_j}\varepsilon_{\hat{z}_{12}}\right)^2 - \sum_{j=1}^{r} g_j\left(\frac{\partial \alpha_{j-1}}{\partial \widehat{y}} z_j + \frac{1}{2g_j}\left|\widehat{d}_{si_1} + \dot{\widehat{d}}_y\right|\right)^2 \\
& - \sum_{j=1}^{r}\frac{1}{4d_j}\left(\varepsilon_{\hat{z}_{11}}^2 + \varepsilon_{\hat{z}_{13}}^2 + \cdots + \varepsilon_{\hat{z}_{1r}}^2\right) - \left(\sqrt{h_1}|z_1| - \sqrt{h_r}|z_r|\right)^2 \\
& - \sqrt{h_1 h_r}\left|z_r(\overline{z}_{11} - \widehat{y}_m) + z_r\left(\varepsilon_{\hat{z}_{11}} - \widehat{d}_y\right)\right| + \left|z_r \widehat{R}(\widetilde{s})\widehat{C}(\widetilde{s})(\overline{z}_{11} - \widehat{y}_m)\right| \le 0,
\end{aligned} \tag{4.35}$$

we arrive at

$$\dot{V}_r \le -\sum_{j=1}^{r} C_j z_j^2 + \left(\frac{1}{2\gamma}\widehat{R}(\widetilde{s})\widehat{C}(\widetilde{s})\left(\varepsilon_{\hat{z}_{11}} - \widehat{d}_y\right)\right)^2 + \sum_{j=1}^{r}\frac{1}{4g_j}\left|\widehat{d}_{si_1} + \dot{\widehat{d}}_y\right|^2 + \sum_{j=1}^{r}\frac{1}{4d_j}\left(\varepsilon^T P\Delta + \Delta^T P\varepsilon\right). \tag{4.36}$$

Equation (4.36) implies that

$$\begin{aligned}
\dot{V}_r \le & -\sum_{j=1}^{r} C_j z_j^2 - \left(\frac{1}{2}\Phi^T\Gamma^{-1}\Phi + \sum_{j=1}^{r}\frac{1}{4d_j}\varepsilon^T P\varepsilon\right) + \left(\frac{1}{2}\Phi^T\Gamma^{-1}\Phi + \sum_{j=1}^{r}\frac{1}{4d_j}\varepsilon^T P\varepsilon\right) \\
& + \left(\frac{1}{2\gamma}\widehat{R}(\widetilde{s})\widehat{C}(\widetilde{s})\left(\varepsilon_{\hat{z}_{11}} - \widehat{d}_y\right)\right)^2 + \sum_{j=1}^{r}\frac{1}{4g_j}\left|\widehat{d}_{si_1} + \dot{\widehat{d}}_y\right|^2 \\
& + \sum_{j=1}^{r}\frac{1}{4d_j}\left|\varepsilon^T P\Delta + \Delta^T P\varepsilon\right| \le -2k_v V_r + C,
\end{aligned} \tag{4.37}$$

where $k_v \triangleq \min\{C_1, \ldots C_r, \lambda_{\min}(\Gamma)\}$, $\lambda_{\min}(\Gamma)$ is the smallest eigenvalue of $\Gamma$ and

$$C = \frac{1}{2}\Phi^T\Gamma^{-1}\Phi + \sum_{j=1}^{r}\frac{1}{4d_j}\varepsilon^T P\varepsilon + \left(\frac{1}{2\gamma}\widehat{R}(\widetilde{s})\widehat{C}(\widetilde{s})\left(\varepsilon_{\widehat{z}_{11}} - \widehat{d}_y\right)\right)^2 + \sum_{j=1}^{r}\frac{1}{4g_j}\left|\widehat{d}_{si_1} + \dot{\widehat{d}}_y\right|^2 + \sum_{j=1}^{r}\frac{1}{4d_j}\left|\varepsilon^T P\Delta + \Delta^T P\varepsilon\right| \tag{4.38}$$

is bounded since $\varepsilon_{\widehat{z}_{11}}$, $\widehat{d}_y$ are bounded and $\Phi^T\Gamma^{-1}\Phi$ is bounded due to the parameter update law specified in (4.19). We conclude that

$$V_r \le e^{-2k_v\theta}V_r(0) + \int_0^\theta Ce^{-2k_v(\theta-\tau)}d\tau \le e^{-2k_v\theta}V_r(0) + \left(1 - e^{-2k_v\theta}\right)\frac{C}{2k_v}. \tag{4.39}$$

As $\theta \to \infty$, we have

$$V_r(\infty) \le \frac{C}{2k_v}, \tag{4.40}$$

which implies that the overall system is stable and the bound $C/(2k_v)$ can be decreased by increasing $k_v$ or increasing $\gamma$. By (4.14), this implies that $z$, $\widetilde{\Theta}$, $\varepsilon$ are bounded. Since $z_1 = \widehat{y} - \widehat{y}_m$, $\widehat{y}$ is also bounded. From (3.11), we can see that $\xi$ and $v_1, \ldots, v_\ell$ are bounded since $\overline{W}_f(\widehat{y})$ and $\overline{W}_g(\widehat{y})$ are bounded. Moreover, we conclude that the virtual inputs $\alpha$ are bounded because they consist of bounded terms. Also, $\overline{z}_1$ is bounded from (3.12) and also $\widehat{z}_1$ from the definition of $\varepsilon$. With the ISS assumption and bounded $\widehat{z}_1$, we conclude that the internal dynamics $\widehat{z}_2$ is bounded. Finally, $\widehat{x}$ is bounded by diffeomorphism, that is, $\widehat{x} = T^{-1}(\widehat{z})$. □

## 5. Illustrative Example

For realistic simulation, we set up a simulation configuration as shown in Figure 2, in which the controller and parametric adaptation operate in the $\theta$-domain whereas the open-loop system operates in the time domain. The proposed spatial domain output feedback adaptive control scheme is applied to a reformulated system in spatial domain expressed as

$$\dot{\widehat{x}} = f(\widehat{x}) + g(\widehat{x})\widehat{u} + \widehat{d}_s, \qquad \widehat{y} = h(\widehat{x}) + \widehat{d}_y, \tag{5.1}$$

where

$$f(\widehat{x}) = \begin{bmatrix} -a_1 + \dfrac{\widehat{x}_2}{\widehat{x}_1} \\ -a_0 \end{bmatrix}, \qquad g(\widehat{x}) = \begin{bmatrix} 0 \\ \dfrac{b_0}{\widehat{x}_1} \end{bmatrix}, \qquad h(\widehat{x}) = \widehat{x}_1, \tag{5.2}$$

with $a_0 = 5155$, $a_1 = 1138$, and $b_0 = 140368$. For verification purpose, the output disturbance is assumed to be a low-pass rectangular periodic signal (with amplitude switching between

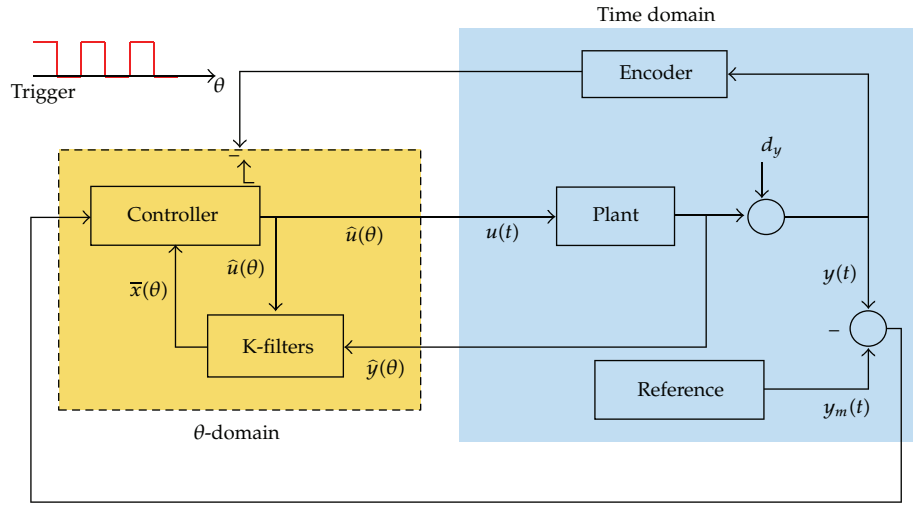


**Figure 2:** The configuration for numerical simulation.

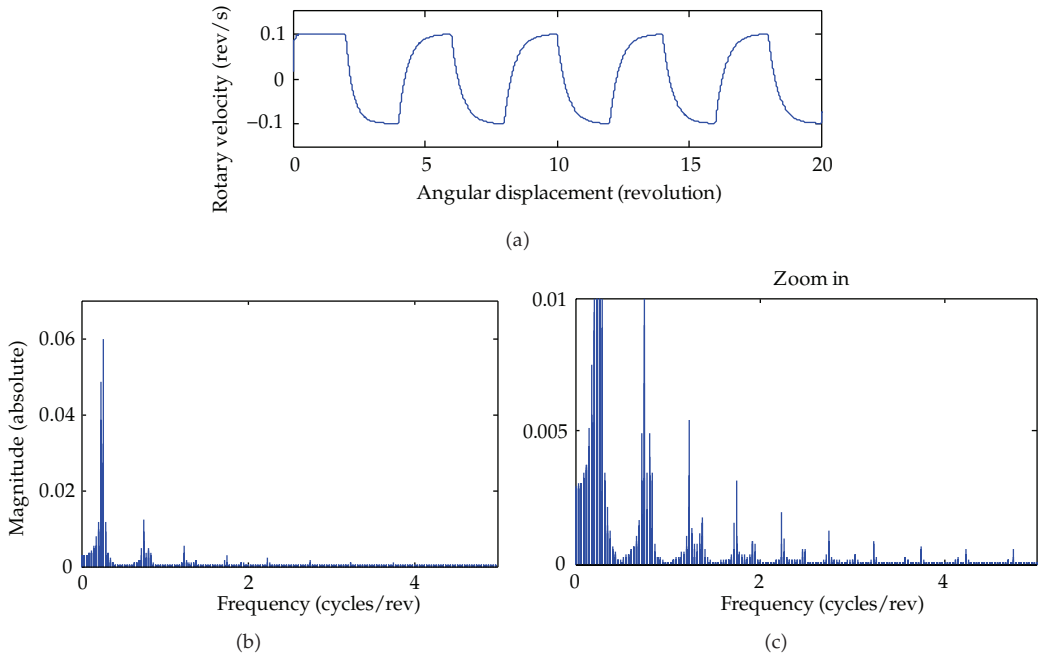


**Figure 3:** The output disturbance and the corresponding frequency spectrum.

−0.1 and 0.1) (see Figure 3), that is,

$$\widehat{d}_y(\theta) = \frac{0.1}{0.0125\widetilde{s}+1}\left[\sum_{l=-\infty}^{\infty}(-1)^l\Pi(\theta-1-l)\right] + \frac{10}{(0.005\widetilde{s}+1)^2}N_0, \tag{5.3}$$

where

$$\Pi(\theta) = \begin{cases} 1 & |\theta| < 1, \\ 0.5 & |\theta| = 1, \\ 0 & \text{otherwise.} \end{cases} \tag{5.4}$$

Note that the disturbance has been low-pass filtered so that it is continuously differentiable. Parameters of the internal model filter are specified to target the fundamental frequency and the first three harmonic frequencies of the periodic disturbance, that is,

$$\widehat{R}(\widetilde{s}) = \prod_{i=1}^{4} \frac{\widetilde{s}^2 + 2\zeta_i \omega_{ni} \widetilde{s} + \omega_{ni}^2}{\widetilde{s}^2 + 2\xi_i \omega_{ni} \widetilde{s} + \omega_{ni}^2}, \tag{5.5}$$

where

$$\begin{gathered} \varsigma_i = 0.2, \qquad \xi_i = 0.0002, \\ \omega_{n1} = 0.25\pi, \qquad \omega_{n2} = 3 \times 0.25\pi, \qquad \omega_{n3} = 5 \times 0.25\pi, \qquad \omega_{n4} = 7 \times 0.25\pi, \end{gathered} \tag{5.6}$$

Furthermore, the stabilizing filter is specified as

$$\widehat{C}(\widetilde{s}) = \frac{100\,000(\widetilde{s}/100 + 1)}{(\widetilde{s}/10\,000 + 1)}. \tag{5.7}$$

The parameters of the $K$-filter are set to $k_1 = 1600$ and $k_2 = 100$. The initial values of the estimated parameters are set to $\widetilde{a}_0 = 1500$, $\widetilde{a}_1 = 500$, and $\widetilde{b}_0 = 1000000$. The allowable parameter variation sets are

$$\begin{aligned} \widetilde{a}_0 &\in \Omega_{\widetilde{a}_0} \triangleq \{\widetilde{a}_0 : 100 \le \widetilde{a}_0 \le 10\,000\}, \\ \widetilde{a}_1 &\in \Omega_{\widetilde{a}_1} \triangleq \{\widetilde{a}_1 : 10 \le \widetilde{a}_1 \le 10\,000\}, \\ \widetilde{b}_0 &\in \Omega_{\widetilde{b}_0} \triangleq \left\{\widetilde{b}_0 : 10\,000 \le \widetilde{b}_0 \le 10\,000\,000\right\}. \end{aligned} \tag{5.8}$$

Note that $d_s(t)$ is set to 0 so that the system performance is not affected by the unstructured uncertainty. Suppose that a variable speed control task demands the system to initially run at 30 rev/s and then speed up to 35 rev/s and finally speed down to 25 rev/s (see Figure 4). To avoid getting infinite value when taking derivative, the reference command is specified to have smooth (instead of instant) change. Figure 5 compares the tracking performance of two scenarios. The figures on the left are for the pure output feedback adaptive backstepping design. The ones on the right are for the proposed output feedback design with internal model control. Without internal model control, the adaptive backstepping design has already shown superb tracking performance. We see that adding the internal model control further reduces the magnitude of the tracking error without noticeable increase in the control input.

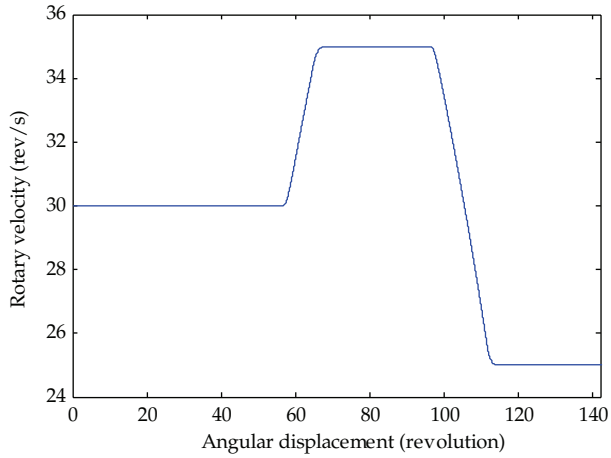


**Figure 4:** The tracking command for a variable speed control task.

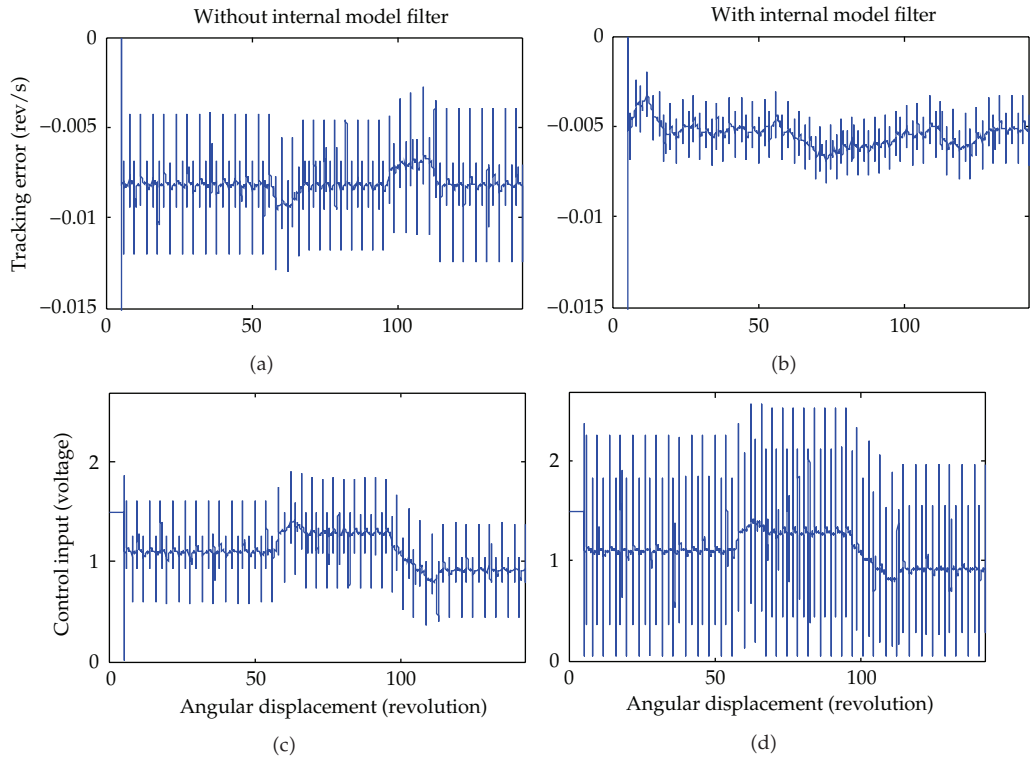


**Figure 5:** Comparison of tracking performance.

## 6. Conclusion

This paper presents the design of a new spatial domain adaptive control system, which can be applied to rotary systems operating at varying speeds and subject to spatially periodic and band-limited disturbances and structured/unstructured parametric uncertainties.

The proposed design integrates two control paradigms, that is, adaptive backstepping and internal model control. The overall output feedback adaptive control system can be shown to be stable and have bounded state estimated error and output tracking error. Feasibility and effectiveness of the proposed design are further justified by a numerical example. Future effort will be dedicated to implementation and verification of the proposed control design to a practical rotary system, for example, a brushless dc-motor-driven control system.

## References

[1] B. A. Francis and W. M. Wonham, "The internal model principle of control theory," *Automatica*, vol. 12, no. 5, pp. 457–465, 1976.

[2] V. O. Nikiforov, "Adaptive non-linear tracking with complete compensation of unknown disturbances," *European Journal of Control*, vol. 4, pp. 132–139, 1998.

[3] Z. Ding, "Adaptive disturbance rejection of nonlinear systems in an extended output feedback form," *IET Control Theory & Applications*, vol. 1, no. 1, pp. 298–303, 2007.

[4] L. Marconi, A. Isidori, and A. Serrani, "Input disturbance suppression for a class of feedforward uncertain nonlinear systems," *Systems & Control Letters*, vol. 45, no. 3, pp. 227–236, 2002.

[5] L. Gentili and L. Marconi, "Robust nonlinear disturbance suppression of a magnetic levitation system," *Automatica*, vol. 39, no. 4, pp. 735–742, 2003.

[6] C. Kravaris, V. Sotiropoulos, C. Georgiou, N. Kazantzis, M. Xiao, and A. J. Krener, "Nonlinear observer design for state and disturbance estimation," *Systems & Control Letters*, vol. 56, no. 11-12, pp. 730–735, 2007.

[7] B. Mahawan and Z.-H. Luo, "Repetitive control of tracking systems with time-varying periodic references," *International Journal of Control*, vol. 73, no. 1, pp. 1–10, 2000.

[8] C. L. Chen, G. T. C. Chiu, and J. Allebach, "Robust spatial-sampling controller design for banding reduction in electrophotographic process," *Journal of Imaging Science and Technology*, vol. 50, no. 6, pp. 530–536, 2006.

[9] C. L. Chen and G. T. C. Chiu, "Spatially periodic disturbance rejection with spatially sampled robust repetitive control," *Journal of Dynamic Systems, Measurement, and Control*, vol. 130, no. 2, pp. 11–21, 2008.

[10] M. Nakano, J. H. She, Y. Mastuo, and T. Hino, "Elimination of position-dependent disturbances in constant-speed-rotation control systems," *Control Engineering Practice*, vol. 4, no. 9, pp. 1241–1248, 1996.

[11] C. L. Chen and Y. H. Yang, "Spatially periodic disturbance rejection for uncertain rotational motion systems using spatial domain adaptive backstepping repetitive control," in *Proceedings of the 33rd Annual Conference of the IEEE Industrial Electronics Society*, pp. 638–643, Taipei, Taiwan, November 2007.

[12] Y. H. Yang and C. L. Chen, "Spatially periodic disturbance rejection using spatial-based output feedback adaptive backstepping repetitive control," in *Proceeding of the American Control Conference*, pp. 4117–4122, 2008.

[13] G. Kreisselmeier, "Adaptive observers with exponential rate of convergence," *IEEE Transactions on Automatic Control*, vol. 22, no. 1, pp. 2–8, 1977.

[14] R. Marino, G. L. Santosuosso, and P. Tomei, "Robust adaptive observers for nonlinear systems with bounded disturbances," *IEEE Transactions on Automatic Control*, vol. 46, no. 6, pp. 967–972, 2001.

[15] S. C. Tong, X. L. He, and H. G. Zhang, "A combined backstepping and small-gain approach to robust adaptive fuzzy output feedback control," *IEEE Transactions on Fuzzy Systems*, vol. 17, no. 5, pp. 1059–1069, 2009.

[16] S. Tong and Y. Li, "Observer-based fuzzy adaptive control for strict-feedback nonlinear systems," *Fuzzy Sets and Systems*, vol. 160, no. 12, pp. 1749–1764, 2009.

[17] S. Tong, C. Li, and Y. Li, "Fuzzy adaptive observer backstepping control for MIMO nonlinear systems," *Fuzzy Sets and Systems*, vol. 160, no. 19, pp. 2755–2775, 2009.

Hindawi Publishing Corporation
Journal of Applied Mathematics
Volume 2012, Article ID 717504, 19 pages
doi:10.1155/2012/717504

*Research Article*

# On Kalman Smoothing for Wireless Sensor Networks Systems with Multiplicative Noises

**Xiao Lu,[1,2] Haixia Wang,[1] and Xi Wang[1]**

[1] *Key Laboratory for Robot & Intelligent Technology of Shandong Province, Shandong University of Science and Technology, Qingdao 266510, China*
[2] *School of Control Science and Engineering, Shandong University, Jinan 250100, China*

Correspondence should be addressed to Xiao Lu, luxiao98@163.com

Received 12 March 2012; Revised 21 May 2012; Accepted 21 May 2012

Academic Editor: Baocang Ding



The paper deals with Kalman (or $H_2$) smoothing problem for wireless sensor networks (WSNs) with multiplicative noises. Packet loss occurs in the observation equations, and multiplicative noises occur both in the system state equation and the observation equations. The Kalman smoothers which include Kalman fixed-interval smoother, Kalman fixedlag smoother, and Kalman fixed-point smoother are given by solving Riccati equations and Lyapunov equations based on the projection theorem and innovation analysis. An example is also presented to ensure the efficiency of the approach. Furthermore, the proposed three Kalman smoothers are compared.

## 1. Introduction

The linear estimation problem has been one of the key research topics of control community according to [1]. As is well known, two indexes are used to investigate linear estimation, one is $H_2$ index, and the other is $H_\infty$ index. Under the performance of $H_2$ index, Kalman filtering [2–4] is an important approach to study linear estimation besides Wiener filtering. In general, Kalman filtering which usually uses state space equation is better than Wiener filtering, since it is recursive, and it can be used to deal with time-variant system [1, 2, 5]. This has motivated many previous researchers to employ Kalman filtering to study linear time variant or linear time-invariant estimation, and Kalman filtering has been a popular and efficient approach for the normal linear system. However, the standard Kalman filtering cannot be directly used in the estimation on wireless sensor networks (WSNs) since packet loss occurs, and sometimes multiplicative noises also occur [6, 7].

Linear estimation for systems with multiplicative noises under $H_2$ index has been studied well in [8, 9]. Reference [8] considered the state optimal estimation algorithm for

singular systems with multiplicative noise, and dynamic noise and noise measurement estimations have been proposed. In [9], we presented the linear filtering for continuous-time systems with time-delayed measurements and multiplicative noises under $H_2$ index.

Wireless sensor networks have been popular these years, and the corresponding estimation problem has attracted many researchers' attention [10–15]. It should be noted that in the above works, only packet loss occurs. Reference [10] which is an important and ground-breaking reference has considered the problem of Kalman filtering of the WSN with intermittent packet loss, and Kalman filter together with the upper and lower bounds of the error covariance is presented. Reference [11] has developed the work of [10], the measurements are divided into two parts which are sent by different channel under different packet loss rate, and the Kalman filter together with the covariance matrix is given. Reference [14] also develops the result of [11], and the stability of the Kalman filter with Markovian packet loss has been given.

However, the above references mainly focus on the linear systems with packet loss, and they cannot be useful when there are multiplicative noises in the system models [6, 7, 16–18]. For the Kalman filtering problem for wireless sensor networks with multiplicative noises, [16–18] give preliminary results, where [16] has given Kalman filter, [17] deals with the Kalman filter for the wireless sensor networks system with two multiplicative noises and two measurements which are sent by different channels and packet-drop rates, and [18] has given the information fusion Kalman filter for wireless sensor networks with packet loss and multiplicative noises.

In this paper, Kalman smoothing problem including fixed-point smoothing [6], fixed-interval smoothing, and fixed-lag smoothing [7] for WSN with packet loss will be studied. Multiplicative noises both occur in the state equation and observation equation, which will extend the result of works of [8] where multiplicative noises only occur in the state equations. Three Kalman smoothers will be given by recursive equations. The smoother error covariance matrices of fixed-interval smoothing and fixed-lag smoothing are given by Riccati equation without recursion, while the smoother error covariance matrix of fixed-point smoothing is given by recursive Riccati equation and recursive Lyapunov equation, which develops the work of [6, 7], where some main theorems with errors on Kalman smoothing are given.

The rest of the paper is organized as follows. In Section 2, we will present the system model and state the problem to be dealt with in the paper. The main results of Kalman smoother will be given in Section 3. In Section 4, a numerical example will be given to show the result of smoothers. Some conclusion will be drawn in Section 5.

## 2. Problem Statement

Consider the following discrete-time wireless sensor network systems with multiplicative noises:

$$\mathbf{x}(t+1) = A\mathbf{x}(t) + B_1\mathbf{x}(t)\mathbf{w}(t) + B_2\mathbf{u}(t), \tag{2.1}$$

$$\overline{\mathbf{y}}(t) = C\mathbf{x}(t) + D\mathbf{x}(t)\mathbf{w}(t) + \mathbf{v}(t), \tag{2.2}$$

$$\mathbf{y}(t) = \gamma(t)\overline{\mathbf{y}}(t), \mathbf{x}(0), \tag{2.3}$$

where $\mathbf{x}(t) \in R^n$ is the state, $\mathbf{y}(t) \in R^p$ is measurement, $\mathbf{u}(t) \in R^r$ is input sequence, $\mathbf{v}(t) \in R^p$ is the white noise of zero means, which is additive noise, and $\mathbf{w}(t) \in R^1$ is the white noise

of zero means, which is multiplicative noise. $A \in \mathcal{R}^{n\times n}$, $B_1 \in \mathcal{R}^{n\times n}$, $B_2 \in \mathcal{R}^{n\times r}$, $C \in \mathcal{R}^{p\times n}$, and $D \in \mathcal{R}^{p\times n}$ are known time-invariant matrices.

*Assumption 2.1.* $\gamma(t)$ $(t \geq 0)$ is Bernoulli random variable with probability distribution

$$p(\gamma(t)) = \begin{cases} \lambda(t), & \gamma(t) = 1, \\ 1 - \lambda(t), & \gamma(t) = 0. \end{cases} \tag{2.4}$$

$\gamma(t)$ is independent of $\gamma(s)$ for $s \neq t$, and $\gamma(t)$ is uncorrelated with $\mathbf{x}(0)$, $\mathbf{u}(t)$, $\mathbf{v}(t)$, and $\mathbf{w}(t)$.

*Assumption 2.2.* The initial states $\mathbf{x}(0)$, $\mathbf{u}(t)$, $\mathbf{v}(t)$, and $\mathbf{w}(t)$ are all uncorrelated white noises with zero means and known covariance matrices, that is,

$$\left\langle \begin{bmatrix} \mathbf{x}(0) \\ \mathbf{u}(t) \\ \mathbf{v}(t) \\ \mathbf{w}(t) \end{bmatrix}, \begin{bmatrix} \mathbf{x}(0) \\ \mathbf{u}(s) \\ \mathbf{v}(s) \\ \mathbf{w}(s) \end{bmatrix} \right\rangle = \begin{bmatrix} \Pi(0) & 0 & 0 & 0 \\ 0 & Q\delta_{t,s} & 0 & 0 \\ 0 & 0 & R\delta_{t,s} & 0 \\ 0 & 0 & 0 & M\delta_{t,s} \end{bmatrix}, \tag{2.5}$$

where $\langle a, b\rangle = \mathcal{E}[ab^*]$, and $\mathcal{E}$ denotes the mathematical expectation.

The Kalman smoothing problem considered in the paper for the system model (2.1)–(2.3) can be stated in the following three cases.

*Problem 1* (fixed-interval smoothing). Given the measurements $\{\mathbf{y}(0), \ldots, \mathbf{y}(N)\}$ and scalars $\{\gamma(0), \ldots, \gamma(N)\}$ for a fixed scalar $N$, find the fixed-interval smoothing estimate $\hat{\mathbf{x}}(t \mid N)$ of $\mathbf{x}(t)$, such that

$$\min \mathcal{E}[\mathbf{x}(t) - \hat{\mathbf{x}}(t \mid N)]' \left[\mathbf{x}(t) - \hat{\mathbf{x}}(t \mid N) \mid \mathbf{y}_0^N, \gamma_0^N, \mathbf{x}(0), \Pi(0)\right], \tag{2.6}$$

where $0 \leq t \leq N$, $\mathbf{y}_0^N \triangleq \{\mathbf{y}(0), \ldots, \mathbf{y}(N)\}$, $\gamma_0^N \triangleq \{\gamma(0), \ldots, \gamma(N)\}$.

*Problem 2* (fixed-lag smoothing). Given the measurements $\{\mathbf{y}(0), \ldots, \mathbf{y}(t)\}$ and scalars $\{\gamma(0), \ldots, \gamma(t)\}$ for a fixed scalar $l$, find the fixed-lag smoothing estimate $\hat{\mathbf{x}}(t - l \mid t)$ of $\mathbf{x}(t - l)$, such that

$$\min \mathcal{E}[\mathbf{x}(t-l) - \hat{\mathbf{x}}(t-l \mid t)]' \left[\mathbf{x}(t-l) - \hat{\mathbf{x}}(t-l \mid t) \mid \mathbf{y}_0^t, \gamma_0^t, \mathbf{x}(0), \Pi(0)\right], \tag{2.7}$$

where $\mathbf{y}_0^t \triangleq [\mathbf{y}(0), \ldots, \mathbf{y}(t)]$, $\gamma_0^t \triangleq [\gamma(0), \ldots, \gamma(t)]$.

*Problem 3* (fixed-point smoothing). Given the measurements $\{\mathbf{y}(0), \ldots, \mathbf{y}(N)\}$ and scalars $\{\gamma(0), \ldots, \gamma(N)\}$ for a fixed time instant $t$, find the fixed-point smoothing estimate $\hat{\mathbf{x}}(t \mid j)$ of $\mathbf{x}(t)$, such that

$$\min \mathcal{E}\left[\mathbf{x}(t) - \hat{\mathbf{x}}(t \mid j)\right]' \left[\mathbf{x}(t) - \hat{\mathbf{x}}(t \mid j) \mid \mathbf{y}_0^j, \gamma_0^j, \mathbf{x}(0), \Pi(0)\right], \tag{2.8}$$

where $0 \leq t < j \leq N$, $\mathbf{y}_0^j \triangleq \{\mathbf{y}(0), \ldots, \mathbf{y}(j)\}$, $\gamma_0^j \triangleq \{\gamma(0), \ldots, \gamma(j)\}$, $j = t+1, t+2, \ldots, N$.

## 3. Main Results

In this section, we will give Kalman fixed-interval smoothing, Kalman fixed-lag smoothing, and Kalman fixed-point smoothing for the system model (2.1)–(2.3) and compare them with each other. Before we give the main result, we first give the Kalman filtering for the system model (2.1)–(2.3) which will be useful in the section. We first give the following definition.

*Definition 3.1.* Given time instants $t$ and $j$, the estimator $\widehat{\xi}(t \mid j)$ is the optimal estimation of $\xi(t)$ given the observation sequences

$$\mathcal{L}\{\mathbf{y}(0),\ldots,\mathbf{y}(t),\mathbf{y}(t+1),\ldots,\mathbf{y}(j);\gamma(0),\ldots,\gamma(t),\gamma(t+1),\ldots,\gamma(j)\}, \tag{3.1}$$

and the estimator $\widehat{\xi}(t)$ is the optimal estimation of $\xi(t)$ given the observation

$$\mathcal{L}\{\mathbf{y}(0),\ldots,\mathbf{y}(t-1);\gamma(0),\ldots,\gamma(t-1)\}. \tag{3.2}$$

*Remark 3.2.* It should be noted that the linear space $\mathcal{L}\{\mathbf{y}(0),\ldots,\mathbf{y}(t-1);\gamma(0),\ldots,\gamma(t-1)\}$ means the linear space $\mathcal{L}\{\mathbf{y}(0),\ldots,\mathbf{y}(t-1)\}$ under the condition that the scalars $\gamma(0),\ldots,\gamma(t-1)$ are known. So is the linear space $\mathcal{L}\{\mathbf{y}(0),\ldots,\mathbf{y}(t),\mathbf{y}(t+1),\ldots,\mathbf{y}(j);\gamma(0),\ldots,\gamma(t),\gamma(t+1),\ldots,\gamma(j)\}$.

Give the following denotations:

$$\widetilde{\mathbf{y}}(t) \triangleq \mathbf{y}(t) - \widehat{\mathbf{y}}(t), \tag{3.3}$$

$$\mathbf{e}(t) \triangleq \mathbf{x}(t) - \widehat{\mathbf{x}}(t), \tag{3.4}$$

$$P(t+1) \triangleq \mathcal{E}\left[\mathbf{e}(t+1)\mathbf{e}^{T}(t+1) \mid \mathbf{y}_0^t, \gamma_0^t\right], \tag{3.5}$$

$$\Pi(t+1) \triangleq \mathcal{E}\left[\mathbf{x}(t+1)\mathbf{x}^{T}(t+1) \mid \mathbf{y}_0^t, \gamma_0^t\right], \tag{3.6}$$

it is clear that $\widetilde{\mathbf{y}}(t)$ is the Kalman filtering innovation sequence for the system (2.1)–(2.3). We now have the following relationships:

$$\widetilde{\mathbf{y}}(t) = \gamma(t)C\mathbf{e}(t) + \gamma(t)D\mathbf{x}(t)\mathbf{w}(t) + \gamma(t)\mathbf{v}(t). \tag{3.7}$$

The following lemma shows that $\{\widetilde{\mathbf{y}}\}$ is the innovation sequence. For the simplicity of discussion, we omitted the $\{\gamma(0),\ldots,\gamma(t-1)\}$ as in Remark 3.2.

**Lemma 3.3.**

$$\{\widetilde{\mathbf{y}}(0),\ldots,\widetilde{\mathbf{y}}(t)\} \tag{3.8}$$

*is the innovation sequence which spans the same linear space consider that*

$$\mathcal{L}\{\mathbf{y}(0),\ldots,\mathbf{y}(t)\}. \tag{3.9}$$

*Proof.* Firstly, from (3.2) in Definition 3.1, we have

$$\hat{\mathbf{y}}(t) = \mathrm{Proj}\{\mathbf{y}(t) \mid \mathbf{y}(0), \ldots, \mathbf{y}(t-1)\}. \tag{3.10}$$

From (3.3) and (3.10), we have $\tilde{\mathbf{y}}(t) \in \mathcal{L}\{\mathbf{y}(0), \ldots, \mathbf{y}(t)\}$ for $t = 0, 1, 2, \ldots$. Thus,

$$\mathcal{L}\{\tilde{\mathbf{y}}(0), \ldots, \tilde{\mathbf{y}}(t)\} \subset \mathcal{L}\{\mathbf{y}(0), \ldots, \mathbf{y}(t)\}. \tag{3.11}$$

Secondly, from inductive method, we have

$$\begin{aligned}
&\mathbf{y}(0) = \tilde{\mathbf{y}}(0) + \mathcal{E}\mathbf{y}(0) \in \mathcal{L}\{\tilde{\mathbf{y}}(0)\},\\
&\mathbf{y}(1) = \tilde{\mathbf{y}}(1) + \mathrm{Proj}\{\mathbf{y}(1) \mid \mathbf{y}(0)\} \in \mathcal{L}\{\tilde{\mathbf{y}}(0), \tilde{\mathbf{y}}(1)\},\\
&\qquad \vdots\\
&\mathbf{y}(t) = \tilde{\mathbf{y}}(t) + \mathrm{Proj}\{\mathbf{y}(t) \mid \mathbf{y}(0), \ldots, \mathbf{y}(t-1)\}\\
&\qquad\quad \in \mathcal{L}\{\tilde{\mathbf{y}}(0), \ldots, \tilde{\mathbf{y}}(t-1)\}.
\end{aligned} \tag{3.12}$$

Thus,

$$\mathcal{L}\{\mathbf{y}(0), \ldots, \mathbf{y}(t)\} \subset \mathcal{L}\{\tilde{\mathbf{y}}(0), \ldots, \tilde{\mathbf{y}}(t)\}. \tag{3.13}$$

So

$$\mathcal{L}\{\mathbf{y}(0), \ldots, \mathbf{y}(t)\} = \mathcal{L}\{\tilde{\mathbf{y}}(0), \ldots, \tilde{\mathbf{y}}(t)\}. \tag{3.14}$$

Next, we show that $\tilde{\mathbf{y}}$ is an uncorrelated sequence. In fact, for any $t, s$ $(t \neq s)$, we can assume that $t > s$ without loss of generality, and it follows from (3.7) that

$$\begin{aligned}
\mathcal{E}\left[\tilde{\mathbf{y}}(t)\tilde{\mathbf{y}}^T(s)\right] = \mathcal{E}\left[\gamma(t)C\mathbf{e}(t)\tilde{\mathbf{y}}^T(s)\right] + \mathcal{E}\left[\gamma(t)D\mathbf{x}(t)\mathbf{w}(t)\tilde{\mathbf{y}}^T(s)\right]\\
+ \mathcal{E}\left[\gamma(t)\mathbf{v}(t)\tilde{\mathbf{y}}^T(s)\right].
\end{aligned} \tag{3.15}$$

Note that $\mathcal{E}[\gamma(t)D\mathbf{x}(t)\mathbf{w}(t)\tilde{\mathbf{y}}^T(s)] = 0$, $\mathcal{E}[\gamma(t)\mathbf{v}(t)\tilde{\mathbf{y}}^T(s)] = 0$. Since $\mathbf{e}(t)$ is the state prediction error, it follows that $\mathcal{E}[\gamma(t)C\mathbf{e}(t)\tilde{\mathbf{y}}^T(s)] = 0$, and thus $\mathcal{E}[\tilde{\mathbf{y}}(t)\tilde{\mathbf{y}}^T(s)] = 0$, which implies that $\tilde{\mathbf{y}}(t)$ is uncorrelated with $\tilde{\mathbf{y}}(s)$. Hence, $\{\tilde{\mathbf{y}}(0), \ldots, \tilde{\mathbf{y}}(t)\}$ is an innovation sequence. This completes the proof of the lemma. □

For the convenience of derivation, we will give the orthogonal projection theorem in form of the next theorem without proof, and readers can refer to [4, 5],

**Theorem 3.4.** *Given the measurements* $\{\mathbf{y}(0),\ldots,\mathbf{y}(t)\}$ *and the corresponding innovation sequence* $\{\tilde{\mathbf{y}}(0),\ldots,\tilde{\mathbf{y}}(t)\}$ *in Lemma 3.3, the projection of the state* $\mathbf{x}$ *can be given as*

$$\begin{aligned}\operatorname{Proj}\{\mathbf{x}\mid \mathbf{y}(0),\ldots,\mathbf{y}(\mathrm{t})\} &= \operatorname{Proj}\{\mathbf{x}\mid \tilde{\mathbf{y}}(0),\ldots,\tilde{\mathbf{y}}(\mathrm{t})\}\\ &= \operatorname{Proj}\{\mathbf{x}\mid \mathbf{y}(0),\ldots,\mathbf{y}(\mathrm{t}-1)\}\\ &\quad+\mathcal{E}\left[x\tilde{\mathbf{y}}^{T}(t)\right]\left[\mathcal{E}\left(\tilde{\mathbf{y}}(t)\tilde{\mathbf{y}}^{T}(t)\right)\right]^{-1}\tilde{\mathbf{y}}(t).\end{aligned}\tag{3.16}$$

According to a reviewer's suggestion, we will give the Kalman filter for the system model (2.1)–(2.3) which has been given in [7]

**Lemma 3.5.** *Consider the system model* (2.1)–(2.3) *with scalars* $\gamma(0),\ldots,\gamma(t+1)$ *and the initial condition* $\hat{\mathbf{x}}(0)=0$*; the Kalman filter can be given as*

$$\begin{aligned}\hat{\mathbf{x}}(t+1\mid t+1) &= \hat{\mathbf{x}}(t+1)+P(t+1)C^{T}\\ &\quad\times\left[CP(t+1)C^{T}+D\Pi(t+1)MD^{T}+R\right]^{-1}\\ &\quad\times\left[\mathbf{y}(t+1)-\gamma(t+1)C\hat{\mathbf{x}}(t+1)\right],\end{aligned}\tag{3.17}$$

$$\begin{aligned}\hat{\mathbf{x}}(t+1) &= A\hat{\mathbf{x}}(t)+K(t)\left[\mathbf{y}(t)-\gamma(t)C\hat{\mathbf{x}}(t)\right],\\ \hat{\mathbf{x}}(0) &= 0,\end{aligned}\tag{3.18}$$

$$\begin{aligned}P(t+1) &= \left[A-\gamma(t)K(t)C\right]P(t)\times\left[A-\gamma(t)K(t)C\right]^{T}\\ &\quad+\left[B_1-\gamma(t)K(t)D\right]\Pi(t)\times\left[B_1-\gamma(t)K(t)D\right]^{T}M\\ &\quad+B_2QB_2^{T}+\gamma(t)K(t)RK^{T}(t),\\ P(0) &= \mathcal{E}\left[\mathbf{x}(0)\mathbf{x}^{T}(0)\mid\gamma(0)\right],\end{aligned}\tag{3.19}$$

$$\Pi(t+1) = A\Pi(t)A^{T}+B_1\Pi(t)B_1^{T}M+B_2QB_2^{T},\qquad \Pi(0)=P(0),\tag{3.20}$$

*where*

$$K(t)\triangleq\left[AP(t)C^{T}+B_1M\Pi(t)D^{T}\right]\times\left[CP(t)C^{T}+D\Pi(t)MD^{T}+R\right]^{-1}.\tag{3.21}$$

*Proof.* Firstly, according to the projection theorem (Theorem 3.4), we have

$$\begin{aligned}\hat{\mathbf{y}}(t) &= \operatorname{Proj}\{\mathbf{y}(t)\mid\tilde{\mathbf{y}}(0),\ldots,\tilde{\mathbf{y}}(t-1);\gamma(0),\ldots,\gamma(t-1)\}\\ &= \operatorname{Proj}\{\gamma(t)C\mathbf{x}(t)+\gamma(t)D\mathbf{x}(t)\mathbf{w}(t)+\gamma(t)\mathbf{v}(t)\mid\tilde{\mathbf{y}}(0),\ldots,\tilde{\mathbf{y}}(t-1);\gamma(0),\ldots,\gamma(t-1)\}\\ &= \gamma(t)C\hat{\mathbf{x}}(t),\end{aligned}\tag{3.22}$$

then from (3.7), we have

$$Q_{\tilde{\mathbf{y}}}(t) \triangleq \langle \tilde{\mathbf{y}}(t), \tilde{\mathbf{y}}(t) \rangle = \gamma(t) C P(t) C^T + \gamma(t) D \Pi(t) M D^T + \gamma(t) R. \tag{3.23}$$

Secondly, according to the projection theorem, we have

$$\begin{aligned}
\hat{\mathbf{x}}(t+1) &= \operatorname{Proj}\{\mathbf{x}(t+1) \mid \tilde{\mathbf{y}}(0), \ldots, \tilde{\mathbf{y}}(t); \gamma(0), \ldots, \gamma(t)\} \\
&= \operatorname{Proj}\{A\mathbf{x}(t) + B_1 \mathbf{x}(t)\mathbf{w}(t) + B_2 \mathbf{u}(t) \mid \tilde{\mathbf{y}}(0), \ldots, \tilde{\mathbf{y}}(t-1); \gamma(0), \ldots, \gamma(t-1)\} \\
&\quad + \operatorname{Proj}\{A\mathbf{x}(t) + B_1 \mathbf{x}(t)\mathbf{w}(t) + B_2 \mathbf{u}(t) \mid \tilde{\mathbf{y}}(t); \gamma(t)\} \\
&= A\hat{\mathbf{x}}(t) + \gamma(t) \times \left[AP(t)C^T + B_1 M \Pi(t) D^T\right] Q_{\tilde{\mathbf{y}}}^{-1}(t) \\
&= A\hat{\mathbf{x}}(t) + \gamma(t) K(t) \\
&\quad \times [C\mathbf{e}(t) + D\mathbf{x}(t)\mathbf{w}(t) + \mathbf{v}(t)] \\
&= A\hat{\mathbf{x}}(t) + K(t)\left[\mathbf{y}(t) - \gamma(t) C \hat{\mathbf{x}}(t)\right],
\end{aligned} \tag{3.24}$$

which is (3.18) by considering (3.21), (3.22), and (3.23).

Thirdly, by considering (3.7) and Theorem 3.4, we also have

$$\begin{aligned}
\hat{\mathbf{x}}(t+1 \mid t+1) &= \operatorname{Proj}\{\mathbf{x}(t+1) \mid \tilde{\mathbf{y}}(0), \ldots, \tilde{\mathbf{y}}(t), \tilde{\mathbf{y}}(t+1); \gamma(0), \ldots, \gamma(t), \gamma(t+1)\} \\
&= \hat{\mathbf{x}}(t+1) + \operatorname{Proj}\{\mathbf{x}(t+1) \mid \tilde{\mathbf{y}}(t+1); \gamma(t+1)\} \\
&= \hat{\mathbf{x}}(t+1) + P(t+1) C^T \times \left[CP(t+1)C^T + D\Pi(t+1)MD^T + R\right]^{-1} \\
&\quad \times \left[\mathbf{y}(t+1) - \gamma(t+1) C \hat{\mathbf{x}}(t+1)\right],
\end{aligned} \tag{3.25}$$

which is (3.17).

From (2.1) and (3.24), we have

$$\begin{aligned}
\mathbf{e}(t+1) &= \mathbf{x}(t+1) - \hat{\mathbf{x}}(t+1) \\
&= \left[A - \gamma(t) K(t) C\right] \mathbf{e}(t) + \left[B_1 - \gamma(t) K(t) D\right] \mathbf{x}(t) \mathbf{w}(t) \\
&\quad + B_2 \mathbf{u}(t) - \gamma(t) K(t) \mathbf{v}(t),
\end{aligned} \tag{3.26}$$

then we have

$$\begin{aligned}
P(t+1) &= \mathcal{E}\left[\mathbf{e}(t+1)\mathbf{e}^T(t+1) \mid \gamma_0^{t+1}\right] \\
&= \left[A - \gamma(t) K(t) C\right] P(t) \times \left[A - \gamma(t) K(t) C\right]^T \\
&\quad + \left[B_1 - \gamma(t) K(t) D\right] \Pi(t) \times \left[B_1 - \gamma(t) K(t) D\right]^T M \\
&\quad + B_2 Q B_2^T + \gamma(t) K(t) R K^T(t),
\end{aligned} \tag{3.27}$$

which is (3.19).

From (2.1), (3.20) can be given directly, and the proof is over. □

*Remark 3.6.* Equation (3.19) is a recursive Riccati equation, and (3.20) is a Lyapunov equation.

### 3.1. Kalman Fixed-Interval Smoother

In this subsection, we will present the Kalman fixed-interval smoother by the projection theorem. First, we define

$$P(t,k) \triangleq \mathcal{E}\left[\mathbf{x}(t)\mathbf{e}^T(t+k) \mid \mathbf{y}_0^{t+k}, \gamma_0^{t+k}\right], \tag{3.28}$$

$$\mathbf{e}(t \mid t+k) \triangleq \mathbf{x}(t) - \widehat{\mathbf{x}}(t \mid t+k), \tag{3.29}$$

$$P(t \mid t+k) \triangleq \mathcal{E}\left[\mathbf{e}(t \mid t+k)\ \mathbf{e}^T(t \mid t+k) \mid \mathbf{y}_0^{t+k}, \gamma_0^{t+k}\right]. \tag{3.30}$$

Then we can give the theorem which develops [6] as follows.

**Theorem 3.7.** *Consider the system* (2.1)–(2.3) *with the measurements* $\{\mathbf{y}(0), \ldots, \mathbf{y}(N)\}$ *and scalars* $\{\gamma(0), \ldots, \gamma(N)\}$*, Kalman fixed-interval smoother can be given by the following backwards recursive equations:*

$$\begin{aligned}\widehat{\mathbf{x}}(t \mid N) = \widehat{\mathbf{x}}(t \mid t) + \sum_{k=1}^{N-t} P(t,k)C^T \left[CP(t+k)C^T + D\Pi(t+k)MD^T + R\right]^{-1} \\ \times \left[\mathbf{y}(t+k) - \gamma(t+k)C\widehat{\mathbf{x}}(t+k)\right], \quad t = 0, 1, \ldots, N,\end{aligned} \tag{3.31}$$

*and the corresponding smoother error covariance matrix can be given as*

$$\begin{aligned}P(t \mid N) = P(t) - \sum_{k=0}^{N-t} \gamma(t+k)P(t,k)C^T \\ \times \left[CP(t+k)C^T + D\Pi(t+k)MD^T + R\right]CP(t,k), \quad t = 0, 1, \ldots, N,\end{aligned} \tag{3.32}$$

*where*

$$P(t,k) = P(t,k-1)\left[A - \gamma(t+k-1)K(t+k-1)C\right]^T, \quad k = 1, \ldots, N-t, \tag{3.33}$$

*with* $P(t,0) = P(t)$*, and* $P(t+k)$*,* $P(t)$*,* $\widehat{\mathbf{x}}(t)$ *can be given from* (3.18)*,* (3.19)*, and* (3.17)*.*

*Proof.* From the projection theorem, we have

$$\begin{aligned}\widehat{\mathbf{x}}(t \mid N) &= \mathrm{Proj}\{\mathbf{x}(t) \mid \mathbf{y}(0), \ldots, \mathbf{y}(t), \mathbf{y}(t+1), \ldots, \mathbf{y}(N)\} \\ &= \mathrm{Proj}\{\mathbf{x}(t) \mid \widetilde{\mathbf{y}}(0), \ldots, \widetilde{\mathbf{y}}(t), \widetilde{\mathbf{y}}(t+1), \ldots, \widetilde{\mathbf{y}}(N)\} \\ &= \mathrm{Proj}\{\mathbf{x}(t) \mid \widetilde{\mathbf{y}}(0), \ldots, \widetilde{\mathbf{y}}(t)\} + \mathrm{Proj}\{\mathbf{x}(t) \mid \widetilde{\mathbf{y}}(t+1), \ldots, \widetilde{\mathbf{y}}(N)\}\end{aligned}$$

$$
\begin{aligned}
&= \widehat{\mathbf{x}}(t \mid t) \ + \sum_{k=1}^{N-t} \mathrm{Proj}\{\mathbf{x}(t) \mid \widetilde{\mathbf{y}}(t+k)\} \\
&= \widehat{\mathbf{x}}(t \mid t) \ + \sum_{k=1}^{N-t} \mathrm{Proj}\{\mathbf{x}(t) \mid \gamma(t+k)[C\mathbf{e}(t+k) D\mathbf{x}(t+k)\mathbf{w}(t+k) + \mathbf{v}(t+k)]\} \\
&= \widehat{\mathbf{x}}(t \mid t) + \sum_{k=1}^{N-t} P(t,k) C^T \Big[CP(t+k)C^T + D\Pi(t+k)\ MD^T + R\Big]^{-1} \\
&\quad \times \big[\mathbf{y}(t+k) - \gamma(t+k) C\widehat{\mathbf{x}}(t+k)\big],
\end{aligned}
\tag{3.34}
$$

which is (3.31).

Noting that $\mathbf{x}(t)$ is uncorrelated with $\mathbf{w}(t+k-1)$, $\mathbf{u}(t+k-1)$, and $\mathbf{v}(t+k-1)$ for $k = 1, \ldots, N-t$, then from (3.5), we have

$$
\begin{aligned}
P(t,k) \ &= \mathcal{E}\Big[\mathbf{x}(t)\mathbf{e}^T(t+k) \mid \mathbf{y}_0^{t+k}, \gamma_0^{t+k}\Big] \\
&= \langle \mathbf{x}(t), \\
&\qquad \big[A - \gamma(t+\mathrm{k}-1) K(t+k-1) C\big]\mathbf{e}(t+k-1) \\
&\qquad + \big[B_1 - \gamma(t+k-1) K(t+k-1) D\big] \times \mathbf{x}(t+k-1)\mathbf{w}(t+k-1) \\
&\qquad + B_2\mathbf{u}(t+k-1) - \gamma(t+k-1) K(t+k-1)\mathbf{v}(t+k-1)\rangle \\
&= P(t,k-1)\big[A - \gamma(t+k-1) K(t+k-1) C\big]^T,
\end{aligned}
\tag{3.35}
$$

which is (3.33).

Next, we will give the proof of covariance matrix $P(t \mid N)$. From the projection theorem, we have $\mathbf{x}(t) = \widehat{\mathbf{x}}(t \mid N) + \mathbf{e}(t \mid N) = \widehat{\mathbf{x}}(t) + \mathbf{e}(t)$, and from (3.34), we have

$$
\mathbf{e}(t \mid N) = \mathbf{e}(t) - \sum_{k=0}^{N-t} P(t,k) C^T \Big[CP(t+k)C^T + D\Pi(t+k) MD^T + R\Big]^{-1} \times \widetilde{\mathbf{y}}(t+k), \tag{3.36}
$$

that is,

$$
\mathbf{e}(t) = \mathbf{e}(t \mid N) + \sum_{k=0}^{N-t} P(t,k) C^T \Big[CP(t+k)C^T + D\Pi(t+k) MD^T + R\Big]^{-1} \times \widetilde{\mathbf{y}}(t+k). \tag{3.37}
$$

Thus, (3.32) can be given. □

*Remark 3.8.* The proposed theorem is based on the theorem in [6]. However, the condition of the theorem in [6] is wrong since multiplicative noises $\mathbf{w}(0), \ldots, \mathbf{w}(t)$ are not known. In addition, the proposed theorem gives the fixed-interval smoother error covariance matrix $P(t \mid N)$ which is an important index in Problem 1 and also useful in the comparison with fixed-lag smoother.

### 3.2. Kalman Fixed-Lag Smoother

Let $t_l = t - l$, and we can give Kalman fixed-lag smoothing estimate for the system model (2.1)–(2.3), which develops [6] in the following theorem.

**Theorem 3.9.** *Consider the system* (2.1)–(2.3)*, given the measurements* $\{\mathbf{y}(0), \ldots, \mathbf{y}(t)\}$ *and scalars* $\{\gamma(0), \ldots, \gamma(t)\}$ *for a fixed scalar* $l$ $(l < t)$*, then Kalman fixed-lag smoother can be given by the following recursive equations:*

$$\begin{aligned}\widehat{\mathbf{x}}(t_l \mid t) = \widehat{\mathbf{x}}(t_l \mid t_l) + \sum_{k=1}^{l} P(t_l, k) C^T \Big[ CP(t_l + k) C^T + D\Pi(t_l + k) M D^T + R \Big]^{-1} \\ \times \big[ \mathbf{y}(t_l + k) - \gamma(t_l + k) C \widehat{\mathbf{x}}(t_l + k) \big], \quad t > l,\end{aligned} \tag{3.38}$$

*and the corresponding smoother error covariance matrix* $P(t_l \mid t)$ *can be given as*

$$P(t_l \mid t) = P(t_l) - \sum_{k=0}^{l} \gamma(t_l + k) P(t_l, k) C^T \Big[ CP(t_l + k) C^T + D\Pi(t_l + k) M D^T + R \Big] CP(t_l, k), \quad t > l, \tag{3.39}$$

*where*

$$P(t_l, k) = P(t_l, k-1) \big[ A - \gamma(t_l + k - 1) K(t_l + k - 1) C \big]^T, \quad k = 1, \ldots, l, \tag{3.40}$$

*with* $P(t_l, 0) = P(t_l)$*, and* $P(t_l + k)$*,* $P(t_l)$*,* $\widehat{\mathbf{x}}(t_l + k)$*, and* $\widehat{\mathbf{x}}(t_l \mid t_l)$ *can be given from Lemma 3.5.*

*Proof.* From the projection theorem, we have

$$\begin{aligned}\widehat{\mathbf{x}}(t_l \mid t) &= \operatorname{Proj}\{\mathbf{x}(t_l) \mid \mathbf{y}(0), \ldots, \mathbf{y}(t_l), \mathbf{y}(t_l + 1), \ldots, \mathbf{y}(t)\} \\ &= \operatorname{Proj}\{\mathbf{x}(t_l) \mid \widetilde{\mathbf{y}}(0), \ldots, \widetilde{\mathbf{y}}(t_l), \widetilde{\mathbf{y}}(t_l + 1), \ldots, \widetilde{\mathbf{y}}(t)\} \\ &= \operatorname{Proj}\{\mathbf{x}(t_l) \mid \widetilde{\mathbf{y}}(0), \ldots, \widetilde{\mathbf{y}}(t_l)\} + \operatorname{Proj}\{\mathbf{x}(t_l) \mid \widetilde{\mathbf{y}}(t_l + 1), \ldots, \widetilde{\mathbf{y}}(t)\} \\ &= \widehat{\mathbf{x}}(t_l \mid t_l) + \sum_{k=1}^{l} \operatorname{Proj}\{\mathbf{x}(t_l) \mid \widetilde{\mathbf{y}}(t_l + k)\} \\ &= \widehat{\mathbf{x}}(t_l \mid t_l) + \sum_{k=1}^{l} \operatorname{Proj}\big\{\mathbf{x}(t_l) \mid \gamma(t_l + k)[C\mathbf{e}(t_l + k) + D\mathbf{x}(t_l + k)\mathbf{w}(t_l + k) + \mathbf{v}(t_l + k)]\big\} \\ &= \widehat{\mathbf{x}}(t_l \mid t_l) \\ &\quad + \sum_{k=1}^{l} P(t_l, k) C^T \Big[ CP(t_l + k) C^T + D\Pi(t_l + k) M D^T + R \Big]^{-1} \\ &\quad \times \big[ \mathbf{y}(t_l + k) - \gamma(t_l + k) C \widehat{\mathbf{x}}(t_l + k) \big],\end{aligned} \tag{3.41}$$

which is (3.38).

Noting that $\mathbf{x}(t)$ is uncorrelated with $\mathbf{w}(t+k-1)$, $\mathbf{u}(t+k-1)$, and $\mathbf{v}(t+k-1)$ for $k=1,\ldots,l$, then from (3.5), we have

$$\begin{aligned} P(t_l,k) &= \mathcal{E}\left[\mathbf{x}(t_l)\mathbf{e}^T(t_l+k) \mid \mathbf{y}_0^{t_l+k}, \gamma_0^{t_l+k}\right] \\ &= \left\langle \mathbf{x}(t_l), \left[A-\gamma(t_l+k-1)K(t_l+k-1)C\right]\times \mathbf{e}(t_l+k-1)\right. \\ &\quad + \left[B_1-\gamma(t_l+k-1)K(t_l+k-1)D\right]\times \mathbf{x}(t_l+k-1)\mathbf{w}(t_l+k-1) \\ &\quad \left. +B_2\mathbf{u}(t_l+k-1)-\gamma(t_l+k-1)K(t_l+k-1)\mathbf{v}(t_l+k-1)\right\rangle \\ &= P(t_l,k-1)\left[A-\gamma(t_l+k-1)K(t_l+k-1)C\right]^T, \end{aligned} \tag{3.42}$$

which is (3.40).

Next, we will give the proof of covariance matrix $P(t_l \mid t)$. Since $\mathbf{x}(t_l)=\hat{\mathbf{x}}(t_l \mid t)+\mathbf{e}(t_l \mid t)=\hat{\mathbf{x}}(t_l)+\mathbf{e}(t_l)$, from (3.41), we have

$$\mathbf{e}(t_l \mid t)=\mathbf{e}(t_l)-\sum_{k=0}^{l}P(t_l,k)C^T\left[CP(t_l+k)C^T+D\Pi(t_l+k)MD^T+R\right]^{-1}\times\tilde{\mathbf{y}}(t_l+k), \tag{3.43}$$

that is,

$$\mathbf{e}(t_l) \;=\mathbf{e}(t_l \mid t)+\sum_{k=0}^{l}P(t_l,k)C^T\left[CP(t_l+k)C^T+D\Pi(t_l+k)MD^T+R\right]^{-1}\times\tilde{\mathbf{y}}(t_l+k). \tag{3.44}$$

Thus, (3.39) can be given. □

*Remark 3.10.* It should be noted that the result of the Kalman smoothing is better than that of Kalman filtering for the normal systems without packet loss since more measurement information is available. However, it is not the case if the measurement is lost, which can be verified in the next section. In addition, in Theorems 3.7 and 3.9, we have changed the predictor type of $\mathbf{x}(t)$ or $\mathbf{x}(t_l)$ in [6] to the filter case of $\mathbf{x}(t \mid t)$ or $\mathbf{x}(t_l \mid t_l)$, which will be more convenient to be compared with Kalman fixed-point smoother (3.45).

### 3.3. Kalman Fixed-Point Smoother

In this subsection, we will present the Kalman fixed-point smoother by the projection theorem and innovation analysis. We can directly give the theorem which develops [7] as follows.

**Theorem 3.11.** *Consider the system* (2.1)–(2.3) *with the measurements* $\{\mathbf{y}(0),\ldots,\mathbf{y}(j)\}$ *and scalars* $\{\gamma(0),\ldots,\gamma(j)\}$*, then Kalman fixed-point smoother can be given by the following recursive equations:*

$$\begin{aligned} \hat{\mathbf{x}}(t \mid j) = \hat{\mathbf{x}}(t \mid t) &+ \sum_{k=1}^{j-t}P(t,k)C^T\left[CP(t+k)C^T+D\Pi(t+k)MD^T+R\right]^{-1} \\ &\times\left[\mathbf{y}(t+k)-\gamma(t+k)C\hat{\mathbf{x}}(t+k)\right], \quad j=t+1,\ldots,N, \end{aligned} \tag{3.45}$$

*and the corresponding smoother error covariance matrix $P(t \mid j)$ can be given as*

$$P(t \mid j) = P(t \mid j-1) - \gamma(j)K(t \mid j) \times \left[CP(j)C^T + D\Pi(j)MD^T + R\right]K^T(t \mid j), \tag{3.46}$$

*where*

$$P(t,k) = P(t,k-1) \times \left[A - \gamma(t+k-1)K(t+k-1)C\right]^T, \quad k = 1,\ldots,j-t, \tag{3.47}$$

$$K(t \mid j) = \gamma(j)P(t)\Psi_1^T(j,t) \times \left[CP(j)C^T + D\Pi(j)MD^T + R\right]^{-1}, \tag{3.48}$$

$$\Psi_1(j,t) = \Psi_1(j-1)\cdots\Psi_1(t), \tag{3.49}$$

*with $P(t,0) = P(t)$, $P(t \mid t-1) = P(t)$, $\Psi_1(t) = A - \gamma(t)K(t)C$, and $P(t+k)$, $P(t)$, and $\hat{\mathbf{x}}(t)$ can be given from* (3.19) *and* (3.18).

*Proof.* The proof of (3.45) and (3.47) can be referred to [7], and we only give the proof of the covariance matrix $P(t \mid j)$. From the projection theorem, we have

$$\begin{aligned}
\hat{\mathbf{x}}(t \mid t+k) &= \mathrm{Proj}\{\mathbf{x}(t) \mid \tilde{\mathbf{y}}(0),\ldots,\tilde{\mathbf{y}}(t),\tilde{\mathbf{y}}(t+1),\ldots,\tilde{\mathbf{y}}(t+k)\} \\
&= \mathrm{Proj}\{\mathbf{x}(t) \mid \tilde{\mathbf{y}}(0),\ldots,\tilde{\mathbf{y}}(t+k-1)\} + \mathrm{Proj}\{\mathbf{x}(t) \mid \tilde{\mathbf{y}}(t+k)\} \\
&= \hat{\mathbf{x}}(t \mid t+k-1) + K(t \mid t+k)\tilde{\mathbf{y}}(t+k),
\end{aligned} \tag{3.50}$$

where

$$K(t \mid t+k) = \mathcal{E}\left[\mathbf{x}(t)\tilde{\mathbf{y}}^T(t+k)\right]Q_{\tilde{\mathbf{y}}}^{-1}(t+k). \tag{3.51}$$

Define $\Psi_1(t) = A - \gamma(t)K(t)C$ and $\Psi_2(t) = B_1 - \gamma(t)K(t)D$, then (3.26) can be rewritten as

$$\mathbf{e}(t+1) = \Psi_1(t)\mathbf{e}(t) + \Psi_2(t)\mathbf{x}(t)\mathbf{w}(t) + B_2\mathbf{u}(t) - \gamma(t)K(t)\mathbf{v}(t), \tag{3.52}$$

and recursively computing (3.52), we have

$$\begin{aligned}
\mathbf{e}(t+k) &= \Psi_1(t+k,t)\mathbf{e}(t) + \Psi_2(t+k,t)\mathbf{x}(t)\mathbf{w}(t) \\
&\quad + \sum_{i=t+1}^{t+k} \Psi_1(t+k,i) \times \left[B_2\mathbf{u}(i-1) - \gamma(i-1)K(i-1)\mathbf{v}(i-1)\right],
\end{aligned} \tag{3.53}$$

where

$$\begin{aligned}
\Psi_1(t+k,i) &= \Psi_1(t+k-1)\cdots\Psi_1(i), \quad i < t+k, \\
\Psi_2(t+k,t) &= \Psi_1(t+k-1)\cdots\Psi_1(t+1)\Psi_2(t), \\
\Psi_1(t+k,t+k) &= I_n.
\end{aligned} \tag{3.54}$$

By considering (3.7), (3.53), and Theorem 3.4,

$$\mathcal{E}\left[\mathbf{x}(t)\tilde{\mathbf{y}}^T(t+k)\right] = \gamma(t+k)P(t)\Psi_1^T(t+k,t), \tag{3.55}$$

so

$$K(t \mid t+k) = \gamma(t+k)P(t)\Psi_1^T(t+k,t) \times \left[CP(t+k)C^T + D\Pi(t+k)MD^T + R\right]^{-1}, \tag{3.56}$$

which is (3.48) by setting $t+k=j$.

From (3.50) and considering $\mathbf{x}(t) = \hat{\mathbf{x}}(t \mid t+k) + \mathbf{e}(t \mid t+k) = \hat{\mathbf{x}}(t \mid t+k-1) + \mathbf{e}(t \mid t+k-1)$, then we have

$$\mathbf{e}(t \mid t+k) = \mathbf{e}(t \mid t+k-1) - K(t \mid t+k)\tilde{\mathbf{y}}(t+k), \tag{3.57}$$

that is,

$$\mathbf{e}(t \mid t+k-1) = \mathbf{e}(t \mid t+k) + K(t \mid t+k)\tilde{\mathbf{y}}(t+k). \tag{3.58}$$

Then according to (3.30), we have

$$P(t \mid t+k-1) = P(t \mid t+k) + K(t \mid t+k)Q_{\tilde{\mathbf{y}}}(t+k)K^T(t \mid t+k), \tag{3.59}$$

Combined with (3.23), we have (3.46) by setting $t+k=j$. □

### 3.4. Comparison

In this subsection, we will give the comparison among the three cases of smoothers. It can be easily seen from (3.31), (3.38), and (3.45) that the smoothers are all given by a Kalman filter and an updated part. To be compared conveniently, the smoother error covariance matrices are given in (3.32), (3.39), and (3.46), which develops the main results in [6, 7] where only Kalman smoothers are given.

It can be easily seen from (3.31) and (3.38) that Kalman fixed-interval smoother is similar to fixed-lag smoother. For (3.31), the computation time is $N-t$, and it is $l$ in (3.38). For Kalman fixed-interval smoother, the $N$ is fixed, and $t$ is variable, so when $t = 0, 1, \ldots, N-1$, the corresponding smoother $\hat{\mathbf{x}}(t \mid N)$ can be given. For Kalman fixed-lag smoother, the $l$ is fixed, and $t$ is variable, so when $t = l+1, l+2, \ldots$, the corresponding smoother $\hat{\mathbf{x}}(t_l \mid t)$ can be given. The two smoothers are similar in the form of (3.31) and (3.38). However, it is hard to see which smoother is better from the smoother error covariance matrix (3.32) and (3.39), which will be verified in numerical example.

For Kalman fixed-point smoother in Theorem 3.7, the time $t$ is fixed, and in this case, we can say that Kalman fixed-point smoother is different from fixed-interval and fixed-lag smoother in itself. $j$ can be equal to $t+1, t+2, \ldots$.

## 4. Numerical Example

In the section, we will give an example to show the efficiency and the comparison of the presented results.

Consider the system (2.1)–(2.3) with $N = 80,\ l = 20$,

$$A = \begin{bmatrix} 0.8 & 0.3 \\ 0 & 0.6 \end{bmatrix}, \qquad B_1 = \begin{bmatrix} 0.2 & 0 \\ 0.1 & 0.9 \end{bmatrix}, \qquad B_2 = \begin{bmatrix} 0.5 \\ 0.8 \end{bmatrix},$$
$$C = \begin{bmatrix} 1 & 2 \end{bmatrix}, \qquad D = \begin{bmatrix} 2 & 2 \end{bmatrix}, \tag{4.1}$$
$$\gamma(t) = \frac{1 + (-1)^t}{2}.$$

The initial state value $\mathbf{x}(0) = \begin{bmatrix} 1 \\ 0.5 \end{bmatrix}$, and noises $\mathbf{u}(t)$ and $\mathbf{w}(t)$ are uncorrelated white noises with zero means and unity covariance matrices, that is, $Q = 1,\ M = 1$. Observation noise $\mathbf{v}(t)$ is of zero means and with covariance matrix $R = 0.01$.

Our aim is to calculate the Kalman fixed-interval smoother $\widehat{\mathbf{x}}(t \mid N)$ of the signal $\mathbf{x}(t)$, Kalman fixed-lag smoother $\widehat{\mathbf{x}}(t_l \mid t)$ of the signal $\mathbf{x}(t_l)$ for $t = l + 1, \ldots, N$, and Kalman fixed-point smoother $\widehat{\mathbf{x}}(t \mid j)$ of the signal $\mathbf{x}(t)$ for $j = t + 1, \ldots, N$ based on observations $\{\mathbf{y}(i)\}_{i=0}^{N}$, $\{\mathbf{y}(i)\}_{i=0}^{t}$ and $\{\mathbf{y}(i)\}_{i=0}^{j}$, respectively. For the Kalman fixed-point smoother $\widehat{\mathbf{x}}(t \mid j)$, we can set $t = 30$.

According to Theorem 3.7, the computation of the Kalman fixed-interval smoother $\widehat{\mathbf{x}}(t \mid N)$ can be summarized in three steps as shown below.

*Step 1.* Compute $\Pi(t + 1)$, $P(t + 1)$, $\widehat{\mathbf{x}}(t + 1)$, and $\widehat{\mathbf{x}}(t + 1 \mid t + 1)$ by (3.20), (3.19), (3.18), and (3.17) in Lemma 3.5 for $t = 0, \ldots, N - 1$, respectively.

*Step 2.* $t \in [0, N]$ is set invariant compute $P(t, k)$ by (3.33) for $k = 1, \ldots, N - t$; with the above initial values $P(t, 0) = P(t)$.

*Step 3.* Compute the Kalman fixed-interval smoother $\widehat{\mathbf{x}}(t \mid N)$ by (3.31) for $t = 0, \ldots, N$ with fixed N.

Similarly, according to Theorem 3.9, the computation of the Kalman fixed-lag smoother $\widehat{\mathbf{x}}(t_l \mid t)$ can be summarized in three steps as shown below.

*Step 1.* Compute $\Pi(t_l + k + 1)$, $P(t_l + k + 1)$, $\widehat{\mathbf{x}}(t_l + k + 1)$, and $\widehat{\mathbf{x}}(t_l + k + 1 \mid t_l + k + 1)$ by (3.20), (3.19), (3.18), and (3.17) in Lemma 3.5 for $t > l$ and $k = 1, \ldots, l$, respectively.

*Step 2.* $t \in [0, N]$ is set invariant; compute $P(t_l, k)$ by (3.40) for $k = 1, \ldots, l$ with the above initial values $P(t_l, 0) = P(t_l)$.

*Step 3.* Compute the Kalman fixed-lag smoother $\widehat{\mathbf{x}}(t_l \mid t)$ by (3.38) for $t > l$.

According to Theorem 3.11, the computation of Kalman fixed-point smoother $\widehat{\mathbf{x}}(t \mid j)$ can be summarized in three steps as shown below.

*Step 1.* Compute $\Pi(t + 1)$, $P(t + 1)$, $\widehat{\mathbf{x}}(t + 1)$, and $\widehat{\mathbf{x}}(t + 1 \mid t + 1)$ by (3.20), (3.19), (3.18) and (3.17) in Lemma 3.5 for $t = 0, \ldots, N - 1$, respectively.

*Step 2.* Compute $P(t, k)$ by (3.47) for $k = 1, \ldots, j - t$ with the initial value $P(t, 0) = P(t)$.

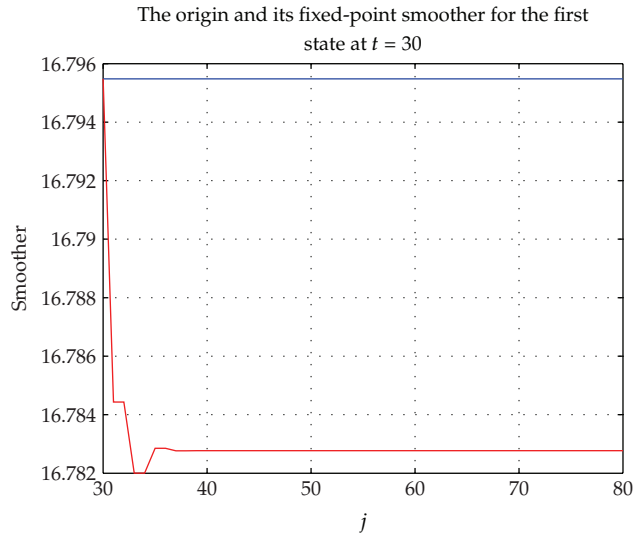


**Figure 1:** The origin and its fixed-point smoother $\hat{x}_1(30 \mid j)$, where the blue line is the origin signal, the red line is the smoother.

*Step 3.* Compute the Kalman fixed-point smoother $\hat{\mathbf{x}}(t \mid j)$ by (3.45) for $j = t+1, \ldots, N$.

The tracking performance of Kalman fixed-point smoother $\hat{\mathbf{x}}(t \mid j) = \begin{bmatrix} \hat{\mathbf{x}}_1(t|j) \\ \hat{\mathbf{x}}_2(t|j) \end{bmatrix}$ is drawn in Figures 1 and 2, and the line is based on the fixed time $t = 30$, and the variable is $j$. It can be easily seen from the above two figures that the smoother is changed much at first, and after the time $j = 35$, the fixed-point smoother is fixed, that is, the smoother at time $t = 30$ will take little effect on $\mathbf{y}(j)$, $\mathbf{y}(j+1), \ldots$ due to packet loss. In addition, at time $j = 30$, the estimation (filter) is more closer to the origin than other $j > 30$, which shows that Kalman filter is better than fixed-point smoother for WSN with packet loss. In fact, the smoothers below are also not good as filter.

The fixed-interval smoother $\hat{\mathbf{x}}(t \mid N) = \begin{bmatrix} \hat{\mathbf{x}}_1(t|N) \\ \hat{\mathbf{x}}_2(t|N) \end{bmatrix}$ is given in Figures 3 and 4, and the tracking performance of the fixed-lag smoother $\hat{\mathbf{x}}(t_l \mid t) = \begin{bmatrix} \hat{\mathbf{x}}_1(t_l|t) \\ \hat{\mathbf{x}}_2(t_l|t) \end{bmatrix}$ is given in Figures 5 and 6. From the above figures, they can estimate the origin signal in general.

In addition, according to the comparison part in the end of last section, we give the comparison of the sum of the error covariance of the fixed-interval and fixed-lag smoother (the fixed-point smoother is different from the above two smoother, so its error covariance is not necessary to be compared with, which has been explained at the end of last section), and we also give the sum of the error covariance of Kalman filter, and they are all drawn in Figure 7. As seen from Figure 7, it is hard to say which smoother is better due to packet loss, and the result of smoothers is not better than filter.

## 5. Conclusion

In this paper, we have studied Kalman fixed-interval smoothing, fixed-lag smoothing [6], and fixed-point smoothing [7] for wireless sensor network systems with packet loss and multiplicative noises. The smoothers are given by recursive equations. The smoother error

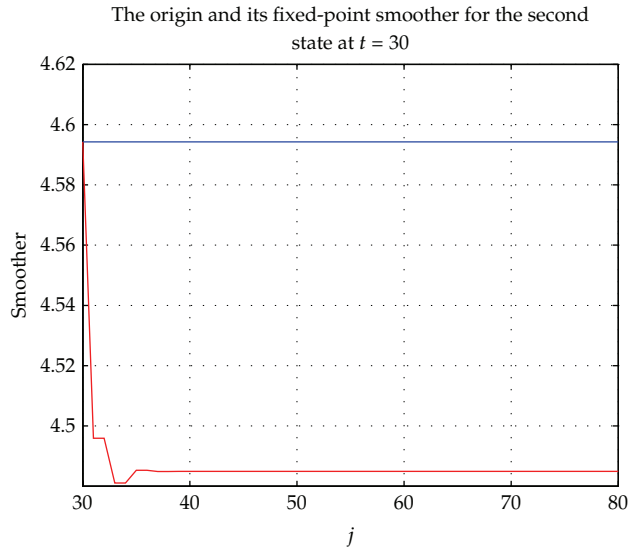


**Figure 2:** The origin and its fixed-point smoother $\hat{x}_2(30 \mid j)$, where the blue line is the origin signal, the red line is the smoother.

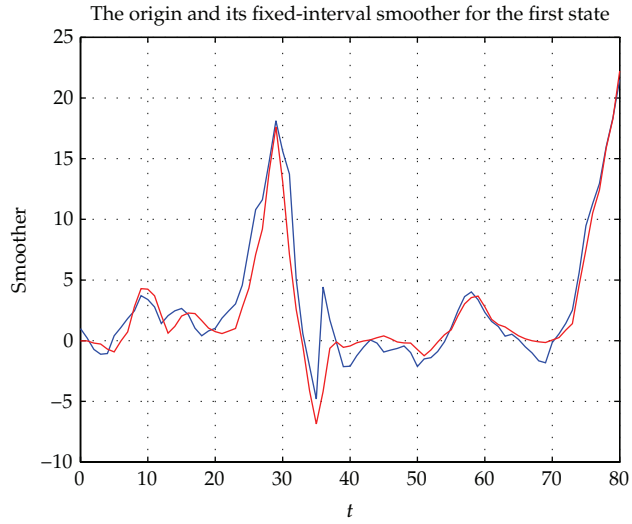


**Figure 3:** The origin and its fixed-interval smoother $\hat{x}_1(t \mid N)$, where the blue line is the origin signal, the red line is the smoother.

covariance matrices of fixed-interval smoothing, and fixed-lag smoothing are given by Riccati equation without recursion, while the smoother error covariance matrix of fixed-point smoothing is given by recursive Riccati equation and recursive Lyapunov equation. The comparison among the fixed-point smoother, fixed-interval smoother and fixed-lag smoother has been given, and numerical example verified the proposed approach. The proposed approach will be useful to study more difficult problems, for example, the WSN with random delay and packet loss [19].

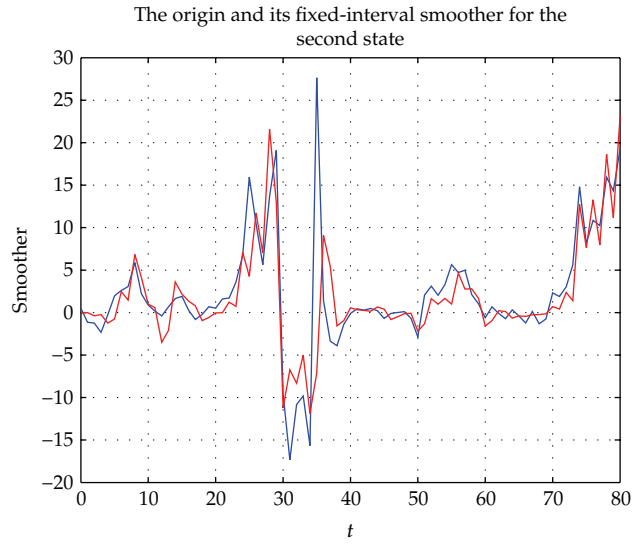


**Figure 4:** The origin and its fixed-interval smoother $\hat{x}_2(t \mid N)$, where the blue line is the origin signal, the red line is the smoother.


**Figure 5:** The origin and its fixed-lag smoother $\hat{x}_1(t-l \mid t)$, where the blue line is the origin signal, the red line is the smoother.

## Disclosure

X. Lu is affiliated with Shandong University of Science and Technology and also with Shandong University, Qingdao, China. H. Wang and X. Wang are affiliated with Shandong University of Science and Technology, Qingdao, China.

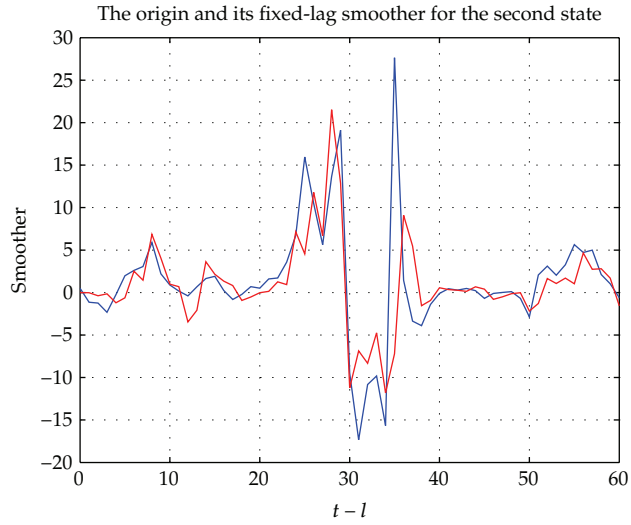


**Figure 6:** The origin and its fixed-lag smoother $\hat{x}_2(t-l \mid t)$, where the blue line is the origin signal, the red line is the smoother.

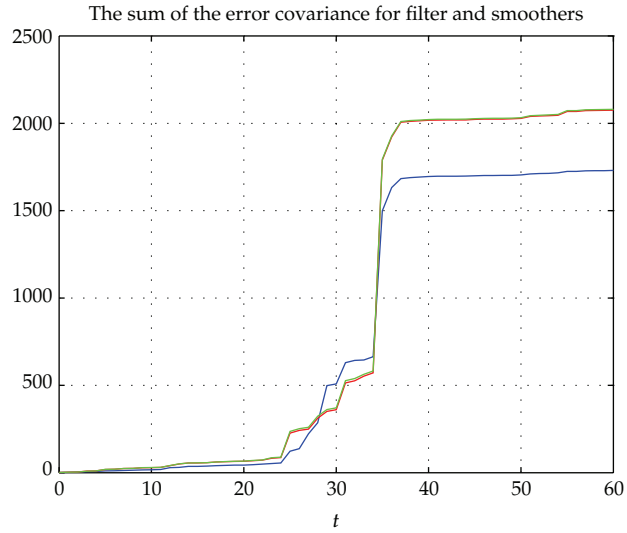


**Figure 7:** The sum of the error covariance for filter, fixed-interval smoother, and fixed-lag smoother, where the blue line is for the filter, the green line is for fixed-interval smoother, and the red line is for the fixed-lag smoother.

## Acknowledgment

This work is supported by National Nature Science Foundation (60804034), the Scientific Research Foundation for the Excellent Middle-Aged and Youth Scientists of Shandong Province (BS2012DX031), the Nature Science Foundation of Shandong Province (ZR2009GQ006), SDUST Research Fund (2010KYJQ105), the Project of Shandong Province

Higher Educational Science, Technology Program (J11LG53) and "Taishan Scholarship" Construction Engineering.

## References

[1] N. Wiener, *Extrapolation Interpolation, and Smoothing of Stationary Time Series*, The Technology Press and Wiley, New York, NY, USA, 1949.
[2] R. E. Kalman, "A new approach to linear filtering and prediction problems," *Journal of Basic Engineering*, vol. 82, no. 1, pp. 35–45, 1960.
[3] T. Kailath, A. H. Sayed, and B. Hassibi, *Linear Estimation*, Prentice-Hall, Englewood Cliffs, NJ, USA, 1999.
[4] B. D. O. Anderson and J. B. Moore, *Optimal Filtering*, Prentice-Hall, Englewood Cliffs, NJ, USA, 1979.
[5] X. Lu, H. Zhang, W. Wang, and K.-L. Teo, "Kalman filtering for multiple time-delay systems," *Automatica*, vol. 41, no. 8, pp. 1455–1461, 2005.
[6] X. Lu, W. Wang, and M. Li, "Kalman fixed-interval and fixed-lag smoothing for wireless sensor systems with multiplicative noises," in *Proceedings of the 24th Chinese Control and Decision Conference (CCDC '12)*, Taiyuan, China, May 2012.
[7] X. Lu and W. Wang, "Kalman fixed-point smoothing for wireless sensor systems with multiplicative noises," in *Proceedings of the 24th Chinese Control Conference (CCDC '12)*, Taiyuan, China, May 2012.
[8] D. S. Chu and S. W. Gao, "State optimal estimation algorithm for singular systems with multiplicative noise," *Periodical of Ocean University of China*, vol. 38, no. 5, pp. 814–818, 2008.
[9] H. Zhang, X. Lu, W. Zhang, and W. Wang, "Kalman filtering for linear time-delayed continuous-time systems with stochastic multiplicative noises," *International Journal of Control, Automation, and Systems*, vol. 5, no. 4, pp. 355–363, 2007.
[10] B. Sinopoli, L. Schenato, M. Franceschetti, K. Poolla, M. I. Jordan, and S. S. Sastry, "Kalman filtering with intermittent observations," *IEEE Transaction on Automatic Control*, vol. 49, no. 9, pp. 1453–1464, 2004.
[11] X. Liu and A. Goldsmith, "Kalman filtering with partial observation losses," in *Proceedings of the 15th International Symposium on the Mathematical Theory of Networks and Systems*, pp. 4180–4183, Atlantis, Bahamas, December 2004.
[12] A. S. Leong, S. Dey, and J. S. Evans, "On Kalman smoothing with random packet loss," *IEEE Transactions on Signal Processing*, vol. 56, no. 7, pp. 3346–3351, 2008.
[13] L. Schenato, "Optimal estimation in networked control systems subject to random delay and packet drop," *IEEE Transactions on Automatic Control*, vol. 53, no. 5, pp. 1311–1317, 2008.
[14] M. Huang and S. Dey, "Stability of Kalman filtering with Markovian packet losses," *Automatica*, vol. 43, no. 4, pp. 598–607, 2007.
[15] L. Schenato, B. Sinopoli, M. Franceschetti, K. Poolla, and S. S. Sastry, "Foundations of control and estimation over lossy networks," *Proceedings of the IEEE*, vol. 95, no. 1, pp. 163–187, 2007.
[16] X. Lu and T. Wang, "Optimal estimation with observation loss and multiplicative noise," in *Proceedings of the 8th World Congress on Intelligent Control and Automation (WCICA '10)*, pp. 248–251, July 2010.
[17] X. Lu, M. Li, and Q. Pu, "Kalman filtering for wireless sensor network with multiple multiplicative noises," in *Proceedings of the 23th Chinese Control and Decision Conference (CCDC '11)*, pp. 2376–2381, May 2011.
[18] X. Lu, X. Wang, and H. Wang, "Optimal information fusion Kalman filtering for WSNs with multiplicative noise," in *Proceedings of the International Conference on System Science and Engineering (ICSSE '12)*, June 2012.
[19] L. Schenato, "Kalman filtering for networked control systems with random delay and packet loss," in *Proceedings of the Conference of Mathematical Theroy of Networks and Systems (MTNSar '06)*, Kyoto, Japan, July 2006.

Hindawi Publishing Corporation
Journal of Applied Mathematics
Volume 2012, Article ID 514504, 22 pages
doi:10.1155/2012/514504

*Research Article*

# Robust Adaptive Switching Control for Markovian Jump Nonlinear Systems via Backstepping Technique

**Jin Zhu,[1] Hongsheng Xi,[1] Qiang Ling,[1] and Wanqing Xie[2]**

[1] *Department of Automation, University of Science and Technology of China, Hefei, Anhui 230027, China*
[2] *Center of Information Science Experiment and Education, University of Science and Technology of China, China*

Correspondence should be addressed to Jin Zhu, jinzhu@ustc.edu.cn

Received 28 March 2012; Accepted 9 May 2012

Academic Editor: Xianxia Zhang



This paper investigates robust adaptive switching controller design for Markovian jump nonlinear systems with unmodeled dynamics and Wiener noise. The concerned system is of strict-feedback form, and the statistics information of noise is unknown due to practical limitation. With the ordinary input-to-state stability (ISS) extended to jump case, stochastic Lyapunov stability criterion is proposed. By using backstepping technique and stochastic small-gain theorem, a switching controller is designed such that stochastic stability is ensured. Also system states will converge to an attractive region whose radius can be made as small as possible with appropriate control parameters chosen. A simulation example illustrates the validity of this method.

## 1. Introduction

The establishment of modern control theory is contributed by state space analysis method which was introduced by Kalman in 1960s. This method, describing the changes of internal system states accurately through setting up the relationship of internal system variables and external system variables in time domain, has become the most important tool in system analysis. However, there remain many complex systems whose states are driven by not only continuous time but also a series of discrete events. Such systems are named hybrid systems whose dynamics vary with abrupt event occurring. Further, if the occurring of these events is governed by a Markov chain, the hybrid systems are called Markovian jump systems. As one branch of modern control theory, the study of Markovian jump systems has aroused lots of attention with fruitful results achieved for linear case, for example, stability analysis [1, 2], filtering [3, 4] and controller design [5, 6], and so forth. But studies are far from complete

because researchers are facing big challenges while dealing with the nonlinear case of such complicated systems.

The difficulties may result from several aspects for the study of Markovian jump nonlinear systems (MJNSs). First of all, controller design largely relies on the specific model of systems, and it is almost impossible to find out one general controller which can stabilize all nonlinear systems despite of their forms. Secondly Markovian jump systems are applied to model systems suffering sudden changes of working environment or system dynamics. For this reason, practical jump systems are usually accompanied by uncertainties, and it is hard to describe these uncertainties with precise mathematical model. Finally, noise disturbance is an important factor to be considered. More often that not, the statistics information of noise is unknown when taking into account the complexity of working environment. Among the achievements of MJNSs, the format of nonlinear systems should be firstly taken into account. As one specific model, the nonlinear system of strict-feedback form is well studied due to its powerful modelling ability of many practical systems, for example, power converter [7], satellite attitude [8], and electrohydraulic servosystem [9]. However, such models should be modified since stochastic structure variations exist in these practical systems, and this specific nonlinear system has been extended to jump case. For Markovian jump nonlinear systems of strict-feedback form, [10, 11] investigated stabilization and tracking problems for such MJNSs, respectively. And [12] studied the robust controller design for such systems with unmodeled dynamics. However, for the MJNSs suffering aforementioned factors in this paragraph, research work has not been performed yet.

Motivated by this, this paper focuses on robust adaptive controller design for a class of MJNSs with uncertainties and Wiener noise. Compared with the existing result in [12], several practical limitations are considered which include the following: the uncertainties are with unmodeled dynamics, and the upper bound of dynamics is not necessarily known. Meanwhile the statistics information of Wiener noise is unknown. Also the adaptive parameter is introduced to the controller design whose advantage has been described in [13]. The control strategy consists of several steps: firstly, by applying generalized *Itô* formula, the stochastic differential equation for MJNS is deduced and the concept of JISpS (jump input-to-state practical stability) is defined. Then with backstepping technology and small-gain theorem, robust adaptive switching controller is designed for such strict-feedback system. Also the upper bound of the uncertainties can be estimated. Finally according to the stochastic Lyapunov criteria, it is shown that all signals of the closed-loop system are globally uniformly bounded in probability. Moreover, system states can converge to an attractive region whose radius can be made as small as possible with appropriate control parameters chosen.

The rest of this paper is organized as follows. Section 2 begins with some mathematical notions including differential equation for MJNS, and we introduce the notion of JISpS and stochastic Lyapunov stability criterion. Section 3 presents the problem description, and a robust adaptive switching controller is given based on backstepping technique and stochastic small-gain theorem. In Section 4, stochastic Lyapunov criteria are applied for the stability analysis. Numerical examples are given to illustrate the validity of this design in Section 5. Finally, a brief conclusion is drawn in Section 6.

## 2. Mathematical Notions

### 2.1. Stochastic Differential Equation of MJNS

Throughout the paper, unless otherwise specified, we denote by $(\Omega, \mathcal{F}, \{\mathcal{F}_t\}_{t\geq 0}, P)$ a complete probability space with a filtration $\{\mathcal{F}_t\}_{t\geq 0}$ satisfying the usual conditions (i.e., it is right

continuous and $\mathcal{F}_0$ contains all $p$-null sets). Let $|x|$ stand for the usual Euclidean norm for a vector $x$, and let $\|x_t\|$ stand for the supremum of vector $x$ over time period $[t_0, t]$, that is, $\|x_t\| = \sup_{t_0 \le s \le t} |x(s)|$. The superscript $T$ will denote transpose and we refer to $\mathrm{Tr}(\cdot)$ as the trace for matrix. In addition, we use $L_2(P)$ to denote the space of Lebesgue square integrable vector.

Take into account the following Markovian jump nonlinear system:

$$dx = f(x, u, t, r(t))dt + g(x, u, t, r(t))d\omega(t), \tag{2.1}$$

where $x \in \mathbb{R}^n$, $u \in \mathbb{R}^m$ are state vector and input vector of the system, respectively. $r(t)$, $t \ge 0$ is named system regime, a right-continuous Markov chain on the probability space taking values in finite state space $S = \{1, 2, \ldots, N\}$. And $\omega(t) = \{\omega_1, \omega_2, \ldots, \omega_l\}$ is $l$-dimensional independent Wiener process defined on the probability space, with covariance matrix $E\{d\omega d\omega^T\} = \Upsilon(t)\Upsilon^T(t)dt$, where $\Upsilon(t)$ is an unknown bounded matrix-value function. Furthermore, we assume that the Wiener noise $\omega(t)$ is independent of the Markov chain $r(t)$. The functions $f : \mathbb{R}^{n+m} \times \mathbb{R}_+ \times S \to \mathbb{R}^n$ and $g : \mathbb{R}^{n+m} \times \mathbb{R}_+ \times S \to \mathbb{R}^{n \times l}$ are locally Lipschitz in $(x, u, r(t) = k) \in \mathbb{R}^{n+m} \times S$ for all $t \ge 0$; namely, for any $h > 0$, there is a constant $K_h \ge 0$ such that

$$\left|f(x_1, u_1, t, k) - f(x_2, u_2, t, k)\right| \vee \left|g(x_1, u_1, t, k) - g(x_2, u_2, t, k)\right| \le K_h(|x_1 - x_2| + |u_1 - u_2|) \tag{2.2}$$

$$\forall (x_1, u_1, t, k), (x_2, u_2, t, k) \in \mathbb{R}^{n+m} \times \mathbb{R}_+ \times S, \quad |x_1| \vee |x_2| \vee |u_1| \vee |u_2| \le h. \tag{2.3}$$

It is known by [2] that with (2.3) standing, MJNS (2.1) has a unique solution.

Considering the right-continuous Markov chain $r(t)$ with regime transition rate matrix $\Pi = [\pi_{kj}]_{N \times N}$, the entries $\pi_{kj}, k, j = 1, 2, \ldots, N$ are interpreted as transition rates such that

$$P\big(r(t + dt) = j \mid r(t) = k\big) = \begin{cases} \pi_{kj}dt + o(dt) & \text{if } k \ne j, \\ 1 + \pi_{kj}dt + o(dt) & \text{if } k = j, \end{cases} \tag{2.4}$$

where $dt > 0$ and $o(dt)$ satisfies $\lim_{dt \to 0}(o(dt)/dt) = 0$. Here $\pi_{kj} > 0 (k \ne j)$ is the transition rate from regime $k$ to regime $j$. Notice that the total probability axiom imposes $\pi_{kk}$ negative and

$$\sum_{j=1}^{N} \pi_{kj} = 0, \quad \forall k \in S. \tag{2.5}$$

For each regime transition rate matrix $\Pi$, there exists a unique stationary distribution $\zeta = (\zeta_1, \zeta_2, \ldots, \zeta_N)$ such that [14]

$$\Pi \cdot \zeta = 0, \qquad \sum_{k=1}^{N} \zeta_k = 1, \quad \zeta_k > 0, \ \forall k \in S. \tag{2.6}$$

Let $C^{2,1}(\mathbb{R}^n \times \mathbb{R}_+ \times S)$ denote the family of all functions $F(x,t,k)$ on $\mathbb{R}^n \times \mathbb{R}_+ \times S$ which are continuously twice differentiable in $x$ and once in $t$. Furthermore, we give the stochastic differentiable equation of $F(x,t,k)$ as

$$\begin{aligned} dF(x,t,k) = {} & \frac{\partial F(x,t,k)}{\partial t}dt + \frac{\partial F(x,t,k)}{\partial x}f(x,u,t,k)dt \\ & + \frac{1}{2}\mathrm{Tr}\left[\Upsilon^T g^T(x,u,t,k)\frac{\partial^2 F(x,t,k)}{\partial x^2}g(x,u,t,k)\Upsilon\right]dt \\ & + \sum_{j=1}^{N}\pi_{kj}F(x,t,j)dt + \frac{\partial F(x,t,k)}{\partial x}g(x,u,t,k)d\omega(t) \\ & + \sum_{j=1}^{N}\left[F(x,t,j) - F(x,t,k)\right]dM_j(t), \end{aligned} \tag{2.7}$$

where $M(t) = (M_1(t), M_2(t), \ldots, M_N(t))$ is a martingale process.

Take the expectation in (2.7), so that the the infinitesimal generator produces [2, 15]

$$\begin{aligned} \mathcal{L}F(x,t,k) = {} & \frac{\partial F(x,t,k)}{\partial t} + \frac{\partial F(x,t,k)}{\partial x}f(x,u,t,k) + \sum_{j=1}^{N}\pi_{kj}F(x,t,j) \\ & + \frac{1}{2}\mathrm{Tr}\left[\Upsilon^T g^T(x,u,t,k)\frac{\partial^2 F(x,t,k)}{\partial x^2}g(x,u,t,k)\Upsilon\right]. \end{aligned} \tag{2.8}$$

*Remark 2.1.* Equation (2.7) is the differential equation of MJNS (2.1). It is given by [12], and the similar result is also achieved in [15]. Compared with the differential equation of general nonjump systems, two parts come forth as differences: transition rates $\pi_{kj}$ and martingale process $M(t)$, which are both caused by the Markov chain $r(t)$. And we will show in the following section that the martingale process also has effects on the controller design.

## 2.2. JISpS and Stochastic Small-Gain Theorem

*Definition 2.2.* MJNS (2.1) is JISpS in probability if for any given $\epsilon > 0$, there exist $\mathcal{KL}$ function $\beta(\cdot,\cdot)$, $\mathcal{K}_\infty$ function $\gamma(\cdot)$, and a constant $d_c \geq 0$ such that

$$P\{|x(t,k)| < \beta(|x_0|,t) + \gamma(\|u_t(k)\|) + d_c\} \geq 1 - \epsilon \quad \forall t \geq 0,\ k \in S,\ x_0 \in \mathbb{R}^n \setminus \{0\}. \tag{2.9}$$

*Remark 2.3.* The definition of ISpS (input-to-state practically stable) in probability for nonjump stochastic system is put forward by Wu et al. [16], and the difference between JISpS in probability and ISpS in probability lies in the expressions of system state $x(t,k)$ and control signal $u_t(k)$. For nonjump system, system state and control signal contain only continuous time $t$ with $k \equiv 1$. While jump systems concern with both continuous time $t$ and discrete regime $k$. For different regime $k$, control signal $u_t(k)$ will differ with different sample taken even at the same time $t$, and that is the reason why the controller is called a switching one.

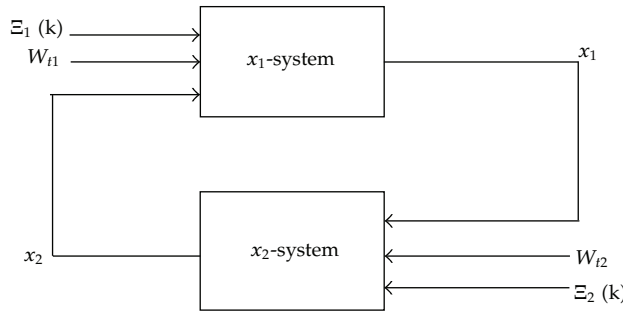


**Figure 1:** Interconnected feedback system.

Based on this, the corresponding stability is called Jump ISpS, and it is an extension of ISpS. Let $k \equiv 1$, and the definition of JISpS will degenerate to ISpS.

Consider the jump interconnected dynamic system described in Figure 1:

$$\begin{aligned} dx_1 &= f_1(x_1, x_2, \Xi_1(r(t)), r(t))dt + g_1(x_1, x_2, \Xi_1(r(t)), r(t))dW_{t1}, \\ dx_2 &= f_2(x_1, x_2, \Xi_2(r(t)), r(t))dt + g_2(x_1, x_2, \Xi_2(r(t)), r(t))dW_{t2}, \end{aligned} \tag{2.10}$$

where $x = (x_1^T, x_2^T)^T \in \mathbb{R}^{n_1+n_2}$ is the state of system, $\Xi_i(r(t))$, $i = 1,2$ denotes exterior disturbance and/or interior uncertainty. $W_{ti}$ is independent Wiener noise with appropriate dimension, and we introduce the following stochastic nonlinear small-gain theorem as a lemma, which is an extension of the corresponding result in Wu et al. [16].

**Lemma 2.4** (stochastic small-gain theorem). *Suppose that both the $x_1$-system and $x_2$-system are JISpS in probability with $(\Xi_1(k), x_2(t,k))$ as input and $x_1(t,k)$ as state and $(\Xi_2(k), x_1(t,k))$ as input and $x_2(t,k)$ as state, respectively; that is, for any given $\epsilon_1, \epsilon_2 > 0$,*

$$\begin{aligned} &P\{|x_1(t,k)| < \beta_1(|x_1(0,k)|,t) + \gamma_1(\|x_2(t,k)\|) + \gamma_{w1}(\|\Xi_{1t}(k)\|) + d_1\} \geq 1 - \epsilon_1, \\ &P\{|x_2(t,k)| < \beta_2(|x_2(0,k)|,t) + \gamma_2(\|x_1(t,k)\|) + \gamma_{w2}(\|\Xi_{2t}(k)\|) + d_2\} \geq 1 - \epsilon_2, \end{aligned} \tag{2.11}$$

*hold with $\beta_i(\cdot,\cdot)$ being $\mathcal{KL}$ function, $\gamma_i$ and $\gamma_{wi}$ being $\mathcal{K}_\infty$ functions, and $d_i$ being nonnegative constants, $i = 1,2$.*

*If there exist nonnegative parameters $\rho_1$, $\rho_2$, $s_0$ such that nonlinear gain functions $\gamma_1$, $\gamma_2$ satisfy*

$$(1+\rho_1)\gamma_1 \circ (1+\rho_2)\gamma_2(s) \leq s, \quad \forall s \geq s_0, \tag{2.12}$$

*the interconnected system is JISpS in probability with $\Xi(k) = (\Xi_1(k), \Xi_2(k))$ as input and $x = (x_1, x_2)$ as state; that is, for any given $\epsilon > 0$, there exist a $\mathcal{KL}$ function $\beta_c(\cdot,\cdot)$, a $\mathcal{K}_\infty$ function $\gamma_w(\cdot)$, and a parameter $d_c \geq 0$ such that*

$$P\{|x(t,k)| < \beta_c(|x_0|,t) + \gamma_w(\|\Xi_t(k)\|) + d_c\} \geq 1 - \epsilon. \tag{2.13}$$

*Remark 2.5.* The previously mentioned stochastic small-gain theorem for jump systems is an extension of nonjump case. This extension can be achieved without any mathematical difficulties, and the proof process is the same as in [16]. The reason is that in Lemma 3.1 we only take into account the interconnection relationship between synthetical system and its subsystems, despite the fact that subsystems are of jump or nonjumpform. If both subsystems are nonjump and ISpS in probability, respectively, the synthetical system is ISpS in probability. By contraries, if both subsystems are jump and JISpS in probability, respectively, the synthetical system is JISpS in probability correspondingly.

## 3. Problem Description and Controller Design

### 3.1. Problem Description

Consider the following Markovian jump nonlinear systems with dynamic uncertainty and noise described by

$$\begin{aligned} d\xi &= q(y,\xi,t,r(t))dt, \\ dx_i &= x_{i+1}dt + f_i^T(X_i,t,r(t))\theta^* dt + \Delta_i(X,\xi,t,r(t))dt + g_i^T(X_i,t,r(t))d\omega, \\ dx_n &= udt + f_n^T(X,t,r(t))\theta^* dt + \Delta_n(X,\xi,t,r(t))dt + g_n^T(X,t,r(t))d\omega \quad i = 1,2,\ldots,n-1, \\ y &= x_1, \end{aligned} \tag{3.1}$$

where $X_i = (x_1, x_2, \ldots, x_i)^T \in \mathbb{R}^i (X \in \mathbb{R}^n)$ is state vector, $u \in \mathbb{R}$ is system input signal, $\xi \in \mathbb{R}^{n_0}$ is unmeasured state vector, and $y$ is output signal. $\theta^* \in \mathbb{R}^{p_0}$ is a vector of unknown adaptive parameters. The Markov chain $r(t) \in S$ and Wiener noise $\omega$ are as defined in Section 2. $f_i : \mathbb{R}^i \times \mathbb{R}_+ \times S \to \mathbb{R}^{p_0}$, $g_i : \mathbb{R}^i \times \mathbb{R}_+ \times S \to \mathbb{R}^l$ are vector-valued smooth functions, and $\Delta_i(X,\xi,t,r(t))$ denotes the unmodeled dynamic uncertainty which could vary with different regime $r(t)$ taken. Both $f_i$, $g_i$ and $\Delta_i$ are locally Lipschitz as in Section 2.

Our design purpose is to find a switching controller $u$ of the form $u(x,t,k)$, $k \in S$ such that the closed-loop jump system could be JISpS in probability and the system output $y$ could be within an attractive region around the equilibrium point. In this paper, the following assumptions are made for MJNS (3.1).

(A1) The $\xi$ subsystem with input $y$ is JISpS in probability; namely, for any given $\epsilon > 0$, there exist $\mathcal{KL}$ function $\beta(\cdot,\cdot)$, $\mathcal{K}_\infty$ function $\gamma(\cdot)$, and a constant $d_c \geq 0$ such that

$$P\{|\xi(t,k)| < \beta(|\xi_0|,t) + \gamma(\|y\|) + d_c\} \geq 1 - \epsilon \quad \forall t \geq 0,\ k \in S,\ \xi_0 \in \mathbb{R}^{n_0} \setminus \{0\}. \tag{3.2}$$

(A2) For each $i = 1,2,\ldots,n$, $k \in S$, there exists an unknown bounded positive constant $p_i^*$ such that

$$|\Delta_i(X,\xi,t,k)| \leq p_i^* \overline{\phi}_{i1}(X_i,k) + p_i^* \overline{\phi}_{i2}(|\xi|,k), \tag{3.3}$$

where $\overline{\phi}_{i1}(\cdot,k)$, $\overline{\phi}_{i2}(\cdot,k)$ are known nonnegative smooth functions for any given $k \in S$. Notice that $p_i^*$ is not unique since any $\overline{p}_i^* > p_i^*$ satisfies inequality (3.3). To avoid

confusion, we define $p_i^*$ the smallest nonnegative constant such that inequality (3.3) is satisfied.

For the design of switching controller, we introduce the following lemmas.

**Lemma 3.1** (Young's inequality [12]). *For any two vectors $x, y \in \mathbb{R}^n$, the following inequality holds*

$$x^T y \leq \frac{\epsilon^p}{p}|x|^p + \frac{1}{q\epsilon^q}|y|^q, \tag{3.4}$$

*where $\epsilon > 0$ and the constants $p > 1$, $q > 1$ satisfy $(p-1)(q-1) = 1$.*

**Lemma 3.2** (martingale representation [17]). *Let $B(t) = [B_1(t), B_2(t), \ldots, B_N(t)]$ be $N$-dimensional standard Wiener noise. Supposing $M(t)$ is an $\mathcal{F}_t^N$-martingale (with respect to $P$) and that $M(t) \in L^2(P)$ for all $t \geq 0$, then there exists a stochastic process $\Psi(t) \in L^2(P)$, such that*

$$dM(t) = \Psi(t) \cdot dB(t). \tag{3.5}$$

### 3.2. Controller Design

Now we seek for the switching controller for MJNS (3.1) so that the closed-loop system could be JISpS in probability, where the parameter $\theta^*$, $p_i^*$ needs to be estimated. Denote the estimation of adaptive parameter $\theta^*$ with $\theta$ and the estimation of upper bound of uncertainty $p_i^*$ with $p_i$. Perform a new transformation as

$$z_i = x_i(k) - \alpha_{i-1}(X_{i-1}, t, \theta, p_i, k) \quad \forall i = 1, 2, \ldots, n,\ k \in S. \tag{3.6}$$

For simplicity, we just denote $\alpha_{i-1}(X_{i-1}, t, \theta, p_i, k)$, $f_i(X_i, t, k)$, $g_i(X_i, t, k)$, $\Delta_i(X, \xi, t, k)$, $q(y, \xi, t, k)$ by $\alpha_{i-1}(k)$, $f_i(k)$, $g_i(k)$, $\Delta_i(k)$, $q(k)$, respectively, where $\alpha_0(k) = 0$, $\alpha_n(k) = u(k)$, for all $k \in S$, and the new coordinate is $Z(k) = (z_1(k), z_2(k), \ldots, z_n(k))$.

According to stochastic differential equation (2.7), one has

$$\begin{aligned}
dz_i &= dx_i - d\alpha_{i-1}(k) \\
&= \left[x_{i+1} + f_i^T(k)\theta^* + \Delta_i(k)\right]dt - \frac{\partial \alpha_{i-1}(k)}{\partial t}dt - \sum_{j=1}^{i-1}\frac{\partial \alpha_{i-1}(k)}{\partial x_j}\left[x_{j+1} + f_j^T(k)\theta^* + \Delta_j(k)\right]dt \\
&\quad - \frac{\partial \alpha_{i-1}(k)}{\partial \theta}\dot{\theta}\,dt - \sum_{j=1}^{i-1}\frac{\partial \alpha_{i-1}(k)}{\partial p_i}\dot{p}_i dt - \frac{1}{2}\sum_{p,q=1}^{i-1}\frac{\partial^2 \alpha_{i-1}(k)}{\partial x_p \partial x_q}g_p^T(k)\Upsilon\Upsilon^T g_q(k)dt - \sum_{j=1}^{N}\pi_{kj}\alpha_{i-1}(j)dt \\
&\quad + \left[g_i^T(k) - \sum_{j=1}^{i-1}\frac{\partial \alpha_{i-1}(k)}{\partial x_j}g_j^T(k)\right]d\omega + \sum_{j=1}^{N}\left[\alpha_{i-1}(k) - \alpha_{i-1}(j)\right]dM_j(t)
\end{aligned}$$

$$
\begin{aligned}
&= \left[z_{i+1} + \alpha_i(k) + \tau_i^T(k)\theta^* + \Lambda_i(k)\right]dt - \frac{\partial \alpha_{i-1}(k)}{\partial t}dt - \frac{\partial \alpha_{i-1}(k)}{\partial \theta}\dot{\theta}\,dt - \sum_{j=1}^{i-1}\frac{\partial \alpha_{i-1}(k)}{\partial p_i}\dot{p}_i dt \\
&\quad - \sum_{j=1}^{i-1}\frac{\partial \alpha_{i-1}(k)}{\partial x_j}x_{j+1}dt - \frac{1}{2}\sum_{p,q=1}^{i-1}\frac{\partial^2 \alpha_{i-1}(k)}{\partial x_p \partial x_q}g_p^T(k)\Upsilon\Upsilon^T g_q(k)dt - \sum_{j=1}^{N}\pi_{kj}\alpha_{i-1}(j)dt \\
&\quad + \rho_i^T(k)d\omega + \Gamma_i(k)dM(t).
\end{aligned} \tag{3.7}
$$

Here we define

$$
\begin{aligned}
\Lambda_i(k) &\triangleq \Delta_i(k) - \sum_{j=1}^{i-1}\frac{\partial \alpha_{i-1}(k)}{\partial x_j}\Delta_j(k), \\
\tau_i(k) &\triangleq f_i(k) - \sum_{j=1}^{i-1}\frac{\partial \alpha_{i-1}(k)}{\partial x_j}f_j(k), \\
\rho_i(k) &\triangleq g_i(k) - \sum_{j=1}^{i-1}\frac{\partial \alpha_{i-1}(k)}{\partial x_j}g_j(k), \\
\Gamma_i(k) &\triangleq [\alpha_{i-1}(k) - \alpha_{i-1}(1), \alpha_{i-1}(k) - \alpha_{i-1}(2), \ldots, \alpha_{i-1}(k) - \alpha_{i-1}(N)].
\end{aligned} \tag{3.8}
$$

From assumption (A2), one gets that there exists nonnegative smooth function $\phi_{i1}$, $\phi_{i2}$ satisfying

$$
|\Lambda_i(k)| \le p_i^*\phi_{i1}(X_i, k) + p_i^*\phi_{i2}(|\xi|, k). \tag{3.9}
$$

The inequality (3.9) could easily be deduced by using Lemma 3.1.

Considering the transformation $z_i$ in (3.7) which contains the martingale process $M(t)$, according to Lemma 3.2, there exist a function $\Psi(t) \in L^2(P)$ and an $N$-dimensional standard Wiener noise $B(t)$ satisfying $dM(t) = \Psi(t)dB(t)$, where $E[\Psi(t)\Psi(t)^T] = \psi(t)\psi(t)^T \le Q < \infty$ and $Q$ is a positive bounded constant. Therefore we have

$$
\begin{aligned}
dz_i = &\left\{ z_{i+1} + \alpha_i(k) + \tau_i^T(k)\theta^* + \Lambda_i(k) - \frac{\partial \alpha_{i-1}(k)}{\partial t} - \frac{\partial \alpha_{i-1}(k)}{\partial \theta}\dot{\theta} - \sum_{j=1}^{i-1}\frac{\partial \alpha_{i-1}(k)}{\partial p_i}\dot{p}_i \right. \\
&\left. - \sum_{j=1}^{i-1}\frac{\partial \alpha_{i-1}(k)}{\partial x_j}x_{j+1} - \frac{1}{2}\sum_{p,q=1}^{i-1}\frac{\partial^2 \alpha_{i-1}(k)}{\partial x_p \partial x_q}g_p^T(k)\Upsilon\Upsilon^T g_q(k) - \sum_{j=1}^{N}\pi_{kj}\alpha_{i-1}(j) \right\}dt \\
&+ \rho_i^T(k)d\omega + \Gamma_i(k)\Psi(t)dB(t).
\end{aligned} \tag{3.10}
$$

Differential equation of new coordinate $Z = (z_1, z_2, \ldots, z_n)$ is deduced by (3.10). The martingale process resulting from Markov process is transformed into Wiener noise by using Martingale representation theorem. To deal with this, quartic Lyapunov function is proposed, and in the controller design, consideration must be taken for the Wiener noise $B(t)$.

Choose the quartic Lyapunov function as

$$V(k) = \frac{1}{4}\sum_{i=1}^{n} z_i^4 + \frac{1}{2\gamma}\tilde{\theta}^T\tilde{\theta} + \sum_{i=1}^{n}\frac{1}{2\sigma_i}\tilde{p}_i^2, \tag{3.11}$$

where $\gamma > 0$, $\sigma_i > 0$ are constants. $\tilde{\theta} = \theta^* - \theta$ and $\tilde{p}_i = p_i^M - p_i$ are parameter estimation errors, where $p_i^M \triangleq \max\{p_i^*, p_i^0\}$ and $p_i^0$ are given positive constants.

In the view of (3.10) and (3.11), the infinitesimal generator of $V$ satisfies

$$\begin{aligned}
\mathcal{L}V(k) = {} & \sum_{i=1}^{n} z_i^3 \Bigg\{ z_{i+1} + \alpha_i(k) + \tau_i^T(k)\theta^* + \Lambda_i(k) - \frac{\partial\alpha_{i-1}(k)}{\partial t} - \frac{\partial\alpha_{i-1}(k)}{\partial\theta}\dot{\theta} - \sum_{j=1}^{i-1}\frac{\partial\alpha_{i-1}(k)}{\partial p_i}\dot{p}_i \\
& - \sum_{j=1}^{i-1}\frac{\partial\alpha_{i-1}(k)}{\partial x_j}x_{j+1} - \frac{1}{2}\sum_{p,q=1}^{i-1}\frac{\partial^2\alpha_{i-1}(k)}{\partial x_p\partial x_q}g_p^T(k)\Upsilon\Upsilon^T g_q(k) - \sum_{j=1}^{N}\pi_{kj}\alpha_{i-1}(j)\Bigg\} \\
& + \frac{3}{2}\sum_{i=1}^{n} z_i^2\rho_i^T(k)\Upsilon\Upsilon^T\rho_i(k) + \frac{3}{2}\sum_{i=1}^{n} z_i^2\Gamma_i(k)\psi\psi^T\Gamma_i^T(k) - \frac{1}{\gamma}\tilde{\theta}^T\dot{\theta} - \sum_{i=1}^{n}\frac{1}{\sigma_i}\tilde{p}_i\dot{p}_i + \sum_{j=1}^{N}\pi_{kj}V(j) \\
\le {} & \sum_{i=1}^{n} z_i^3 \Bigg\{ \left(\frac{3}{4}\delta_i^{4/3} + \frac{1}{4\delta_{i-1}^4}\right) z_i + \alpha_i(k) + \tau_i^T(k)\theta - \frac{\partial\alpha_{i-1}(k)}{\partial t} - \frac{\partial\alpha_{i-1}(k)}{\partial\theta}\dot{\theta} - \sum_{j=1}^{i-1}\frac{\partial\alpha_{i-1}(k)}{\partial p_i}\dot{p}_i \\
& - \sum_{j=1}^{i-1}\frac{\partial\alpha_{i-1}(k)}{\partial x_j}x_{j+1} + \lambda z_i^3\sum_{p,q=1}^{i-1}\left[\frac{\partial^2\alpha_{i-1}(k)}{\partial x_p\partial x_q}\right]^2\left[g_p^T(k)g_q(k)\right]^2 + \mu_1 z_i\left[\rho_i^T(k)\rho_i(k)\right]^2 \\
& + \mu_2 z_i\left[\Gamma_i(k)\Gamma_i^T(k)\right]^2 - \sum_{j=1}^{N}\pi_{kj}\alpha_{i-1}(j)\Bigg\} + \left[\frac{(n-1)n(2n-1)}{96\lambda} + \frac{9n}{16\mu_1}\right]|\Upsilon|^4 \\
& + \frac{9n}{16\mu_2}Q^2 - \tilde{\theta}^T\left[\frac{1}{\gamma}\dot{\theta} - \sum_{i=1}^{n} z_i^3\tau_i(k)\right] - \sum_{i=1}^{n}\left[\frac{1}{\sigma_i}\tilde{p}_i\dot{p}_i - z_i^3\Lambda_i(k)\right] + \sum_{j=1}^{N}\pi_{kj}V(j).
\end{aligned} \tag{3.12}$$

The following inequalities could be deduced by using Young's inequality and norm inequalities with the help of changing the order of summations or exchanging the indices of the summations:

$$\begin{aligned}
& \sum_{i=1}^{n} z_i^3 z_{i+1} \le \frac{3}{4}\sum_{i=1}^{n-1}\delta_i^{4/3}z_i^4 + \frac{1}{4}\sum_{i=1}^{n-1}\frac{1}{\delta_i^4}z_{i+1}^4 = \sum_{i=1}^{n}\left(\frac{3}{4}\delta_i^{4/3} + \frac{1}{4\delta_{i-1}^4}\right)z_i^4 \\
& - \frac{1}{2}\sum_{i=1}^{n} z_i^3\sum_{p,q=1}^{i-1}\frac{\partial^2\alpha_{i-1}(k)}{\partial x_p\partial x_q}g_{\mathrm{p}}^T(k)\Upsilon\Upsilon^T g_q(k)
\end{aligned}$$

$$\begin{aligned}
&\le \sum_{i=1}^{n}\lambda z_i^6 \sum_{p,q=1}^{i-1}\left[\frac{\partial^2\alpha_{i-1}(k)}{\partial x_p\partial x_q}\right]^2 g_p^T(k)g_p(k)g_q^T(k)g_q(k) + \sum_{i=1}^{n}\sum_{p,q=1}^{i-1}\frac{1}{16\lambda}\left|\Upsilon\Upsilon^T\right|^2 \\
&= \sum_{i=1}^{n}\lambda z_i^6 \sum_{p,q=1}^{i-1}\left[\frac{\partial^2\alpha_{i-1}(k)}{\partial x_p\partial x_q}\right]^2 \left[g_p^T(k)g_q(k)\right]^2 + \frac{\left|\Upsilon\Upsilon^T\right|^2}{96\lambda}(n-1)n(2n-1), \\
&\frac{3}{2}\sum_{i=1}^{n} z_i^2\rho_i^T(k)\Upsilon\Upsilon^T\rho_i(k) \\
&\quad\le \sum_{i=1}^{n}\mu_1 z_i^4\left[\rho_i^T(k)\rho_i(k)\right]^2 + \sum_{i=1}^{n}\frac{9}{16\mu_1}\left|\Upsilon\Upsilon^T\right|^2 \\
&\quad= \sum_{i=1}^{n}\mu_1 z_i^4\left[\rho_i^T(k)\rho_i(k)\right]^2 + \frac{9n}{16\mu_1}\left|\Upsilon\Upsilon^T\right|^2, \\
&\frac{3}{2}\sum_{i=1}^{n} z_i^2\Gamma_i(k)\psi\psi^T\Gamma_i^T(k) \\
&\quad\le \frac{3}{2}\sum_{i=1}^{n} z_i^2\Gamma_i(k)Q\Gamma_i^T(k) \\
&\quad\le \sum_{i=1}^{n}\mu_2 z_i^4\left[\Gamma_i(k)\Gamma_i^T(k)\right]^2 + \sum_{i=1}^{n}\frac{9}{16\mu_2}Q^2 \\
&\quad= \sum_{i=1}^{n}\mu_2 z_i^4\left[\Gamma_i(k)\Gamma_i^T(k)\right]^2 + \frac{9n}{16\mu_2}Q^2,
\end{aligned} \tag{3.13}$$

where $\delta_0 = \infty$, $\delta_n = 0$ and $\lambda > 0$, $\mu_1 > 0$, $\mu_2 > 0$, $\delta_i > 0$, $i = 1, 2, \ldots, n$ are design parameters to be chosen.

Here we suggest the following adaptive laws [18]:

$$\begin{aligned}
\dot{\theta} &= \gamma\left[\sum_{i=1}^{n} z_i^3\tau_i(k) - a\left(\theta - \theta^0\right)\right], \\
\dot{p}_i &= \sigma_i\left[z_i^3\varpi_i(k) - m_i\left(p_i - p_i^0\right)\right].
\end{aligned} \tag{3.14}$$

Here $a > 0$, $\theta^0 \in \mathbb{R}^{p_0}$, $m_i > 0$, $i = 1, 2, \ldots, n$ are design parameters to be chosen. And define function $\beta(k)$ as

$$\begin{aligned}
\varpi_i(k) &= \phi_{i1}(X_i, k)\cdot\tanh\left[\frac{z_i^3\phi_{i1}(X_i, k)}{\varepsilon_i}\right] + z_i^3\tanh\left(\frac{z_i^6}{\upsilon_i}\right), \\
\beta_i(k) &= p_i\cdot\varpi_i(k),
\end{aligned} \tag{3.15}$$

where $\varepsilon_i > 0$, $\upsilon_i > 0$, $i = 1, 2, \ldots, n$ are control parameters to be chosen, and let the virtual control signal be

$$\begin{aligned}\alpha_i(k) = & -c_i z_i - \left(\frac{3}{4}\delta_i^{4/3} + \frac{1}{4\delta_{i-1}^4}\right) z_i - \tau_i^T(k)\theta + \frac{\partial \alpha_{i-1}(k)}{\partial t} + \frac{\partial \alpha_{i-1}(k)}{\partial \theta}\dot{\theta} + \sum_{j=1}^{i-1}\frac{\partial \alpha_{i-1}(k)}{\partial p_i}\dot{p}_i \\ & + \sum_{j=1}^{i-1}\frac{\partial \alpha_{i-1}(k)}{\partial x_j}x_{j+1} - \lambda z_i^3 \sum_{p,q=1}^{i-1}\left[\frac{\partial^2 \alpha_{i-1}(k)}{\partial x_p \partial x_q}\right]^2 \left[g_p^T(k) g_q(k)\right]^2 - \mu_1 z_i \left[\rho_i^T(k)\rho_i(k)\right]^2 \\ & - \mu_2 z_i \left[\Gamma_i(k)\Gamma_i^T(k)\right]^2 + \sum_{j=1}^{N}\pi_{kj}\alpha_{i-1}(j) - \beta_i(k).\end{aligned} \tag{3.16}$$

Thus the real control signal $u(k)$ satisfies $u(k) = \alpha_n(k)$ such that

$$\begin{aligned}\mathcal{L}V \le & -\sum_{i=1}^{n} c_i z_i^4 + a\tilde{\theta}\left(\theta - \theta^0\right) + \sum_{i=1}^{n} z_i^3\left[\Lambda_i(k) - p_i^M \varpi_i(k)\right] + \sum_{i=1}^{n} m_i \tilde{p}_i\left(p_i - p_i^0\right) \\ & + \left[\frac{(n-1)n(2n-1)}{96\lambda} + \frac{9n}{16\mu_1}\right]|\Upsilon|^4 + \frac{9n}{16\mu_2}Q^2 + \sum_{j=1}^{N}\pi_{kj}V(j).\end{aligned} \tag{3.17}$$

Based on assumption (A2) and (3.9), we obtain the following inequality by applying Lemma 3.1:

$$\begin{aligned} z_i^3\Lambda_i(k) - p_i^M z_i^3 \varpi_i(k) &\le \left|z_i^3\Lambda_i(k)\right| - p_i^M z_i^3 \phi_{i1}(X_i, k)\cdot \tanh\left[\frac{z_i^3\phi_{i1}(X_i,k)}{\varepsilon_i}\right] - p_i^M z_i^6 \tanh\left(\frac{z_i^6}{\upsilon_i}\right) \\ &\le \left|z_i^3\right| * \left[p_i^* \phi_{i1}(X_i,k) + p_i^* \phi_{i2}(|\xi|,k)\right] - p_i^M z_i^3 \phi_{i1}(X_i,k) \\ &\quad \cdot \tanh\left[\frac{z_i^3\phi_{i1}(X_i,k)}{\varepsilon_i}\right] - p_i^M z_i^6 \tanh\left(\frac{z_i^6}{\upsilon_i}\right) \\ &\le \left|z_i^3\right| p_i^* \phi_{i1}(X_i,k) - p_i^M z_i^3 \phi_{i1}(X_i,k)\cdot \tanh\left[\frac{z_i^3\phi_{i1}(X_i,k)}{\varepsilon_i}\right] \\ &\quad + p_i^M \left|z_i^3\right| \phi_{i2}(|\xi|,k) - p_i^M z_i^6 \tanh\left(\frac{z_i^6}{\upsilon_i}\right) \\ &\le p_i^M\left[\left|z_i^3\phi_{i1}(X_i,k)\right| - z_i^3\phi_{i1}(X_i,k)\cdot \tanh\left[\frac{z_i^3\phi_{i1}(X_i,k)}{\varepsilon_i}\right]\right] \\ &\quad + p_i^M\left[z_i^6 - z_i^6 \tanh\left(\frac{z_i^6}{\upsilon_i}\right) + \frac{1}{4}\phi_{i2}^2(|\xi|,k)\right] \\ &\le \frac{\varepsilon_i + \upsilon_i}{2}p_i^M + \frac{p_i^M}{4}\phi_{i2}^2(|\xi|,k). \end{aligned} \tag{3.18}$$

In (3.18), the following inequality is applied:

$$0 \le |\eta| - \eta \cdot \tanh\left(\frac{\eta}{\epsilon}\right) \le \frac{1}{2}\epsilon. \tag{3.19}$$

Notice the fact that

$$\begin{aligned} a\tilde{\theta}^T\left(\theta-\theta^0\right) &= -\frac{1}{2}a\tilde{\theta}^T\tilde{\theta} - \frac{1}{2}a\left(\theta-\theta^0\right)^T\left(\theta-\theta^0\right) + \frac{1}{2}a\left(\theta^*-\theta^0\right)^T\left(\theta^*-\theta^0\right) \\ &\le -\frac{1}{2}a\tilde{\theta}^T\tilde{\theta} + \frac{1}{2}a\left(\theta^*-\theta^0\right)^T\left(\theta^*-\theta^0\right), \\ m_i\tilde{p}_i\left(p_i-p_i^0\right) &= -\frac{1}{2}m_i\tilde{p}_i^2 - \frac{1}{2}m_i\left(p_i-p_i^0\right)^2 + \frac{1}{2}m_i\left(p_i^M-p_i^0\right)^2 \\ &\le -\frac{1}{2}m_i\tilde{p}_i^2 + \frac{1}{2}m_i\left(p_i^M-p_i^0\right)^2. \end{aligned} \tag{3.20}$$

Submitting (3.18), (3.20) into (3.12), there is

$$\begin{aligned} \mathcal{L}V(k) \le & -\sum_{i=1}^{n}c_iz_i^4 - \frac{1}{2}a\tilde{\theta}^T\tilde{\theta} - \sum_{i=1}^{n}\frac{1}{2}m_i\tilde{p}_i^2 + \frac{1}{2}a\left(\theta^*-\theta^0\right)^T\left(\theta^*-\theta^0\right) + \sum_{i=1}^{n}\frac{1}{2}m_i\left(p_i^M-p_i^0\right)^2 \\ & + \left[\frac{(n-1)n(2n-1)}{96\lambda} + \frac{9n}{16\mu_1}\right]|\Upsilon|^4 + \frac{9n}{16\mu_2}Q^2 + \sum_{i=1}^{n}\frac{\varepsilon_i+\upsilon_i}{2}p_i^M \\ & + \sum_{i=1}^{n}\frac{p_i^M}{4}\phi_{i2}^2(|\xi|,k) + \sum_{j=1}^{N}\pi_{kj}V(j) \\ \le & -\alpha_1V(k) + V_\xi(|\xi|,k) + d_z + \sum_{j=1}^{N}\pi_{kj}V(j). \end{aligned} \tag{3.21}$$

Here parameter $\alpha_1$, $d_z$ and $\mathcal{K}_\infty$ function $V_\xi(|\xi|,k)$ is chosen to satisfy

$$\begin{aligned} & V_\xi(|\xi|,k) \ge \sum_{i=1}^{n}\frac{p_i^M}{4}\phi_{i2}^2(|\xi|,k), \qquad \alpha_1 = \min\{4c_i, a\cdot\gamma, m\cdot\sigma_i\}, \\ d_z = & \frac{1}{2}a(\theta^*-\theta^0)^T(\theta^*-\theta^0) + \sum_{i=1}^{n}\frac{1}{2}m_i\left(p_i^M-p_i^0\right)^2 + \left[\frac{(n-1)n(2n-1)}{96\lambda} + \frac{9n}{16\mu_1}\right]|\Upsilon|^4 \\ & + \frac{9n}{16\mu_2}Q^2 + \sum_{i=1}^{n}\frac{\varepsilon_i+\upsilon_i}{2}p_i^M. \end{aligned} \tag{3.22}$$

## 4. Stochastic Stability Analysis

**Theorem 4.1.** *Considering the MJNS* (3.1) *with Assumptions (A2) standing, the X-subsystem is JISpS in probability with the adaptive laws* (3.14) *and switching control law* (3.16) *adopted; meanwhile all solutions of closed-loop X-subsystem are ultimately bounded.*

*Proof.* Considering the MJNS (3.1) with Lyapunov function (3.11), the following equations hold according to [10]:

$$EV(r(t)) = \sum_{l=1}^{N} EV(l)\zeta_l, \qquad E\mathcal{L}V(r(t)) = \sum_{l=1}^{N} E(\mathcal{L}V(l))\zeta_l. \tag{4.1}$$

Thus (3.21) can be written as

$$\begin{aligned} E\mathcal{L}V(r(t)) &= \sum_{l=1}^{N} E(\mathcal{L}V(l))\zeta_l \\ &\le \sum_{l=1}^{N} E\left\{-\alpha_1\zeta_l V(l) + \zeta_l V_\xi(|\xi|, l) + \zeta_l d_z + \zeta_l \sum_{j=1}^{N} \pi_{lj} V(j)\right\} \\ &= -\alpha_1 \sum_{l=1}^{N} \zeta_l EV(l) + E\left\{\sum_{l=1}^{N}\zeta_l \sum_{j=1}^{N} \pi_{lj} V(j)\right\} + \sum_{l=1}^{N} \zeta_l EV_\xi(|\xi|, l) + d_z \\ &\le -\alpha EV(r(t)) + \chi(|\xi(t)|) + d_z, \end{aligned} \tag{4.2}$$

where positive scalar $\alpha$ is given as

$$\begin{aligned} \alpha &\triangleq \alpha_1 - \max_{l,j\in S}\left\{\frac{\zeta_l}{\zeta_j}\right\} * \max_{j\in S}\left\{\sum_{l=1}^{N} \pi_{lj}\right\} \\ \chi(|\xi(t)|) &\triangleq \sum_{l=1}^{N} \zeta_l EV_\xi(|\xi|, l). \end{aligned} \tag{4.3}$$

It is easily seen that $\chi(|\xi(t)|)$ is a $\mathcal{K}_\infty$ function with $r(t)$ given, and appropriate control parameter $c_i$, $l \cdot \gamma$, $m \cdot \sigma_i$ can be chosen to satisfy $\alpha > 0$.

For each integer $h \ge 1$, define a stopping time as

$$\tau_h = \inf\{t \ge 0 : |z(t)| \ge h\} \tag{4.4}$$

Obviously, $\tau_h \to \infty$ almost surely as $h \to \infty$. Noticing that $0 < |z(t)| \le h$ if $0 \le t < \tau_h$, we can apply the generalized $It\hat{o}$ formula to derive that for any $t \ge 0$,

$$\begin{aligned} E\left[e^{\alpha\cdot(t\wedge\tau_h)} V(r(t\wedge\tau_h))\right] &= V(z_0, 0, r(0)) + \int_0^{t\wedge\tau_h} e^{\alpha s}[\alpha EV(r(s)) + E\mathcal{L}V(r(s))]ds \\ &\le V(r(0)) + \int_0^{t\wedge\tau_h} e^{\alpha s}\left[\alpha EV(r(s)) - \alpha EV(r(s)) + \chi(|\xi(t)|) + d_z\right]ds \\ &= V(r(0)) + \int_0^{t\wedge\tau_h} e^{\alpha s}\left[\chi(|\xi(t)|) + d_z\right]ds. \end{aligned} \tag{4.5}$$

Let $h \to \infty$, apply Fatou's lemma to (4.5), and we have

$$E\left[e^{\alpha t}V(r(t))\right] \le V(r(0)) + E\int_0^t e^{\alpha s}\left[\chi(|\xi(t)|) + d_z\right]ds. \tag{4.6}$$

By using mean value theorem for integration, there is

$$\begin{aligned} E\left[e^{\alpha t}V(x(t),t,k)\right] &= e^{\alpha t}EV(r(t)) \\ &\le V(r(0)) + \sup_{0\le s\le t}\left[\chi(|\xi(s)|) + d_z\right]\cdot\int_0^t e^{\alpha s}ds. \end{aligned} \tag{4.7}$$

According to the property of $\mathcal{K}_\infty$ function, the following inequality is deduced:

$$\begin{aligned} e^{\alpha t}EV(r(t)) &\le V(r(0)) + \left\{\chi\left(\sup_{0\le s\le t}|\xi(s)|\right) + d_z\right\}\cdot\int_0^t e^{\alpha s}ds \\ &= V(r(0)) + \left[\chi(\|\xi(t)\|) + d_z\right]\cdot\left(\frac{1}{\alpha}\right)\left(e^{\alpha t} - 1\right) \\ &\le V(r(0)) + \left[\chi(\|\xi(t)\|) + d_z\right]\cdot\left(\frac{1}{\alpha}\right)e^{\alpha t}. \end{aligned} \tag{4.8}$$

According to (3.11), one gives

$$e^{\alpha t}\sum_{j=1}^{N}\frac{1}{4}E\left\{z_i^4\right\} \le e^{\alpha t}EV(r(t)) \le EV(r(0)) + \left[\chi(\|\xi(t)\|) + d_z\right]\cdot\left(\frac{1}{\alpha}\right)e^{\alpha t}. \tag{4.9}$$

Consequently,

$$\sum_{i=1}^{N}E\left\{z_i^4\right\} \le 4e^{-\alpha t}V(r(0)) + \frac{4}{\alpha}\left\{\chi(\|\xi(t)\|) + d_z\right\}. \tag{4.10}$$

Defining $\mathcal{KL}$ function $\beta(\cdot,\cdot)$, $\mathcal{K}_\infty$ function $\gamma(\cdot)$, and nonnegative number $d_c$ as:

$$\beta(|z_0|,t) = 4e^{-\lambda t}V(r(0)), \qquad \gamma(\|\xi(t)\|) = \frac{4}{\alpha}\chi(\|\xi(t)\|), \qquad d_c = \frac{4}{\alpha}d_z. \tag{4.11}$$

and applying Chebyshev's inequality, we have that the $X$-subsystem of MJNS (3.1) is JISpS in probability.

The proof is completed. □

**Theorem 4.2.** *Considering the MJNS* (3.1) *with Assumptions (A1), (A2) holding, the interconnected Markovian jump system is JISpS in probability with adaptive laws* (3.14) *and switching control law*

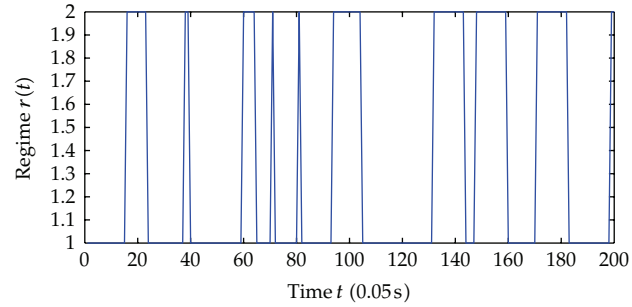


**Figure 2:** Regime transition $r(t)$.

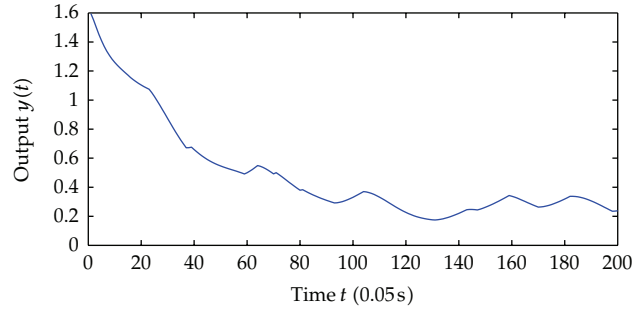


**Figure 3:** System output $y$.

(3.16) *adopted; meanwhile all solutions of closed-loop system are ultimately bounded. Furthermore, the system output could be regulated to an arbitrarily small neighborhood of the equilibrium point in probability within finite time.*

*Proof.* From Assumption (A1), the $\xi$ subsystem is JISpS in probability. And it has been shown in Theorem 4.1 that the $X$ subsystem is JISpS in probability. Similar to the proof in [12], we have that the entire MJNS (3.1) is JISpS in probability; that is, for any given $\epsilon > 0$, there exists $T > 0$ and $\delta > 0$ such that if $t > T$, the output of jump system $y$ satisfies

$$P\{|y(t)| < \delta\} \geq 1 - \epsilon. \tag{4.12}$$

Meanwhile $\delta$ can be made as small as possible by appropriate control parameters chosen. □

## 5. Simulation

With loss of generality, in this section we consider a two-order Markovian jump nonlinear system with regime transition space $S = \{1, 2\}$, and the system with unmodeled dynamics and noise is as follows:

$$d\xi = q(x_1, \xi, t, r(t))dt,$$

$$dx_1 = x_2 dt + f_1(x_1, t, r(t))\theta^* dt + \Delta_1(X, \xi, t, r(t))dt + x_1^{1/3} d\omega,$$

$$dx_2 = udt + f_2(X,t,r(t))\theta^* dt + \Delta_2(X,\xi,t,r(t))dt,$$
$$y = x_1,$$
(5.1)

where the transition rate matrix is $\Pi = \left[\begin{smallmatrix}\pi_{11} & \pi_{12}\\ \pi_{21} & \pi_{22}\end{smallmatrix}\right] = \left[\begin{smallmatrix}-2 & 2\\ 3 & -3\end{smallmatrix}\right]$ with stationary distribution $\zeta_1 = \zeta_2 = 0.5$.

Here let noise covariance be $E\{d\omega d\omega^T\} = 1$ and system dynamics for each mode as

$$\begin{aligned}
q(x_1,\xi,t,1) &= -0.5\xi + 0.3x_1, \qquad q(x_1,\xi,t,2) = -0.4\xi + 0.3x_1\cos t,\\
f_1(x_1,t,1) &= x_1^2, \qquad f_1(x_1,t,2) = -x_1\cos x_1,\\
\Delta_1(X,\xi,t,1) &= 0.5\xi + 0.4x_1\sin 2t, \qquad \Delta_1(X,\xi,t,2) = x_1\xi,\\
f_2(X,t,1) &= x_1\sin x_2 + x_2, \qquad f_2(X,t,2) = x_1 + 2x_2,\\
\Delta_2(X,\xi,t,1) &= 0.4\xi\sin t + 0.3x_1. \qquad \Delta_2(X,\xi,t,2) = x_1|\xi|^{1/2}.
\end{aligned}$$
(5.2)

From Assumption (A2), we have

$$\begin{aligned}
\Delta_1(X,\xi,t,1) &\le p_1^*|\xi| + p_1^*|x_1|, \qquad \Delta_1(X,\xi,t,2) \le p_1^*|\xi|^2 + p_1^*|x_1|^2,\\
\Delta_2(X,\xi,t,1) &\le p_2^*|\xi| + p_2^*|x_1|, \qquad \Delta_2(X,\xi,t,2) \le p_2^*|\xi| + p_2^*|x_1|^2,
\end{aligned}$$
(5.3)

where $p_1^* \le 0.5$ and $p_2^* \le 0.5$ and the $\xi$ subsystem satisfies

$$\mathcal{L}V_0(\xi,t,k) \le -\frac{4}{10}|\xi|^2 + \chi_0(|x_1|) + d_0,$$
(5.4)

where $V_0 = (1/2)\xi^2$, $\chi_0(|x_1|) = 0.15|x_1|^2$, $d_0 = 0.125$, and it can be checked which satisfies the stochastic small-gain theorem. Thus the control law is taken as follows (here $\delta_1 = 1$ ).

*Case 1.* The system regime is $k = 1$:

$$\begin{aligned}
\alpha_1(1) = {} & -\left(c_1 + \frac{3}{4}\right)x_1 - x_1^2\theta - \mu_1 x_1^{7/3} - p_1 x_1\tanh\left(\frac{x_1^4}{\epsilon_1}\right) - x_1^3\tanh\left(\frac{x_1^6}{v_i}\right)\\
\alpha_2(1) = {} & -\left(c_2 + \frac{1}{4}\right)z_2(1) - x_1\sin x_2 - u_1 z_2^3(1)x_1^2 - \frac{1}{4}z_2^3(1) - \left(c_1 + \frac{3}{4} + 2x_1 + \frac{3}{4}x_1^2x_1^4\right)\\
& \times\left(x_1^2 + x_2\right) + \pi_{11}\alpha_1(1) + \pi_{12}\alpha_1(2) - \mu_2 z_2(1)[\alpha_1(1) - \alpha_1(2)]^4 - \tau_2(1)\theta - \tau_1(1)\dot\theta\\
& - p_1\tanh\left(\frac{x_1^4}{\epsilon_1}\right) - 3x_1^2\tanh\left(\frac{x_1^6}{v_i}\right) - 4p_1x_1^4\operatorname{sech}^2\left(\frac{x_1^4}{\epsilon_1}\right) - x_1^8\operatorname{sech}^2\left(\frac{x_1^6}{v_i}\right) - p_2\varpi_1(2),
\end{aligned}$$

$$
\begin{aligned}
z_2(1) &= x_2 - \alpha_1(1),\\
\dot{\theta} &= \gamma\left[\sum_{i=1}^{2} z_i^3 \tau_i(1) - a\left(\theta - \theta^0\right)\right],\\
\dot{p}_1 &= \sigma_1\left[x_1^3 \varpi_i(1) - m_1\left(p_1 - p_1^0\right)\right],\\
\dot{p}_2 &= \sigma_2\left[z_2^3(1)\varpi_2(1) - m_2\left(p_2 - p_2^0\right)\right].
\end{aligned}
\tag{5.5}
$$

*Case 2.* The system regime is $k = 2$:

$$
\begin{aligned}
\alpha_1(2) &= -\left(c_1 + \frac{3}{4}\right)x_1 - x_1 \sin x_1 - x_2 - p_1 x_1 \tanh\left(\frac{x_1^4}{\epsilon_1}\right) - x_1^3 \tanh\left(\frac{x_1^6}{v_i}\right),\\
\alpha_2(2) &= -\left(c_2 + \frac{1}{4}\right)z_2(2) - \mu_1 z_2^3(2) x_1^4 - \frac{1}{4} z_2^3(2) - \left(c_1 + \frac{11}{4} + \frac{3}{4}x_1^2 + x_1^6\right)(x_1 + x_2)\\
&\quad + \pi_{21}\alpha_1(1) + \pi_{22}\alpha_1(2) - \mu_2 z_2(2)[\alpha_1(1) - \alpha_1(2)]^4 - \tau_2(2)\theta - \tau_1(2)\dot{\theta}\\
&\quad - p_1 \tanh\left(\frac{x_1^4}{\epsilon_1}\right) - 3x_1^2 \tanh\left(\frac{x_1^6}{v_i}\right) - 4p_1 x_1^4 \operatorname{sech}^2\left(\frac{x_1^4}{\epsilon_1}\right) - x_1^8 \operatorname{sech}^2\left(\frac{x_1^6}{v_i}\right) - p_2 \varpi_2(2),\\
z_2(2) &= x_2 - \alpha_1(2),\\
\dot{\theta} &= \gamma\left[\sum_{i=1}^{2} z_i^3 \tau_i(2) - a\left(\theta - \theta^0\right)\right],\\
\dot{p}_1 &= \sigma_1\left[x_1^3 \varpi_i(2) - m_1\left(p_1 - p_1^0\right)\right],\\
\dot{p}_2 &= \sigma_2\left[z_2^3(2)\varpi_2(2) - m_2\left(p_2 - p_2^0\right)\right].
\end{aligned}
\tag{5.6}
$$

In computation, we set the initial value to be $x_1 = 1.6$, $x_2 = -2.7$, $\theta = 0$, $p_1 = p_2 = 0$ let parameter $\theta^0 = 1$, $\gamma = 1$, $a = 1$, $p^0 = 0.7$, $\epsilon_i = v_i = 0.5$, $m_i = 1$, $\mu_1 = \mu_2 = 1$ and the time step to be 0.05 s. For comparison, two groups of different control parameters are given. First we take the parameter with values $c_1 = c_2 = 0.7$, $\sigma_1 = \sigma_2 = 2$, and the simulation results are as follows. Figure 2 shows the regime transition of the jump system, Figure 3 shows the system output $y$ which is defined as the system state $x_1$, and Figure 4 shows system state $x_2$. Figure 5 shows the corresponding switching controller $u$; finally Figure 6 shows the trajectory of adaptive parameter $\theta$ and Figure 7; Figure 8 shows the trajectory of parameter $p_1$, $p_2$, respectively.

Now we choose different control parameters as $c_1 = c_2 = 2$, $\sigma_1 = \sigma_2 = 5$ and repeat the simulation. The simulation results are as follows. Figure 9 shows the regime transition of the jump system, Figure 10 shows the system output $y$ which is defined as the system state $x_1$ and, Figure 11 shows system state $x_2$, and Figure 12 shows the corresponding switching

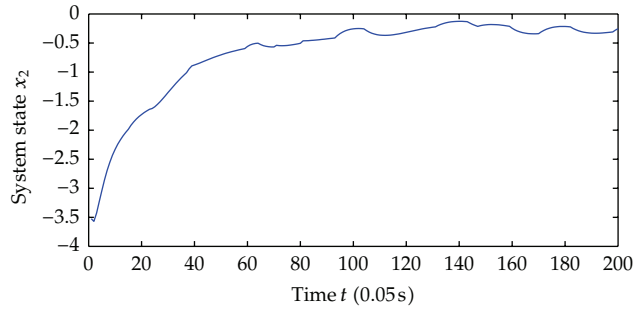


**Figure 4:** System state $x_2$.

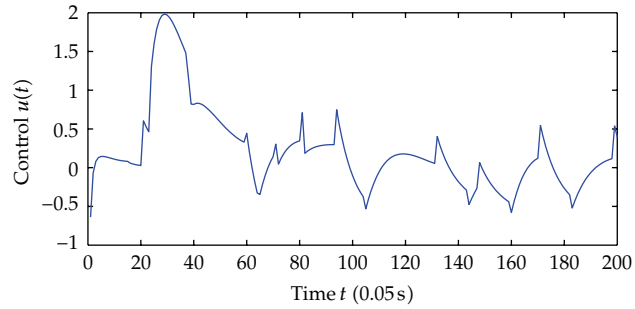


**Figure 5:** Switching controller $u$.

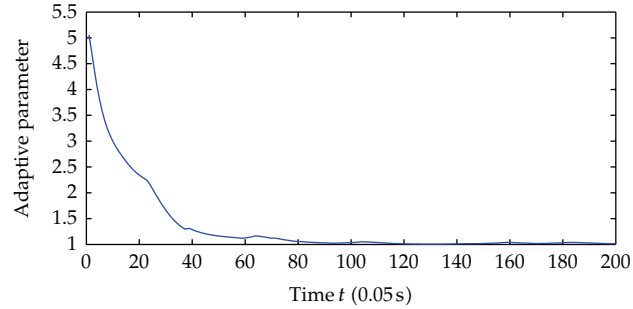


**Figure 6:** Adaptive parameter $\theta$.

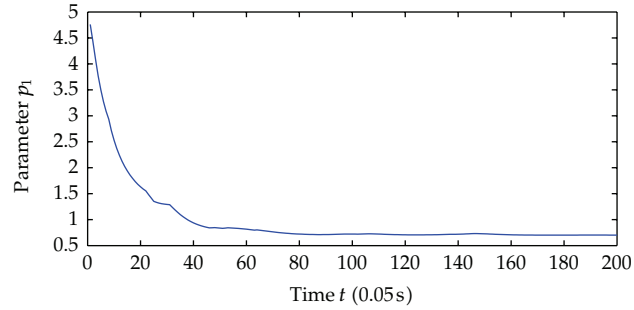


**Figure 7:** Parameter $p_1$.

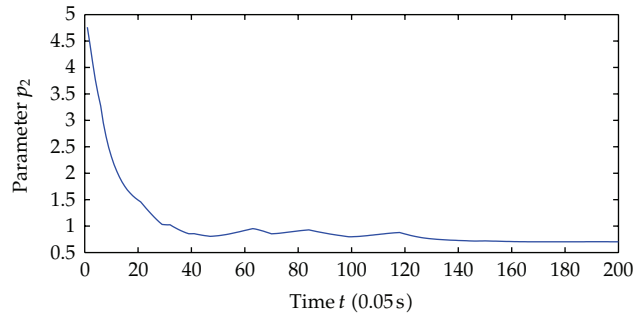


**Figure 8:** Parameter $p_2$.

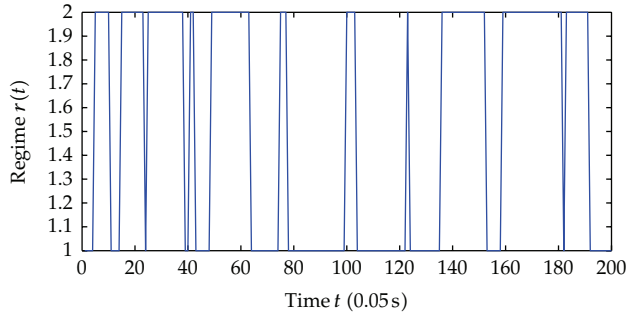


**Figure 9:** Regime transition $r(t)$.

controller $u$; the trajectory of adaptive parameter $\theta$ is shown in Figures 13 and 14; Figure 15 shows the trajectory of parameter $p_1$, $p_2$, respectively.

Comparing the results from two simulations, all the signals of closed-loop system are globally uniformly ultimately bounded, and the system output can be regulated to a neighborhood near the equilibrium point despite different jump samples. As could be seen from the figures, larger values of $c_1$, $c_2$, $\sigma_1$, $\sigma_2$ help to increase the convergence speed of system states. This reason is that the increase of these parameters increases the value of $\alpha$, which determines the system states convergence speed. Also adaptive parameters $\theta$ and $p_1$, $p_2$ approach convergence faster with the increasing of aforementioned parameters.

*Remark 5.1.* Much research work has been performed towards the study of nonlinear system by using small-gain theorem [16, 19]. In contrast to their contributions, this paper considers a more general form than nonjump systems. The controller $u(k)$ varies with different regime $r(t) = k$ taken, and it differs in two aspects (see (3.16)): the coupling of regimes $\pi_{kj}\alpha_{i-1}(j)$ and $\mu_2 z_i[\Gamma_i(k)\Gamma_i^T(k)]^2$, which are both caused by the Markovian jumps. The switching controller will degenerate to an ordinary one if $r(t) \equiv 1$. This controller design method can also be applied for the nonjump nonlinear system.

## 6. Conclusion

In this paper, the robust adaptive switching controller design for a class of Markovian jump nonlinear system is studied. Such MJNSs, suffering from unmodeled dynamics and noise

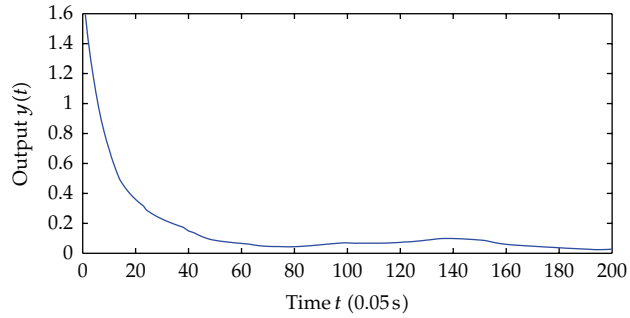


**Figure 10:** System output $y$.

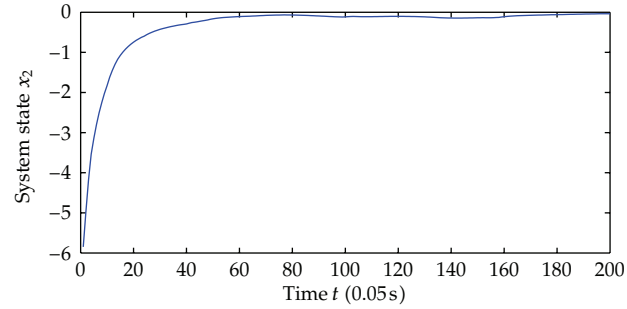


**Figure 11:** System state $x_2$.

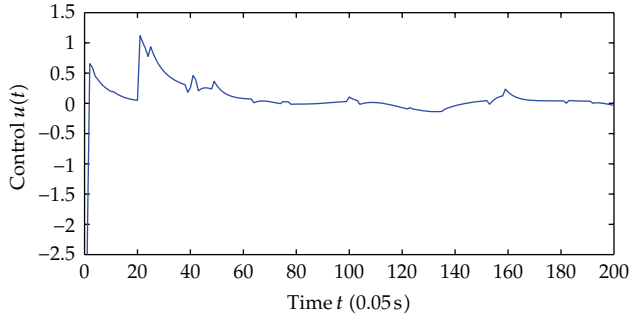


**Figure 12:** Switching controller $u$.

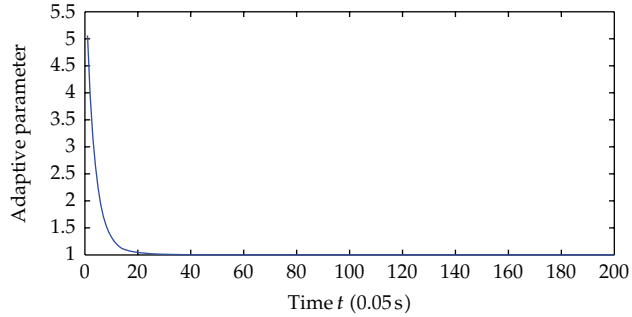


**Figure 13:** Adaptive parameter $\theta$.

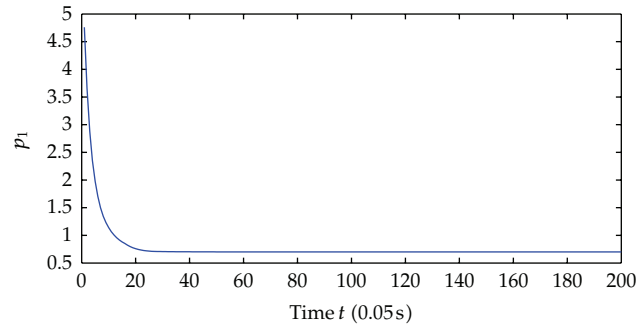


**Figure 14:** Parameter $p_1$.

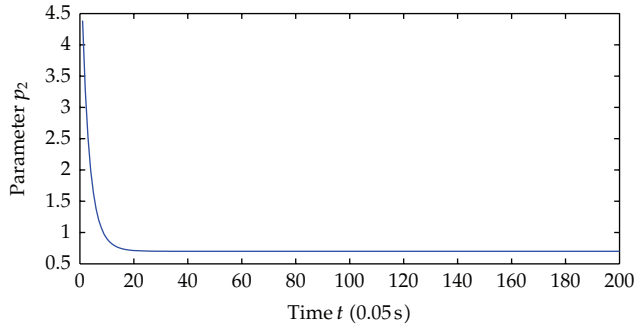


**Figure 15:** Parameter $p_2$.

of unknown covariance, are of the strict feedback form. With the extension of input-to-state stability (ISpS) to jump case as well as the small-gain theorem, stochastic Lyapunov stability criterion is put forward. By using backstepping technique, a switching controller is designed which ensures the jump nonlinear system to be jump ISpS in probability. Moreover the upper bound of uncertainties can be estimated, and system output will converge to an attractive region around the equilibrium point, whose radius can be made as small as possible with appropriate control parameters chosen. Numerical examples are given to show the effectiveness of the proposed design.

## Acknowledgment

This work is supported by the National Natural Science Foundation of China under Grants 60904021 and the Fundamental Research Funds for the Central Universities under Grants WK2100060004.

## References

[1] M. Mariton, *Jump Linear Systems in Automatic Control*, Marcel-Dekker, New York, NY, USA, 1990.
[2] X. Mao, "Stability of stochastic differential equations with Markovian switching," *Stochastic Processes and Their Applications*, vol. 79, no. 1, pp. 45–67, 1999.
[3] C. E. de Souza, A. Trofino, and K. A. Barbosa, "Mode-independent $H_\infty$ filters for Markovian jump linear systems," *IEEE Transactions on Automatic Control*, vol. 51, no. 11, pp. 1837–1841, 2006.
[4] S. Xu, J. Lam, and X. Mao, "Delay-dependent $H_\infty$ control and filtering for uncertain Markovian jump systems with time-varying delays," *IEEE Transactions on Circuits and Systems. I. Regular Papers*, vol. 54, no. 9, pp. 2070–2077, 2007.

[5] N. Xiao, L. Xie, and M. Fu, "Stabilization of Markov jump linear systems using quantized state feedback," *Automatica*, vol. 46, no. 10, pp. 1696–1702, 2010.
[6] T. Hou, W. Zhang, and H. Ma, "Finite horizon $H_2/H_\infty$ control for discrete-time stochastic systems with Markovian jumps and multiplicative noise," *IEEE Transactions on Automatic Control*, vol. 55, no. 5, pp. 1185–1191, 2010.
[7] H. Sira-Ramírez, M. Rios-Bolivar, and A. S. I. Zinober, "Adaptive dynamical input-output linearization of dc to dc power converters: a backstepping approach," *International Journal of Robust and Nonlinear Control*, vol. 7, no. 3, pp. 279–296, 1997.
[8] R. Kristiansen, P. J. Nicklasson, and J. T. Gravdahl, "Satellite attitude control by quaternion-based backstepping," *IEEE Transactions on Control Systems Technology*, vol. 17, no. 1, pp. 227–232, 2009.
[9] C. Kaddissi, J. P. Kenne, and M. Saad, "Indirect adaptive control of an electrohydraulic Servo system based on nonlinear backstepping," *IEEE/ASME Transactions on Mechatronics*, vol. 16, no. 6, pp. 1171–1177, 2010.
[10] Z.-J. Wu, X.-J. Xie, P. Shi, and Y.-Q. Xia, "Backstepping controller design for a class of stochastic nonlinear systems with Markovian switching," *Automatica*, vol. 45, no. 4, pp. 997–1004, 2009.
[11] Z. J. Wu, J. Yang, and P. Shi, "Adaptive tracking for stochastic nonlinear systems with Markovian switching," *IEEE Transactions on Automatic Control*, vol. 55, no. 9, pp. 2135–2141, 2010.
[12] J. Zhu, J. Park, K.-S. Lee, and M. Spiryagin, "Switching controller design for a class of Markovian jump nonlinear systems using stochastic small-gain theorem," *Advances in Difference Equations*, vol. 2009, Article ID 896218, 23 pages, 2009.
[13] D. Dong, C. Chen, J. Chu, and T. J. Tarn, "Robust quantum-inspired reinforcement learning for robot navigation," *IEEE/ASME Transactions on Mechatronics*, vol. 17, no. 1, pp. 86–97, 2012.
[14] D. W. Stroock, *An Introduction to Markov Processes*, vol. 230 of *Graduate Texts in Mathematics*, Springer, Berlin, Germany, 2005.
[15] C. Yuan and X. Mao, "Robust stability and controllability of stochastic differential delay equations with Markovian switching," *Automatica*, vol. 40, no. 3, pp. 343–354, 2004.
[16] Z.-J. Wu, X.-J. Xie, and S.-Y. Zhang, "Adaptive backstepping controller design using stochastic small-gain theorem," *Automatica*, vol. 43, no. 4, pp. 608–620, 2007.
[17] B. Øsendal, *Stochastic Differential Equations*, Springer, New York, NY, USA, 2000.
[18] M. M. Polycarpou and P. A. Ioannou, "A robust adaptive nonlinear control design," *Automatica*, vol. 32, no. 3, pp. 423–427, 1996.
[19] Z.-P. Jiang, "A combined backstepping and small-gain approach to adaptive output feedback control," *Automatica*, vol. 35, no. 6, pp. 1131–1139, 1999.

Hindawi Publishing Corporation
Journal of Applied Mathematics
Volume 2012, Article ID 945240, 11 pages
doi:10.1155/2012/945240

*Research Article*

# Robust Stability of Uncertain Systems over Network with Bounded Packet Loss

**Yafeng Guo[1] and Tianhong Pan[2]**

[1] *Department of Control Science and Engineering, School of Electronics and Information Engineering, Tongji University, Shanghai 201804, China*
[2] *Department of Chemical and Materials Engineering, University of Alberta, Edmonton, AB, Canada T6G 2G6*

Correspondence should be addressed to Tianhong Pan, thpan888@hotmail.com

Received 26 February 2012; Revised 20 April 2012; Accepted 23 April 2012

Academic Editor: Baocang Ding



This paper investigates the problem of robust stability of uncertain linear discrete-time system over network with bounded packet loss. A new Lyapunov functional is constructed. It can more fully utilize the characteristics of the packet loss; hence the established stability criterion is more effective to deal with the effect of packet loss on the stability. Numerical examples are given to illustrate the effectiveness and advantage of the proposed methods.

## 1. Introduction

A networked control system (NCS) is a system whose feedback loop or (and) control loop is (are) connected via a communication network, which may be shared with other devices. The main advantages of NCS are low cost, reduced weight, high reliability, simple installation, and maintenance. As a result, the NCSs have been applied in many fields, such as mobile sensor networks, manufacturing systems, teleoperation of robots, and aircraft systems [1].

However, the insertion of the communication networks in control loops will bring some new problems. One of the most common problems in NCSs, especially in wireless sensor networks, is packet dropout, that is, packets can be lost due to communication noise, interference, or congestion [2]. Some results on this issue have been available. Generally, in these results there are two types of packet-loss model. One is stochastic packet loss ([2–5]; etc), another is arbitrary but bounded packet loss ([6–9]; etc).

Here, we are concerned about the arbitrary but bounded packet loss. For this case, there are two approaches available. One approach is based on switched system theory;

another one is based on the theory of time-varying-delay system. Yu et al. [7] modeled the packet-loss process as an arbitrary but finite switching signal. This enables them to apply the theory from switched systems to stabilize the NCS. However, Yu et al. [7] adopted a common Lyapunov function and the results are quadratic. Xiong and Lam [9] utilized a packet-loss-dependent Lyapunov function to establish the stabilization condition, which is less conservative than that of Yu et al. [7]. Unfortunately, however, in the stability condition of their approaches the system matrices appear in the forms of power and cross-multiplication among them. Therefore, it is difficult to deal with the systems with parametric uncertainty by using these approaches. In contrast, if utilizing the delay system approach, the system matrices are affine in the stability condition. Hence, this approach suits the uncertain systems. However, it may be very conservative if directly using the existing delay system approaches (e.g., [10–14]) to deal with the bounded packet loss. The main reason is that the existing approaches can not fully utilize the characteristic of packet loss. Therefore, for the systems in the simultaneous presence of parameter uncertainties and bounded packet loss, the problem of robust stability has not been fully investigated and remains to be challenging, which motivates the present study.

In this paper, we study the robust stability problem for uncertain discrete-time systems with bounded networked packet loss. First, we transform the packet loss into a time-varying input delay. Second, we note that the considered time-varying delay has a new characteristic. It is different with the general time-varying delay, that is, the considered time delay will change with some laws in the interval of two consecutive successful transmissions of the network, which is not possessed by general time-varying delay. In order to utilize this characteristic, we define a new Lyapunov functional. It does not only depend on the bound of the delay, but also on the rate of its change. Due to more fully utilizing the properties of the packet loss (that is the time-varying delay induced by the packet loss), the established stability criterion shows its less conservativeness. The construction of Lyapunov functional is inspired by Fridman [15], where the stability of sampled-data control systems is considered. It does not mean that the method developed in this paper is trivial. In fact, as it is shown in the Section 3 of this paper that the properties of induced-delay are more complicate than that in Fridman [15], such that the method of Fridman [15] cannot directly be applied to the problem considered in this paper. Finally, three examples are provided to illustrate the effectiveness of the developed results.

## 2. Problem Formulation

The framework of NCSs considered in the paper is depicted in Figure 1. The plant to be controlled is modeled by linear discrete-time system:

$$x(k+1) = (A + \Delta A)x(k) + (B + \Delta B)u(k), \tag{2.1}$$

where $k \in \mathbb{Z}_+$ is the time step, $x(k) \in \mathbb{R}^{n_x}$ and $u(k) \in \mathbb{R}^{n_u}$ are the system state and control input, respectively. $x_0 \triangleq x(0)$ is the initial state. $A$ and $B$ are known real constant matrices with appropriate dimension. $\Delta A$ and $\Delta B$ are unknown matrices describing parameter uncertainties.

In this paper, the parameter uncertainties are assumed to be of the form $\begin{bmatrix} \Delta A & \Delta B \end{bmatrix} = DF(k)\begin{bmatrix} E_1 & E_2 \end{bmatrix}$, where $D$, $E_1$, and $E_2$ are known real constant matrices of appropriate

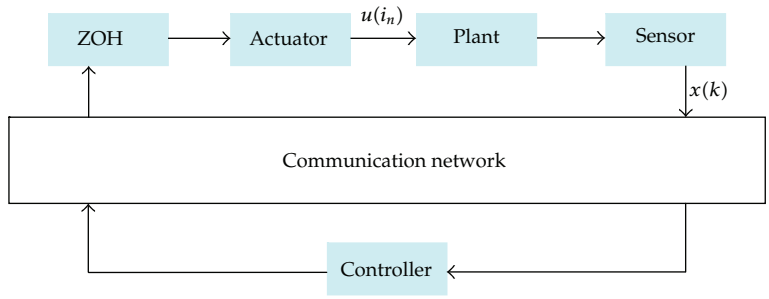


**Figure 1:** Networked control systems with packet loss.

dimensions, and $F(k)$ is an unknown real-valued time-varying matrix satisfying $F(k)F^T(k) \leq I$.

Networks exist between sensor and controller and between controller and zero-order holder (ZOH). The sensor is clock driven, the controller and ZOH are event driven and the data are transmitted in a single packet at each time step. As have been mentioned in Section 1, this paper only considers the network packet loss. Then it is assumed that there is not any network-induced delay.

Let $\mathbb{S} \triangleq \{i_1, i_2, i_3, \ldots\} \subset \{0, 1, 2, 3, \ldots\}$ denote the sequence of time points of successful data transmissions from the sensor to the zero-order hold at the actuator side and $i_n < i_{n+1}$ for any $n = 1, 2, 3, \ldots$.

*Assumption 2.1.* The number of consecutive packet loss in the network is less than $\overline{m}$, that is

$$i_{n+1} - i_n - 1 \leq \overline{m}, \quad \forall n \in \{1, 2, 3, \ldots\}. \tag{2.2}$$

*Remark 2.2.* Assumption 2.1 is similar to that in Liu et al. [8]. From the physical point of view, it is natural to assume that only a finite number of consecutive packet losses can be tolerated in order to avoid the NCS becoming open loop. Thus, the number of consecutive packet loss in the networks should be less than the finite number $\overline{m}$.

The networked controller is a state-feedback controller:

$$u = Kx. \tag{2.3}$$

From the viewpoint of the ZOH, the control input is

$$u(k) = u(i_n) = Kx(i_n), \quad i_n \leq k < i_{n+1}. \tag{2.4}$$

The initial inputs are set to zero: $u(k) = 0$, $0 \leq k < i_1$. Hence the closed-loop system becomes

$$x(k+1) = (A + \Delta A)x(k) + (B + \Delta B)Kx(i_n), \tag{2.5}$$

for $k \in [i_n, i_{n+1})$. The objective of this paper is to analyze the robust stability of NCS (2.5).

*Remark 2.3.* The packet loss process can take place in the sensor-controller link and the controller-actuator link. Since the considered controller is static in this paper, it is equivalent to incorporate the double-sided packet loss as a single-packet loss process. This is just the reason that this paper only considers the single-packet loss process. However, if the controller is online implemented, then one should clearly consider the double-sided packet loss rather than incorporate them as a single-packet loss process. For such case, readers can be referred to Ding [16], which systematically addressed the modeling and analysis methods for double-sided packet loss process.

## 3. Stability of Networked Control Systems

In this section, we analyze the stability property of NCSs. Here we firstly investigate the stability of NCS (2.5) when the plant (2.1) without any uncertainty, that is, $\Delta A = 0$ and $\Delta B = 0$. we have the following result.

**Theorem 3.1.** *Assuming $\Delta A = 0$ and $\Delta B = 0$, NCS (2.5) with arbitrary packet-loss process is asymptotically stable if there exist matrices $P > 0$, $Z > 0$, $Q_1$, $Q_2$, $M$, $N$, and $S$ such that the following LMI holds*

$$\Phi_1 \triangleq \Xi_1 + \Xi_2 + \Xi_2^T + \overline{m}(\Xi_3 + \Xi_5) - (\overline{m}+1)\Xi_4 < 0, \tag{3.1}$$

$$\begin{bmatrix} \widetilde{\Phi}_2 & N \\ * & -\dfrac{1}{\overline{m}-1}Z \end{bmatrix} < 0, \tag{3.2}$$

$$\Phi_3 \triangleq \Xi_1 + \Xi_6 + \Xi_6^T - \Xi_4 - \frac{1}{\overline{m}}\Xi_7 < 0, \tag{3.3}$$

$$\begin{bmatrix} P + (\overline{m}+1)\Lambda_1 & (\overline{m}+1)\Lambda_2 \\ * & (\overline{m}+1)\Lambda_3 \end{bmatrix} > 0, \tag{3.4}$$

*where* $\widetilde{\Phi}_2 \triangleq \Xi_1 + \Xi_2 + \Xi_2^T + \Xi_3 + \Xi_5 - 2\Xi_4$ *and*

$$\begin{aligned}
&\Xi_1 = \operatorname{diag}\{P, -P, 0\}, \qquad \Xi_6 = \begin{bmatrix} S & -SA & -SBK \end{bmatrix}, \\
&\Xi_2 = \begin{bmatrix} M & -MA+N & -MBK & -N \end{bmatrix}, \quad \Lambda_1 = \frac{Q_1 + Q_1^T}{2}, \\
&\Lambda_2 = -Q_1 + Q_2, \quad \Lambda_3 = \frac{Q_1 + Q_1^T}{2} - Q_2 - Q_2^T, \\
&\Xi_3 = \begin{bmatrix} \Lambda_1 & 0 & \Lambda_2 \\ * & 0 & 0 \\ * & * & \Lambda_3 \end{bmatrix}, \qquad \Xi_4 = \begin{bmatrix} 0 & 0 & 0 \\ * & \Lambda_1 & \Lambda_2 \\ * & * & \Lambda_3 \end{bmatrix}, \\
&\Xi_5 = \begin{bmatrix} Z & -Z & 0 \\ * & Z & 0 \\ * & * & 0 \end{bmatrix}, \qquad \Xi_7 = \begin{bmatrix} 0 & 0 & 0 \\ * & Z & -Z \\ * & * & Z \end{bmatrix}.
\end{aligned} \tag{3.5}$$

*Proof.* Define

$$d_k = k - i_n, \quad i_n \le k < i_{n+1}, \tag{3.6}$$

then the NCS (2.5) can be represented as a delay system:

$$x(K+1) = Ax(K) + BKx(k - d_k), \quad k \in [i_n, i_{n+1}). \tag{3.7}$$

Inspired by Fridman [15], we construct the following new functional candidate as:

$$V(k) \triangleq V_1(k) + V_2(k) + V_3(k), \tag{3.8}$$

with $V_1(k) = x^T(k)Px(k)$ and

$$\begin{aligned} V_2(k) =& (i_{n+1} - i_n - d_k) \begin{bmatrix} x(k) \\ x(k-d_k) \end{bmatrix}^T \\ & \times \begin{bmatrix} \dfrac{Q_1 + Q_1^T}{2} & -Q_1 + Q_2 \\ * & \dfrac{Q_1 + Q_1^T}{2} - Q_2 - Q_2^T \end{bmatrix} \begin{bmatrix} x(k) \\ x(k-d_k) \end{bmatrix}, \\ V_3(k) =& (i_{n+1} - i_n - d_k) \sum_{i=k-d_k}^{k-1} \eta^T(i) Z \eta(i), \end{aligned} \tag{3.9}$$

where $\eta(i) = x(i+1) - x(i)$ and $P > 0$, $Z > 0$, $Q_1$, $Q_2$ are to be determined.

From (2.2) and (3.6), we know that $d_k \le \overline{m}$. Therefore, similar with the discussion of Fridman [15], it can be seen that (3.4) guarantees (3.8) to be a Lyapunov functional. For $k \in [i_n, i_{n+1})$, we, respectively, calculate the forward difference of the functional (3.8) along the solution of system (3.7) by two cases.

*Case* 1 ($i_n \le k < i_{n+1} - 1$). In this case, we have $d_{k+1} = d_k + 1$. Then,

$$\Delta V_1(k) = x^T(k+1)Px(k+1) - x^T(k)Px(k), \tag{3.10}$$

$$\begin{aligned} \Delta V_2(k) =& (i_{n+1} - i_n - d_k - 1)\xi^T(k)\Xi_3\xi(k) \\ & - (i_{n+1} - i_n - d_k)\xi^T(k)\Xi_4\xi(k), \\ \Delta V_3(k) =& (i_{n+1} - i_n - d_k - 1)[x(k+1) - x(k)]^T \\ & \times Z[x(k+1) - x(k)] - \sum_{i=k-d_k}^{k-1} \eta^T(i) Z \eta(i), \end{aligned} \tag{3.11}$$

where $\xi(k) = [x\ (k+1)^T\ x(k)^T\ x(k-d_k)^T]^T$.

In addition, for any appropriately dimensioned matrices $M$ and $N$ the following relationships always hold:

$$0 = 2\xi^T(k)\mathrm{M}[x(k+1) - Ax(k) - BKx(k-d_k)]\ , \tag{3.12}$$

$$\begin{aligned} 0 \le{}& 2\xi^T(k)N[x(k) - x(k-d_k)], \\ &+ d_k\xi^T(k)NZ^{-1}N^T\xi(k) + \sum_{i=k-d_k}^{k-1}\eta^T(i)Z\eta(i). \end{aligned} \tag{3.13}$$

Then, from (3.10)–(3.13), we have

$$\Delta V(k) \le \xi^T(k)\Omega\xi(k), \tag{3.14}$$

where $\Omega = \Xi_1 + \Xi_2 + \Xi_2^T + (i_{n+1} - i_n - d_k - 1)(\Xi_3 + \Xi_5) - (i_{n+1} - i_n - d_k)\Xi_4 + d_kNZ^{-1}N^T$.

Now we prove (3.1) and (3.2) guaranteeing that $\Omega < 0$. By Schur complement, (3.2) is equivalent to

$$\Phi_2 \triangleq \widetilde{\Phi}_2 + (\overline{m} - 1)NZ^{-1}N^T < 0. \tag{3.15}$$

Then from (3.1) and (3.15), we know that $\Phi_1 < 0$ and $\Phi_2 < 0$. Hence for any scalar $\alpha \in [0,1]$, the following inequality holds:

$$\alpha\Phi_1 + (1-\alpha)\Phi_2 < 0. \tag{3.16}$$

Noting that in this case $0 \le d_k \le i_{n+1} - i_n - 2$, then we have $0 \le i_{n+1} - i_n - 2 - d_k \le \overline{m} - 1$. Therefore, $0 \le (i_{n+1} - i_n - d_k - 2)/(\overline{m} - 1) \le 1$. By setting $\alpha = (i_{(n+1)} - i_n - d_k - 2)/(\overline{m} - 1)$, from (3.16) we obtain that $\Omega + (\overline{m} - (i_{n+1} - i_n - 1))NZ^{-1}N^T < 0$. Due to $\overline{m} - (i_{n+1} - i_n - 1) \ge 0$, the inequality above implies $\Omega < 0$ holds. Therefore, in this case $\Delta V(k) < 0$ holds.

*Case* 2 ($k = i_{n+1} - 1$). In this case, we have $d_k = i_{n+1} - i_n - 1$ and $d_{k+1} = 0$. The

$$\Delta V_1(k) = x^T(k+1)Px(k+1) - x^T(k)Px(k), \tag{3.17}$$

$$\begin{aligned} \Delta V_2(k) &= -\xi^T(k)\Xi_4\xi(k), \\ \Delta V_3(k) &= -\sum_{i=k-d_k}^{k-1}\eta^T(i)Z\eta(i). \end{aligned} \tag{3.18}$$

By the Jensen's inequality [17], we have

$$\begin{aligned} &-\sum_{i=k-d_k}^{k-1}\eta^T(i)Z\eta(i) \\ &\quad\le -\frac{1}{\overline{m}}(x(k) - x(k-d_k))^T Z(x(k) - x(k-d_k)). \end{aligned} \tag{3.19}$$

In addition, for any appropriately dimensioned matrix $S$ the following relationship always holds:

$$0 = 2\xi^T(k)S[x(k+1) - Ax(k) - BKx(k-d_k)]. \tag{3.20}$$

Then, from (3.17)–(3.20), we have

$$\Delta V(k) \le \xi^T(k)\left[\Xi_1 + \Xi_6 + \Xi_6^T - \Xi_4 - \frac{1}{\overline{m}}\Xi_7\right]\xi^T(k). \tag{3.21}$$

In this case, we can see that (3.3) guarantees $\Delta V(k) < 0$.

From both Cases 1 and 2, we can conclude $\Delta V(k) < 0$ for $k \in [i_n, i_{n+1})$, for all $n \in \{1, 2, 3, \ldots\}$. Then, from the Lyapunov stability theory, the NCS (2.5) with arbitrary packet-loss process satisfying (2.2) is asymptotically stable. □

*Remark 3.2.* The proposed stability criterion in Theorem 3.1 is dependent on the bound of the packet loss. Furthermore, from the proof of Theorem 3.1, we can see that the varying rate of packet-loss-induced delays is fully utilized to obtain the stability condition. According to the difference of induced delays' varying rates, we separate $k \in [i_n, i_{n+1})$ into two parts, that is $i_n \le k < i_{n+1} - 1$ and $k = i_{n+1} - 1$. For the two cases, we, respectively, calculate the forward difference of the functional and guarantee it less than zero, such that the NCS is asymptotically stable. Theorem 3.1 is more effective to deal with packet loss than the existing time-varying delay system approaches in the sense that Theorem 3.1 can allow a larger upper bound of the packet loss, which will be demonstrated in an example in next section.

*Remark 3.3.* In Fridman [15], the continuous-time sampled control system is considered. The varying rate of sampling-induced delays is constant when the derivative of the Lyapunov functional is calculated. However, in our paper, the varying rate of packet-loss-induced delays will be changing when the difference of the Lyapunov functional is calculated. Therefore, the method of Fridman [15] for continuous-time domain cannot directly be applied to the problem of discrete-time domain considered in this paper.

Note that in LMIs (3.1)–(3.3) the system matrices $A$ and $B$ appear in affine form, thus the stability condition presented in Theorem 3.1 can be readily extended to cope with uncertain systems (2.1). By using Theorem 3.4 and the well-known $S$-procedure, we can easily obtain the following theorem, and hence its proof is omitted.

**Theorem 3.4.** *NCS* (2.5) *is robustly asymptotically if there exist matrices* $P > 0$, $Z > 0$, $Q_1$, $Q_2$, $M$, $N$, $S$ *and scalar* $\varepsilon_1$, $\varepsilon_2$, $\varepsilon_3$ *satisfying* (3.4) *and the following LMIs:*

$$\begin{bmatrix} \Phi_1 & MD & \varepsilon_1\Pi^T \\ * & -\varepsilon_1 I & 0 \\ * & * & -\varepsilon_1 I \end{bmatrix} < 0, \quad \begin{bmatrix} \Phi_3 & SD & \varepsilon_3\Pi^T \\ * & -\varepsilon_3 I & 0 \\ * & * & -\varepsilon_3 I \end{bmatrix} < 0, \quad \begin{bmatrix} \tilde{\Phi}_2 & N & MD & \varepsilon_2\Pi^T \\ * & -\dfrac{1}{\overline{m}-1}Z & 0 & 0 \\ * & * & -\varepsilon_2 I & 0 \\ * & * & * & -\varepsilon_2 I \end{bmatrix} < 0, \tag{3.22}$$

*where* $\Phi_1$, $\tilde{\Phi}_2$, $\Phi_3$ *are given in* (3.5) *and* $\Pi = \begin{bmatrix} 0 & -E_1 & -E_2K \end{bmatrix}$.

*Remark 3.5.* Because the LMIs of Theorem 3.1 are affine in the system matrices $A$ and $B$, it is readily extended to deal with the systems with norm-bounded parameter uncertainty (i.e., Theorem 3.4). With similar reason it can also be easily extended to deal with the systems with polytopic-type uncertainty. The reason why we only consider one of the cases is to avoid the paper being too miscellaneous.

*Remark 3.6.* It is worth to reiterate that if there is only packet loss, the method of this paper is more suitable than the general time-delay method. However, if there simultaneously exist network-induced delay and packet loss, the method of this paper is not applicable, but the general time-delay method is still valid. For example, Yue et al. [18], Gao and Chen [19], and Huang and Nguang [20] considered the networked control systems with both network-induced delay and packet loss, where Yue et al. [18] and Gao and Chen [19] are the methods of continuous-time domain, Huang and Nguang [20] is the method of discrete-time domain. Yue et al. [18] investigated the $H_\infty$ regulating control for network-based uncertain systems. Gao and Chen [19] studied the $H_\infty$ output tracking control for network-based uncertain systems. For the uncertain networked control system with random time delays, Huang and Nguang [20] analyzed robust disturbance attenuation performance and proposed the corresponding design method for the controllers.

## 4. Numerical Examples

In this section, three examples are provided to illustrate the effectiveness and advantage of the proposed stability results.

*Example 4.1.* Borrow the system considered by Gao and Chen [10], where $\Delta A = 0$, $\Delta B = 0$ and

$$A = \begin{bmatrix} 1.0078 & 0.0301 \\ 0.5202 & 1.0078 \end{bmatrix}, \qquad B = \begin{bmatrix} -0.0001 \\ -0.0053 \end{bmatrix}. \tag{4.1}$$

Here we are interested in the allowable maximum bound of dropout loss that guarantees the asymptotic stability of the closed-loop system. For extensive comparison purpose, we let the controller gain matrices take two different values: $K_1 = \begin{bmatrix} 105.2047 & 25.3432 \end{bmatrix}$ and $K_2 = \begin{bmatrix} 110.6827 & 34.6980 \end{bmatrix}$. By using different methods, the calculated results are presented in Table 1. From the table, it is easy to see that the method proposed in this paper is more effective than the others. But it is never to say that the proposed method in this paper is more suitable to deal with the time-delay; it is only to show that the proposed method is more suitable to deal with the packet-loss than the general time-delay methods.

*Example 4.2.* Borrow the system considered by Wang et al. [14], where $\Delta A = 0$, $\Delta B = 0$ and

$$A = \begin{bmatrix} 1 & 0.01 & 0 & 0 \\ 0 & 1 & 0 & 0 \\ 0 & 0 & 1 & 0.01 \\ 0 & 0 & 0 & 1 \end{bmatrix}, \qquad B = \begin{bmatrix} 0 & 0 \\ 0.01 & 0 \\ 0 & 0 \\ 0 & 0.01 \end{bmatrix}, \tag{4.2}$$

$$K = \begin{bmatrix} -0.0166 & -0.2248 & 0.0006 & 0.0016 \\ 0.0004 & 0.0016 & -0.0165 & -0.2271 \end{bmatrix}.$$

**Table 1:** Calculated maximum bound of dropout loss.

| Controller gain matrix | $K = K_1$ | $K = K_2$ |
|---|---|---|
| [10, Theorem 1] | 7 | 5 |
| [11, Theorem 1] | 6 | 5 |
| [12, Theorem 1] | 6 | 4 |
| [13, Theorem 1] | 7 | 5 |
| Theorem 3.1 in this paper | 13 | 10 |

When lower bound of the equivalent delay is 0, the allowable maximum upper bound of the equivalent delay is 13 as reported in Wang et al. [14]. Therefore, if there is only bounded packet loss, by using the method of Wang et al. [14], the allowable maximum bound of dropout loss is 13. However, by using Theorem 3.1 of this paper, one can obtain that the allowable maximum bound of dropout loss is 190. This example shows again that the proposed method is more suitable to deal with the packet-loss than the general time-delay methods.

*Example 4.3.* Consider the following uncertain system:

$$x(k+1) = \begin{bmatrix} 1.0078 + \alpha(k) & 0.0301 \\ 0.5202 & 1.0078 \end{bmatrix} x(k) + \begin{bmatrix} -0.1 \\ -5.3 + \alpha(k) \end{bmatrix} u(k), \tag{4.3}$$

where $|\alpha(k)| \leq \overline{\alpha}$. The system matrices can be written in the form of (2.1) with matrices given by

$$\begin{aligned} A &= \begin{bmatrix} 1.0078 & 0.0301 \\ 0.5202 & 1.0078 \end{bmatrix}, \qquad B = \begin{bmatrix} -0.1 \\ -5.3 \end{bmatrix}, \qquad D = \overline{\alpha}, \\ E_1 &= \begin{bmatrix} 1 & 0 \\ 0 & 0 \end{bmatrix}, \qquad E_2 = \begin{bmatrix} 0 \\ 1 \end{bmatrix}, \qquad F(k) = \frac{\alpha(k)}{\overline{\alpha}}. \end{aligned} \tag{4.4}$$

Now assume that the controller gain matrix is $K = \begin{bmatrix} 0.1052 & 0.0253 \end{bmatrix}$, and our purpose is to determine the upper value of $\overline{\alpha}$ such that the closed-loop system is robustly stable. By using Theorem 3.4, the detail calculated result is shown in Table 2.

In the following, we will present some simulation results. Assume the initial condition to be $x(k) = [1 \; -1]^T$ for $k \leq 0$. Let $\alpha(k)$ changes randomly between −0.0027 and 0.0027, which is shown in Figure 2(a). In addition, let the upper of dropout loss is 13, which is shown in Figure 2(b). Then, the state response of the close-loop system is given in Figure 2(c). It can be seen from this figure that the system is robustly asymptotically stable, which shows the validity of the method proposed in this paper.

## 5. Conclusions

The problem of robust stability analysis for uncertain systems over network with bounded packet loss has been considered in this paper. A new Lyapunov functional is constructed.

**Table 2:** Calculated upper values of $\overline{\alpha}$ for different cases.

| $\overline{m}$ | 3 | 5 | 7 | 9 | 11 | 13 |
|---|---|---|---|---|---|---|
| Upper value of $\overline{\alpha}$ | 0.0105 | 0.0104 | 0.0101 | 0.0096 | 0.0077 | 0.0027 |

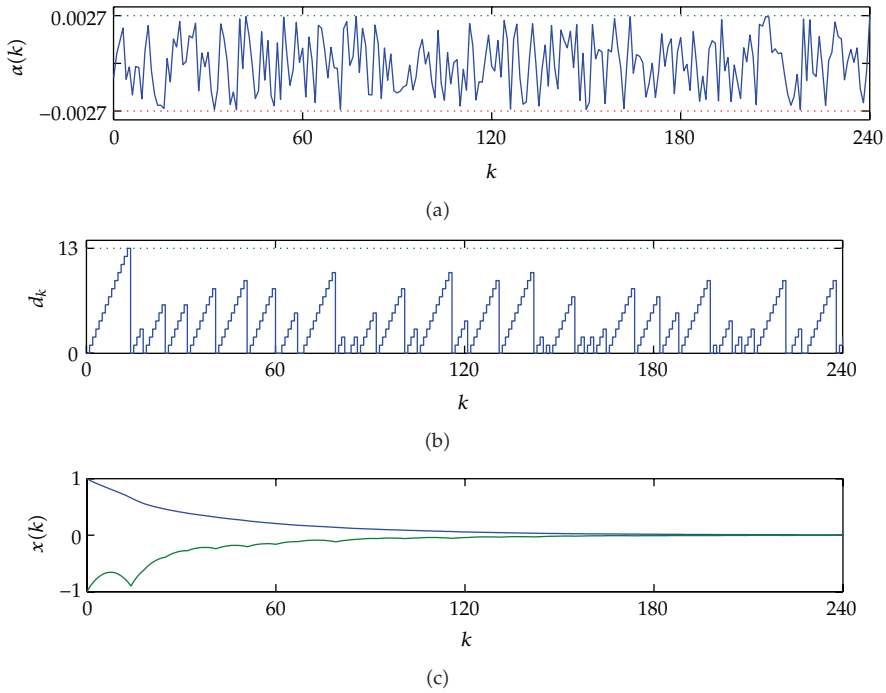


**Figure 2:** Simulation results.

This Lyapunov functional not only utilizes the bound of the packet loss but also utilizes the varying rate of the packet-loss-induced delays, which aims at reducing the conservatism of the results. Numerical examples are also presented to demonstrate the effectiveness and advantages of the proposed approach.

## Acknowledgments

This work was supported by National Natural Science Foundation of China (61104115 and 60904053), Research Fund for the Doctoral Program of Higher Education of China (20110072120018), and the Fundamental Research Funds for the Central Universities.

## References

[1] G. C. Walsh, H. Ye, and L. G. Bushnell, "Stability analysis of networked control systems," *IEEE Transactions on Control System Technology*, vol. 10, no. 3, pp. 438–446, 2002.

[2] L. Schenato, "To zero or to hold control inputs with lossy links?" *IEEE Transactions on Automatic Control*, vol. 54, no. 5, pp. 1093–1099, 2009.

[3] O. C. Imer, S. Yüksel, and T. Başar, "Optimal control of LTI systems over unreliable communication links," *Automatica*, vol. 42, no. 9, pp. 1429–1439, 2006.

[4] B. Sinopoli, L. Schenato, M. Franceschetti, K. Poolla, M. I. Jordan, and S. S. Sastry, "Kalman filtering with intermittent observations," *IEEE Transactions on Automatic Control*, vol. 49, no. 9, pp. 1453–1464, 2004.
[5] S. Hu and W.-Y. Yan, "Stability robustness of networked control systems with respect to packet loss," *Automatica*, vol. 43, no. 7, pp. 1243–1248, 2007.
[6] G.-P. Liu, J. X. Mu, D. Rees, and S. C. Chai, "Design and stability analysis of networked control systems with random communication time delay using the modified MPC," *International Journal of Control*, vol. 79, no. 4, pp. 288–297, 2006.
[7] M. Yu, L. Wang, T. Chu, and G. Xie, "Stabilization of networked control systems with data packet dropout and network delays via switching system approach," in *Proceedings of the 43rd IEEE Conference on Decision and Control*, pp. 3539–3544, Atlantis, Bahamas, 2004.
[8] G.-P. Liu, Y. Xia, J. Chen, D. Rees, and W. Hu, "Networked predictive control of systems with random network delays in both forward and feedback channels," *IEEE Transactions on Industrial Electronics*, vol. 54, no. 3, pp. 1282–1297, 2007.
[9] J. Xiong and J. Lam, "Stabilization of linear systems over networks with bounded packet loss," *Automatica*, vol. 43, no. 1, pp. 80–87, 2007.
[10] H. Gao and T. Chen, "New results on stability of discrete-time systems with time-varying state delay," *IEEE Transactions on Automatic Control*, vol. 52, no. 2, pp. 328–334, 2007.
[11] B. Zhang, S. Xu, and Y. Zou, "Improved stability criterion and its applications in delayed controller design for discrete-time systems," *Automatica*, vol. 44, no. 11, pp. 2963–2967, 2008.
[12] J. Xiong and J. Lam, "Stabilization of networked control systems with a logic ZOH," *IEEE Transactions on Automatic Control*, vol. 54, no. 2, pp. 358–363, 2009.
[13] X. Meng, J. Lam, B. Du, and H. Gao, "A delay-partitioning approach to the stability analysis of discrete-time systems," *Automatica*, vol. 46, pp. 610–614, 2010.
[14] P. Wang, C. Han, and B. Ding, "Stability of discrete-timenetworked control systems and its extension for robust $H_\infty$ control," *International Journal of Systems Science*. In press.
[15] E. Fridman, "A refined input delay approach to sampled-data control," *Automatica*, vol. 46, no. 2, pp. 421–427, 2010.
[16] B. Ding, "Stabilization of linear systems over networks with bounded packet loss and its use in model predictive control," *Automatica*, vol. 47, no. 11, pp. 2526–2533, 2011.
[17] K. Gu, "An integral inequality in the stability problem of time-delay systems," in *Proceedings of the 39th IEEE Conference on Decision and Control*, pp. 2805–2810, Sydney, Australia, 2000.
[18] D. Yue, Q.-L. Han, and J. Lam, "Network-based robust $H_\infty$ control of systems with uncertainty," *Automatica*, vol. 41, no. 6, pp. 999–1007, 2005.
[19] H. Gao and T. Chen, "Network-based $H_\infty$ output tracking control," *IEEE Transactions on Automatic Control. Transactions on Automatic Control*, vol. 53, no. 3, pp. 655–667, 2008.
[20] D. Huang and S. K. Nguang, "Robust disturbance attenuation for uncertain networked control systems with random time delays," *IET Control Theory & Applications*, vol. 2, no. 11, pp. 1008–1023, 2008.

Hindawi Publishing Corporation
Journal of Applied Mathematics
Volume 2012, Article ID 987975, 20 pages
doi:10.1155/2012/987975

*Research Article*

# Optimal Control of Polymer Flooding Based on Maximum Principle

**Yang Lei,[1] Shurong Li,[1] Xiaodong Zhang,[1] Qiang Zhang,[1] and Lanlei Guo[2]**

[1] *College of Information and Control Engineering, China University of Petroleum, Qingdao, 266580, China*
[2] *Research Institute of Geological Science, Sinopec Shengli Oilfield Company, Dongying 257000, China*

Correspondence should be addressed to Yang Lei, yutian_hdpu2003@163.com

Received 8 March 2012; Accepted 29 May 2012

Academic Editor: Xianxia Zhang



Polymer flooding is one of the most important technologies for enhanced oil recovery (EOR). In this paper, an optimal control model of distributed parameter systems (DPSs) for polymer injection strategies is established, which involves the performance index as maximum of the profit, the governing equations as the fluid flow equations of polymer flooding, and the inequality constraint as the polymer concentration limitation. To cope with the optimal control problem (OCP) of this DPS, the necessary conditions for optimality are obtained through application of the calculus of variations and Pontryagin's weak maximum principle. A gradient method is proposed for the computation of optimal injection strategies. The numerical results of an example illustrate the effectiveness of the proposed method.

## 1. Introduction

It is of increasing necessity to produce oil fields more efficiently and economically because of the ever-increasing demand for petroleum worldwide. Since most of the significant oil fields are mature fields and the number of new discoveries per year is decreasing, the use of EOR processes is becoming more and more imperative. At present, polymer flooding technology is the best method for chemically EOR [1]. It could reduce the water-oil mobility ratio and improve sweep efficiency [2–5].

Because of the high cost of chemicals, it is essential to optimize polymer injection strategies to provide the greatest oil recovery at the lowest cost. The optimization procedure involves maximizing the objective function (cumulative oil production or profit) from a polymer flooding reservoir by adjusting the injection concentration. One way of solving this problem is direct optimization with the reservoir simulator. Numerical models are

used to evaluate the complex interactions of variables affecting development decisions, such as reservoir and fluid properties and economic factors. Even with these models, the current practice is still the conventional trial and error approach. In each trial, the polymer concentration of an injection well is selected based on the intuition of the reservoir engineer. This one-well-at-a-time approach may lead to suboptimal decisions because engineering and geologic variables affecting reservoir performance are often nonlinearly correlated. And the problem definitely compounds when multiple producers and injectors are involved in a field development case. The use of the optimal control method offers a way out.

The optimal control method has been researched in EOR techniques in recent years. Ramirez et al. [6] firstly applied the theory of optimal control to determine the best possible injection strategies for EOR processes. Their study was motivated by the high operation costs associated with EOR projects. The objective of their study was to develop an optimization method to minimize injection costs while maximizing the amount of oil recovered. The performance of their algorithm was subsequently examined for surfactant injection as an EOR process in a one-dimensional core flooding problem [7]. The control for the process was the surfactant concentration of the injected fluid. They observed a significant improvement in the ratio of the value of the oil recovered to the cost of the surfactant injected from 1.5 to about 3.4. Optimal control was also applied to steam flooding by Liu et al. [8]. They developed an approach using optimal control theory to determine operating strategies to maximize the economic attractiveness of steam flooding process. Their objective was to maximize a performance index which is defined as the difference between oil revenue and the cost of injected steam. Their optimization method also obtained significant improvement under optimal operation. Ye et al. [9] were involved in the study of optimal control of gas-cycling in condensate reservoirs. It was shown that both the oil recovery and the total profit of a condensate reservoir can be enhanced obviously through optimization of gas production rate, gas injection rate, and the mole fractions of each component in injection gas. Daripa et al. [10–15] researched the basic physical mechanisms that contribute to poor oil recovery by EOR technologies and how to individually control each of these physical mechanisms. Brouwer and Jansen [16] and Sarma et al. [17] used the optimal control theory as an optimization algorithm for adjusting the valve setting in smart wells of water flooding. The water flooding scheme that maximized the profit was numerically obtained by combining reservoir simulation with control theory practices of implicit differentiation. They were able to achieve improved sweep efficiency and delayed water breakthrough by dynamic control of the valve setting.

For the previous work on optimal control of polymer flooding, Guo et al. [18] applied the iterative dynamic programming algorithm to solve the OCP of a one-dimensional core polymer flooding. However, the optimal control model used in their study is so simple that it is not adapted for practical oilfield development. As a result of the complicated nature of reservoir models with nonlinear constraints, it is very tedious and troublesome to cope with a large number of grid points for the state variables and control variables. To avoid these difficulties, Li et al. [19] and Lei et al. [20] used the genetic algorithms to determine the optimal injection strategies of polymer flooding and the reservoir model equations were treated as a "black box." The genetic algorithms are capable of finding the global optimum on theoretical sense, but, as Sarma et al. [17] point out, they require tens or hundreds of thousand reservoir simulation runs of very large model and are not able to guarantee monotonic maximization of the objective function.

In this paper, an optimal control model of DPS for polymer flooding is established which maximizes the profit by adjusting the injection concentration. Then the determination

of polymer injection strategies turns to solve this OCP of DPS. Necessary conditions for optimality are obtained by Pontryagin's weak maximum principle. A gradient numerical method is presented for solving the OCP. Finally, an example of polymer flooding project involving a heterogeneous reservoir case is investigated and the results show the efficiency of the proposed method.

## 2. Mathematical Formulation of Optimal Control

### 2.1. Performance Index

Let $\Omega \in R^2$ denote the domain of reservoir with boundary $\partial\Omega$, $n$ be the unit outward normal on $\partial\Omega$, and $(x, y) \in \Omega$ be the coordinate of a point in the reservoir. Given a fixed final time $t_f$, we set $\Psi = \Omega \times [0, t_f]$, $\Gamma = \partial\Omega \times [0, t_f]$, and suppose that there exist $N_w$ injection wells and $N_o$ production wells in the oilfield. The injection and production wells are located at $L_w = \{(x_{wi}, y_{wi}) \mid i = 1, 2, \ldots, N_w\}$ and $L_o = \{(x_{oj}, y_{oj}) \mid j = 1, 2, \ldots, N_o\}$, respectively. This descriptive statement of the cost functional must be translated into a mathematical form to use quantitative optimization techniques. The oil value can be formulated as

$$\int_0^{t_f} \iint_\Omega \xi_o (1 - f_w) q_{\text{out}} d\sigma\, dt, \tag{2.1}$$

where $\xi_o$ is the cost of oil per unit mass ($10^4$ \$/m$^3$), $f_w(x, y, t)$ is the fractional flow of water, and $q_{\text{out}}(x, y, t)$ is the flow velocity of production fluid (m/day). We define $q_{\text{out}}(x, y, t) \geq 0$ at $(x, y) \in L_o$ and $q_{\text{out}}(x, y, t) \equiv 0$ at $(x, y) \notin L_o$.

The polymer cost is expressed mathematically as

$$\int_0^{t_f} \iint_\Omega \xi_p q_{\text{in}} c_{\text{pin}} d\sigma\, dt, \tag{2.2}$$

where $\xi_p$ is the cost of oil per unit volume ($10^4$ \$/m$^3$), $c_{\text{pin}}(x, y, t)$ is the polymer concentration of the injection fluid (g/L), and $q_{\text{in}}(x, y, t)$ is the flow velocity of injection fluid (m/day). We define $q_{\text{in}}(x, y, t) \geq 0$ at $(x, y) \in L_w$ and $q_{\text{in}}(x, y, t) \equiv 0$ at $(x, y) \notin L_w$.

The objective functional is, therefore,

$$\max J = \int_0^{t_f} \iint_\Omega \left[\xi_o (1 - f_w) q_{\text{out}} - \xi_p q_{\text{in}} c_{\text{pin}}\right] d\sigma\, dt. \tag{2.3}$$

### 2.2. Governing Equations

The maximization of the cost functional $J$ given by (2.3) is not totally free but is constrained by the system process dynamics. The governing equations of the polymer flooding process must therefore be developed to describe the flow of both the aqueous and oil phases through the porous media of a reservoir formation. The equations used in this paper allow for the adsorption of polymer onto the solid matrix in addition to the convective and dispersive mechanisms of mass transfer. Let $p(x, y, t)$, $S_w(x, y, t)$ and $c_p(x, y, t)$ denote the pressure, water saturation, and polymer concentration of the oil reservoir, respectively, at a point

$(x, y) \in \Omega$ and a time $t \in [0, t_f]$, then $p(x, y, t)$, $S_w(x, y, t)$, and $c_p(x, y, t)$ satisfy the following partial differential equations (PDEs).

(i) The flow equation for oil phase

$$\frac{\partial}{\partial x}\left(k_p r_o \frac{\partial p}{\partial x}\right) + \frac{\partial}{\partial y}\left(k_p r_o \frac{\partial p}{\partial y}\right) - (1 - f_w) q_{\text{out}} = h \frac{\partial a_o}{\partial t}, \quad (x, y, t) \in \Psi. \tag{2.4}$$

(ii) The flow equation for water phase

$$\frac{\partial}{\partial x}\left(k_p r_w \frac{\partial p}{\partial x}\right) + \frac{\partial}{\partial y}\left(k_p r_w \frac{\partial p}{\partial y}\right) + q_{\text{in}} - f_w q_{\text{out}} = h \frac{\partial a_w}{\partial t}, \quad (x, y, t) \in \Psi. \tag{2.5}$$

(iii) The flow equation for polymer component

$$\begin{aligned} &\frac{\partial}{\partial x}\left(k_d r_d \frac{\partial c_p}{\partial x}\right) + \frac{\partial}{\partial x}\left(k_p r_c \frac{\partial p}{\partial x}\right) + \frac{\partial}{\partial y}\left(k_d r_d \frac{\partial c_p}{\partial y}\right) + \frac{\partial}{\partial y}\left(k_p r_c \frac{\partial p}{\partial y}\right) + q_{\text{in}} c_{\text{pin}} - f_w q_{\text{out}} c_p \\ &\quad = h \frac{\partial a_c}{\partial t}, \quad (x, y, t) \in \Psi. \end{aligned} \tag{2.6}$$

(iv) The boundary conditions and initial conditions

$$\left.\frac{\partial p}{\partial n}\right|_{\partial\Omega} = 0, \quad \left.\frac{\partial S_w}{\partial n}\right|_{\partial\Omega} = 0, \quad \left.\frac{\partial c_p}{\partial n}\right|_{\partial\Omega} = 0, \quad (x, y, t) \in \Gamma, \tag{2.7}$$

$$\begin{gathered} p(x, y, 0) = p^0(x, y), \quad S_w(x, y, 0) = S_w^0(x, y), \\ c_p(x, y, 0) = c_p^0(x, y), \quad (x, y) \in \Omega, \end{gathered} \tag{2.8}$$

where the corresponding parameters are defined as

$$k_p = Kh, \qquad k_d = Dh, \tag{2.9}$$

$$r_o = \frac{k_{ro}}{B_o \mu_o}, \qquad r_w = \frac{k_{rw}}{B_w R_k \mu_w}, \qquad r_c = \frac{k_{rw} c_p}{B_w R_k \mu_p}, \qquad r_d = \frac{\phi_p S_w}{B_w}, \tag{2.10}$$

$$a_o = \frac{\phi(1 - S_w)}{B_o}, \qquad a_w = \frac{\phi S_w}{B_w}, \qquad a_c = \frac{\phi_p S_w c_p}{B_w} + \rho_r (1 - \phi) C_{rp}. \tag{2.11}$$

The constant coefficient $K(x, y)$ is the absolute permeability ($\mu\text{m}^2$), $h$ is the thickness of the reservoir bed (m), $D$ is the diffusion coefficient of polymer ($\text{m}^2/\text{s}$), $\rho_r$ ($\text{kg}/\text{m}^3$) is the rock density, and $\mu_o$ (mPa·s) is the oil viscosity.

The oil volume factor $B_o$, the water volume factor $B_w$, the rock porosity $\phi$, and the effective porosity to polymer $\phi_p$ are expressed as functions of the reservoir pressure $p$:

$$\begin{aligned} B_o &= \frac{B_{or}}{\left[1 + C_o(p - p_r)\right]}, \\ B_w &= \frac{B_{wr}}{\left[1 + C_w(p - p_r)\right]}, \\ \phi &= \phi_r\left[1 + C_R(p - p_r)\right], \\ \phi_p &= f_a\phi, \end{aligned} \tag{2.12}$$

where $p_r$ is the reference pressure (MPa), $\phi_r$, $B_{or}$, and $B_{wr}$ denote the porosity, the oil, and water volume factor under the condition of the reference pressure, respectively, $f_a$ is the effective pore volume coefficient, $C_o$, $C_w$, and $C_R$ denote the compressibility factors of oil, water, and rock, respectively.

Functions relating values of the oil and water relative permeabilities $k_{ro}$ and $k_{rw}$ to the water saturation $S_w$ are

$$\begin{aligned} k_{rw} &= k_{rwro}\left(\frac{S_w - S_{wc}}{1 - S_{wc} - S_{or}}\right)^{n_w}, \\ k_{ro} &= k_{rocw}\left(\frac{1 - S_w - S_{or}}{1 - S_{wc} - S_{or}}\right)^{n_o}, \end{aligned} \tag{2.13}$$

where $k_{rwro}$ is the oil relative permeability at the irreducible water saturation $S_{wc}$, $k_{rwcw}$ is the water relative permeability at the residual oil saturation and $S_{or}$, $n_w$, and $n_o$ are constant coefficients.

The polymer solution viscosity $\mu_p$ (mPa·s), the permeability reduction factor $R_k$, and the amount adsorbed per unit mass of the rock $C_{rp}$ (mg/g) which depend on the polymer concentration $c_p$ are given by

$$\begin{aligned} \mu_p &= \mu_w\left[1 + \left(ap_1c_p + ap_2c_p^2 + ap_p^3\right)\right], \\ R_k &= 1 + \frac{(R_{k\max} - 1)\cdot b_{rk}\cdot c_p}{1 + b_{rk}\cdot c_p}, \\ C_{rp} &= \frac{ac_p}{1 + bc_p}, \end{aligned} \tag{2.14}$$

where $\mu_w$ is the viscosity of the aqueous phase with no polymer (mPa·s), $ap_1, ap_2, ap_3$, $R_{k\max}, b_{rk}$, and $a$ ($\mathrm{cm}^3/\mathrm{g}$) and $b$ (g/L) are constant coefficients.

The fractional flow of water $f_w$ is given by,

$$f_w = \frac{r_w}{r_o + r_w}. \tag{2.15}$$

### 2.3. Constraint

Since the negative and overhigh injection polymer concentrations are not allowed, the constraint in polymer flooding is expressed mathematically as

$$0 \le c_{\text{pin}} \le c_{\max}, \tag{2.16}$$

where $c_{\max}$ is the maximum injection polymer concentration.

### 2.4. Optimal Control Formulation

The reservoir pressure $p$, the water saturation $S_w$ and the polymer concentration $c_p$ are the three state variables for the problem as formulated. The system state vector is denoted by

$$\mathbf{u}(x,y,t) = \left[p, S_w, c_p\right]^T. \tag{2.17}$$

The control for the process is the polymer concentration of injected fluid

$$v(x,y,t) = c_{\text{pin}}, \quad (x,y) \in L_w. \tag{2.18}$$

Then the OCP of DPS for polymer flooding has the general form,

$$\max_v J = \int_0^{t_f} \iint_\Omega F(\mathbf{u}, v)\, d\sigma\, dt, \tag{2.19}$$

$$\text{s.t. } \mathbf{f}\left(\dot{\mathbf{u}}, \mathbf{u}, \mathbf{u}_x, \mathbf{u}_y, \mathbf{u}_{xx}, \mathbf{u}_{yy}, v\right) = 0, \quad (x,y,t) \in \Psi, \tag{2.20}$$

$$\mathbf{g}\left(\mathbf{u}, \mathbf{u}_x, \mathbf{u}_y, \mathbf{u}_{xx}, \mathbf{u}_{yy}\right) = 0, \quad (x,y,t) \in \Gamma, \tag{2.21}$$

$$\mathbf{u}(x,y,0) = \mathbf{u}^0(x,y), \quad (x,y) \in \Omega, \tag{2.22}$$

$$0 \le v \le v_{\max}, \tag{2.23}$$

where $\dot{\mathbf{u}} = \partial \mathbf{u}/\partial t$, $\mathbf{u}_l = \partial \mathbf{u}/\partial l$, $\mathbf{u}_{ll} = \partial^2 \mathbf{u}/\partial l^2$, $l = x, y$, (2.19) denotes the performance index (2.3), (2.20) expresses the governing equations (2.4)–(2.6), (2.21) and (2.22) denote the boundary and initial conditions, respectively, and (2.23) denotes the injection polymer concentration constraint (2.16).

## 3. Necessary Conditions of Optimal Control

### 3.1. Maximum Principle of DPS

We desire to find a set of necessary conditions for the state vector, $\mathbf{u}$, and the control, $v$, to be extremals of the functional $J$ (2.19) subject to the PDEs (2.20)~(2.22) and the constraint (2.23). A convenient way to cope with such an OCP of DPS (2.19)~(2.23) is through the use

of distributed adjoint variables. The first step is to form an augmented functional by adjoining the governing equations to the performance index $J$. We define the Hamiltonian as

$$H = F + \lambda^T \mathbf{f}, \tag{3.1}$$

where $\boldsymbol{\lambda}(x, y, t)$ is the adjoint vector. Then the argument functional is given by,

$$J_A = J + \int_0^{t_f} \iint_\Omega \boldsymbol{\lambda}^T \mathbf{f}(\dot{\mathbf{u}}, \mathbf{u}, \mathbf{u}_x, \mathbf{u}_y, \mathbf{u}_{xx}, \mathbf{u}_{yy}, v)\, d\sigma\, dt = \int_0^{t_f} \iint_\Omega H(\dot{\mathbf{u}}, \mathbf{u}, \mathbf{u}_x, \mathbf{u}_y, \mathbf{u}_{xx}, \mathbf{u}_{yy}, v)\, d\sigma\, dt. \tag{3.2}$$

Following the standard procedure of the calculus of variables, the increment of $J_A$, denoted by $\Delta J_A$, is formed by introducing variations $\delta\mathbf{u}$, $\delta\mathbf{u}_x$, $\delta\mathbf{u}_y$, $\delta\mathbf{u}_{xx}$, $\delta\mathbf{u}_{yy}$, $\delta\dot{\mathbf{u}}$, and $\delta v$ giving

$$\begin{aligned} \Delta J_A = {} & J_A(\mathbf{u} + \delta\mathbf{u}, \mathbf{u}_x + \delta\mathbf{u}_x, \mathbf{u}_y + \delta\mathbf{u}_y, \mathbf{u}_{xx} + \delta\mathbf{u}_{xx}, \mathbf{u}_{yy} + \delta\mathbf{u}_{yy}, \dot{\mathbf{u}} + \delta\dot{\mathbf{u}}, v + \delta v) \\ & - J_A(\mathbf{u}, \mathbf{u}_x, \mathbf{u}_y, \mathbf{u}_{xx}, \mathbf{u}_{yy}, \dot{\mathbf{u}}, v). \end{aligned} \tag{3.3}$$

This formulation assumes that the final time, $t_f$, is fixed.

Expanding (3.3) in a Taylor series and retaining only the linear terms give the variation of the functional, $\delta J_A$,

$$\begin{aligned} \delta J_A = \int_0^{t_f} \iint_\Omega \Bigg[ & \left(\frac{\partial H}{\partial \mathbf{u}}\right)^T \delta\mathbf{u} + \left(\frac{\partial H}{\partial \mathbf{u}_x}\right)^T \delta\mathbf{u}_x + \left(\frac{\partial H}{\partial \mathbf{u}_{xx}}\right)^T \delta\mathbf{u}_{xx} + \left(\frac{\partial H}{\partial \mathbf{u}_y}\right)^T \delta\mathbf{u}_y \\ & + \left(\frac{\partial H}{\partial \mathbf{u}_{yy}}\right)^T \delta\mathbf{u}_{yy} + \left(\frac{\partial H}{\partial \dot{\mathbf{u}}}\right)^T \delta\dot{\mathbf{u}} + \left(\frac{\partial H}{\partial v}\right)\delta v \Bigg] d\sigma\, dt. \end{aligned} \tag{3.4}$$

Since the variations $\delta\mathbf{u}$, $\delta\mathbf{u}_l$, $\delta\mathbf{u}_{ll}$ $(l = x, y)$, and $\delta\dot{\mathbf{u}}$ are not independent can be expressed in terms of the variations $\delta\mathbf{u}$ by integrating the following three terms by parts:

$$\iint_\Omega \left[\left(\frac{\partial H}{\partial \mathbf{u}_l}\right)^T \delta\mathbf{u}_l\right] d\sigma = \iint_\Omega \frac{\partial}{\partial l}\left[\left(\frac{\partial H}{\partial \mathbf{u}_l}\right)^T \delta\mathbf{u}\right] d\sigma - \iint_\Omega \left[\frac{\partial}{\partial l}\left(\frac{\partial H}{\partial \mathbf{u}_l}\right)^T \delta\mathbf{u}\right] d\sigma, \tag{3.5}$$

$$\begin{aligned} \iint_\Omega \left[\left(\frac{\partial H}{\partial \mathbf{u}_{ll}}\right)^T \delta\mathbf{u}_{ll}\right] d\sigma = {} & \iint_\Omega \left[\frac{\partial^2}{\partial l^2}\left(\frac{\partial H}{\partial \mathbf{u}_{ll}}\right)\right]^T \delta\mathbf{u}\, d\sigma \\ & + \iint_\Omega \frac{\partial}{\partial l}\left[\left(\frac{\partial H}{\partial \mathbf{u}_{ll}}\right)^T \delta\mathbf{u}_l - \frac{\partial}{\partial l}\left(\frac{\partial H}{\partial \mathbf{u}_{ll}}\right)^T \delta\mathbf{u}\right] d\sigma, \end{aligned} \tag{3.6}$$

$$\int_0^{t_f} \left(\frac{\partial H}{\partial \dot{\mathbf{u}}}\right)^T \delta\dot{\mathbf{u}} = \left[\left(\frac{\partial H}{\partial \dot{\mathbf{u}}}\right)^T \delta\mathbf{u}\right]\Bigg|_0^{t_f} - \int_0^{t_f} \frac{\partial}{\partial t}\left(\frac{\partial H}{\partial \dot{\mathbf{u}}}\right)^T \delta\mathbf{u}\, dt. \tag{3.7}$$

Using the Green's formula in (3.5) and (3.6), we obtain

$$\begin{aligned}
&\iint_{\Omega} \sum_{l=x,y} \left[ \left( \frac{\partial H}{\partial \mathbf{u}_l} \right)^T \delta \mathrm{u}_l + \left( \frac{\partial H}{\partial \mathbf{u}_{ll}} \right)^T \delta \mathbf{u}_{ll} \right] d\sigma \\
&\quad = \iint_{\Omega} \sum_{l=x,y} \left[ -\frac{\partial}{\partial l} \left( \frac{\partial H}{\partial \mathbf{u}_l} \right) + \frac{\partial^2}{\partial l^2} \left( \frac{\partial H}{\partial \mathbf{u}_{ll}} \right) \right]^T \delta \mathbf{u} \, d\sigma \\
&\qquad + \oint_{\partial\Omega} \left\{ \left[ \left( \frac{\partial H}{\partial \mathbf{u}_x} - \frac{\partial}{\partial x} \frac{\partial H}{\partial \mathbf{u}_{xx}} \right)^T \delta \mathbf{u} + \left( \frac{\partial H}{\partial \mathbf{u}_{xx}} \right)^T \delta \mathbf{u}_x \right] dy \right. \\
&\qquad \left. - \left[ \left( \frac{\partial H}{\partial \mathbf{u}_y} - \frac{\partial}{\partial y} \frac{\partial H}{\partial \mathbf{u}_{yy}} \right)^T \delta \mathbf{u} + \left( \frac{\partial H}{\partial \mathbf{u}_{yy}} \right)^T \delta \mathbf{u}_y \right] dx \right\}.
\end{aligned} \tag{3.8}$$

By substituting the above equations (3.7) and (3.8) into (3.4), the first variation $\delta J_A$ is expressed as

$$\begin{aligned}
\delta J_A = &\int_{t_0}^{t_f} \iint_{\Omega} \left( \frac{\partial H}{\partial \mathbf{u}} - \frac{\partial}{\partial x} \frac{\partial H}{\partial \mathbf{u}_x} - \frac{\partial}{\partial y} \frac{\partial H}{\partial \mathbf{u}_y} + \frac{\partial^2}{\partial x^2} \frac{\partial H}{\partial \mathbf{u}_{xx}} + \frac{\partial^2}{\partial y^2} \frac{\partial H}{\partial \mathbf{u}_{yy}} - \frac{\partial}{\partial t} \frac{\partial H}{\partial \dot{\mathbf{u}}} \right)^T \delta \mathbf{u} \, d\sigma \, dt \\
&+ \int_{t_0}^{t_f} \oint_{\partial\Omega} \left\{ \left[ \left( \frac{\partial H}{\partial \mathbf{u}_x} - \frac{\partial}{\partial x} \frac{\partial H}{\partial \mathbf{u}_{xx}} \right)^T \delta \mathbf{u} + \left( \frac{\partial H}{\partial \mathbf{u}_{xx}} \right)^T \delta \mathbf{u}_x \right] dy \right. \\
&\qquad \left. - \left[ \left( \frac{\partial H}{\partial \mathbf{u}_y} - \frac{\partial}{\partial y} \frac{\partial H}{\partial \mathbf{u}_{yy}} \right)^T \delta \mathbf{u} + \left( \frac{\partial H}{\partial \mathbf{u}_{yy}} \right)^T \delta \mathbf{u}_y \right] dx \right\} dt \\
&+ \iint_{\Omega} \left[ \left( \frac{\partial H}{\partial \dot{\mathbf{u}}} \right)^T \delta \mathbf{u} \right]_0^{t_f} d\sigma + \int_{t_0}^{t_f} \iint_{\Omega} \left( \frac{\partial H}{\partial v} \right) \delta v \, d\sigma \, dt.
\end{aligned} \tag{3.9}$$

When the state and control regions are not bounded, the variation of the functional must vanish at an extremal (the fundamental theorem of the calculus of variations). When the control region is constrained by a boundary, then the necessary condition for optimality is to maximize the performance index $J_A$ with respect to the control $v$. This means that the variation $\delta J_A$ is

$$\delta J_A(v^*, \delta v) \geq 0, \tag{3.10}$$

where $v^*$ denotes the optimal control. Equation (3.10) is the weak minimum principle of Pontryagin. The necessary conditions for these two cases are the same except for the term involving the variation of the control, $\delta v$. For polymer flooding problem there are higher and lower bounds on the control variable $v$ given as (2.16).

The following necessary conditions for optimality are obtained when we apply Pontryagin's maximum principle.

*(1) Adjoint Equations*

Since the variation $\delta\mathbf{u}$ is free and not zero, the coefficient terms involving the $\delta\mathbf{u}$ variation in the first term of (3.9) are set to zero. This results in the adjoint equations as given by

$$\frac{\partial H}{\partial \mathbf{u}} - \sum_{l=x,y}\left(\frac{\partial}{\partial l}\frac{\partial H}{\partial \mathbf{u}_l} + \frac{\partial^2}{\partial l^2}\frac{\partial H}{\partial \mathbf{u}_{ll}}\right) - \frac{\partial}{\partial t}\frac{\partial H}{\partial \dot{\mathbf{u}}} = 0. \tag{3.11}$$

Substitute the Hamiltonian (3.1) into (3.11) and the adjoint equations become

$$\begin{aligned}&\frac{\partial F}{\partial \mathbf{u}} + \left(\frac{\partial \mathbf{f}}{\partial \mathbf{u}} - \frac{\partial}{\partial t}\frac{\partial \mathbf{f}}{\partial \dot{\mathbf{u}}}\right)^T \boldsymbol{\lambda} \\ &\quad + \sum_{l=x,y}\left[\left(\frac{\partial^2}{\partial l^2}\frac{\partial \mathbf{f}}{\partial \mathbf{u}_{ll}} - \frac{\partial}{\partial l}\frac{\partial \mathbf{f}}{\partial \mathbf{u}_l}\right)^T \boldsymbol{\lambda} + \left(2\frac{\partial}{\partial l}\frac{\partial \mathbf{f}}{\partial \mathbf{u}_{ll}} - \frac{\partial \mathbf{f}}{\partial \mathbf{u}_l}\right)^T \frac{\partial \boldsymbol{\lambda}}{\partial l} + \left(\frac{\partial \mathbf{f}}{\partial \mathbf{u}_{ll}}\right)^T \frac{\partial^2 \boldsymbol{\lambda}}{\partial l^2}\right] \\ &\quad - \left(\frac{\partial \mathbf{f}}{\partial \dot{\mathbf{u}}}\right)^T \frac{\partial \boldsymbol{\lambda}}{\partial t} = 0.\end{aligned} \tag{3.12}$$

Equation (3.12) is a set of PDEs with nonconstant coefficients.

*(2) Transversality Boundary Conditions*

The adjoint boundary conditions are obtained from the second term of (3.9):

$$\left[\left(\frac{\partial H}{\partial \mathbf{u}_l} - \frac{\partial}{\partial l}\frac{\partial H}{\partial \mathbf{u}_{ll}}\right)^T \delta\mathbf{u} + \left(\frac{\partial H}{\partial \mathbf{u}_{ll}}\right)^T \delta\mathbf{u}_l\right]\Bigg|_{\partial\Omega} = 0, \quad l = x, y. \tag{3.13}$$

*(3) Transversality Terminal Conditions*

Since the initial state is specified, the variation $\delta\mathbf{u}|_{t=0}$ of (3.9) is zero. However, the final state is not specified; therefore, the variation $\delta\mathbf{u}|_{t=t_f}$ is free and nonzero. This means that the following relation must be zero:

$$\frac{\partial H}{\partial \dot{\mathbf{u}}} = \left(\frac{\partial f}{\partial \dot{\mathbf{u}}}\right)^T \boldsymbol{\lambda} = 0, \text{ at } t = t_f. \tag{3.14}$$

*(4) Optimal Control*

With all the previous terms vanishing, the variation of the functional $\delta J_A$ becomes

$$\delta J_A = \int_0^{t_f} \iint_\Omega \left(\frac{\partial H}{\partial v}\right) \delta v \, d\sigma \, dt. \tag{3.15}$$

This equation expresses the direct influence of variation $\delta v$ on $\delta J_A$. A necessary condition for the optimality of $v^*$ is that $\delta J_A \geq 0$ for all possible small variations, $\delta v$. Since there are lower

and higher bounds on the control $v$ (2.9), we use the weak maximum principle to assert the following necessary conditions for optimality:

$$\frac{\partial H}{\partial v} = 0 \quad \text{for } 0 \le v^* \le v_{\max}, \tag{3.16}$$

when the control vector is unconstrained. Because the variation $\delta v$ can only be negative along the lower bound, we have

$$\frac{\partial H}{\partial v} \le 0 \quad \text{for } v^* = 0. \tag{3.17}$$

And because the variation $\delta v$ can only be positive along the higher bound, we have

$$\frac{\partial H}{\partial v} \ge 0 \quad \text{for } v^* = v_{\max}. \tag{3.18}$$

### 3.2. Necessary Conditions of OCP for Polymer Flooding

Let $\boldsymbol{\lambda}(x, y, t) = (\lambda_1, \lambda_2, \lambda_3)^T$ denote the adjoint vector of OCP for polymer flooding. Applying the theory developed in Section 3.1 and substituting the governing equations (2.4)–(2.6) into (3.12), the adjoint equations, given by (3.12), reduce for the polymer flooding problem under consideration as given in,

$$\begin{aligned}
&\sum_{l=x,y} \left\{ \frac{\partial}{\partial l}\left(k_p r_o \frac{\partial \lambda_1}{\partial l}\right) + \frac{\partial}{\partial l}\left(k_p r_w \frac{\partial \lambda_2}{\partial l}\right) + \frac{\partial}{\partial l}\left(k_p r_c \frac{\partial \lambda_3}{\partial l}\right) \right. \\
&\qquad \left. - \left[ k_p \frac{\partial r_o}{\partial p}\frac{\partial p}{\partial l}\frac{\partial \lambda_1}{\partial l} + k_d \frac{\partial r_w}{\partial p}\frac{\partial p}{\partial l}\frac{\partial \lambda_2}{\partial l} + \left( k_p \frac{\partial r_c}{\partial p}\frac{\partial p}{\partial l} + k_d \frac{\partial r_d}{\partial p}\frac{\partial c_p}{\partial l}\right)\frac{\partial \lambda_3}{\partial l} \right] \right\} \\
&\quad - q_{\text{out}}\left( \xi_o \frac{\partial f_w}{\partial p} - \frac{\partial f_w}{\partial p}\lambda_1 + \frac{\partial f_w}{\partial p}\lambda_2 + c_p \frac{\partial f_w}{\partial p}\lambda_3 \right) \\
&\quad + \frac{\partial a_o}{\partial p}\frac{\partial \lambda_1}{\partial t} + \frac{\partial a_w}{\partial p}\frac{\partial \lambda_2}{\partial t} + \frac{\partial a_c}{\partial p}\frac{\partial \lambda_3}{\partial t} = 0, \quad (x, y, t) \in \Psi, \\
&\sum_{l=x,y} \left[ -k_p \frac{\partial p}{\partial l}\left( \frac{\partial r_o}{\partial S_w}\frac{\partial \lambda_1}{\partial l} + \frac{\partial r_w}{\partial S_w}\frac{\partial \lambda_2}{\partial l} + \frac{\partial r_c}{\partial S_w}\frac{\partial \lambda_3}{\partial l} \right) - k_d \frac{\partial r_d}{\partial S_w}\frac{\partial c_p}{\partial l}\frac{\partial \lambda_3}{\partial l} \right] \\
&\quad - q_{\text{out}}\left( \xi_o \frac{\partial f_w}{\partial S_w} - \frac{\partial f_w}{\partial S_w}\lambda_1 + \frac{\partial f_w}{\partial S_w}\lambda_2 + c_p \frac{\partial f_w}{\partial S_w}\lambda_3 \right) + \frac{\partial a_o}{\partial S_w}\frac{\partial \lambda_1}{\partial t} + \frac{\partial a_w}{\partial S_w}\frac{\partial \lambda_2}{\partial t} \\
&\quad + \frac{\partial a_c}{\partial S_w}\frac{\partial \lambda_3}{\partial t} = 0, \quad (x, y, t) \in \Psi,
\end{aligned}$$

$$\sum_{l=x,y}\left[\frac{\partial}{\partial l}\left(k_d r_d \frac{\partial \lambda_3}{\partial l}\right) - k_p \frac{\partial p}{\partial l}\left(\frac{\partial r_w}{\partial c_p}\frac{\partial \lambda_2}{\partial l} + \frac{\partial r_c}{\partial c_p}\frac{\partial \lambda_3}{\partial l}\right)\right]$$
$$- q_{\text{out}}\left[\xi_o \frac{\partial f_w}{\partial c_p} - \frac{\partial f_w}{\partial c_p}\lambda_1 + \frac{\partial f_w}{\partial c_p}\lambda_2 + \left(c_p \frac{\partial f_w}{\partial c_p} + f_w\right)\lambda_3\right]$$
$$+ \frac{\partial a_c}{\partial c_p}\frac{\partial \lambda_3}{\partial t} = 0, \quad (x, y, t) \in \Psi. \tag{3.19}$$

The boundary conditions (2.7) of the DPS result in $(\partial \mathbf{u}/\partial l)|_{\partial\Omega} = 0$ and $\delta \mathbf{u}_l|_{\partial\Omega} = 0, l = x, y$, in (3.13). The coefficients of the arbitrary variation $\delta \mathbf{u}_l|_{\partial\Omega}$ terms must be zero and yield the boundary conditions for the adjoint equations as given by

$$\frac{\partial H}{\partial \mathbf{u}_l} - \frac{\partial}{\partial l}\frac{\partial H}{\partial \mathbf{u}_{ll}} = 0, \quad l = x, y. \tag{3.20}$$

By substituting the governing equations (2.4)–(2.6) into (3.20), the boundary conditions of adjoint equations for the polymer flooding OCP are expressed as

$$\left(r_o \frac{\partial \lambda_1}{\partial l} + r_w \frac{\partial \lambda_2}{\partial l}\right)\Big|_{\partial\Omega} = 0, \quad \frac{\partial \lambda_3}{\partial l}\Big|_{\partial\Omega} = 0, \quad l = x, y, \ (x, y, t) \in \Gamma. \tag{3.21}$$

The following transversality terminal conditions at $t = t_f$ are obtained by substituting the governing equations (2.4)–(2.6) into (3.14):

$$-\frac{\partial a_o}{\partial p}\lambda_1 - \frac{\partial a_w}{\partial p}\lambda_2 - \frac{\partial a_c}{\partial p}\lambda_3 = 0,$$
$$-\frac{\partial a_o}{\partial S_w}\lambda_1 - \frac{\partial a_w}{\partial S_w}\lambda_2 - \frac{\partial a_c}{\partial S_w}\lambda_3 = 0, \qquad -\frac{\partial a_c}{\partial c_p}\lambda_3 = 0. \tag{3.22}$$

Since the coefficient terms involving the adjoint variables in (3.22) are not zero, the terminal conditions of adjoint equations in the OCP of polymer flooding can be simplified to

$$\lambda_1(x, y, t_f) = 0, \quad \lambda_2(x, y, t_f) = 0, \quad \lambda_3(x, y, t_f) = 0, \quad (x, y) \in \Omega. \tag{3.23}$$

Equation (3.23) shows that the adjoint variables are known at the final time $t_f$. Since the state variables are known at the initial time and the adjoint variables are known at the final time, the OCP is a split two-point boundary-value problem.

The variation of the performance index, $J$, reduces to the following simplified functional of the control variation:

$$\delta J_A = \int_0^{t_f} \iint_\Omega q_{\text{in}}(\xi_p + \lambda_3)\delta v \, d\sigma \, dt. \tag{3.24}$$

From the results of (3.16)–(3.18), the necessary condition for optimality of polymer flooding problem is

$$q_{\text{in}}(\xi_p + \lambda_3)\begin{cases} = 0, & \text{for } 0 \le v^* \le v_{\max}, \\ \le 0, & \text{for } v^* = 0, \\ \ge 0, & \text{for } v^* = v_{\max}. \end{cases} \tag{3.25}$$

## 4. Numerical Solution

We propose an iterative numerical technique for determining the optimal injection strategies of polymer flooding. The computational procedure is based on adjusting estimates of control function $v$ to improve the value of the objective functional. For a control to be optimal, the necessary condition given by (3.25) must be satisfied. If the control $v$ is not optimal, then a correction $\delta v$ is determined so that the functional is made lager, that is, $\delta J_A > 0$. If $\delta v$ is selected as

$$\delta v = w q_{\text{in}}(\xi_p + \lambda_3), \tag{4.1}$$

where $w$ is an arbitrary positive weighting factor, the functional variation becomes

$$\delta J_A = \int_0^{t_f} \iint_{\Omega} w\left[q_{\text{in}}(\xi_p + \lambda_3)\right]^2 d\sigma dt \ge 0. \tag{4.2}$$

Thus, choosing $\delta v$ in the gradient direction ensures a local improvement in the objective functional, $J_A$. At the higher and lower bounds on $v$, we must make the appropriate weighting terms equal to zero to avoid leaving the allowable region.

The computational algorithm of control iteration based on gradient direction is as follows.

*(1) Initialization*

Make an initial guess for the control function, $v(x, y, t), (x, y) \in L_w, t \in [0, t_f]$.

*(2) Resolution of the State Equations*

Using stored current value of $v(x, y, t), (x, y) \in L_w$, integrate the governing equations forward in time with known initial state conditions. We use the finite difference method of a full implicit scheme for the PDEs as discussed in [21, 22]. The profit functional is evaluated, and the coefficients involved in the adjoint equations which are function of the state solution are computed and stored.

*(3) Resolution of the Adjoint Equations*

Using the stored coefficients, integrate the adjoint equations numerically backward in time with known final time adjoint conditions by (3.23). Compute and store $\delta v$ as defined by (4.1).

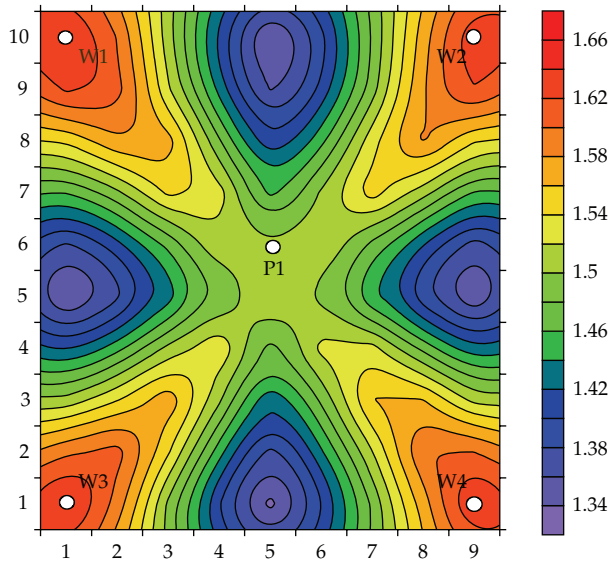


**Figure 1:** Permeability ($\mu m^2$) distribution.

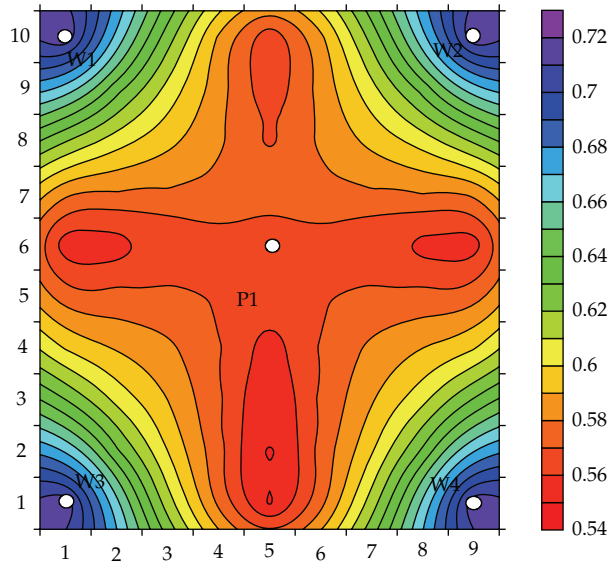


**Figure 2:** Initial water saturation contour map.

*(4) Computation of the New Control*

Using the evaluated $\delta v$, an improved function is computed as

$$v(x,y,t)^{\text{new}} = v(x,y,t)^{\text{old}} + \delta v(x,y,t), \quad (x,y) \in L_w, \tag{4.3}$$

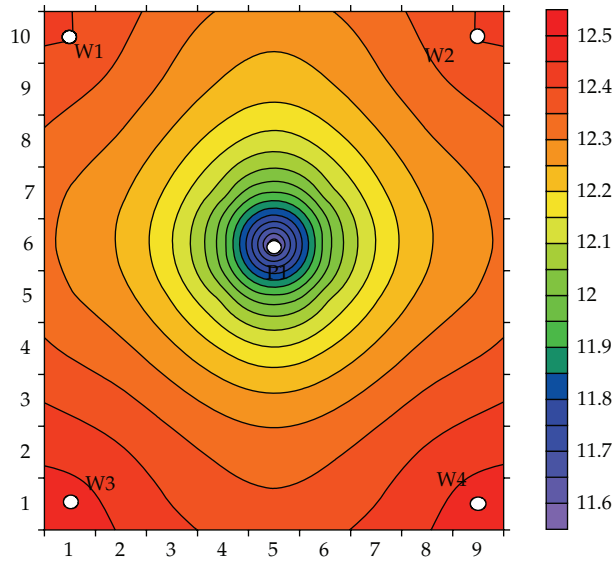


**Figure 3:** Initial reservoir pressure (MPa) contour map.

**Table 1:** Parameters of reservoir description used in the example.

| Parameters | Values |
|---|---|
| Number of production well, $N_p$ | 1 |
| Number of injection wells, $N_w$ | 4 |
| Thickness of the reservoir bed, $h$ (m) | 5 |
| Reference pressure, $p_r$ (MPa) | 12 |
| Porosity under the condition of the reference pressure, $\phi_r$ | 0.31 |
| Rock density, $\rho_r$ (kg/m$^3$) | 2000 |
| Rock compressibility factor, $C_R$ (1/MPa) | $9.38 \times 10^{-6}$ |
| Irreducible water saturation, $S_{or}$ | 0.25 |
| Residual oil saturation, $S_{wc}$ | 0.22 |
| Oil relative permeability at the irreducible water saturation, $k_{rwro}$ | 0.5228 |
| Water relative permeability at the residual oil saturation, $k_{rocw}$ | 0.9 |
| Index of oil relative permeability curve, $n_o$ | 4.287 |
| Index of water relative permeability curve, $n_w$ | 2.3447 |

where $0 \leq v^{\text{new}} \leq v_{\max}$. A single variable search strategy can be used to find the value of the positive weighting factor $w$ which maximizes the improvement in the performance functional using (4.3).

*(5) Termination*

The optimization algorithm is stopped when the variation $\delta v$ is too small to effectively change the performance measure, that is, when

$$\left| J^{\text{new}} - J^{\text{old}} \right| < \varepsilon, \tag{4.4}$$

where $\varepsilon$ is a small positive number.

**Table 2:** Fluid data used in the example.

| Parameters | Values |
|---|---|
| Oil viscosity, $\mu_o$ (mPa·s) | 50 |
| Compressibility factors of oil, $C_o$ (1/MPa) | $5 \times 10^{-6}$ |
| Oil volume factor under the condition of the reference pressure, $B_{or}$ | 1 |
| Aqueous phase viscosity with no polymer, $\mu_w$ (mPa·s) | 0.458 |
| Compressibility factors of water, $C_w$ (1/MPa) | $4.6 \times 10^{-6}$ |
| Water volume factor under the condition of the reference pressure, $B_{wr}$ | 1 |
| Polymer absorption parameter, $a$ (g/cm$^3$) | 0.03 |
| Polymer absorption parameter, $b$ (g/cm$^3$) | 3.8 |
| Diffusion coefficient, $D$ (m$^2$/s) | $1 \times 10^{-5}$ |
| Effective pore volume coefficient, $f_a$ | 1 |
| Permeability reduction parameter, $R_{k\,\max}$ | 1.15 |
| Permeability reduction parameter, $b_{rk}$ | 1.2 |
| Viscosity parameter, $ap_1$ | 15.426 |
| Viscosity parameter, $ap_2$ | 0.4228 |
| Viscosity parameter, $ap_3$ | 0.2749 |

## 5. Case Study

In this section we present a numerical example of optimal control for polymer flooding done with the proposed iterative gradient method.

The two-phase flow of oil and water in a heterogeneous two-dimensional reservoir is considered. The reservoir covers an area of $421.02 \times 443.8\,\text{m}^2$ and has a thickness of 5 m and is discretized into $90(9 \times 10 \times 1)$ grid blocks. The production model is a five-spot pattern, with one production well P1 located at the center of the reservoir $(5, 6)$ and four injection wells W1~W4 placed at the four corners $(1, 10)$, $(9, 10)$, $(1, 1)$, and $(9, 1)$ as shown in the permeability distribution map of Figure 1. Polymer is injected when the fractional flow of water for the production well comes to 97% after water flooding. The time domain of polymer injection is 0~1440 days and the polymer flooding project life is $t_f = 5500$ (days). Figures 2 and 3 show the contour maps of the initial water saturation $S_w^0$ and the initial reservoir pressure $p^0$, respectively. The initial polymer concentration is $c_p^0 = 0$ (g/L). In the performance index calculation, we use the price of oil $\xi_o = 0.0503$ ($10^4$ \$/m$^3$) (80 (\$/bbl)), and the cost of polymer $\xi_p = 2.5 \times 10^{-4}$ ($10^4$ \$/kg). The fluid velocity of production well is $q_{\text{out}} = 7.225 \times 10^{-3}$ (m/day), and the fluid velocity of every injection well is $q_{\text{in}} = 2.89 \times 10^{-2}$ (m/day). The PDEs are solved by full implicit finite difference method with step size 10 days. For the constraint (29), the maximum injection polymer concentration is $c_{\max} = 2.2$ (g/L). The parameters of the reservoir description and the fluid data are shown in Tables 1 and 2, respectively.

The polymer injection strategies obtained by the conventional engineering judgment method (trial and error) are the same 1.8 (g/L) for all injection wells. The performance index is $J = \$1.592 \times 10^7$ with oil production 32429 m$^3$ and polymer injection 155520 kg. For comparison, the results obtained by engineering judgment method are considered as the initial control strategies of the proposed iterative gradient method. A backtracking search strategy [23] is used to find the appropriate weighting term $w$ and the stopping criterion is chosen as $\varepsilon = 1 \times 10^{-5}$. By using the proposed algorithm, we obtain a cumulative oil of 33045 m$^3$ and a cumulative polymer of 151618 kg yielding the profit of $J^* = \$1.624 \times 10^7$

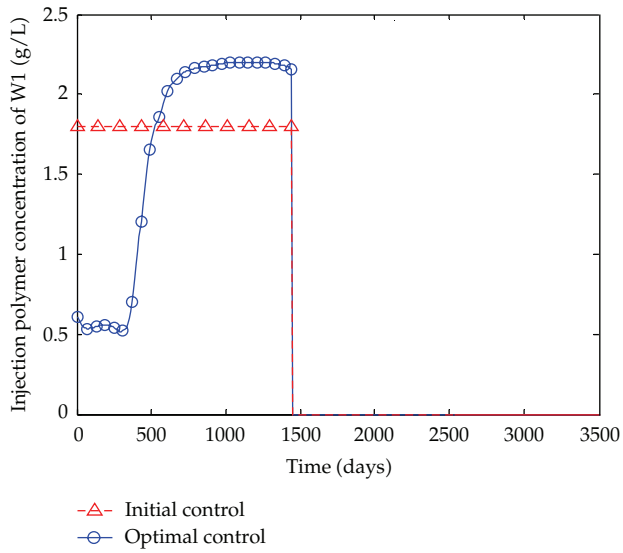


**Figure 4:** Injection polymer concentration of well W1.

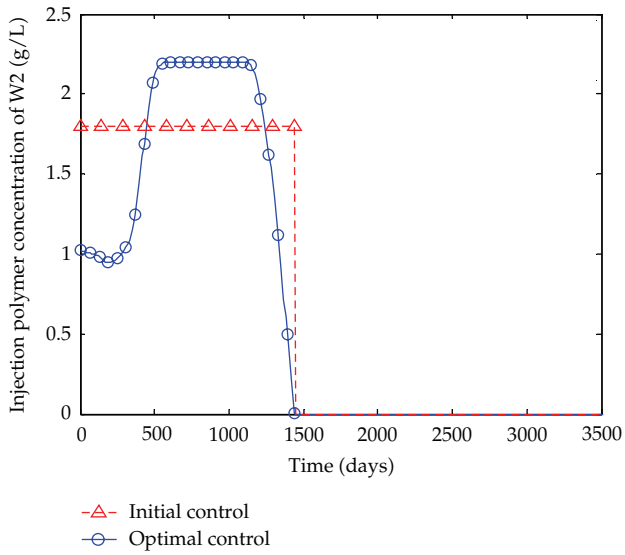


**Figure 5:** Injection polymer concentration of well W2.

over the polymer flooding project life of the reservoir. The results show an increase in performance index of $\$3.2 \times 10^5$. Figures 8 and 9 show the fractional flow of water in production well and the cumulative oil production curves of the two methods, respectively. It is obvious that the fractional flow of water obtained by iterative gradient method is lower than that by engineering judgment. Therefore, with the less cumulative polymer injection, the proposed method gets more oil production and higher recovery ratio. Figure 4 to Figure 7 show the optimal control policies of the injection wells W1~W4. As a result, the optimal injection polymer concentration profiles of W1 and W2 are significantly different

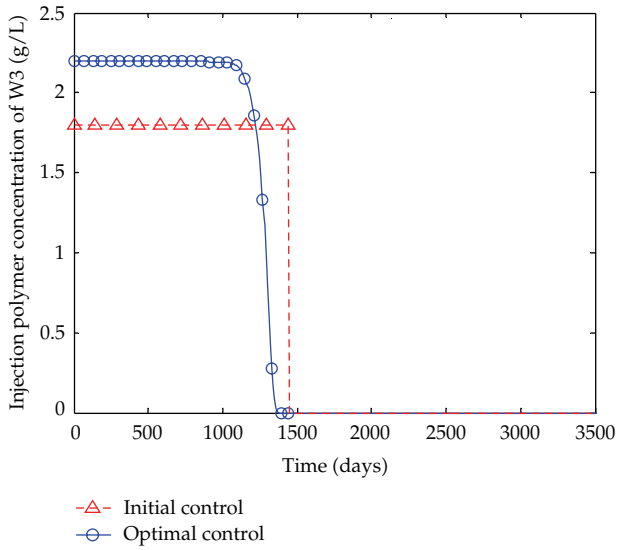


**Figure 6:** Injection polymer concentration of well W3.

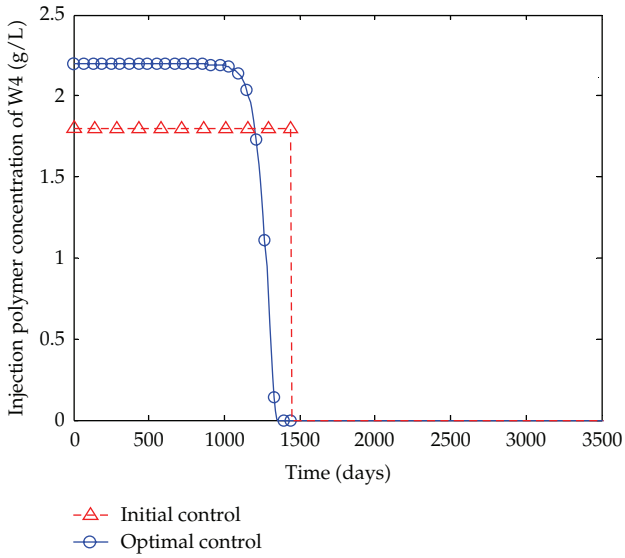


**Figure 7:** Injection polymer concentration of well W4.

from those of W3, W4. It is mainly due to the differences of the well positions and the distance to the production well, as well as the reservoir heterogeneity and the uniform initial water saturation distribution.

## 6. Conclusion

In this work, a new optimal control model of DPS is established for the dynamic injection strategies making of polymer flooding. Necessary conditions of this OCP are obtained by

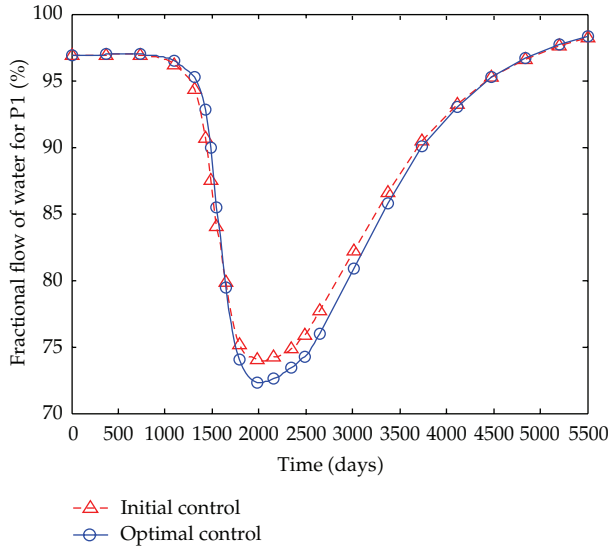


**Figure 8:** Fractional flow of water for the production well P1.

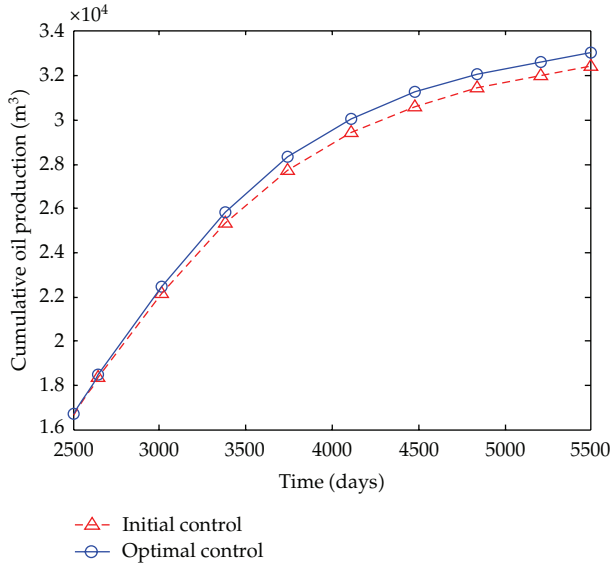


**Figure 9:** Cumulative oil production.

using the calculus of variations and Pontryagin's weak maximum principle. An iterative computational algorithm is proposed for the determination of optimal injection strategies. The optimal control model of polymer flooding and the proposed method are used for a reservoir example and the optimum injection concentration profiles for each well are offered. The results show that the profit is enhanced by the proposed method. Meanwhile, more oil production and higher recovery ratio are obtained. And the injection strategies chosen by engineering judgment are same for all the wells, whereas the optimal control policies by the

proposed method are different from each other as a result of the reservoir heterogeneity and the uniform initial conditions.

In conclusion, given the properties of an oil reservoir and the properties of a polymer solution, optimal polymer flooding injection strategies to maximize profit can be designed by using distributed-parameter control theory. The approach used is a powerful tool that can aid significantly in the development of operational strategies for EOR processes.

## Acknowledgments

This work was supported by the Natural Science Foundation of China under Grant 60974039, the Natural Science Foundation of Shandong Province of China under Grant ZR2011FM002, the Fundamental Research Funds for the Central Universities under Grant 27R1105018A, and the Postgraduate Innovation Funds of China University of Petroleum.

## References

[1] Y. Qing, D. Caili, W. Yefei, T. Engao, Y. Guang, and Z. Fulin, "A study on mass concentration determination and property variations of produced polyacrylamide in polymer flooding," *Petroleum Science and Technology*, vol. 29, no. 3, pp. 227–235, 2011.

[2] B. K. Maitin, "Performance analysis of several polyacrylamide floods in North German oil fields," in *Proceedings of the SPE/DOE Enhanced Oil Recovery Symposium*, pp. 159–165, 1992.

[3] M. A. de Melo, C. R. C. de Holleben, I. P. G. da Silva et al., "Evaluation of polymer injection projects in Brazil," in *Proceedings of the SPE Latin American and Caribbean Petroleum Engineering Conference*, pp. 1–17, 2005.

[4] Q. Yu, H. Jiang, and C. Zhao, "Study of interfacial tension between oil and surfactant polymer flooding," *Petroleum Science and Technology*, vol. 28, no. 18, pp. 1846–1854, 2010.

[5] H. Jiang, Q. Yu, and Z. Yi, "The influence of the combination of polymer and polymer-surfactant flooding on recovery," *Petroleum Science and Technology*, vol. 29, no. 5, pp. 514–521, 2011.

[6] W. F. Ramirez, Z. Fathi, and J. L. Cagnol, "Optimal injection policies for enhanced oil recovery: part 1 theory and computational strategies," *Society of Petroleum Engineers Journal*, vol. 24, no. 3, pp. 328–332, 1984.

[7] Z. Fathi and W. F. Ramirez, "Use of optimal control theory for computing optimal injection policies for enhanced oil recovery," *Automatica*, vol. 22, no. 1, pp. 33–42, 1986.

[8] W. Liu, W. F. Ramirez, and Y. F. Qi, "Optimal control of steamflooding," *SPE Advanced Technology Series*, vol. 1, no. 2, pp. 73–82, 1993.

[9] J. Ye, Y. Qi, and Y. Fang, "Application of optimal control theory to making gas-cycling decision of condensate reservoir," *Chinese Journal of Computational Physics*, vol. 15, no. 1, pp. 71–76, 1998.

[10] P. Daripa, J. Glimm, B. Lindquist, and O. McBryan, "Polymer floods: a case study of nonlinear wave analysis and of instability control in tertiary oil recovery," *SIAM Journal on Applied Mathematics*, vol. 48, no. 2, pp. 353–373, 1988.

[11] P. Daripa and G. Paşa, "An optimal viscosity profile in enhanced oil recovery by polymer flooding," *International Journal of Engineering Science*, vol. 42, no. 19-20, pp. 2029–2039, 2004.

[12] P. Daripa and G. Paşa, "Stabilizing effect of diffusion in enhanced oil recovery and three-layer Hele-Shaw flows with viscosity gradient," *Transport in Porous Media*, vol. 70, no. 1, pp. 11–23, 2007.

[13] P. Daripa and G. Pasa, "On diffusive slowdown in three-layer Hele-Shaw flows," *Quarterly of Applied Mathematics*, vol. 68, no. 3, pp. 591–606, 2010.

[14] P. Daripa, "Studies on stability in three-layer Hele-Shaw flows," *Physics of Fluids*, vol. 20, no. 11, pp. 1–11, 2008.

[15] P. Daripa, "Hydrodynamic stability of multi-layer Hele-Shaw flows," *Journal of Statistical Mechanics*, vol. 12, pp. 1–32, 2008.

[16] D. R. Brouwer and J. D. Jansen, "Dynamic optimization of water flooding with smart wells using optimal control theory," in *Proceedings of the SPE European Petroleum Conference*, pp. 391–402, 2002.

[17] P. Sarma, K. Aziz, and L. J. Durlofsky, "Implementation of adjoint solution for optimal control of smart wells," in *Proceedings of the SPE Reservoir Simulation Symposium*, pp. 1–17, 2005.

[18] L. L. Guo, S. R. Li, Y. B. Zhang, and Y. Lei, "Solution of optimal control of polymer flooding based on parallelization of iterative dynamic programming," *Journal of China University of Petroleum*, vol. 33, no. 3, pp. 167–174, 2009, (Edition of Natural Science).

[19] S. R. Li, Y. Lei, X. D. Zhang, and Q. Zhang, "Optimal control solving of polymer flooding based on a hybrid genetic algorithm," in *Proceedings of the 29th Chinese Control Conference*, pp. 5194–5198, 2010.

[20] Y. Lei, S. R. Li, and X. D. Zhang, "Optimal control solving of polymer flooding based on real-coded genetic algorithm," in *Proceedings of the 8th World Congress on Intelligent Control and Automation*, pp. 5111–5114, 2010.

[21] K. Aziz and A. Settari, *Fundamentals of Reservoir Simulation*, Elsevier Applied Science, New York, NY, USA, 1986.

[22] P. Sarma, W. H. Chen, L. J. Durlofsky, and K. Aziz, "Production optimization with adjoint models under nonlinear control-state path inequality constraints," in *Proceedings of the SPE Intelligent Energy Conference and Exhibition*, pp. 1–19, 2006.

[23] J. Nocedal and S. J. Wright, *Numerical Optimization*, Springer, New York, NY, USA, 2000.

Hindawi Publishing Corporation
Journal of Applied Mathematics
Volume 2012, Article ID 710904, 11 pages
doi:10.1155/2012/710904

*Research Article*

# Finite-Time $H_\infty$ Filtering for Linear Continuous Time-Varying Systems with Uncertain Observations

**Huihong Zhao[1] and Chenghui Zhang[2]**

[1] *Department of Electromechanical Engineering, Dezhou University, No. 566 University Road West, Dezhou 253023, China*
[2] *School of Control Science and Engineering, Shandong University, 17923 Jingshi Road, Jinan 250061, China*

Correspondence should be addressed to Huihong Zhao, huihong1980@163.com

Received 29 March 2012; Revised 3 June 2012; Accepted 6 June 2012

Academic Editor: Qiang Ling



This paper is concerned with the finite-time $H_\infty$ filtering problem for linear continuous time-varying systems with uncertain observations and $\mathcal{L}_2$-norm bounded noise. The design of finite-time $H_\infty$ filter is equivalent to the problem that a certain indefinite quadratic form has a minimum and the filter is such that the minimum is positive. The quadratic form is related to a Krein state-space model according to the Krein space linear estimation theory. By using the projection theory in Krein space, the finite-time $H_\infty$ filtering problem is solved. A numerical example is given to illustrate the performance of the $H_\infty$ filter.

## 1. Introduction

Most of the literatures on estimation problem always assume the observations contain the signal to be estimated [1–8]. In [5], the linear matrix inequality technique was applied to solve the finite-time $H_\infty$ filtering problem of singular Markovian jump systems. In [6], new stability and robust stability results for 2D discrete stochastic systems were proposed based on weaker conservative assumptions. In [7], an observer was incorporated to the vaccination control rule for an SEIR propagation disease model. In [8], two linear observer prototypes for a class of linear hybrid systems were proposed based on the prediction error. However, in practice, the observation may contain the signal in a random manner, that is, the observation consists of noise alone in a nonzero probability, and it is commonly called uncertain observations or missing measurements [9, 10]. In this paper, the finite-time $H_\infty$ filtering problem is investigated for linear continuous time-varying systems with uncertain observations and $\mathcal{L}_2$-norm bounded noises.

The $H_2$-based optimal filtering has been well studied for linear systems with uncertain observations [9–13]. In [9], the recursive least-squares estimator was proposed for linear discrete-time systems with uncertain observations. The robust optimal filter for discrete time-varying systems with missing measurements and norm-bounded parameter uncertainties was designed by optimizing the upper bound of the state estimation error variance in [10]. Using the covariance information, the recursive least-squares filtering and fixed-point smoothing algorithms for linear continuous-time systems with uncertain observations were proposed in [11]. Linear and nonlinear one-step prediction algorithms for discrete-time systems with uncertain observations were presented from a covariance assignment viewpoint in [12]. The statistical convergence properties of the estimation error covariance were studied, and the existence of a critical value for the arrival rate of the observations was shown in [13]. In recent years, due to the fact that the $H_\infty$-based estimation approach does not require the information on statistics of input noise, it has received more and more attention for linear systems with uncertain observations [14–16]. Using Lyapunov function approach, the $H_\infty$ filtering algorithms in terms of linear matrix inequalities were proposed for systems with missing measurements in [14–16]. To authors' best knowledge, research on finite-time $H_\infty$ filtering for linear continuous time-varying systems with uncertain observations has not been fully investigated and remains to be challenging, which motivates the present study.

Although the Krein space linear estimation theory [1, 3] has been applied to fault detection and nonlinear estimation [17, 18], no results have been developed for systems with uncertain observations, which will be an interesting research topic in the future. In this paper, the problem of finite-time $H_\infty$ filtering will be investigated for linear continuous time-varying systems with uncertain observations and $\mathcal{L}_2$-norm bounded input noise. Based on the knowledge of Krein space linear estimation theory [1, 3], a new approach in Krein space will be developed to handle the $H_\infty$ filtering problem for linear continuous time-varying systems with uncertain observations. It will be shown that the $H_\infty$ filtering problem for linear continuous time-varying systems with uncertain observations is partially equivalent to an $H_2$ filtering problem for a certain Krein space state-space model. Through employing projection theory, both the existence condition and a solution of the $H_\infty$ filtering can be obtained in terms of a differential Riccati equation. The major contribution of this paper can be summarized as follows: (i) it shows that the $H_\infty$ filtering problem for systems with uncertain observations can be converted into an $H_2$ optimal estimation problem subject to a fictitious Krein space stochastic systems; (ii) it develops a Kalman-like robust estimator for linear continuous time-varying systems with uncertain observations.

*Notation.* Elements in a Krein space will be denoted by **boldface** letters, and elements in the Euclidean space of complex numbers will be denoted by normal letters. The superscripts "$-1$" and "$*$" stand for the inverse and complex conjugation of a matrix, respectively. $\delta(t-\tau)=0$ for $t\neq\tau$ and $\delta(t-\tau)=1$ for $t=\tau$. $\mathbb{R}^n$ denotes the $n$-dimensional Euclidean space. $I$ is the identity matrix with appropriate dimensions. For a real matrix, $P>0$ (resp., $P<0$) means that $P$ is symmetric and positive (resp., negative) definite. $\langle\cdot,\cdot\rangle$ denotes the inner product in Krein space. diag$\{\cdots\}$ denotes a block-diagonal matrix. $\theta(t)\in\mathcal{L}_2[0,T]$ means $\int_{t=0}^{T}\theta^*(t)\theta(t)dt<\infty$. $\mathcal{L}\{\cdots\}$ denotes the linear space spanned by sequence $\{\cdots\}$. An abstract vector space $\{\mathcal{K},\langle\cdot,\cdot\rangle\}$ that satisfies the following requirements is called a **Krein space** [1].

(i) $\mathcal{K}$ is a linear space over $\mathcal{C}$, the field of complex numbers.

(ii) There exists a bilinear form $\langle\cdot,\cdot\rangle\in\mathcal{C}$ on $\mathcal{K}$ such that

(a) $\langle \mathbf{y}, \mathbf{x} \rangle = \langle \mathbf{x}, \mathbf{y} \rangle^*$,
(b) $\langle a\mathbf{x} + b\mathbf{y}, \mathbf{z} \rangle = a\langle \mathbf{x}, \mathbf{z} \rangle + b\langle \mathbf{y}, \mathbf{z} \rangle$,

for any $\mathbf{x}, \mathbf{y}, \mathbf{z} \in \mathcal{K}$, $a, b \in \mathcal{C}$, and where $*$ denotes complex conjugation.

(iii) The vector space $\mathcal{K}$ admits a direct orthogonal sum decomposition

$$\mathcal{K} = \mathcal{K}_+ \oplus \mathcal{K}_- \tag{1.1}$$

such that $\{\mathcal{K}_+, \langle \cdot, \cdot \rangle\}$ and $\{\mathcal{K}_-, -\langle \cdot, \cdot \rangle\}$ are Hilbert spaces, and

$$\langle \mathbf{x}, \mathbf{y} \rangle = 0 \tag{1.2}$$

for any $\mathbf{x} \in \mathcal{K}_+$ and $\mathbf{y} \in K_-$.

## 2. System Model and Problem Formulation

In this paper, we consider the following linear continuous time-varying system with uncertain observations

$$\begin{aligned} \dot{x}(t) &= A(t)x(t) + B(t)w(t), \\ y(t) &= r(t)C(t)x(t) + v(t), \\ z(t) &= L(t)x(t), \\ x(0) &= x_0, \end{aligned} \tag{2.1}$$

where $x(t) \in \mathbb{R}^n$ is the state vector, $w(t) \in \mathbb{R}^p$ is an exogenous disturbance belonging to $\mathcal{L}_2[0,T]$, $y(t) \in \mathbb{R}^m$ is the observation, $v(t) \in \mathbb{R}^m$ is the observation noise belonging to $\mathcal{L}_2[0,T]$, $z(t) \in \mathbb{R}^q$ is the signal to be estimated, and $A(t)$, $B(t)$, $C(t)$, and $L(t)$ are known real time-varying matrices with appropriate dimensions.

The stochastic variable $r(t) \in \mathbb{R}$ takes the values of 0 and 1 with

$$\begin{aligned} \text{Prob}\{r(t) = 1\} &= E_r\{r(t)\} = p(t), \\ \text{Prob}\{r(t) = 0\} &= 1 - E_r\{r(t)\} = 1 - p(t), \\ E_r\{r(t)r(s)\} &= p(t)p(s), \quad t \neq s, \\ E_r\left\{r^2(t)\right\} &= p(t) \end{aligned} \tag{2.2}$$

[11]. Note that many literatures associated with observer design are based on the assumption that $p(t) = 1$ [1–4], it can be unreasonable in many practical applications [9, 10, 13]. In this paper, we assume that $p(t)$ is a known positive scalar.

The finite-time $H_\infty$ filtering problem under investigation is stated as follows: given a scalar $\gamma > 0$, a matrix $P_0 > 0$, and the observation $\{y(s)|_{0\le s\le t}\}$, find an estimate of the signal $z(t)$, denoted by $\check{z}(t) = \mathcal{F}\{y(s)|_{0\le s\le t}\}$, such that

$$J_{\mathcal{F}} = E_r\left\{\|x_0\|^2_{P_0^{-1}} + \int_0^T \|w(t)\|^2 dt + \int_0^T \|v(t)\|^2 dt - \gamma^{-2}\int_0^T \|e_f(t)\| dt\right\} > 0, \tag{2.3}$$

where $e_f(t) = \check{z}(t) - z(t)$.

Thus, the finite-time $H_\infty$ filtering problem can be equivalent to the following:

(I) $J_{\mathcal{F}}$ has a minimum with respect to $\{x_0, w(t)|_{0\le t\le T}\}$;

(II) $\check{z}(t)$ can be chosen such that the value of $J_{\mathcal{F}}$ at its minimum is positive.

## 3. Main Results

In this section, through introducing a fictitious Krein space-state space model, we construct a partially equivalent Krein space projection problem. By using innovation analysis approach, we derive the finite-time $H_\infty$ filter and its existence condition.

### 3.1. Construct a Partially Equivalent Krein Space Problem

To begin with, we introduce the following state transition matrix:

$$\frac{d}{dt}\Phi(t,\tau) = A(t)\Phi(t,\tau), \quad \Phi(\tau,\tau) = I, \tag{3.1}$$

it follows from the state-space model (2.1) that

$$y(t) = r(t)C(t)\Phi(t,0)x_0 + r(t)C(t)\int_0^t \Phi(t,\tau)B(\tau)w(\tau)d\tau + v(t), \tag{3.2}$$

$$\check{z}(t) = L(t)\Phi(t,0)x_0 + L(t)\int_0^t \Phi(t,\tau)B(\tau)w(\tau)d\tau + e_f(t). \tag{3.3}$$

Thus, we can rewrite $J_{\mathcal{F}}$ as

$$
\begin{aligned}
J_{\mathcal{F}} &= E_r\left\{\|x_0\|^2_{P_0^{-1}} + \int_0^T \|w(t)\|^2 dt + \int_0^T \|v(t)\|^2 dt - \gamma^{-2}\int_0^T \left\|e_f(t)\right\|^2 dt\right\} \\
&= x_0^* P_0^{-1} x_0 + \int_0^T w^*(t)w(t)dt \\
&\quad + E_r\left\{\int_0^T \left(y(t) - r(t)C(t)\Phi(t,0)x_0 - r(t)C(t)\int_0^t \Phi(t,\tau)B(\tau)w(\tau)d\tau\right)^* \right. \\
&\qquad \left. \times\left(y(t) - r(t)C(t)\Phi(t,0)x_0 - r(t)C(t)\int_0^t \Phi(t,\tau)B(\tau)w(\tau)d\tau\right)dt\right\} \\
&\quad - \gamma^{-2}\int_0^T \left(\check{z}(t) - L(t)\Phi(t,0)x_0 - L(t)\int_0^t \Phi(t,\tau)B(\tau)w(\tau)d\tau\right)^* \\
&\quad \times\left(\check{z}(t) - L(t)\Phi(t,0)x_0 - L(t)\int_0^t \Phi(t,\tau)B(\tau)w(\tau)d\tau\right)dt \\
&= x_0^* P_0^{-1} x_0 + \int_0^T w^*(t)w(t)dt \\
&\quad + \int_0^T \left(y_0(t) - C_1(t)\Phi(t,0)x_0 - C_1(t)\int_0^t \Phi(t,\tau)B(\tau)w(\tau)d\tau\right)^* \\
&\quad \times\left(y_0(t) - C_1(t)\Phi(t,0)x_0 - C_1(t)\int_0^t \Phi(t,\tau)B(\tau)w(\tau)d\tau\right)dt \\
&\quad + \int_0^T \left(y_s(t) - C_2(t)\Phi(t,0)x_0 - C_2(t)\int_0^t \Phi(t,\tau)B(\tau)w(\tau)d\tau\right)^* \\
&\quad \times\left(y_s(t) - C_2(t)\Phi(t,0)x_0 - C_2(t)\int_0^t \Phi(t,\tau)B(\tau)w(\tau)d\tau\right)dt \\
&\quad - \gamma^{-2}\int_0^T \left(\check{z}(t) - L(t)\Phi(t,0)x_0 - L(t)\int_0^t \Phi(t,\tau)B(\tau)w(\tau)d\tau\right)^* \\
&\quad \times\left(\check{z}(t) - L(t)\Phi(t,0)x_0 - L(t)\int_0^t \Phi(t,\tau)B(\tau)w(\tau)d\tau\right)dt,
\end{aligned}
\tag{3.4}
$$

where

$$
C_1(t) = p(t)C(t), \qquad C_2(t) = \sqrt{p(t)\left(1-p(t)\right)}C(t), \qquad y_0(t) = y(t), \qquad y_s(t) \equiv 0. \tag{3.5}
$$

Moreover, we introduce the following Krein space stochastic system

$$\begin{aligned}
\dot{\mathbf{x}}(t) &= A(t)\mathbf{x}(t) + B(t)\mathbf{w}(t),\\
\mathbf{y}_0(t) &= C_1(t)\mathbf{x}(t) + \mathbf{v}(t),\\
\mathbf{y}_s(t) &= C_2(t)\mathbf{x}(t) + \mathbf{v}_s(t),\\
\check{\mathbf{z}}(t) &= L(t)\mathbf{x}(t) + \mathbf{e}_f(t),\\
\mathbf{x}(0) &= \mathbf{x}_0,
\end{aligned} \tag{3.6}$$

where $\mathbf{x}_0$, $\mathbf{w}(t)$, $\mathbf{v}(t)$, $\mathbf{v}_s(t)$, and $\mathbf{e}_f(t)$ are mutually uncorrelated white noises with zero means and known covariance matrices as

$$\left\langle \begin{bmatrix} \mathbf{x}_0 \\ \mathbf{w}(t) \\ \mathbf{v}(t) \\ \mathbf{v}_s(t) \\ \mathbf{e}_f(t) \end{bmatrix}, \begin{bmatrix} \mathbf{x}_0 \\ \mathbf{w}(\tau) \\ \mathbf{v}(\tau) \\ \mathbf{v}_s(\tau) \\ \mathbf{e}_f(\tau) \end{bmatrix} \right\rangle = \begin{bmatrix} P_0 & 0 & 0 & 0 & 0 \\ 0 & I\delta(t-\tau) & 0 & 0 & 0 \\ 0 & 0 & I\delta(t-\tau) & 0 & 0 \\ 0 & 0 & 0 & I\delta(t-\tau) & 0 \\ 0 & 0 & 0 & 0 & -\gamma^2 I\delta(t-\tau) \end{bmatrix}. \tag{3.7}$$

Let

$$\begin{aligned}
y_0(t) &= C_1(t)x(t) + v(t),\\
y_s(t) &= C_2(t)x(t) + v_s(t),
\end{aligned} \tag{3.8}$$

then it follows from (3.1), (3.3), (3.4), and (3.7) that

$$\begin{aligned}
J_{\mathcal{T}} = {} & x_0^*\langle \mathbf{x}_0, \mathbf{x}_0\rangle^{-1}x_0 + \int_0^T w^*(t)\langle \mathbf{w}(t), \mathbf{w}(t)\rangle^{-1}w(t)dt + \int_0^T v^*(t)\langle \mathbf{v}(t), \mathbf{v}(t)\rangle^{-1}v(t)dt \\
& + \int_0^T v_s^*(t)\langle \mathbf{v}_s(t), \mathbf{v}_s(t)\rangle^{-1}v_s(t)dt + \int_0^T e_f^*(t)\langle \mathbf{e}_f(t), \mathbf{e}_f(t)\rangle^{-1}e_f(t)dt.
\end{aligned} \tag{3.9}$$

According to [1] and [3], we have the following results.

**Lemma 3.1.** *Consider system* (2.1)*, given a scalar* $\gamma > 0$ *and a matrix* $P_0 > 0$*, then* $J_{\mathcal{T}}$ *in* (2.3) *has the minimum over* $\{x_0, w(t)|_{0\le t\le T}\}$ *if and only if the innovation* $\tilde{\mathbf{y}}_z(t)$ *exists for* $0 \le t \le T$*, where*

$$\tilde{\mathbf{y}}_z(t) = \mathbf{y}_z(t) - \hat{\mathbf{y}}_z(t), \tag{3.10}$$

$\mathbf{y}_z(t) = [\mathbf{y}_0^*(t) \;\; \mathbf{y}_s^*(t) \;\; \check{\mathbf{z}}^*(t)]^*$, *and* $\widehat{\mathbf{y}}_z(t)$ *denote the projection of* $\mathbf{y}_z(t)$ *onto* $\mathcal{L}\{\{\mathbf{y}_z(\tau)\}|_{0\le\tau<t}\}$. *In this case the minimum value of* $J_{\mathcal{F}}$ *is*

$$\begin{aligned}\min J_{\mathcal{F}} = &\int_0^T \big(y_0(t) - C_1(t)\widehat{x}(t)\big)^*\big(y_0(t) - C_1(t)\widehat{x}(t)\big)dt \\ &+ \int_0^T \big(y_s(t) - C_2(t)\widehat{x}(t)\big)^*\big(y_s(t) - C_2(t)\widehat{x}(t)\big)dt \\ &- \gamma^{-2}\int_0^T (\check{z}(t) - L(t)\widehat{x}(t))^*(\check{z}(t) - L(t)\widehat{x}(t))dt,\end{aligned} \tag{3.11}$$

*where* $\widehat{x}(t)$ *is obtained from the Krein space projection of* $\mathbf{x}(t)$ *onto* $\mathcal{L}\{\{\mathbf{y}_z(j)\}|_{0\le\tau<t}\}$.

*Remark 3.2.* By analyzing the indefinite quadratic form $J_{\mathcal{F}}$ in (3.4) and using the Krein space linear estimation theory [1], it has been shown that the $H_\infty$ filtering problem for linear systems with uncertain observations is equivalent to the $H_2$ estimation problem with respect to a Krein space stochastic system, which is new as far as we know. In this case, Krein space projection method can be applied to derive an $H_\infty$ estimator for linear systems with uncertain observations, which is more simple and intuitive than previous versions.

### 3.2. Solution of the Finite-Time $H_\infty$ Filtering Problem

By applying the standard Kalman filter formula to system (3.6), we have the following lemma.

**Lemma 3.3.** *Consider the Krein space stochastic system* (3.6), *the prediction* $\widehat{\mathbf{x}}(t)$ *is calculated by*

$$\dot{\widehat{\mathbf{x}}}(t) = A(t)\widehat{\mathbf{x}}(t) + K(t)\widetilde{\mathbf{y}}_z(t), \tag{3.12}$$

*where*

$$\begin{aligned}\widetilde{\mathbf{y}}_z(t) &= \mathbf{y}_z(t) - H(t)\widehat{\mathbf{x}}(t), \\ H(t) &= \big[C_1^*(t) \;\; C_2^*(t) \;\; L^*(t)\big]^*, \\ K(t) &= P(t)H^*(t)R_{\widetilde{y}z}^{-1}(t), \\ R_{\widetilde{y}z}(t) &= \operatorname{diag}\Big\{I, I, -\gamma^2 I\Big\},\end{aligned} \tag{3.13}$$

*and* $P(t)$ *is computed by*

$$\begin{aligned}\dot{P}(t) &= A(t)P(t) + P(t)A^*(t) + B(t)B^*(t) - K(t)R_{\widetilde{y}_z}(t)K^*(t), \\ P(0) &= P_0.\end{aligned} \tag{3.14}$$

Now we are in the position to present the main results of this subsection.

**Theorem 3.4.** *Consider system* (2.1)*, given a scalar* $\gamma > 0$ *and a matrix* $P_0 > 0$*, and suppose* $P(t)$ *is the bounded positive definite solution to Riccati differential equation* (3.14)*. Then, one possible level-*$\gamma$ *finite-time* $H_\infty$ *filter that achieves* (2.3) *is given by*

$$\check{z}(t) = L(t)\hat{x}(t), \quad 0 \le t \le T, \tag{3.15}$$

*where*

$$\begin{aligned} \dot{\hat{x}}(t) &= A(t)\hat{x}(t) + P(t)C_f^*(t)\big(y_f(t) - C_f(t)\hat{x}(t)\big), \\ \hat{x}(0) &= 0 \end{aligned} \tag{3.16}$$

*with* $y_f(t) = [y_0^*(t) \;\; y_s^*(t)]^*$, $C_f(t) = [C_1^*(t) \;\; C_2^*(t)]^*$.

*Proof.* It follows from Lemma 3.3 that if $P(t)$ is a bounded positive definite solution to Riccati differential equation (3.14), then the projection $\hat{\mathbf{x}}(t)$ exists. According to Lemma 3.1, it is obvious that the $H_\infty$ filter that achieves (2.3) exists. If this is the case, the minimum value of $J_{\mathcal{F}}$ is given by (3.11). In order to achieve $\min J_{\mathcal{F}} > 0$, one natural choice is to set

$$\check{z}(t) - L(t)\hat{x}(t) = 0 \tag{3.17}$$

thus the finite-time $H_\infty$ filter can be given by (3.15).

On the other hand, from (3.12) and (3.15), It is easy to verify that (3.16) holds. □

*Remark 3.5.* Let

$$e(t) = x(t) - \hat{x}(t), \tag{3.18}$$

it follows from (2.1) and (3.16) that

$$\dot{e}(t) = (A(t) - \Gamma(t)C(t))e(t) + B(t)w(t) - P(t)C_f^*(t)v_z(t), \tag{3.19}$$

where

$$\Gamma(t) = P(t)C_f^*(t)\left[\frac{p(t)I}{\sqrt{p(t)(1-p(t))}I}\right], \qquad v_z(t) = \begin{bmatrix} v(t) \\ v_s(t) \end{bmatrix}. \tag{3.20}$$

Unlike [14–16], the parameter matrices in the filtering error equation (3.19) do not contain the stochastic variable $r(t)$, which is an interesting phenomenon. As mentioned in Definition 1 in [19], it is obvious that, if $(C(t), A(t))$ is detectable, then the filtering error equation (3.19) is exponentially stable. Based on the above analysis, it can be concluded that the following assumptions are necessary for the finite-time $H_\infty$ filter design in this paper:

(i) $(C(t), A(t))$ is detectable,

(ii) $w(t), v(t) \in \mathcal{L}_2[0, T]$.

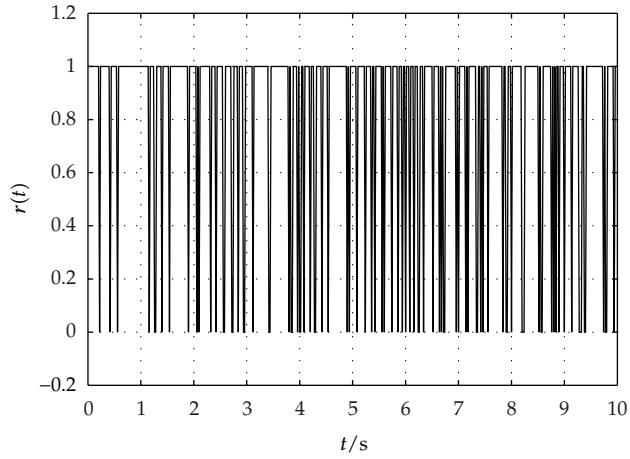


**Figure 1:** Stochastic variable $r(t)$.

## 4. A Numerical Example

We consider system (2.1) with the following parameters:

$$A(t) = \begin{bmatrix} -10 & 6 \\ 2 & -5 \end{bmatrix}, \quad B(t) = \begin{bmatrix} 2.8 \\ 1.6 \end{bmatrix}, \quad C(t) = [18 \;\; 9.5], \quad L(t) = [1 \;\; 1] \tag{4.1}$$

and set $\gamma = 1.1$, $x(0) = [0 \;\; 0]^*$, $p(t) = 0.8$, and $P_0 = I$. In addition, we suppose that the noises $w(t)$ and $v(t)$ are generated by Gaussian with zero means and covariances $Q_w = 1$, $Q_v = 0.02$, the sampling time is 0.02 s, and the stochastic variable $r(t)$ is simulated as in Figure 1. Based on Theorem 3.4, we design the finite-time $H_\infty$ filter. Figure 2 shows the true value of signal $z(t)$ and its $H_\infty$ filtering estimate, and Figure 3 shows the estimation error $\tilde{z}(t) = z(t) - \check{z}(t)$. It can be observed from the simulation results that the finite-time $H_\infty$ filter has good tracking performance.

## 5. Conclusions

In this paper, we have proposed a new finite-time $H_\infty$ filtering technique for linear continuous time-varying systems with uncertain observations. By introducing a Krein state-space model, it is shown that the $H_\infty$ filtering problem can be partially equivalent to a Krein space $H_2$ filtering problem. A sufficient condition for the existence of the finite-time $H_\infty$ filter is given, and the filter is derived in terms of a differential Riccati equation.

Future research work will extend the proposed method to investigate the $H_\infty$ multistep prediction and fixed-lag smoothing problem for linear continuous time-varying systems with uncertain observations.

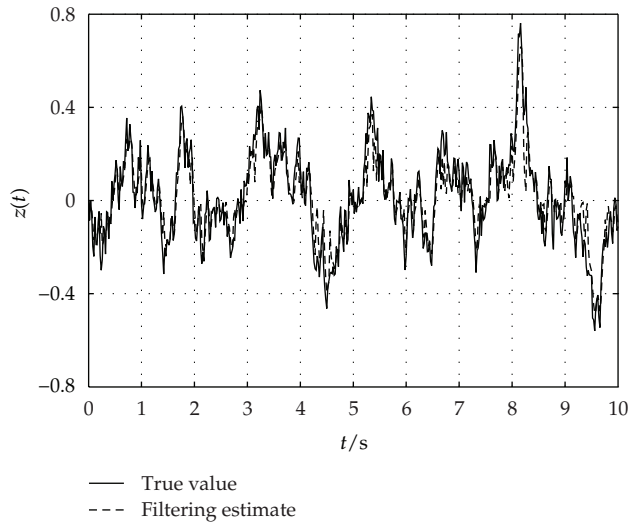


**Figure 2:** True value of signal $z(t)$ (solid line) and its $H_\infty$ filtering estimate (dashed line).

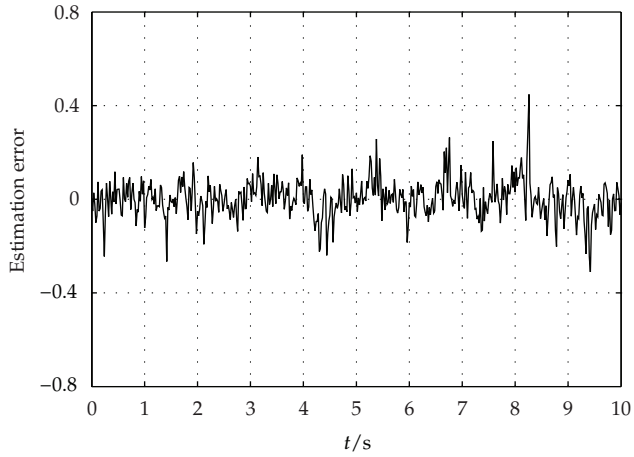


**Figure 3:** Estimation error $\tilde{z}(t)$.

## Acknowledgments

The authors sincerely thank the anonymous reviewers for providing valuable comments and useful suggestions aimed at improving the quality of this paper. The authors also thank the editor for the efficient and professional processing of their paper. This work is supported by the National Natural Science Foundation of China (60774004, 61034007, and 60874016) and the Independent Innovation Foundation of Shandong University, China (2010JC003).

## References

[1] B. Hassibi, A. H. Sayed, and T. Kailath, *Indefinite-Quadratic Estimation and Control: A Unified Approach to $H_2$ and $H_\infty$ Theories*, SIAM, New York, NY, USA, 1999.

[2] T. Kailath, "A view of three decades of linear filtering theory," *IEEE Transactions on Information Theory*, vol. 20, no. 2, pp. 146–181, 1974.
[3] H. Zhang and L. Xie, *Control and Estimation of Systems with Input/Output Delays*, vol. 355, Springer, Berlin, Germany, 2007.
[4] B. D. O. Anderson and J. B. Moore, *Optimal Filtering*, Prentice-Hall, Englewood Cliffs, NJ, USA, 1979.
[5] C. X. Liu, Y. Q. Zhang, and H. X. Sun, "Finite-time $H_\infty$ filtering for singular stochastic systems," *Journal of Applied Mathematics*, vol. 2012, Article ID 615790, 16 pages, 2012.
[6] J.-R. Cui, G.-D. Hu, and Q. Zhu, "Stability and robust stability of 2D discrete stochastic systems," *Discrete Dynamics in Nature and Society*, vol. 2011, Article ID 545361, 11 pages, 2011.
[7] M. De la Sen, A. Ibeas, and S. Alonso-Quesada, "Observer-based vaccination strategy for a true mass action SEIR epidemic model with potential estimation of all the populations," *Discrete Dynamics in Nature and Society*, vol. 2011, Article ID 743067, 19 pages, 2011.
[8] M. De La Sen and N. Luo, "Design of linear observers for a class of linear hybrid systems," *International Journal of Systems Science*, vol. 31, no. 9, pp. 1077–1090, 2000.
[9] N. E. Nahi, "Optimal recursive estimation with uncertain observation," *IEEE Transactions on Information Theory*, vol. 15, no. 4, pp. 457–462, 1969.
[10] Z. Wang, F. Yang, D. W. C. Ho, and X. Liu, "Robust finite-horizon filtering for stochastic systems with missing measurements," *IEEE Signal Processing Letters*, vol. 12, no. 6, pp. 437–440, 2005.
[11] S. Nakamori, "Estimation of signal using covariance information given uncertain observations in continuous-time systems," *IEICE Transactions on Fundamentals of Electronics, Communications and Computer Sciences*, vol. E79-A, no. 6, pp. 736–744, 1996.
[12] W. NaNacara and E. E. Yaz, "Recursive estimator for linear and nonlinear systems with uncertain observations," *Signal Processing*, vol. 62, no. 2, pp. 215–228, 1997.
[13] B. Sinopoli, L. Schenato, M. Franceschetti, K. Poolla, M. I. Jordan, and S. S. Sastry, "Kalman filtering with intermittent observations," *IEEE Transactions on Automatic Control*, vol. 49, no. 9, pp. 1453–1464, 2004.
[14] W. Wang and F. W. Yang, "$H_\infty$ filter design for discrete-time systems with missing measurements," *Acta Automatica Sinica*, vol. 32, no. 1, pp. 107–111, 2006.
[15] Z. Wang, F. Yang, D. W. C. Ho, and X. Liu, "Robust $H_\infty$ filtering for stochastic time-delay systems with missing measurements," *IEEE Transactions on Signal Processing*, vol. 54, no. 7, pp. 2579–2587, 2006.
[16] H. Zhang, Q. Chen, H. Yan, and J. Liu, "Robust $H_\infty$ filtering for switched stochastic system with missing measurements," *IEEE Transactions on Signal Processing*, vol. 57, no. 9, pp. 3466–3474, 2009.
[17] H. Zhao, M. Zhong, and M. Zhang, "$H_\infty$ fault detection for linear discrete time-varying systems with delayed state," *IET Control Theory & Applications*, vol. 4, no. 11, pp. 2303–2314, 2010.
[18] H. Zhao, C. Zhang, G. Wang, and G. Xing, "$H_\infty$ estimation for a class of Lipschitz nonlinear discrete-time systems with time delay," *Abstract and Applied Analysis*, vol. 2011, Article ID 970978, 22 pages, 2011.
[19] K. M. Nagpal and P. P. Khargonekar, "Filtering and smoothing in an $H_\infty$ setting," *IEEE Transactions on Automatic Control*, vol. 36, no. 2, pp. 152–166, 1991.

Hindawi Publishing Corporation
Journal of Applied Mathematics
Volume 2012, Article ID 840873, 13 pages
doi:10.1155/2012/840873

*Research Article*

# Distributed Containment Control of Networked Fractional-Order Systems with Delay-Dependent Communications

**Xueliang Liu,[1,2] Bugong Xu,[1,2] and Lihua Xie[3]**

[1] *College of Automation Science and Engineering, South China University of Technology, Guangzhou 510640, China*
[2] *Key Laboratory of Autonomous Systems and Network Control, Ministry of Education, Guangzhou 510640, China*
[3] *School of Electrical and Electronic Engineering, Nanyang Technological University, Singapore 639798*

Correspondence should be addressed to Bugong Xu, aubgxu@scut.edu.cn

Received 5 March 2012; Accepted 26 May 2012

Academic Editor: Baocang Ding



This paper is concerned with a containment problem of networked fractional-order system with multiple leaders under a fixed directed interaction graph. Based on the neighbor rule, a distributed protocol is proposed in delayed communication channels. By employing the algebraic graph theory, matrix theory, Nyquist stability theorem, and frequency domain method, it is analytically proved that the whole follower agents will flock to the convex hull which is formed by the leaders. Furthermore, a tight upper bound on the communication time-delay that can be tolerated in the dynamic network is obtained. As a special case, the interconnection topology under the undirected case is also discussed. Finally, some numerical examples with simulations are presented to demonstrate the effectiveness and correctness of the theoretical results.

## 1. Introduction

In recent years, coordination of multiagent systems has attracted considerable interest in the control community due to their wide application areas in formation control [1–3], flocking/swarming [4, 5], consensus [6–9], sensor networks [10, 11], synchronization of complex networks [12, 13], and distributed computation [14]. A common character of these applications is that each individual agent lacks a global knowledge of the whole system and can only send and/or obtain state information from its neighbors through local communications. Significant progress has been made in the coordination problem (see, e.g., [11, 15, 16] and the references therein).

As a special case of coordination control, containment control means to drive the followers to be in the convex hull which is spanned by the leaders. Different from general leader-following consensus problems, where there exist multiple leaders and multiple followers in containment problems. The coordinate objective is likely to be one or several target sets in multiagent coordination control. These target sets may be a biological communities, a team of robots, a food enrichment area, and so on. For example, a kind of biological group hunts another kind of biological communities, a team of biological group cooperatively builds their nest, and several agents lead a team of agents avoiding hazardous obstacles. Thus, how to control a multiagent system to achieve a common target becomes an interesting problem.

The idea of fractional calculus has been known since the development of the regular calculus, with the first reference probably being dated back to the seventeenth century [17], where the meaning of derivative of order one-half was first mentioned. Although it has a long history, the fractional calculus applications to physics and engineering are just a recent focus of interest. Moreover, fractional derivatives provide an excellent tool for the description of memory and hereditary properties of various materials and processes. As pointed out by many researchers, many physical systems are more suitable to be modeled by fractional-order dynamic equations [18]. Many systems are known to display fractional-order dynamics, such as viscoelastic systems, electromagnetic waves, and quantum evolution of complex systems. In additional, integer-order systems can be regarded as a special case of fractional-order systems.

More recently, many interesting agent-related consensus problems are under investigation, and fractional-order consensus becomes a hot topic. The consensus problem of fractional-order systems is first proposed and investigated by Cao et al. [19, 20], where three different cases of coordination models are introduced. By employing a varying-order fractional coordination strategy, a higher convergence performance is obtained. Sun et al. [21] study the consensus problem for fractional-order systems under undirected scale-free networks. They also compared the convergence rate of fractional-order dynamics and the integer-order dynamics. In order to increase the convergence speed and ensure the exponential convergence, a switching order consensus protocol is employed. Shen et al. [22, 23] consider the consensus problem of fractional-order systems with nonuniform input and/or communication delays over directed networks. Based on the Nyquist stability criterion and frequency domain approach, some sufficient conditions are obtained to ensure the fractional-order consensus. Formation control problems for fractional-order systems were discussed in [24]. However, little research work has been done toward the problem of containment control of fractional-order system, which is the main focus of this paper.

Motivated by the above discussion, in this paper, we consider the containment problem of networked fractional-order systems over directed topologies. Different from generally leader-following consensus problem, there exist multiple leaders in a containment control problem. The objective is to drive the followers to be in the convex hull formed by the leaders. On the other hand, in practice delays unavoidably exist due to the finite speed of transmission, acquisition, and traffic congestions. Therefore, studying the agents with the form of fractional-order dynamics over delayed communication channel becomes very significant.

The rest of the paper is organized as follows. Section 2 gives some preliminaries on algebraic graph theory and Caputo fractional operator and formulates the problem under investigation. In Section 3, containment control under fixed directed topologies and delayed

communication channels is investigated. In Section 4, two examples are provided to verify the theoretical analysis. Finally, some concluding remarks will be drawn in Section 5.

Some remarks on the notation are given as follows: $[\alpha]$ stands for the integer part of $\alpha$, $\mathbf{1}_n$ is an $n$-dimension column vector with all ones. $I_N$ is the identity matrix with dimension $N \times N$. $\mathbb{R}^{N\times N}$ and $\mathbb{R}^N$, respectively, denote the family of all $N \times N$ dimensional matrices and the $N$ dimensional column vector. The notation $A > 0\,(A \geq 0)$ means that matrix $A$ is positive definite (semidefinite). "$\|x\|$" stands for the Euclidean norm of vector $x$. $\lambda_i(A)$ and $\rho(A)$ denote the $i$th eigenvalue of matrix $A$ and spectral radius of matrix $A$, respectively. diag $\{\cdots\}$ stands for a block diagonal matrix. $A\otimes B$ means the Kronecker product of matrices $A$ and $B$. A set $\Theta \in \mathbb{R}^N$ is convex if the line segment between any two elements in $\Theta$ lies in $\Theta$, that is, if for any $x, y \in \Theta$ and any $\gamma$ with $0 \leq \gamma \leq 1$, we have $\gamma x + (1-\gamma)y \in \Theta$. Similarly, a vector sum $\gamma_1 x_1 + \gamma_2 x_2 + \cdots + \gamma_n x_n$ is called a convex combination of $x_1, x_2, \ldots, x_n$ if the coefficients satisfy $\gamma_i \geq 0$ and $\sum_{i=1}^{n} \gamma_i = 1$. The convex hull of $\Theta$ denoted by co$\{\Theta\}$ is the intersection of all convex sets containing $\Theta$. For nonempty set $E$, the Euclid distance between point $x$ and set $E$ is defined as $d_E(x) = \inf_{y\in E}\|x - y\|$. $\mathcal{O} = \{1, 2, \ldots, N\}$.

## 2. Preliminary

Before formulating our problem, we introduce some basic concepts in graph theory and the Caputo fractional operator for fractional-order networks.

### 2.1. Algebraic Graph Theory

Algebraic graph theory is a natural framework for analyzing coordination problems. Let the interaction topology of information exchanged between $N$ agents be described by a directed graph $\mathcal{G} = \{\mathcal{V}, \mathcal{E}, \mathcal{A}\}$, where $\mathcal{V} = \{1, 2, \ldots, N\}$ is the set of vertices, vertex $i$ represents the $i$th agent, $\mathcal{E} \subset \mathcal{V} \times \mathcal{V}$ is the set of edge. An edge in $\mathcal{G}$ is denoted by an ordered pair $(j, i)$, representing that agent $i$ can receive information from agent $j$. The neighborhood of the $i$th agent is denoted by $\mathcal{N}_i = \{j \in \mathcal{V} \mid (j, i) \in \mathcal{E}\}$. $\mathcal{A} = [a_{ij}]_{N\times N} \in R^N$ is called the weighted adjacency matrix of $\mathcal{G}$ with nonnegative elements where $a_{ii} = 0$ and $a_{ij} \geq 0$ with $a_{ij} > 0$ for $j \in \mathcal{N}_i$. The in-degree of agent $i$ is defined as $\deg_{\text{in}}(i) = \sum_{j=1}^{N} a_{ij}$, and the out-degree of agent $i$ is defined as $\deg_{\text{out}}(i) = \sum_{j=1}^{N} a_{ji}$. The Laplacian matrix of $\mathcal{G}$ is defined as $L = \mathfrak{D} - \mathcal{A}$, where $\mathfrak{D} = \text{diag}\{\deg_{\text{in}}(1), \deg_{\text{in}}(2), \ldots, \deg_{\text{in}}(N)\}$. A sequence of edges $(i_1, i_2), (i_2, i_3), \ldots, (i_{k-1}, i_k)$ is called a path from agent $i_1$ to agent $i_k$. A directed tree is a directed graph, where every agent has exactly one neighbor except one agent has no neighbors. A spanning tree of $\mathcal{G}$ is a directed tree whose vertex set is $\mathcal{V}$ and whose edge set is a subset of $\mathcal{E}$. In undirected graphs, if there is a path between any two vertices of a graph $\mathcal{G}$, then $\mathcal{G}$ is connected, otherwise disconnected.

### 2.2. Caputo Fractional Operator

For an arbitrary real number $\alpha$, the Riemann-Liouville and Caputo fractional derivatives are defined, respectively, as

$$ {}_aD_t^{\alpha} f(t) = \frac{1}{\Gamma(m-\alpha)} \frac{d^m}{dt^m} \int_a^t (t-\tau)^{m-\alpha-1} f(\tau) d\tau, \tag{2.1} $$

$$ {}_a^C D_t^{\alpha} f(t) = \frac{1}{\Gamma(m-\alpha)} \int_a^t \frac{f^m(\tau)}{(t-\tau)^{\alpha+1-m}} d\tau, \tag{2.2} $$

where $m = [\alpha] + 1$ is the first integer which is not less than $\alpha$ and $\Gamma(\cdot)$ is the Euler's gamma function.

It is worth pointing out that the advantage of Caputo approach is that the initial conditions for fractional-order differential equations with Caputo derivatives take on the same form as that for integer-order differential equations. For details, please refer to [17]. Therefore, we will only use the Caputo fractional operator in this paper to model the system dynamics. For notational simplicity, we rewrite ${}_a^C D_t^\alpha f(t)$ as $f^{(\alpha)}(t)$ in the rest of the paper.

### 2.3. Laplace Transform

In the following, we will introduce the Laplace transform of the caputo fractional derivative which will fascinate the development of the subsequent results:

$$\mathcal{L}\left\{f^{(\alpha)}(t)\right\} = \begin{cases} s^\alpha F(s) - s^{\alpha-1} f(0), & \alpha \in (0,1]; \\ s^\alpha F(s) - s^{\alpha-1} f(0) - s^{\alpha-2}\dot{f}(0), & \alpha \in (1,2]. \end{cases} \tag{2.3}$$

### 2.4. Problem Formulation

Consider a networked fractional-order system consisting of $N + m$ agents, where $N$ agents labeled by $1, 2, \ldots, N$ are referred to as the follower agents and the other agents labeled by $N + 1, \ldots, N + m$ act as leaders of the team. The information interaction topology among $N$ following-agents is described by the graph $\mathcal{G} = (\mathcal{V}, \mathcal{E}, \mathcal{A})$, and the whole system involving $N + m$ agents is conveniently modeled by a weighted directed graph $\overline{\mathcal{G}} = (\overline{\mathcal{V}}, \overline{\mathcal{E}}, \overline{\mathcal{A}})$ with $\overline{\mathcal{V}} = \{1, 2, \ldots, N + m\}$ and $\overline{\mathcal{A}} = a_{ij} \in \mathbb{R}^{(N+m)\times(N+m)}$, $i, j = 1, 2, \ldots, N + m$, where the lower block submatrix of order $N$ can be regarded as $\mathcal{A}$. In this paper, we regard the convex hull spanned by multiple leaders as a virtual leader. The graph $\overline{\mathcal{G}}$ has a spanning tree meaning that there exits a path from the virtual leader to every follower agent. In general, the dynamic of each leader is independent of the follower agents. $\overline{x}_k$ represents the position state of the leader $k$ and keeps being a constant.

The dynamic of follower agent $i$ takes the following form:

$$x_i^{(\alpha)}(t) = u_i(t), \quad i \in \mathcal{I}, \tag{2.4}$$

where $x_i(t) \in \mathbb{R}^n$ is the position state, $u_i(t) \in \mathbb{R}^n$ is the control input of agent $i$, and $x_i^{(\alpha)}(t) \in \mathbb{R}^n$ is the $\alpha$th derivative of $x_i(t)$. In practice, the fractional order $\alpha$ often lies in $(0, 1]$, so we assume that the order $\alpha$ is a positive real number but not more than 1 in this paper.

For the aforementioned fractional-order dynamics, the following control rule will be used for follower agent $i$:

$$u_i(t) = \sum_{j \in \mathcal{N}_i} a_{ij}\big(x_j(t-\tau) - x_i(t-\tau)\big) + \sum_{k=N+1}^{N+m} b_k^i(\overline{x}_k(t-\tau) - x_i(t-\tau)), \tag{2.5}$$

where $b_k^i \geq 0$, $b_k^i > 0$ if and only if the leader $k$ ($k = N + 1, N + 2, \ldots, N + m$) is a neighbor of agent $i$. Let $\mathcal{B} = [\mathcal{B}_{N+1}, \mathcal{B}_{N+2}, \ldots, \mathcal{B}_{N+m}]$, where $\mathcal{B}_k \in \mathbb{R}^{N\times N}$ is a diagonal matrix with $b_k^i$ ($i = 1, 2, \ldots, N$) as its diagonal entry. Assume the time delay in (2.5) satisfies $0 < \tau \leq h$.

Inserting the control rule (2.5) into each follower agent dynamic (2.4), the dynamics of agent $i$ becomes

$$x^{(\alpha)}(t) = -(\mathcal{H} \otimes I_n)x(t-\tau) + [\mathcal{B}(I_m \otimes \mathbf{1}_N)] \otimes I_n \overline{x}(t-\tau), \tag{2.6}$$

where $x(t) = [x_1^T(t), x_2^T(t), \ldots, x_N^T(t)]^T$, $\overline{x}(t) = [\overline{x}_{N+1}^T(t), \overline{x}_{N+2}^T(t), \ldots, \overline{x}_{N+m}^T(t)]^T$, $\mathcal{H} = \mathcal{L} + \mathcal{B}(\mathbf{1}_m \otimes I_N)$.

Our objective is to let the $N$ follower agents move into the polytope region formed by the leaders; that is, for any $x_i(t)$ $(i = 1, 2, \ldots, N)$ it can be represented as a convex hull of $\overline{x}_k(t)$ $(k = N+1, N+2, \ldots, N+m)$ when $t \to +\infty$, namely:

$$\lim_{t \to +\infty} d_\Theta(x_i(t)) = 0, \quad i = 1, 2, \ldots, N, \tag{2.7}$$

where $\Theta = \{\mu \mid \mu \in \mathrm{co}\{\overline{x}_{N+1}(t), \overline{x}_{N+2}(t), \ldots, \overline{x}_{N+m}(t)\}\}$.

## 3. Convergence Analysis

Before starting our main results, we begin with the following lemmas which will play an important role in the proof of main results.

**Lemma 3.1.** *If graph $\overline{\mathcal{G}}$ has a spanning tree, then the matrix $\mathcal{H}$ associated with $\overline{\mathcal{G}}$ is a positive stable matrix; that is, all the eigenvalues of $\mathcal{H}$ lie in the open right hand plane.*

*Proof.* This lemma follows from Lemma 4 in [9] by considering the convex region formed by the leaders as a virtual leader. □

**Lemma 3.2** (see [25]). *The following autonomous system:*

$$\frac{d^\alpha x(t)}{dt^\alpha} = Ax(t), \quad x(0) = x_0, \tag{3.1}$$

*with $0 < \alpha \leq 1$, $x \in R^n$, and $A \in R^{n \times n}$, is asymptotically stable if and only if $|\arg(\rho(A))| > \alpha\pi/2$ is satisfied for all eigenvalues of matrix $A$. Also, this system is stable if and only if $|\arg(\rho(A))| \geq \alpha\pi/2$ is satisfied for all eigenvalues of matrix $A$ with those critical eigenvalues satisfying $|\arg(\rho(A))| = \alpha\pi/2$ having geometric multiplicity of one. The geometric multiplicity of an eigenvalue $\lambda$ of the matrix $A$ is the dimension of the subspace of vectors $v$ for which $Av = \lambda v$.*

When the time delay $\tau = 0$, the dynamic network degenerates to the delay-free case, and the dynamic (2.6) can be rewritten as

$$x^{(\alpha)}(t) = -(\mathcal{H} \otimes I_n)x(t) + [\mathcal{B}(I_m \otimes \mathbf{1}_N)] \otimes I_n \overline{x}(t). \tag{3.2}$$

Then, we have the following theorem.

**Theorem 3.3.** *For the fractional-order dynamic system* (3.2)*, the follower agents can enter the region spanned by the leaders if the fixed interaction graph $\overline{\mathcal{G}}$ has a directed spanning tree.*

*Proof .* By Lemma 3.1, we learn that matrix $\mathscr{H}$ is invertible. Let $\delta(t) = x(t) - [\mathscr{H}^{-1}\mathcal{B}(I_m \otimes \mathbf{1}_N)] \otimes \mathbf{I}_n \overline{x}(t)$. Then, we get the following error system:

$$\delta^{(\alpha)}(t) = -(\mathscr{H} \otimes I_n)\delta(t). \tag{3.3}$$

Since all the eigenvalues of matrix $\mathscr{H}$ lie in the open right hand plane, then, $|\arg(-\mathscr{H}))| \in (\pi/2, \pi]$ and $2\arg(\rho(\mathscr{H}))/\pi > 1$ hold. It follows from Lemma 3.2 that system (3.3) is asymptotically stable for any $\alpha \in (0, 1]$.

In the sequel, we will prove that all the follower agents can be aggregated in a polytope region formed by the leaders. In other words, we need only to prove that for any vector $\overline{x}_i^*(t) \in \mathbb{R}^n$ $(i = 1, 2, \ldots, N)$, the region can be expressed as a convex hull of $\overline{x}_k(t) \in \mathbb{R}^n (k = N+1, N+2, \ldots, N+m)$. This problem can be transformed to prove that matrix $[\mathscr{H}^{-1}\mathcal{B}(I_m \otimes \mathbf{1}_N)] \otimes I_n$ is a row stochastic matrix that is, it is a nonnegative matrix, and the sum of the items in every row is 1.

Since all the eigenvalues of $\mathscr{H}$ have positive real parts, there exist a positive scalar $\kappa > 0$ and nonnegative matrix $Z$ such that $\mathscr{H} = \kappa I - Z$ holds. Obviously, $\kappa > \rho(Z)$ and $\lambda_i(\mathscr{H}) = \kappa - \lambda_i(Z), \forall i = 1, 2, \ldots, N$. Therefore,

$$\mathscr{H}^{-1} = (\kappa I - Z)^{-1} = \frac{1}{\kappa}\left(I + \frac{1}{\kappa}Z + \frac{1}{\kappa^2}Z^2 + \cdots\right) \geq 0. \tag{3.4}$$

It can be seen that matrix $\mathscr{H}^{-1} \otimes I_n$ is a nonnegative matrix and so is $[\mathscr{H}^{-1}\mathcal{B}(I_m \otimes \mathbf{1}_N)] \otimes I_n$. Notice that $\mathscr{H} = L + \mathcal{B}(\mathbf{1}_m \otimes I_N)$ and $L\mathbf{1}_N = 0$; we obtain

$$\begin{aligned}(\mathscr{H} \otimes I_n)(\mathbf{1}_N \otimes \mathbf{1}_n) &= ((L + \mathcal{B}(\mathbf{1}_m \otimes I_N)) \otimes I_n)(\mathbf{1}_N \otimes \mathbf{1}_n) \\ &= \left(\sum_{i=N+1}^{N+m} \mathcal{B}_i \mathbf{1}_N\right) \otimes \mathbf{1}_n.\end{aligned} \tag{3.5}$$

Thus,

$$\begin{aligned}\left(\left[\mathscr{H}^{-1}\mathcal{B}(I_m \otimes \mathbf{1}_N)\right] \otimes I_n\right)(\mathbf{1}_m \otimes \mathbf{1}_n) &= \left((\mathscr{H} \otimes I_n)^{-1}[\mathcal{B}(I_m \otimes \mathbf{1}_N)] \otimes I_n\right)(\mathbf{1}_m \otimes \mathbf{1}_n) \\ &= (\mathscr{H} \otimes I_n)^{-1}\left(\sum_{i=N+1}^{N+m} \mathcal{B}_i \mathbf{1}_N\right) \otimes \mathbf{1}_n \\ &= \mathbf{1}_N \otimes \mathbf{1}_n.\end{aligned} \tag{3.6}$$

It is obvious that $[\mathscr{H}^{-1}\mathcal{B}(I_m \otimes \mathbf{1}_N)] \otimes I_n$ is a row stochastic matrix. Thus, the conclusion of Theorem 3.3 holds. □

*Remark 3.4.* This result coincides with the existing results in [26] and has been extended to fractional order cases.

In what follows, we will focus on the convergence analysis of (2.6) under fixed and directed interconnection topologies in delayed communication channels.

**Theorem 3.5.** *For the fractional-order dynamic system* (2.6)*, the follower agents can enter the region spanned by the leaders if the fixed interaction graph* $\overline{\mathcal{G}}$ *has a directed spanning tree and* $\tau < \tau^*$*, where*

$$\tau^* = \min_{i\in\mathcal{O}} \frac{\pi - (\alpha\pi/2) + \eta_i}{\left(|\mu_i|\right)^{1/\alpha}}, \tag{3.7}$$

$\mu_i, i \in \mathcal{O}$ *is the* $i$*th eigenvalue of matrix* $\mathcal{H}$, $\eta_i = \arctan(\mathrm{Im}(\mu_i)/\,\mathrm{Re}(\mu_i))$.

*Proof.* Since the communication topology $\overline{\mathcal{G}}$ has a spanning tree, all the eigenvalues of $\mathcal{H}$ have positive real parts by Lemma 3.1. Therefore, matrix $\mathcal{H}$ is invertible. Let $\delta(t) = x(t) - x^*(t)$, $x^*(t) = [\mathcal{H}^{-1}\mathcal{B}(I_m \otimes \mathbf{1}_N)] \otimes I_n \overline{x}(t)$. Then, we get the following error system

$$\delta^{(\alpha)}(t) = -(\mathcal{H} \otimes I_n)\delta(t - \tau). \tag{3.8}$$

Taking Laplace transform of system (3.8), it yields that

$$s^\alpha \xi(s) - s^{\alpha-1}\xi(0) = -e^{-\tau s}(\mathcal{H} \otimes I_n)\xi(s), \tag{3.9}$$

where $\xi(s)$ is the Laplace transforms of position states $\delta(t)$. After some simple manipulation we obtain

$$\xi(s) = (\Delta(s))^{-1}\xi(0), \tag{3.10}$$

where $\Delta(s) = s^\alpha I + e^{-\tau s}(\mathcal{H} \otimes I_n)$, which is called a characteristic matrix in [27]. The distribution of $\det(\Delta(s))$'s eigenvalues totally determines the stability of system (3.8). Thus, a sufficient condition for the error dynamics (3.8) which converges to zero is that all the poles of $\Delta(s)$ are located at the open left half plane or $s = 0$.

Then, the characteristic equation of (3.8) is

$$s^\alpha + e^{-\tau s}\mu_i = 0, \tag{3.11}$$

where $\mu_i$ is the $i$th eigenvalue of matrix $\mathcal{H}$.

Obviously, $s \neq 0$. Now, we turn to prove that the poles of (3.11) are located at the open left half plane. Since the directed graph $\overline{\mathcal{G}}$ has a spanning tree, all the eigenvalues of $\mathcal{H}$ have positive real parts. Without loss of generality, we assume that the eigenvalues satisfy $0 < \mathrm{Re}(\mu_1) \leq \mathrm{Re}(\mu_2) \leq \cdots \leq \mathrm{Re}(\mu_n)$. Based on the Nyquist stability theorem, all the roots of (3.11) lie in the open left half complex plane, if and only if the Nyquist curve $e^{-\tau s}\mu_i/s^\alpha$ does not enclose the point $(-1, 0\mathbf{i})$ for any $w \in \mathbb{R}$, where $\mathbf{i}$ is the imaginary unit.

Therefore, assume that $s = \mathbf{i}w = w(\cos(\pi/2) + \mathbf{i}\sin(\pi/2))$ $(w > 0)$ is a root of (3.11); we have

$$w^\alpha\left(\cos\frac{\alpha\pi}{2} + \mathbf{i}\sin\frac{\alpha\pi}{2}\right) + |\mu_i|\left(\cos(\eta_i - w\tau) + \mathbf{i}\sin(\eta_i - w\tau)\right) = 0, \tag{3.12}$$

where $\eta_i = \arctan(\mathrm{Im}(\mu_i)/\,\mathrm{Re}(\mu_i))$. Separating the real and imaginary parts of (3.12) yields

$$\begin{aligned} w^{\alpha}\cos\frac{\alpha\pi}{2} + |\mu_i|\cos(\eta_i - w\tau) &= 0, \\ w^{\alpha}\sin\frac{\alpha\pi}{2} + |\mu_i|\sin(\eta_i - w\tau) &= 0. \end{aligned} \tag{3.13}$$

From the above two equations, one gets

$$w^{2\alpha} + |\mu_i|^2 + 2|\mu_i| w^{\alpha}\cos\left(\frac{\alpha\pi}{2} - \eta_i + w\tau\right) = 0, \tag{3.14}$$

that is

$$\left(w^{\alpha} - |\mu_i|\right)^2 + 2|\mu_i| w^{\alpha}\left[1 + \cos\left(\frac{\alpha\pi}{2} - \eta_i + w\tau\right)\right] = 0. \tag{3.15}$$

Obviously, the two terms in the left-hand side of (3.15) are nonnegative the equality holds if and only if both the two terms are zero, namely:

$$w^{\alpha} = |\mu_i|, \tag{3.16}$$

$$1 + \cos\left(\frac{\alpha\pi}{2} - \eta_i + w\tau\right) = 0. \tag{3.17}$$

Thus, combining (3.16) and (3.17), we can easily obtain that

$$\pi + 2k\pi = \left(|\mu_i|\right)^{1/\alpha}\tau + \frac{\alpha\pi}{2} - \eta_i, \quad k = 0, 1, 2, \ldots. \tag{3.18}$$

Therefore, the smallest time-delay $\tau > 0$ occurs at $k = 0$ and satisfies

$$\tau = \frac{\pi - (\alpha\pi/2) + \eta_i}{\left(|\mu_i|\right)^{1/\alpha}}. \tag{3.19}$$

Similarly, one can repeat the very argument for the case that $w < 0$ and get similar conclusion.

Thus, the Nyquist plot of $e^{-\tau s}\mu_i/s^{\alpha}$ does not enclose the point $(-1, 0\mathbf{i})$ for all $i > 1$ if

$$\tau < \frac{\pi - (\alpha\pi/2) + \eta_i}{\left(|\mu_i|\right)^{1/\alpha}}. \tag{3.20}$$

Then all the roots of $\det(\Delta(s))$ lie in the open left hand plan. Therefore, the error system (3.8) is asymptotically stable, that is, $x \to x^* = [\mathscr{H}^{-1}\mathcal{B}(I_m \otimes \mathbf{1}_N)] \otimes I_n\overline{x}$, as $t \to +\infty$. The rest of the proof is similar to that of Theorem 3.3 and hence is omitted.

For the case of the considered undirected graph, that is, agent $i$ and agent $j$ can receive information from each other when there exists an edge between $i$ and $j$; we can get the following result. □

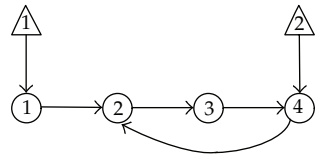


**Figure 1:** Directed graph $\mathcal{G}_1$ and $\overline{\mathcal{G}}_1$.

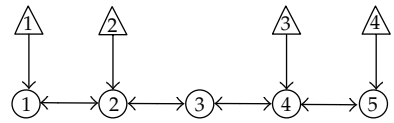


**Figure 2:** Directed graph $\mathcal{G}_2$ and $\overline{\mathcal{G}}_2$.

**Theorem 3.6.** *Under an undirected time-invariant interaction graph $\overline{\mathcal{G}}$, that is, strongly connected, the follower agents can enter the region spanned by the leaders if $\tau < \overline{\tau}^*$, where*

$$\overline{\tau}^* = \min_{i\in\mathcal{I},\mu_i>0} \frac{\pi - (\alpha\pi/2)}{\left(|\mu_i|\right)^{1/\alpha}}, \tag{3.21}$$

*$\mu_i$, $i \in \mathcal{I}$ is the ith eigenvalue of matrix $\mathcal{H}$.*

*Proof*. The proof of Theorem 3.6 is similar to that of the Theorem 3.5 by noting that the eigenvalues of $\mathcal{H}$ are nonnegative real number, and hence omitted. □

## 4. Numerical Examples

In this section, two numerical simulations will be presented to illustrate the effectiveness of the theoretical results obtained in the previous sections. In all the simulations, all dynamics of agent are integrated with a fixed time step 0.05. The following two directed graphs with 0-1 weights will be needed in the analysis of this section. Circle and triangle stand for follower agent and leader, respectively.

*Example 4.1.* Consider a dynamic fractional-order network of four follower agents and two leaders with a fixed topology given in Figure 1. Obviously, the topology $\overline{\mathcal{G}}_1$ has a spanning tree. Suppose that all the agents are moving in a horizontal line and each follower agent can receive the state information of its neighbors precisely. The matrix $\mathcal{H}$ is $\begin{pmatrix} 2 & -1 & 0 & 0 \\ 0 & 2 & -1 & -1 \\ 0 & 0 & 1 & -1 \\ 0 & 0 & 0 & 1 \end{pmatrix}$, and its four eigenvalues are $0.2451, 1.0000, 1.8774 + 0.7449\mathbf{i}, 1.8774 - 0.7449\mathbf{i}$, respectively. The initial position states of follower agents are generated randomly in $[1, 6]$, and leaders are chosen as $\overline{x}_1(0) = 0.5, \overline{x}_2(0) = -0.5$. Let $\alpha = 0.92$ and $u_0(t) = 0.2$. The state trajectories of the fractional-order close-loop systems (2.6) are shown in Figure 3. It can be easily seen that as time goes on, the whole follower agents will be flocked in the segment $[-0.5, 0.5]$, which is formed by the two leaders.

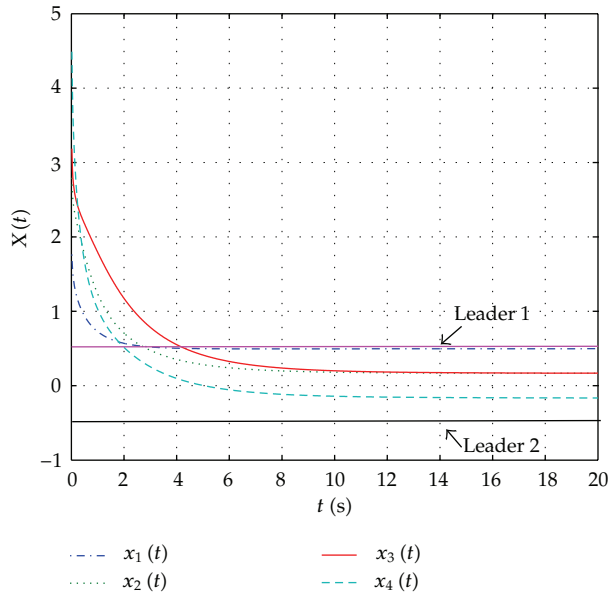


**Figure 3:** State trajectories of four follower agents and two leaders under the topology $\overline{\mathcal{G}}_1$.

*Example 4.2.* Consider a dynamic fractional-order network of five follower agents and four leaders moving in a plane. The interconnection topology among the above agents is given in Figure 2. Clearly, $\overline{\mathcal{G}}_2$ is strongly connected. The matrix $\mathcal{H}$ is

$$\begin{pmatrix} 2 & -1 & 0 & 0 & 0 \\ -1 & 3 & -1 & 0 & 0 \\ 0 & -1 & 2 & -1 & 0 \\ 0 & 0 & -1 & 3 & -1 \\ 0 & 0 & 0 & -1 & 2 \end{pmatrix}, \tag{4.1}$$

and its five eigenvalues are $0.6972, 1.3820, 2.0000, 3.6180, 4.3028$, respectively. The initial position states of agents and leaders are given as follows:

$$\begin{gathered} x_1(0) = (0,2)^T, \quad x_2(0) = (0,3)^T, \quad x_3(0) = (0,4)^T, \quad x_4(0) = (0,5)^T, \quad x_5(0) = (0,6)^T, \\ \overline{x}_1(0) = (4,5)^T, \quad \overline{x}_2(0) = (5,6)^T, \quad \overline{x}_3(0) = (6,5)^T, \quad \overline{x}_4(0) = (5,4)^T. \end{gathered} \tag{4.2}$$

Take the fractional order $\alpha = 0.96$ in (2.1). Then, it can be seen from Theorem 3.6 that all the followers will enter into the region formed by the leaders if $\tau < 0.3573$. Figures 4 and 5 depict the simulation results for position trajectories under different time delays. From these simulations, one can easily find that the containment control is realized via protocol (2.5) as long as the time delay doesnot exceed the upper bound. These simulations are consistent with the theoretical result in Section 3.

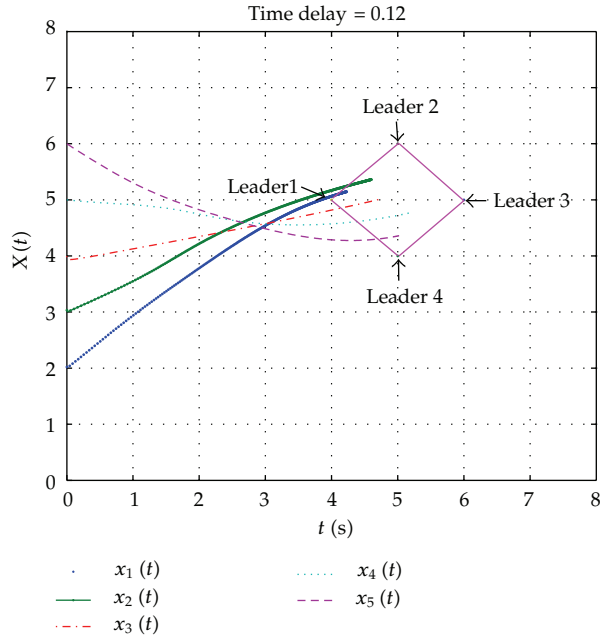


**Figure 4:** State trajectories of five follower agents and four leaders under the topology $\overline{\mathcal{G}}_2$ and time delay $\tau = 0.12$.

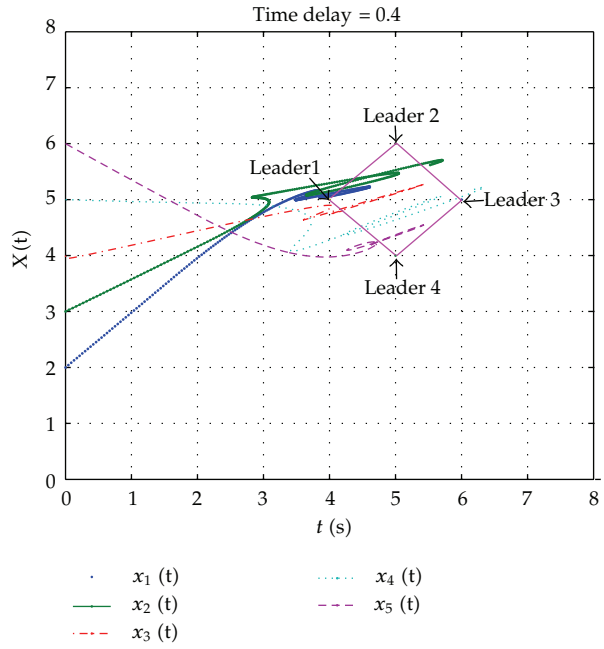


**Figure 5:** State trajectories of five follower agents and four leaders under the topology $\overline{\mathcal{G}}_2$ and time delay $\tau = 0.4$.

## 5. Conclusion

In this paper, the containment control problem of multiple leaders has been considered for networks of fractional-order dynamics with delay-dependent communication channels. Utilizing algebraic graph theory, matrix theory, Nyquist stability theorem, and frequency domain method, some sufficient conditions are obtained. It is shown that all the follower agents will ultimately move into the convex hull which is spanned by the leaders, for appropriate communication time delay if the topology of weighted network has a spanning tree. Moreover, two numerical simulations are provided to validate the effectiveness of our theoretical analysis.

## Acknowledgments

This work was supported by the National Natural Science Foundation of China under Grant no. 61174070, the Specialized Research Found for the Doctoral Program no. 20110172110033, the NSFC-Guangdong Joint Foundation Key Project under Grant no. U0735003, the Oversea Cooperation Foundation under Grant 60828006 and the Key Laboratory of Autonomous Systems and Network Control, Ministry of Education.

## References

[1] F. Xiao, L. Wang, J. Chen, and Y. Gao, "Finite-time formation control for multi-agent systems," *Automatica*, vol. 45, no. 11, pp. 2605–2611, 2009.

[2] R. Vidal, O. Shakernia, and S. Sastry, "Formation control of nonholonomic mobile robots with omnidirectional visual servoing and motion segmentation," in *Proceedings of the IEEE Conference on Robotics and Automation (ICRA '03)*, pp. 584–589, Taipei, Taiwan, September 2003.

[3] J. A. Fax and R. M. Murray, "Information flow and cooperative control of vehicle formations," *IEEE Transactions on Automatic Control*, vol. 49, no. 9, pp. 1465–1476, 2004.

[4] F. Cucker and S. Smale, "Emergent behavior in flocks," *IEEE Transactions on Automatic Control*, vol. 52, no. 5, pp. 852–862, 2007.

[5] R. Olfati-Saber, "Flocking for multi-agent dynamic systems: algorithms and theory," *IEEE Transactions on Automatic Control*, vol. 51, no. 3, pp. 401–420, 2006.

[6] L. Xiao, S. Boyd, and S. Lall, "A scheme for robust distributed sensor fusion based on average consensus," in *Proceedings of the 4th International Conference on Information Process in Sensor Networks*, pp. 63–70, Los Angeles, Calif, USA, April 2005.

[7] R. Saber and J. Shamma, "Consensus filters for sensor networks and distributed sensor fusion," in *Proceedings of the 44th IEEE Conference on Decision and Control, and the European Control Conference (CDC-ECC '05)*, pp. 6698–6703, Seville, Spain, 2005.

[8] T. Li and J. Zhang, "Mean square average-consensus under measurement noise and fixed topologies: necessary and sufficient conditions," *Automatica*, vol. 45, no. 8, pp. 1929–1936, 2009.

[9] J. Hu and Y. Hong, "Leader-following coordination of multi-agent systems with coupling time delays," *Physica A*, vol. 374, no. 2, pp. 853–863, 2007.

[10] W. Ren, R. W. Beard, and D. Kingston, "Multi-agent kalman consensus with relative uncertainty," in *Proceedings of the American Control Conference*, pp. 1865–1870, Portland, Ore, USA, June 2005.

[11] R. Olfati-Saber and R. M. Murray, "Consensus problems in networks of agents with switching topology and time-delays," *IEEE Transactions on Automatic Control*, vol. 49, no. 9, pp. 1520–1533, 2004.

[12] W. Yu, G. Chen, and J. Cao, "Adaptive synchronization of uncertain coupled stochastic complex networks," *Asian Journal of Control*, vol. 13, no. 3, pp. 418–429, 2011.

[13] M. Barahona and L. Pecora, "Synchronization in small-world systems," *Physical Review Letters*, vol. 89, no. 5, Article ID 054101-4, 2002.

[14] N. A. Lynch, *Distributed Algorithms*, The Morgan Kaufmann Series in Data Management Systems, Morgan Kaufmann, San Francisco, Calif, USA, 1996.

[15] W. Ren and R. W. Beard, *Distributed Consensus in Multi-Vehicle Cooperative Control*, Springer, London, UK, 2008.
[16] M. Cao, A. S. Morse, and B. D. O. Anderson, "Agreeing asynchronously," *IEEE Transactions on Automatic Control*, vol. 53, no. 8, pp. 1826–1838, 2008.
[17] I. Podlubny, *Fractional Differential Equations: An Introduction to Fractional Derivatives, Fractional Differential Equations, to Methods of Their Solution and Some of Their Applications*, vol. 198 of *Mathematics in Science and Engineering*, Academic Press, New York, NY, USA, 1999.
[18] K. Oldham and J. Spanier, *The Fractional Calculus*, Academic Press, New York, NY, USA, 1974.
[19] Y. Cao, Y. Li, W. Ren, and Y. Chen, "Distributed coordination algorithms for multiple fractional-order systems," in *Proceedings of the IEEE Conference on Decision and Control (CDC '08)*, pp. 2920–2925, Cancun, Mexico, December 2008.
[20] Y. Cao, Y. Li, W. Ren, and Y. Chen, "Distributed coordination of networked fractional-order systems," *IEEE Transactions on Systems, Man, and Cybernetics B*, vol. 40, no. 2, pp. 362–370, 2010.
[21] W. Sun, Y. Li, C. Li, and Y. Chen, "Convergence speed of a fractional order consensus algorithm over undirected scale-free networks," *Asian Journal of Control*, vol. 13, no. 6, pp. 936–946, 2011.
[22] J. Shen, J. D. Cao, and J. Lu, "Consenus of fractional-order systems with non-uniform input and communication delays," *Journal of Systems and Control Engineering*, vol. 226, no. 2, pp. 271–283, 2012.
[23] J. Shen and J. Cao, "Necessary and sufficient conditions for consenus of delayed fractional-order systems over directed graph," 2011, http://www.paper.edu.cn/.
[24] Y. Cao and W. Ren, "Distributed formation control for fractional-order systems: dynamic interaction and absolute/relative damping," *Systems & Control Letters*, vol. 59, no. 3-4, pp. 233–240, 2010.
[25] D. Matignon, "Stability result on fractional differential equations with applications to control processing," in *Proceedings of the IMACSSMC*, pp. 963–968, Lille, France, 1996.
[26] Y. Cao and W. Ren, *Distributed Coordination of Multi-agent Networks Emergent Problems, Models, and Issues*, Springer, London, UK, 2011.
[27] W. Deng, C. Li, and J. Lü, "Stability analysis of linear fractional differential system with multiple time delays," *Nonlinear Dynamics*, vol. 48, no. 4, pp. 409–416, 2007.

Hindawi Publishing Corporation
Journal of Applied Mathematics
Volume 2012, Article ID 435924, 13 pages
doi:10.1155/2012/435924

*Research Article*

# Energy-Driven Image Interpolation Using Gaussian Process Regression

**Lingling Zi[1,2] and Junping Du[1]**

[1] *Beijing Key Laboratory of Intelligent Telecommunication Software and Multimedia, School of Computer Science, Beijing University of Posts and Telecommunications, Beijing 100876, China*
[2] *School of Electronic and Information Engineering, Liaoning Technical University, Huludao 125105, China*

Correspondence should be addressed to Junping Du, junpingdu@126.com

Received 1 March 2012; Accepted 27 April 2012

Academic Editor: Baocang Ding



Image interpolation, as a method of obtaining a high-resolution image from the corresponding low-resolution image, is a classical problem in image processing. In this paper, we propose a novel energy-driven interpolation algorithm employing Gaussian process regression. In our algorithm, each interpolated pixel is predicted by a combination of two information sources: first is a statistical model adopted to mine underlying information, and second is an energy computation technique used to acquire information on pixel properties. We further demonstrate that our algorithm can not only achieve image interpolation, but also reduce noise in the original image. Our experiments show that the proposed algorithm can achieve encouraging performance in terms of image visualization and quantitative measures.

## 1. Introduction

Image interpolation is a very important aspect of image processing and involves the use of a known pixel set to produce an unknown pixel set, resulting in an image of higher resolution [1, 2]. This technique is widely used in remote sensing, aerospace, infrared imaging, low-light level night imagery, and other fields [3–5]. However, maintaining image quality during image interpolation is still a difficult issue [6]. To address this, many image interpolation methods have been proposed. For example, traditional bilinear interpolation computes the unknown pixel value using the location information between the adjacent pixels. This technique does not consider the contents of the image, so edge blurring will occur in the interpolated image [7, 8]. In order to capture image details more clearly, an artifact-free image upscaling method called ICBI [9] has recently been proposed, which uses

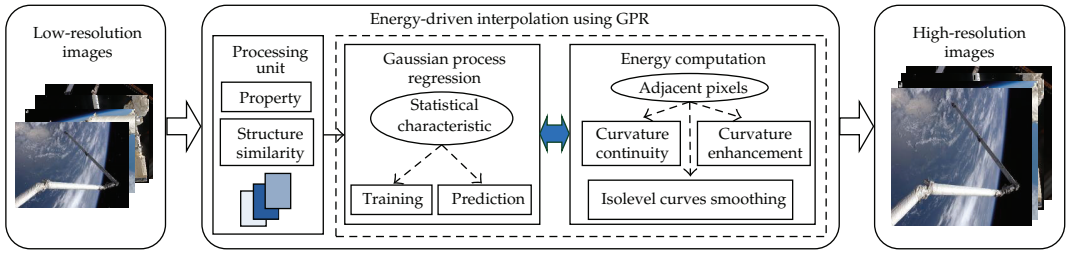


**Figure 1:** Overview of our approach for image interpolation.

iterative curvature-based interpolation to obtain a high image quality, but does not take into account underlying local information between image patches. Local image information can be mined according to its structural redundancy characteristic, as proposed by Glasner et al. [10]. This characteristic can lay the foundations for the training and predicting of a statistical model [11, 12]. A statistical model known as Gaussian process regression (GPR) was first applied in the reconstruction of high-resolution images in 2011 and has been shown to be capable of generating an image with sharp edges by extracting the necessary information from a low-resolution image [13]. However, it should be noted that this method only uses the local structural information for each pixel's neighborhood, so it can still generate unexpected details. To develop the above techniques, we propose here a novel energy-driven interpolation algorithm employing Gaussian process regression (EGPR) (Figure 1). This algorithm not only emphasizes the influence of adjacent pixel properties on interpolated values, but also brings into full play the role of the statistical model.

Our contribution is twofold. Firstly, we propose a framework for both magnification and deblurring in order to fulfill the interpolation task for low-resolution images with low noise. Secondly, we demonstrate an energy-driven approach based on the properties of adjacent pixels within this framework. In addition, we define the processing unit and its properties for better implementation of the EGPR algorithm.

The rest of the paper is structured as follows. Section 2 discusses GPR. Section 3 illustrates the proposed EGPR algorithm. Section 4 presents experimental work carried out to demonstrate the effectiveness of our algorithm. Section 5 concludes the paper.

## 2. Gaussian Process Regression

In recent years, GPR has become a hot issue in the field of machine learning and has attracted great academic interest [14–16]. It has many advantages, including its rigorous underlying statistical learning theory, easy regression process implementation, few parameters, and improved model interpretability [17–19]. As a result of these benefits, it has been used in many areas [20–23]; however, to the best of our knowledge, it has not yet been fully utilized in image interpolation. Rasmussen and Williams [24] defined the Gaussian process and noted in particular that a Gaussian process is completely specified by its mean and covariance functions ((2.1) and (2.2), resp.):

$$\mu(x) = E[Y(x)], \tag{2.1}$$

$$\mathrm{COV}(x, x') = E\left[\left(Y(x) - \mu(x)\right)\left(Y(x') - \mu(x')\right)\right], \tag{2.2}$$

where $x$ and $x'$ are any random variables. In particular, they could represent n-dimensional input or output vectors. The Gaussian process can be written as follows:

$$g(x) \sim GP(\mu(x), \mathrm{COV}(x, x')). \tag{2.3}$$

There are a variety of covariance functions, of which one of the most commonly used is the squared exponential (SE) covariance function

$$\mathrm{COV}(g(x_p), g(x_q)) = \exp\left(-\frac{1}{2}\left|x_p - x_q\right|^2\right). \tag{2.4}$$

In Gaussian processes, the marginal likelihood $p(y \mid X)$ at a point is very useful and is the integral of the likelihood multiplied by the prior probability

$$p(y \mid X) = \int p(y \mid g, X) p(g \mid X) dg. \tag{2.5}$$

We can rewrite (2.5) as follows:

$$\log p(g \mid X) = -\frac{1}{2} g^T \mathrm{COV}^{-1} g - \frac{1}{2} \log|\mathrm{COV}| - \frac{n}{2} \log 2\pi. \tag{2.6}$$

We can make use of Gaussian identities to obtain (2.7), in order to compute the log marginal likelihood. The conjugate gradients method has been applied to solve this equation. Using this approach, we can obtain the hyperparameters of the covariance function. Further details of GPR can be found in [24] as follows:

$$\log p(g \mid X) = -\frac{1}{2} y^T \left(\mathrm{COV}(X, X) + \sigma_n^2 I\right)^{-1} y - \frac{1}{2} \log\left|\mathrm{COV}(X, X) + \sigma_n^2 I\right| - \frac{n}{2} \log 2\pi. \tag{2.7}$$

## 3. The Proposed Algorithm

In this paper, we combine the energy-driven approach with GPR to accomplish the task of image interpolation. The proposed algorithm models low-resolution image data as a function of a probability distribution that satisfies a local static Gaussian process. This algorithm framework is shown in Figure 2 and is broadly divided into the training process and prediction process. Firstly, the GPR model can be established using the low-resolution image data. Next, this model is used to predict the unknown pixel values of a high-resolution image by adopting an energy computation approach. Through the above two steps, we produce a high-quality enlarged image. The process is further clarified by the following:

$$L' = d * L, \qquad H' = L'\uparrow^s, \qquad H = f * H', \tag{3.1}$$

where $L$ and $H$ denote the input low-resolution image with a little noise and the output high-resolution image, respectively, $L'$ denotes the noise-free low-resolution image, $H'$ denotes the initial high-resolution image, $s$denotes the upsampling factor, and $d$ and $f$ denote the clear transfer function and energy transfer function, respectively.

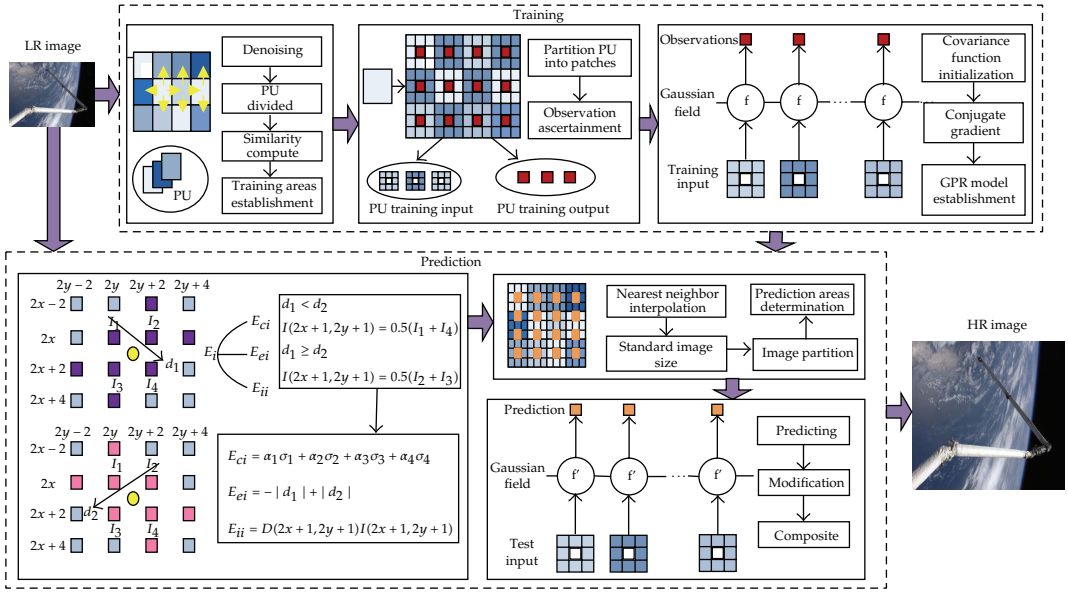


**Figure 2:** Architecture of the proposed algorithm.

## 3.1. Training

The following definitions are used in the EGPR algorithm.

*Definition 3.1.* A given image $L$ is divided into many regions of equal size, and each region is defined as a processing unit (PU). Each PU is also divided into $3 \times 3$ overlapping image patches (the total number is $M$). The center of each patch is defined as an output vector $Y_{TR}$ of PU, where $Y_{TR} = (y_1, y_2, \ldots y_M)^T$, while the nearest eight values are defined as an input vector $X_{TR}$ of PU, where

$$X_{TR} = \left\{ \begin{array}{c} x_{11}, x_{12} \ldots, x_{18} \\ x_{21}, x_{22} \ldots, x_{28} \\ \ldots. \\ x_{M1}, x_{M2} \ldots, x_{M8} \end{array} \right\}. \tag{3.2}$$

*Definition 3.2.* Given a total of $N$ pixels in each PU, the pixels are sorted and denoted as $I_1, I_2 \ldots I_N$. $I_{\max\ ave}$, $I_{\min\ ave}$, and $I_{ave}$ are defined using the following formulae:

$$I_{\max\ ave} = \sum_{i=1}^{\text{Top}} \frac{I_i}{\text{Top}}, \qquad I_{\min\ ave} = \sum_{i=1}^{\text{Below}} \frac{I_i}{\text{Below}}, \qquad I_{ave} = \sum_{i=1}^{N} \frac{I_i}{N}, \tag{3.3}$$

where top represents the number of the largest pixels used and below the number of the smallest pixels used. Then $I_{\max\ ave}$, $I_{\min\ ave}$, and $I_{ave}$ are called basic properties of PU.

To facilitate the operation of the PU, it is necessary to introduce some properties in advance.

*Property 1.* Given a number $N$ in each PU, if $I_{\max\ \mathrm{ave}} = 0$, then pixel value $I_i = 0$, where $i \leq N$.

*Property 2.* Given $x_{ij}$, if $x_{ij} = a$, then its corresponding output vector value is $y_{ij} = a$, where $y_{ij} \in Y_{TR}, i \in M, j = 1$.

Denoising is the first step in the EGPR algorithm, and we use the following formula (3.4) to obtain noise-free images:

$$I_i = \begin{cases} I_{\mathrm{neighbor}}, & (I_{\max\ \mathrm{ave}} - I_{\min\ \mathrm{ave}}) \langle \theta \,\&\, I_i \rangle (I_{\mathrm{ave}} + B), \\ I_i, & \text{otherwise}, \end{cases} \tag{3.4}$$

where $\theta$ and $B$ represent empirical values, and $I_{\mathrm{neighbor}}$ represents the adjacent pixel value.

Before applying GPR, we can obtain the particular relationship between the input and output vectors of PU according to Properties 1 and 2. Pixels with this relationship need not be included in the following GPR training, so the predicted values can be directly obtained, saving time and speeding up the EGPR algorithm.

Training plays an important role in the EGPR algorithm, and we adopt a different approach from that used in [13]. Our algorithm contains two processes: training domain establishment and GPR model foundation. In the first stage, we search possible training domains along the four directions of each specific PU. Next, we compute the structural similarity between directions to determine the definite training domain. Inspired by the concept of image SSIM, we define the PU structural similarity as follows.

*Definition 3.3* (*PU structural similarity*). Given two processing units $P$ and $Q$, their structural similarity is defined as

$$S(P,Q) = \frac{(2m_P m_Q + C_1)(2\varphi_{PQ} + C_2)}{\left(m_P^2 + m_Q^2 + C_1\right)\left(\varphi_P^2 + \varphi_Q^2 + C_2\right)}, \tag{3.5}$$

where $C_1$ and $C_2$ are constants, and the other components are calculated as follows:

$$m_P = \frac{1}{N}\sum_{i=1}^{N} p_i, \quad p_i \in P, \qquad m_Q = \frac{1}{N}\sum_{i=1}^{N} q_i, \quad q_i \in Q, \qquad \varphi_P = \left(\frac{1}{N-1}\sum_{i=1}^{N}(p_i - m_p)^2\right)^{1/2},$$
$$\varphi_Q = \left(\frac{1}{N-1}\sum_{i=1}^{N}(q_i - m_q)^2\right)^{1/2}, \qquad \varphi_{PQ} = \frac{1}{N-1}\sum_{i=1}^{N}(p_i - m_p)(q_i - m_q). \tag{3.6}$$

When the search step count reaches the predefined number, or if the PU structure similarity falls below a certain value, the first stage is complete. In the second stage, we apply a Gaussian process prior probability and establish the GPR model with Gaussian noise $\gamma$ (see (3.7) below) using the image data from training domains. In (3.7), "$GP$" denotes a Gaussian process

$$y = g(X) + \gamma, \quad \gamma \sim GP\left(0, \sigma_n^2\right). \tag{3.7}$$

(a) Iteration = 50 (b) Iteration = 100

**Figure 3:** Images obtained after adaptation with different numbers of iterations. In (a), many black points are observed, each indicating a zero prediction for the pixels. In (b), the black points have been eliminated.

When aiming to achieve high-quality images, the conjugate gradients method is chosen to obtain the model hyperparameters, including mean, variance, and log marginal likelihood. Notice that different iteration numbers in the conjugate gradients method may lead to different prediction accuracies. Figure 3 shows the interpolation images obtained after 50 iterations and 100 iterations, where it can be seen that the latter is better than the former.

### *3.2. Prediction*

Inspired by the ICBI algorithm, we firstly compute the initial pixel value $H'(2x+1, 2y+1)$ according to the following formulae:

$$\begin{aligned} \tau_1 &= I(2x+4, 2y) + I(2x+2, 2y-2) + I(2x, 2y+4) + I(2x-2, 2y+2), \\ \tau_2 &= I(2x+4, 2y+2) + I(2x+2, 2y+4) + I(2x, 2y-2) + I(2x-2, 2y), \end{aligned} \tag{3.8}$$

$$\begin{aligned} d_1(2x+1, 2y+1) &= \tau_1 + I(2x+2, 2y+2) + I(2x, 2y) - 3\big(I(2x, 2y+2) + I(2x+2, 2y)\big), \\ d_2(2x+1, 2y+1) &= \tau_2 + I(2x+2, 2y) + I(2x, 2y+2) - 3\big(I(2x, 2y) + I(2x+2, 2y+2)\big), \end{aligned} \tag{3.9}$$

$$H'(2x+1, 2y+1) = \begin{cases} \dfrac{1}{2}\big(I(2x, 2y) + I(2x+2, 2y+2)\big), & d_1(2x+1, 2y+1) < d_2(2x+1, 2y+1), \\ \dfrac{1}{2}\big(I(2x+2, 2y) + I(2x, 2y+2)\big), & d_1(2x+1, 2y+1) \geq d_2(2x+1, 2y+1). \end{cases} \tag{3.10}$$

However, the pixel value obtained is only a roughly estimated value and needs further refinement. Following [9], we establish (3.11) to calculate the energy of each interpolated pixel, and the initial estimate can be modified accordingly,

$$E(2x+1,2y+1) = cE_c(2x+1,2y+1) + eE_e(2x+1,2y+1) + iE_i(2x+1,2y+1), \quad (3.11)$$

where $c$, $e$, and $i$ are chosen to adjust the energy contributions from the three parts.

$E_c$ represents the curvature continuity energy and can be computed with the following formulae:

$$\begin{aligned}
\sigma_1 &= \left|d_1(2x,2y) - d_1(2x+1,2y+1)\right| + \left|d_2(2x,2y) - d_2(2x+1,2y+1)\right|,\\
\sigma_2 &= \left|d_1(2x,2y) - d_1(2x+1,2y-1)\right| + \left|d_2(2x,2y) - d_2(2x+1,2y-1)\right|,\\
\sigma_3 &= \left|d_1(2x,2y) - d_1(2x-1,2y+1)\right| + \left|d_2(2x,2y) - d_2(2x-1,2y+1)\right|,\\
\sigma_4 &= \left|d_1(2x,2y) - d_1(2x-1,2y-1)\right| + \left|d_2(2x,2y) - d_2(2x-1,2y-1)\right|,\\
E_c(2x+1,2y+1) &= \alpha_1\sigma_1 + \alpha_2\sigma_2 + \alpha_3\sigma_3 + \alpha_4\sigma_4,
\end{aligned} \quad (3.12)$$

where $\alpha_i (i = 1 \ldots 4)$ are weight values (see (3.13)), and $d_1$ and $d_2$ have the same meanings as above. $\theta$ is set as the threshold

$$\alpha_i = \begin{cases} 1 & \text{if } \sigma_i < \theta, \\ 0, & \text{otherwise.} \end{cases} \quad (3.13)$$

The second energy term $E_b$ represents the curvature enhancement energy and can be computed by

$$E_e(2x+1,2y+1) = \left|d_2(2x+1,2y+1)\right| - \left|d_1(2x+1,2y+1)\right|. \quad (3.14)$$

The third energy term, $E_i$, represents the isolevel curves smoothing energy and can be computed with

$$E_i(2x+1,2y+1) = D(2x+1,2y+1)I(2x+1,2y+1), \quad (3.15)$$

where $D(2x+1,2y+1)$ can be computed as follows:

$$\begin{aligned} D(2x+1,2y+1) = {} & \frac{2d_3(2x+1,2y+1)d_4(2x+1,2y+1)d_5(2x+1,2y+1)}{d_3(2x+1,2y+1)^2 + d_4(2x+1,2y+1)^2} \\ & + \frac{-d_3(2x+1,2y+1)^2 d_2 - {d_2}^2 d_3(2x+1,2y+1)}{d_3(2x+1,2y+1)^2 + d_4(2x+1,2y+1)^2}, \\ d_3(2x+1,2y+1) = {} & \frac{1}{2}(I(2x,2y) - I(2x+2,2y+2)), \\ d_4(2x+1,2y+1) = {} & \frac{1}{2}(I(2x,2y+2) - I(2x+2,2y)), \\ d_5(2x+1,2y+1) = {} & \frac{1}{2}(I(2x+1,2y-1) + I(2x+1,2y+3) \\ & - I(2x-1,2y+1) - I(2x+3,2y+1)). \end{aligned} \tag{3.16}$$

Suppose that the low-resolution image $L_{ij}$ is of size $m \times n$ and that it is changed to the corresponding interpolated image $H_{ij'}$ of size $((m \times 2^{\text{scale}}) - (2^{\text{scale}} - 1)) \times ((n \times 2^{\text{scale}}) - (2^{\text{scale}} - 1))$, where "scale" denotes the magnification factor. Then we use the nearest interpolation algorithm for the missing pixels in order to obtain the image $H_{ij'}$ of size $(m \times 2^{\text{scale}}) \times (n \times 2^{\text{scale}})$.

Similarly, we partition $H_{ij'}$ into overlapping processing units. The eight adjacent pixels of each pixel are treated as GPR model test input data based on the model $M$ which was obtained from the training process. Note that if PU has Property 1 or Property 2, then we can directly obtain the corresponding pixel values. Otherwise, we capture the prediction distribution of unknown pixels in the initial high-resolution image. The joint distribution of the training domain output $y$ and the test output $f'$ is given by the following equation:

$$\begin{bmatrix} y \\ g' \end{bmatrix} \sim GP\left(0, \begin{bmatrix} \text{COV}(X,X) + \sigma_n^2 I, \text{COV}(X,X') \\ \text{COV}(X',X), \text{COV}(X',X') \end{bmatrix}\right), \tag{3.17}$$

where $X$ denotes the GPR training data matrix, $X'$ is the test matrix, and $\text{COV}(X,X')$ is the $n \times n$ matrix of covariances. Therefore, we can derive the predictive distribution based on the obtained model $M$:

$$\begin{aligned} g' \mid X, y, X' &\sim GP\left(\overline{g'}, V\left(\overline{g'}\right)\right), \\ \overline{g'} &= \text{COV}(X',X)\left[\text{COV}(X,X) + \sigma_n^2 I\right]^{-1} y, \\ V\left(\overline{g'}\right) &= \text{COV}(X',X') - \text{COV}(X',X)\left[\text{COV}(X,X) + \sigma_n^2 I\right]^{-1} \text{COV}(X,X'). \end{aligned} \tag{3.18}$$

During the prediction of high-resolution image pixels, two rules should be obeyed. Firstly, the PU divided by the initial high-resolution image should correspond to that divided by the low-resolution image. Secondly, the gradient algorithm should satisfy the common positive definite matrix. If not, it will lead to a zero prediction, and the prediction value

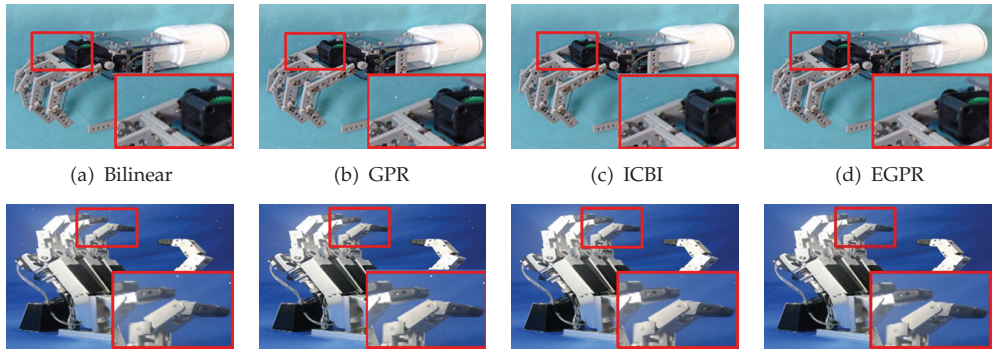

(a) Bilinear (b) GPR (c) ICBI (d) EGPR

(e) Bilinear (f) GPR (g) ICBI (h) EGPR

**Figure 4:** Comparison of images obtained using four methods, with scale = 1. Parts (a)–(d) show image 1. Parts (e)–(h) show image 2.

will need modifying. The modification method can be utilized to maintain the original interpolated pixel value. Finally, we combine all the processing units together in a smooth manner to obtain the high-resolution images without noise.

## 4. Experimental Results and Discussion

In this section, we compare the experimental results obtained using the proposed algorithm with those obtained using the bilinear algorithm, GPR algorithm [13], and ICBI algorithm [9]. Each algorithm was run in MATLAB. In order to evaluate algorithm performance, we first downsampled original high-quality images to acquire low-resolution images. Then we enlarged these low-resolution images by utilizing the different interpolation algorithms and compared the enlarged images with the original high-quality images. In all experiments, we set the PU size to $30 \times 30$, but this may be increased according to the magnification factor. At the same time, we used zero mean and square exponential functions as the respective mean and covariance functions in the EGPR. The covariance function required two hyperparameters: a characteristic length scale, the default value of which was 0.21, and the standard deviation of the signal, the default value of which was 0.08. In addition, to achieve color image interpolation, we trained and predicted the GPR model separately for each of the R, G, and B channels.

Figure 4 shows the interpolation results from the four algorithms when "scale" was set as 1. Figures 4(a)–4(d) are comparisons of image 1, and Figures 4(e)–4(h) are comparisons of image 2. In the enlarged red-bordered region, it can be seen that the bilinear method introduces jaggy effects, the GPR method reduces these jaggy effects, and the ICBI method achieves a clear edge but is still a little blurry. By employing the energy computation based on properties of adjacent pixels, our new method generates a clearer image without noise.

Similarly, Figures 5 and 6 demonstrate the interpolation results with scales of 2 and 3, respectively. From these figures, it can be seen that our method achieved the clearest and smoothest enlarged image of the four methods tested, for example, along edges on the root hand in Figure 6(h). Moreover, the advantages of our proposed algorithm become more enhanced at greater enlargement factors.

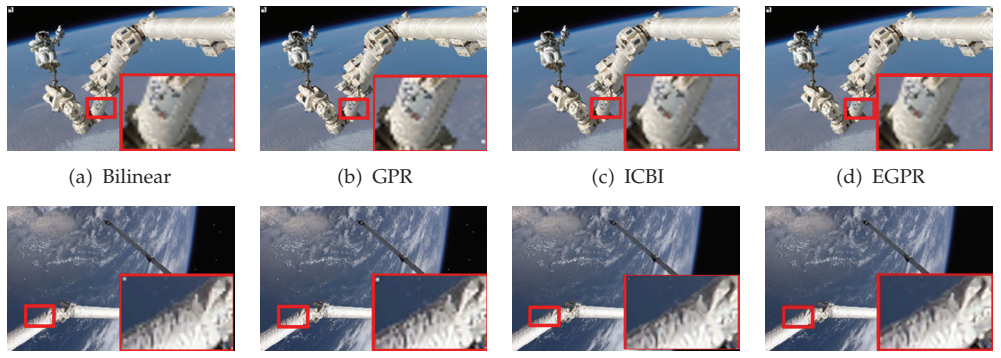

(a) Bilinear (b) GPR (c) ICBI (d) EGPR

(e) Bilinear (f) GPR (g) ICBI (h) EGPR

**Figure 5:** Comparison of images obtained using four methods, with scale = 2. Parts (a)–(d) show image 3. Parts (e)–(h) show image 4.

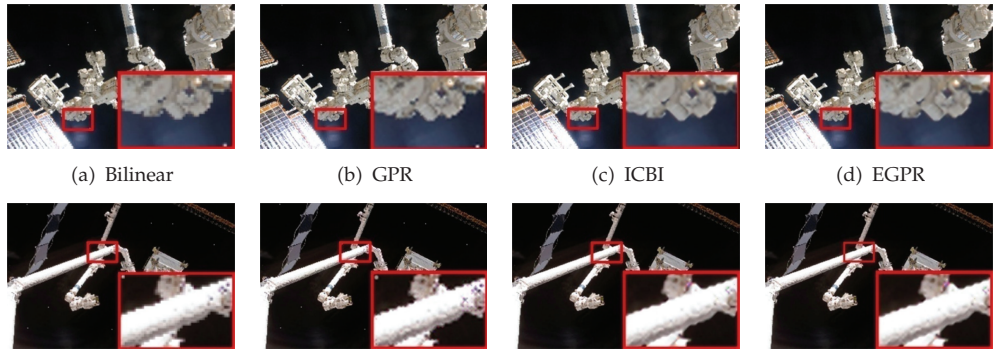

(a) Bilinear (b) GPR (c) ICBI (d) EGPR

(e) Bilinear (f) GPR (g) ICBI (h) EGPR

**Figure 6:** Comparison of images obtained using four methods, with scale = 3. Parts (a)–(d) show image 5. Parts (e)–(h) show image 6.

**Table 1:** Comparison of PSNR for the four interpolation methods when applied to test images.

| Image | Scale | Bilinear | GPR | ICBI | EGPR |
|---|---|---|---|---|---|
| Image 1 | 1 | 32.9940 | 33.2792 | 33.3456 | 33.3986 |
| Image 2 | 1 | 30.6314 | 30.7861 | 31.3684 | 31.4594 |
| Image 3 | 2 | 29.5738 | 29.4194 | 29.7173 | 29.7213 |
| Image 4 | 2 | 27.7717 | 27.4767 | 27.8485 | 27.8625 |
| Image 5 | 3 | 23.4038 | 24.4366 | 24.7153 | 24.7171 |
| Image 6 | 3 | 24.3122 | 25.1477 | 25.6880 | 25.6909 |

**Table 2:** Comparison of RMS for the four interpolation methods when applied to test images.

| Image | Scale | Bilinear | GPR | ICBI | EGPR |
|---|---|---|---|---|---|
| Image 1 | 1 | 16.4437 | 15.8419 | 15.7032 | 15.6004 |
| Image 2 | 1 | 21.1046 | 20.3410 | 19.1890 | 18.9614 |
| Image 3 | 2 | 24.9225 | 24.8861 | 24.4329 | 24.4191 |
| Image 4 | 2 | 31.0516 | 32.1427 | 30.6882 | 30.6118 |
| Image 5 | 3 | 50.8161 | 44.8762 | 43.3017 | 43.2633 |
| Image 6 | 3 | 45.9833 | 41.5720 | 39.0571 | 39.0412 |

**Table 3:** Comparison of MSSIM for the four interpolation methods when applied to test images.

| Image | Scale | Bilinear | GPR | ICBI | EGPR |
|---|---|---|---|---|---|
| Image 1 | 1 | 0.936 | 0.937 | 0.938 | 0.940 |
| Image 2 | 1 | 0.946 | 0.947 | 0.953 | 0.955 |
| Image 3 | 2 | 0.905 | 0.906 | 0.909 | 0.910 |
| Image 4 | 2 | 0.812 | 0.808 | 0.815 | 0.816 |
| Image 5 | 3 | 0.818 | 0.837 | 0.850 | 0.851 |
| Image 6 | 3 | 0.857 | 0.865 | 0.878 | 0.879 |

To further validate our algorithm, we also provide objective measurements. Peak signal-to-noise ratio (PSNR) and root mean square (RMS) error are traditional quantitative measures of accuracy, and by comparing their values for the above images, we can conclude that the proposed EGPR algorithm yields interpolated pixel values that are much closer to their original high-quality values than those obtained with the bilinear algorithm, GPR algorithm, and ICBI algorithm. Tables 1 and 2 summarize the PSNR and RMS values for each algorithm at different magnification factors and for each image. It can be observed that the PSNR values for images obtained using the EGPR algorithm are the highest, and those using the bilinear algorithm are the lowest. Further, RMS values for images obtained using the EGPR algorithm are the lowest, and those using the bilinear algorithm are the highest. Overall, it can be clearly demonstrated that our new method outperforms the other three algorithms.

MSSIM [25] is an image quality assessment index which assesses the image visibility quality from an image formation point of view under the assumption of the correlation between human visual perception and image structural information. We compared the MSSIM obtained using the EGPR algorithm at different scale values with the corresponding values obtained using the bilinear, GPR, and ICBI algorithms, as shown in Table 3. It is noted that our new algorithm achieves a greater MSSIM than the other three algorithms, and the results show that the images obtained using our algorithm are closer to the original high-resolution images in terms of image structure similarity.

In addition, Figure 7 clearly demonstrates the quantitative assessment results for each image at different magnification levels. In this figure, the blue dots represent the quality scores of the images obtained using the comparison algorithms, and the red dots represent those obtained using our algorithm. Our interpolation algorithm is notably superior to the other algorithms, according to all three objective measurements. The proposed algorithm therefore yielded encouraging performance in terms of image visualization and quantitative quality assessment, making it a competitive image interpolation algorithm.

## 5. Conclusions

In this paper, we have presented a novel EGPR method for image interpolation. The main feature of this new algorithm is its ability to obtain relatively high prediction accuracy of the unknown pixels by fully utilizing underlying image patch information. The implementation process involves two steps: training and prediction. The former creates a GPR model using only single-image data as the training set, and the latter combines energy computation with the acquired model to produce a high-resolution image. Experiments have shown that our algorithm can yield encouraging performance not only in terms of image visualization

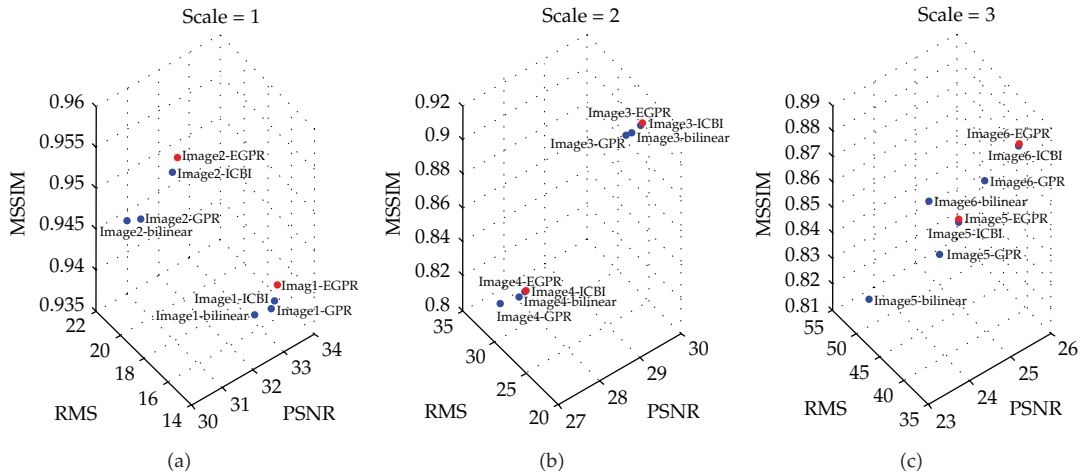


**Figure 7:** Quantitative quality assessment results for the four interpolation methods.

but also in terms of PSNR, RMS, and MSSIM quality measures. However, better image interpolation comes at the expense of greater algorithm complexity. Methods of improving the algorithm efficiency need further investigation. In future, we can improve this algorithm to address the problem of the interpolation of image sequences. Images in the same sequence are also subject to the recurrence phenomenon, whereby images contain spatial-temporal correlation [26]. We believe that this problem can be addressed using the improved EGPR algorithm by finding an appropriate energy-driven computation and training mode.

## Acknowledgments

This work was supported by the National Basic Research Program of China (973 Program) 2012CB821200 (2012CB821206), the National Natural Science Foundation of China (no. 91024001, no. 61070142), and the Beijing Natural Science Foundation (no. 4111002).

## References

[1] P. Thevenaz, T. Blu, and M. Unser, "Interpolation revisited," *IEEE Transactions on Medical Imaging*, vol. 19, no. 7, pp. 739–758, 2000.

[2] K. S. Ni and T. Q. Nguyen, "An adaptable *k*-nearest neighbors algorithm for MMSE image interpolation," *IEEE Transactions on Image Processing*, vol. 18, no. 9, pp. 1976–1987, 2009.

[3] Z. Hou and Q. Zhang, "Interpolation algorithm for recovering the missing phase values in 3D measurement," *Optik*, vol. 121, no. 14, pp. 1324–1329, 2010.

[4] J. W. Han, J. H. Kim, S. H. Cheon, J. O. Kim, and S. J. Ko, "A novel image interpolation method using the bilateral filter," *IEEE Transactions on Consumer Electronics*, vol. 56, no. 1, pp. 175–181, 2010.

[5] T. Nagata, "Smooth local interpolation of surfaces using normal vectors," *Journal of Applied Mathematics*, vol. 2010, Article ID 952420, 24 pages, 2010.

[6] Y. W. Tai, S. Liu, M. S. Brown, and S. Lin, "Super resolution using edge prior and single image detail synthesis," in *Proceedings of the IEEE Computer Society Conference on Computer Vision and Pattern Recognition (CVPR '10)*, pp. 2400–2407, June 2010.

[7] W. S. Tam, C. W. Kok, and W. C. Siu, "Modified edge-directed interpolation for images," *Journal of Electronic Imaging*, vol. 19, no. 1, Article ID 013011, pp. 1–20, 2010.

[8] J. Sun, J. Sun, Z. Xu, and H. Y. Shum, "Image super-resolution using gradient profile prior," in *Proceedings of the 26th IEEE Conference on Computer Vision and Pattern Recognition (CVPR '08)*, pp. 1–8, June 2008.
[9] A. Giachetti and N. Asuni, "Real-time artifact-free image upscaling," *IEEE Transactions on Image Processing*, vol. 20, no. 10, pp. 2760–2768, 2011.
[10] D. Glasner, S. Bagon, and M. Irani, "Super-resolution from a single image," in *Proceedings of the 12th International Conference on Computer Vision (ICCV '09)*, pp. 349–356, October 2009.
[11] K. I. Kim and Y. Kwon, "Example-based learning for single-image super-resolution," in *Proceedings of the 30th DAGM symposium on Pattern Recognition*, pp. 456–465, 2008.
[12] R. Fattal, "Image upsampling via imposed edge statistics," *ACM Transactions on Graphics*, vol. 26, no. 3, Article ID 1276496, pp. 95-1–95-8, 2007.
[13] H. He and W.-C. Siu, "Single image super-resolution using Gaussian process regression," in *Proceedings of the 26th IEEE Conference on Computer Vision and Pattern Recognition (CVPR '11)*, pp. 449–456, 2011.
[14] H. Asheri, H. R. Rabiee, N. Pourdamghani, and M. H. Rohban, "A gaussian process regression framework for spatial error concealment with adaptive kernels," in *Proceedings of the 20th International Conference on Pattern Recognition (ICPR '10)*, pp. 4541–4544, August 2010.
[15] G. Salimi-Khorshidi, T. E. Nichols, S. M. Smith, and M. W. Woolrich, "Using gaussian-process regression for meta-analytic neuroimaging inference based on sparse observations," *IEEE Transactions on Medical Imaging*, vol. 30, no. 7, pp. 1401–1416, 2011.
[16] J. Pasi, V. Jarno, and V. Aki, "Robust Gaussian process regression with a student-t likelihood," *Journal of Machine Learning Research*, vol. 12, pp. 3227–3257, 2011.
[17] L. You, V. Brusic, M. Gallagher, and M. Bodén, "Using Gaussian process with test rejection to detect T-cell epitopes in pathogen genomes," *IEEE/ACM Transactions on Computational Biology and Bioinformatics*, vol. 7, no. 4, pp. 741–751, 2010.
[18] S. Sun and X. Xu, "Variational inference for infinite mixtures of Gaussian processes with applications to traffic flow prediction," *IEEE Transactions on Intelligent Transportation Systems*, vol. 12, no. 2, pp. 466–475, 2011.
[19] R. Zimmermann, "Asymptotic behavior of the likelihood function of covariance matrices of spatial Gaussian processes," *Journal of Applied Mathematics*, vol. 2010, Article ID 494070, 17 pages, 2010.
[20] A. Ranganathan, M.-H. Yang, and J. Ho, "Online sparse Gaussian process regression and its applications," *IEEE Transactions on Image Processing*, vol. 20, no. 2, pp. 391–404, 2011.
[21] O. Rudovic and M. Pantic, "Shape-constrained Gaussian process regression for facial-point-based head-pose normalization," in *Proceedings of the International Conference on Computer Vision (ICCV '11)*, pp. 1495–1502, 2011.
[22] A. M. Feng, L. M. Fang, and M. Lin, "Gaussian process regression and its application in near-infrared spectroscopy analysis," *Spectroscopy and Spectral Analysis*, vol. 31, no. 6, pp. 1514–1517, 2011.
[23] M. M. Atia, A. Noureldin, and M. Korenberg, "Gaussian process regression approach for bridging GPS outages in integrated navigation systems," *Electronics Letters*, vol. 47, no. 1, pp. 52–53, 2011.
[24] C. E. Rasmussen and C. K. I. Williams, *Gaussian Processes for Machine Learning*, Adaptive Computation and Machine Learning, MIT Press, Cambridge, Mass, USA, 2006.
[25] Z. Wang, A. C. Bovik, H. R. Sheikh, and E. P. Simoncelli, "Image quality assessment: from error visibility to structural similarity," *IEEE Transactions on Image Processing*, vol. 13, no. 4, pp. 600–612, 2004.
[26] J.-W. Roh and B.-K. Yi, "Efficient indexing of interval time sequences," *Information Processing Letters*, vol. 109, no. 1, pp. 1–12, 2008.

Hindawi Publishing Corporation
Journal of Applied Mathematics
Volume 2012, Article ID 920260, 19 pages
doi:10.1155/2012/920260

*Research Article*

# On Robust Hybrid Force/Motion Control Strategies Based on Actuator Dynamics for Nonholonomic Mobile Manipulators

**Yongxin Zhu[1] and Liping Fan[1,2]**

[1] *School of Microelectronics, Shanghai Jiao Tong University, Shanghai 200240, China*
[2] *School of Medical Instrument and Food Engineering, University of Shanghai for Science and Technology, Shanghai 200093, China*

Correspondence should be addressed to Liping Fan, fanlipingsds@gmail.com

Received 1 March 2012; Accepted 25 May 2012

Academic Editor: Weihai Zhang



Robust force/motion control strategies are presented for mobile manipulators under both holonomic and nonholonomic constraints in the presence of uncertainties and disturbances. The controls are based on structural knowledge of the dynamics of the robot, and the actuator dynamics is also taken into account. The proposed control is robust not only to structured uncertainty such as mass variation but also to unstructured one such as disturbances. The system stability and the boundness of tracking errors are proved using Lyapunov stability theory. The proposed control strategies guarantee that the system motion converges to the desired manifold with prescribed performance. Simulation results validate that not only the states of the system asymptotically converge to the desired trajectory, but also the constraint force asymptotically converges to the desired force.

## 1. Introduction

Mobile manipulators refer to robotic manipulators mounted on mobile platforms. Such systems combine the advantages of mobile platforms and robotic arms and reduce their drawbacks [1–4]. For instance, the mobile platform extends the arm workspace, whereas the arm offers much operational functionality. Applications for such systems could be found in mining, construction, forestry, planetary exploration, teleoperation, and military [5–11].

Mobile manipulators possess complex and strongly coupled dynamics of mobile platforms and manipulators [12–16]. A control approach by nonlinear feedback linearization was presented for the mobile platform so that the manipulator is always positioned at the preferred configurations measured by its manipulability [17]. In [14], the effect of the dynamic interaction on the tracking performance of a mobile manipulator was studied, and

nonlinear feedback control for the mobile manipulator was developed to compensate the dynamic interaction. In [18], a basic framework for the coordination and control of vehicle-arm systems was presented, which consists of two basic task-oriented control: end-effector task control and platform self-posture control. The standard definition of manipulability was generalized to the case of mobile manipulators, and the optimization of criteria inherited from manipulability considerations were given to generate the controls of the system when its end-effector motion was imposed [19]. In [20], a unified model for mobile manipulator was derived, and nonlinear feedback was applied to linearize and decouple the model, and decoupled force/position control of the end-effector along the same direction for mobile manipulators was proposed and applied to nonholonomic cart pushing. The previously mentioned literature concerning with control of the mobile manipulator requires the precise information on the dynamics of the mobile manipulator; there may be some difficulty in implementing them on the real system in practical applications.

Different researchers have investigated adaptive controls to deal with dynamics uncertainty of mobile manipulators. Adaptive neural-network- (NN-) based controls for the arm and the base had been proposed for the motion control of a mobile manipulator [21, 22]; each NN control output comprises a linear control term and a compensation term for parameter uncertainty and disturbances. Adaptive control was proposed for trajectory/force control of mobile manipulators subjected to holonomic and nonholonomic constraints with unknown inertia parameters [23, 24], which ensures the state of the system to asymptotically converge to the desired trajectory and force. The principal limitation associated with these schemes is that controllers are designed at the velocity input level or torque input level, and the actuator dynamics are excluded.

As demonstrated in [25–27], actuator dynamics constitute an important component of the complete robot dynamics, especially in the case of high-velocity movement and highly varying loads. Many control methods have therefore been developed to take into account the effects of actuator dynamics (see, e.g., [28–30]). However, the literature is sparse on the control of the nonholonomic mobile manipulators including the actuator dynamics. In most of the research works for controlling mobile manipulators, joint torques are control inputs though in reality joints are driven by actuators (e.g., DC motors), and therefore using actuator input voltages as control inputs is more realistic. To this effect, actuator dynamics is combined with the mobile manipulator's dynamics in this paper.

This paper addresses the problem of stabilization of force/motion control for a class of mobile manipulator systems with both holonomic and nonholonomic constraints in the parameter uncertainties and external disturbances.

Unlike the force/motion control presented in [31–37], which is proposed for the mechanical systems subject to either holonomic or nonholonomic constraints, in our paper, the control is to deal with the system subject to both holonomic and nonholonomic constraints. After the dynamics based on decoupling force/motion is first presented, the robust motion/force control is proposed for the system under the consideration of the actuator dynamics uncertainty to complete the trajectory/force tracking. The paper has main contributions listed as follows.

(i) Decoupling robust motion/force control strategies are presented for mobile manipulator with both holonomic and nonholonomic constraints in the parameter uncertainties and external disturbances, and nonregressor-based control design is developed in a unified manner without imposing any restriction on the system dynamics.

(ii) The actuators (e.g., DC motor) dynamics of both the mobile platform and the arm are integrated with mobile manipulator dynamics and kinematics so that the actuator input voltages are the control inputs thus making the system more realistic.

Simulation results are described in detail that show the effectiveness of the proposed control law.

The rest of the paper is organized as follows. The system description of mobile manipulator subject to nonholonomic constraints and holonomic is briefly described in Section 2. Problem statement for the system control is given in Section 4. The main results of robust adaptive control design are presented in Section 5. Simulation studies are presented by comparison between the proposed robust control with nonrobust control in Section 6. Concluding remarks are given in Section 7.

## 2. System Description

Consider an $n$ DOF mobile manipulator with nonholonomic mobile base. The constrained mechanical system can be described as

$$M(q)\ddot{q} + C(q,\dot{q})\dot{q} + G(q) + d(t) = B(q)\tau + f, \tag{2.1}$$

where $q = [q_1, \ldots, q_n]^T \in R^n$ denote the generalized coordinates; $M(q) \in R^{n\times n}$ is the symmetric bounded positive definite inertia matrix; $C(\dot{q},q)\dot{q} \in R^n$ denotes the Centripetal and Coriolis torques; $G(q) \in R^n$ is the gravitational torque vector; $d(t)$ denotes the external disturbances; $\tau \in R^m$ is the control inputs; $B(q) \in R^{n\times m}$ is a full rank input transformation matrix and is assumed to be known because it is a function of fixed geometry of the system; $f \in R^m$ denotes the vector of constraint forces; $J \in R^{n\times m}$ is Jacobian matrix; $\lambda = [\lambda_n, \lambda_h] \in R^m$ is Lagrange multipliers corresponding to the nonholonomic and holonomic constraints.

The generalized coordinates may be separated into two sets $q = [q_v, q_a]^T$, where $q_v \in R^v$ describes the generalized coordinates for the mobile platform, $q_a \in R^r$ is the coordinates of the manipulator, and $n = v + r$.

*Assumption 2.1* (see [38–40]). The mobile manipulator is subject to known nonholonomic constraints.

*Assumption 2.2.* The system (2.8) is subjected to $k$ independent holonomic constraints, which can be written as

$$h(q) = 0, \quad h(q) \in R^k, \tag{2.2}$$

where $h(q)$ is full rank, then $J(q) = \partial h/\partial q$.

*Remark 2.3.* In actual implementation, we can adopt the methods of producing enough friction between the wheels of the mobile platform and the ground such that this assumption holds [41–43].

The vehicle is subjected to nonholonomic constraints, the $l$ nonintegrable and independent velocity constraints can be expressed as

$$A(q_v)\dot{q}_v = 0, \tag{2.3}$$

where $A(q_v) = [A_1^T(q_v), \ldots, A_l^T(q_v)]^T : R^v \rightarrow R^{l\times v}$ is the kinematic constraint matrix which is assumed to have full rank $l$. In the paper, the vehicle is assumed to be completely nonholonomic. The effect of the constraints can be viewed as a restriction of the dynamics on the manifold $\Omega_n$ as

$$\Omega_n = \{(q_v, \dot{q}_v) \mid A(q_v)\dot{q}_v = 0\}. \tag{2.4}$$

The generalized constraint forces for the nonholonomic constraints can be given by

$$f_n = A^T(q_v)\lambda_n. \tag{2.5}$$

Assume that the annihilator of the codistribution spanned by the covector fields $A_1(q_v), \ldots, A_l(q_v)$ is a $(v-l)$-dimensional smooth nonsingular distribution $\Delta$ on $R^v$. This distribution $\Delta$ is spanned by a set of $(v-l)$ smooth and linearly independent vector fields $H_1(q_v), \ldots, H_{v-l}(q_v)$; that is, $\Delta = \text{span}\{H_1(q_v), \ldots, H_{v-l}(q)\}$, which satisfy, in local coordinates, the following relation:

$$H^T(q_v)A^T(q_v) = 0, \tag{2.6}$$

where $H(q_v) = [H_1(q_v), \ldots, H_{n_v-l}(q_v)] \in R^{v\times(v-l)}$. Note that $H^TH$ is of full rank. Constraints (2.3) imply the existence of vector $\dot{\eta} \in R^{v-l}$ [44], such that

$$\dot{q}_v = H(q_v)\dot{\eta}. \tag{2.7}$$

Considering the nonholonomic constraints (2.3) and its derivative, the dynamics of mobile manipulator can be expressed as

$$\begin{bmatrix} H^TM_vH & H^TM_{va} \\ M_{av}H & M_a \end{bmatrix}\begin{bmatrix} \ddot{\eta} \\ \ddot{q}_a \end{bmatrix} + \begin{bmatrix} H^TM_v\dot{H} + H^TC_vH & H^TC_{va} \\ M_{av}\dot{H} + C_{av}H & C_a \end{bmatrix}\begin{bmatrix} \dot{\eta} \\ \dot{q}_a \end{bmatrix} + \begin{bmatrix} H^TG_v \\ G_a \end{bmatrix} + \begin{bmatrix} H^Td_v \\ d_a \end{bmatrix} = \begin{bmatrix} H^TB_v\tau_v \\ B_a\tau_a \end{bmatrix} + \begin{bmatrix} 0 & 0 \\ J_v & J_a \end{bmatrix}^T\begin{bmatrix} 0 \\ \lambda_h \end{bmatrix}. \tag{2.8}$$

From Assumption 2.2, the holonomic constraint force $f_h$ can be converted to the joint space as $f_h = J^T\lambda_h$. Hence, the holonomic constraint on the robot's end effector can be viewed as restricting only the dynamics on the constraint manifold $\Omega_h$ defined by $\Omega_h = \{(q, \dot{q}) \mid h(q) = 0, J(q)\dot{q} = 0\}$. The vector $q_a$ can be further rearranged and partitioned

into $q_a = [q_a^1, q_a^2]^T$; $q_a^1 \in R^{r-k}$ describes the constrained motion of the manipulator, and $q_a^2 \in R^k$ denotes the remaining joint variable. Then,

$$J(q) = \left[\frac{\partial h}{\partial \eta}, \frac{\partial h}{\partial q_a^1}, \frac{\partial h}{\partial q_a^2}\right]. \tag{2.9}$$

From [45], it could be concluded $q$ is the function of $\zeta = [\eta, q_a^1]^T$, that is, $q = q(\zeta)$, and we have $\dot{q} = L(\zeta)\dot{\zeta}$, where $L(\zeta) = \partial q/\partial\zeta$, $\ddot{q} = L(\zeta)\ddot{\zeta} + \dot{L}(\zeta)\dot{\zeta}$, and $L(\zeta)$, $J^1(\zeta) = J(q(\zeta))$ satisfy the relationship

$$L^T(\zeta)J^{1T}(\zeta) = 0. \tag{2.10}$$

The dynamic model (2.8), when it restricted to the constraint surface, can be transformed into the reduced model:

$$M^1 L(\zeta)\ddot{\zeta} + C^1\dot{\zeta} + G^1 + d^1(t) = u + J^{1T}\lambda_h, \tag{2.11}$$

where

$$\begin{gathered}
M^1 = \begin{bmatrix} H^T M_v H & H^T M_{va} \\ M_{av} H & M_a \end{bmatrix}, \\
C^1 = \begin{bmatrix} H^T M_v \dot{H} & H^T M_{va} \\ M_{av} H & M_a \end{bmatrix} \dot{L}(\zeta) + \begin{bmatrix} H^T M_v \dot{H} + H^T C_v H & H^T C_{va} \\ M_{av}\dot{H} + C_{av} & C_a \end{bmatrix} L(\zeta), \\
G^1 = \begin{bmatrix} H^T G_v \\ G_a \end{bmatrix}, \qquad d^1(t) = \begin{bmatrix} H^T d_v \\ d_a \end{bmatrix}, \\
u = B^1\tau, \qquad B^1 = \begin{bmatrix} H^T B_v & 0 \\ 0 & B_a \end{bmatrix}, \qquad \zeta = \begin{bmatrix} \eta \\ q_a^1 \end{bmatrix}.
\end{gathered} \tag{2.12}$$

Multiplying $L^T$ by both sides of (2.11), we can obtain

$$M_L(\zeta)\ddot{\zeta} + C_L(\zeta, \dot{\zeta})\dot{\zeta} + G_L + d_L(t) = L^T B^1 \tau. \tag{2.13}$$

The force multipliers $\lambda_h$ can be obtained by (2.11):

$$\lambda_h = Z(\zeta)\left(C^1(\zeta, \dot{\zeta})\dot{\zeta} + G^1 + d^1(t) - B^1\tau\right), \tag{2.14}$$

where $M_L = L^T M^1 L$, $C_L = L^T C^1$, $G_L = L^T G^1$, $Z = (J^1(M^1)^{-1}J^{1T})^{-1}J^1(M^1)^{-1}$.

*Property 1.* The matrix $M_L$ is symmetric and positive definite.

*Property 2.* The matrix $\dot{M}_L - 2C_L$ is skew symmetric.

*Property 3* (see [46]). For holonomic systems, matrices $J^1(\zeta)$, $L(\zeta)$ are uniformly bounded and uniformly continuous if $\zeta$ is uniformly bounded and continuous, respectively.

*Property 4.* There exist some finite positive constants $c_i > 0$ $(1 \le i \le 4)$ and finite nonnegative constant $c_i \ge 0$ $(i = 5)$ such that for all $\zeta \in R^n$, for all $\dot{\zeta} \in R^n$, $\|M_L(\zeta)\| \le c_1$, $\|C_L(\zeta, \dot{\zeta})\| \le c_2 + c_3\|\dot{\zeta}\|$, $\|G_L(\zeta)\| \le c_4$, and $\sup_{t\ge 0}\|d_L(t)\| \le c_5$.

## 3. Actuator Dynamics

The joints of the mobile manipulators are assumed to be driven by DC motors. Consider the following notations used to model a DC motor: $v \in R^m$ represents the control input voltage vector; $I$ denotes an $m$-element vector of motor armature current; $K_N \in R^{m\times m}$ is a positive definite diagonal matrix which characterizes the electromechanical conversion between current and torque; $L_a = \text{diag}[L_{a1}, L_{a2}, L_{a3}, \ldots, L_{am}]$, $R_a = \text{diag}[R_{a1}, R_{a2}, R_{a3}, \ldots, R_{am}]$, $K_e = \text{diag}[K_{e1}, K_{e2}, K_{e3}, \ldots, K_{em}]$, $\omega = [\omega_1, \omega_2, \ldots, \omega_m]^T$ represent the equivalent armature inductances, resistances, back EMF constants, angular velocities of the driving motors, respectively; $G_r = \text{diag}(g_{ri}) \in R^{m\times m}$ denotes the gear ratio for $m$ joints; $\tau_m$ are the torque exerted by the motor. In order to apply the DC servomotors for actuating an $n$-DOF mobile manipulator, assuming no energy losses, a relationship between the $i$th joint velocity $\dot{q}_i$ and the motor shaft velocity $\omega_i$ can be presented as $g_{ri} = \omega_i/\dot{q}_i = \tau_i/\tau_{mi}$ with the gear ratio of the $i$th joint $g_{ri}$, the $i$th motor shaft torque $\tau_{mi}$, and the $i$th joint torque $\tau_i$. The motor shaft torque is proportional to the motor current $\tau_m = K_N I$. The back EMF is proportional to the angular velocity of the motor shaft; then we can obtain

$$L_a \frac{dI}{dt} + R_a I + K_e \omega = v. \tag{3.1}$$

In the actuator dynamics (3.1), the relationship between $\omega$ and $\dot{\zeta}$ is dependent on the type of mechanical system and can be generally expressed as

$$\omega = G_r T \dot{\zeta}. \tag{3.2}$$

The structure of $T$ depends on the mechanical systems to be controlled. For instance, in the simulation example, a two-wheel differential drive 2-DOF mobile manipulator is used to illustrate the control design. From [47], we have

$$\begin{aligned} v &= \frac{\left(r\dot{\theta}_l + r\dot{\theta}_r\right)}{2}, \\ \dot{\theta} &= \frac{\left(r\dot{\theta}_r - r\dot{\theta}_l\right)}{2l}, \\ \dot{\theta}_1 &= \dot{\theta}_1, \\ \dot{\theta}_2 &= \dot{\theta}_2, \end{aligned} \tag{3.3}$$

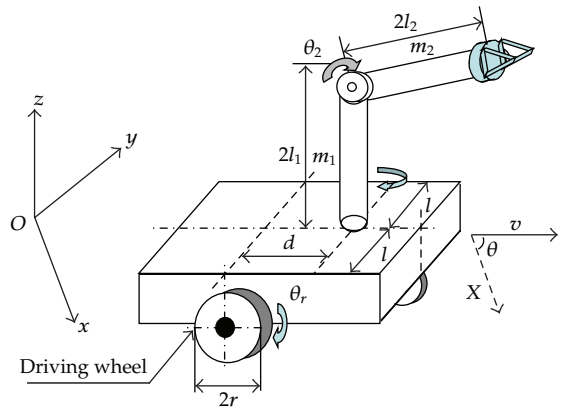


**Figure 1:** The 2-DOF mobile manipulator.

where $\dot{\theta}_l$ and $\dot{\theta}_r$ are the angular velocities of the two wheels, respectively, and $v$ is the linear velocity of the mobile platform, as shown in Figure 1. Since $\dot{y} = v\cos\theta$, we have

$$\begin{gathered}\left[\dot{\theta}_l \;\; \dot{\theta}_r \;\; \dot{\theta}_1 \;\; \dot{\theta}_2\right]^T = T\left[\dot{y} \;\; \dot{\theta} \;\; \dot{\theta}_1 \;\; \dot{\theta}_2\right]^T, \\ T = \begin{bmatrix} \dfrac{1}{r\cos\theta} & \dfrac{l}{r} & 0 & 0 \\ \dfrac{1}{r\cos\theta} & -\dfrac{l}{r} & 0 & 0 \\ 0 & 0 & 1 & 0 \\ 0 & 0 & 0 & 1 \end{bmatrix},\end{gathered} \tag{3.4}$$

where $r$ and $l$ are shown in Figure 1.

Eliminating $\omega$ from the actuator dynamics (3.1) by substituting (3.2), one obtains

$$L^T B^1 G_r K_N I = M_L(\zeta)\ddot{\zeta} + C_L\left(\zeta, \dot{\zeta}\right)\dot{\zeta} + G_L + d_L(t), \tag{3.5}$$

$$\lambda_h = Z(\zeta)\left(C_2\dot{\zeta} + G_2 + d_2(t) - B^1 G_r K_N I\right), \tag{3.6}$$

$$v = L_a\frac{dI}{dt} + R_a I + K_e G_r T\dot{\zeta}. \tag{3.7}$$

Until now we have brought the kinematics (2.3), dynamics (3.5), (3.6) and actuator dynamics (3.7) of the considered nonholonomic system from the generalized coordinate system $q \in R^n$ to feasible independent generalized velocities $\zeta \in R^{n-l-k}$ without violating the nonholonomic constraint (2.3).

## 4. Problem Statement

Since the system is subjected to the nonholonomic constraint (2.3) and holonomic constraint (2.2), the states $q_v$, $q_a^1$, $q_a^2$ are not independent. By a proper partition of $q_a$, $q_a^2$ is uniquely determined by $\zeta = [\eta, q_a^1]^T$. Therefore, it is not necessary to consider the control of $q_a^2$.

Given a desired motion trajectory $\zeta^d(t) = [\eta^d q_a^{1\,d}]^T$ and a desired constraint force $f_d(t)$, or, equivalently, a desired multiplier $\lambda_h(t)$, the trajectory and force tracking control is to determine a control law such that for any $(\zeta(0), \dot{\zeta}(0)) \in \Omega$, $\zeta$, $\dot{\zeta}$, $\lambda$ asymptotically converge to a manifold $\Omega_d$ specified as $\Omega$ where

$$\Omega_d = \left\{ (\zeta, \dot{\zeta}, \lambda_h) \mid \zeta = \zeta_d,\ \dot{\zeta} = \dot{\zeta}_d,\ \lambda = \lambda_d \right\}. \tag{4.1}$$

The controller design will consist of two stages: (i) a virtual adaptive control input $I^d$ is designed so that the subsystems (3.5) and (3.6) converge to the desired values, and (ii) the actual control input $v$ is designed in such a way that $I \to I^d$. In turn, this allows $\zeta - \zeta^d$ and $\lambda - \lambda^d$ to be stabilized to the origin.

*Assumption 4.1.* The desired reference trajectory $\zeta^d(t)$ is assumed to be bounded and uniformly continuous and has bounded and uniformly continuous derivatives up to the second order. The desired Lagrangian multiplier $\lambda_d(t)$ is also bounded and uniformly continuous.

## 5. Robust Control Design

### 5.1. Kinematic and Dynamic Subsystems

Let $e_\zeta = \zeta - \zeta^d$, $\dot{\zeta}_r = \dot{\zeta}^d - k_\zeta e_\zeta$, $r = \dot{e}_\zeta + k_\zeta e_\zeta$ with $k_\zeta > 0$, $e_\beta = \lambda - \lambda^d$. A decoupled control scheme is introduced to control generalized position and constraint force separatively.

Consider the virtual control input $I$ is designed as

$$I = K_N^{-1} G_r^{-1} B^{1^{-1}} \tau. \tag{5.1}$$

Let the control $u$ be as the form

$$\begin{aligned} u &= L^{+T} u_a - J^{1T} u_b, \\ u_a &= B^1 G_r K_{Na} I_a, \\ u_b &= B^1 G_r K_{Nb} I_b, \end{aligned} \tag{5.2}$$

where $u_a$, $I_a \in R^{n-l-k}$ and $u_b$, $I_b \in R^k$ and $L^{+T} = (L^T L)^{-1} L^T$. Then, (2.13) and (2.14) can be changed to

$$M_L(\zeta)\ddot{\zeta} + C_L(\zeta, \dot{\zeta})\dot{\zeta} + G_L + d_L(t) = B^1 G_r K_{Na} I_a, \tag{5.3}$$

$$Z(\zeta)\left(C^1(\zeta, \dot{\zeta})\dot{\zeta} + G^1 + d^1(t) - L^{+T} \mathrm{B}^1 G_r K_{Na} I_a\right) + B^1 G_r K_{Nb} I_b = \lambda_h. \tag{5.4}$$

Consider the following control laws:

$$B^1 G_r K_{Na} I_a^d = -K_p r - K_i \int r dt - \frac{r\Phi^2}{\Phi\gamma(\|r\|) + \delta}, \tag{5.5}$$

$$\Phi = C^T \Psi, \tag{5.6}$$

$$B^1 G_r K_{Nb} I_b^d = \frac{\chi^2}{\chi + \delta} + \lambda_h^d - K_f e_\lambda, \tag{5.7}$$

$$\chi = c_1 \|Z(\zeta)\| \left\| L^{+T} \right\| \left\| \frac{d}{dt} \left[ \dot{\zeta}^d \right] \right\|, \tag{5.8}$$

where $C = \begin{bmatrix} c_1 & c_2 & c_3 & c_4 & c_5 \end{bmatrix}$; $\Psi = \begin{bmatrix} \|(d/dt)[\dot{\zeta}_r]\| & \|\dot{\zeta}_r\| & \|\dot{\zeta}\| & \|\dot{\zeta}_r\| & 11 \end{bmatrix}^T$; $K_p, K_i, K_f$ are positive definite. $\gamma(\|r\|)$ can be defined as follows: if $\|r\| \le \rho$, $\gamma(\|r\|) = \rho$, else $\gamma(\|r\|) = \|r\|$, $\rho$ is a small value, $\delta(t)$ is a time-varying positive function converging to zero as $t \to \infty$, such that $\int_0^t \delta(\omega) d\omega = a < \infty$. There are many choices for $\delta(t)$ that satisfies the condition.

### 5.2. Control Design at the Actuator Level

Till now, we have designed a virtual controller $I$ and $\zeta$ for kinematic and dynamic subsystems. $\zeta$ tending to $\zeta^d$ can be guaranteed, if the actual input control signal of the dynamic system $I$ be of the form $I^d$ which can be realized from the actuator dynamics by the design of the actual control input $\nu$. On the basis of the above statements we can conclude that if $\nu$ is designed in such a way that $I$ tends to $I^d$, then $(\zeta - \zeta^d) \to 0$ and $(\lambda - \lambda^d) \to 0$.

Defining $I = e_I + I^d$ and substituting $I$ and $\dot{\zeta}$ of (3.7) one gets

$$L_a \dot{e}_I + R_a e_I + K_e G_r T \dot{e}_\zeta = -L_a \dot{I}^d - R_a I^d - K_e G_r T \dot{\zeta}^d + \nu. \tag{5.9}$$

The actuator parameters $K_N$, $L_a$, $R_a$, and $K_e$ are considered unknown for control design; however, there exist $L_0$, $R_0$, and $K_{e0}$, such that

$$\|L_a - L_0\| \le \alpha_1, \qquad \|R_a - R_0\| \le \alpha_2, \qquad \|K_e - K_{e0}\| \le \alpha_3. \tag{5.10}$$

Consider the robust control law

$$\nu = \nu_0 - \sum_{i=1}^{3} \frac{e_I \mu_i^2}{\|e_I\| \mu_i + \delta} - K_d e_I, \tag{5.11}$$

where

$$\begin{aligned} v_0 &= L_0\dot{I}^d + R_0 I^d + K_{e0} G_r T \dot{\zeta}^d, \\ \mu_1 &= \alpha_1 \left\| \left( \frac{d}{dt} \right) I^d \right\|, \\ \mu_2 &= \alpha_2 \left\| I^d \right\|, \\ \mu_3 &= \alpha_3 \left\| \left( \frac{d}{dt} \right) \zeta^d \right\|. \end{aligned} \tag{5.12}$$

### 5.3. Stability Analysis for the System

**Theorem 5.1.** *Consider the mechanical system described by* (2.1), (2.3), *and* (2.2); *using the control law* (5.5) *and* (5.7), *the following hold for any* $(q(0), \dot{q}(0)) \in \Omega_n \cap \Omega_h$:

(i) $r$ *and* $e_I$ *converge to a set containing the origin with the convergence rate as* $t \to \infty$;

(ii) $e_q$ *and* $\dot{e}_q$ *asymptotically converge to* 0 *as* $t \to \infty$;

(iii) $e_\lambda$ *and* $\tau$ *are bounded for all* $t \geq 0$.

*Proof.* (i) By combing (3.5) with (5.5), the closed-loop system dynamics can be rewritten as

$$M_L \dot{r} = B^1 G_r K_{Na} I_a^d + B^1 G_r K_{Na} e_I - \left( M_L \ddot{\zeta}_r + C_L \dot{\zeta}_r + G_L + d_L \right) - C_L r. \tag{5.13}$$

Substituting (5.5) into (5.13), the closed-loop dynamic equation is obtained:

$$M_L \dot{r} = -K_p r - K_i \int r\, dt - \frac{r\Phi^2}{\Phi\gamma(\|r\|) + \delta} - \mu - C_L r + B^1 G_r K_{Na} e_I, \tag{5.14}$$

where $\mu = M_L \ddot{\zeta}_r + C_L \dot{\zeta}_r + G_L + d_L$.

Consider the function

$$\begin{aligned} V &= V_1 + V_2, \\ V_1 &= \frac{1}{2} r^T M_L r + \frac{1}{2} \left( \int r dt \right)^T K_i \int r dt + e_\zeta^T k_\zeta K_{Na} K_p e_\zeta, \\ V_2 &= \frac{1}{2} e_I^T K_{Na} L_a e_I. \end{aligned} \tag{5.15}$$

Then, differentiating $V_1$ with respect to time, we have

$$\dot{V}_1 = r^T \left( M_L \dot{r} + \frac{1}{2} \dot{M}_L r + K_i \int r dt \right) + 2 e_\zeta^T k_\zeta K_{Na} K_p \dot{e}_\zeta. \tag{5.16}$$

From Property 1, we have $(1/2)\lambda_{\min}(M_L)r^T r \le V \le (1/2)\lambda_{\max}(M_L)r^T r$. By using Property 2, the time derivative of $V$ along the trajectory of (5.14) is

$$\begin{aligned}
\dot{V}_1 &= -r^T K_p r - r^T \mu - \frac{\|r\|^2\Phi^2}{\Phi\gamma(\|r\|)+\delta} + 2e_\zeta^T k_\zeta K_{Na} K_p \dot{e}_\zeta + r^T B^1 G_r K_{Na} e_I \\
&\le -r^T K_p r - \frac{\|r\|^2\Phi^2}{\Phi\gamma(\|r\|)+\delta} + \|r\|\Phi + 2e_\zeta^T k_\zeta K_{Na} K_p \dot{e}_\zeta + r^T B^1 G_r K_{Na} e_I \\
&\le -r^T K_p r - \frac{\|r\|^2\Phi^2 - \gamma(\|r\|)\Phi^2\|r\| - \|r\|\Phi\delta}{\Phi\gamma(\|r\|)+\delta} + 2e_\zeta^T k_\zeta K_{Na} K_p \dot{e}_\zeta + r^T B^1 G_r K_{Na} e_I,
\end{aligned} \tag{5.17}$$

when $\|r\| \ge \rho$; therefore,

$$\dot{V}_1 \le -r^T K_p r + \delta + 2e_\zeta^T k_\zeta K_{Na} K_d r - 2e_\zeta^T k_\zeta K_{Na} K_p k_\zeta e_\zeta + r^T B^1 G_r K_{Na} e_I. \tag{5.18}$$

Differentiating $V_2(t)$ with respect to time, using (3.7), one has

$$\dot{V}_2 = -e_I^T K_{Na}\left[L_a \dot{I}_a^d + R_a I_a^d + K_e G_r T \dot{\zeta}^d + R_a e_I + K_e G_r T \dot{e}_\zeta - \nu\right]. \tag{5.19}$$

Substituting $\nu$ in (5.19) by the control law (5.11), one has

$$\begin{aligned}
\dot{V}_2 = & -e_I^T K_{Na}(K_d + R_a)e_I - e_I^T K_{Na} K_e G_r T \dot{e}_\zeta - e_I^T K_{Na}(L_a - L_0)\dot{I}^d \\
& - e_I^T K_{Na}(R_a - R_0) I^d - e_I^T K_{Na}(K_e - K_{e0}) G_r T \dot{\zeta}^d - e_I^T K_{Na} \sum_{i=1}^{3} \frac{\mu_i^2 e_I}{\|e_I\|\mu_i + \delta} \\
\le & -e_I^T K_{Na}(K_d + R_a)e_I - e_I^T K_{Na} K_e G_r T \dot{e}_\zeta + \alpha_1 K_{Na}\|e_I\|\left\|\dot{I}^d\right\| \\
& + \alpha_2 K_{Na}\|e_I\|\left\|I_a^d\right\| + \alpha_3 K_{Na} G_r T \|e_I\|\left\|\zeta^d\right\| - K_{Na}\sum_{i=1}^{3}\frac{\|e_I\|^2\mu_i^2}{\|e_I\|\mu_i + \delta} \\
\le & -e_I^T K_{Na}(K_d + R_a)e_I - \mathrm{e}_I^T K_{Na} K_e G_r T \dot{e}_\zeta + K_{Na}\sum_{i=1}^{3}\alpha_i\delta \\
= & -e_I^T K_{Na}(K_d + R_a)e_I - e_I^T K_N K_e G_r T r + e_I^T K_{Na} K_e G_r T k_\zeta e_\zeta + K_{Na}\delta\sum_{i=1}^{3}\alpha_i.
\end{aligned} \tag{5.20}$$

Integrating (5.18) and (5.20), $\dot{V}$ can be expressed as

$$\begin{aligned}
\dot{V} \le & -r^T K_p r + \delta + 2e_\zeta^T k_\zeta K_{Na} K_p r - 2e_\zeta^T k_\zeta K_{Na} K_p k_\zeta e_\zeta + r^T B^1 G_r K_{Na} e_I \\
& - e_I^T K_{Na}(K_d + R_a)e_I - e_I^T K_{Na} K_e G_r T r + e_I^T K_{Na} K_e G_r T k_\zeta e_\zeta + K_{Na}\delta\sum_{i=1}^{3}\alpha_i.
\end{aligned} \tag{5.21}$$

We can obtain

$$\dot{V} \le -\begin{bmatrix} r^T & e_\zeta & e_I \end{bmatrix} Q \begin{bmatrix} K_{Na} & 0 & 0 \\ 0 & K_{Na} & 0 \\ 0 & 0 & K_{Na} \end{bmatrix} \begin{bmatrix} r \\ e_\zeta \\ e_I \end{bmatrix}, \tag{5.22}$$

where

$$Q = \begin{bmatrix} K_p & -K_p k_\zeta & \frac{1}{2} G_r \left( K_e T - B^1 \right) \\ -k_\zeta K_p & 2 k_\zeta K_p T k_\zeta & -\frac{1}{2} K_e G_r T k_\zeta \\ \frac{1}{2} G_r \left( K_e T - B^1 \right) & -\frac{1}{2} K_e G_r T k_\zeta & \left( K_d + R_a \right) \end{bmatrix}. \tag{5.23}$$

The term $Q$ on the right-hand side (5.22) can always be negative definite by choosing suitable $K_p$ and $K_d$. Since $[K_{na}]$ is positive definite, we only need to choose $K_p$ and $K_d$ such that $Q$ is positive definite. Therefore, $K_d$ and $K_p$ can always be chosen to satisfy

$$\left( K_d + R \right) > K_p^{-1} \begin{bmatrix} \frac{1}{2} G_r \left( K_e T - B^1 \right) & -\frac{1}{2} K_e G_r T k_\zeta \end{bmatrix} \begin{bmatrix} 2I & k_\zeta^{-1} \\ k_\zeta^{-1} & k_\zeta^{-1} T^{-1} k_\zeta^{-1} \end{bmatrix} \begin{bmatrix} \frac{1}{2} G_r \left( K_e T - B^1 \right) \\ -\frac{1}{2} K_e G_r T k_\zeta \end{bmatrix}. \tag{5.24}$$

If $\|r\| \le \rho$, it is easy to obtain $\dot{V} \le 0$. $r$, $e_\zeta$, and $e_I$ converge to a set containing the origin with $t \to \infty$.

(ii) $V$ is bounded, which implies that $r \in L_\infty^{n-k}$. From $r = \dot{e}_\zeta + k_\zeta e_\zeta$, it can be obtained that $e_\zeta, \dot{e}_\zeta \in L_\infty^{n-k}$. As we have established $e_\zeta, \dot{e}_\zeta \in L_\infty$, from Assumption 4.1, we conclude that $\zeta(t), \dot{\zeta}(t), \dot{\zeta}_r(t), \ddot{\zeta}_r(t) \in L_\infty^{n-k}$ and $\dot{q} \in L_\infty^n$.

Therefore, all the signals on the right hand side of (5.14) are bounded, and we can conclude that $\dot{r}$ and therefore $\ddot{\zeta}$ are bounded. Thus, $r \to 0$ as $t \to \infty$ can be obtained. Consequently, we have $e_\zeta \to 0$, $\dot{e}_\zeta \to 0$ as $t \to \infty$. It follows that $e_q, \dot{e}_q \to 0$ as $t \to \infty$.

(iii) Substituting the control (5.5) and (5.7) into the reduced order dynamic system model (5.4) yields

$$\begin{aligned} \left( 1 + K_f \right) e_\lambda &= Z(\zeta) \left( C^1(\zeta, \dot{\zeta}) \dot{\zeta} + G^1 + d^1(t) - L^{+T} G_r K_{Na} I_a \right) + B^1 G_r K_{Nb} I_b^d + B^1 G_r K_{Nb} e_I \\ &= -Z(\zeta) L^{+T} M_L(\zeta) \left( \ddot{\zeta} \right) + \frac{\chi^2}{\chi + \delta} + B^1 G_r K_{Nb} e_I. \end{aligned} \tag{5.25}$$

Since $\dot{\zeta} = 0$ when $I \in R^k$, (3.7) could be changed as

$$L_a \frac{dI_b}{dt} + R_a I_b = v_b. \tag{5.26}$$

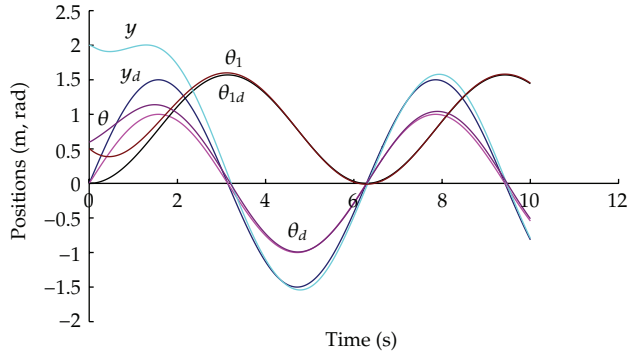


**Figure 2:** The positions of the joints.

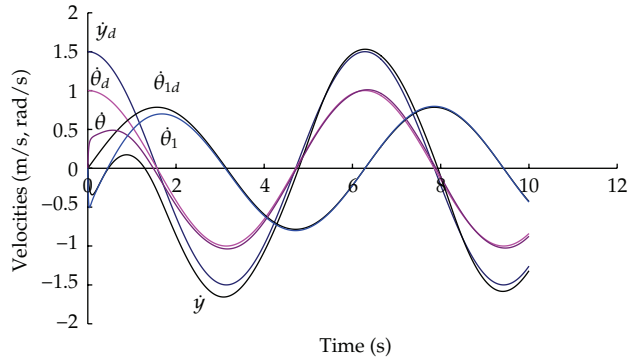


**Figure 3:** The velocities of the joints.

Therefore, $r = 0$ and $e_\zeta = 0$ in the force space; (5.20) could be changed as

$$\dot{V}_2 = -e_I^T K_{Nb}(K_d + R)e_I + K_{Nb}\delta\sum_{i=1}^{3}\alpha_i. \tag{5.27}$$

Since $K_{Nb}$ is bounded, $\dot{V} < 0$, we can obtain $e_I \to 0$ as $t \to \infty$. The proof is completed by noticing that $\dot{\zeta}$, $Z(q)$, $K_{Nb}$ and $e_I$ are bounded. Moreover, $\zeta \to \zeta^d$, and $-Z(\zeta)L^{+T}M_L(\zeta)(\ddot{\zeta}^d) + \chi^2/(\chi + \delta) \le \delta$, $e_I \to 0$, the right-hand side terms of (5.25), tend uniformly asymptotically to zero; then it follows that $e_\lambda \to 0$, then $f(t) \to f_d(t)$.

Since $r$, $\zeta$, $\dot{\zeta}$, $\zeta_r$, $\dot{\zeta}_r$, $\ddot{\zeta}_r$, $e_\lambda$ and $e_I$ are all bounded, it is easy to conclude that $\tau$ is bounded from (5.2). □

## 6. Simulations

To verify the effectiveness of the proposed control algorithm, let us consider a 2-DOF manipulator mounted on two-wheels-driven mobile base [23] shown in Figure 1. The mobile manipulator is subjected to the following constraints: $\dot{x}\cos\theta + \dot{y}\sin\theta = 0$. Using Lagrangian

approach, we can obtain the standard form with $q_v = [x, y, \theta]^T$, $q_a = [\theta_1, \theta_2]^T$, $q = [q_v, q_a]^T$, and $A_v = [\cos\theta, \sin\theta, 0]^T$:

$$M_v = \begin{bmatrix} m_{p12} + \dfrac{2I_w \sin^2\theta}{r^2} & -\dfrac{2I_w}{r^2}\sin\theta\cos\theta & -m_{12}d\sin\theta \\ -\dfrac{2I_w}{r^2}\sin\theta\cos\theta & m_{p12} + \dfrac{2I_w\cos^2\theta}{r^2} & m_{12}d\cos\theta \\ -m_{12}d\sin\theta & m_{12}d\cos\theta & M_{11}^1 \end{bmatrix},$$

$$M_{11}^1 = I_p + I_{12} + m_{12}d^2 + \frac{2I_w L^2}{r^2}, \qquad M_a = \operatorname{diag}[I_{12}, I_2],$$

$$M_{va} = \begin{bmatrix} 0.0 & 0.0 \\ 0.0 & 0.0 \\ I_{12} & 0.0 \end{bmatrix},$$

$$B = \begin{bmatrix} \dfrac{\sin\theta}{r} & -\dfrac{\sin\theta}{r} & 0.0 & 0.0 \\ -\dfrac{\cos\theta}{r} & \dfrac{\cos\theta}{r} & 0.0 & 0.0 \\ -\dfrac{l}{r} & \dfrac{l}{r} & 0.0 & 0.0 \\ 0.0 & 0.0 & 1.0 & 0.0 \\ 0.0 & 0.0 & 0.0 & 1.0 \end{bmatrix}, \tag{6.1}$$

$$C_v = \begin{bmatrix} \dfrac{2I_w}{r^2}\dot\theta\sin\theta\cos\theta & \dfrac{2I_w}{r^2}\dot\theta\sin^2\theta & -m_{12}d\dot\theta\cos\theta & 0.0 \\ -\dfrac{2I_w}{r^2}\dot\theta\cos^2\theta & \dfrac{2I_w}{r^2}\dot\theta\sin\theta\cos\theta & m_{12}d\dot\theta\cos\theta & 0.0 \\ 0.0 & 0.0 & 0.0 & 0.0 \end{bmatrix},$$

$$C_{va} = 0.0, \qquad C_a = 0.0, \qquad G_v = [0.0, 0.0, 0.0]^T, \qquad G_a = \left[0.0, m_2 g l_2 \sin\theta_2\right]^T,$$

$$H = \begin{bmatrix} -\tan\theta & 0.0 & 0.0 & 0.0 \\ 1.0 & 0.0 & 0.0 & 0.0 \\ 0.0 & 1.0 & 0.0 & 0.0 \\ 0.0 & 0.0 & 1.0 & 0.0 \\ 0.0 & 0.0 & 0.0 & 1.0 \end{bmatrix},$$

$$\tau_v = [\tau_l, \tau_r]^T, \qquad \tau_a = [\tau_1, \tau_2]^T,$$

$$m_{p12} = m_p + m_{12}, \qquad m_{12} = m_1 + m_2, \qquad I_{12} = I_1 + I_2.$$

Let the desired trajectory $q_d = [x_d, y_d, \theta_d, \theta_{1d}, \theta_{2d}]^T$ and the end effector be subject to the geometric constraint $\Phi = l_1 + l_2\sin(\theta_2) = 0$, and $y_d = 1.5\sin(t)$, $\theta_d = 1.0\sin(t)$, $\theta_{1d} = \pi/4(1 - \cos(t))$, $\lambda_d = 10.0N$.

The trajectory and force tracking control problem is to design control law $\tau$ such that (4.1) holds and all internal signals are bounded.

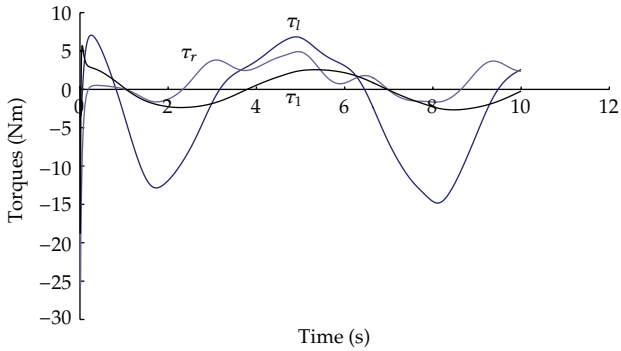


**Figure 4:** The torques of the joints.

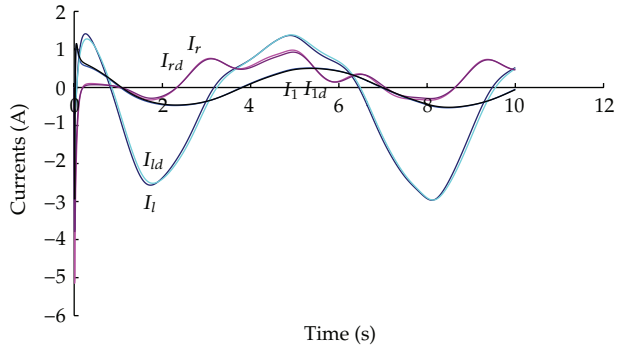


**Figure 5:** Tracking the desired currents.

In the simulation, we assume the parameter $m_p = m_1 = m_2 = 1.0$, $I_w = I_p = 1.0$, $2I_1 = I_2 = 1.0$, $I = 0.5$, $d = L = R = 1.0$, $2l_1 = 1.0$, $2l_2 = 0.6$, $q(0) = [0, 2.0, 0.6, 0.5]^T$, $\dot{q}(0) = [0.0, 0.0, 0.0, 0.0]^T$, $K_N = \text{diag}[0.01]$, $G_r = \text{diag}[100]$, $L_a = [0.005, 0.005, 0.005, 0.005]^T$, $R_a = [2.5, 2.5, 2.5, 2.5]^T$, and $K_e = [0.02, 0.02, 0.02, 0.02]^T$. The disturbance on the mobile base is set $0.1\sin(t)$ and $0.1\cos(t)$. By Theorem 5.1, the control gains are selected as $K_p = \text{diag}[1.0, 1.0, 1.0]$, $k_\xi = \text{diag}[1.0, 1.0, 1.0]$, $K_i = 0.0$ and $K_f = 0.995$, $C = [8.0, 8.0, 8.0, 8.0, 8.0]^T$, $K_N = 0.1$, $K_d = \text{diag}[10, 10, 10, 10]$, $\alpha_1 = 0.008$, $\alpha_2 = 4.0$, $\alpha_3 = 0.03$. The disturbance on the mobile base is set $0.1\sin(t)$ and $0.1\cos(t)$. The simulation results for motion/force are shown in Figures 2, 3, 4, 5, 6, 7, 8, and 9. The desired currents tracking and input voltages on the motors are shown in Figures 5, 6, 8, and 9. The simulation results show that the trajectory and force tracking errors asymptotically tend to zero, which validate the effectiveness of the control law in Theorem 5.1.

## 7. Conclusion

In this paper, effective robust control strategies have been presented systematically to control the holonomic constrained nonholonomic mobile manipulator in the presence of uncertainties and disturbances, and actuator dynamics is considered in the robust control. All control strategies have been designed to drive the system motion converge to the desired

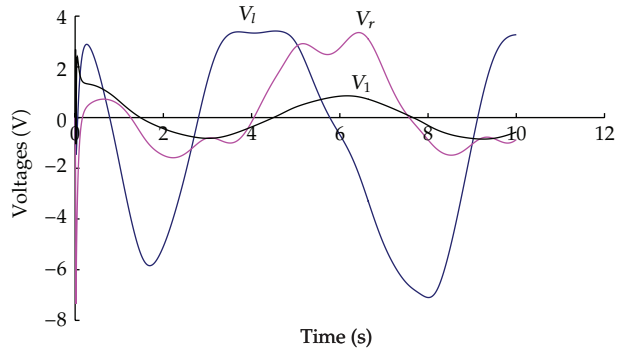


**Figure 6:** The input voltages.

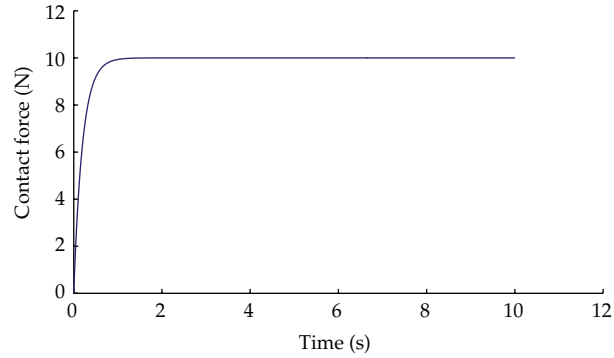


**Figure 7:** The constraint force.

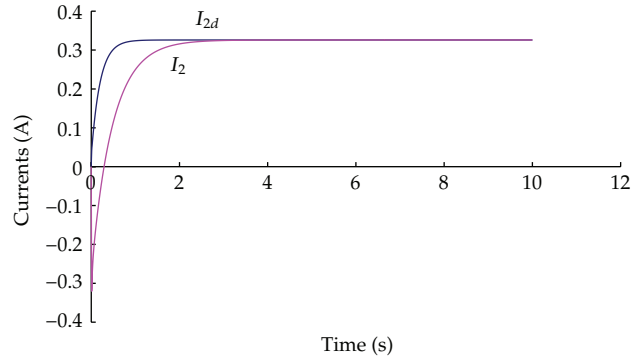


**Figure 8:** Tracking the desired current of the joint 2.

manifold and at the same time guarantee the boundedness of the constrained force. The proposed controls are nonregressor based and require no information on the system dynamics. Simulation studies have verified the effectiveness of the proposed controller.

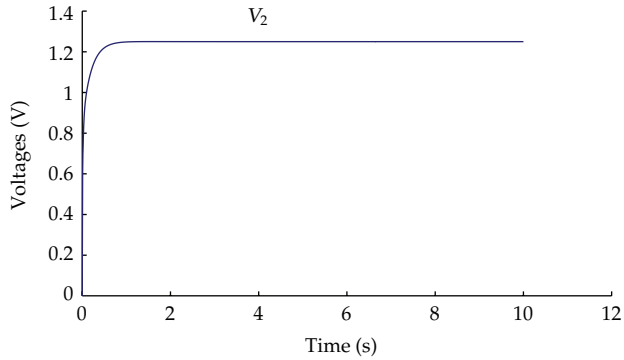


**Figure 9:** The input voltage of the joint 2.

## Acknowledgment

The authors are thankful to the Ministry of Science and Technology of China as the paper is partially sponsored by the National High-Technology Research and Development Program of China (863 Program) (no. 2009AA012201).

## References

[1] Z. Li, P. Y. Tao, S. S. Ge, M. Adams, and W. S. Wijesoma, "Robust adaptive control of cooperating mobile manipulators with relative motion," *IEEE Transactions on Systems, Man, and Cybernetics, Part B*, vol. 39, no. 1, pp. 103–116, 2009.

[2] Z. Li, S. S. Ge, and A. Ming, "Adaptive robust motion/force control of holonomic-constrained nonholonomic mobile manipulators," *IEEE Transactions on Systems, Man, and Cybernetics, Part B*, vol. 37, no. 3, pp. 607–616, 2007.

[3] Z. Li, C. Yang, J. Luo, Z. Wang, and A. Ming, "Robust motion/force control of nonholonomic mobile manipulators using hybrid joints," *Advanced Robotics*, vol. 21, no. 11, pp. 1231–1252, 2007.

[4] Z. Li, A. Ming, N. Xi, J. Gu, and M. Shimojo, "Development of hybrid joints for the compliant arm of human-symbiotic mobile manipulator," *International Journal of Robotics and Automation*, vol. 20, no. 4, pp. 260–270, 2005.

[5] V. A. Pavlov and A. V. Timofeyev, "Construction and stabilization of programmed movements of a mobile robot-manipulator," *Engineering Cybernetics*, vol. 14, no. 6, pp. 70–79, 1976.

[6] J. H. Chung and S. A. Velinsky, "Modeling and control of a mobile manipulator," *Robotica*, vol. 16, no. 6, pp. 607–613, 1998.

[7] K. Watanabe, K. Sato, K. Izumi, and Y. Kunitake, "Analysis and control for an omnidirectional mobile manipulator," *Journal of Intelligent and Robotic Systems*, vol. 27, no. 1-2, pp. 3–20, 2000.

[8] Z. Li, C. Yang, and N. Ding, "Robust adaptive motion control for remotely operated vehicles with velocity constraints," *International Journal of Control, Automation, and System*, vol. 10, no. 2, pp. 421–429, 2012.

[9] Y. Kang, Z. Li, W. Shang, and H. Xi, "Control design for tele-operation system with time-varying and stochastic communication delays," *International Journal of Innovative Computing, Information and Control*, vol. 8, no. 1, pp. 61–74, 2012.

[10] Y. Kang, Z. Li, W. Shang, and H. Xi, "Motion synchronisation of bilateral teleoperation systems with mode-dependent time-varying communication delays," *IET Control Theory & Applications*, vol. 4, no. 10, pp. 2129–2140, 2010.

[11] Z. Li, X. Cao, and N. Ding, "Adaptive fuzzy control for synchronization of nonlinear teleoperators with stochastic time-varying communication delays," *IEEE Transactions on Fuzzy Systems*, vol. 19, no. 4, pp. 745–757, 2011.

[12] Z. Li and W. Chen, "Adaptive neural-fuzzy control of uncertain constrained multiple coordinated nonholonomic mobile manipulators," *Engineering Applications of Artificial Intelligence*, vol. 21, no. 7, pp. 985–1000, 2008.

[13] Z. Li, S. S. Ge, and Z. Wang, "Robust adaptive control of coordinated multiple mobile manipulators," *Mechatronics*, vol. 18, no. 5-6, pp. 239–250, 2008.
[14] Y. Yamamoto and X. Yun, "Effect of the dynamic interaction on coordinated control of mobile manipulators," *IEEE Transactions on Robotics and Automation*, vol. 12, no. 5, pp. 816–824, 1996.
[15] Z. Li, W. Chen, and J. Luo, "Adaptive compliant force-motion control of coordinated non-holonomic mobile manipulators interacting with unknown non-rigid environments," *Neurocomputing*, vol. 71, no. 7–9, pp. 1330–1344, 2008.
[16] Z. Li, J. Gu, A. Ming, C. Xu, and M. Shimojo, "Intelligent compliant force/motion control of non-holonomic mobile manipulator working on the nonrigid surface," *Neural Computing and Applications*, vol. 15, no. 3-4, pp. 204–216, 2006.
[17] Y. Yamamoto and X. Yun, "Coordinating locomotion and manipulation of a mobile manipulator," *IEEE Transactions on Automatic Control*, vol. 39, no. 6, pp. 1326–1332, 1994.
[18] O. Khatib, "Mobile manipulation: the robotic assistant," *Robotics and Autonomous Systems*, vol. 26, no. 2-3, pp. 175–183, 1999.
[19] B. Bayle, J. Y. Fourquet, and M. Renaud, "Manipulability of wheeled mobile manipulators: application to motion generation," *International Journal of Robotics Research*, vol. 22, no. 7-8, pp. 565–581, 2003.
[20] J. Tan, N. Xi, and Y. Wang, "Integrated task planning and control for mobile manipulators," *International Journal of Robotics Research*, vol. 22, no. 5, pp. 337–354, 2003.
[21] S. Lin and A. A. Goldenberg, "Neural-network control of mobile manipulators," *IEEE Transactions on Neural Networks*, vol. 12, no. 5, pp. 1121–1133, 2001.
[22] Z. Li, C. Yang, and J. Gu, "Neuro-adaptive compliant force/motion control of uncertain constrained wheeled mobile manipulators," *International Journal of Robotics and Automation*, vol. 22, no. 3, pp. 206–214, 2007.
[23] W. Dong, "On trajectory and force tracking control of constrained mobile manipulators with parameter uncertainty," *Automatica*, vol. 38, no. 9, pp. 1475–1484, 2002.
[24] Z. Li, S. S. Ge, M. Adams, and W. S. Wijesoma, "Robust adaptive control of uncertain force/motion constrained nonholonomic mobile manipulators," *Automatica*, vol. 44, no. 3, pp. 776–784, 2008.
[25] M. C. Good, L. M. Sweet, and K. L. Strobel, "Dynamic models for control system design of integrated robot and drive systems," *Journal of Dynamic Systems, Measurement and Control*, vol. 107, no. 1, pp. 53–59, 1985.
[26] Z. Li, S. S. Ge, M. Adams, and W. S. Wijesoma, "Adaptive robust output-feedback motion/force control of electrically driven nonholonomic mobile manipulators," *IEEE Transactions on Control Systems Technology*, vol. 16, no. 6, pp. 1308–1315, 2008.
[27] Z. Li, J. Li, and Y. Kang, "Adaptive robust coordinated control of multiple mobile manipulators interacting with rigid environments," *Automatica*, vol. 46, no. 12, pp. 2028–2034, 2010.
[28] J. H. Yang, "Adaptive robust tracking control for compliant-join mechanical arms with motor dynamics," in *Proceedings of the 38th IEEE Conference on Decision & Control*, pp. 3394–3399, December 1999.
[29] R. Colbaugh and K. Glass, "Adaptive regulation of rigid-link electrically-driven manipulators," in *Proceedings of the IEEE International Conference on Robotics & Automation. Part 1*, pp. 293–299, May 1995.
[30] C. Y. Su and Y. Stepanenko, "Hybrid adaptive/robust motion control of rigid-link electrically-driven robot manipulators," *IEEE Transactions on Robotics & Automation*, vol. 11, no. 3, pp. 426–432, 1995.
[31] Z. P. Wang, S. S. Ge, and T. H. Lee, "Robust motion/force control of uncertain holonomic/non-holonomic mechanical systems," *IEEE/ASME Transactions on Mechatronics*, vol. 9, no. 1, pp. 118–123, 2004.
[32] S. S. Ge, J. Wang, T. H. Lee, and G. Y. Zhou, "Adaptive robust stabilization of dynamic nonholonomic chained systems," *Journal of Robotic Systems*, vol. 18, no. 3, pp. 119–133, 2001.
[33] S. S. Ge, Z. Wang, and T. H. Lee, "Adaptive stabilization of uncertain nonholonomic systems by state and output feedback," *Automatica*, vol. 39, no. 8, pp. 1451–1460, 2003.
[34] W. Dong, W. L. Xu, and W. Huo, "Trajectory tracking control of dynamic non-holonomic systems with unknown dynamics," *International Journal of Robust and Nonlinear Control*, vol. 9, no. 13, pp. 905–922, 1999.
[35] Z. Li, Y. Yang, and J. Li, "Adaptive motion/force control of mobile under-actuated manipulators with dynamics uncertainties by dynamic coupling and output feedback," *IEEE Transactions on Control Systems Technology*, vol. 18, no. 5, pp. 1068–1079, 2010.
[36] Z. Li and C. Xu, "Adaptive fuzzy logic control of dynamic balance and motion for wheeled inverted pendulums," *Fuzzy Sets and Systems*, vol. 160, no. 12, pp. 1787–1803, 2009.
[37] Z. Li and J. Luo, "Adaptive robust dynamic balance and motion controls of mobile wheeled inverted pendulums," *IEEE Transactions on Control Systems Technology*, vol. 17, no. 1, pp. 233–241, 2009.

[38] Y. Kang, Z. Li, Y. Dong, and H. Xi, "Markovian-based fault-tolerant control for wheeled mobile manipulators," *IEEE Transactions on Control Systems Technology*, vol. 20, no. 1, pp. 266–276, 2012.
[39] Z. Li, "Adaptive fuzzy output feedback motion/force control for wheeled inverted pendulums," *IET Control Theory & Applications*, vol. 5, no. 10, pp. 1176–1188, 2011.
[40] Z. Li and Y. Kang, "Dynamic coupling switching control incorporating support vector machines for wheeled mobile manipulators with hybrid joints," *Automatica*, vol. 46, no. 5, pp. 832–842, 2010.
[41] Z. Li and Y. Zhang, "Robust adaptive motion/force control for wheeled inverted pendulums," *Automatica*, vol. 46, no. 8, pp. 1346–1353, 2010.
[42] Z. Li, Y. Zhang, and Y. Yang, "Support vector machine optimal control for mobile wheeled inverted pendulums with unmodelled dynamics," *Neurocomputing*, vol. 73, no. 13–15, pp. 2773–2782, 2010.
[43] Z. Li, J. Zhang, and Y. Yang, "Motion control of mobile under-actuated manipulators by implicit function using support vector machines," *IET Control Theory & Applications*, vol. 4, no. 11, pp. 2356–2368, 2010.
[44] C. Y. Su and Y. Stepanenko, "Robust motion/force control of mechanical systems with classical nonholonomic constraints," *IEEE Transactions on Automatic Control*, vol. 39, no. 3, pp. 609–614, 1994.
[45] N. H. McClamroch and D. Wang, "Feedback stabilization and tracking of constrained robots," *IEEE Transactions on Automatic Control*, vol. 33, no. 5, pp. 419–426, 1988.
[46] S. S. Ge, Z. Li, and H. Yang, "Data driven adaptive predictive control for holonomic constrained under-actuated biped robots," *IEEE Transactions on Control Systems Technology*, vol. 20, no. 3, pp. 787–795, 2012.
[47] C. M. Anupoju, C. Y. Su, and M. Oya, "Adaptive motio tracking control of uncertainonholonomic mechanical systems including actuator dynamics," *IEE Proceedings Control Theory & Applications*, vol. 152, no. 5, pp. 575–580, 2005.

Hindawi Publishing Corporation
Journal of Applied Mathematics
Volume 2012, Article ID 414315, 24 pages
doi:10.1155/2012/414315

*Research Article*

# Adaptive Sliding Mode Control of Mobile Manipulators with Markovian Switching Joints

**Liang Ding, Haibo Gao, Kerui Xia, Zhen Liu, Jianguo Tao, and Yiqun Liu**

*State Key Laboratory of Robotics and System, Harbin Institute of Technology, Harbin 150080, China*

Correspondence should be addressed to Liang Ding, liangding@hit.edu.cn

Received 22 February 2012; Accepted 6 April 2012

Academic Editor: Xianxia Zhang



The hybrid joints of manipulators can be switched to either active (actuated) or passive (underactuated) mode as needed. Consider the property of hybrid joints, the system switches stochastically between active and passive systems, and the dynamics of the jump system cannot stay on each trajectory errors region of subsystems forever; therefore, it is difficult to determine whether the closed-loop system is stochastically stable. In this paper, we consider stochastic stability and sliding mode control for mobile manipulators using stochastic jumps switching joints. Adaptive parameter techniques are adopted to cope with the effect of Markovian switching and nonlinear dynamics uncertainty and follow the desired trajectory for wheeled mobile manipulators. The resulting closed-loop system is bounded in probability and the effect due to the external disturbance on the tracking errors can be attenuated to any preassigned level. It has been shown that the adaptive control problem for the Markovian jump nonlinear systems is solvable if a set of coupled linear matrix inequalities (LMIs) have solutions. Finally, a numerical example is given to show the potential of the proposed techniques.

## 1. Introduction

The hybrid joint shown in Figure 1 was first proposed in [1–5], which is with one clutch and one brake. When the clutch is released, the link is free, and the passive link is directly controlled by the dynamic coupling of mobile manipulators; when it is on, the joint is actuated by the motor. Moreover, the passive link can be locked by the brake embedded in the joint as needed. The robot with hybrid joints is called the hybrid actuated robot.

One of the advantages of using hybrid actuated robots is that they may consume less energy than the fully-actuated ones. For example, hyperredundant robots, such as snake-like robots or multilegged mobile robots [6], need large redundancy for dexterity and specific task

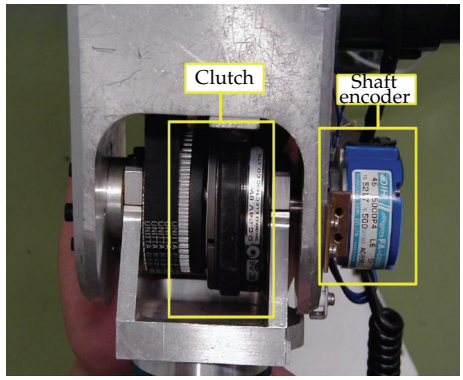


**Figure 1:** The hybrid joint.

completion while underactuation structure allows a more compact design and much simpler control and communication schemes. The hybrid actuated robot concept is also useful for the reliability or fault-tolerant design of fully-actuated robots working in hazardous areas or with dangerous materials. If any of the joint actuators of such a device fails, one degree of freedom of the system would be lost. It is important, in these cases, that the passive (failed) joint can still be controlled via the dynamic coupling with the active ones, so the system can still make use of all of its degrees of freedom originally planned.

Hybrid actuated mobile manipulator is the robot manipulator consisting of hybrid joints mounting on a wheeled mobile robot, which first appeared in [1–5]. Hybrid actuated mobile manipulators are different from full-actuated mobile manipulators in [7–26], due to simultaneously integrating both kinematic constraints and dynamic constraints. For these reasons, increasing effort needs to be made towards control design that guarantee stability and robustness for hybrid actuated mobile manipulators with the consideration of joint switching. The hybrid joint is also with the characteristic of underactuated the joints [27–34], for example, the hybrid joints in the free mode, which can rotate freely, can be indirectly driven by the effect of the dynamic coupling between the active and passive joints. The zero torque at the hybrid joints results in a second-order nonholonomic constraint [35, 36].

The mobile manipulator using Markovian switching hybrid joint can be loosely defined as a system that involves the interaction of both discrete events (represented by finite automata) and continuous-time dynamics (represented by differential equations). The joint switching seems to be stochastic and the switching may appear in any joints of the robot which need to develop Markovian jump linear system (MJLS) [37] to incorporate abrupt changes in the joints of mobile manipulators and use the Markovian jumping systems to guarantee the stochastic stability. Therefore, the discrete part (switching part) can be regarded as a continuous-time Markov process representing the modes of the system and the continuous part represents the dynamics state of the system, which evolves according to the differential dynamic equation when the mode is fixed. The hybrid formulation provides a powerful framework for modeling and analyzing the systems subject to abrupt joint switching variations, which are partly due to the inherently vulnerability to abrupt changes caused by component failures, sudden environmental disturbances, abrupt variation of the operation point of mobile manipulator, and so on.

The joint switching seems to be stochastic and the switching may appear in any joints of the robot, while simple switching approach cannot handle all the possibility. In this paper,

to avoid the necessity of stopping the robot as the joint switches, MJLS method used to model and analyze switching robotic systems is an effective but challenging work.

To our best knowledge, there are few works considering MJLS method used to model and analyze switching robotic systems. In this paper, we consider the problem of adaptive control for stochastic jump systems with matched uncertainties and disturbances. The jumping parameters are treated as continuous-time discrete-state Markov process. Note that adaptive control method is one of the most popular techniques of nonlinear control design [8]. However, adaptive control for stochastic nonlinear mechanical dynamics systems with Markovian switching has received relatively little attention. Therefore, this paper will be concerned with the design of adaptive control for mobile manipulators using Markovian switching joints. There exist parameter uncertainties, nonlinearities, and external disturbance in the systems and environments under consideration. First, we design a reduced model for the wheeled mobile manipulator with switching joints. After introducing continuous-time Markov chain, adaptive control is adopted to cope with the effect of Markovian switching and nonlinear dynamics uncertainty and drive wheeled mobile manipulators following the desired trajectory. The resulting closed-loop system is bounded in probability and the effect due to the external disturbance on the tracking error can be attenuated to any pre-assigned level. Moreover, unknown upper bounds of dynamics uncertainties and disturbances can be estimated by adaptive updated law. The mechanical system with matched disturbances and Markov jumping is solved in terms of a finite set of coupled LMIs. It has been shown that the adaptive control problem for the Markovian jump nonlinear systems is solvable if a set of coupled LMIs have solutions. Finally, a numerical example is given to show the potential of the proposed techniques.

The main contributions of this paper lie in:

(i) developing a reduced model for mobile manipulators such that it could be transformed into the framework of MJLS with modeling system dynamics uncertainties;

(ii) designing an adaptive sliding mode control (SMC) for wheeled mobile manipulators with hybrid joints with Markovian switching;

(iii) the system with matched disturbances and Markov jumping is solved in terms of a finite set of coupled LMIs.

## 2. Preliminary

**Lemma 2.1** (see [38]). *Let $e = H(s)r$ with $H(s)$ representing an $(n \times m)$-dimensional strictly proper exponentially stable transfer function, $r$ and $e$ denoting its input and output, respectively. Then $r \in L_2^m \bigcap L_\infty^m$ implies that $e, \dot{e} \in L_2^n \bigcap L_\infty^n$, $e$ is continuous, and $e \to 0$ as $t \to \infty$. If, in addition, $r \to 0$ as $t \to \infty$, then $\dot{e} \to 0$.*

**Lemma 2.2** (see [39]). *For the matrix $A$ and $B$ with appropriate dimensions, if $(I + AB)$ is nonsingular, then $(I + AB)^{-1} = I - A(I + BA)^{-1}B$.*

**Theorem 2.3.** *Given a Markov jump linear system with the system parameter matrices $A_i$, $B_i$, $C_i$, $D_i$, and $I > \eta^2 D_i^T D_i$, for $\eta \geq 0$, $\Phi(t)$ is unknown but satisfying $\|\Phi(t)\| \leq \eta$,*

$$\dot{x} = \left[A_i + B_i[I - \Phi(t)D_i]^{-1}\Phi(t)C_i\right]x, \tag{2.1}$$

*if there exits $P_i > 0$ satisfies the following inequality for each $i \in S = 1, 2, \ldots, N$,*

$$\begin{bmatrix} P_iA_i + A_i^TP_i + \sum_{j=1}^{N}\pi_{ij}P_j & \eta P_iB_i & C_i^T \\ \eta B_i^TP_i^T & -I & \eta D_i^T \\ C_i & \eta D_i & -I \end{bmatrix} < 0, \tag{2.2}$$

*then the system* (2.1) *is stable in the mean square sense.*

*Proof.* If there exists a positive definite matrix $P_i$ satisfying Lyapunov inequality (2.3), then the indefinite system (2.1) is asymptotically stable:

$$P_iA_i + A_i^TP_i + P_iB_i[I - \Phi(t)D_i]^{-1}\Phi(t)C_i + \left(A_i + B_i[I - \Phi(t)D_i]^{-1}\Phi(t)C_i\right)^TP_i^T + \sum_{j=0}^{N}\pi_{ij}P_j < 0. \tag{2.3}$$

Let $p_i = [I - \Phi(t)D_i]^{-1}\Phi(t)C_ix$, then $p_i$ can be represented as $p_i = \Phi(t)[C_ix + D_ip_i]$. Then, from the inequality $\|\Phi(t)\| \le \eta$, we can achieve $p_i^Tp_i \le \eta^2[C_ix + D_ip_i]^T[C_ix + D_ip_i]$. Since

$$\begin{aligned} 2x^TP_iB_i(I - \Phi(t)D_i)^{-1}\Phi(t)C_ix &= 2x^TP_iB_ip_i \\ &\le 2x^TP_iB_ip_i + [C_ix + D_ip_i]^T[C_ix + D_ip_i] - \eta^{-2}p_i^Tp_i \\ &= x^TC_i^TC_ix + 2x^T\left[P_iB_i + C_i^TD_i\right]p_i \\ &\quad - \eta^{-2}p_i^T\left[I - \eta^2D_i^TD_i\right]p_i. \end{aligned} \tag{2.4}$$

Assume that $a_i^T = x^T(P_iB_i + C_i^TD_i)$, $b_i = p_i$, $W_i = \eta^2(I - \eta^2D_i^TD_i)^{-1}$, using inequality (2.4) and Lemma 2.1, there is

$$\begin{aligned} &2x^TP_iB_i(I - \Phi(t)D_i)^{-1}\Phi(t)C_ix \\ &\quad \le x^TC_i^TC_ix + \eta^2x^T\left(P_iB_i + C_i^TD_i\right)\left(I - \eta^2D_i^TD_i\right)^{-1}\left(P_iB_i + C_i^TD_i\right)^Tx. \end{aligned} \tag{2.5}$$

If the following inequality stands, then inequality (2.3) holds:

$$P_iA_i + A_i^TP_i + \sum_{j=0}^{N}\pi_{ij}P_j + C_i^TC_i + \eta^2\left(P_iB_i + C_i^TD_i\right)\left(I - \eta^2D_i^TD_i\right)^{-1}\left(P_iB_i + C_i^TD_i\right)^T < 0. \tag{2.6}$$

With Schur Complement, it is easy to transfer (2.6) into (2.2), namely, the system (2.1) is stable. The proof is completed. □

*Definition 2.4.* A stochastic process $v(t)$ is said to be bounded in probability if the random variables $|v(t)|$ are bounded in probability uniformly in $t$, that is,

$$\lim_{r\to\infty}\sup_{t>0} P|v(t)| > r = 0. \tag{2.7}$$

## 3. System Description

### 3.1. Dynamics

Consider an $n_a$ DOF robotic manipulator mounted on a two-wheeled driven mobile platform, the dynamics can be described as:

$$M(q)\ddot{q} + V(q,\dot{q})\dot{q} + G(q) + d(t) = B(q)\tau + f, \tag{3.1}$$

where $q = [q_v^T, q_a^T]^T \in \mathbb{R}^n$ with $q_v = [x, y, \vartheta]^T \in \mathbb{R}^{n_v}$ denoting the generalized coordinates for the mobile platform and $q_a \in \mathbb{R}^{n_a}$ denoting the coordinates of the robotic manipulator joints, and $n = n_v + n_a$. The symmetric positive definite inertia matrix $M(q) \in \mathbb{R}^{n\times n}$, the Centripetal and Coriolis torques $V(q,\dot{q}) \in \mathbb{R}^{n\times n}$, the gravitational torque vector $G(q) \in \mathbb{R}^n$, the known input transformation matrix $B(q) \in \mathbb{R}^{n\times m}$, the control inputs $\tau \in \mathbb{R}^m$, and the generalized constraint forces $f \in \mathbb{R}^n$ could be represented as, respectively,

$$\begin{aligned} M(q) &= \begin{bmatrix} M_v & M_{va} \\ M_{av} & M_a \end{bmatrix}, \qquad V(q,\dot{q}) = \begin{bmatrix} V_v & V_{va} \\ V_{av} & V_a \end{bmatrix}, \qquad f = \begin{bmatrix} J_v^T\lambda_n \\ 0 \end{bmatrix}, \\ G(q) &= \begin{bmatrix} G_v \\ G_a \end{bmatrix}, \qquad B(q)\tau = \begin{bmatrix} \tau_v \\ \tau_a \end{bmatrix}, \qquad d(t) = \begin{bmatrix} d_v \\ d_a \end{bmatrix}, \end{aligned} \tag{3.2}$$

where $M_v$ and $M_a$ describe the inertia matrices for the mobile platform and the links, respectively, $M_{va}$ and $M_{av}$ are the coupling inertia matrices of the mobile platform and the links; $V_v$, $V_a$ denote the Centripetal and Coriolis torques for the mobile platform, the links, respectively; $V_{va}$, $V_{av}$ are the coupling Centripetal and Coriolis torques of the mobile platform, the links. $G_v$ and $G_a$ are the gravitational torque vectors for the mobile platform, the links, respectively; $\tau_v$ is the input vector associated with the left driven wheel and the right driven wheel, respectively; and $\tau_a$ are the control input vectors for the joints of the manipulator; $d_v$, $d_a$ denote the external disturbances on the mobile platform, the links, respectively; $J_v \in \mathbb{R}^{l\times n_v}$ is the kinematic constraint matrix related to nonholonomic constraints; $\lambda_n \in \mathbb{R}^l$ is the associated Lagrangian multipliers with the generalized nonholonomic constraints. We assume that the mobile manipulator is subject to known nonholonomic constraints. A method of modeling the dynamics of wheeled robots considering wheel-soil interaction mechanics is presented in [40, 41]. For the reason of simplification, we can adopt the methods of producing enough friction between the wheels of the mobile platform and the ground.

### 3.2. Reduced System

When the system is subjected to nonholonomic constraints, the $(n - m)$ nonintegrable and independent velocity constraints can be expressed as

$$J_v(q)\dot{q}_v = 0. \tag{3.3}$$

The constraint (3.3) is referred to as the classical nonholonomic constraint when it is not integrable. In the paper, constraint (3.3) is assumed to be completely nonholonomic and exactly known.

Since $J_v(q) \in \mathbb{R}^{(n_v-m)\times n}$ introduce $J_a \in \mathbb{R}^{n_a \times n}$, and $J = [J_v, J_a]^T \in \mathbb{R}^{(n-m)\times n}$, such that it is possible to find a $m + n_a$ rank matrix $R(q) \in \mathbb{R}^{n\times(m+n_a)}$ formed by a set of smooth and linearly independent vector fields spanning the null space of $J(q)$, that is,

$$R^T(q)J^T(q) = 0, \tag{3.4}$$

where $R(q) = [r_1(q), \ldots, r_m(q), r_{m+1}(q), \ldots, r_{m+n_a}(q)]$. Define an auxiliary time function $\dot{z}(t) \in \mathbb{R}^{m+n_a}$, and $\dot{z}(t) = [\dot{z}_1(t), \ldots, \dot{z}_m(t), \dot{z}_{m+1}(t), \ldots, \dot{z}_{m+n_a}(t)]^T$ such that

$$\dot{q} = R(q)\dot{z}(t) = r_1(q)\dot{z}_1(t) + \cdots + r_m(q)\dot{z}_m(t) + r_{m+1}(q)\dot{z}_{m+1}(t) + \cdots + r_{m+n_a}(q)\dot{z}_{m+n_a}(t). \tag{3.5}$$

Equation (3.5) is the kinematic model for the wheeled inverted pendulums. Usually, $\dot{z}(t)$ has physical meaning, consisting of the angular velocity $\omega$, the linear velocity $v$, and the joint angle vector $\theta_a$, that is, $\dot{z}(t) = [v\ \omega\ \dot{\theta}_a^T]^T$. Equation (3.5) describes the kinematic relationship between the motion vector $q$ and the velocity vector $\dot{z}(t)$.

Differentiating (3.5) yields

$$\ddot{q} = \dot{R}(q)\dot{z} + R(q)\ddot{z}. \tag{3.6}$$

From (3.5), $\dot{z}$ can be obtained from $q$ and $\dot{q}$ as

$$\dot{z} = \left[R^T(q)R(q)\right]^{-1}R^T(q)\dot{q}. \tag{3.7}$$

The dynamic equation (3.1), which satisfies the nonholonomic constraint (3.3), can be rewritten in terms of the internal state variable $\dot{z}$ as

$$M(q)R(q)\ddot{z} + V^*\dot{z} + G(q) + d(t) = B(q)\tau + J^T(q)\lambda, \tag{3.8}$$

with $V^* = [M(q)\dot{R}(q) + V(q,\dot{q})R(q)]$, $\lambda = [\lambda_n, 0]^T$.

**Table 1:** The modes of operation.

| Mode | The modes of hybrid joints | | | | | |
|---|---|---|---|---|---|---|
| | Right wheel | Left wheel | Joint 1 | Joint 2 | ⋯ | Joint $n_a$ |
| 1 | normal | normal | normal | normal | ⋯ | normal |
| 2 | normal | underactuated | normal | normal | ⋯ | normal |
| 3 | normal | underactuated | underactuated | normal | ⋯ | normal |
| 4 | normal | underactuated | normal | underactuated | ⋯ | normal |
| ⋮ | ⋮ | ⋮ | ⋮ | ⋮ | ⋮ | ⋮ |
| $2^{n_a+1}$ | normal | underactuated | underactuated | underactuated | ⋯ | underactuated |

Substituting (3.5) and (3.6) into (3.1), and then premultiplying (3.1) by $R^T(q)$, the constraint matrix $J^T(q)\lambda$ can be eliminated by virtue of (3.4). As a consequence, we have the transformed nonholonomic system

$$\mathcal{M}(q)\ddot{z} + \mathcal{V}(q,\dot{q})\dot{z} + \mathcal{G}(q) + \mathfrak{D} = \mathcal{U}, \tag{3.9}$$

where $\mathcal{M}(q) = R^T M(q) R$, $\mathcal{V}(q,\dot{q}) = R^T[M(q)\dot{R} + V(q,\dot{q})R]$, $\mathcal{G}(q) = R^T G(q)$, $\mathfrak{D} = R^T d(t)$, $\mathcal{U} = R^T B(q)\tau$, which is more appropriate for the controller design as the constraint $\lambda$ has been eliminated from the dynamics.

*Remark 3.1.* In this paper, we choose $z = [\theta_r\ \theta_l\ \theta_1\ \theta_2, \ldots, \theta_{n_a}]^T$, where $\theta_r$, $\theta_l$ denote the rotation angle of the left wheel and the right wheel of the mobile platform, respectively, and $\theta_1, \ldots, \theta_{n_a}$ denote the joint angles of the link $1, 2, \ldots, n_a$, respectively, and $\tau = [\tau_r, \tau_l, \tau_1, \ldots, \tau_{n_a}]$.

*Remark 3.2.* The total degree of freedom for a two-wheeled driven mobile manipulator is $n_q = n_a + 2$.

### 3.3. Switching Dynamics

The hybrid joint is within each actuator of the wheels and links of the mobile manipulator, such that switching may appear in every joint independently. Since the left wheel and right wheel are symmetric, for simplification, we assume that the switching appears in the left wheel and each joint of the manipulator independently. Therefore, there are $2^{n_a+1}$ modes of operation, which are listed in Table 1 depending on which hybrid joint is in the active (actuated) or passive (underactuated) mode.

Let $h_p$ be the number of passive hybrid joints that have not already reached their set point in a given instant. If $h_p > h_a$, $h_a$ passive joints are controlled and grouped in the vector $z_p \in \mathbb{R}^{h_a}$, the remaining passive hybrid joints, if any, are kept locked by the brakes, and the active joints are grouped in the vector $z_a \in \mathbb{R}^{h_a}$. If $h_p < h_a$, the $h_p$ passive hybrid joints are controlled applying torques in $h_a$ active hybrid joints. In this case, $z_p \in \mathbb{R}^{h_p}$ and $z_a \in \mathbb{R}^{h_a}$. The strategy is to control all passive hybrid joints until they reach the desired position, considering the conditions exposed above, and then turn on the clutch. After that, all the active hybrid joints are controlled by themselves as a fully-actuated robot.

The dynamics (3.9) can be partitioned into two parts, the actuated part and the passive part, represented by "$a$" and "$p$," respectively. Then we can rewrite the dynamics (3.9) as

$$\begin{bmatrix} \mathcal{M}_a(\zeta) & \mathcal{M}_{ap}(\zeta) \\ \mathcal{M}_{pa}(\zeta) & \mathcal{M}_p(\zeta) \end{bmatrix} \begin{bmatrix} \ddot{z}_a \\ \ddot{z}_p \end{bmatrix} + \begin{bmatrix} \mathcal{V}_a & \mathcal{V}_{ap} \\ \mathcal{V}_{pa} & \mathcal{V}_p \end{bmatrix} \begin{bmatrix} \dot{z}_a \\ \dot{z}_p \end{bmatrix} + \begin{bmatrix} \mathcal{G}_a \\ \mathcal{G}_p \end{bmatrix} + \begin{bmatrix} \mathfrak{D}_a(t) \\ \mathfrak{D}_p(t) \end{bmatrix} = \begin{bmatrix} \mathcal{U}_a \\ \mathcal{U}_p \end{bmatrix}, \tag{3.10}$$

where

(i) $\mathcal{M}_a \in \mathbb{R}^{h_a \times h_a}$, $\mathcal{M}_p \in \mathbb{R}^{h_p \times h_p}$: the inertia matrices of the actuated parts and the passive parts, respectively;

(ii) $\mathcal{M}_{ap} \in \mathbb{R}^{h_a \times h_p}$, $\mathcal{M}_{pa} \in \mathbb{R}^{h_p \times h_a}$: the coupling inertia matrices of the actuated parts and the passive parts, respectively;

(iii) $\mathcal{V}_a \in \mathbb{R}^{h_a \times h_a}$, $V_p \in \mathbb{R}^{h_p \times h_p}$: the Centripetal and Coriolis torque matrices of the actuated parts and the passive parts, respectively;

(iv) $\mathcal{V}_{ap} \in \mathbb{R}^{h_a \times h_p}$, $\mathcal{V}_{pa} \in \mathbb{R}^{h_p \times h_a}$: the coupling Centripetal and Coriolis torques of the actuated parts and the passive parts, respectively;

(v) $\mathcal{G}_a \in \mathbb{R}^{h_a}$, $\mathcal{G}_p \in \mathbb{R}^{h_p}$: the gravitational torque vector for the actuated parts and the passive parts, respectively;

(vi) $\mathfrak{D}_a(t) \in \mathbb{R}^{h_a}$, $\mathfrak{D}_p(t) \in \mathbb{R}^{h_p}$: the bounded external disturbance from the environments on the actuated parts and the passive parts, respectively;

(vii) $\mathcal{U}_a \in \mathbb{R}^{h_a}$: the control input torque vector for the actuated parts of the joints;

(viii) $\mathcal{U}_p \in \mathbb{R}^{h_p}$: the control input torque vector for the passive parts of the joints satisfying $\mathcal{U}_p = 0$.

After some simple manipulation, we can further obtain

$$\mathcal{U}_a = \overline{M}(z)\ddot{z}_p + \overline{H}(z, \dot{z}) + \overline{D}(t), \tag{3.11}$$

where

$$\begin{aligned} \overline{M} &= \mathcal{M}_a - \mathcal{M}_a \mathcal{M}_{pa}^{-1} \mathcal{M}_p, \\ \overline{H} &= \overline{V}_1 \dot{z}_a + \overline{V}_2 \dot{z}_p + \mathcal{G}_a - \mathcal{M}_a \mathcal{M}_{pa}^{-1} \mathcal{G}_p, \\ \overline{D}(t) &= \mathfrak{D}_a - \mathcal{M}_a \mathcal{M}_{pa}^{-1} \mathfrak{D}_p, \\ \overline{V}_1 &= V_a - \mathcal{M}_a \mathcal{M}_{pa}^{-1} V_{pa}, \\ \overline{V}_2 &= V_{ap} - \mathcal{M}_a \mathcal{M}_{pa}^{-1} V_p. \end{aligned} \tag{3.12}$$

## 4. Control Design

### 4.1. Model-Based Control with Unmodeled Dynamics

Define the tracking errors as

$$\begin{aligned} e &= z_p - z_{pd}, \\ \dot{e} &= \dot{z}_p - \dot{z}_{pd}, \end{aligned} \tag{4.1}$$

where $\ddot{z}_{pd}$, $\dot{z}_{pd}$ and $z_{pd}$ denote the desired trajectories vectors of passive joint accelerations, velocities, and positions, respectively.

The parameters $\overline{M}$, $\overline{H}$, and $\overline{D}(t)$ in dynamical model (3.11) are functions of physical parameters of mobile manipulators like links masses, links lengths, moments of inertial, and so on. The precise values of these parameters are difficult to acquire due to measuring errors and environment and payloads variations. Therefore, it is assumed that actual value $\overline{M}$, $\overline{H}$, and $\overline{D}(t)$ can be separated as nominal parts denoted by $\overline{M}_0$, $\overline{H}_0$, and $\overline{D}_0(t)$ and uncertain parts denoted by $\Delta\overline{M}$, $\Delta\overline{H}$, and $\Delta\overline{D}(t)$, respectively. These variables satisfy the following relationships:

$$\begin{aligned} \overline{M} &= \overline{M}_0 + \Delta M, \\ \overline{H} &= \overline{H}_0 + \Delta H, \\ \overline{D} &= \overline{D}_0 + \Delta D. \end{aligned} \tag{4.2}$$

Suppose that the dynamical models of robot manipulators are known precisely and unmodeled dynamics are excluded, that is, $\Delta M$, $\Delta H$, and $\Delta D$ in (3.11) are all zeros. At this time, dynamical models (3.11) can be converted into the following nominal models:

$$\overline{M}_0(z)\ddot{z}_p + \overline{H}_0(z, \dot{z}) + \overline{D}_0 = \mathcal{U}_0. \tag{4.3}$$

Consider the control law as

$$\mathcal{U}_0 = \overline{M}_0(z)\left(\ddot{z}_{pd} - K_v\dot{e} - K_p e\right) + \overline{H}_0(z, \dot{z}) + \overline{D}_0, \tag{4.4}$$

where $K_v$ and $K_p$ are positive definite matrices. Substituting (4.4) into (4.3) yields

$$\ddot{e} + K_v\dot{e} + K_p e = 0. \tag{4.5}$$

From Lemma 2.1, it is obvious that errors $\dot{e}$ and $\ddot{e}$ will asymptotically if proportional gain $K_p$ and derivative gain $K_v$ are chosen in the favorable situation.

According to (4.4), the proposed control is effective based on the strong assumptions that exact knowledge of robot dynamics is precisely known and unmodeled dynamics has to be ignored, which is difficult to obtain in practices. Therefore, we need to approximate dynamics nonlinear functions. One can imagine that model-based control is used to control

nominal system and another adaptive based control attaching to model-based control for uncertain system can be designed. In this way, applying (4.4) to original systems (3.11) yields

$$\ddot{e} + K_v\dot{e} + K_p e = \Xi, \tag{4.6}$$

$$\Xi = -\overline{M}_0^{-1}\left(\Delta M\ddot{z}_p + \Delta H(z,\dot{z}) + \Delta D(t)\right), \tag{4.7}$$

which $\Xi$ is a function of joint variables, physical parameters, parameters variations, unmodeled dynamics, and so on and denotes the structured uncertainty and unstructured uncertainty.

Up to now, the control objective can be restated as: seek a control law based on nominal parameters and adaptive-based compensator such that joint motions of robotic systems (3.11) can follow desired trajectories. The overall control law can be written as

$$\mathcal{U}_a = \mathcal{U}_0 + \mathcal{U}_c, \tag{4.8}$$

where $\mathcal{U}_c$ is an adaptive-based controller serving as a compensator for model-based control and designed later. Using control law (4.8), the closed-loop system becomes:

$$\ddot{e} + K_v\dot{e} + K_p e = \overline{M}_0^{-1}\mathcal{U}_c + \Xi. \tag{4.9}$$

Supposed that the state vector is defined as $x = [e^T, \dot{e}^T]^T$, the state space equation has form as

$$\dot{x} = Ax + BU, \tag{4.10}$$

$$A = \begin{bmatrix} 0 & I \\ -K_p & -K_v \end{bmatrix}, \qquad B = \begin{bmatrix} 0 \\ I \end{bmatrix}, \qquad U = \overline{M}_0^{-1}\mathcal{U}_c + \Xi. \tag{4.11}$$

### 4.2. Stochastic Control Design

Since the hybrid joints can be switched among different modes, considering the Markovian jumping, we can rewrite (4.10) by integrating Markovian jumping parameters as

$$\dot{x}(t) = A(r_t)x(t) + B(r_t)U, \tag{4.12}$$

where $r_t = j$, and $j$ is one of the Markovian jumping parameters in the limited set $S = \{1, 2, \ldots, N\}$ with the mode transition rate matrix $\prod = (\pi_{j\iota}), (k, \iota \in N)$. The jump transition probability can be defined as

$$P(r_{t+\Delta t} = \iota \mid r_t = k) = \begin{cases} \pi_{k\iota}\Delta t + o(\Delta t), & k \neq \iota, \\ 1 + \pi_{kk}\Delta t + o(\Delta t), & \iota = k, \end{cases} \tag{4.13}$$

where $\sum_{\iota=1,\iota\neq k}^{N}\pi_{k\iota} = -\pi_{k\iota},\ \pi_{k\iota}\geq 0,\ \forall\ \iota,k\in\Omega,\ \iota\neq k$. Here, $\Delta t>0$ and $\lim_{\Delta t\to 0} o(\Delta t)/\Delta t = 0$. The model of the form (4.12) is a hybrid system in which one state $x(t)$ takes values continuously and another state $r_t$, referred to as the mode or operating form, takes values discretely in $S$.

For $V(t,x)\in C^1$, let us introduce the weak infinitesimal operator $\mathcal{L}V$ of the process $\{x(t),\eta_t,t\geq 0\}$ at the point $\{t,x,j\}$,

$$\mathcal{L}V = \frac{\partial V}{\partial t} + \frac{\partial V}{\partial x}\dot{x}(t) + \sum_{k=1}^{N}\pi_{kj}V(x,j). \tag{4.14}$$

For each possible value $r_t = j$, $j\in S$, we will denote the system matrices associated with mode $j$ by

$$A(r_t) = A(j) = A_j, \qquad B(r_t) = B(j) = B_j, \tag{4.15}$$

where $A_j$, $B_j$ are known real constant matrices of appropriate dimensions which describe the nominal system.

**Theorem 4.1.** *If the linear matrix inequalities* (4.16) *have the solution* $X_j$ *for given* $A_j$, $B_j$, $X_j>0$, *and*

$$\begin{bmatrix}\widetilde{B}_j & 0 & 0\\ 0 & I & 0\\ 0 & 0 & I\end{bmatrix}^T\begin{bmatrix}\left(A_jX_j + X_jA_j^T + \sum_{k=1}^{N}\pi_{kj}X_j\right) & * & *\\ \eta & -I & \eta I\\ A_jX_j & \eta I & -I\end{bmatrix}\begin{bmatrix}\widetilde{B}_j & 0 & 0\\ 0 & I & 0\\ 0 & 0 & I\end{bmatrix} < 0, \tag{4.16}$$

*and define the sliding surface as*

$$\sigma_j = S_jx_j + \gamma\int_0^t S_jx_j\,dt, \tag{4.17}$$

$$S_j = \left(B_j^TX_j^{-1}B_j\right)^{-1}B_j^TX_j^{-1}. \tag{4.18}$$

*Consider the adaptive control as*

$$\mathcal{U}_c = -\overline{M}_0K\sigma_j - \overline{M}_0\left(S_jA_jx_j + \gamma S_jx_j\right) - \overline{M}_0\frac{1}{b}\sum_{i=1}^{5}\frac{\sigma_j\widehat{c}_i\Phi_i^2}{\|\sigma_j\|\Phi_i+\delta}, \tag{4.19}$$

*with the adaptive law*

$$\dot{\widehat{c}}_i = -\varpi_i\widehat{c}_i + \frac{\omega_i\Phi_i^2\|\sigma_j\|^2}{\|\sigma_j\|\Phi_i+\delta_i}, \qquad i=1,\ldots,5, \tag{4.20}$$

*where* $\widehat{C} = [\widehat{c}_1, \ldots, \widehat{c}_5]^T$, *and* $\Phi = [\|\ddot{z}_{pr}\|, 1, \|\dot{z}\|, 1, \|\dot{z}\|]^T$, $\omega_i > 0$, $K$ *is positive definite,* $\delta_i > 0$ *and* $\varpi_i > 0$ ( $1 \le i \le 5$) *satisfying:* $\lim_{t\to\infty}\delta_i(t) = 0$, $\int_0^\infty \delta_i(s)ds = \rho_{i\delta} < \infty$, $\lim_{t\to\infty}\varpi_i(t) = 0$, $\int_0^\infty \varpi_i(s)ds = \rho_{i\varpi} < \infty$ *with the constants* $\rho_{i\delta}$ *and* $\rho_{i\varpi}$, *and* $b$ *will be defined later. Then, a stable sliding mode exists from the initial time, and the sliding dynamics is stable.*

*Proof.* Define the transfer matrix $T_j$ and the related vector $\nu$, we have

$$T_j = \begin{bmatrix} \left(\widetilde{B}_j X_j \widetilde{B}_j\right)\widetilde{B}_j^T \\ \left(B_j^T X_j^{-1} B_j\right)^{-1} B_j^T X_j^{-1} \end{bmatrix}, \tag{4.21}$$

$$\nu = \begin{bmatrix} \nu_1 & \nu_2 \end{bmatrix}^T = T_j x_j, \tag{4.22}$$

where $\nu_1 \in R^{n-m}$, and $\nu_2 \in R^m$, $\widetilde{B}_j$ is any basis of the null space of $B_j^T$, that is, $B_j$ is an orthogonal complement of $B_j$, Note that given any $B_j$, $\widetilde{B}_j$ is not unique. Moreover, $T_j^{-1} = [\, X_j\widetilde{B}_j \;\; B_j \,]$.

Consider (4.22), it is easy to have

$$\dot{\sigma}_j = \dot{\nu}_2 + \gamma\nu_2. \tag{4.23}$$

From the definition of $\sigma_j$, we have

$$\dot{\sigma}_j = S_j\left(A_j x_j + B_j U\right) + \gamma S_j x_j. \tag{4.24}$$

Consider (4.11) and (4.18), we can rewrite (4.24) as

$$\dot{\sigma}_j = S_j A_j x_j + S_j B_j \overline{M}_0^{-1}\mathcal{U}_c + S_j B_j \Xi + \gamma S_j x_j = S_j A_j x_j + \overline{M}_0^{-1}\mathcal{U}_c + \Xi + \gamma S_j x_j. \tag{4.25}$$

with $S_j B_j = I$.

Consider (4.7), and $\ddot{z}_p = \ddot{z}_r + \dot{\sigma}_j$ with $\ddot{z}_r = \ddot{z}_{pd} - \gamma\nu_2$ and $\dot{\sigma}_j = \dot{\nu}_2 + \gamma\nu_2$, we can rewrite it as

$$\begin{aligned} \Xi &= -\overline{M}_0^{-1}\left(\Delta M\ddot{z}_p + \Delta H(z,\dot{z}) + \Delta D(t)\right) \\ &= -\overline{M}_0^{-1}\Delta M\ddot{z}_r - \overline{M}_0^{-1}\Delta M\dot{\sigma}_j - \overline{M}_0^{-1}\Delta H(z,\dot{z}) - \overline{M}_0^{-1}\Delta D. \end{aligned} \tag{4.26}$$

Let $\Gamma = (I + \overline{M}_0^{-1}\Delta M)^{-1}$, then we have

$$\dot{\sigma}_j = \Gamma\left(S_j A_j x_j + \gamma S_j x_j + \overline{M}_0^{-1}\mathcal{U}_c - \overline{M}_0^{-1}\Delta M\ddot{z}_r - \overline{M}_0^{-1}\Delta H(z,\dot{z}) - \overline{M}_0^{-1}\Delta D\right). \tag{4.27}$$

Let us consider the Lyapunov function as

$$V_1 = \sigma_j^T\sigma_j. \tag{4.28}$$

Taking the derivative (4.28) and integrating (4.27), we have

$$\begin{aligned}\dot{V}_1 &= \sigma_j^T \dot{\sigma}_j + \dot{\sigma}_j^T \sigma_j \\ &= 2\sigma_j^T \Gamma\left(S_j A_j x_j + \gamma S_j x_j + \overline{M}_0^{-1}\mathcal{U}_c - \overline{M}_0^{-1}\Delta M\ddot{z}_r - \overline{M}_0^{-1}\Delta H(z,\dot{z}) - \overline{M}_0^{-1}\Delta D\right).\end{aligned} \tag{4.29}$$

Substituting (4.19) into (4.29), we have

$$\begin{aligned}\dot{V}_1 &= -2\sigma_j^T \Gamma K\sigma_j + 2\sigma_j^T \Gamma \\ &\quad\times\left(-\frac{1}{b}\sum_{i=1}^{5}\frac{\sigma_j\widehat{c}_i\Phi_i^2}{\|\sigma_j\|\Phi_i+\delta} - \overline{M}_0^{-1}\Delta M\ddot{z}_r - \overline{M}_0^{-1}\Delta H(z,\dot{z}) - \overline{M}_0^{-1}\Delta D\right) \\ &= -2\sigma_j^T\Gamma K\sigma_j - 2\sigma_j^T\Gamma\frac{1}{b}\sum_{i=1}^{5}\frac{\sigma\widehat{c}_i\Phi_i^2}{\|\sigma_j\|\Phi_i+\delta} - 2\sigma_j^T\Gamma\overline{M}_0^{-1}\Delta M\ddot{z}_r \\ &\quad - 2\sigma_j^T\Gamma\overline{M}_0^{-1}\Delta H(z,\dot{z}) - 2\sigma_j^T\Gamma\overline{M}_0^{-1}\Delta D \\ &\le -2\sigma_j^T\Gamma K\sigma_j - 2\Gamma\frac{1}{b}\sum_{i=1}^{5}\frac{\|\sigma_j\|^2\widehat{c}_i\Phi_i^2}{\|\sigma_j\|\Phi_i+\delta} + 2\|\sigma_j\|\|\Gamma\|\left\|\overline{M}_0^{-1}\Delta M\right\|\|\ddot{z}_r\| \\ &\quad + 2\|\sigma_j\|\|\Gamma\|\left\|\overline{M}_0^{-1}\right\|\|\Delta H(z,\dot{z})\| + 2\|\sigma_j\|\|\Gamma\|\left\|\overline{M}_0^{-1}\right\|\|\Delta D\|.\end{aligned} \tag{4.30}$$

*Assumption 4.2.* There exist some finite positive constants $c_i > 0$ $(1 \le i \le 5)$ such that $\forall z \in R^{n-l}, \forall \dot{z} \in R^{n-l}$, $\|\Gamma\|\|\overline{M}_0^{-1}\Delta M\| \le c_1$, $\|\Gamma\|\|\overline{M}_0^{-1}\|\|\Delta H(z,\dot{z})\| \le c_2 + c_3\|\dot{z}\|$, $\|\Gamma\|\|\overline{M}_0^{-1}\|\|\Delta D\| \le c_4 + c_5\|\dot{z}\|$.

*Remark 4.3.* For simplification, we assume that $\Delta M > 0$. There exist the minimum and maximum eigenvalues $\lambda_{\min}(\Gamma)$ and $\lambda_{\max}(\Gamma)$, such that for all $x \in R^{(n-l-n_p)}$, there exists the known positive parameter $b$ satisfying $0 < b \le \lambda_{\min}(\Gamma)$, that is, $x^T bIx \le x^T\lambda_{\min}(\Gamma)Ix$.

*Remark 4.4.* In reality, these constants $c_i, 1 \le i \le 5$ cannot be obtained beforehand. Although any fixed large $c_i$ can guarantee good performance, it is not practical as large $c_i$ imply, in general, high noise amplification and high cost of control. Therefore, it is necessary to develop an adaptive law which can approximate the knowledge of $c_i, 1 \le i \le 5$.

Choose the Lyapunov function candidate $V_3 = V_1 + V_2$ with

$$V_2 = \widetilde{C}^T\Omega^{-1}\widetilde{C}, \tag{4.31}$$

where $\widetilde{C} = C - \widehat{C}$, and $\Omega = \mathrm{diag}[\omega_i]$, $i = 1, \ldots, 5$, therefore, we have

$$\begin{aligned}V_3 &\le -2\sigma_j^T\Gamma K\sigma_j - 2\Gamma\frac{1}{b}\sum_{i=1}^{5}\frac{\|\sigma_j\|^2\widehat{c}_i\Phi_i^2}{\|\sigma_j\|\Phi_i+\delta} + 2\|\sigma_j\|\|\Gamma\|\left\|\overline{M}_0^{-1}\Delta M\right\|\|\ddot{z}_r\| \\ &\quad + 2\|\sigma_j\|\|\Gamma\|\left\|\overline{M}_0^{-1}\right\|\|\Delta H(z,\dot{z})\| + 2\|\sigma_j\|\|\Gamma\|\left\|\overline{M}_0^{-1}\right\|\|\Delta D\| + 2\dot{\widetilde{C}}^T\Omega^{-1}\widetilde{C}.\end{aligned} \tag{4.32}$$

Integrating (4.20) into (4.32), we have

$$\begin{aligned} V_3 &\le -2\sigma_j^T \Gamma K \sigma_j - 2\Gamma \frac{1}{b} \sum_{i=1}^{5} \frac{\|\sigma_j\|^2 \hat{c}_i \Phi_i^2}{\|\sigma_j\| \Phi_i + \delta} + 2\|\sigma_j\| \|\Gamma\| \left\| \overline{M}_0^{-1} \Delta M \right\| \|\ddot{z}_r\| \\ &\quad + 2\|\sigma_j\| \|\Gamma\| \left\| \overline{M}_0^{-1} \right\| \|\Delta H(z, \dot{z})\| + 2\|\sigma_j\| \|\Gamma\| \left\| \overline{M}_0^{-1} \right\| \|\Delta D\| \\ &\quad + 2\sum_{i=1}^{5} \hat{c}_i^T \varpi_i \omega_i^{-1} \tilde{c}_i - 2\sum_{i=1}^{5} \frac{\tilde{c}_i \Phi_i^2 \|\sigma_j\|^2}{\|\sigma_j\| \|\Phi_i\| + \delta_i} \\ &\le -2\sigma_j^T \Gamma K \sigma_j + 2\sum_{i=1}^{5} \hat{c}_i^T \varpi_i \omega_i^{-1} \tilde{c}_i + \sum_{i=1}^{5} 2\delta_i \\ &\le -2\lambda_{\min}(\Gamma K) \|\sigma_j\|^2 + \sum_{i=1}^{5} \frac{\varpi_i}{2\omega_i} c_i^2 + \sum_{i=1}^{5} 2\delta_i, \end{aligned} \tag{4.33}$$

with $\tilde{c}_i \hat{c}_i = -(\hat{c}_i - (1/2)c_i)^2 + (1/4)c_i^2$. Therefore, $\dot{V}_3 \le -\lambda_{\min}(\Gamma K)\|\sigma_j\|^2 + \sum_{i=1}^{5}(\varpi_i/2\omega_i)c_i^2 + \sum_{i=1}^{5} 2\delta_i$. Since $\sum_{i=1}^{5}(\varpi_i/2\omega_i)c_i^2 + \sum_{i=1}^{5} 2\delta_i$ is bounded, there exists $t > t_1$, $\sum_{i=1}^{5}(\varpi_i/2\omega_i)c_i^2 + \sum_{i=1}^{5} 2\delta_i \le \rho_1$ with the finite constant $\rho_1$, when $\|\sigma_j\| \ge \sqrt{\rho_1/\lambda_{\min}(\Gamma K)}$, then $\dot{V}_3 \le 0$. For $\|\sigma_j\| \ge \sqrt{\rho_1/\lambda_{\min}(\Gamma K)}$, and $\sigma_j$ will converge to a compact set denoted by

$$\Upsilon_j := \left\{ \sigma_j : |\sigma_j| \le \sqrt{\frac{\rho_1}{\lambda_{\min}(\Gamma K)}} \right\}. \tag{4.34}$$

From all the above, $\sigma_j$ converges to a small set containing the origin as $t \to \infty$. Moreover, $\sigma_j \to 0$ as $t \to \infty$ because of $\lim_{t\to\infty}\delta_i(t) = 0$, $\lim_{t\to\infty}\varpi_i(t) = 0$, therefore, $\Upsilon_j$ converges to the origin, there $\sigma_j \to 0$, therefore, $\dot{\nu}_2 \to 0$ and $\nu_2 \to 0$.

Consider (4.21) and (4.22), we have

$$\dot{\nu} = T_j \dot{x}_j. \tag{4.35}$$

Consider Theorem 2.3 and (4.23), and let $\dot{\sigma} = 0$, it is easy to have

$$\dot{\nu} = \begin{bmatrix} \dot{\nu}_1 \\ \dot{\nu}_2 \end{bmatrix} = \overline{A}_j \nu, \tag{4.36}$$

where

$$\overline{A}_j = \begin{bmatrix} \Lambda_{j1} & \Lambda_{j2} \\ 0 & -\gamma I \end{bmatrix} = \begin{bmatrix} \left(\tilde{B}_j^T X \tilde{B}_j\right)^{-1} \tilde{B}_j^T A_j X_j \tilde{B} & \left(\tilde{B}_j^T X \tilde{B}_j\right)^{-1} \tilde{B}_j^T A_j B_j \\ 0 & -\gamma I \end{bmatrix}, \tag{4.37}$$

Therefore, we can partition the state equation as as

$$\begin{aligned} \dot{\nu}_1 &= \Lambda_{j1} \nu_1 + \Lambda_{j2} \nu_2, \\ \dot{\nu}_2 &= -\gamma \nu_2, \end{aligned} \tag{4.38}$$

Since $\nu_2 \to 0$ and $\dot{\nu}_2 \to 0$, we only consider the stability of $\dot{\nu}_1 = \Lambda_{j1}\nu_1$. It is easy to obtain that if there exists a positive-define matrix $P_j = \widetilde{B}_j^T X_j \widetilde{B}_j$ enabling the following inequality to hold:

$$\begin{bmatrix} P_j\Lambda_{j1} + \Lambda_{j1}^T P_j + \sum_{k=1}^{N} \pi_{kj} P_j & * & * \\ \eta\widetilde{B}_j & -I & * \\ C_j & \eta I & -I \end{bmatrix} < 0, \tag{4.39}$$

where $C_j = A_j X_j \widetilde{B}_j$, then the system

$$\dot{\nu}_1 = \Lambda_{j1}\nu_1 \tag{4.40}$$

is asymptotically stable, where $X$ is a solution matrix to the LMIs (4.16), which implies that the sliding-mode dynamics (4.36) is asymptotically stable. This implies that (4.39) holds if the matrix inequality shown in (4.16) holds. □

*Remark 4.5.* Note that Theorem 4.1 provides a solution to the problem of adaptive control for mechanical nonlinear systems with Markovian jump parameters. It is worth mentioning that the work conducted in this paper is the attempt to overcome the dynamics uncertainty arising in the sliding mode control for dynamics nonlinear systems with Markovian jump parameters and adopt adaptive control for dynamics nonlinear systems with Markovian jump parameters. The results obtained could be extended to general dynamics systems.

### 4.3. Switching Stability

For the system switching stability between the two different modes, we give the following theorems.

**Theorem 4.6.** *Consider the switching system* (4.13) *if the system is both stable before and after the switching phase using the control law* (4.19). *Assume that there exists no external impacts during the switching, the system is also stable during the switching phase.*

*Proof.* Since $\mathbb{V}_1$ and $\mathbb{V}_2$ are decreasing from Theorem 4.1, we know the system is stable no matter the hybrid joint is either actuated or underactuated. In the preceding, we have shown that the Lyapunov function is nonincreasing during the switching. Let $\mathbb{V}_{12}^- = (1/2\,)(\dot{\zeta}^- - \dot{\zeta})\mathfrak{D}(\dot{\zeta}^- - \dot{\zeta})$ and $\mathbb{V}_{12}^+ = (1/2)\,(\dot{\zeta}^+ - \dot{\zeta})\mathfrak{D}(\dot{\zeta}^+ - \dot{\zeta})$ denote the Lyapunov function before and after the switching, and $\dot{\zeta}^+$ and $\dot{\zeta}^-$ represent the post- and preswitch velocities, respectively. The Lyapunov function change during the switching can be simplified as follows:

$$\Delta\mathbb{V} = \mathbb{V}^+ - \mathbb{V}^- = \frac{1}{2}(\dot{\zeta}^+ - \dot{\zeta})\mathfrak{D}(\dot{\zeta}^+ - \dot{\zeta}) - \frac{1}{2}(\dot{\zeta}^- - \dot{\zeta})\mathfrak{D}(\dot{\zeta}^- - \dot{\zeta}). \tag{4.41}$$

There is no external impact during the switching, which means that there are no extra energy injected into the system. Since the inertia properties of the switching joint and link exist,

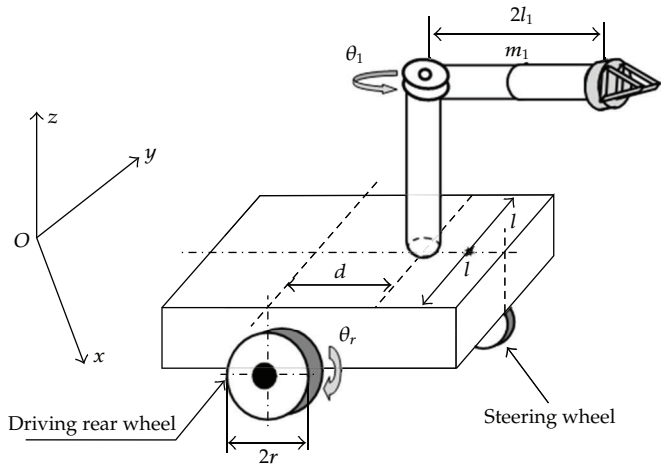


**Figure 2:** The wheeled mobile manipulator in the simulation.

during the switching joint, if the switching joint is switched from the active mode to the passive mode without considering the friction, the motion of the link should be continuous, that is, $\dot{\zeta}^+ = \dot{\zeta}^- = \dot{\zeta}$. Therefore, during the switching, the Lyapunov function is nonincreasing. If considering the friction, the Lyapunov function is decreasing, that is, $\Delta\mathbb{V} \leq 0$, the motion is stable during the switching. Similarly, if the switching joint is switched from the passive mode to the active mode, although the joint torque is added, since the motion of the system is continuous because of the inertia, that is, $\Delta\mathbb{V} \leq 0$, the motion of the system is also stable. □

## 5. Simulation Studies

To verify the effectiveness of the proposed control algorithm, let us consider a wheeled mobile underactuated manipulator shown in Figure 2.

The following variables have been chosen to describe the vehicle (see also Figure 2),

(i) $\tau_l, \tau_r$: the torques of two wheels;

(ii) $\tau_1$: the torques of joint 1;

(iii) $\theta_l, \theta_r$: the rotation angle of the left wheel and the right wheel of the mobile platform;

(iv) $v$: the forward velocity of the mobile platform;

(v) $\theta$: the direction angle of the mobile platform;

(vi) $\omega$: the rotation velocity of the mobile platform, and $\omega = \dot{\theta}$;

(vii) $\theta_1$: the joint angle of the underactuated link;

(viii) $m_1, I_1, l_1$: the mass, the inertia moment, and the length for the link;

(ix) $r$: the radius of the wheels;

(x) $l$: the distance of the wheels;

(xi) $l_G$: the distance between the wheel and joint 1;

(xii) $m$: the mass of the mobile platform;

(xiii) $I$: the inertia moment of the mobile platform;

(xiv) $I_w$: the inertia moment of each wheel;

(xv) $g$: gravity acceleration.

The mobile underactuated manipulator is subject to the following constraint: $\dot{x}\cos\theta - \dot{y}\sin\theta + \dot{\theta}l_G = 0$. Using the Lagrangian approach, we can obtain the dynamic model with $q = [\theta_l, \theta_r, \theta_1]^T$, then we could obtain

$$\begin{gathered} M(q)\ddot{q} + C(q,\dot{q})\dot{q} + G(q) = B\tau, \\ M(q) = \begin{bmatrix} m_{11}(q) & m_{12}(q) & m_{13}(q) \\ * & m_{22}(q) & m_{23}(q) \\ * & * & m_{33}(q) \end{bmatrix}, \qquad C(q,\dot{q}) = \begin{bmatrix} c_1(q,\dot{q}) \\ c_2(q,\dot{q}) \\ c_3(q,\dot{q}) \end{bmatrix}, \\ B = \begin{bmatrix} 1 & 0 & 0 \\ 0 & 1 & 0 \\ 0 & 0 & 1 \end{bmatrix}, \end{gathered} \tag{5.1}$$

where

$$\begin{aligned} m_{11}(q) &= 2p_1 + \frac{2p_3}{l^2}\tan^2\theta_r, \\ m_{12}(q) &= \frac{p_4}{l}\tan\theta_r - p_8\sin\theta_l, \\ m_{13}(q) &= 0, \quad m_{22}(q) = 2p_2, \\ m_{23}(q) &= p_6, \quad m_{33}(q) = 2p_5, \\ c_1(q,\dot{q}) &= \frac{4p_3}{l^2}\tan\theta_r\sec^2\theta_r\dot{\theta}_r^2\dot{\theta}_l + \frac{p_4}{l}\sec\theta_r\dot{\theta}_r^2 - 2p_7\sec\theta_r\sin\theta_1\dot{\theta}_l\dot{\theta}_r^2 \\ &\quad -2p_7\sec^2\theta_r\cos\theta_1\dot{\theta}_1\dot{\theta}_l - p_8\cos\theta_1\dot{\theta}_1\dot{\theta}_r, \\ c_2(q,\dot{q}) &= \frac{p_4}{l}\sec^2\theta_r\dot{\theta}_l\theta_r - p_8\cos\theta_1\theta_l\theta_1, \\ c_3(q,\dot{q}) &= p_7\tan\theta_r\cos\theta_1\dot{\theta}_l\dot{\theta}_1 + p_8\cos\theta_1\dot{\theta}_l\dot{\theta}_r\dot{\theta}_1, \\ p_1 &= \frac{1}{2}\left(m + m_1 + \frac{I_w}{r^2}\right), \quad p_2 = \frac{1}{2}\left(I + I_m + m_1l_1^2 + I_1\right), \quad p_3 = \frac{1}{2}(I_m + I_w), \\ p_4 &= I_m, \quad p_5 = \frac{1}{2}\left(m_1l_1^2 + I_1\right), \quad p_6 = m_1l_1^2 + I_1, \quad p_7 = \frac{m_1l_1}{l_1}, \quad p_8 = m_1l_1. \end{aligned} \tag{5.2}$$

As discussed in Section 2, we set the fully operational configuration represented by OOO while three possible configurations can occur: $AAP$, $APA$, and $APP$, where $A$ represents actuated joints and $P$ represents passive joints. For example, if we find that a switching occurs in $\tau_{\theta_1}$, then the switching configuration to validate the proposed methodology is the $AAP$ configuration. We consider a workspace with a positioning domain which range from $-8°$ to $12°$, with the velocities set to $1°/s$, and use 2 sectors of position in each joint, denoted as I($-8° : 2°$) and II($2° : 12°$), to map the mobile manipulator workspace. The linearization points with respect to I and II are chosen as $-3°$ and $7°$, respectively. Then, according to Section 3.2, 8 linearization points with 32 modes are found. For simplification, we select the 8 modes in simulation, which are shown in Table 2. There exist 8 modes for the

**Table 2:** Simulation modes.

| Mode | Joint status | Mode | Joint status | Linearization Section | | |
|---|---|---|---|---|---|---|
| | | | | $\theta_r$ | $\theta_l$ | $\theta_1$ |
| 1 | $AAA$ | 5 | $AAP$ | I | I | I |
| 2 | $AAA$ | 6 | $AAP$ | II | I | I |
| 3 | $APA$ | 7 | $APP$ | II | I | II |
| 4 | $APA$ | 8 | $APP$ | II | II | II |

simulation example, which means an $8 \times 8$ dimension transition rate matrix $\Pi$ is needed, so $\Pi$ is defined as

$$\Pi = \begin{bmatrix} -0.72 & 0.15 & 0.22 & 0.21 & 0.14 & 0 & 0 & 0 \\ 0.2 & -0.7 & 0.2 & 0.2 & 0 & 0.1 & 0 & 0 \\ 0.16 & 0.22 & -0.68 & 0.2 & 0 & 0 & 0.1 & 0 \\ 0.22 & 0.3 & 0.2 & -0.82 & 0 & 0 & 0 & 0.1 \\ 0 & 0 & 0 & 0 & -0.78 & 0.26 & 0.26 & 0.26 \\ 0 & 0 & 0 & 0 & 0.26 & -0.78 & 0.26 & 0.26 \\ 0 & 0 & 0 & 0 & 0.26 & 0.26 & -0.78 & 0.26 \\ 0 & 0 & 0 & 0 & 0.26 & 0.26 & 0.26 & -0.78 \end{bmatrix}. \tag{5.3}$$

The system parameters are chosen as $G = 0\,\text{kg}$, $B = I$, $m = 10.0\,\text{kg}$, $m_1 = 2.0\,\text{kg}$, $I = 1.0\,\text{kg} \cdot m^2$, $I_1 = 1.0\,\text{kg} \cdot m^2$, $I_m = 2.0\,\text{kg} \cdot m^2$, $I_w = 2.0\,\text{kg} \cdot m^2$, $l = 1.0\ m$, $l_1 = 1.0\ m$, $r = 0.5\ m$.

Assume that the nominal models are obtained as:

$$A_1 = \begin{bmatrix} 0 & 0 & 1.0000 & 0 \\ 0 & 0 & 0 & 1.0000 \\ 0.0040 & 0.0012 & 0.0653 & -0.0728 \\ -0.0047 & -0.0010 & -0.0717 & 0.0647 \end{bmatrix}, \quad B_1 = \begin{bmatrix} 0 & 0 \\ 0 & 0 \\ 0.0003 & 0.3354 \\ -0.0003 & -0.0020 \end{bmatrix},$$

$$A_2 = \begin{bmatrix} 0 & 0 & 1.0000 & 0 \\ 0 & 0 & 0 & 1.0000 \\ 0.0040 & 0.0012 & 0.0653 & -0.0728 \\ -0.0047 & -0.0010 & -0.0717 & 0.0647 \end{bmatrix}, \quad B_2 = \begin{bmatrix} 0 & 0 \\ 0 & 0 \\ 0.0003 & 0.3354 \\ -0.0003 & 0.3333 \end{bmatrix},$$

$$A_3 = \begin{bmatrix} 0 & 0 & 1.0000 & 0 \\ 0 & 0 & 0 & 1.0000 \\ 0.0057 & 0.0014 & 0.0725 & -0.0764 \\ -0.0064 & -0.0011 & -0.0790 & 0.0676 \end{bmatrix}, \quad B_3 = \begin{bmatrix} 0 & 0 \\ 0 & 0 \\ 0.0035 & 0.3582 \\ -0.0035 & -0.0249 \end{bmatrix},$$

$$A_4 = \begin{bmatrix} 0 & 0 & 1.0000 & 0 \\ 0 & 0 & 0 & 1.0000 \\ 0.0057 & 0.0014 & 0.0725 & -0.0764 \\ -0.0064 & -0.0011 & -0.0790 & 0.0676 \end{bmatrix}, \quad B_4 = \begin{bmatrix} 0 & 0 \\ 0 & 0 \\ 0.0035 & 0.3582 \\ -0.0035 & 0.3333 \end{bmatrix},$$

$$A_5 = \begin{bmatrix} 0 & 0 & 1.0000 & 0 \\ 0 & 0 & 0 & 1.0000 \\ 0.0042 & 0.0016 & 0.0628 & -0.0686 \\ -0.0048 & -0.0013 & -0.0691 & 0.0606 \end{bmatrix}, \quad B_5 = \begin{bmatrix} 0 & 0 \\ 0 & 0 \\ -0.0022 & 0.3175 \\ 0.0022 & 0.0158 \end{bmatrix},$$

$$A_6 = \begin{bmatrix} 0 & 0 & 1.0000 & 0 \\ 0 & 0 & 0 & 1.0000 \\ 0.0042 & 0.0016 & 0.0628 & -0.0686 \\ -0.0048 & -0.0013 & -0.0691 & 0.0606 \end{bmatrix}, \quad B_6 = \begin{bmatrix} 0 & 0 \\ 0 & 0 \\ -0.0022 & 0.3175 \\ 0.0022 & 0.3333 \end{bmatrix},$$

$$A_7 = \begin{bmatrix} 0 & 0 & 1.0000 & 0 \\ 0 & 0 & 0 & 1.0000 \\ 0.0055 & 0.0010 & 0.0753 & -0.0809 \\ -0.0062 & -0.0008 & -0.0819 & 0.0719 \end{bmatrix}, \quad B_7 = \begin{bmatrix} 0 & 0 \\ 0 & 0 \\ 0.0068 & 0.3808 \\ -0.0068 & -0.0475 \end{bmatrix},$$

$$A_8 = \begin{bmatrix} 0 & 0 & 1.0000 & 0 \\ 0 & 0 & 0 & 1.0000 \\ 0.0055 & 0.0010 & 0.0753 & -0.0809 \\ -0.0062 & -0.0008 & -0.0819 & 0.0719 \end{bmatrix}, \quad B_8 = \begin{bmatrix} 0 & 0 \\ 0 & 0 \\ 0.0068 & 0.3808 \\ -0.0068 & 0.3333 \end{bmatrix}. \tag{5.4}$$

The parameters in (4.19) are set as $C(0) = [0.00002, \ldots, 0.00002]^T$, for $i = 1, 2, \ldots, 8$, $M_0 = I$, $\omega_i = 0.5$, $\alpha_i = \delta = 1/(t+1)^2$, $K = \text{diag}[1.0]$, $b = 1.0$, $\gamma = 1.0$. The initial condition we used for simulation is $x_0 = [0.3, 0.3, 0.2, -0.1, 0.1, -0.15]^T$. Via LMI optimization with the data $A_j, B_j$, we can get the following solution to the LMIs (4.16) as:

$$X_1 = 10^4 \begin{bmatrix} 1.9625 & 0.0001 & -0.0012 & 0.0011 \\ 0.0001 & 1.9620 & -0.0003 & 0.0002 \\ -0.0012 & -0.0003 & 1.0267 & 0.0000 \\ 0.0011 & 0.0002 & 0.0000 & 1.0267 \end{bmatrix},$$

$$X_2 = 10^3 \begin{bmatrix} 2.7094 & -0.0148 & -0.0022 & 0.0015 \\ -0.0148 & 2.7654 & -0.0004 & -0.0003 \\ -0.0022 & -0.0004 & 4.8496 & -0.0000 \\ 0.0015 & -0.0003 & -0.0000 & 4.8496 \end{bmatrix},$$

$$X_3 = 10^3 \begin{bmatrix} 2.4313 & -0.0153 & -0.0028 & 0.0020 \\ -0.0153 & 2.4918 & -0.0005 & -0.0002 \\ -0.0028 & -0.0005 & 4.8077 & -0.0000 \\ 0.0020 & -0.0002 & -0.0000 & 4.8077 \end{bmatrix},$$

$$X_4 = 10^3 \begin{bmatrix} 2.2073 & -0.0145 & -0.0026 & 0.0018 \\ -0.0145 & 2.2639 & -0.0004 & -0.0003 \\ -0.0026 & -0.0004 & 4.7749 & -0.0000 \\ 0.0018 & -0.0003 & -0.0000 & 4.7749 \end{bmatrix},$$

$$X_5 = 10^3 \begin{bmatrix} 2.8110 & -0.0160 & -0.0023 & 0.0016 \\ -0.0160 & 2.8679 & -0.0005 & -0.0002 \\ -0.0023 & -0.0005 & 4.8654 & -0.0000 \\ 0.0016 & -0.0002 & -0.0000 & 4.8654 \end{bmatrix},$$

$$X_6 = 10^3 \begin{bmatrix} 5.2731 & -0.0149 & -0.0037 & 0.0030 \\ -0.0149 & 5.3153 & -0.0010 & 0.0003 \\ -0.0037 & -0.0010 & 5.3202 & -0.0000 \\ 0.0030 & 0.0003 & -0.0000 & 5.3202 \end{bmatrix},$$

$$X_7 = 10^3 \begin{bmatrix} 5.2363 & -0.0123 & -0.0054 & 0.0045 \\ -0.0123 & 5.3133 & -0.0007 & 0.0000 \\ -0.0054 & -0.0007 & 5.3153 & -0.0000 \\ 0.0045 & 0.0000 & -0.0000 & 5.3153 \end{bmatrix},$$

$$X_8 = \begin{bmatrix} -0.6928 & -0.0000 & -0.0000 & -0.0000 \\ -0.0000 & -0.6928 & -0.0000 & -0.0000 \\ -0.0000 & -0.0000 & -0.6928 & -0.0000 \\ -0.0000 & -0.0000 & -0.0000 & -0.6928 \end{bmatrix}. \tag{5.5}$$

So we can obtain the solution of $S_i$, for $i = 1, 2, \ldots, 8$. Torque disturbances $D(t)$ are introduced to verify the robustness of the controllers

$$\begin{bmatrix} d_r(t) \\ d_l(t) \\ d_1(t) \end{bmatrix} = \begin{bmatrix} 0.023\sin(4t) \\ 0.007\sin(3t) + 0.009\cos^2 t \\ 0.015\cos(5t) \end{bmatrix}. \tag{5.6}$$

The disturbance is turned off after the switching introduction in corresponding joint or wheel.

The system switches among the 8 modes randomly during operation. From Figure 3, we can see that firstly the system switches from mode 1 to mode 4, then from mode 4 to mode 1, finally, it switches from mode 1 to modes 4, 6, and 7. Figure 4 shows that the system is stabilized during operation. From Figures 5, 6, and 7, it can be noticed that the torque inputs are bounded. The simulation results demonstrate the tracking error decays to the equilibrium point under the designed mode-dependent controller.

## 6. Conclusion

In this paper, we consider stochastic stability and sliding mode control for mobile manipulators using stochastic jumps switching joints. Adaptive parameter techniques are adopted to cope with the effect of the Markovian switching and nonlinear dynamics uncertainty and follow the desired trajectory for wheeled mobile manipulators. The resulting closed-loop system is bounded in probability and the effect due to the external disturbance on the tracking errors can be attenuated to any preassigned level. It has been shown that the adaptive control problem for the Markovian jump nonlinear systems is solvable if a set of coupled LMIs have solutions. Finally, a numerical example is given to show the potential of the proposed techniques.

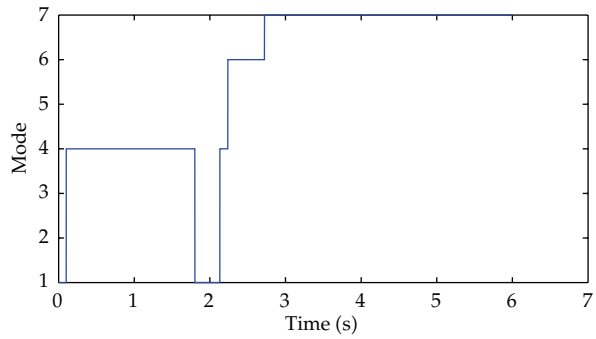


**Figure 3:** Mode jumping.

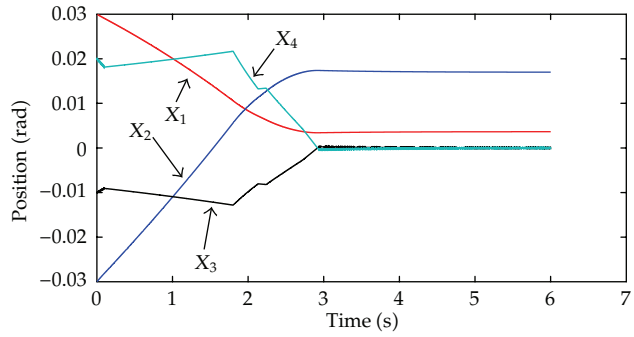


**Figure 4:** States.

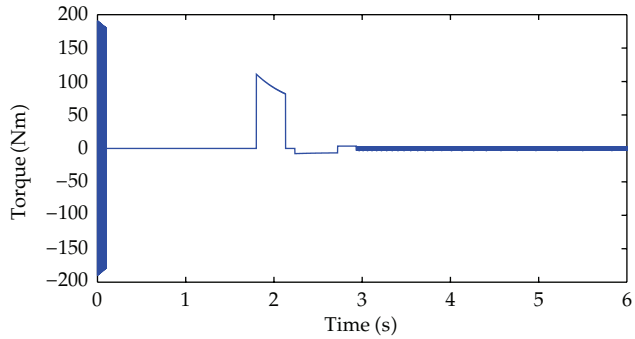


**Figure 5:** The input control $u_1$.

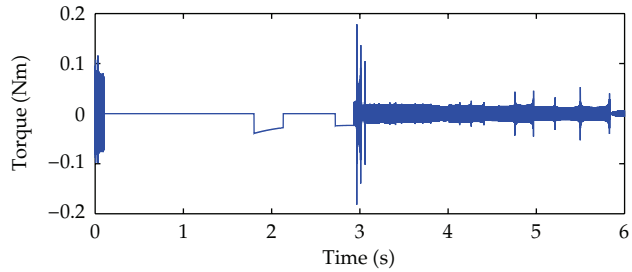


**Figure 6:** The input control $u_2$.

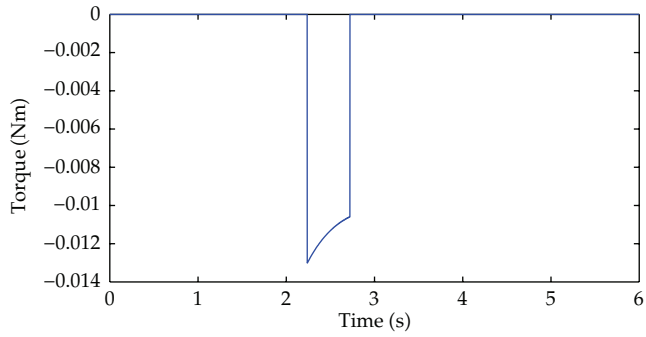


**Figure 7:** The input control $u_3$.

## 7. Acknowledgment

This study was partially supported by the National Natural Science Foundation of China (Grant no. 61005080), Special Postdoctoral Foundation of China (Grant no. 201104405), Postdoctoral Foundation of China (20100480994), and the "111" Project (B07018). The authors would like to express their acknowledgment to Dr. Z. J. Li for his help in theory and literature.

## References

[1] Z. Li, A. Ming, N. Xi, and M. Shimojo, "Motion control of nonholonomic mobile underactuated manipulator," in *Proceedings of the IEEE International Conference on Robotics and Automation*, pp. 3512–3519, May 2006.

[2] Z. Li, A. Ming, N. Xi, J. Gu, and M. Shimojo, "Development of hybrid joints for the complaint arm of human-symbiotic mobile manipulator," *International Journal of Robotics and Automation*, vol. 20, no. 4, pp. 260–270, 2005.

[3] Z. Li, C. Yang, J. Luo, Z. Wang, and A. Ming, "Robust motion/force control of nonholonomic mobile manipulatorsusing hybrid joints," *Advanced Robotics*, vol. 21, no. 11, pp. 1231–1252, 2007.

[4] Z. Li and Y. Kang, "Dynamic coupling switching control incorporating support vector machines for wheeled mobile manipulators with hybrid joints," *Automatica*, vol. 46, no. 5, pp. 785–958, 2010.

[5] Z. Li, Y. Yang, and J. Li, "Adaptive motion/force control of mobile under-actuated manipulators with dynamics uncertainties by dynamic coupling and output feedback," *IEEE Transactions Control System Technology*, vol. 18, no. 5, pp. 1068–1079, 2010.

[6] S. S. Ge and Z. Li, "Data driven adaptive predictive control for holonomic constrained under-actuated biped robots," *IEEE Transactions on Control Systems Technology*, vol. 20, no. 3, pp. 787–795, 2012.

[7] S. Lin and A. A. Goldenberg, "Neural-network control of mobile manipulators," *IEEE Transaction on Neural Network*, vol. 12, no. 5, pp. 1121–1133, 2001.

[8] Z. Li, S. S. Ge, and A. Ming, "Adaptive robust motion/force control of holonomic-constrained nonholonomic mobile manipulator," *IEEE Transactions System, Man, and Cybernetics B*, vol. 37, no. 3, pp. 607–617, 2007.

[9] Z. Li, J. Li, and Y. kang, "Adaptive robust coordinated control of multiple mobile manipulators interacting with rigid environments," *Automatica*, vol. 46, pp. 2028–2034, 2010.

[10] W. Dong, "On trajectory and force tracking control of constrained mobile manipulators with parameter uncertainty," *Automatica*, vol. 38, no. 9, pp. 1475–1484, 2002.

[11] Z. Li, P. Tao, S. S. Ge, M. D. Adams, and W. S. Wijesoma, "Robust adaptive control of cooperating mobile manipulators with relative motion," *IEEE Transactions System, Man, and Cybernetics B*, vol. 39, no. 1, pp. 103–116, 2009.

[12] Z. Li, W. Chen, and J. Luo, "Adaptive compliant force-motion control of coordinated nonholonomic mobile manipulators interacting with unknown non-rigid environments," *Neurocomputing*, vol. 71, no. 7–9, pp. 1330–1344, 2008.

[13] Y. Yamamoto and X. Yun, "Unified analysis on mobility and manipulability of mobile manipulators," in *Proceedings of the IEEE International Conference on Robotics and Automation*, pp. 1200–1206, 1999.
[14] Z. Li, J. Gu, A. Ming, and C. Xu, "Intelligent complaint force/motion control of nonholonomic mobile manipulator working on the non-rigid surface," *Neural Computing and Applications*, vol. 15, no. 3-4, pp. 204–216, 2006.
[15] Z. Li, C. Yang, and J. Gu, "Neuro-adaptive compliant force/ motion control for uncertain constrained wheeled mobile manipulator," *International Journal of Robotics and Automation*, vol. 22, no. 3, pp. 206–214, 2007.
[16] Z. Li, S. S. Ge, M. Adams, and W. S. Wijesoma, "Robust adaptive control of uncertain force/motion constrained nonholonomic mobile manipulators," *Automatica*, vol. 44, no. 3, pp. 776–784, 2008.
[17] Y. Liu and Y. Li, "Robust adaptive neuro-fuzzy control for nonholonomic mobile modular manipulats in task space," in *Proceedings of the IEEE International Conference on Robotics and Biomimetics*, pp. 66–71, 2005.
[18] K. Tchon, "Repeatability of inverse kinematics algorithms for mobile manipulators," *Institute of Electrical and Electronics Engineers*, vol. 47, no. 8, pp. 1376–1380, 2002.
[19] Z. Li and W. Chen, "Adaptive neural-fuzzy control of uncertain constrained multiple coordinated nonholonomic mobile manipulators," *Engineering Applications of Artificial Intelligence*, vol. 21, no. 7, pp. 985–1000, 2008.
[20] J. G. Tao, X. Li, F. Yang, and Z. Q. Deng, "A wheel-arm reconfigurable mobile robot design and its reconfigurable configuration," in *Proceedings of the ASME/IFToMM International Conference on Reconfigurable Mechanisms and Robots*, pp. 550–557, 2008.
[21] Z. Li, S. S. Ge, M. Adams, and W. S. Wijesoma, "Adaptive robust output-feedback motion/force control of electrically driven nonholonomic mobile manipulators," *IEEE Transactions on Control Systems Technology*, vol. 16, no. 6, pp. 1308–1315, 2008.
[22] Z. Li, S. S. Ge, and Z. Wang, "Robust adaptive control of coordinated multiple mobile manipulators," *Mechatronics*, vol. 18, pp. 239–250, 2008.
[23] R. Brooks, L. Aryanada, A. Edsinger et al., "Sensing and manipulating built-for-human environments," *International Journal of Humanoid Robotics*, vol. 1, no. 1, pp. 1–28, 2004.
[24] S. S. Ge, J. Wang, T. H. Lee, and G. Y. Zhou, "Adaptive robust stabilization of dynamic nonholonomic chained systems," *Journal of Robotic System*, vol. 18, no. 3, pp. 119–133, 2001.
[25] S. S. Ge, Z. Wang, and T. H. Lee, "Adaptive stabilization of uncertain nonholonomic systems by state and output feedback," *Automatica*, vol. 39, no. 8, pp. 1451–1460, 2003.
[26] A. De Luca and G. Oriolo, "Trajectory planning and control for planar robots with passive last joint," *The International Journal of Robotics Research*, vol. 21, no. 5-6, pp. 575–590, 2002.
[27] H. Arai and K. Tanie, "Nonholonomic control of a three-DOF planar underactuted manipulator," *IEEE Transactions Robotics and Automation*, vol. 14, no. 5, pp. 681–694, 1998.
[28] M. Bergerman, C. Lee, and Y. Xu, "A dynamic coupling index for underactuated manipulators," *Journal of Robotic Systems*, vol. 12, no. 10, pp. 693–707, 1995.
[29] Z. Li, J. Zhang, and Y. Yang, "Motion control of mobile under-actuated manipulators by implicit function using support vector machines," *IET Control Theory & Applications*, vol. 4, no. 11, pp. 2356–2368, 2010.
[30] Z. Li, "Adaptive fuzzy output feedback motion/force control for wheeled inverted pendulums," *IET Control Theory & Applications*, vol. 5, no. 10, pp. 1176–1188, 2011.
[31] M. W. Spong, "The swing up control problem for the Acrobot," *IEEE Control Systems*, vol. 15, pp. 49–55, 1995.
[32] Z. Li, Y. Zhang, and Y. Yang, "Support vector machine optimal control for mobile wheeled inverted pendulums with unmodelled dynamics," *Neurocomputing*, vol. 73, pp. 2773–2782, 2010.
[33] Z. Li and C. Xu, "Adaptive fuzzy logic control of dynamic balance and motion for wheeled inverted pendulums," *Fuzzy Sets and Systems*, vol. 160, no. 12, pp. 1787–1803, 2009.
[34] Z. Li and J. Luo, "Adaptive robust dynamic balance and motion controls of mobile wheeled inverted pendulums," *IEEE Transactions on Control Systems Technology*, vol. 17, no. 1, pp. 233–241, 2009.
[35] Y. Liu, Y. Xu, and M. Bergerman, "Cooperation control of multiple manipulators with passive joints," *IEEE Transactions Robotics and Automation*, vol. 15, no. 2, pp. 258–267, 1999.
[36] R. Tinos, M. H. Terra, and J. Y. Ishihara, "Motion and force control of cooperative robotic manipulators with passive joints," *IEEE Transactions Control Systems Technology*, vol. 14, no. 4, pp. 725–734, 2006.
[37] Y. Kang, Z. Li, Y. Dong, and H. Xi, "Markovian based fault-tolerant control for wheeled mobile manipulators," *IEEE Transactions Control System Technology*, vol. 20, no. 1, pp. 266–276, 2012.

[38] S. S. Ge, T. H. Lee, and C. J. Harris, *Adaptive Neural Network Control of Robot Manipulators*, World Scientific, London, UK, 1998.
[39] A. Weinmann, *Uncertain Models and Robust Control*, Springer, New York, NY, USA, 1991.
[40] L. Ding, K. Nagatani, K. Sato et al., "Terramechanics-based high-fidelity dynamics simulation for wheeled mobile robot on deformable rough terrain," *IEEE International Conference on Robotics and Automation*, pp. 4922–4927, 2010.
[41] L. Ding, H. Gao, Z. Deng, and W. Li, "Advances in simulation of planetary wheeled mobile robots," in *Mobile Robots-Current Trends*, chapter 18, pp. 375–402, Intech Press, 2011.

Hindawi Publishing Corporation
Journal of Applied Mathematics
Volume 2012, Article ID 642480, 10 pages
doi:10.1155/2012/642480

*Research Article*

# A New Proof to the Necessity of a Second Moment Stability Condition of Discrete-Time Markov Jump Linear Systems with Real States

**Qiang Ling[1] and Haojiang Deng[2]**

[1] *Department of Automation, University of Science and Technology of China, Anhui, Hefei 230027, China*
[2] *National Network New Media Engineering Research Center, Institute of Acoustics, Chinese Academy of Science, Beijing 100190, China*

Correspondence should be addressed to Qiang Ling, qling@ustc.edu.cn

Received 12 February 2012; Accepted 28 March 2012

Academic Editor: Baocang Ding



This paper studies the second moment stability of a discrete-time jump linear system with real states and the system matrix switching in a Markovian fashion. A sufficient stability condition was proposed by Fang and Loparo (2002), which only needs to check the eigenvalues of a deterministic matrix and is much more computationally efficient than other equivalent conditions. The proof to the necessity of that condition, however, is a challenging problem. In the paper by Costa and Fragoso (2004), a proof was given by extending the state domain to the complex space. This paper proposes an alternative necessity proof, which does not need to extend the state domain. The proof in this paper demonstrates well the essential properties of the Markov jump systems and achieves the desired result in the real state space.

## 1. Introduction

### 1.1. Background of the Discrete-Time Markov Jump Linear Systems

This paper studies the stability condition of discrete-time jump linear systems in the real state domain. In a jump linear system, the system parameters are subject to abrupt jumps. We are concerned with the stability condition when these jumps are governed by a finite Markov chain. A general model is shown as follows:

$$\begin{aligned} x[k+1] &= A\big[q[k]\big]x[k], \\ x[0] &= x_0, \qquad q[k] = q_0, \end{aligned} \tag{1.1}$$

where $x[k] \in R^n$ is the state and $\{q[k]\}$ is a discrete-time Markov chain with a finite state space $\{q_1, q_2, \ldots, q_N\}$ and a transition matrix $Q = (q_{ij})_{N\times N}$, where $q_{ij} = P(q[k+1] = q_j \mid q[k] = q_i)$. $x_0 \in R^n$ is the initial state. $q_0$ is the initial Markov state, whose distribution is denoted as $p = [p_1 \;\; p_2 \;\; \cdots \;\; p_N]$ with $p_i = P(q_0 = q_i)$. $\{q[k]\}$ is assumed to be a *time-homogeneous aperiodic* Markov chain. When $q[k] = q_i$, $A[q[k]] = A_i (i = 1, \ldots, N)$, that is, $A[q[k]]$ switches among $\{A_i\}_{i=1}^N$. A compound matrix is constructed from $A_i$ as

$$A_{[2]} = \left(Q^T \otimes I_{n^2}\right) \operatorname{diag}\left(A_i \otimes A_i\right)_{i=1}^N, \tag{1.2}$$

where $I_{n^2}$ denotes an identity matrix with the order of $n^2$ and $\otimes$ denotes the Kronecker product [1]. A brief introduction on the Kronecker product will be given in Section 2.1.

For the jump linear system in (1.1), the first question to be asked is *"is the system stable?"* There has been plenty of work on this topic, especially in 90s, [2–6]. Recently this topic has caught academic interest again because of the emergence of networked control systems [7]. Networked control systems often suffer from the network delay and dropouts, which may be modelled as Markov chains, so that networked control systems can be classified into discrete-time jump linear systems [8–11]. Therefore, the stability of the networked control systems can be determined through studying the stability of the corresponding jump linear systems. Before proceeding further, we review the related work.

### 1.2. Related Work

At the beginning, the definitions of stability of jump linear systems are considered. In [6], three types of second moment stability are defined.

*Definition 1.1.* For the jump linear system in (1.1), the equilibrium point 0 is

(1) *stochastically stable*, if, for every initial condition $(x[0] = x_0, q[0] = q_0)$,

$$\mathbf{E}\left[\sum_{k=0}^{\infty} \|x[k]\|^2 \mid x_0, q_0\right] < \infty, \tag{1.3}$$

where $\|\cdot\|$ denotes the 2-norm of a vector;

(2) *mean square stable* (MSS), if, for every initial condition $(x_0, q_0)$,

$$\lim_{k\to\infty} \mathbf{E}\left[\|x[k]\|^2 \mid x_0, q_0\right] = 0; \tag{1.4}$$

(3) *exponentially mean square stable*, if, for every initial condition $(x_0, q_0)$, there exist constants $0 < \alpha < 1$ and $\beta > 0$ such that for all $k \geq 0$,

$$\mathbf{E}\left[\|x[k]\|^2 \mid x_0, q_0\right] < \beta\alpha^k \|x_0\|^2, \tag{1.5}$$

where $\alpha$ and $\beta$ are independent of $x_0$ and $q_0$.

In [6], the above 3 types of stabilities are proven to be equivalent. So we can study mean square stability without loss of generality. In [6], a necessary and sufficient stability condition is proposed.

**Theorem 1.2** (see [6]). *The jump linear system in* (1.1) *is mean square stable, if and only if, for any given set of positive definite matrices* $\{W_i : i = 1, \ldots, N\}$*, the following coupled matrix equations have unique positive definite solutions* $\{M_i : i = 1, \ldots, N\}$*:*

$$\sum_{j=1}^{N} q_{ij} A_i^T M_j A_i - M_i = -W_i. \tag{1.6}$$

*Although the above condition is necessary and sufficient, it is difficult to verify because it claims validity for any group of positive definite matrices* $\{W_i : i = 1, \ldots, N\}$*. A more computationally efficient testing criterion was, therefore, pursued [3, 4, 12–15]. Theorem 1.3 gives a sufficient mean square stability condition.*

**Theorem 1.3** (see [4, 12]). *The jump linear system in* (1.1) *is mean square stable, if all eigenvalues of the compound matrix* $A_{[2]}$ *in* (1.2) *lie within the unit circle.*

*Remark 1.4.* By Theorem 1.3, the mean square stability of a jump linear system can be reduced to the stability of a deterministic system in the form $y_{k+1} = A_{[2]} y_k$ [13]. Thus the complexity of the stability problem is greatly reduced. Theorem 1.3 only provides a sufficient condition for stability. The condition was conjectured to be necessary as well [2, 15]. In the following, we briefly review the research results related to Theorem 1.3.

In [14], Theorem 1.3 was proven to be necessary and sufficient for a scalar case, that is, $A_i (i = 1, \ldots, N)$ are scalar. In [15], the necessity of Theorem 1.3 was proven for a special case with $N = 2$ and $n = 2$. In [4, 12], Theorem 1.3 was asserted to be necessary and sufficient for more general jump linear systems. Specifically, Bhaurucha [12] considered a random sampling system with the sampling intervals governed by a Markov chain while Mariton [4] studied a continuous-time jump linear system. Although their sufficiency proof is convincing, their necessity proof is incomplete.

The work in [3] may shed light on the proof of the necessity of Theorem 1.3. In [3], a jump linear system model being a little different from (1.1) is considered. The difference lies in

(i) $x[k] \in C^n$, where $C$ stands for the set of complex numbers,

(ii) $x_0 \in S_c$, where $S_c$ is the set of complex vectors with finite second-order moments in the complex state space.

The mean square stability in [3] is defined as

$$\lim_{k \to \infty} \mathbf{E}\left[x[k] x^*[k] \mid x_0, q_0\right] = 0, \quad \forall x_0 \in S_c, \forall q_0, \tag{1.7}$$

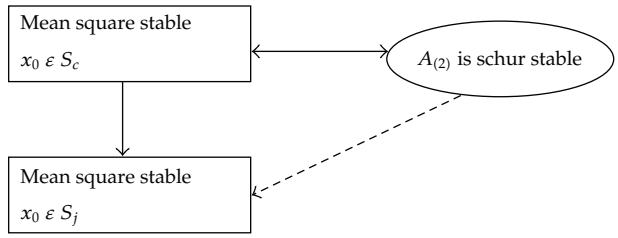


**Figure 1:** Relationship between different senses of mean square stability.

where * stands for the conjugate transpose. Corresponding to the definition in (1.7), the mean square stability in (1.4) can be eewritten into (because $x[k] \in R^n$ in (1.4), there is no difference between $x^T[k]$ and $x^*[k]$),

$$\lim_{k\to\infty} \mathbf{E}\left[x[k]x^*[k] \mid x_0, q_0\right] = 0, \quad \forall x_0 \in S_j, \forall q_0, \tag{1.8}$$

where $S_j$ is the set of all vectors in $R^n$. For any vector $x \in R^n$, we can treat it as a random vector with a single element in $R^n$, and also a random vector in $C^n$. Of course, such random vectors have finite second-order moments. Therefore, we know

$$S_j \subset S_c, \qquad S_j \cap S_c \neq S_c. \tag{1.9}$$

It can be seen that the mean square stability in (1.7) requires *stronger* condition ($x_0 \in S_c$) than the one in (1.8) ($x_0 \in S_j$). When $A_i (i = 1, \ldots, N)$ are real matrices, a necessary and sufficient stability condition was given in the complex state domain.

**Theorem 1.5** (see [3]). *The jump linear system in* (1.1) *(with complex states) is mean square stable in the sense of* (1.7) *if and only if* $A_{[2]}$ *is Schur stable.*

*Due to the relationship of* $S_j \subset S_c$ *and Theorem 1.5, we can establish the relationship diagram in Figure 1. As it shows, the Schur stability of* $A_{[2]}$ *is a sufficient condition for mean square stability with* $x_0 \in S_j$ *at the first look.*

We are still wondering *"whether the condition in Theorem 1.3 is necessary too?"* the answer is definitely *"yes."* That necessity was conjectured in [2]. A proof to the necessity of that condition was first given in [16], which extends the state domain to the complex space and establishes the desired necessity in the stability sense of (1.7). As mentioned before, our concerned stability (in the sense of (1.8)) is weaker than that in (1.7). This paper proves that the weaker condition in (1.8) still yields the schur stability of $A_{[2]}$, that is, the necessity of theorem 1.3 is confirmed. This paper confines the state to the real space domain and makes the best use of the essential properties of the markov jump linear systems to reach the desired necessity goal. In Section 2, a necessary and sufficient version of Theorem 1.3 is stated and its necessity is strictly proven. In Section 3, final remarks are placed.

## 2. A Necessary and Sufficient Condition for Mean Square Stability

This section will give a necessary and sufficient version of Theorem 1.3. Throughout this section, we will define mean square stability in the sense of (1.4) ($x_0 \in S_j$). At the beginning, we will give a brief introduction to the Kronecker product and list some of its properties. After then, the main result, a necessary and sufficient condition for the mean square stability, is presented in Theorem 2.1 and its necessity is proven by direct matrix computations.

### 2.1. Mathematical Preliminaries

Some of the technical proofs in this paper make use of the *Kronecker product*, $\otimes$ [1]. The Kronecker product of two matrices $A = (a_{ij})_{M\times N}$, $B = (b_{pq})_{P\times Q}$ is defined as

$$A \otimes B = \begin{bmatrix} a_{11}B & a_{12}B & \cdots & a_{1N}B \\ a_{21}B & a_{22}B & \cdots & a_{2N}B \\ \vdots & \vdots & \ddots & \vdots \\ a_{M1}B & a_{M2}B & \cdots & a_{MN}B \end{bmatrix}_{MP\times NQ}. \tag{2.1}$$

For simplicity, $A \otimes A$ is denoted as $A^{[2]}$ and $A \otimes A^{[n]}$ is denoted as $A^{[n+1]}(n \geq 2)$.

For two vectors $x$ and $y$, $x \otimes y$ simply rearranges the columns of $xy^T$ into a vector. So for two stochastic processes $\{x[n]\}$ and $\{y[n]\}$, $\lim_{n\to\infty}\mathbf{E}[x[n] \otimes y[n]] = 0$ if and only if $\lim_{n\to\infty}\mathbf{E}[x[n]y^T[n]] = 0$. Furthermore, if $\lim_{n\to\infty}\mathbf{E}[x^{[2]}[n]] = 0$ and $\lim_{n\to\infty}\mathbf{E}[y^{[2]}[n]] = 0$, then

$$\lim_{n\to\infty}\mathbf{E}\left[x[n] \otimes y[n]\right] = 0. \tag{2.2}$$

The following property of the Kronecker product will be frequently used in the technical proofs

$$(A_1A_2\cdots A_n) \otimes (B_1B_2\cdots B_n) = (A_1 \otimes B_1)(A_2 \otimes B_2)\cdots(A_n \otimes B_n), \tag{2.3}$$

where $A_i$, $B_i(i = 1, 2, \ldots, n)$ are all matrices with appropriate dimensions.

Our computations need two linear operators, **vec** and **devec**. The **vec** operator transforms a matrix $A = (a_{ij})_{M\times N}$ into a vector as

$$\mathrm{vec}(A) = [a_{11}\cdots a_{M1}a_{12}\cdots a_{M2}\cdots a_{1N}\cdots a_{MN}]^T. \tag{2.4}$$

The **devec** operator inverts the **vec** operator for a square matrix, that is,

$$\mathrm{devec}(\mathrm{vec}(A)) = A, \tag{2.5}$$

where $A$ is a square matrix.

### 2.2. Main Results

**Theorem 2.1.** *The jump linear system in* (1.1) *is mean square stable if and only if* $A_{[2]}$ *is Schur stable, that is, all eigenvalues of* $A_{[2]}$ *lie within the unit circle.*

*There are already some complete proofs for sufficiency of Theorem 2.1, [3, 12, 13]. So we will focus on the necessity proof. Throughout this section, the following notational conventions will be followed.*

The initial condition of the jump linear system in (1.1) is denoted as $x[0] = x_0, q[0] = q_0$ and the distribution of $q_0$ is denoted as $p = [p_1 \;\; p_2 \;\; \cdots \;\; p_N]$ $(P(q[0] = q_i \mid q_0) = p_i)$.

The system transition matrix in (1.1) is defined as

$$\Phi(k;m) = \begin{cases} \prod_{l=m}^{k-1} A\left[q[l]\right], & \text{if } m < k, \\ I_n, & \text{if } m \geq k, \end{cases} \tag{2.6}$$

where $I_n$ is an identity matrix with the order of $n$. With this matrix, the system's state at time instant $k$ can be expressed as

$$x[k] = \Phi(k;0)x_0. \tag{2.7}$$

A conditional expectation is defined as

$$\Phi_i[k] = P(q[k] = q_i \mid q_0)\mathbf{E}\left[(\Phi(k;0))^{[2]} \mid q[k] = q_i, q_0\right], \tag{2.8}$$

where $i = 1, 2, \ldots, N$. Specially $\Phi_i[0] = p_i I_{n^2}$ $(i = 1, \ldots, N)$. Based on the definition of $\Phi_i[k]$, we obtain

$$\mathbf{E}\left[(\Phi(k;0))^{[2]} \mid q_0\right] = \sum_{i=1}^{N} \Phi_i[k]. \tag{2.9}$$

By combining all $\Phi_i[k] (i = 1, 2, \ldots, N)$ into a bigger matrix, we define

$$V_\Phi[k] = \left[\Phi_1^T[k] \;\; \Phi_2^T[k] \;\; \cdots \;\; \Phi_N^T[k]\right]^T. \tag{2.10}$$

Thus, $V_\Phi[0] = p^T \otimes I_{n^2}$.

The necessity proof of Theorem 2.1 needs the following three preliminary Lemmas.

**Lemma 2.2.** *If the jump linear system in* (1.1) *is mean square stable, then*

$$\lim_{k \to \infty} \mathbf{E}\left[(\Phi[k;0])^{[2]} \mid q_0\right] = 0, \quad \forall q_0. \tag{2.11}$$

*Proof of Lemma 2.2.* Because the system is mean square stable, we get

$$\lim_{k\to\infty} \mathbf{E}\left[x^{[2]}[k] \mid x_0, q_0\right] = 0, \quad \forall x_0,\, q_0. \tag{2.12}$$

The expression of $x[k] = \Phi(k;0)x_0$ yields

$$\lim_{k\to\infty} \mathbf{E}\left[(\Phi(k;0)x_0)^{[2]} \mid x_0, q_0\right] = 0. \tag{2.13}$$

$\Phi(k;0)$ is an $n \times n$ matrix. So we can denote it as $\Phi(k;0) = [a_1(k), a_2(k), \ldots, a_n(k)]$, where $a_i(k)$ is a column vector. By choosing $x_0 = e_i$ ($e_i$ is an $R^{n\times 1}$ vector with the $i$th element as 1 and the others as 0), (2.13) yields

$$\lim_{k\to\infty} \mathbf{E}\left[a_i^{[2]}[k] \mid q_0\right] = 0, \quad i = 1, 2, \ldots, n. \tag{2.14}$$

By the definition of the Kronecker product, we know

$$(\Phi(k;0))^{[2]} = [a_1[k] \otimes a_1[k], \ldots, a_1[k] \otimes a_n[k], \ldots, a_n[k] \otimes a_1[k], \ldots, a_n[k] \otimes a_n[k]]. \tag{2.15}$$

So (2.14) yields

$$\lim_{k\to\infty} \mathbf{E}\left[(\Phi[k;0])^{[2]} \mid q_0\right] = 0, \quad \forall q_0. \tag{2.16}$$

□

**Lemma 2.3.** *If the jump linear system in* (1.1) *is mean square stable, then*

$$\lim_{k\to\infty} \Phi_i[k] = 0, \quad i = 1, \ldots, N, \forall q_0. \tag{2.17}$$

*Proof of Lemma 2.3.* Choose any $z_0, w_0 \in R^n$. Lemma 2.2 guarantees

$$\lim_{k\to\infty} \mathbf{E}\left[\left(z_0^{[2]}\right)^T (\Phi(k;0))^{[2]} w_0^{[2]} \mid q_0\right] = 0. \tag{2.18}$$

By the definition of the Kronecker product, we know

$$\mathbf{E}\left[\left(z_0^{[2]}\right)^T (\Phi(k;0))^{[2]} w_0^{[2]} \mid q_0\right] = \mathbf{E}\left[\left(z_0^T \Phi(k;0) w_0\right)^2 \mid q_0\right]. \tag{2.19}$$

By (2.8), (2.9), and (2.19), we get

$$\mathbf{E}\left[\left(z_0^T \Phi[k;0] w_0\right)^2 \mid q_0\right] = \sum_{i=1}^{N} P(q[k] = q_i \mid q_0)\, \mathbf{E}\left[\left(z_0^T \Phi[k,0] w_0\right)^2 \mid q[k] = q_i, q_0\right]. \tag{2.20}$$

Because $P(q[k] = q_i \mid q_0) \geq 0$ and $\mathbf{E}[(z_0^T \Phi[k;0] w_0)^2 \mid q[k] = q_i, q_0] \geq 0$, the combination of (2.18) and (2.20) yields

$$\lim_{k\to\infty} P(q[k] = q_i \mid q_0)\mathbf{E}\left[\left(z_0^T \Phi(k;0) w_0\right)^2 \mid q[k] = q_i, q_0\right] = 0. \tag{2.21}$$

$\Phi(k;0)$ is an $n \times n$ matrix. So it can be denoted as $\Phi(k;0) = (a_{mj}(k))_{m=1,\ldots,n;j=1,\ldots,n}$. In (2.21), we choose $z_0 = e_m$ and $w_0 = e_j$ and get

$$\lim_{k\to\infty} P(q[k] = q_i \mid q_0)\mathbf{E}\left[\left(a_{mj}(n)\right)^2 \mid q[k] = q_i, q_0\right] = 0, \tag{2.22}$$

where $i = 1, 2, \ldots, N$, $m = 1, \ldots, n$ and $j = 1, \ldots, n$. By the definition of $\Phi_i[k]$, we know the elements of $\Phi_i[k]$ take the form of

$$P(q[k] = q_i \mid q_0)\mathbf{E}\left[a_{m_1 j_1}(k) a_{m_2 j_2}(k) \mid q[k] = q_i, q_0\right], \tag{2.23}$$

where $m_1, m_2, j_1, j_2 = 1, \ldots, n$. So (2.22) guarantees

$$\lim_{k\to\infty} \Phi_i[k] = 0, \quad \forall q_0. \tag{2.24}$$

□

**Lemma 2.4.** *$V_\Phi[k]$ is governed by the following dynamic equation*

$$V_\Phi[k] = A_{[2]} \qquad V_\Phi[k-1], \tag{2.25}$$

*with $V_\Phi[0] = p^T \otimes I_{n^2}$.*

*Proof of Lemma 2.4.* By the definition in (2.8), we can recursively compute $\Phi_i[k]$ as follows:

$$\begin{aligned}
\Phi_i[k] &= P(q[k] = q_i \mid q_0)\mathbf{E}\left[\left(A\left[q[k-1]\right]\Phi(k-1;0)\right)^{[2]} \mid q[k] = q_i, q_0\right] \\
&= P(q[k] = q_i \mid q_0)\mathbf{E}\left[\left(A\left[q[k-1]\right]\right)^{[2]} (\Phi(k-1;0))^{[2]} \mid q[k] = q_i, q_0\right] \\
&= P(q[k] = q_i \mid q_0)\sum_{j=1}^{N} P(q[k-1] = q_j \mid q[k] = q_i, q_0) \\
&\qquad \times \mathbf{E}\left[\left(A\left[q[k-1]\right]\right)^{[2]} (\Phi(k-1;0))^{[2]} \mid q[k] = q_i, q[k-1] = q_j, q_0\right] \\
&= \sum_{j=1}^{N} A_j^{[2]} P(q[k] = q_i \mid q_0) P(q[k-1] = q_j \mid q[k] = q_i, q_0) \\
&\qquad \times \mathbf{E}\left[(\Phi(k-1;0))^{[2]} \mid q[k] = q_i, q[k-1] = q_j, q_0\right].
\end{aligned} \tag{2.26}$$

Because $\Phi(k-1;0)$ depends on only $\{q[k-2], q[k-3], \ldots, q[0]\}$ and the jump sequence $\{q[k]\}$ is Markovian, we know

$$\mathbf{E}\Big[(\Phi(k-1;0))^{[2]} \mid q[k] = q_i, q[k-1] = q_j, q_0\Big] = \mathbf{E}\Big[(\Phi(k-1;0))^{[2]} \mid q[k-1] = q_j, q_0\Big]. \quad (2.27)$$

$P(q[k] = q_i \mid q_0)P(q[k-1] = q_j \mid q[k] = q_i, q_0)$ can be computed as

$$\begin{aligned} &P(q[k] = q_i \mid q_0)P(q[k-1] = q_j \mid q[k] = q_i, q_0) \\ &\quad = P(q[k-1] = q_j, q[k] = q_i \mid q_0) \\ &\quad = P(q[k] = q_i \mid q[k-1] = q_j, q_0)P(q[k-1] = q_j \mid q_0) \\ &\quad = P(q[k] = q_i \mid q[k-1] = q_j)P(q[k-1] = q_j \mid q_0) \\ &\quad = q_{ji}P(q[k-1] = q_j \mid q_0). \end{aligned} \quad (2.28)$$

Substituting (2.27) and (2.28) into the expression of $\Phi_i[k]$, we get

$$\Phi_i[k] = \sum_{j=1}^{N} q_{ji} A_j^{[2]} \Phi_j[k-1]. \quad (2.29)$$

After combining $\Phi_i[k] (i = 1, 2, \ldots, N)$ into $V_\Phi[k]$ as (2.10), we get

$$V_\Phi[k] = A_{[2]} V_\Phi[k-1]. \quad (2.30)$$

We can trivially get $V_\Phi[0]$ from $\Phi_i[0]$ by (2.10). □

*Proof of Necessity of Theorem 2.1.* By Lemma 2.3, we get

$$\lim_{k\to\infty} V_\Phi[k] = 0. \quad (2.31)$$

By Lemma 2.4, we get $V_\Phi[k] = A_{[2]}^k V_\Phi[0]$ and $V_\Phi[0] = p^T \otimes I_{n^2}$. Therefore, (2.31) yields

$$\lim_{k\to\infty} A_{[2]}^k \left(p^T \otimes I_{n^2}\right) = 0, \quad (2.32)$$

for any $p$ (the initial distribution of $q_0$).

$A_{[2]}^k$ is an $Nn^2 \times Nn^2$ matrix. We can write $A_{[2]}^k$ as $A_{[2]}^k = [A^1(k), A^2(k), \ldots, A^N(k)]$ where $A^i(n) (i = 1, \ldots, N)$ is an $Nn^2 \times n^2$ matrix. By taking $p_i = 1$ and $p_j = 0 (j = 1, \ldots, i-1, i+1, \ldots, N)$, (2.32) yields

$$\lim_{k\to\infty} A^i(k) = 0. \quad (2.33)$$

Thus we can get

$$\lim_{k\to\infty} A_{[2]}^k = 0. \quad (2.34)$$

So $A_{[2]}$ is Schur stable. The proof is completed. □

## 3. Conclusion

This paper presents a necessary and sufficient condition for the second moment stability of a discrete-time Markovian jump linear system. Specifically this paper provides proof for the necessity part. Different from the previous necessity proof, this paper confines the state domain to the real space. It investigates the structures of relevant matrices and make a good use of the essential properties of Markov jump linear systems, which may guide the future research on such systems.

## Acknowledgment

This work was supported in part by the National Natural Science Foundation of China (60904012), the Program for New Century Excellent Talents in University (NCET-10-0917) and the Doctoral Fund of Ministry of Education of China (20093402120017).

## References

[1] R. Bellman, *Introduction to Matrix Analysis*, McGraw-Hill, New York, NY, USA, 1960.

[2] Y. Fang and K. A. Loparo, "Stochastic stability of jump linear systems," *IEEE Transactions on Automatic Control*, vol. 47, no. 7, pp. 1204–1208, 2002.

[3] O. L. V. Costa and M. D. Fragoso, "Stability results for discrete-time linear systems with Markovian jumping parameters," *Journal of Mathematical Analysis and Applications*, vol. 179, no. 1, pp. 154–178, 1993.

[4] M. Mariton, *Jump Linear Systems in Automatic Control*, Marcel Dekker, 1990.

[5] X. Feng, K. A. Loparo, Y. Ji, and H. J. Chizeck, "Stochastic stability properties of jump linear systems," *IEEE Transactions on Automatic Control*, vol. 37, no. 1, pp. 38–53, 1992.

[6] Y. Ji, H. J. Chizeck, X. Feng, and K. A. Loparo, "Stability and control of discrete-time jump linear systems," *Control Theory and Advanced Technology*, vol. 7, no. 2, pp. 247–270, 1991.

[7] O. Beldiman, G. C. Walsh, and L. Bushnell, "Predictors for networked control systems," in *American Control Conference*, pp. 2347–2351, June 2000.

[8] J. Nilsson, *Real-time control systems with delays*, Ph.D. dissertation, Lund Institute of Technology, 1998.

[9] W. Zhang, M. S. Branicky, and S. M. Phillips, "Stability of networked control systems," *IEEE Control Systems Magazine*, vol. 21, no. 1, pp. 84–97, 2001.

[10] P. Seiler and R. Sengupta, "Analysis of communication losses in vehicle control problems," in *American Control Conference*, pp. 1491–1496, June 2001.

[11] B. Lincoln and A. Cervin, "Jitterbug: a tool for analysis of real-time control performance," in *IEEE Conference on Decision and Control*, pp. 1319–1324, December 2002.

[12] B. Bhaurucha, *On the stability of randomly varying systems*, Ph.D. dissertation, University of California, Berkeley, Calif, USA, 1961.

[13] Y. Fang, *Stability analysis of linear control systems with uncertain parameters*, Ph.D. dissertation, Case Western Reserve University, 1994.

[14] W. S. Gray, O. R. Gonzàlez, and S. Patilkulkarni, "Stability of digital control systems subject to jump linear random perturbations," in *IEEE Confernce on Decision and Control*, pp. 1154–1159, December 2000.

[15] X. Dong, "Stochastic stability of discrete-time jump linear systems," in *Chinese Control Conference*, 2003.

[16] O. L. V. Costa and M. D. Fragoso, "Comments on: 'Stochastic stability of jump linear systems'," *IEEE Transactions on Automatic Control*, vol. 49, no. 8, pp. 1414–1416, 2004.

Hindawi Publishing Corporation
Journal of Applied Mathematics
Volume 2012, Article ID 365923, 17 pages
doi:10.1155/2012/365923

*Research Article*

# Robust Speed Tracking of Networked PMSM Servo Systems with Uncertain Feedback Delay and Load Torque Disturbance

**Qiang Ling,[1] Jing Li,[1] and Haojiang Deng[2]**

[1] *Department of Automation, University of Science and Technology of China, Hefei, Anhui 230027, China*
[2] *National Network New Media Engineering Research Center, Institute of Acoustics, Chinese Academy of Science, Beijing 100190, China*

Correspondence should be addressed to Qiang Ling, qling@ustc.edu.cn

Received 28 February 2012; Revised 30 March 2012; Accepted 31 March 2012

Academic Editor: Baocang Ding



This paper considers a class of networked Permanent Magnet Synchronous Motors (PMSMs), whose feedback loops are closed over a shared data network. Although the installation and maintenance cost of the networked PMSM system can be lowered by replacing the conventional point-to-point feedback cables with a network, the network packet dropouts and transmission delay may degrade the system's performance and even destabilize it. The load torque disturbance is another source to deteriorate the PMSM system's performance. To investigate the effects of the data network and the torque disturbance on the speed tracking of a PMSM system is one major task of this paper. In particular, we derive a sufficient stability condition for this system in an LMI (linear matrix inequality) form and provides a way to bound the system's $H_\infty$ performance. Moreover, we adopt an iterative LMI method to design the speed controller of the PMSM system, which can robustly guarantee stability and performance against the network-induced delays, packet dropouts, and the torque disturbance. Simulations are done to verify the effectiveness of the obtained results.

## 1. Introduction

In the high-performance applications, such as robotics, aeronautic devices, and precision machine tools, the positioning accuracy is required to be higher and higher so that an alternative better than the traditional induction motors is needed. The permanent magnet synchronous motor (PMSM) is one wise choice to meet this accuracy challenge in the low-to-medium power servo systems. Because the PMSM's rotor is a permanent magnet and the flux linkage is constant [1], it possesses many advantages, like superior power density, large torque-to-inertia ratio, and high efficiency. Consequently, the PMSM has received

widespreading acceptance in industrial applications and is recognized as one of the key components in automation applications.

In PMSM applications, speed tracking is of great importance [2]. The existence of the load torque disturbance, however, makes speed tracking a rather tough task. In fact, it is impossible to measure the disturbance directly in real application. One way is to estimate the disturbance and actively cancel it [3]. Such methods may complicate the system design and increase the system's cost. We take another way, that is, designing a robust controller that can guarantee the system's performance is less sensitive to the disturbance.

Conventionally, a PMSM servo system includes a small number of PMSMs, which are connected to controllers by point-to-point cables to close the control loops. The modern industry, however, demands more and more PMSMs that could be located in geographically separated areas. Thus the direct cable connection architecture is inconvenient for the installation and maintenance. Instead, we can close the feedback loops of PMSMs over a digital network to form a networked control system (NCS), which is a newly developed technology being able to reduce the system's wiring cost, simplify the system's diagnosis and maintenance, and improve the system's agility [4]. The use of network will, however, induce intermittent losses and delays of the feedback information, may deteriorate the system's performance, and even cause instability [5]. There are many results on NCSs, some of which are introduced here (see more in the survey [6]). Reference [7] investigates the problem of robust stabilization and disturbance for the NCSs with random communication network-induced delays. Reference [8] Considers $H_\infty$ output tracking for NCSs with delays and data packet dropouts. In [9], the discrete-time NCSs is studied and a state feedback controller with less conservatism is given. Moreover, a modified optimization algorithm is also proposed in [9] to cope with Bilinear Matrix Inequalities (BMIs).

As an important field of NCSs, networked servo systems are also well studied in recent years. In [10], fuzzy logic control is used to enhance the performance of networked servo systems with delays. To compensate the noise in the transmission channels, two-degrees-of-freedom control is utilized in [11]. Predictive control [12] is implemented to suppress the negative effects of delays and dropouts induced by the network. These results mainly focus on servo systems with DC motors or AC induction motors. Nevertheless, PMSM, as one of the main actuators in servo systems, is rarely mentioned in the previous NCS research. Due to its great potential in the industry, the networked PMSM servo systems could be one of the hot research topics in the future. Though a networked PMSM servo system has the same problems of data packet dropouts and transmission delay as typical networked servo systems, it has its own characteristics due to the employment of field-orientation mechanism and the special motor structures [13]. So when we design a controller for such a system, the specific properties should be taken into account to achieve less conservative results. The load torque disturbance, as a common disturbance in applications, should also be considered in the networked PMSM servo system.

This paper is organized as follows. In Section 2, we establish the mathematical model for the networked PMSM servo systems, which suffers the uncertain network-induced delay and data dropouts as well as the load torque disturbance. A sufficient stability condition of the system is given and proven in Section 3 based on the Lyapunov-Krasovskii techniques. Moreover, a bound on the system's $H_\infty$ performance is also provided in Section 3. An iterative LMI method is proposed to design a robust controller in Section 4, which can guarantee both the stability and performance under the torque perturbation and the network-induced delay and dropouts. Simulations are done in Section 5 to verify the effectiveness of the obtained results. Some final remarks are placed in Section 6.

## 2. Problem Formulation

### 2.1. PMSM Dynamics

In the synchronously rotating rotor $d$-$q$ coordinate, a PMSM drive can be modeled as [2]

$$\begin{aligned} u_d &= Ri_d + L_d\frac{di_d}{dt} - n_p\omega L_q i_q, \\ u_q &= Ri_q + L_q\frac{di_q}{dt} + n_p\omega L_d i_d + n_p\omega\phi_a, \\ J\frac{d\omega}{dt} &+ B_0\omega + T_l = n_p\phi_a, \end{aligned} \tag{2.1}$$

where $\omega$ is the rotating speed; $i_d$ and $i_q$ are the $d$- and $q$-axes stator currents, respectively; $u_d$ and $u_q$ are the $d$- and $q$-axes stator voltages, respectively; $R$ is the stator resistance per phase; $L_d$ and $L_q$ are the $d$- and $q$-axes stator inductances, respectively, and $L_d = L_q = L$ in the surface-mounted PMSM; $n_p$ is the number of poles; $\phi_a = \sqrt{3/2}\phi_f$, with $\phi_f$ being the flux linkage of the permanent magnet rotor; $J$ is the total moment of inertia of the motor and load, and $B_0$ is the friction coefficient of the motor; $T_l$ is the load torque.

A well-known strategy for a PMSM drive is the field-oriented vector control approach. Under this scheme, a practical structure of cascaded control loops, including a speed loop and two current loops, is usually employed [14]. In order to approximately eliminate the coupling between the $d$- and $q$-axes currents, the $d$-axis reference current $i_d^*$ is set at zero and $i_d$ is regulated via a PI controller, as is shown in Figure 1.

Design the current controller of the $q$-axis as

$$u_q = Ri_{qr} + n_p\phi_a\omega, \tag{2.2}$$

where $i_{qr}$ is the reference current of the $q$-axis, which is computed by the speed controller. Then the state-space equation of a PMSM can be represented as

$$\begin{bmatrix} \dfrac{di_q}{dt} \\ \dfrac{d\omega}{dt} \end{bmatrix} = \begin{bmatrix} -\dfrac{R}{L} & 0 \\ \dfrac{n_p\phi_a}{J} & -\dfrac{B_0}{J} \end{bmatrix} \begin{bmatrix} i_q \\ \omega \end{bmatrix} + \begin{bmatrix} \dfrac{R}{L} \\ 0 \end{bmatrix} i_{qr} + \begin{bmatrix} 0 \\ -\dfrac{T_l}{J} \end{bmatrix}. \tag{2.3}$$

To proceed further, we need to make the following two definitions.

*Definition 2.1.* The tracking errors of speed, the $q$-axis current $i_q$, and the reference current $i_{qr}$ are defined as

$$e(t) = \omega^* - \omega, \qquad e_q(t) = i_q^* - i_q, \qquad e_{qr}(t) = i_{qr}^* - i_{qr}, \tag{2.4}$$

where $\omega^*$, $i_q^*$, $i_{qr}^*$ are the corresponding reference values.

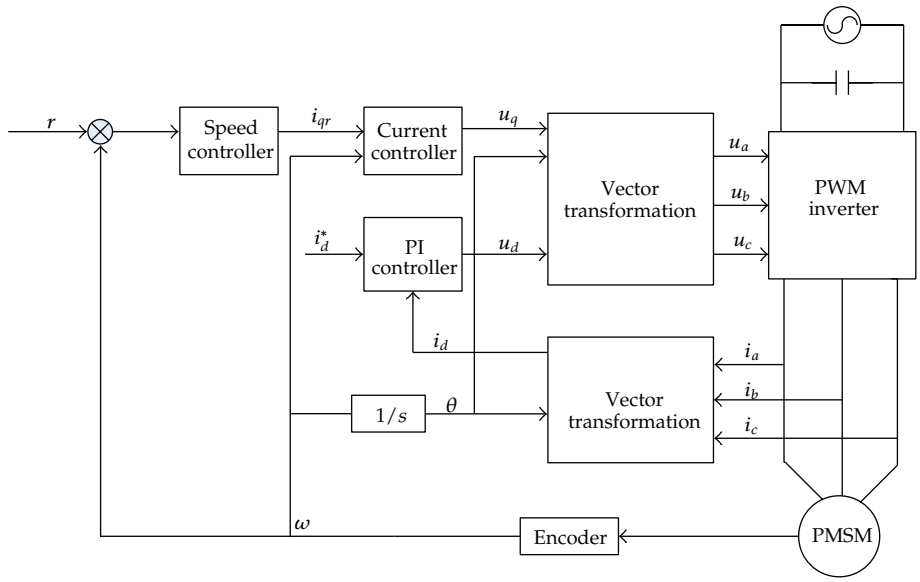


**Figure 1:** Configuration of a PMSM Servo System.

By Definition 2.1, the state-space equation (2.3) can be rewritten into a compact form as

$$\dot{x}(t) = Ax(t) + B(u(t) + d(t)), \tag{2.5}$$

where

$$x(t) = \left[e_q(t)\ e(t)\right]^T, \qquad u(t) = \left[e_{qr}(t)\ 0\right]^T, \qquad d(t) = \left[0\ \Delta T_l(t)\right]^T,$$
$$A = \begin{bmatrix} -\dfrac{R}{L} & 0 \\ \dfrac{n_p\phi_a}{J} & -\dfrac{B_0}{J} \end{bmatrix}, \qquad B = \begin{bmatrix} \dfrac{R}{L} & 0 \\ 0 & \dfrac{1}{J} \end{bmatrix}. \tag{2.6}$$

$\Delta T_l(t)$ represents the load torque disturbance, which is bounded and perhaps time-varying.

*Definition 2.2.* The disturbance suppressing performance of the system is evaluated by the following signal:

$$z(t) = e(t). \tag{2.7}$$

We want to design a robust controller for a networked PMSM to satisfy the following requirements.

(1) When the load torque disturbance $d(t) = 0$, the system is asymptotically stable under any initial state, namely,

$$\lim_{t\to\infty} z(t) = 0. \tag{2.8}$$

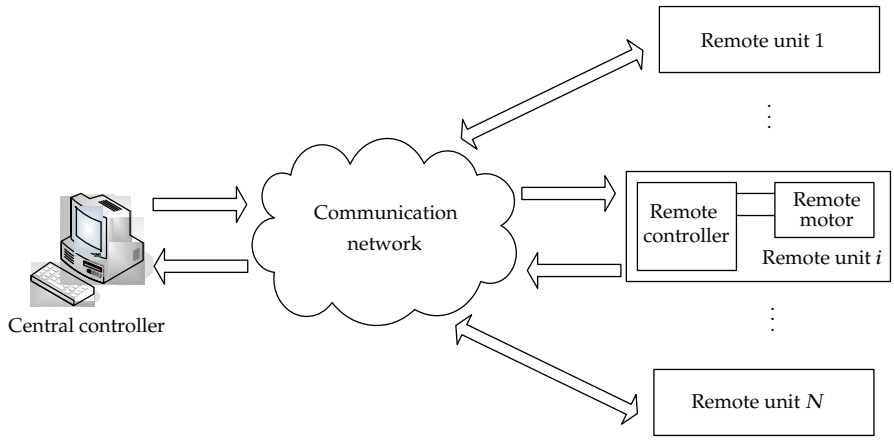


**Figure 2:** The diagram of a typical networked servo system.

(2) When the load torque disturbance $d(t) \neq 0$, the closed-loop system has the ability to suppress disturbance, namely,

$$\|z(t)\|_2 \leq \gamma \|d(t)\|_2, \tag{2.9}$$

where $\|\cdot\|_2$ stands for the $L_2$ norm of a continuous-time signal and $\gamma$ is a quantitative measure of the disturbance attenuation. The smaller $\gamma$, the better disturbance attenuation.

## 2.2. Structure of Networked PMSM Servo Systems

A typical networked servo system is shown in Figure 2, which can be divided into three parts:

(1) the remote unit containing a remote controller and a remote motor,
(2) the central controller,
(3) the communication network.

The remote unit and the central controller exchange feedback information through the communication network.

When the remote motors are PMSMs, we get a networked PMSM servo system as shown in Figure 3. Each distributed remote controller receives control signals from the communication network and then convert them into PWM signals to drive the motor. It also sends local measurements, such as rotating speed, motor current, and local environment information, back to the central controller via the shared data network. The central controller is usually a sophisticated controller and can provide advanced real-time control strategies to the remote units.

## 2.3. System Modeling

Because of the limited bandwidth of the network, data packet dropouts are unavoidable. When a dropout occurs, it might be more advantageous to drop the old packet and transmit a new one than to retransmit the old one [15]. Network-induced delays are also considered here. The model of the concerned networked PMSM servo system is shown in Figure 4.

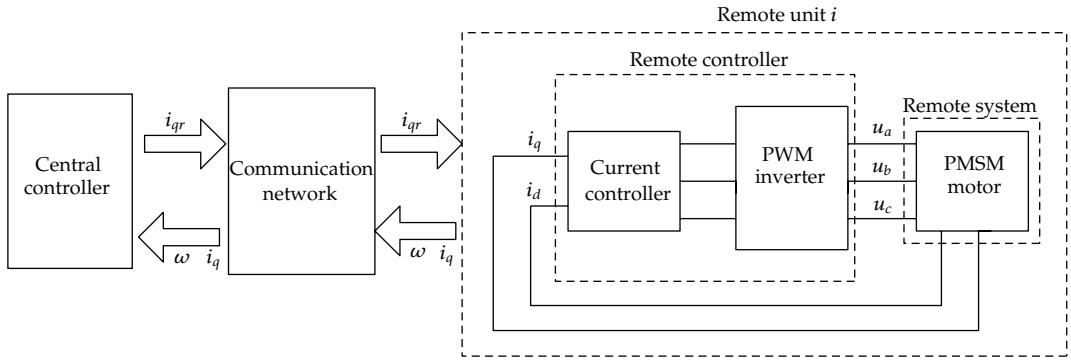


**Figure 3:** The diagram of a networked PMSM servo system.

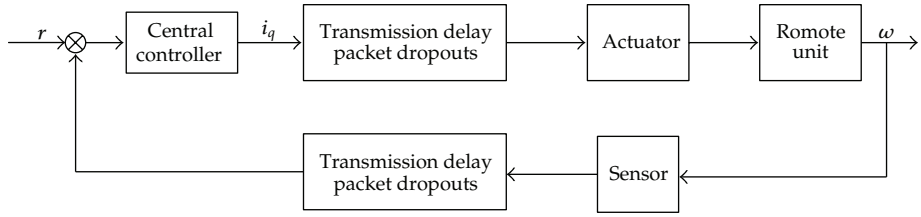


**Figure 4:** The model of the networked PMSM servo system.

The following assumptions are placed on the networked PMSM servo system.

(1) The sensor is clock driven, and the controller and actuator are event driven.

(2) The sampling period is a positive constant scalar $h$.

(3) The controller-to-actuator and the sensor-to-controller delays are denoted as $\tau_{ca}$ and $\tau_{sc}$, respectively. The state feedback controller is static (see (2.14)). So these two delays can be lumped as

$$\tau_k = \tau_{sc} + \tau_{ca}. \tag{2.10}$$

Moreover, $\tau_k$ is less than $h$, that is, $0 \leq \tau_k \leq \overline{\tau} \leq h$, where $\overline{\tau}$ is the upper bound of delays. Due to the static feedback controller, we can assume that the transmission from the controller to the actuator is delay free and all delays come from the transmissions from the sensor to the controller, that is, $\tau_{sc} = \tau_k$ and $\tau_{ca} = 0$, in Figure 4.

(4) The maximum numbers of the consecutive controller-to-actuator and sensor-to-controller data dropouts are denoted as $d_{ca}$ and $d_{sc}$, respectively. They can also be lumped as

$$d_k = d_{ca} + d_{sc}. \tag{2.11}$$

$d_k$ is bounded as $0 \leq d_k \leq \overline{d}$. Similar to $\tau_k$, $d_k$ is also assumed to only come from the transmissions from the sensor to the controller, that is, $d_{sc} = d_k$ and $d_{ca} = 0$.

If only delays exist in the system, the sampled signal at $kh$ ($\forall k \in \mathcal{N}$) will arrive at the controller at the time $kh + \tau_k$. So the delay is $\eta(t) = t - kh$ and its range is

$$\eta(t) \in [0, h + \overline{\tau}], \tag{2.12}$$

When the data dropouts also exist, they can be treated as delays and yield the following overall delay range:

$$\eta(t) \in \left[0, \left(\overline{d} + 1\right)h + \overline{\tau}\right] = [0, \overline{\eta}]. \tag{2.13}$$

It is well known that time-varying delay is more difficult to handle than constant delay from the control system's perspective. The actuator can know the total delay $\eta(t)$ by the time stamping technique. In the present paper, the actuator is assumed to purposefully postpone to implement the received control variable by the time of $\overline{\eta} - \eta(t)$ and yields a constant overall delay of $\overline{\eta}$, which is easier to deal with. We choose a static state feedback controller. Due to the constant delay strategy, our controller takes the following form:

$$u(t) = Kx\left(t - \overline{\eta}\right), \tag{2.14}$$

where $K$ is the feedback gain to be designed. By substituting (2.14) into (2.5), we get the following state-space equation of the networked PMSM servo system:

$$\begin{aligned} \dot{x}(t) &= Ax(t) + BKx\left(t - \overline{\eta}\right) + Bd, \\ z(t) &= Cx(t). \end{aligned} \tag{2.15}$$

## 3. Analysis of Networked PMSM Servo Systems

### 3.1. A Sufficient Stability Condition

In industry applications, the stability of a servo system is crucial. So we first have to guarantee that the system is stable. Here stability means the asymptotic stability when the disturbance is zero, that is, $d(t) = 0$. Under the delay and dropout conditions in (2.13), we get the following stability condition, which is expressed in an LMI (linear matrix inequality) form and easy to verify.

**Theorem 3.1.** *Under the given controller gain $K$ and the upper bound $\overline{\eta} > 0$ (in (2.13)), the system (2.15) is asymptotically stable if there exist matrices $P > 0$, $Q > 0$, $Z > 0$, $Y$ and $W$ such that the following matrix inequality (3.1) holds:*

$$\begin{bmatrix} W_1 & W_2 & -\overline{\eta}Y & A^T \\ * & W_3 & -\overline{\eta}W & K^T B^T \\ * & * & -\overline{\eta}Z & 0 \\ * & * & * & -\overline{\eta}^{-1}Z^{-1} \end{bmatrix} < 0, \tag{3.1}$$

*where $W_1 = PA + A^T P + Y + Y^T + Q$, $W_2 = PBK - Y + W^T$, and $W_3 = -Q - W - W^T$.*

*Proof.* We construct the following Lyapunov-Krasovskii function:

$$V(t) = V_1(t) + V_2(t) + V_3(t), \tag{3.2}$$

where $V_1(t) = x^T(t)Px(t)$, $V_2(t) = \int_{t-\overline{\eta}}^{t} x^T(\alpha)Qx(\alpha)d\alpha$, and $V_3(t) = \int_{-\overline{\eta}}^{0}\int_{t+\beta}^{t} \dot{x}^T(s)Z\dot{x}(s)ds\,d\beta$. By the Newton-Leibniz formula, we get

$$x\left(t-\overline{\eta}\right) = x(t) - \int_{t-\overline{\eta}}^{t} \dot{x}(\alpha)d\alpha. \tag{3.3}$$

The derivatives of $V_1$, $V_2$, and $V_3$ are computed as follows:

$$\begin{aligned}
\dot{V}_1(t) &= 2x^T(t)P\left[Ax(t) + BKx\left(t-\overline{\eta}\right)\right] \\
&= 2x^T(t)P(A+BK)x(t) - 2x^T(t)PBK\int_{t-\overline{\eta}}^{t}\dot{x}(\alpha)d\alpha \\
&= 2x^T(t)P(A+BK)x(t) \\
&\quad + 2x^T(t)(Y-PBK)\int_{t-\overline{\eta}}^{t}\dot{x}(\alpha)d\alpha + 2x^T\left(t-\overline{\eta}\right)W\int_{t-\overline{\eta}}^{t}\dot{x}(\alpha)d\alpha \\
&\quad - \left[2x^T(t)Y\int_{t-\overline{\eta}}^{t}\dot{x}(\alpha)d\alpha + 2x^T\left(t-\overline{\eta}\right)W\int_{t-\overline{\eta}}^{t}\dot{x}(\alpha)d\alpha\right] \\
&= 2x^T(t)P(A+BK)x(t) + 2x^T(t)(Y-PBK)\left[x(t) - x\left(t-\overline{\eta}\right)\right] \\
&\quad + 2x^T\left(t-\overline{\eta}\right)W\left[x(t) - x\left(t-\overline{\eta}\right)\right] \\
&\quad - \left[2x^T(t)Y\int_{t-\overline{\eta}}^{t}\dot{x}(\alpha)d\alpha + 2x^T\left(t-\overline{\eta}\right)W\int_{t-\overline{\eta}}^{t}\dot{x}(\alpha)d\alpha\right] \\
&= \frac{1}{\overline{\eta}}\int_{t-\overline{\eta}}^{t}\Big[2x^T(t)(PA+Y)x(t) + 2x^T(t)\Big(PBK - Y + W^T\Big)x\left(t-\overline{\eta}\right) \\
&\qquad -2x^T\left(t-\overline{\eta}\right)Wx\left(t-\overline{\eta}\right) - 2x^T(t)\overline{\eta}Y\dot{x}(\alpha) - 2x^T\left(t-\overline{\eta}\right)\overline{\eta}W\dot{x}(\alpha)\Big]d\alpha, \\
\dot{V}_2(t) &= x^T(t)Qx(t) - x^T\left(t-\overline{\eta}\right)Qx\left(t-\overline{\eta}\right) \\
&= \frac{1}{\overline{\eta}}\int_{t-\overline{\eta}}^{t}\Big[x^T(t)Qx(t) - x^T\left(t-\overline{\eta}\right)Qx\left(t-\overline{\eta}\right)\Big]d\alpha, \\
\dot{V}_3(t) &= \int_{-\overline{\eta}}^{0}\Big[\dot{x}^T(t)Z\dot{x}(t) - \dot{x}\left(t+\beta\right)Z\dot{x}\left(t+\beta\right)\Big]d\beta \\
&= \int_{t-\overline{\eta}}^{t}\Big[\dot{x}^T(t)Z\dot{x}(t) - \dot{x}(\alpha)Z\dot{x}(\alpha)\Big]d\alpha \\
&= \frac{1}{\overline{\eta}}\int_{t-\overline{\eta}}^{t}\Big[x^T(t)\overline{\eta}A^TZAx(t) + 2x^T(t)\overline{\eta}A^TZBKx\left(t-\overline{\eta}\right) \\
&\qquad +x^T\left(t-\overline{\eta}\right)\overline{\eta}K^TB^TZBKx\left(t-\overline{\eta}\right) - \dot{x}^T(\alpha)\overline{\eta}Z\dot{x}(\alpha)\Big]d\alpha.
\end{aligned} \tag{3.4}$$

Finally, we have

$$\dot{V}(t) = \frac{1}{\overline{\eta}} \int_{t-\overline{\eta}}^{t} \zeta^T(t,\alpha)\Phi\zeta(t,\alpha)d\alpha, \tag{3.5}$$

where

$$\zeta(t,\alpha) = \begin{bmatrix} x(t) \\ x(t-\overline{\eta}) \\ \dot{x}(\alpha) \end{bmatrix}, \qquad \Phi = \begin{bmatrix} W_1 + \overline{\eta}A^T Z A & W_2 + \overline{\eta}A^T Z B K & -\overline{\eta}Y \\ * & W_3 + \overline{\eta}K^T B^T Z B K & -\overline{\eta}W \\ * & * & -\overline{\eta}Z \end{bmatrix}. \tag{3.6}$$

By the Schur complement theorem, we get from (3.1) that there must exist $\epsilon > 0$ such that

$$\Phi < -\epsilon I, \tag{3.7}$$

where $I$ represents an identity matrix of an appropriate dimension. Substituting (3.7) into (3.5) yields

$$\dot{V}(t) < -\epsilon\|x(t)\|^2. \tag{3.8}$$

According to Lyapunov-Krasovskii theorem, if there exist $\epsilon > 0$ such that $\dot{V}(t) < -\varepsilon\|x\|^2$, the system (2.15) is asymptotic stable. So if the matrix inequality (3.1) holds, the system (2.15) is asymptotically stable. This completes the proof. □

### 3.2. Robust Performance Analysis

*Definition 3.2.* A stable system in (2.15) is said to satisfy the $H_\infty$ performance index $\gamma > 0$ if under the zero initial condition,

$$\|z(t)\|_2 \le \gamma\|d(t)\|_2. \tag{3.9}$$

We can verify whether the performance requirement in (3.9) is satisfied through the following theorem.

**Theorem 3.3.** *Under the given controller gain $K$ and the upper bound $\overline{\eta} > 0$ (in (2.13)), the system (2.15) satisfies the performance index $\gamma$ in (3.9) if there exist matrices $P > 0$, $Q > 0$, $Z > 0$, $Y$ and $W$ such that the following matrix inequality holds:*

$$\begin{bmatrix} W_1 & W_2 & -\overline{\eta}Y & PB & A^T & C^T \\ * & W_3 & -\overline{\eta}W & 0 & K^T B^T & 0 \\ * & * & -\overline{\eta}Z & 0 & 0 & 0 \\ * & * & * & -\gamma^2 I & B^T & 0 \\ * & * & * & * & -\overline{\eta}^{-1}Z^{-1} & 0 \\ * & * & * & * & * & -I \end{bmatrix} < 0, \tag{3.10}$$

*where $W_1 = PA + A^T P + Y + Y^T + Q$, $W_2 = PBK - Y + W^T$, and $W_3 = -Q - W - W^T$.*

*Proof.* Equation (3.10) implies (3.1). By Theorem 3.1, we know the system is stable.

Define $J_{zd} = \int_0^\infty [z^T(t)z(t) - \gamma^2 d^T(t)d(t)]dt$. $J_{zd}$ can be modified into

$$J_{zd} = \int_0^\infty \left[z^T(t)z(t) - \gamma^2 d^T(t)d(t) + \dot{V}(t)\right]dt + V(t)|_{t=0} - V(t)|_{t=\infty}. \tag{3.11}$$

Under the zero initial condition, $V(t)|_{t=0} = 0$. Because of $V(t)|_{t=\infty} \geq 0$, we get

$$\begin{aligned} J_{zd} &\leq \int_0^\infty \left[z^T(t)z(t) - \gamma^2 d^T(t)d(t) + \dot{V}(t)\right]dt \\ &\leq \frac{1}{\overline{\eta}} \int_0^\infty \int_{t-\overline{\eta}}^t \begin{bmatrix} x(t) \\ x(t-\overline{\eta}) \\ \dot{x}(\alpha) \\ d(t) \end{bmatrix}^T \Xi \begin{bmatrix} x(t) \\ x(t-\overline{\eta}) \\ \dot{x}(\alpha) \\ d(t) \end{bmatrix}, \end{aligned} \tag{3.12}$$

where

$$\Xi = \begin{bmatrix} W_1 + C^T C & W_2 & -\overline{\eta}Y & PB \\ * & W_3 & -\overline{\eta}W & 0 \\ * & * & -\overline{\eta}Z & 0 \\ * & * & * & -\gamma^2 I \end{bmatrix} + \begin{bmatrix} A^T \\ K^T B^T \\ 0 \\ B^T \end{bmatrix} \overline{\eta} Z \begin{bmatrix} A^T \\ K^T B^T \\ 0 \\ B^T \end{bmatrix}^T. \tag{3.13}$$

By the Schur complement theorem, we know that (3.10) implies $\Xi < 0$. Therefore, $J_{z\omega} < 0$, that is,

$$\int_0^\infty \left[z^T(t)z(t) - \gamma^2 d^T(t)d(t)\right]dt < 0. \tag{3.14}$$

After simple manipulations, the above equation yields

$$\|z(t)\|_2^2 \leq \gamma^2 \|d(t)\|_2^2. \tag{3.15}$$

Equation (3.15) is equivalent to (3.9). □

In (3.9), the left side variable $z(t)$ and the right one $d(t)$ have different units. So the ratio between them, $\gamma$, does not have a clear physical meaning. In order to overcome this difficulty, we introduce the following relative sensitive functions.

*Definition 3.4.* The sensitive functions of the speed tracking error and the load torque disturbance are defined as

$$S_z = \frac{\|Z\|_2}{\omega_{\text{ref}}}, \qquad S_T = \frac{\|\Delta T_l\|_2}{\mathrm{T}_{l0}}, \tag{3.16}$$

where $\omega_{\text{ref}}$ is the reference tracking speed and $T_{l0}$ is the nominal load torque.

Based on the above definition, (3.15) can be rewritten into

$$S_z \le \tilde{\gamma} S_T, \tag{3.17}$$

where $\tilde{\gamma} = (T_{l0}/\omega_{\text{ref}})\gamma$.

*Remark 3.5.* In (3.17), both units of $S_z$ and $S_T$ are percentage. So (3.17) means how much percent of load torque disturbance yields how much percent of speed tracking error. $\tilde{\gamma}$ is exactly the gain between two percentage variables ($S_z$ and $S_T$) and can quantitatively reflect the capability to attenuate the load torque disturbance attenuation. $\tilde{\gamma}$ is determined by the system's delay in (2.13) and the controller gain $K$ in (2.14). Although we cannot change the system's delay, we do have freedom to choose an appropriate $K$ to yield a better (smaller) $\tilde{\gamma}$, which is the major task of the next section.

## 4. The Design of the Robust Controller

When we design the robust controller, the controller gain $K$ is unknown. So the matrix inequalities in Theorems 3.1 and 3.3 are bilinear matrix inequalities (BMIs). As a result, we cannot find a maximum $\overline{\eta}$ or the minimum $\gamma$ using convex optimization algorithms. In the subsequent part, we propose some methods to resolve this issue.

Define $X = P^{-1}$ and $\Delta = \text{diag}\{X, X, X, I, I, I\}$. Pre- and postmultiply (3.10) by $\Delta$, we obtain

$$\begin{bmatrix} \widetilde{W}_1 & \widetilde{W}_2 & -\overline{\eta}\widetilde{Y} & B & XA^T & XC^T \\ * & \widetilde{W}_3 & -\overline{\eta}\widetilde{W} & 0 & F^TB^T & 0 \\ * & * & -\overline{\eta}XS^{-1}X & 0 & 0 & 0 \\ * & * & * & -\gamma^2 I & B^T & 0 \\ * & * & * & * & -\overline{\eta}^{-1}S & 0 \\ * & * & * & * & * & -I \end{bmatrix} < 0, \tag{4.1}$$

where $\widetilde{W}_1 = AX + XA^T + \widetilde{Y} + \widetilde{Y}^T + \widetilde{Q}$, $\widetilde{W}_2 = BF - \widetilde{Y} + \widetilde{W}^T$, $\widetilde{W}_3 = -\widetilde{Q} - \widetilde{W} - \widetilde{W}^T$, $\widetilde{Y} = XYX$, $\widetilde{Q} = XQX$, $\widetilde{W} = XWX$, $F = KX$, and $S = Z^{-1}$.

Define a matrix variable $M < XS^{-1}X$, then matrix inequality (4.1) is equivalent to the combination of matrix inequalities (4.2), (4.3) and(4.4)

$$\begin{bmatrix} \widetilde{W}_1 & \widetilde{W}_2 & -\overline{\eta}\widetilde{Y} & B & XA^T & XC^T \\ * & \widetilde{W}_3 & -\overline{\eta}\widetilde{W} & 0 & F^TB^T & 0 \\ * & * & -\overline{\eta}M & 0 & 0 & 0 \\ * & * & * & -\gamma^2 I & B^T & 0 \\ * & * & * & * & -\overline{\eta}^{-1}S & 0 \\ * & * & * & * & * & -I \end{bmatrix} < 0, \tag{4.2}$$

$$\begin{bmatrix} -Z & P \\ P & -N \end{bmatrix} < 0, \tag{4.3}$$

$$S = Z^{-1}, \qquad N = M^{-1}, \qquad P = X^{-1}. \tag{4.4}$$

Based on the above transformation, a robust controller can be designed as follows.

**Theorem 4.1.** *Under the given $\overline{\eta} > 0$ and $\gamma > 0$, the system* (2.15) *satisfies the performance index $\gamma$ if there exist matrices $X > 0$, $P > 0$, $Q > 0$, $Z > 0$, $M > 0$, $S > 0$, $N > 0$, $Y$ and $W$ such that matrix inequalities* (4.2), (4.3) *and* (4.4) *hold. In this case, a robust $H_\infty$ state feedback controller gain can be chosen as $K = FX^{-1}$.*

It is noted that the conditions in Theorem 4.1 are not LMI because of the inverse matrix constraints in (4.3) and (4.4). Fortunately, there are some methods to efficiently solve these inequalities. In [16], a method is given to obtain the suboptimal delay $\overline{\eta}$ or the suboptimal $\gamma$ by setting $S = X$. With more computational efforts, better results can be obtained by an iterative algorithm in [17]. That iterative algorithm is called cone complementary linearization (CCL) method. By adopting the CCL method, we get the following algorithm to cope with the nonlinear minimization problem subject to LMIs.

*Algorithm 4.2.* There are 4 steps.

*Step 1.* Choose a sufficiently large initial variable $\gamma > 0$ such that there exists a feasible solution to matrix inequalities (4.2) and (4.3) and (4.4). Set $\gamma_{\min} = \gamma$.

*Step 2.* Find a feasible set $(X_0, P_0, Q_0, Z_0, M_0, S_0, N_0, Y_0, W_0)$ satisfying (4.2) and (4.3), and the matrix inequality in (4.5) (One way to get a feasible set is by setting $S = X$ as the aforementioned suboptimal solution). Set $k = 0$,

$$\begin{bmatrix} S & I \\ I & Z \end{bmatrix} < 0, \qquad \begin{bmatrix} N & I \\ I & M \end{bmatrix} < 0, \qquad \begin{bmatrix} P & I \\ I & X \end{bmatrix} < 0. \tag{4.5}$$

*Step 3.* Solve the LMI problem in (4.6),

$$\begin{aligned} &\operatorname{Min}_{X,P,Q,Z,M,S,N,Y,W} \ \operatorname{tr}(S_k Z + S Z_k + N M_k + P_k X + P X_k) \\ &\text{s.t.} \quad \text{equations (4.2),(4.3), and (4.5).} \end{aligned} \tag{4.6}$$

Set $X_{k+1} = X$, $P_{k+1} = P$, $Q_{k+1} = Q$, $Z_{k+1} = Z$, $M_{k+1} = M$, $S_{k+1} = S$, $N_{k+1} = N$, $Y_{k+1} = Y$, and $W_{k+1} = W$.

*Step 4.* If (3.10) holds, then set $\gamma_{\min} = \gamma$ and return to Step 2 after decreasing $\gamma$ to some extent. If (3.10) is not satisfied within a specified number of iterations, to say $k_{\max}$, then we stop the above iterations. Otherwise, set $k = k + 1$ and go back to Step 3.

**Table 1:** The nominal parameters of a PMSM.

| $R$ | $L$ | $\phi_f$ | $B_0$ |
|---|---|---|---|
| 2.875 Ω | 0.0085 H | 0.0816 Wb | 0.00185 N · m · s |
| $J$ | $n_p$ | $T_l$ | |
| 0.0008 N · m · s | 4 | 2 N · m | |

**Table 2:** The relationship between the speed tracking error and $\overline{\eta}$.

| Speed error percentage | 6% | 5.6% | 5.2% | 4.8% | 4.4% | 4.0% |
|---|---|---|---|---|---|---|
| $\overline{\eta}$ | 0.082 | 0.075 | 0.068 | 0.061 | 0.055 | 0.049 |
| Speed error percentage | 3.6% | 3.2% | 2.8% | 2.4% | 2.0% | |
| $\overline{\eta}$ | 0.043 | 0.037 | 0.032 | 0.026 | 0.005 | |

## 5. Simulation Results

To verify the results in Theorems 3.1, 3.3, and 4.1, a MATLAB/SIMULINK simulation platform of networked PMSM servo systems is built up, which is shown in Figure 1. The sampling period $h$ is 10 ms. The tracking reference speed is set to 1500 r/min. The nominal parameters of a PMSM is shown in Table 1.

In the following simulations, the load torque disturbance is no larger than 30% of the nominal value. According to Theorem 4.1 and Definition 3.4, we obtain the relationship between the speed tracking error and $\overline{\eta}$, which is demonstrated in Table 2.

*Remark 5.1.* The data in Table 2 shows the relationship between the speed tracking error and the maximum delay $\overline{\eta}$. When the networked PMSM servo system needs higher tracking accuracy, it can tolerate less transmission delay and data packet dropouts. If the speed tacking error is less than 2.0%, $\overline{\eta}$ is equal to 0.005 s, which means that the system cannot tolerate even one data packet dropout under this circumstance.

In the sequel, we simulate 3 cases to demonstrate the effectiveness of the obtained results. In these simulations, the maximum relative speed tracking error is 5%, and the load torque disturbance is no larger than 30% of the nominal value. According to Definition 3.4, we get

$$\gamma \leq \gamma_{\min} = 125. \tag{5.1}$$

By Theorem 4.1 (with $\gamma = \gamma_{\min}$), we try to maximize $\overline{\eta}$ and reach a suboptimal solution with $\overline{\eta} = 0.064$ s and the corresponding controller gain of $K = [0, -0.0212]$.

### 5.1. Stability of System

*Case 1.* The first simulation is to verify the stability of the networked PMSM servo system. $\overline{\eta}$ is set to 0.064 s. Figure 5 shows the speed tracking error trajectory. After approximate 0.15 s, the speed tracking error is almost zero. So this result demonstrates the correctness of the stability condition in Theorem 3.1.

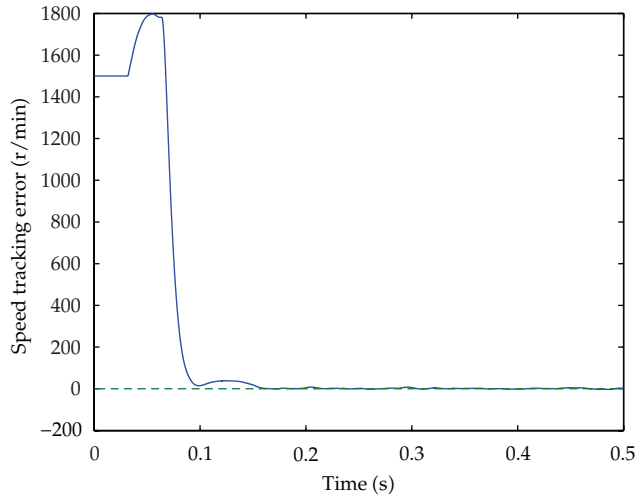


**Figure 5:** The speed tracking error.

### 5.2. Robustness against Transmission Delay and Data Dropouts

*Case 2.* In the second case, performance comparison is made between two approaches, the robust controller proposed in this paper and the PID controller.

*The PID Controller*

Its parameters are tuned to perform well under the network-delay-free situation. In the simulation, the network-induced delay is set to 0.1 h (= 0.001 s).

*Robust Controller*

The robust controller is then applied as the central controller to regulate the speed loop. The network-induced delay $\overline{\eta}$ is set to be 0.064 s. $\overline{\eta} = 0.064\,\text{s} = 6.4\,\text{h}$ means that the system can tolerate 5 dropouts among any 6 consecutive data packets.

The results of this case are shown in Figure 6.

Although the PID controller suffers a much smaller delay than the robust controller, it generates much worse tracking performance than the robust controller. The reason lies in that the design of the robust controller takes the delay into account, while the design of the PID controller does not. So the effectiveness of Theorems 3.3 and 4.1 is confirmed.

### 5.3. Robustness against Load Torque Disturbance

*Case 3.* The purpose of the third simulation is to verify that the proposed robust controller can effectively suppress the load torque disturbance. Under the worst condition of five consecutive data packet dropouts and network-induced delay up to 0.4 h, a 30% load torque disturbance occurs at time 0.5 s and disappears at time 0.55 s. Figure 7 shows the simulation results.

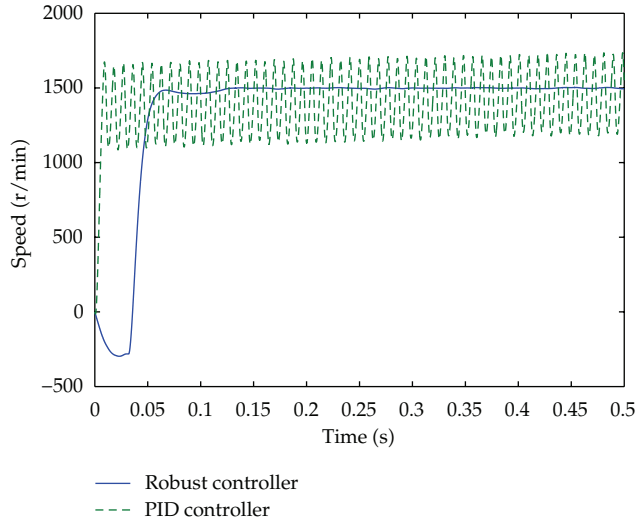


**Figure 6:** Speed response under the network delays and dropouts.

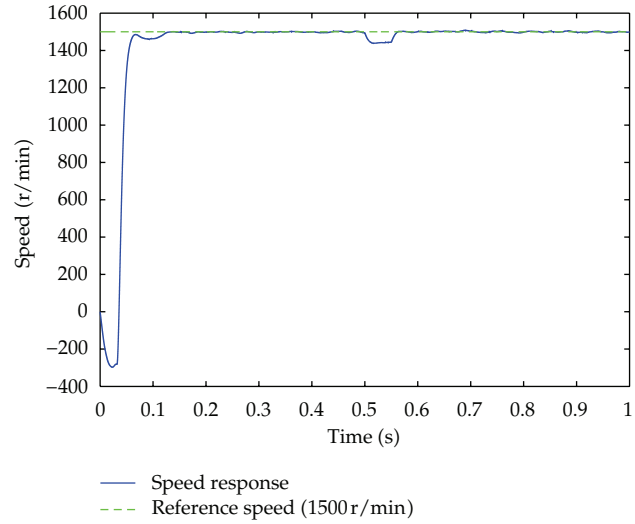


**Figure 7:** Speed response under the network delays and dropouts and the load torque disturbance.

As we see in Figure 7, when the load torque disturbance starts at time 0.5 s, the speed deviates from the reference speed of 1500 r/min. However, after the disturbance disappears at time 0.55 s, the speed of PMSM quickly returns back to the reference speed in about 0.03 s. From the speed response curve, we can also see that the speed tracking error is less than 5% during the whole process. These simulation results confirm that the robust controller designed in this paper satisfies the accuracy demand and can effectively suppress the load torque disturbance.

## 6. Conclusion

The networked PMSM servo system has a promising future in industry applications. However, its performance may be degraded by the network delays and data packet dropouts.

The load disturbance is also a detrimental factor for the control performance. In this paper, we propose a sufficient stability condition by the Lyapunov-Krasovskii method, quantitatively investigate the robustness of the system's performance against the load torque disturbance, and give a way to design a robust controller, which can either tolerate larger network delay or give better $H_\infty$ performance. The simulations are done to verify the correctness of the stability result and demonstrate the superiority of the obtained controller in terms of performance robustness against the data packet dropouts and transmission delay as well as the load torque disturbance.

## Acknowledgments

This paper was supported in part by the National Natural Science Foundation of China (60904012), the Program for New Century Excellent Talents in University (NCET0-10-0917), and the Doctoral Fund of Ministry of Education of China (20093402120017).

## References

[1] C. F. J. Kuo, C. H. Hsu, and C. C. Tsai, "Control of a permanent magnet synchronous motor with a fuzzy sliding-mode controller," *International Journal of Advanced Manufacturing Technology*, vol. 32, no. 7-8, pp. 757–763, 2007.

[2] S. S. Yang and Y. S. Zhong, "Robust speed tracking of permanent magnet synchronous motor servo systems by equivalent disturbance attenuation," *IET Control Theory and Applications*, vol. 1, no. 3, pp. 595–603, 2007.

[3] K. H. Kim, I. C. Baik, G. W. Moon, and M. J. Youn, "A current control for a permanent magnet synchronous motor with a simple disturbance estimation scheme," *IEEE Transactions on Control Systems Technology*, vol. 7, no. 5, pp. 630–633, 1999.

[4] W. Zhang, M. S. Branicky, and S. M. Phillips, "Stability of networked control systems," *IEEE Control Systems Magazine*, vol. 21, no. 1, pp. 84–99, 2001.

[5] P. Seiler and R. Sengupta, "An $H_\infty$ approach to networked control," *IEEE Transactions on Automatic Control*, vol. 50, no. 3, pp. 356–364, 2005.

[6] J. P. Hespanha, P. Naghshtabrizi, and Y. Xu, "A survey of recent results in networked control systems," *Proceedings of the IEEE*, vol. 95, no. 1, pp. 138–162, 2007.

[7] D. Huang and S. K. Nguang, "Robust disturbance attenuation for uncertain networked control systems with random time delays," *IET Control Theory & Applications*, vol. 2, no. 11, pp. 1008–1023, 2008.

[8] H. Gao and T. Chen, "Network-based $H_\infty$ output tracking control," *IEEE Transactions on Automatic Control*, vol. 53, no. 3, pp. 655–667, 2008.

[9] P. Wang, C.Z. Han, and B.C. Ding, "Stability of discrete-time networked control systems and its extension for robust $H_\infty$ control," *International Journal of Systems Science*. In press.

[10] K. C. Lee, S. Lee, and M. H. Lee, "Remote fuzzy logic control of networked control system via profibus-DP," *IEEE Transactions on Industrial Electronics*, vol. 50, no. 4, pp. 784–792, 2003.

[11] T. Li and Y. Fujimoto, "Control system with high-speed and real-time communication links," *IEEE Transactions on Industrial Electronics*, vol. 55, no. 4, pp. 1548–1557, 2008.

[12] S. Chai, G. P. Liu, D. Rees, and Y. Xia, "Design and practical implementation of internet-based predictive control of a servo system," *IEEE Transactions on Control Systems Technology*, vol. 16, no. 1, pp. 158–168, 2008.

[13] W. Leonhard, "Microcomputer control of high dynamic performance ac-drives-A survey," *Automatica*, vol. 22, no. 1, pp. 1–19, 1986.

[14] M. N. Uddin, M. A. Abido, and M. A. Rahman, "Development and implementation of a hybrid intelligent controller for interior permanent-magnet synchronous motor drives," *IEEE Transactions on Industry Applications*, vol. 40, no. 1, pp. 68–76, 2004.

[15] M. Yu, L. Wang, T. Chu, and F. Hao, "An LMI approach to networked control systems with data packet dropout and transmission delays," in *Proceedings of the 43rd IEEE Conference on Decision and Control (CDC '04)*, pp. 3545–3550, December 2004.

[16] Y. S. Lee, Y. S. Moon, W. H. Kwon, and P. G. Park, "Delay-dependent robust $H_\infty$ control for uncertain systems with a state-delay," *Automatica*, vol. 40, no. 1, pp. 65–72, 2004.
[17] Y. S. Moon, P. Park, W. H. Kwon, and Y. S. Lee, "Delay-dependent robust stabilization of uncertain state-delayed systems," *International Journal of Control*, vol. 74, no. 14, pp. 1447–1455, 2001.

Hindawi Publishing Corporation
Journal of Applied Mathematics
Volume 2012, Article ID 715497, 9 pages
doi:10.1155/2012/715497

*Research Article*

# Stability Analysis of Predator-Prey System with Fuzzy Impulsive Control

**Yuangan Wang**

*School of Mathematics and Computer Science, Qinzhou University, Qinzhou, Guangxi 535000, China*

Correspondence should be addressed to Yuangan Wang, 6180738@qq.com

Received 14 December 2011; Revised 22 March 2012; Accepted 11 April 2012

Academic Editor: Xianxia Zhang



Having attracted much attention in the past few years, predator-prey system provides a good mathematical model to present the correlation between predators and preys. This paper focuses on the robust stability of Lotka-Volterra predator-prey system with the fuzzy impulsive control model, and Takagi-Sugeno (T-S) fuzzy impulsive control model as well. Via the T-S model and the Lyapunov method, the controlling conditions of the asymptotical stability and exponential stability are established. Furthermore, the numerical simulation for the Lotka-Volterra predator-prey system with impulsive effects verifies the effectiveness of the proposed methods.

## 1. Introduction

Since Volterra presented the differential equation to solve the issue of the sharp change of the population of the sharks (predator) and the minions (prey) in 1925, the predator-prey system has been applied into many areas and played an important role in the biomathematics. Much attention has been attracted to the stability of the predator-prey system. Brauer and Soudack studied the global behavior of a predator-prey system under constant-rate prey harvesting with a pair of nonlinear ordinary differential equations [1]. Xu and his workmates concluded that a short-time delay could ensure the stability of the predator-prey system [2]. After analyzing the different capability between the mature and immature predator, Wang and his workmates obtained the global stability with the small time-delay system [3]. Li and his partners studied the impulsive control of Lotka-Volterra predator-prey system and established sufficient conditions of the asymptotic stability with the method of Lyapunov functions [4]. Liu and Zhang studied the coexistence and stability of predator-prey model with Beddington-DeAngelis functional response and stage structure [5]. Li did some work on the predator-prey system with Holling II functional response and obtained the existence,

uniqueness and global asymptotic stability of the in random perturbation [6]. Furthermore, Ko and Ryu studied the qualitative behavior of nonconstant positive solutions on a general Gauss-type predator-prey model with constant diffusion rates under homogenous Neumann boundary condition [7]. Additionally, many papers discussed the predator-prey system with other different methods, such as LaSalle's invariance principle method [8], Liu and Chen's impulsive perturbations method [9], and Moghadas and Alexander's generalized Gauss-type predator–prey model [10].

In recent years, fuzzy impulsive theory has been applied to the stability analysis of the non-linear differential equations [11–15]. However, it should be admitted that the stability of fuzzy logic controller (FLC) is still an open problem. It is well-known that the parallel distributed compensation technique has been the most popular controller design approach and belongs to a continuous input control way. It is important to point out that there exist many systems, like the predator-prey system, which cannot commonly endure continuous control inputs, or they have impulsive dynamical behavior due to abrupt jumps at certain instants during the evolving processes. In this sense, it is the same with communication networks, biological population management, chemical control, and so forth [16–23]. Hence, it is necessary to extend FLC and reflect these impulsive jump phenomena in the predator-prey system. Until recently, few papers talk about the stability of Lotka-Volterra predator-prey system with fuzzy impulsive control. In this paper, the writer will study the robustness of the predator-prey system by the fuzzy impulsive control based on the T-S mathematical model.

The rest of this paper is organized as follows. Section 2 describes the Lotka-Volterra predator-prey system and T-S fuzzy system with impulsive control. In Section 3, the theoretic analysis and design algorithm on stability of the impulsive fuzzy system are performed. Numerical simulations for the predator-prey system with impulsive effects are carried out with respect to the proposed method in Section 4. Finally, some conclusions are made in Section 5.

## 2. Problem Equation

The Lotka-Volterra predator-prey system is expressed with the following differential equation:

$$\begin{aligned} \dot{x}_1(t) &= x_1(t)\big(\mu_1 - r_{12}x_2(t)\big), \\ \dot{x}_2(t) &= x_2(t)\big(-\mu_2 + r_{21}x_1(t)\big), \end{aligned} \tag{2.1}$$

where $x_1(t), x_2(t)$ $(x_1(t) > 0, x_2(t) > 0)$ denote the species density of the preys and the predators in the group at time $t$ respectively. The coefficient $\mu_1 > 0$ denotes the birth rate of the preys, and $\mu_2 > 0$ denotes the death rate of the predators. The other two coefficients $r_{12}$ and $r_{21}$ (both positive) describe interactions between the species.

In order to discuss the stability of the system, a matrix differential equation is presented as follows:

$$\dot{x} = Ax + \Phi(x), \quad \text{where } A = \begin{bmatrix} \mu_1 & 0 \\ 0 & -\mu_2 \end{bmatrix}, \ \Phi(x) = \begin{bmatrix} -r_{12}x_1x_2 \\ r_{21}x_1x_2 \end{bmatrix}. \tag{2.2}$$

**Lemma 2.1.** *$\dot{x} = f(x(t))$, where $x(t) \in R^n$ is the state variable, and $f \in C[R^n, R^n]$ satisfies $f(0) = 0$, is a vector field defined over a compact region $W \subseteq R^n$. By using the methods introduced in [24], one can construct fuzzy model for system (2.1) as follows.*

*Control Rule $i$ ($i = 1, 2, \ldots, r$): IF $z_1(t)$ is $M_{i1}$, $z_2(t)$ is $M_{i2}\ldots$, and $z_p(t)$ is $M_{ip}$, THEN $\dot{x}(t) = A_i x(t)$, where $r$ is the number of T-S fuzzy rules, and $z_1(t), z_2(t), \ldots, z_p(t)$ are the premise variables, each $M_{ij}$ ($j = 1, 2, \ldots, p$) is a fuzzy set, and $A_i \in R^{n\times n}$ is a constant matrix.*

*Thus, the nonlinear equation can be transformed to the following linear equation.*

*If $x_2(t)$ is $M_i$*

$$\begin{aligned} \dot{x} &= A_i x(t), \quad t \neq \tau_j, \\ \Delta x|_{t=\tau_j} &= K_{i,j} x(t), \quad t = \tau_j, \\ i &= 1, 2, \ldots, r, \quad j = 1, 2 \ldots, \end{aligned} \tag{2.3}$$

*where*

$$A_i = \begin{bmatrix} \mu_1 - d_i r_{12} & 0 \\ d_i r_{21} & -\mu_2 \end{bmatrix}, \tag{2.4}$$

*and $d_i$ is related to the value of $x_2(t)$ (here, $d_i = x_2(t)$). $M_i, x(t), A_i \in R^{2\times 2}$, $r$ is the number of the IF-THEN rules, $K_{i,j} \in R^{2\times 2}$ denotes the control of the $j$ th impulsive instant, $\Delta x|_{t=\tau_j} \equiv x(\tau_j^+ - \tau_j^-)$.*

*Correspondently, with center-average defuzzifier, the overall T-S fuzzy impulsive system can be represented as follows:*

$$\begin{aligned} \dot{x}(t) &= \sum_{i=1}^{r} h_i(x_2(t))(A_i x(t)), \quad t \neq \tau_j, \\ \Delta x|_{t=\tau_j} &= \sum_{i=1}^{r} h_i(x_2(t)) K_{i,j} x, \quad t = \tau_j, \end{aligned} \tag{2.5}$$

*where $h_i(x_2(t)) = \omega_i(x_2(t)) / \sum_{i=1}^{r} \omega_i(x_2(t))$ and $\omega_i(x_2(t)) = \prod_{j=1}^{p} M_{i,j}(x_2(t))$.*

Obviously, $h_i(x_2(t)) \geq 0$, $\sum_{i=1}^{r} h_i(x_2(t)) = 1$, $i = 1, 2, \ldots, r$.

**Lemma 2.2.** *If $P$ is a real semipositive matrix, then a real matrix $C$ exists, making $P = C^T C$.*

## 3. Stability Analysis

**Theorem 3.1.** *Assume that $\lambda_i$ is the maximum eigenvalue of $[A_i^T + A_i]$ ($i = 1, 2, \ldots, r$), let $\lambda(\alpha) = \max_i\{\lambda_i\}$, $0 < \delta_j = \tau_j - \tau_{j-1} < \infty$ is impulsive distance [25]. If $\lambda(\alpha) \geq 0$ and there exists a constant scalar $\varepsilon > 1$ and a semipositive matrix $P$, such that*

$$\ln(\varepsilon\beta_j) + \lambda(\alpha)\delta_j \leq 0, \qquad PA_i = A_i P, \tag{3.1}$$

*where*

$$P = C^T C, \qquad \beta_j = \max_i \left\| C\left(I + K_{i,j}\right) \right\|. \tag{3.2}$$

*Then the system* (2.5) *is stable globally and asymptotically.*

*Proof.* Let the candidate Lyapunov function be in the form of

$$V(x) = \frac{1}{2} x^T P x. \tag{3.3}$$

Clearly, for $t \neq \tau_j$,

$$\begin{aligned} \dot{V}(x) &= \frac{1}{2} \sum_{i=1}^{r} h_i(x_2(t)) x^T \left[ A_i^T P + P A_i \right] x \\ &= \frac{1}{2} \sum_{i=1}^{r} h_i(x_2(t)) x^T P \left[ P^{-1} A_i^T P + A_i \right] x \\ &\leq \frac{1}{2} \lambda(\alpha) x^T P \sum_{i=1}^{r} h_i(x_2(t)) x \\ &= \frac{1}{2} \lambda(\alpha) x^T P x \\ &= \lambda(\alpha) V(x(t)), \end{aligned} \tag{3.4}$$

where $t \in (\tau_{j-1}, \tau_j]$ $(j = 1, 2, \ldots)$.

For $t = \tau_j$, we have

$$\begin{aligned} V\left(x\left(\tau_j^+\right)\right) &= \frac{1}{2} \sum_{i=1}^{r} h_i(x_2(t)) \left[ \left(I + K_{i,j}\right) x(\tau_j) \right]^T P \left[ \left(I + K_{i,j}\right) x(\tau_j) \right] \\ &= \frac{1}{2} \sum_{i=1}^{r} h_i(x_2(t)) \left[ \left(I + K_{i,j}\right) x(\tau_j) \right]^T C^T C \left[ \left(I + K_{i,j}\right) x(\tau_j) \right] \\ &= \frac{1}{2} \sum_{i=1}^{r} h_i(x_2(t)) \left\| C\left(I + K_{i,j}\right) x(\tau_j) \right\| \\ &\leq \frac{1}{2} \sum_{i=1}^{r} h_i(x_2(t)) \left\| C\left(I + K_{i,j}\right) \right\| \left\| x(\tau_j) \right\| \\ &\leq \frac{1}{2} \sum_{i=1}^{r} h_i(x_2(t)) \beta_j \left\| x(\tau_j) \right\| \\ &= \beta_j V\left(x(\tau_j)\right), \quad j \in N. \end{aligned} \tag{3.5}$$

Let $j = 1$, for any $t \in (\tau_0, \tau_1]$, by (3.4), we obtain

$$V(x(t)) \leq V(x(\tau_0)) \exp(\lambda(\alpha)(t - \tau_0)). \tag{3.6}$$

Then

$$V(x(\tau_1)) \leq V(x(\tau_0)) \exp(\lambda(\alpha)(\tau_1 - \tau_0)). \tag{3.7}$$

From (3.5) and (3.7), we obtain

$$V\left(x\left(\tau_1^+\right)\right) \leq \beta_1 V(x(\tau_1)) \leq \beta_1 V(x(\tau_0)) \exp(\lambda(\alpha)(\tau_1 - \tau_0)). \tag{3.8}$$

In the same way, for any $t \in (\tau_1, \tau_2]$, we have

$$V(t, x) \leq V\left(\tau_1^+, x\right) \exp(\lambda(\alpha)(t - \tau_1)) \leq \beta_1 V(\tau_0, x) \exp(\lambda(\alpha)(t - \tau_0)). \tag{3.9}$$

Similarly, for all $k$ and $t \in (\tau_k, \tau_{k+1}]$, we obtain

$$V(t, x) \leq \beta_k \cdots \beta_2 \beta_1 V(\tau_0, x) \exp(\lambda(\alpha)(t - \tau_0)). \tag{3.10}$$

From (3.2), we obtain

$$\beta_k \exp(\lambda(\alpha)\delta_k) \leq \frac{1}{\varepsilon}, \quad k \in N. \tag{3.11}$$

Thus, for $t \in (\tau_k, \tau_{k+1}]$, $k \in N$, we have

$$\begin{aligned} V(x(t)) &\leq V(x(\tau_0))\beta_1\beta_2 \cdots \beta_k \exp(\lambda(\alpha)(t - \tau_0)) \\ &= V(x(\tau_0))\left[\beta_1 \exp(\lambda(\alpha)\delta_1)\right] \cdots \left[\beta_k \exp(\lambda(\alpha)\delta_k)\right] \exp(\lambda(\alpha)(t - \tau_k)) \\ &\leq V(x(\tau_0)) \frac{1}{\varepsilon^k} \exp(\lambda(\alpha)(t - \tau_k)). \end{aligned} \tag{3.12}$$

So, if $t \to \infty$, then $k \to \infty$ and $V(t, x) \to 0$. So the system (2.5) is stable globally and asymptotically. □

**Theorem 3.2.** *Assume that $\lambda_i$ is the maximum eigenvalue of $[A_i + A_i^T](i = 1, 2, \ldots, r)$, let $\lambda(\alpha) = \max_i\{\lambda_i\}$, $0 < \delta_j = \tau_j - \tau_{j-1} < \infty$ is impulsive distance. If $\lambda(\alpha) < 0$ and a constant scalar $0 \leq \varepsilon < -\lambda(\alpha)$ exists, such that*

$$\ln(\beta) - \varepsilon\delta_j \leq 0, \quad PA_i = A_i P, \tag{3.13}$$

*where $P = C^T C$ and $\beta_j = \max_i \|C(I + K_{i,j})\|$.*

*Then the system* (2.5) *is stable globally and exponentially.*

*Proof.* Let the candidate Lyapunov function be in the form of

$$V(x) = \frac{1}{2}x^T Px. \tag{3.14}$$

Firstly, (3.4)–(3.10) hold.

From (3.13), we obtain

$$\beta_k \exp(-\varepsilon\sigma_k) \le 1, \quad k \in N. \tag{3.15}$$

Thus, for $t \in (\tau_k, \tau_{k+1}], k \in N$,

$$\begin{aligned} V(x(t)) &\le V(x(t_0))\beta_1\beta_2\cdots\beta_k \exp(\lambda(\alpha)(t-t_0)) \\ &= V(x(t_0))\beta_1\beta_2\cdots\beta_k \exp((-\varepsilon)(t-t_0)) \exp((\lambda(\alpha)+\varepsilon)(t-t_0)) \\ &= V(x(t_0))\left[\beta_1 \exp(-\varepsilon(t_1-t_0))\right]\cdots\left[\beta_j \exp(-\varepsilon(t-t_k))\right] \exp((\lambda(\alpha)+\varepsilon)(t-t_0)) \\ &\le V(x(t_0)) \exp((\lambda(\alpha)+\varepsilon)(t-t_0)). \end{aligned} \tag{3.16}$$

Note that $0 \le \varepsilon < -\lambda(\alpha)$, thus $\lambda(\alpha) + \varepsilon < 0$. So the system (2.5) is stable globally and exponentially.

Next, we consider some special cases of the two theorems. Assume that $K = K_{i,j}$ and $\sigma = \sigma_j$ in the two theorems above, so we can have the following corollary. □

**Corollary 3.3.** *Let $\lambda_i$ be the largest eigenvalue of $[A + A^T], (i = 1, 2, \ldots, r), \lambda(\alpha) = \max_i\{\lambda_i\} > 0$. If there exists a constant $\varepsilon > 1$ and a real semi-positive $P$ such that*

$$\ln(\varepsilon\beta) + \lambda(a)\delta \le 0, \quad PA_i = A_iP, \tag{3.17}$$

*where $P = C^TC$, $\beta_j = \max_i\|C(I + K_{i,j})\|$, and $0 < \delta = \tau_j - \tau_{j-1} < \infty$ $(j \in N)$ is impulsive distance. Then the system (2.5) is stable globally and asymptotically.*

**Corollary 3.4.** *Let $\lambda_i$ be the largest eigenvalue of $[A + A^T](i = 1, 2, \ldots, r), \lambda(\alpha) = \max_i\{\lambda_i\} < 0$. If there exists a constant $0 \le \varepsilon < -\lambda(\alpha)$ and a real semi-positive $P$ such that*

$$\ln(\beta) - \varepsilon\delta \le 0, \quad PA_i = A_iP, \tag{3.18}$$

*where $P = C^TC, \beta_j = \max_i\|C(I + K_{i,j})\|$, and $0 < \delta = \tau_j - \tau_{j-1} < \infty (j \in N)$ is impulsive distance. Then the system (2.5) is stable globally and exponentially.*

## 4. Numerical Simulation

In this section, we present a design example to show how to perform the impulsive fuzzy control on the Lotka-Volterra predator-prey systems with impulsive effects. Especially, the biological systems are very complex, nonlinear, and uncertain. As a result, they should be represented by fuzzy logical method with linguistic description.

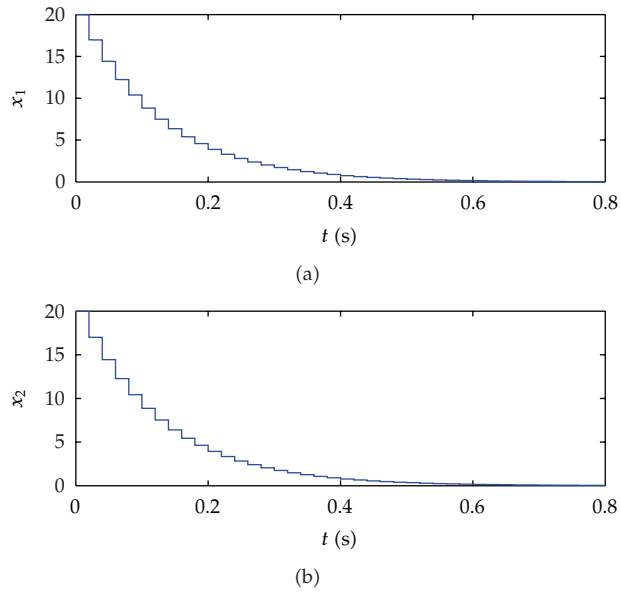


**Figure 1:** The phase portrait of the system with fuzzy impulsive control.

Now, consider a predator-prey system with impulsive effects as follows:

$$\dot{x} = Ax + \Phi(x), \tag{4.1}$$

where,

$$A = \begin{bmatrix} \mu_1 & 0 \\ 0 & -\mu_2 \end{bmatrix}, \quad \Phi(x) = \begin{bmatrix} -r_{12}x_1x_2 \\ r_{21}x_1x_2 \end{bmatrix}. \tag{4.2}$$

*Solving*

From (2.3), we have the following impulsive fuzzy control for the above predator-prey model.

*Rule i*

IF $x_2(t)$ is $M_i$, then

$$\begin{cases} \dot{x}(t) = A_i x(t) & t \neq \tau_j, \\ \Delta x = K_{i,j} x(t) & t = \tau_j, \end{cases} \quad i = 1, 2, \quad j \in N, \tag{4.3}$$

where,

$$A_1 = \begin{bmatrix} \mu_1 - dr_{12} & 0 \\ dr_{21} & -\mu_2 \end{bmatrix}, \quad A_2 = \begin{bmatrix} \mu_1 - (1/2)dr_{12} & 0 \\ (1/2)dr_{21} & -\mu_2 \end{bmatrix}, \tag{4.4}$$

due to $x_2(t) \in [0, d] = [0, 0.12]$, and $M_1(x_2(t)) = x_2(t)/d$, $M_2(x_2(t)) = -x_2(t)/d$.

Let $\varepsilon = 1.2$, $\delta = 0.05$, $P = I$, $\mu_1 = 0.2$, $\mu_2 = 0.16$, $r_{12} = 0.10$, $r_{21} = 0.31$.
From Theorem 3.1 and Corollary 3.3, we can get that $\lambda(\alpha) = 0.194$.
Thus, we have chosen diag $([-0.82, -0.82])$ as impulsive control matrix, such that

$$\beta = \|I + K\| = 0.18, \qquad \ln(\varepsilon\beta) + \lambda(\alpha)\delta = -1.316 \leq 0. \tag{4.5}$$

Thus, from Theorem 3.1 and Corollary 3.3, we can conclude that the numerical example is globally stable. The phase portrait of the system with impulsive control is shown in Figure 1.

## 5. Conclusions

The impulsive control technique, which was proved to be suitable for complex and nonlinear system with impulsive effects, was applied to analyzing the framework of the fuzzy systems based on T-S model and the proposed design approach. First, the robustness of the Lotka-Volterra predator-prey system based on the fuzzy impulsive control was carefully analyzed. Then, the overall impulsive fuzzy system was obtained by blending local linear impulsive system. Meanwhile, the asymptotical stability and exponential stability of the impulsive fuzzy system were derived by Lyapunov method. Finally, a numerical example for predator-prey systems with impulsive effects was given to illustrate the application of impulsive fuzzy control. The simulation results show that the proposed method was effective.

## Acknowledgments

This work was supported by the National Natural Science Foundation of China, Project no. 50975300 and the Foundation of Education Department of Guangxi, China, Project no. 200808MS079.

## References

[1] F. Brauer and A. C. Soudack, "Stability regions in predator-prey systems with constant-rate prey harvesting," *Journal of Mathematical Biology*, vol. 8, no. 1, pp. 55–71, 1979.
[2] J. Xu, L. Pei, and Z. Lu, "Lyapunov stability for a class of predator-prey model with delayed nutrient recycling," *Chaos, Solitons and Fractals*, vol. 28, no. 1, pp. 173–181, 2006.
[3] W. Wang, G. Mulone, F. Salemi, and V. Salone, "Permanence and stability of a stage-structured predator-prey model," *Journal of Mathematical Analysis and Applications*, vol. 262, no. 2, pp. 499–528, 2001.
[4] D. Li, S. Wang, X. Zhang, and D. Yang, "Impulsive control of uncertain Lotka-Volterra predator-prey system," *Chaos, Solitons and Fractals*, vol. 41, no. 4, pp. 1572–1577, 2009.
[5] S. Liu and J. Zhang, "Coexistence and stability of predator-prey model with Beddington-DeAngelis functional response and stage structure," *Journal of Mathematical Analysis and Applications*, vol. 342, no. 1, pp. 446–460, 2008.
[6] Y. Li and H. Gao, "Existence, uniqueness and global asymptotic stability of positive solutions of a predator-prey system with Holling II functional response with random perturbation," *Nonlinear Analysis. Theory, Methods & Applications*, vol. 68, no. 6, pp. 1694–1705, 2008.
[7] W. Ko and K. Ryu, "A qualitative study on general Gause-type predator-prey models with constant diffusion rates," *Journal of Mathematical Analysis and Applications*, vol. 344, no. 1, pp. 217–230, 2008.
[8] J. K. Hale, *Ordinary Differential Equations*, Wiley-Interscience Press, New York, NY, USA, 1969.
[9] X. Liu and L. Chen, "Complex dynamics of Holling type II Lotka-Volterra predator-prey system with impulsive perturbations on the predator," *Chaos, Solitons and Fractals*, vol. 16, no. 2, pp. 311–320, 2003.

[10] S. M. Moghadas and M. E. Alexander, "Dynamics of a generalized Gause-type predator-prey model with a seasonal functional response," *Chaos, Solitons and Fractals*, vol. 23, no. 1, pp. 55–65, 2005.
[11] B. Liu, G. Chen, K. L. Teo, and X. Liu, "Robust global exponential synchronization of general Lur'e chaotic systems subject to impulsive disturbances and time delays," *Chaos, Solitons and Fractals*, vol. 23, no. 5, pp. 1629–1641, 2005.
[12] C.-F. Chuang, W.-J. Wang, and Y.-J. Chen, "$H_\infty$ synchronization of fuzzy model based chen chaotic systems," in *Proceedings of the IEEE International Conference on Control Applications (CCA '10)*, pp. 1199–1204, September 2010.
[13] C.-W. Park, C.-H. Lee, and M. Park, "Design of an adaptive fuzzy model based controller for chaotic dynamics in Lorenz systems with uncertainty," *Information Sciences*, vol. 147, no. 1-4, pp. 245–266, 2002.
[14] X. P. Guan and C. C. Hua, "Synchronization of uncertain time delay chaotic systems using the adaptive fuzzy method," *Chinese Physics Letters*, vol. 19, no. 8, pp. 1031–1034, 2002.
[15] L. Dong, W. Shi-long, Z. Xiao-Hong, D. Yang, and H. Wang, "Fuzzy impulsive control of permanent magnet synchronous motors," *Chinese Physics Letters*, vol. 25, no. 2, pp. 401–404, 2008.
[16] Z. Xiang and G. Chen, "Stability analysis and robust $H_\infty$ control of switched stochastic systems with time-varying delay," *Journal of Applied Mathematics*, vol. 2012, Article ID 202916, 17 pages, 2012.
[17] Z.-H. Guan, R.-Q. Liao, F. Zhou, and H. O. Wang, "On impulsive control and its application to Chen's chaotic system," *International Journal of Bifurcation and Chaos in Applied Sciences and Engineering*, vol. 12, no. 5, pp. 1191–1197, 2002.
[18] S. Y. Tang and L. S. Chen, "Multiple attractors in stage-structured population models with birth pulses," *Bulletin of Mathematical Biology*, vol. 65, no. 3, pp. 479–495, 2003.
[19] S. Y. Xiang, W. Pan, L. Yan, B. Luo, N. Jiang, and K. Wen, "Using polarization properties to enhance performance of chaos synchronization communication between vertical-cavity surface-emitting lasers," *Optics and Laser Technology*, vol. 42, no. 4, pp. 674–681, 2010.
[20] S. Y. Tang and L. Chen, "Density-dependent birth rate, birth pulses and their population dynamic consequences," *Journal of Mathematical Biology*, vol. 44, no. 2, pp. 185–199, 2002.
[21] X. Li, R. Rakkiyappan, and P. Balasubramaniam, "Existence and global stability analysis of equilibrium of fuzzy cellular neural networks with time delay in the leakage term under impulsive perturbations," *Journal of the Franklin Institute*, vol. 348, no. 2, pp. 135–155, 2011.
[22] R. Rakkiyappan and P. Balasubramaniam, "On exponential stability results for fuzzy impulsive neural networks," *Fuzzy Sets and Systems*, vol. 161, no. 13, pp. 1823–1835, 2010.
[23] A. A. Martynyuk, "Stability in the models of real world phenomena," *Nonlinear Dynamics and Systems Theory*, vol. 11, no. 1, pp. 7–52, 2011.
[24] K. Tanaka and H. Wang, *Fuzzy Control Systems Design and Analysis, a Linear Matrix Inequality Approach*, Wiley, New York, NY, USA, 2001.
[25] Y. Wang, Y. U. Honglin, X. Zhang, and D. Li, "Stability analysis and design of time-varying nonlinear systems based on impulsive fuzzy model," *Discrete Dynamics in Nature and Society*, vol. 2012, Article ID 192546, 16 pages, 2012.

Hindawi Publishing Corporation
Journal of Applied Mathematics
Volume 2012, Article ID 467412, 16 pages
doi:10.1155/2012/467412

*Research Article*

# Spatial Images Feature Extraction Based on Bayesian Nonlocal Means Filter and Improved Contourlet Transform

**Pengcheng Han and Junping Du**

*Beijing Key Laboratory of Intelligent Telecommunication Software and Multimedia, School of Computer Science, Beijing University of Posts and Telecommunications, Beijing 100876, China*

Correspondence should be addressed to Junping Du, junpingdu@126.com

Received 1 March 2012; Accepted 6 April 2012

Academic Editor: Baocang Ding



Spatial images are inevitably mixed with different levels of noise and distortion. The contourlet transform can provide multidimensional sparse representations of images in a discrete domain. Because of its filter structure, the contourlet transform is not translation-invariant. In this paper, we use a nonsubsampled pyramid structure and a nonsubsampled directional filter to achieve multidimensional and translation-invariant image decomposition for spatial images. A nonsubsampled contourlet transform is used as the basis for an improved Bayesian nonlocal means (NLM) filter for different frequencies. The Bayesian model adds a sigma range in image *a priori* operations, which can be more effective in protecting image details. The NLM filter retains the image edge content and assigns greater weight to similarities for edge pixels. Experimental results both on standard images and spatial images confirm that the proposed algorithm yields significantly better performance than nonsubsampled wavelet transform, contourlet, and curvelet approaches.

## 1. Introduction

In spatial rendezvous and docking, spatial images are obtained by multisource remote sensors. Spatial images are inevitably mixed with different levels of noise and distortion. The accurate image feature extraction will be helpful for spatial object recognition and can directly influence the success of spatial rendezvous and docking [1, 2]. Image feature extraction of spatial images is based on the definition of image features; to some extent, it can be said that it is based on sensitivity changes to image grayscale values for the human eye. Multidimensional image representation can process images for the sparsest representation, especially for 2D image signals [3, 4]. This approach identifies optimal high-dimensional

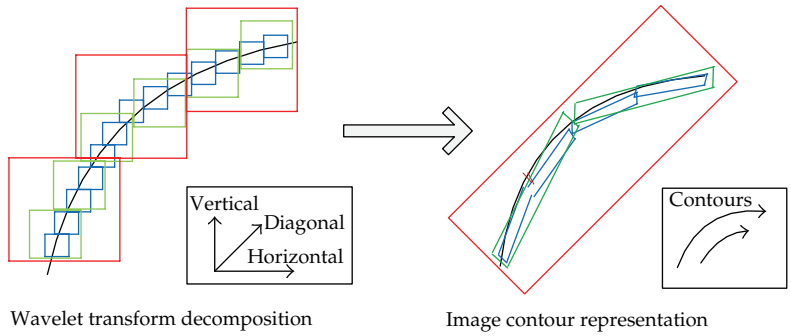


**Figure 1:** Multidimensional image decomposition.

function representation for an image and yields superior image-processing results for an effective solution. A nonlocal means (NLM) filter uses redundant image information on the basis that structural similarity superimposed on pixel noise is random and noise can be effectively removed using weighted averages [5, 6]. Compared to traditional statistical filtering methods, NLM filtering overcomes the constraint of the local neighborhood and extends pixel similarity to block-based similarity, so it is very suitable to deal with spatial images.

In this paper, we use a nonsubsampled pyramid structure and a nonsubsampled directional filter to achieve multidimensional and translation-invariant image decomposition for spatial images. A nonsubsampled contourlet transform is used as the basis for an improved Bayesian nonlocal means (NLM) filter for different frequencies. The Bayesian model adds a sigma range in image *a priori* operations, which can be more effective in protecting image details. The NLM filter retains the image edge content and assigns greater weight to similarities for edge pixels. Experimental results both on standard images and spatial images confirm that the proposed algorithm yields significantly better performance than nonsubsampled wavelet transform, contourlet, and curvelet approaches.

The rest of this paper is organized as follows. Section 2 describes multidimensional image decomposition, with a focus on contourlet and nonsubsampled contourlet transforms (NSCTs). Section 3 outlines application of an NLM filter and proposes an improved NLM algorithm based on a Bayesian model. Section 4 applies the improved NLM filter to NSCT, especially NSDFB, to process image features for further extraction. Section 5 compares feature extraction results for the proposed algorithm and other algorithms. Section 6 concludes the paper.

## 2. Contourlet Transform Decomposition

### 2.1. Multidimensional Image Decomposition

The target of image multidimensional representation is to provide a description of image with less characteristic information. The wavelet transform is a classic image multidimensional representation algorithm that has a good effect on image edge points [7, 8]. However, the wavelet transform can capture only limited direction information in the horizontal, vertical, and diagonal directions, as shown in the left side of Figure 1. It is difficult to express image smoothness contours; a better image representation is shown in the right side of Figure 1.

Other well-known multidimensional image decomposition algorithms include bandlets, brushlets, edge multidimensional transform, complex wavelets, and wedgelet. However, these algorithms require image edge detection and then summarize a representative adaptive coefficient. A decomposition algorithm that can transform an image into fixed decomposition coefficients is desirable. These coefficients can then be used in a broader context that does rely on edge detection alone but also includes better directional image decomposition.

In 2004, Candès and Donoho proposed a curvelet transform that uses a value approximation algorithm for a continuous 2D spatial domain and adds a smooth signal on the basis of a 1D Fourier transform [9]. The best approximation deviation is $O((\log M)^3 M^{-2})$ for curvelet and $O(M^{-1})$ for wavelet transforms. The curvelet transform is first applied to a continuous signal and then combines a multidimensional filter and ridgelet transformation. A second curvelet transform is based on frequency segments and extreme judgment. The curvelet transform is universally applicable to continuous signals, but there will be parallel noise in discrete fields [10]. It is also biased in directional image decomposition. The reason is that the typical rectangular sampling mode leads to *a priori* geometric deviation in decomposition of discrete image signals, especially in the horizontal and vertical directions. This limitation prompted researchers to develop a new multiscale decomposition algorithm that does not depend on edge detection and can decompose images in cross-scale multidimensions.

## 2.2. Contourlet Transform

The contourlet transform is a multidimensional decomposition algorithm proposed by Do and Vetterli in 2005 [11]. The transform can be directly used for multidimensional decomposition of discrete image signals. It has a dual filter for image decomposition and yields a smoother sparse representation of the original image. The two filters are a Laplacian pyramid (LP) filter [12, 13] and a directional filter bank (DFB) [14]. The LP yields nonconsecutive image points, and then the DFB connects consecutive points into a nonlinear structure. The process is shown in Figure 2.

A subsample contourlet transform uses a relevance factor $M$ for image subsampling at each decomposition level. A 2D filter is evolved from the 1D filter. For complete image reconstruction, the following relationship holds for the 1D filter:

$$M_0(z)N_0(z) + M_1(z)N_1(z) = 2,$$
$$S_m = \begin{cases} D(2^{l-1}, 2), & \text{for } 0 \le m \le 2^{l-1} - 1, \\ D(2, 2^{l-1}), & \text{for } 2^{l-1} \le m \le 2^l - 1, \end{cases} \tag{2.1}$$

where $M_0(z)$ and $M_1(z)$ represent low- and high-pass analysis filters, and $N_0(z)$ and $N_1(z)$ represent low- and high-pass synthesis filters, respectively. Downsampling matrices $S_m$ are shown above. For 2D complete decomposition,

$$M_0(M'(z))N_0(M'(z)) + M_1(M'(z))N_1(M'(z)) = 2. \tag{2.2}$$

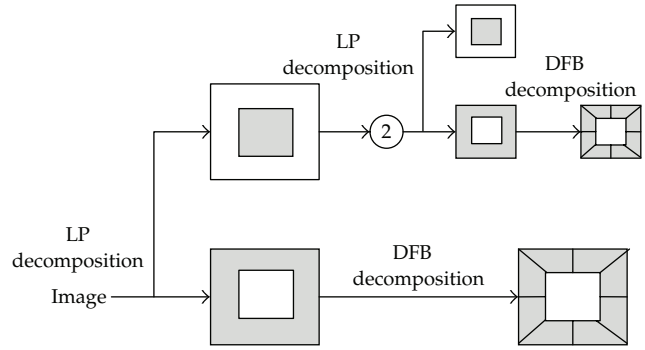


**Figure 2:** Contourlet transform.

$M'(z)$ represents discrete properties of the heterogeneous domain, which can help to reduce the filter complexity from $O(N^2)$ to $O(N)$. In two dimensions, the first DFB step is construction of the spectrum in the frequency domain using two-channel quincunx filter banks to decompose an image into horizontal and vertical directions [15]. The DFB equivalent parallel family is

$$\left\{D_k^{(l)}\left[n - S_m^{(l)}\right]\right\}_{0\le m\le 2^l, m\in L^2}. \tag{2.3}$$

Cutting operations on both directions for the decomposition spectrum provide 2D directional and segmental image decomposition. Like the discrete wavelet transform, the discrete downsampling contourlet transform is shift-invariant [16].

### 2.3. Nonsubsampled Contourlet Transform

NSCT is a fast implementation of the contourlet transform that provides a shift-invariant and multidimensional image representation [17]. Compared with subsampled contourlet transforms, NSCT is closer to the nonredundant wavelet transform [18]. NSCT uses a 2D nonsubsampled filter bank and can be expressed as

$$M_0(z)N_0(z) + M_1(z)N_1(z) = 1, \tag{2.4}$$

where $M(z)$ represents a 2D filter of the $z$ transform, $M_0(z)$ and $M_1(z)$ represent 2D low- and high-pass analysis filters, and $N_0(z)$ and $N_1(z)$ represent 2D low- and high-pass synthesis filters, respectively. There are also other limitations for the filter design.

NSCT involves two steps: multidimensional representation and directional decomposition. Multidimensional representation is achieved by nonsubsampled pyramid decomposition. This step is similar to the 1D discrete nonsubsampled wavelet transform (NSWT), which

uses the à trous method [19]. Compared to NSWT, NSCT uses a nonsubsampled 2D filter. The frame bound of an NSCT directional decomposition is

$$P_1 \le \underbrace{|M_0(e^{\varepsilon})| + |M_1(e^{\varepsilon})|}_{t(e^{\varepsilon})} \le P_2,$$
$$P_1 = \text{ess inf } t(e^{\varepsilon}), \qquad P_2 = \text{ess sup } t(e^{\varepsilon}), \quad \varepsilon \in [-\pi, \pi]^2. \tag{2.5}$$

After decomposition of the first layer, the sampling filter banks provide multiscale decomposition of the underlying properties. The process for two-layer nonsubsampled pyramid decomposition is shown in Figure 3.

The frequency domain for layer $j$ supported by a low-pass filter is $[-(\pi/2^j), -(\pi/2^j)]$; the replacement domain is from $[-(\pi/2^{j-1}), -(\pi/2^{j-1})]$ to $[-(\pi/2^j), -(\pi/2^j)]$, which is supported by a high-pass filter.

Each step in NSWT image decomposition involves three directions. The total image redundancy is $3J + 1$; in NSP, the result redundancy is $J + 1$ [20]. The second NSCT step provides directional information via the nonsubsampled filter, which combines two-channel quincunx sampling filters and a resampling operation for 2D frequency division on directional edges [21]. More accurate directional details can be sampled discretely on a sample stage. Sampling uses a quincunx matrix $Q$ and considers image direction alignment. The process is shown in Figure 4.

## 3. NLM Filter Based on a Bayesian Approach

### 3.1. NLM Filter

Different frequency components play different roles in an image structure. Low-frequency components account for most image energy, forming basic local gradation areas, but play a small role in image content or structure. High-frequency components form the main image edges and determine its basic content or structure and are thus the most important components. Changes in high-frequency information lead to changes in the basic image content or structure, and information extracted from the image by the human eye will thus be subject to major changes. Thus, high-frequency components play the most important role in image perception by the human eye.

At present, many image filters only consider adjacent pixels; some filters take into account information for neighboring pixels, such as Yaroslavsky neighborhood filters [22] and bilateral filters [23]. A nonlinear filter involves additive white noise and can effectively handle image redundancy [24].

The NLM algorithm takes advantage of grayscale image redundancy and structural redundancy through a weighted average of pixel values to estimate the current pixel value. The value of each pixel is calculated using the Gaussian-weighted Euclidean distance between subblocks; a pixel as taken as the right center of the corresponding subblock. This ensures that pixels with a similar structure are assigned greater weight. For an original image $v = \{v(i) \mid i \in I\}$, the expression for the image processed using the NLM filter, $NL(v)$, is

$$NL(v, i) = \sum_{j \in I} w(i, j) v(j), \tag{3.1}$$

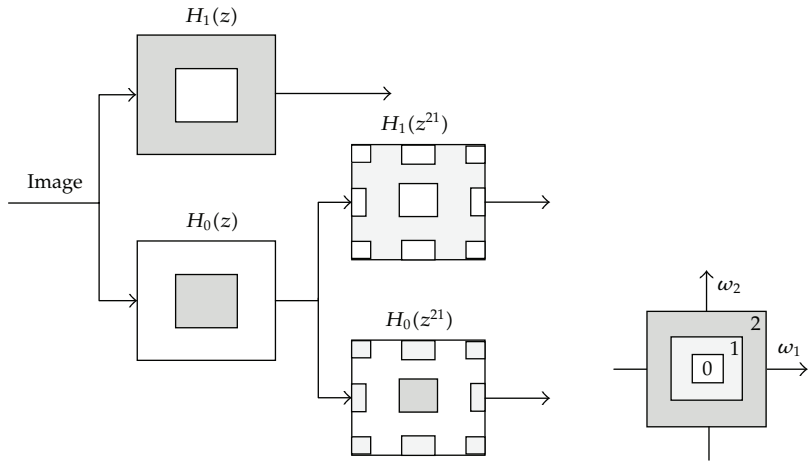


**Figure 3:** Non-subsampled pyramid decomposition.

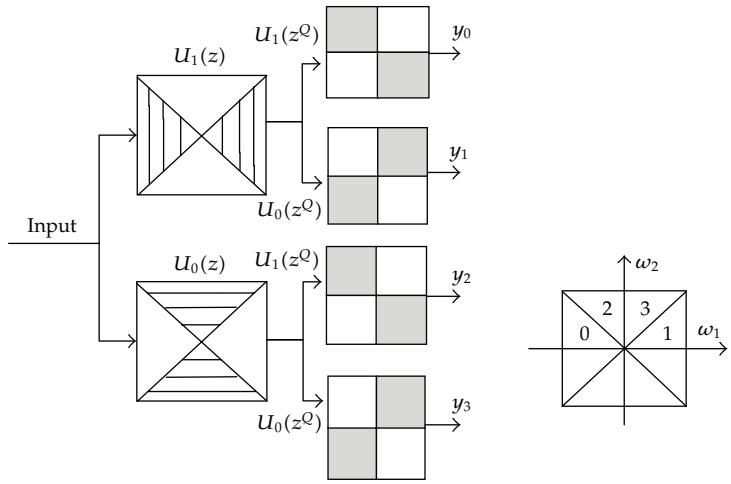


**Figure 4:** Nonsubsampled directional filter banks.

where $w(i,j)$ is the Gaussian-weighted Euclidean distance between pixels $i$ and $j$, which represents the similarity of the image subblocks with $i$ and $j$ as centers:

$$w(i,j) = \frac{1}{Z(i)} \exp\left[-\frac{\left\|v(N_i)_{d\times d} - v(N_j)_{d\times d}\right\|^2}{h^2}\right],$$

$$Z(i) = \sum_j \exp\left[-\frac{\left\|v(N_i)_{d\times d} - v\left(N_j\right)_{d\times d}\right\|_{2a}^2}{h^2}\right], \tag{3.2}$$

$$h^2 = \frac{1}{\sigma^2(1+r^2)} \sum_i^N \sum_j^N \left(rN_i - N_j\right)^2,$$

where $Z(i)$ is a normalization factor, $v(N_i)$ is a set of subblocks with pixel $i$ as the center, $\|\cdot\|_{2a}$ is a Gaussian-weighted Euclidean distance function, $a$ is Gaussian kernel standard deviation, and $h$ is a filter parameter that controls the degree of smoothing. The weight $w(i,j)$ meets $0 \le w(i,j) \le 1$, if neighborhood pixels are more similar with $v(N_i)$, the weight of center pixel is greater.

### 3.2. NLM Filter Combined with a Bayesian Method

The traditional NLM algorithm is very similar in both grayscale and structure content for smooth neighborhood areas. The algorithm yields the best results in flat areas, where better denoising effects can be obtained. At image edges and in texture-rich regions, the algorithm performs poorly because these regions have many repeat structures, the difference in grayscale content is greater, and the larger Euclidean distance makes the weights very small and reduces denoising capability, especially the ability to retain image detail [25]. To improve the edge retention capacity of the NLM algorithm, a Bayesian algorithm was added to make use of image edge information and adjust the similarity of the neighborhood structure so that the center pixel of edge contents that are similar can be given greater weight. This provides a more effective approach for protecting image detail.

The Bayesian NLM filter is expressed as

$$n(x) = \frac{\sum_{y\in\Delta(x)} p(v(x) \mid u(y))p(u(y))u(y)}{\sum_{y\in\Delta(x)} p(v(x) \mid u(y))p(u(y))}, \tag{3.3}$$

where $v(x)$ represents noise data, $u(x)$ represents nonnoise image data, $n(x)$ is the average pixel precision weight for gray value $u(y)$ at a rate of change $\Delta x$, and $p(v(x) \mid u(y))p(u(y))$ is the similarity between $v(x)$ and $u(y)$. Equation (5) can then be rewritten as

$$w(i,j) = \frac{1}{Z(i)} \exp\left[-\frac{\left\|v(N_i)_{d\times d} - v(N_j)_{d\times d}\right\|_{2a}^2}{h^2} - \frac{\left\|n(x_i)_{d\times d} - n(x_j)_{d\times d}\right\|_{2a}^2}{h'}\right]. \tag{3.4}$$

### 3.3. Improved Bayesian NLM Filter

We propose an improved Bayesian NLM filter in which a sigma range is added to the prior image operation for more effective protection of image details [26]. The first step is analysis of the probability density for pixel levels, which takes the average variance for the improved Bayesian filter. Considering the independence and integrity of an image, its conditional probability distribution can be expressed as

$$p(v(x) \mid u(y)) = \sum_{m=1}^{M\times M} p(v_m(x) \mid u_m(y)), \tag{3.5}$$

where $v_m(x)$ and $u_m(y)$ are the image probability densities at pixel $m$ and $v_m(y)$ is a subset of $u_m(y)$. For $L$-level image decomposition, the conditional probability density function is

$$p(v_m(x) \mid u_m(y)) = \frac{v_m(x)^{L-1}}{F(L)} \left( \frac{L}{u_m(y)} \right) \exp\left( -\frac{L v_m(x)}{u_m(y)} \right), \tag{3.6}$$

$$F(L) = \sqrt{G_a(L)} \sum_{l}^{L} \exp\left( u_m(y)^{l-1} - v_m(x)^{l-1} \right). \tag{3.7}$$

Because of multiscale features, we assume that the prior probability $p(u(y))$ is continuous and uniform, $p(u(y)) = 1/|\Delta x|$. The proposed algorithm uses an iterative technique, which takes the observed value $v(x)$ as the initial value $u(y)$. This treatment can process data directly but takes longer, and details can become fuzzy. If the frequency window is too large, the result will have too much edge details and point targets become even more blurred. Experimental results confirmed that $3 \times 3$ window is an appropriate choice. The algorithm uses an *a priori* estimate mean $u'(y)$ to replace $u(y)$ to reduce image noise bias and $\Delta x$ is replaced by $N(x)$. The new Bayesian filter can be expressed as

$$n(x) = \frac{\sum_{y \in \Delta(x)} p(v(x) \mid u'(y)) p(u'(y)) u'(y)}{\sum_{y \in \Delta(x)} p(v(x) \mid u'(y)) p(u'(y))}. \tag{3.8}$$

$N(x)$ can be expressed as $N(x) = \Delta x \cap N_1(x) \cap N_2(x)$, where $N_1(x)$ and $N_2(x)$ are *a priori* regional image characteristics and pixel features, respectively. The *a priori* regional characteristic is image region $\Delta x$, and unrelated points are removed using a region similarity algorithm. The *a priori* pixel feature is the set obtained by comparing the similarity of adjacent pixels [27]. *A priori* pixel characteristics are generally always overlooked in NLM filter processes. In fact, *a priori* pixel characteristics are good for excluding pixel noise [28].

The sigma range between pixel $x$ and the *a priori* mean $u'(x)$ can be defined as $(u'(x)I_1, u'(x)I_2)$ and the range $(I_1, I_2)$ meets $\xi = \int_{I_1}^{I_2} p(s)ds$, where $p(s)$ is the image probability density function. For different sigma values $\xi \in \{0.1, 0.2, \ldots, 0.9\}$, the range can be calculated by pixel search [29].

It is desirable to have a greater sigma weight; however, under conditional probability, the sigma range cannot be greater than the maximum upper boundary, $u'(x)I_2 < V_{\max}$, where $V_{\max}$ is the maximum image density. It has been demonstrated that *a priori* pixel characteristics can have a good effect on retention of image edges, but there will be some situations in which isolated pixels are ignored. To solve this problem, the proposed algorithm uses a threshold $T = V_{\max}/2$ to separate two pixels [30]. For *a priori* pixels, only $u'(x) < T$ are retained.

## 4. Image Feature Extraction Based on the Contourlet Transform

The proposed algorithm can improve the accuracy and completeness of image feature extraction based on direct contourlet decomposition. An image is first processed by the contourlet transform to yield a multidimensional domain, with multiple-resolution

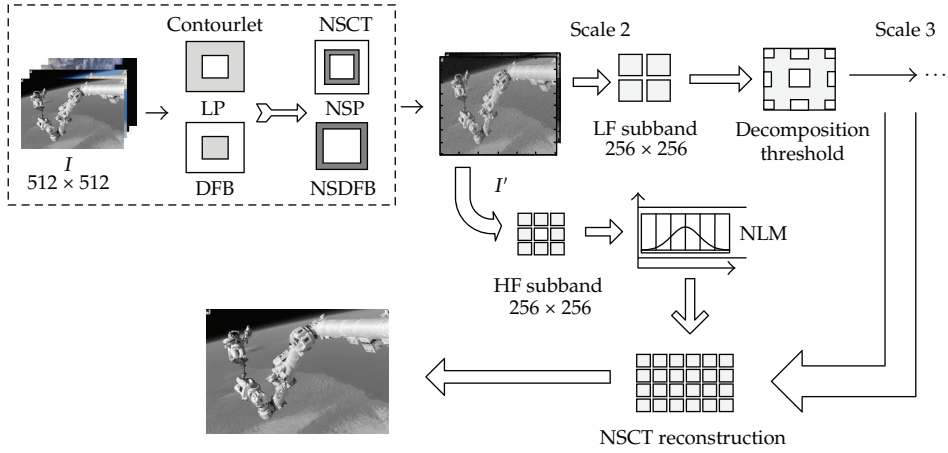


**Figure 5:** Image feature extraction based on the contourlet transform.

decomposition coefficients for large-scale details (low-frequency signal) and finer image details (high-frequency signal). Next, the algorithm applies deeper decomposition to the large-scale approximation. The whole process can be repeated until the algorithm yields the detail required.

Figure 5 shows the two-layer decomposition, where $I$ is the observed image, $I'$ is the image processed using the contourlet transform, LP is a Laplacian pyramid decomposition filter, DFB is a direction filter bank, LF is the low-frequency signal and HF is the high-frequency signal.

The decomposition coefficients for different frequencies are processed using the Bayesian-based NLM filter with a decomposition threshold. In particular, we use the wavelet threshold approach for the low-frequency part and the NLM approach for the high-frequency part. The specific steps in the algorithm are as follows.

*Step 1.* Decompose image I using the nonsubsampled contourlet transform.

*Step 2.* Apply the decomposition threshold method to the low-frequency part for noise suppression and feature extraction.

*Step 3.* Apply the improved Bayesian NLM filter to the high-frequency part for feature extraction.

*Step 4.* Reconstruct the high-frequency and low-frequency parts of the image processed using the contourlet transform.

For the low-frequency part, threshold decomposition is used to remove image noise. First, the threshold value $T$ is set. Decomposition coefficients smaller than $T$ are considered to be noise and thus are set to zero; coefficients greater than $T$ are reserved. The decomposition threshold is

$$T = \frac{\theta_n}{2^k}\sqrt{2\log N}, \quad \theta_n = \frac{M(d1)}{0.6745}, \quad M(d1) = \sum_{i=0}^{N}\sum_{n\in z^2} d1[2n + k_i], \tag{4.1}$$

where $k$ is the number of layers for wavelet decomposition, $\theta_n$ is a function for estimating mean absolute deviation, where $d1$ is the high-frequency coefficient for first-layer contourlet decomposition. The high-frequency part of the first layer usually contains few signal components and comprises mainly noise. For the high-frequency part, $G[D_k(x)]$ and $G[D_k(y)]$ are two blocks for image I. $G\,[D_k(p)]$ represents the rectangular neighborhood around $p$ as center. The proposed algorithm uses an improved Bayesian NLM image filter and a Euclidean distance to represent similarity between high-frequency image blocks. The similarity is represented by $w(x, y)$, which is defined as

$$w(x,y) = \frac{1}{Z(x)} e^{-(\|G[D_k(x)]-G[D_k(y)]\|^2/h^2),}$$
$$Z(x) = \sum_{x,y\in I} e^{-(\|G[D_k(x)]-G[D_k(y)]\|^2/h^2)}, \tag{4.2}$$

where $h$ is a constant used to control the exponential decay rate. Compared with the original NLM filter, the contourlet transform decomposes the image at different resolutions and the proposed approach uses different algorithm to process an image: threshold decomposition is used for the low-frequency part, and an improved Bayesian NLM filter is used for the high-frequency part. The NLM filter involves time-consuming calculations. If an image is decomposed by the contourlet transform for $k$ levels, the improved algorithm only has to process $1/2^k$ of the original size. This not only reduces the computational complexity but also greatly improves the accuracy of feature extraction.

## 5. Experimental Results

Spatial image can directly influence the success of spatial rendezvous and docking. We must ensure that the most accurate image feature can be extracted from spatial images. The proposed algorithm can also be applied to general image processing. To verify the performance of the algorithm, we carried out experiments both on Spatial images and standard images.

### *5.1. Performance Evaluation Based on Spatial Images*

Tests were carried out on image I and image II for an image size of 512 × 512. Multidimensional contourlet and curvelet decomposition algorithms were used for comparison. The same parameters were used for all algorithms.

Image feature extraction results were evaluated according to subjective and objective standards. Figure 6 shows the processing results for image I, and Figure 7 shows the results for image II. It is evident that the proposed algorithm yields a better subjective visual effect compared with the curvelet and contourlet algorithms.

The results show that feature extraction with the curvelet transform leads to confusion for some background information, and the contourlet transform yields a blurry image. By contrast, the proposed algorithm effectively suppresses noise and displays the main features of the image. Finer image details are shown in Figure 8.

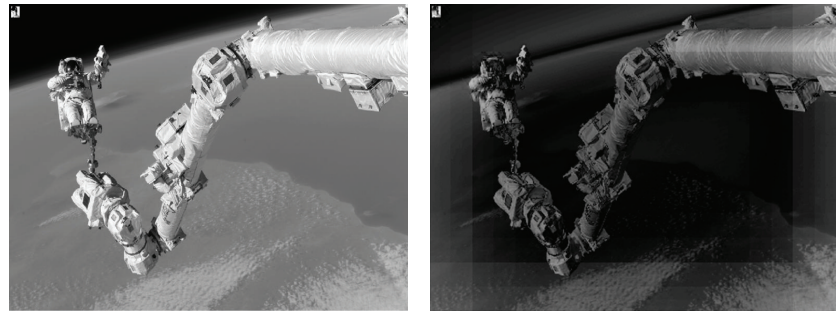

(a) Original image (b) Curvelet transform

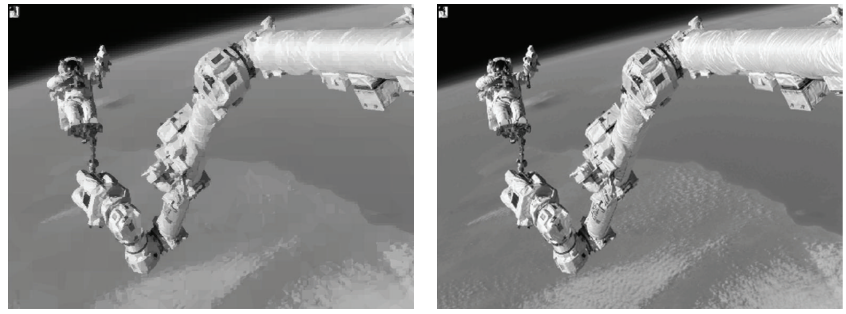

(c) Contourlet transform (d) Contourlet + NL-means

**Figure 6:** Process results for image I.

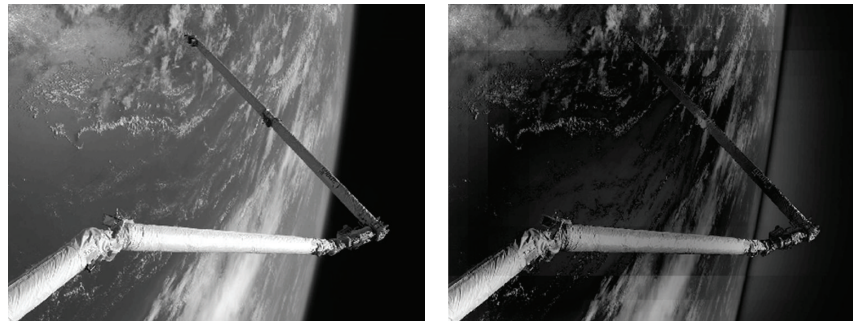

(a) Original image (b) Curvelet transform

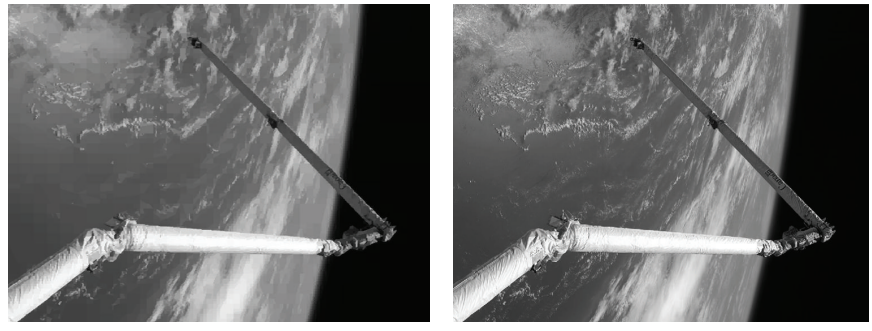

(c) Contourlet transform (d) Contourlet + NL-means

**Figure 7:** Process results for image II.

(a) Original (b) Noisy (c) Curvelet (d) Contourlet

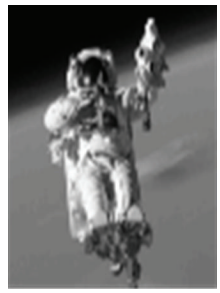

(e) Contourlet + NL-means

**Figure 8:** Process results for image II.

### *5.2. Performance Evaluation Based on Standard Images*

Figures 9 and 10 show the processing results for image as III, IV. Image as III and IV are standard images for an image size of 512 × 512. It is shown that our algorithm also provides better performance than that of Curvelet transform and Contourlet transform.

Results are objectively evaluated using the peak signal-to-noise ratio (PSNR) and structural similarity (SSIM), defined as follows:

$$\begin{aligned} \mathrm{PSNR} &= 10\log_{10}\frac{(L-1)^2}{\sum_{i=1}^{M}\sum_{j=1}^{N}\left[R(i,j)-F(i,j)\right]^2}, \\ \mathrm{SSIM}(x,y) &= \frac{(2u_xu_y+C_1)(2\sigma_{xy}+C_2)}{(u_x^2+u_y^2+C_1)(\sigma_x^2+\sigma_y^2+C_2)}, \\ \mathrm{MSSIM}(X,Y) &= \frac{1}{W}\sum_{r=1}^{W}\mathrm{SSIM}(X_r,Y_r), \end{aligned} \tag{5.1}$$

where $u_x$ and $u_y$ are the mean and $\sigma_x$ and $\sigma_y$ are the standard deviation for the original and processed images, respectively, $\sigma_{xy}$ is the covariance for the original and processed images, and $C_1$ and $C_2$ are constants. MSSIM is mean SSIM, and $W$ is the number of image subblocks. For greater PSNR and MSSIM ($0 \leq \mathrm{MSSIM} \leq 1$), the processed image is closer to the original.

(a) Original image (b) Curvelet transform

(c) Contourlet transform (d) Contourlet + NL-means

**Figure 9:** Process results for image III.

Table 1 compares the feature extraction performance for images I and II for several algorithms and different noise levels. The PSNR results show that the contourlet transform is superior to the curvelet transform for image I by almost 0.5 dB. Both the contourlet and curvelet transforms provide good edge detection. The proposed CT+NLM algorithm showed even better performance (~1.1 dB) compared with the contourlet transform but retained the good edge detection of the latter method (Table 1).The proposed algorithm uses an NLM filter for adaptive image expression. The MSSIM results show that the proposed algorithm yields the best performance for Gaussian, Poisson, Salt and Pepper and Speckle noise (Table 2).

Our algorithm uses a nonsubsampled key point filter for which $J+1$ redundancy is the most efficient. In pyramid decomposition, a lesser extent of image loss can be considered as an effective means to reduce redundancy. The proposed algorithm, which uses a nonsubsampled pyramid filter and a directional filter, leads to some image loss in reducing redundancy. Search windows of 16 × 16, 32 × 32, and 64 × 64 were applied to images I and II. The size of the search window can affect the computational complexity of the NLM filter.

Comparison of the experimental results for different window sizes reveals that the proposed algorithm delivers better noise suppression and feature extraction than the other algorithms. It provides a maximum PSNR value and a minimum MSSIM value for all windows (Table 3).

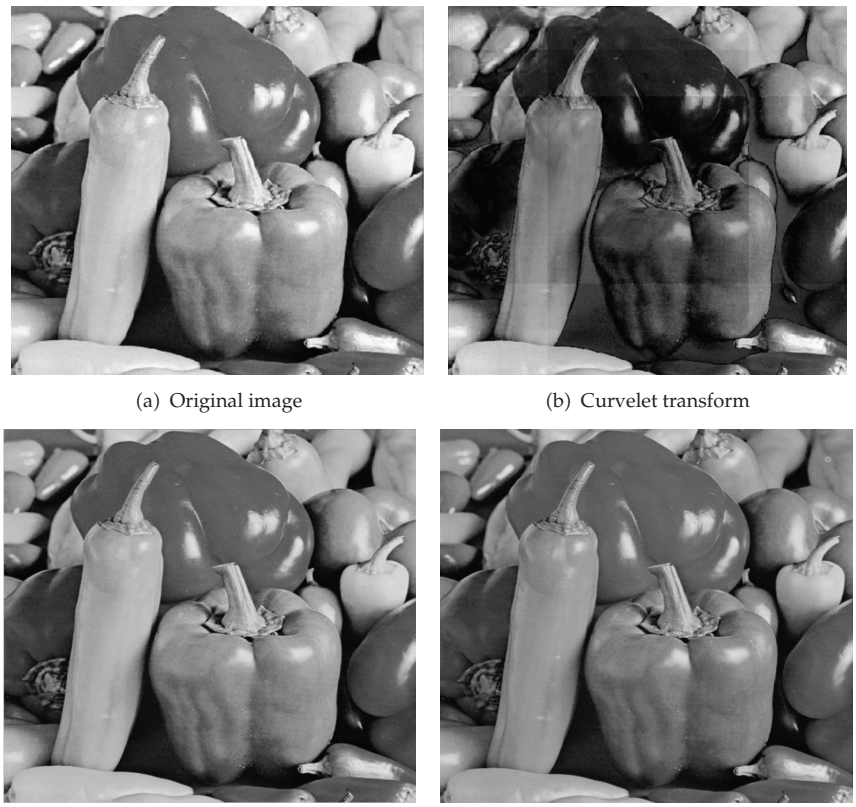

(a) Original image (b) Curvelet transform

(c) Contourlet transform (d) Contourlet + NL-means

**Figure 10:** Process results for image IV.

**Table 1:** PSNR results.

| Noise $\sigma$ | | PSNR (dB) | | | | |
|---|---|---|---|---|---|---|
| | | Noisy | Original | Curvelet | Contourlet | CT + NLM |
| 10 | Image I | 31.22 | 32.93 | 33.01 | 33.58 | 34.62 |
| | Image II | 32.98 | 33.53 | 33.89 | 34.21 | 35.40 |
| 20 | Image I | 31.16 | 31.89 | 32.75 | 33.01 | 34.19 |
| | Image II | 32.49 | 33.14 | 33.19 | 33.82 | 34.89 |
| 30 | Image I | 30.78 | 31.56 | 32.13 | 32.78 | 33.76 |
| | Image II | 31.98 | 32.75 | 32.82 | 33.21 | 34.17 |
| 40 | Image I | 30.56 | 31.01 | 31.74 | 32.53 | 33.61 |
| | Image II | 31.20 | 32.11 | 32.42 | 32.91 | 33.98 |
| 50 | Image I | 29.88 | 30.54 | 31.29 | 31.74 | 32.83 |
| | Image II | 30.77 | 31.56 | 31.98 | 32.17 | 33.28 |

## 6. Conclusions

Focusing on the actual needs of spatial images analysis, an improved contourlet transform, consisting of a nonsubsampled pyramid transform and nonsubsampled directional filter banks, was used to reduce the filter design problem of spatial images. The improved

**Table 2:** MSSIM results.

| Noise | | MSSIM | | | | |
|---|---|---|---|---|---|---|
| | | Noisy | Original | Curvelet | Contourlet | CT + NLM |
| Gaussian | Image I | 0.2979 | 0.3128 | 0.3524 | 0.4277 | 0.5185 |
| | Image II | 0.3014 | 0.3256 | 0.3688 | 0.4316 | 0.5220 |
| Poisson | Image I | 0.5744 | 0.6231 | 0.6827 | 0.7173 | 0.8219 |
| | Image II | 0.5891 | 0.6349 | 0.7028 | 0.7339 | 0.8551 |
| Salt and pepper | Image I | 0.2948 | 0.3239 | 0.3740 | 0.4157 | 0.5255 |
| | Image II | 0.3001 | 0.3398 | 0.3829 | 0.4254 | 0.5345 |
| Speckle | Image I | 0.2953 | 0.3321 | 0.3974 | 0.4309 | 0.5312 |
| | Image II | 0.3021 | 0.3476 | 0.4012 | 0.4452 | 0.5422 |

**Table 3:** Experimental results for different search windows.

| Scheme | Search window 16 × 16 | | | | Search window 32 × 32 | | | | Search window 64 × 64 | | | |
|---|---|---|---|---|---|---|---|---|---|---|---|---|
| | Image I | | Image II | | Image I | | Image II | | Image I | | Image II | |
| | PSNR | SSIM | PSNR | SSIM | PSNR | SSIM | PSNR | SSIM | PSNR | SSIM | PSNR | SSIM |
| Original | 30.53 | 0.658 | 31.45 | 0.679 | 30.09 | 0.669 | 31.21 | 0.685 | 29.89 | 0.675 | 31.09 | 0.703 |
| Curvelet | 30.78 | 0.697 | 31.66 | 0.722 | 30.12 | 0.701 | 31.39 | 0.737 | 29.91 | 0.688 | 31.15 | 0.749 |
| Contourlet | 31.23 | 0.759 | 31.98 | 0.784 | 30.35 | 0.762 | 31.65 | 0.791 | 30.17 | 0.744 | 31.23 | 0.806 |
| CT + NLM | 32.38 | 0.783 | 32.89 | 0.802 | 31.37 | 0.788 | 32.68 | 0.811 | 31.23 | 0.796 | 32.22 | 0.835 |

contourlet transform uses a mapping approach to solve the 2D filter design problem. The algorithm uses a Bayesian NLM filter for high-frequency information to suppress noise and improve the accuracy of image feature extraction. Experimental results confirm that the NLM filter can effectively retain structural information and reduce the residual structure. In the NSCT domain, the proposed algorithm showed better denoising and enhancement effects compared with the contourlet transform. Moreover, in comparison with NSWT, the algorithm is a more mature and sophisticated image-processing method.

## Acknowledgments

This work was supported by the National Basic Research Program of China (973 Program) (2012CB821206), the National Natural Science Foundation of China (no. 91024001, no. 61070142), and the Beijing Natural Science Foundation (no. 4111002).

## References

[1] P. Liu, F. Huang, G. Li, and Z. Liu, "Remote-sensing image denoising using partial differential equations and auxiliary images as priors," *IEEE Geoscience and Remote Sensing Letters*, vol. 9, no. 3, Article ID 6061940, pp. 358–362, 2012.

[2] H. Demirel and G. Anbarjafari, "Discrete wavelet transform-based satellite image resolution enhancement," *IEEE Transactions on Geoscience and Remote Sensing*, vol. 49, no. 6, pp. 1997–2004, 2011.

[3] P. Pan and D. Schonfeld, "Image reconstruction and multidimensional field estimation from randomly scattered sensors," *IEEE Transactions on Image Processing*, vol. 17, no. 1, pp. 94–99, 2008.

[4] F. Kamalabadi, "Multidimensional image reconstruction in astronomy," *IEEE Signal Processing Magazine*, vol. 27, no. 1, pp. 86–96, 2010.

[5] M. Mahmoudi and G. Sapiro, "Fast image and video denoising via nonlocal means of similar neighborhoods," *IEEE Signal Processing Letters*, vol. 12, no. 12, pp. 839–842, 2005.
[6] A. Buades, B. Coll, and J. M. Morel, "A review of image denoising algorithms, with a new one," *Multiscale Modeling & Simulation*, vol. 4, no. 2, pp. 490–530, 2005.
[7] D. L. Donoho, M. Vetterli, R. A. DeVore, and I. Daubechies, "Data compression and harmonic analysis," *IEEE Transactions on Information Theory*, vol. 44, no. 6, pp. 2435–2476, 1998.
[8] S. Mallat, *A Wavelet Tour of Signal Processing*, Elsevier/Academic Press, Amsterdam, The Netherlands, 3rd edition, 2009.
[9] E. J. Candès and D. L. Donoho, "Curvelets—a surprisingly effective nonadaptive representation for objects with edges," in *Curve and Surface Fitting*, A. Cohen, C. Rabut, and L.L. Schumaker, Eds., pp. 105–120, Vanderbilt University Press, Nashville, Tenn, USA, 1999.
[10] E. J. Candès and D. L. Donoho, "New tight frames of curvelets and optimal representations of objects with piecewise $C^2$ singularities," *Communications on Pure and Applied Mathematics*, vol. 57, no. 2, pp. 219–266, 2004.
[11] M. N. Do and M. Vetterli, "The contourlet transform: an efficient directional multiresolution image representation," *IEEE Transactions on Image Processing*, vol. 14, no. 12, pp. 2091–2106, 2005.
[12] P. J. Burt and E. H. Adelson, "The Laplacian pyramid as a compact image code," *IEEE Transactions on Communications*, vol. 31, no. 4, pp. 532–540, 1983.
[13] M. N. Do and M. Vetterli, "Framing pyramids," *IEEE Transactions on Signal Processing*, vol. 51, no. 9, pp. 2329–2342, 2003.
[14] R. H. Bamberger and M. J. T. Smith, "A filter bank for the directional decomposition of images: theory and design," *IEEE Transactions on Signal Processing*, vol. 40, no. 4, pp. 882–893, 1992.
[15] R. Eslami and H. Radha, "Translation-invariant contourlet transform and its application to image denoising," *IEEE Transactions on Image Processing*, vol. 15, no. 11, pp. 3362–3374, 2006.
[16] D. D.-Y. Po and M. N. Do, "Directional multiscale modeling of images using the contourlet transform," *IEEE Transactions on Image Processing*, vol. 15, no. 6, pp. 1610–1620, 2006.
[17] A. L. da Cunha, J. Zhou, and M. N. Do, "The nonsubsampled contourlet transform: theory, design, and applications," *IEEE Transactions on Image Processing*, vol. 15, no. 10, pp. 3089–3101, 2006.
[18] J. H. McClellan, "The design of two-dimensional digital filters by transformation," in *Proceedings of the 7th Annual Princeton Conference on Information Sciences and Systems*, pp. 247–251, 2003.
[19] M. J. Shensa, "The discrete wavelet transform: wedding the atrous and Mallat algorithms," *IEEE Transactions on Signal Processing*, vol. 40, no. 10, pp. 2464–2482, 1992.
[20] R. H. Bamberger and M. J. T. Smith, "A filter bank for the directional decomposition of images: theory and design," *IEEE Transactions on Signal Processing*, vol. 40, no. 4, pp. 882–893, 1992.
[21] E. P. Simoncelli, W. T. Freeman, E. H. Adelson, and D. J. Heeger, "Shiftable multiscale transforms," *IEEE Transactions on Information Theory*, vol. 38, no. 2, pp. 587–607, 1992.
[22] T. Tasdizen, "Principal neighborhood dictionaries for nonlocal means image denoising," *IEEE Transactions on Image Processing*, vol. 18, no. 12, pp. 2649–2660, 2009.
[23] J. Orchard, M. Ebrahimi, and A. Wong, "Efficient nonlocal-means denoising using the SVD," in *IEEE International Conference on Image Processing (ICIP '08)*, pp. 1732–1735, October 2008.
[24] N. Dowson and O. Salvado, "Hashed nonlocal means for rapid image filtering," *IEEE Transactions on Pattern Analysis and Machine Intelligence*, vol. 33, no. 3, pp. 485–499, 2011.
[25] M. Protter, M. Elad, H. Takeda, and P. Milanfar, "Generalizing the nonlocal-means to super-resolution reconstruction," *IEEE Transactions on Image Processing*, vol. 18, no. 1, pp. 36–51, 2009.
[26] P. Coupé, P. Hellier, C. Kervrann, and C. Barillot, "Nonlocal means-based speckle filtering for ultrasound images," *IEEE Transactions on Image Processing*, vol. 18, no. 10, pp. 2221–2229, 2009.
[27] W. L. Zeng and X. B. Lu, "Region-based non-local means algorithm for noise removal," *Electronics Letters*, vol. 47, no. 20, pp. 1125–1127, 2011.
[28] H. Zhong, Y. Li, and L. Jiao, "SAR image despeckling using bayesian nonlocal means filter with sigma preselection," *IEEE Geoscience and Remote Sensing Letters*, vol. 8, no. 4, pp. 809–813, 2011.
[29] R. Lai and Y. T. Yang, "Accelerating non-local means algorithm with random projection," *Electronics Letters*, vol. 47, no. 3, pp. 182–183, 2011.
[30] N. A. Thacker, J. V. Manjon, and P. A. Bromiley, "Statistical interpretation of non-local means," *IET Computer Vision*, vol. 4, no. 3, pp. 162–172, 2010.

Hindawi Publishing Corporation
Journal of Applied Mathematics
Volume 2012, Article ID 101353, 10 pages
doi:10.1155/2012/101353

*Research Article*

# State Estimators for Uncertain Linear Systems with Different Disturbance/Noise Using Quadratic Boundedness

**Longge Zhang,[1,2] Xiangjie Liu,[2] and Xiaobing Kong[2]**

[1] *Department of Mathematics and Physics, North China Electric Power University, Baoding 071003, China*
[2] *State Key Laboratory of Alternate Electrical Power System with Renewable Energy Sources, North China Electric Power University, Beijing 102206, China*

Correspondence should be addressed to Longge Zhang, longgexd@163.com

Received 28 February 2012; Revised 8 April 2012; Accepted 10 April 2012

Academic Editor: Baocang Ding



This paper designs state estimators for uncertain linear systems with polytopic description, different state disturbance, and measurement noise. Necessary and sufficient stability conditions are derived followed with the upper bounding sequences on the estimation error. All the conditions can be expressed in the form of linear matrix inequalities. A numerical example is given to illustrate the effectiveness of the approach.

## 1. Introduction

In many control systems, the state variables are usually not accessible for direct connection. In this case, it is necessary to design a state estimator, so that its output will generate an estimate of those states. Generally speaking, there are two kinds of estimators for dynamic systems: observers and filters. The former is under the supposition of the perfect knowledge of system and measurement equations, and the latter can be applied to the system with disturbance. Many literatures focus on the design of state estimators for linear system, for example, a sliding mode and a disturbance detector for a discrete Kalman filter [1], the quantized measurement method [2], the least squares estimation for linear singular systems [3], stochastic disturbances and deterministic unknown inputs on linear time-invariant systems [4], and the bounded disturbances on a dynamic system [5].

The concept of quadratic boundedness (QB) is first defined for an uncertain nonlinear dynamical system [6], and then its necessary and sufficient conditions for a class of nominally linear systems [7] and a class of linear systems which contain norm-bounded uncertainties

[8] are obtained. For discrete system, QB is applied mainly two regions: the receding horizon control (RHC) and the design of estimator. In RHC research, Ding utilizes QB to characterize the stability properties of the controlled system [9–13]. Alessandri et al. find the upper bounds on the norm of the estimation error by means of invariant sets, and these upper bounds can be expressed in terms of linear matrix inequalities [14]. Paper in [5] designs a filter by searching a suitable tradeoff between the transient and asymptotic behaviors of the estimation error. The designed filter is for the linear discrete systems with the identical state disturbance and measurement noise. For the discrete linear systems, the disturbance and noise are different in general. Nevertheless, little work has been done on the design of the state estimators for uncertain linear systems with different disturbance/noise. So how to design state estimators for uncertain linear systems with different state disturbance and measurement noise is important work.

The existing research work on state estimation usually constructs a filter for uncertain systems with bounded disturbance/noise, with no consideration of input or state constraint. Since the disturbance and noise are not assumed exactly identical, the stability station of the estimator is different from that in the paper [5]. For the above reasons, the situation becomes more complicated and the extension of the method is not straightforward.

This paper designs state estimators for uncertain linear systems with polytopic description. The problem is constructed in the form of linear matrix inequalities (LMIs). The organization of the paper is as follows. The earlier results are presented in the Section 2. The new robust estimator for uncertain linear systems with different disturbance/noise is designed in Section 3. A numerical simulation example is followed in Section 4. And some conclusions are given in the end.

*Notations.* For any vector $x$ and a positive-defined matrix $Q$, $\mathcal{E}_Q$ is the ellipsoid which is defined as $\{x \mid x'Qx \le 1\}$; $Q'$ is the transpose of matrix $Q$. $||x||$ is the Euclid norm of vector $x$. The symbol * induces a symmetric structure in LMIs.

## 2. Earlier Results

In this section, some results presented by Alessandri et al. [5, 14] are briefly introduced.

For a given discrete-time dynamic system,

$$x_{t+1} = A_t x_t + G_t w_t, \quad t = 0, 1, \ldots, \tag{2.1}$$

where $x_t \in R^n$ is the state vector and $w_t \in \mathcal{E}_Q \subset R^p$ is the noise vector. The definition of strictly quadratically bounded with a common Lyapunov matrix of a system and positively invariant set are defined by Alessandri et al. [5, 14], and the following theorem is proved.

**Theorem 2.1** (see [14]). *The following facts are equivalent:*

(i) *System* (2.1) *is strictly quadratically bounded with a common Lyapunov matrix* $P > 0$ *for all allowable* $w_t \in \mathcal{E}_Q$ *and* $(A_t, G_t) \in \varphi, t = 0, 1, \ldots$, *where* $\varphi$ *is a known bounded set.*

(ii) *The ellipsoid* $\mathcal{E}_P$ *is a positively invariant set for system* (2.1) *for all allowable* $w_t \in \mathcal{E}_Q$ *and* $(A_t, G_t) \in \varphi, t = 0, 1, \ldots$.

(iii) *There exists* $\alpha_t \in (0, 1)$ *such that for any* $(A_t, G_t) \in \varphi$,

$$\begin{bmatrix} A'_tPA_t - P + \alpha_t P & A'_tPG_t \\ * & G'_tPG_t - \alpha_t Q \end{bmatrix} \leq 0. \tag{2.2}$$

*For a discrete-time linear system with the same state disturbance and noise,*

$$\begin{aligned} x_{t+1} &= A_t x_t + B_t w_t, \\ y_t &= C_t x_t + D_t w_t, \\ z_t &= L_t x_t, \end{aligned} \tag{2.3}$$

*for* $t = 0, 1, \ldots$, *where* $x_t \in R^n, y_t \in R^m, z_t \in R^r$ *are the state vector, the measured output and the signal will be estimated, respectively, and* $w_t \in \mathcal{E}_Q \subset R^p$ *is the disturbance/noise vector.* $A_t, B_t, C_t, D_t, L_t$ *are the system matrixes with the proper dimensions. We consider the disturbance/noise to be unknown, and the system matrixes are supposed to be unknown and time varying but belonging to a polytopic set* $\mathcal{P}$, *that is,* $(A_t, B_t, C_t, D_t, L_t) \in \mathcal{P}$, $t = 0, 1, \ldots$, *where*

$$\mathcal{P} \triangleq \left\{ (A, B, C, D, L) = \sum_{i=1}^{N} \lambda_i \left( A^{(i)}, B^{(i)}, C^{(i)}, D^{(i)}, L^{(i)} \right); \sum_{i=1}^{N} \lambda_i = 1, \lambda_i \geq 0, i = 1, 2, \ldots N \right\}. \tag{2.4}$$

*Here* $(A^{(i)}, B^{(i)}, C^{(i)}, D^{(i)}, L^{(i)})$ $i = 1, 2, \ldots N$ *are vertexes of the polytope* $\mathcal{P}$.

*Definition 2.2* (see [5]). A sequence of vectors $\xi_t$ is said to be exponentially bounded with constants $\beta \in (0, 1)$, $k_1 \geq 0$, and $k_2 > -k_1$ if

$$\|\xi_t\| \leq k_1 + k_2 (1 - \beta)^t, \quad t = 0, 1, \ldots. \tag{2.5}$$

It is easy to see that $\beta$ determines the convergence speed and $k_1^{1/2}$ represents an upper bound of the sequence $\xi_t$.

**Theorem 2.3** (see [5]). *Consider two scalars* $\alpha \in (0, 1)$ *and* $\gamma > 0$. *The following facts are equivalent.*

(i) *There exist* $\widehat{A}, \widehat{B}, \widehat{L}$, *and* $P > 0$ *such that the following conditions are satisfied for any* $(A, B, C, D, L) \in \mathcal{P}$:

$$\begin{aligned} &\widetilde{C} P^{-1} \widetilde{C}' - \gamma^2 I < 0, \\ &\begin{bmatrix} A'PA - P + \alpha P & A'PG \\ * & G'PG - \alpha Q \end{bmatrix} < 0. \end{aligned} \tag{2.6}$$

(ii) *There exist* $V, W, X > 0, Y > 0$, *and* $Z$ *such that*

$$\begin{bmatrix} \gamma^2 I & L - W & L \\ * & X & X \\ * & * & Y \end{bmatrix} > 0,$$
$$\begin{bmatrix} (1-\alpha)X & (1-\alpha)X & 0 & A'X & A'Y + C'Z' + V' \\ * & (1-\alpha)Y & 0 & A'X & A'Y + C'Z' \\ * & * & \alpha Q & B'X & D'Z + B'Y \\ * & * & * & X & X \\ * & * & * & * & Y \end{bmatrix} > 0, \tag{2.7}$$

*for* $(A, B, C, D, L) = (A^{(i)}, B^{(i)}, C^{(i)}, D^{(i)}, L^{(i)})$, $i = 1, 2, \ldots N$.

*Then, the cost* $J(r, \alpha) \triangleq \mu\gamma - (1-\mu)\alpha$ *can be minimized over* $V, W, X > 0$, $Y > 0$, $Z, \alpha \in (0, 1)$ *and* $\gamma > 0$ *under the constrains* (2.7).

## 3. A Robust Estimator for Uncertain Linear Systems with Different Noises

Let us consider the discrete-time linear system with different disturbance/noise:

$$\begin{aligned} x_{t+1} &= A_t x_t + B_t w_t, \\ y_t &= C_t x_t + D_t v_t, \\ z_t &= L_t x_t, \end{aligned} \tag{3.1}$$

where the matrixes and vectors are the same as (2.3) except $w_t \in \mathcal{E}_{Q_1}, v_t \in \mathcal{E}_{Q_2}$, which are the vectors of the state disturbance and measurement noise, respectively.

To estimate the signal $z_t$, the linear filter is introduced which has the following form:

$$\begin{aligned} \widehat{x}_{t+1} &= \widehat{A}\widehat{x}_t + \widehat{B}y_t, \\ \widehat{z}_t &= \widehat{L}\widehat{x}_t, \end{aligned} \tag{3.2}$$

for $t = 0, 1, \ldots$, where $\widehat{x}_t \in R^n$ is the filter state vector and $\widehat{z}_t \in R^r$ is the estimation of the signal $z_t$.

Define the estimation error $e_t$, the augmented state vector, and the augmented disturbance/noise as

$$e_t \triangleq z_t - \widehat{z}_t, \qquad \widetilde{x}_t \triangleq \begin{bmatrix} x_t \\ \widehat{x}_t \end{bmatrix}, \qquad \widetilde{w}_t = \begin{bmatrix} w_t \\ v_t \end{bmatrix} \tag{3.3}$$

and the dynamic system associated with the estimation error

$$\tilde{x}_{t+1} = \underbrace{\begin{bmatrix} A & 0 \\ \widehat{B}C_t & \widehat{A} \end{bmatrix}}_{\tilde{A}} \tilde{x}_t + \underbrace{\begin{bmatrix} B_t & 0 \\ 0 & \widehat{B}D_t \end{bmatrix}}_{\tilde{B}} \tilde{w}_t, \tag{3.4}$$

$$e_t = \underbrace{\begin{bmatrix} L_t & -\widehat{L} \end{bmatrix}}_{\tilde{C}} \tilde{x}_t, \tag{3.5}$$

for $t = 0, 1, \ldots$.

The objective is to find an estimate $\widehat{z}_t$ of the signal $z_t$ such that the estimation error $e_t = z_t - \widehat{z}_t$ is exponentially bounded for any $x_0 \in R^n$, $w_t \in \mathcal{E}_{Q_1}$, $v_t \in \mathcal{E}_{Q_2}$, and $(A_t, B_t, C_t, D_t, L_t) \in \mathcal{D}$, $t = 0, 1, \ldots$. Then the following problem has to be solved.

*Problem 1.* Find matrices $\widehat{A}, \widehat{B}, \widehat{L}$ such that, for any $x_0 \in R^n$, $w_t \in \mathcal{E}_{Q_1}$, $v_t \in \mathcal{E}_{Q_2}$ and $(A_t, B_t, C_t, D_t, L_t) \in \mathcal{D}$, $t = 0, 1, \ldots$; the estimation error $e_t$ is exponentially bounded with constants $\beta \in (0, 1)$, $k_1 \geq 0$, and $k_2 > -k_1$.

In order to solve Problem 1, we now exploit the results on quadratic boundedness. More specifically, the following proposition holds.

**Proposition 3.1.** *Suppose there exist matrices $\widehat{A}, \widehat{B}, \widehat{L}$, a symmetric matrix $P > 0$, and two scalars $\gamma > 0$ and $\alpha \in (0, 1)$ such that, for any $(A, B, C, D, L) \in \mathcal{D}$,*

$$\tilde{C} P^{-1} \tilde{C}' - \gamma^2 I < 0, \tag{3.6}$$

$$\begin{bmatrix} \tilde{A}' P \tilde{A} - P + \alpha P & \tilde{A}' P \tilde{B} \\ * & \tilde{B}' P \tilde{B} - \alpha R \end{bmatrix} < 0, \tag{3.7}$$

*where $R = \operatorname{diag}\{Q_1, Q_2\}$. Then, for any $x_0 \in R^n$, $w_t \in \mathcal{E}_{Q_1}$, $v_t \in \mathcal{E}_{Q_2}$, and $(A_t, B_t, C_t, D_t, L_t) \in \mathcal{D}$, $t = 0, 1, \ldots$, the estimation error is exponentially bounded with constants*

$$\beta = \alpha, \qquad k_1 = \gamma^2, \qquad k_2 = \gamma^2 (\tilde{x}_0' P \tilde{x}_0 - 1). \tag{3.8}$$

*Hence the matrices $\widehat{A}, \widehat{B}$, and $\widehat{L}$ are a solution of Problem 1.*

*Remark 3.2.* We can see that condition (3.7) ensures system (3.1) is strictly bounded with a common Lyapunov matrix $P$, and from Corollary 2 of paper [5], it is clearly, $\gamma$ is a bound. But its feasibility cannot be easily verified. The following theorem transposes them into the equivalent LMI conditions.

**Theorem 3.3.** *Consider two scalars $\alpha \in (0, 1)$ and $\gamma > 0$. The following facts are equivalent.*

(i) *There exist $\widehat{A}, \widehat{B}, \widehat{L}$, and $P > 0$ such that conditions* (3.6) *and* (3.7) *are satisfied for any $(A, B, C, D, L) \in \mathcal{D}$.*

(ii) *There exist $V, W, X > 0, Y > 0$, and $Z$ such that*

$$\begin{bmatrix} \gamma^2 I & L-W & L \\ * & X & X \\ * & * & Y \end{bmatrix} > 0, \tag{3.9}$$

$$\begin{bmatrix} (1-\alpha)X & (1-\alpha)X & 0 & 0 & A'X & A'Y + C'Z' + V' \\ * & (1-\alpha)Y & 0 & 0 & A'X & A'Y + C'Z' \\ * & * & \alpha Q_1 & 0 & B'X & B'Y \\ * & * & 0 & \alpha Q_2 & 0 & D'Z \\ * & * & * & * & X & X \\ * & * & * & * & * & Y \end{bmatrix} > 0. \tag{3.10}$$

*Proof.* The proof of (3.6)⇔(3.9) is the same as Theorem 2 of reference [5]; here it is omitted for brevity.

(3.7)⇒(3.10) suppose the condition (3.7) is satisfied. The matrix $P$ and matrix $P^{-1}$ are partitioned as

$$P = \begin{bmatrix} P_{11} & P_{12} \\ P_{21} & P_{22} \end{bmatrix}, \qquad P^{-1} = \begin{bmatrix} S_{11} & S \\ S_{21} & S \end{bmatrix}, \tag{3.11}$$

with $P_{11} \in R^{n\times n}$ and $S_{11} \in R^{n\times n}$. Clearly $PP^{-1} = P^{-1}P = I$, so we have

$$S_{12}P'_{12} = I - S_{11}P_{11}, \qquad S_{11}P_{12} + S_{12}P_{22} = 0. \tag{3.12}$$

Moreover, (3.7) is strict inequality, and we can assume, without loss of generality, that $I - S_{11}P_{11}$ is invertible [15]. Hence $S_{12}$ and $P_{12}$ are invertible. Using the Schur complement, we can rewrite (3.7) as

$$\begin{bmatrix} (1-\alpha)P & 0 & \widetilde{A}'P \\ 0 & \alpha R & \widetilde{B}'P \\ * & * & P \end{bmatrix} > 0. \tag{3.13}$$

Define

$$T \triangleq \begin{bmatrix} H' & 0 & 0 \\ 0 & I & 0 \\ 0 & 0 & H' \end{bmatrix}, \tag{3.14}$$

where $H' = \begin{bmatrix} I & I \\ S'_{12}S_{11}^{-1} & 0 \end{bmatrix}$, so

$$T' \begin{bmatrix} (1-\alpha)P & 0 & \widetilde{A}'P \\ 0 & \alpha R & \widetilde{B}'P \\ * & * & P \end{bmatrix} T = \begin{bmatrix} H & 0 & 0 \\ 0 & I & 0 \\ 0 & 0 & H \end{bmatrix} \begin{bmatrix} (1-\alpha)P & 0 & \widetilde{A}'P \\ 0 & \alpha R & \widetilde{B}'P \\ * & * & P \end{bmatrix} \begin{bmatrix} H' & 0 & 0 \\ 0 & I & 0 \\ 0 & 0 & H' \end{bmatrix}$$

$$= \begin{bmatrix} (1-\alpha)HP & 0 & H\widetilde{A}'P \\ 0 & \alpha R & \widetilde{B}'P \\ HPA & HP\widetilde{B} & HP \end{bmatrix} \begin{bmatrix} H' & 0 & 0 \\ 0 & I & 0 \\ 0 & 0 & H' \end{bmatrix} = \begin{bmatrix} (1-\alpha)HPH' & 0 & H\widetilde{A}'PH' \\ 0 & \alpha R & \widetilde{B}'PH' \\ HPAH' & HP\widetilde{B} & HPH' \end{bmatrix},$$

$$HPH' = \begin{bmatrix} I & S_{11}^{-1}S_{12} \\ I & 0 \end{bmatrix} \begin{bmatrix} P_{11} & P_{12} \\ P_{21} & P_{22} \end{bmatrix} \begin{bmatrix} I & I \\ S'_{12}S_{11}^{-1} & 0 \end{bmatrix}$$

$$= \begin{bmatrix} P_{11} + S_{11}^{-1}S_{12}P_{21} + \left(P_{12} + S_{11}^{-1}S_{12}P_{22}\right)S'_{12}S_{11}^{-1} & P_{11} + S_{11}^{-1}S_{12}P_{21} \\ P_{11} + P_{12}S'_{12}S_{11}^{-1} & P_{11} \end{bmatrix}. \tag{3.15}$$

Using condition (3.12), we can get

$$HPH' = \begin{bmatrix} S_{11}^{-1} & S_{11}^{-1} \\ S_{11}^{-1} & P_{11} \end{bmatrix} = \begin{bmatrix} X & X \\ X & Y \end{bmatrix}, \tag{3.16}$$

where $X \triangleq S_{11}^{-1}, Y \triangleq P_{11}$:

$$\begin{aligned} H\widetilde{A}'PH' &= \begin{bmatrix} I & S_{11}^{-1}S_{12} \\ I & 0 \end{bmatrix} \begin{bmatrix} A' & C'\widehat{B}' \\ 0 & \widehat{A}' \end{bmatrix} \begin{bmatrix} P_{11} & P_{12} \\ P_{21} & P_{22} \end{bmatrix} \begin{bmatrix} I & I \\ S'_{12}S_{11}^{-1} & 0 \end{bmatrix} \\ &= \begin{bmatrix} A' & C'\widehat{B}' + S_{11}^{-1}S_{12}\widehat{A}' \\ A' & C'\widehat{B}' \end{bmatrix} \begin{bmatrix} P_{11} + P_{12}S'_{12}S_{11}^{-1} & P_{11} \\ P_{21} + P_{22}S'_{12}S_{11}^{-1} & P_{21} \end{bmatrix} \\ &= \begin{bmatrix} A'X & A'Y + C'Z' + V' \\ A'X & A'Y + C'Z' \end{bmatrix}. \end{aligned} \tag{3.17}$$

Here we define $V \triangleq P_{12}\widehat{A}S'_{12}S_{11}^{-1}, Z \triangleq P_{12}\widehat{B}$:

$$\begin{aligned} \widetilde{B}'PH' &= \begin{bmatrix} B' & 0 \\ 0 & D'\widehat{B}' \end{bmatrix} \begin{bmatrix} P_{11} & P_{12} \\ P_{21} & P_{22} \end{bmatrix} \begin{bmatrix} I & I \\ S'_{12}S_{11}^{-} & 0 \end{bmatrix} \\ &= \begin{bmatrix} B'P_{11} & B'P_{12} \\ D'\widehat{B}'P_{21} & D'\widehat{B}'P_{22} \end{bmatrix} \begin{bmatrix} I & I \\ S'_{12}S_{11}^{-} & 0 \end{bmatrix} = \begin{bmatrix} B'P_{11} + B'P_{12}S'_{12}S_{11}^{-1} & B'P_{11} \\ D'\widehat{B}'P_{21} + D'\widehat{B}'P_{22}S'_{12}S_{11}^{-1} & D'\widehat{B}'P_{21} \end{bmatrix} \\ &= \begin{bmatrix} B'X & B'Y \\ 0 & D'Z' \end{bmatrix}. \end{aligned} \tag{3.18}$$

So we can get condition (3.10).

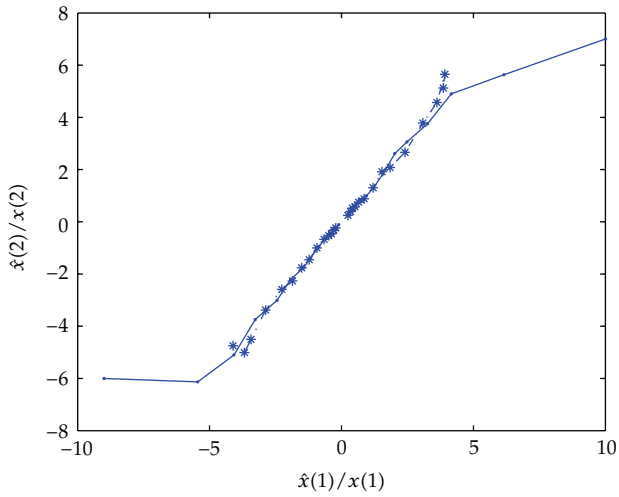


**Figure 1:** The state and estimator trajectories.

(3.10)⇒(3.7) suppose there exist $V, X > 0$, $Y > 0$ and $Z$ satisfied condition (3.4), as condition (3.4) holds at every vertex $(A^{(i)}, B^{(i)}, C^{(i)}, D^{(i)}, L^{(i)})$ of the polytope $\mathcal{D}$, and it also holds for every system matrice $(A, B, C, D, L) \in \mathcal{D}$.

We can obtain $\left[\begin{smallmatrix} X & X \\ X & Y \end{smallmatrix}\right] > 0$ from condition (3.10), and based on the Schur complement, the result of $I - X^{-1}Y < 0$ can be deduced. Then there exist two square invertible matrixes $M$ and $N$ such that $M'N' = I - X^{-1}Y$. Choosing $P_{11} = Y, S_{11} = X^{-1}, S'_{12} = M$ and $P_{12} = N$, condition (3.7) can be obtained by premultiplying and postmultiplying condition (3.10) by $(T')^{-1}$and $T^{-1}$. If we apply the change of variable

$$\begin{aligned} \widehat{A} &= N^{-1}VX^{-1}M^{-1}, \qquad \widehat{B} = N^{-1}Z, \\ \widehat{L} &= WX^{-1}M^{-1}, \qquad P = \begin{bmatrix} Y & N \\ N' & -N'X^{-1}M^{-1} \end{bmatrix}. \end{aligned} \tag{3.19}$$

so, we can get the linear filter (3.2). □

*Remark 3.4.* In paper [5], the estimators for uncertain systems propose that the state disturbance and measurement noise are identical with the time. Ordinarily, they are different in practice, so the result in our paper is the general case.

## 4. A Numerical Example

Let us consider the system [12] in the form of (3.1) with

$$\begin{aligned} A_t &= \begin{bmatrix} 0.385 & 0.33 \\ 0.21 + a_t & 0.59 \end{bmatrix}, \qquad B_t = \begin{bmatrix} 0.3 \\ 0.3 \end{bmatrix}, \\ C_t &= \begin{bmatrix} 0.2 & 0.2 + a_t \end{bmatrix}, \qquad D_t = 0.3, \qquad L_t = [10], \end{aligned} \tag{4.1}$$

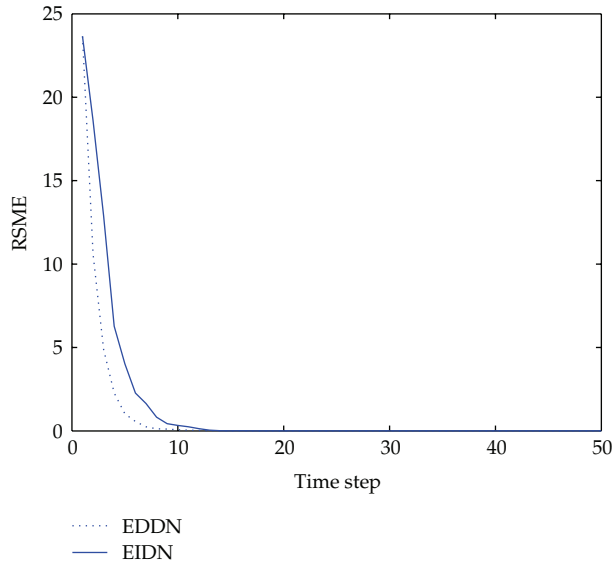


**Figure 2:** Plots of the RSME for the considered filters.

where $a_t$ is an uncertain parameter satisfying $|a_t| \leq 0.11$. Suppose the state disturbance satisfies the condition $|w_t| \leq 0.25$ and the measurement noise satisfies $|v_t| \leq 0.1$ (i.e., $Q_1 = 16, Q_2 = 100$).

As this kind of uncertainty is of the polytopic type described in Section 3, the proposed method is used to obtain a linear filter. In the context, we will refer to this filter as the "filter with different disturbance/noise" (FDDN). Choose two sets of initial states: $\widehat{x}_0 = \{[8 \quad 6]^T, [-11 \quad 7]^T\}, x_0 = \{[10 \quad 7]^T, [-9 \quad -6]^T\}$. The resulting state trajectories are shown in Figure 1 by the marked solid line, followed with the estimator state trajectories shown by the marked dotted line. Figure 1 indicates that the designed estimator can track the systems' states effectively.

The performance of the filter can be further studied by using an average measure of the estimation error, such as the expected quadratic estimation error. Comparison was then made between the FDDN and the "filter with identity disturbance/noise" (FIDN), to evaluate the performance achieved when the different disturbance/noise is taken into account in the synthesis of the filter. At each time instant, the uncertain parameters were chosen to be within, with equal probability, one of their limit values. We assumed $x_0, w_t$ and $v_t, t = 0, 1, \ldots$, to be independent random vectors, and the initial states are in the ball of radius 10 (i.e., $||x_0|| \leq 10$). Figure 2 shows the plots of the "root mean square error" (RMSE), computed over $10^3$ randomly chosen simulations, for the considered filters. The performance of the FDDN turns out to be better from the point of view of the asymptotic behavior when there is large difference between the disturbance and noise.

## 5. Conclusions

The main contribution of this work is the method of constructing an estimator for the uncertain system with the different state disturbance and measurement noise. The stability of

the estimator is analyzed using quadratic boundness. Moreover, the estimator can be got by LMI procedures.

## Acknowledgments

This work was supported by National Natural Science Foundation of China under Grant 60974051, Natural Science Foundation of Beijing under Grant 4122071, Fundamental Research Funds for the Central Universities under Grant 12MS143, and the Construction Project from Beijing Municipal Commission of Education. The authors would like to thank the reviewers for their pertinent comments.

## References

[1] J. H. Kim and J. H. Oh, "Robust state estimator of stochastic linear systems with unknown disturbances," *IEE Proceedings*, vol. 147, no. 2, pp. 224–228, 2000.

[2] M. Fu and C. E. de Souza, "State estimation for linear discrete-time systems using quantized measurements," *Automatica*, vol. 45, no. 12, pp. 2937–2945, 2009.

[3] B. Boulkroune, M. Darouach, and M. Zasadzinski, "Moving horizon state estimation for linear discrete-time singular systems," *IET Control Theory and Applications*, vol. 4, no. 3, pp. 339–350, 2010.

[4] S. Pillosu, A. Pisano, and E. Usai1, "Decentralised state estimation for linear systems with unknown inputs: a consensus-based approach," *IET Control Theory & Applications*, vol. 5, no. 3, pp. 498–506, 2011.

[5] A. Alessandri, M. Baglietto, and G. Battistelli, "Design of state estimators for uncertain linear systems using quadratic boundedness," *Automatica*, vol. 42, no. 3, pp. 497–502, 2006.

[6] M. L. Brockman and M. Corless, "Quadratic boundedness of nonlinear dynamical systems," in *Proceedings of the 34th IEEE Conference on Decision and Control*, pp. 504–509, New Orleans, La, USA, December 1995.

[7] M. L. Brockman and M. Corless, "Quadratic boundedness of nominally linear systems," *International Journal of Control*, vol. 71, no. 6, pp. 1105–1117, 1998.

[8] M. L. Ni and M. J. Er, "Design of linear uncertain systems guaranteeing quadratic boundedness," in *Proceedings of the Americal Control Conference*, pp. 3832–3836, Chicago, Ill, USA, June 2000.

[9] B. Ding and L. Xie, "Dynamic output feedback robust model predictive control with guaranteed quadratic boundedness," in *Proceedings of the 48th IEEE Conference on Decision and Control (CDC/CCC '09)*, pp. 8034–8039, Shanghai, China, December 2009.

[10] B. Ding, "Quadratic boundedness via dynamic output feedback for constrained nonlinear systems in Takagi-Sugeno's form," *Automatica*, vol. 45, no. 9, pp. 2093–2098, 2009.

[11] B. Ding, "Dynamic output feedback predictive control for nonlinear systems represented by a takagi–sugeno model," *IEEE Transactions on Fuzzy Systems*, vol. 19, no. 5, pp. 831–843, 2011.

[12] B. Ding, Y. Xi, M. T. Cychowski, and T. O'Mahony, "A synthesis approach for output feedback robust constrained model predictive control," *Automatica*, vol. 44, no. 1, pp. 258–264, 2008.

[13] B. Ding, "New formulation of dynamic output feedback robust model predictive control with guaranteed quadratic boundedness," in *Proceedings of the 30th Chinese Control Conference*, pp. 3346–3351, Yantai, China, July 2011.

[14] A. Alessandri, M. Baglietto, and G. Battistelli, "On estimation error bounds for receding-horizon filters using quadratic boundedness," *IEEE Transactions on Automatic Control*, vol. 49, no. 8, pp. 1350–1355, 2004.

[15] M. Chilali and P. Gahinet, "$H_\infty$ design with pole placement constraints: an LMI approach," *IEEE Transactions on Automatic Control*, vol. 41, no. 3, pp. 358–367, 1996.

Hindawi Publishing Corporation
Journal of Applied Mathematics
Volume 2012, Article ID 324296, 16 pages
doi:10.1155/2012/324296

*Research Article*

# Measurement Feedback Self-Tuning Weighted Measurement Fusion Kalman Filter for Systems with Correlated Noises

**Xin Wang and Shu-Li Sun**

*Department of Automation, Heilongjiang University, Harbin 150080, China*

Correspondence should be addressed to Xin Wang, wangxin@hlju.edu.cn

Received 26 February 2012; Accepted 19 March 2012

Academic Editor: Baocang Ding



For the linear discrete stochastic systems with multiple sensors and unknown noise statistics, an online estimators of the noise variances and cross-covariances are designed by using measurement feedback, full-rank decomposition, and weighted least squares theory. Further, a self-tuning weighted measurement fusion Kalman filter is presented. The Fadeeva formula is used to establish ARMA innovation model with unknown noise statistics. The sampling correlated function of the stationary and reversible ARMA innovation model is used to identify the noise statistics. It is proved that the presented self-tuning weighted measurement fusion Kalman filter converges to the optimal weighted measurement fusion Kalman filter, which means its asymptotic global optimality. The simulation result of radar-tracking system shows the effectiveness of the presented algorithm.

## 1. Introduction

With the development of scientific technology, the scale of a control system has become more and more complex and tremendous, and the accuracy, fault-tolerance, and robustness of a system are required much higher, so that single sensor has been unable to satisfy the demands of high scientific technologies. Thus, the multisensor information fusion technology has been paid great attention to and become an important research issue.

In early 1980s, Shalom [1, 2] presented the computation formula of cross-covariance matrix by studying the correlation of two sensor subsystems with independent noises. Carlson [3] presented the famous federated Kalman filter by using the upper bound of noise variance matrix to replace noise variance matrix and supposing that the initial local estimation errors are not correlated. Kim [4] proposed the maximum likelihood fusion estimation algorithm by requiring the hypothesis that random variables obey normal distributions.

The universal weighted least squares method and the best linear unbiased fusion estimation algorithm were presented by Li et al. [5] on the basis of a unified linear model for three estimation fusion architectures of centralized filter, distributed filter, and hybrid filter. Three weighted fusion algorithms of matrix-weighted, diagonal-matrix-weighted, and scalar-weighted in the linear minimum variance sense were proposed by Sun and Deng [6], Sun [7], where the matrix-weighted fusion algorithm, maximum likelihood fusion algorithm [4], and distributed best linear unbiased estimation algorithm [5] have the same result and avoid the derivation on the basis of hypothesis of normal distribution and linear model. The shortcomings of methods presented in [3–7] are that they have larger calculation burdens and the fusion accuracy is global suboptimal.

Based on Kalman filtering, Gan and Chris [8] discussed two kinds of multisensor measurement fusion method: the centralized measurement fusion (CMF) and the weighted measurement fusion (WMF). The former is to directly merge the multisensor data through the augmented measurement vector to calculate the estimation. Its advantage is that it can obtain globally optimal state estimator. Its shortcoming is that the computational burden is large since the measurement dimension is high. So it is unsuitable for real-time application. The latter is to weigh local sensor measurements to obtain a low-dimensional measurement equation, and then to use a single Kalman filter to obtain the final fused state estimation. Its advantages are that the computational burden can be obviously reduced and the globally optimal state estimation can be obtained [8–12].

It is known that the existing information fusion Kalman filtering is only effective when the model parameters and noise statistics are exactly known. But this restricts its applications in practice. In real applications, the model parameters and noise statistics are completely or partially unknown in general. The filtering problem for systems with unknown model parameters and/or noise statistics yields the self-tuning filtering. Its basic principle is the optimal filter plus a recursive identifier of model parameters and/or noise statistics [13].

For self-tuning fusion filters, there are two methods of self-tuning weighted state fusion and self-tuning measurement fusion. Weighted state fusion method is used by Sun [14] and Deng et al. [15], respectively, but the used distributed state fusion algorithm is globally suboptimal and the acquired self-tuning estimator cannot reach globally asymptotic optimality. For the self-tuning measurement fuser, [9, 16] considered the uncorrelated input noise and measurement noise. Ran and Deng [17] presented a self-tuning measurement fusion Kalman filter under the assumption that all sensors have the same measurement matrices.

This paper is concerned with the self-tuning filtering problem for a multisensor system with unknown noise variances, different measurement matrices, and correlated noises. Firstly, transform the system with correlated input noise and measurement noise into one with uncorrelated input noise and measurement noise by using the measurement feedback and taking measurement data as a part of system control item. Then, weigh all the measurements by using full-rank decomposition and weighted least squares theory. The Fadeeva formula is used to establish ARMA innovation model with unknown noise covariance matrices and the sampling correlated function of a stationary and reversible ARMA innovation model is used to identify the noise covariance matrices. It is rigorously proved that the presented self-tuning weighted measurement fusion Kalman filter converges to the optimal weighted measurement fusion Kalman filter, that is, it has asymptotic global optimality.

## 2. Problem Formulation

Consider the controlled multisensor time-invariant systems with correlated noises:

$$x(t+1) = \Phi x(t) + Bu(t) + \Gamma w(t), \tag{2.1}$$

$$y_i(t) = H_i x(t) + v_i(t), \quad i = 1, \ldots, L, \tag{2.2}$$

where $x(t) \in R^n$ is the state, $u(t) \in R^p$ is the given control, $y_i(t) \in R^{m_i}$ is the measurement of the sensor $i$, $w(t) \in R^r$ is the input noise, and $v_i(t) \in R^{m_i}$ is the measurement noise. $L$ is the number of sensors, $H_i \in R^{m_i \times n}$ is the measurement matrix of the sensor $i$. $\Phi$, $B$, and $\Gamma$ are constant matrices with compatible dimensions.

*Assumption 2.1.* $w(t)$ and $v_i(t)$ are correlated Gaussian white noise with zero means, and

$$E\left\{ \begin{bmatrix} w(t) \\ v_i(t) \end{bmatrix} \begin{bmatrix} w^{\mathrm{T}}(k) & v_j^{\mathrm{T}}(k) \end{bmatrix} \right\} = \begin{bmatrix} Q_w & S_j \\ S_i^{\mathrm{T}} & R_{ij} \end{bmatrix} \delta_{tk}, \quad i = 1, \ldots, L, \tag{2.3}$$

where the symbol $E$ denotes the expectation, $\delta_{tk}$ is Kronecker delta function, that is, $\delta_{tt} = 1$, $\delta_{tk} = 0$ $(t \neq k)$. The variance matrix of $v_i(t)$ is $R_{ii} = R_i$. Combining $L$ measurement equations of (2.2) yields

$$y^{(\mathrm{I})}(t) = H^{(\mathrm{I})} x(t) + v^{(\mathrm{I})}(t), \tag{2.4}$$

where $y^{(\mathrm{I})}(t) = [y_1^{\mathrm{T}}(t), \ldots, y_L^{\mathrm{T}}(t)]^{\mathrm{T}}$, $H^{(\mathrm{I})} = [H_1^{\mathrm{T}}, \ldots, H_L^{\mathrm{T}}]^{\mathrm{T}}$ and $v^{(\mathrm{I})}(t) = [v_1^{\mathrm{T}}(t), \ldots, v_L^{\mathrm{T}}(t)]^{\mathrm{T}}$. Let the variance of $v^{(\mathrm{I})}(t)$ be $R^{(\mathrm{I})} = (R_{ij}) > 0$ and the cross covariance of $w(t)$ and $v^{(\mathrm{I})}(t)$ be $S = [S_1, \ldots, S_L]$.

*Assumption 2.2.* $(\Phi, H^{(\mathrm{I})})$ is a detectable pair and $(\Phi, \Gamma)$ is a controllable pair, or $\Phi$ are stable.

*Assumption 2.3.* Measurement data $y_i(t)$ is bounded, that is,

$$\left\| y_i(t) \right\| < c, \quad i = 1, \ldots, L, \tag{2.5}$$

where $\| \cdot \|$ is the norm of a vector and $c > 0$ is a positive real number.

### 2.1. CMF and WMF Kalman Filter

To convert the systems (2.1) and (2.4) into the uncorrelated system, (2.1) is equivalent to

$$x(t+1) = \Phi x(t) + Bu(t) + \Gamma w(t) + J\left[ y^{(\mathrm{I})}(t) - H^{(\mathrm{I})} x(t) - v^{(\mathrm{I})}(t) \right], \tag{2.6}$$

where $J$ is a pending matrix. (2.6) can be converted into

$$x(t+1) = \overline{\Phi} x(t) + \overline{u}(t) + \overline{w}(t), \tag{2.7}$$

where $\overline{\Phi} = \Phi - JH^{(\mathrm{I})}$, $\overline{u}(t) = Bu(t) + Jy^{(\mathrm{I})}(t)$, $\overline{w}(t) = \Gamma w(t) - Jv^{(\mathrm{I})}(t)$. $Jy^{(\mathrm{I})}(t)$ as an output feedback becomes a part of the control item. Then, primary system formulae (2.1) and (2.2) are equivalent to the system formed by formulae (2.4) and (2.7). To make $E[\overline{w}(t)v^{(\mathrm{I})\mathrm{T}}(t)] = 0$, introduce $J = \Gamma S R^{(\mathrm{I})-1}$ which ensures that $\overline{w}(t)$ and $v^{(\mathrm{I})}(t)$ are not correlated. Then, variance matrix of $\overline{w}(t)$ is yielded as $\overline{Q}_w = \Gamma(Q_w - SR^{(\mathrm{I})}S^{\mathrm{T}})\Gamma^{\mathrm{T}}$. From [18], we know that any nonzero matrix $H^{(\mathrm{I})}$ has full-rank decomposition:

$$H^{(\mathrm{I})} = FH^{(\mathrm{II})}, \tag{2.8}$$

where $F$ is a full column-rank matrix with the rank $r$, and $H^{(\mathrm{II})}$ is a full row-rank matrix with the rank $r$, then measurement model (2.4) can be represented as

$$y^{(\mathrm{I})}(t) = FH^{(\mathrm{II})}x(t) + v^{(\mathrm{I})}(t). \tag{2.9}$$

Given that $F$ is a full column-rank matrix, it follows that $F^{\mathrm{T}}R^{(\mathrm{I})}F$ is nonsingular. Then, the weighted least squares (WLS) [19] method is used and the Gauss-Markov estimate of $H^{(\mathrm{II})}x(t)$ is yielded as

$$y^{(\mathrm{II})}(t) = \left(F^{\mathrm{T}}R^{(\mathrm{I})-1}F\right)^{-1}F^{\mathrm{T}}R^{(\mathrm{I})-1}y^{(\mathrm{I})}(t), \tag{2.10}$$

substituting (2.9) into (2.10) yields

$$y^{(\mathrm{II})}(t) = H^{(\mathrm{II})}x(t) + v^{(\mathrm{II})}(t), \tag{2.11}$$

$$v^{(\mathrm{II})}(t) = \left(F^{\mathrm{T}}R^{(\mathrm{I})-1}F\right)^{-1}F^{\mathrm{T}}R^{(\mathrm{I})-1}v^{(\mathrm{I})}(t). \tag{2.12}$$

The variance matrix $R^{(\mathrm{II})} = \mathrm{E}[v^{(\mathrm{II})}(t)v^{(\mathrm{II})\mathrm{T}}(t)]$ of $v^{(\mathrm{II})}(t)$ is given by

$$R^{(\mathrm{II})} = \left(F^{\mathrm{T}}R^{(\mathrm{I})-1}F\right)^{-1}. \tag{2.13}$$

For systems (2.4) and (2.7), and (2.7) and (2.11), respectively, using standard Kalman filtering algorithm [20], we can obtain CMF and WMF Kalman estimators $\hat{x}^{(i)}(t \mid t+j)$, $i = \mathrm{I}$, II, $j = 0$, $j < 0$, and $j > 0$, and their error variance matrices $P^{(i)}(t \mid t+j)$. It is proved in [11] that the weighted measurement fusion steady-state Kalman filter $\hat{x}^{(\mathrm{II})}(t \mid t)$ for the weighted measurement fusion system (2.7) and (2.11) has the global optimality, that is, it is numerically identical to the CMF steady-state Kalman filter $\hat{x}^{(\mathrm{I})}(t \mid t)$ if they have the same initial values.

The above WMF method can obviously reduce the computational burden since the dimension of the measurement vector for the centralized measurement fusion is $m \times 1$, $m = m_1 + m_2 + \cdots + m_L$, while that for the weighted measurement fusion is $r \times 1$, and $m$ is much larger than $r$ generally.

### 2.2. Optimal Measurement Fusion Steady-State Kalman Filter

By the above WMF methods, the corresponding optimal steady-state Kalman filter is given as [21]

$$\begin{aligned}
\hat{x}^{(\mathrm{II})}(t+1 \mid t+1) &= \hat{x}^{(\mathrm{II})}(t+1 \mid t) + K_f^{(\mathrm{II})}\varepsilon^{(\mathrm{II})}(t+1),\\
\hat{x}^{(\mathrm{II})}(t+1 \mid t) &= \Psi_p^{(\mathrm{II})}\hat{x}^{(\mathrm{II})}(t \mid t-1) + \overline{K}_p^{(\mathrm{II})}y^{(\mathrm{II})}(t) + \overline{u}(t),\\
\hat{x}^{(\mathrm{II})}(t \mid t+N) &= \hat{x}^{(\mathrm{II})}(t \mid t) + \sum_{j=1}^{N} K^{(\mathrm{II})}(j)\varepsilon^{(\mathrm{II})}(t+j), \qquad N > 0,\\
\overline{u}(t) &= Bu(t) + Jy^{(\mathrm{I})}(t),\\
J &= \Gamma S R^{(\mathrm{I})-1},\\
\varepsilon^{(\mathrm{II})}(t) &= y^{(\mathrm{II})}(t) - H^{(\mathrm{II})}\hat{x}^{(\mathrm{II})}(t \mid t-1),\\
K_f^{(\mathrm{II})} &= \Sigma^{(\mathrm{II})}H^{(\mathrm{II})\mathrm{T}}\left(H^{(\mathrm{II})}\Sigma^{(\mathrm{II})}H^{(\mathrm{II})\mathrm{T}} + R^{(\mathrm{II})}\right)^{-1},\\
\overline{K}_p^{(\mathrm{II})} &= \overline{\Phi}\Sigma^{(\mathrm{II})}H^{(\mathrm{II})\mathrm{T}}\left(H^{(\mathrm{II})}\Sigma^{(\mathrm{II})}H^{(\mathrm{II})\mathrm{T}} + R^{(\mathrm{II})}\right)^{-1},\\
\Psi_p^{(\mathrm{II})} &= \overline{\Phi} - \overline{K}_p^{(\mathrm{II})}H^{(\mathrm{II})},\\
K^{(\mathrm{II})}(j) &= \Sigma^{(\mathrm{II})}\left(\left(I_n - K_f^{(\mathrm{II})}H^{(\mathrm{II})}\right)^{\mathrm{T}}\overline{\Phi}^{\mathrm{T}}\right)^{j}H^{(\mathrm{II})\mathrm{T}}\left(H^{(\mathrm{II})}\Sigma^{(\mathrm{II})}H^{(\mathrm{II})\mathrm{T}} + R^{(\mathrm{II})}\right)^{-1},\\
P^{(\mathrm{II})} &= \left[I_n - K_f^{(\mathrm{II})}H^{(\mathrm{II})}\right]\Sigma^{(\mathrm{II})},
\end{aligned} \tag{2.14}$$

where $\Psi_p^{(\mathrm{II})}$ is a stable matrix [19] and $\Sigma^{(\mathrm{II})}$ satisfies the following Riccati equation:

$$\Sigma^{(\mathrm{II})} = \overline{\Phi}\left[\Sigma^{(\mathrm{II})} - \Sigma^{(\mathrm{II})}H^{(\mathrm{II})\mathrm{T}}\left(H^{(\mathrm{II})}\Sigma^{(\mathrm{II})}H^{(\mathrm{II})\mathrm{T}} + R^{(\mathrm{II})}\right)^{-1}H^{(\mathrm{II})}\Sigma^{(\mathrm{II})}\right]\overline{\Phi}^{\mathrm{T}} + \overline{Q}_w. \tag{2.15}$$

When noise variance matrices $Q_w$, $S_i$, and $R_{ij}(i, j = 1, \ldots, L)$ are unknown, the problem is to find a self-tuning WMF Kalman filter $\hat{x}^{(\mathrm{II})s}(t \mid t)$ for the fused system (2.7) and (2.11). Then, the key to the problem is how to find the consistent estimates of the noise variance and cross-covariance matrices $Q_w$, $S_i$, and $R_{ij}$.

## 3. Online Estimators of Variances and Cross-Covariances

**Lemma 3.1** (matrix inverse Fadeeva formula [13]). *The matrix inverse formula is given by*

$$\left(I_n - q^{-1}\Phi\right)^{-1} = \frac{\mathrm{adj}\left(I_n - q^{-1}\Phi\right)}{\det\left(I_n - q^{-1}\Phi\right)} = \frac{\overline{F}\left(q^{-1}\right)}{\overline{A}\left(q^{-1}\right)}, \tag{3.1}$$

*where $\Phi$ is an $n \times n$ matrix, $q^{-1}$ is a backward shift operator, $I_n$ is an $n \times n$ unit matrix, and*

$$\overline{A}\left(q^{-1}\right) = 1 + \overline{a}_1 q^{-1} + \cdots + \overline{a}_n q^{-n}, \qquad \overline{F}\left(q^{-1}\right) = I_n + \overline{F}_1 q^{-1} + \cdots + \overline{F}_{n-1} q^{-(n-1)} \tag{3.2}$$

*then the coefficients $\overline{a}_i$ and $\overline{F}_i$ can be computed recursively as*

$$\begin{aligned} \overline{a}_i &= -\frac{1}{i}\operatorname{trace}\left(\Phi \overline{F}_{i-1}\right), \quad i = 1, \ldots, n, \\ \overline{F}_i &= \Phi \overline{F}_{i-1} + \overline{a}_i I_n, \quad i = 1, \ldots, n-1, \quad F_0 = I_n, \quad a_0 = 1. \end{aligned} \tag{3.3}$$

*Suppose the greatest common factor of $\overline{A}(q^{-1})$ and $\overline{F}(q^{-1})$ as scalar polynomial of $\mu(q^{-1})$, that is,*

$$\begin{aligned} \overline{F}\left(q^{-1}\right) &= \mu\left(q^{-1}\right) F\left(q^{-1}\right), \\ \overline{A}\left(q^{-1}\right) &= \mu\left(q^{-1}\right) A\left(q^{-1}\right). \end{aligned} \tag{3.4}$$

*Eliminate the greatest common factor $\mu(q^{-1})$ of numerator and denominator in* (3.1)*, we have the irreducible Fadeeva formula:*

$$\begin{aligned} \left(I_n - q^{-1}\Phi\right)^{-1} &= \frac{F(q^{-1})}{A(q^{-1})}, \\ F\left(q^{-1}\right) &= I_n + F_1 q^{-1} + \cdots + F_{n_f} q^{-n_f}, \\ A\left(q^{-1}\right) &= 1 + a_1 q^{-1} + \cdots + a_{n_a} q^{-n_a}, \quad a_{n_a} \neq 0,\ n_a \leq n - n_\mu, \\ F_i &= \Phi F_{i-1} + a_i I_n, \quad i = 1, \ldots, n_f,\ F_0 = I_n,\ n_f = n - n_\mu - 1. \end{aligned} \tag{3.5}$$

**Theorem 3.2.** *For the ith subsystem of systems* (2.1) *and* (2.2) *under the Assumptions of 2.1, 2.2, and 2.3, the innovation model of CARMA*

$$A_i\left(q^{-1}\right) y_i(t) = C_i\left(q^{-1}\right) u(t) + D_i\left(q^{-1}\right) \varepsilon_i(t) \tag{3.6}$$

*is stable. The innovation $\varepsilon_i(t) \in R^{m_i}$ is a white noise with zero mean and variance matrix $Q_{\varepsilon_i}$,*

$$\begin{aligned} C_i\left(q^{-1}\right) &= H_i F\left(q^{-1}\right) B q^{-1}, \\ B_i\left(q^{-1}\right) &= H_i F\left(q^{-1}\right) \Gamma q^{-1}, \end{aligned} \tag{3.7}$$

*where the polynomial matrices of $D_i(q^{-1})$, $A_i(q^{-1})$, $C_i(q^{-1})$, and $B_i(q^{-1})$ have the form as*

$$X_i\left(q^{-1}\right) = X_{i0} + X_{i1} q^{-1} + \cdots + X_{in_{xi}} q^{-n_{xi}}, \quad i = 1, 2, \ldots, L; \tag{3.8}$$

*with*

$$A_{i0} = I_{m_i}, \qquad D_{i0} = I_{m_i}, \qquad B_{i0} = 0, \tag{3.9}$$

*we have*

$$D_i\left(q^{-1}\right)\varepsilon_i(t) = B_i\left(q^{-1}\right)w(t) + A_i\left(q^{-1}\right)v_i(t). \tag{3.10}$$

*Proof.* From (2.1) and (2.2), we have

$$y_i(t) = H_i\left(I_n - q^{-1}\Phi\right)^{-1}q^{-1}[Bu(t) + \Gamma w(t)] + v_i(t). \tag{3.11}$$

Applying the extended Fadeeva formula of (3.5), we have

$$A_i\left(q^{-1}\right)y_i(t) = C_i\left(q^{-1}\right)u(t) + B_i\left(q^{-1}\right)w(t) + A_i\left(q^{-1}\right)v_i(t). \tag{3.12}$$

Suppose $(A_i(q^{-1})I_{m_i}, C_i(q^{-1}), B_i(q^{-1}))$ left-coprime, and $(B_i(q^{-1}), A_i(q^{-1})I_{m_i})$ or their greatest left factor's determinant has no zero point on the unit circles. Note that it needs to be left-coprime factorization if it is not left-coprime. Then, there is an MA process of $D_i(q^{-1})\varepsilon_i(t)$, which makes (3.10) hold and guarantees $D_i(q^{-1})$ stable. We have (3.6) from (3.10) and (3.12). The proof is completed. □

Define a new measurement process:

$$z_i(t) = A_i\left(q^{-1}\right)y_i(t) - C_i\left(q^{-1}\right)u(t). \tag{3.13}$$

From (3.6), we have

$$z_i(t) = D_i\left(q^{-1}\right)\varepsilon_i(t). \tag{3.14}$$

From (3.10), we have

$$z_i(t) = B_i\left(q^{-1}\right)w(t) + A_i\left(q^{-1}\right)v_i(t). \tag{3.15}$$

*Remark 3.3.* When the noise variances $Q_w$ and $R_i$ are known, the Gevers-Wouters [20] algorithm can be used to construct ARMA innovation model and obtain $D_i(q^{-1})$ and $Q_{\varepsilon_i}$.

In (3.14), $z_i(t)$ is a stationary stochastic process, whose correlated function $R_{z_{ij}}(k)$ has cut-off property, and suppose it be cut-off at $n_{z_{ij}}$, that is,

$$\begin{aligned} R_{z_{ij}}(k) &= \mathrm{E}\left[z_i(t)z_j^{\mathrm{T}}(t-k)\right], \quad k = 0, 1, \ldots, n_{z_{ij}}, \\ R_{z_{ij}}(k) &= 0, \quad k > n_{z_{ij}}, \quad i, j = 1, 2, \ldots, L. \end{aligned} \tag{3.16}$$

At the end of time $t$, the sampling estimation of the correlated function $R_{z_{ij}}(k)$ $(k = 0, 1, \ldots, n_{z_{ij}})$ based on measurements $(z_i(t), z_i(t-1), z_i(t-2), \ldots)$ can be defined as

$$\widehat{R}^t_{z_{ij}}(k) = \frac{1}{t}\sum_{\alpha=1}^{t} z_i(\alpha)z_j^{\mathrm{T}}(\alpha - k), \tag{3.17}$$

then we have its recursive form:

$$\widehat{R}^t_{z_{ij}}(k) = \widehat{R}^{t-1}_{z_{ij}}(k) + \frac{1}{t}\left[z_i(t)z_j^{\mathrm{T}}(t-k) - \widehat{R}^{t-1}_{z_{ij}}(k)\right], \quad t = 2, 3, \ldots, \tag{3.18}$$

with the initial value $\widehat{R}^1_{z_{ij}}(k) = z_i(1)z_j^{\mathrm{T}}(1-k)$.

Computing the correlated function on both sides of (3.14), we have

$$\begin{aligned} R_{z_{ij}}(k) = \sum_{u=k}^{n_0} B_{iu}Q_w B^{\mathrm{T}}_{j,u-k} + \sum_{u=k}^{n_0} A_{iu}S_i^{\mathrm{T}} B^{\mathrm{T}}_{j,u-k} + \sum_{u=k}^{n_0} B_{iu}S_j A^{\mathrm{T}}_{j,u-k} + \sum_{u=k}^{n_0} A_{iu}R_{ij}A^{\mathrm{T}}_{j,u-k}, \\ k = 0, 1, \ldots, n_{z_{ij}}, \quad i, j = 1, \ldots, L, \end{aligned} \tag{3.19}$$

where $n_0 = \max(n_{ai}, n_{bi}, n_{aj}, n_{bj})$. $A_{ij}$ and $B_{ij}$ are known, $B_{ij} = 0 (j > n_{bi})$, $A_{ij} = 0 (j > n_{ai})$.

However (3.19) is a matrix equations set. Substituting the sampling estimates at the time $t\widehat{R}^t_{z_{ij}}(k)$ $(k = 0, \ldots, n_{z_{ij}})$ into (3.19), and solving the matrix equations set, then we have the estimates $\widehat{S}_i(t)$, $\widehat{Q}_w(t)$, and $\widehat{R}_{ij}(t)$ at the time $t$.

From the ergodicity of the stationary stochastic process (3.14) and the Assumption 2.3, when $t \to \infty$, we have $\widehat{S}_i(t) \to S_i$, $\widehat{Q}_w(t) \to Q_w$ and $\widehat{R}_{ij}(t) \to R_{ij}$.

## 4. Self-Tuning WMF Kalman Filter

When the statistical features of the noise are unknown, the self-tuning weighted measurement fusion Kalman estimator can be obtained through the following three steps.

*Step 1.* For different sensor systems, (3.16)– (3.19) are used to identify online the estimates $\widehat{Q}_w(t)$, $\widehat{R}_{ij}(t)$, and $\widehat{S}_i(t)$, $i, j = 1, \ldots, L$, of noise variances of $Q_w$, $R_{ij}$, and $S_i$ at the time $t$, which

will yield the following available estimates at the time $t$:

$$\begin{aligned}
\widehat{S} &= \left[\widehat{S}_1, \ldots, \widehat{S}_L\right], \\
\widehat{R}^{(\mathrm{I})} &= \begin{bmatrix} \widehat{R}_{11} & \cdots & \widehat{R}_{1L} \\ \vdots & & \vdots \\ \widehat{R}_{L1} & \cdots & \widehat{R}_{LL} \end{bmatrix}, \\
\widehat{J} &= \Gamma \widehat{S} \widehat{R}^{(\mathrm{I})-1}, \\
\widehat{\overline{u}}(t) &= Bu(t) + \widehat{J} y^{(\mathrm{I})}(t), \\
\widehat{Q} &= \widehat{Q}_w - \widehat{S} \widehat{R}^{(\mathrm{I})-1} \widehat{S}^{\mathrm{T}}, \quad \widehat{\overline{Q}}_w = \Gamma \widehat{Q} \Gamma^{\mathrm{T}}, \\
\widehat{y}^{(\mathrm{II})}(t) &= \widehat{\Omega} y^{(\mathrm{I})}(t), \\
\widehat{\Omega} &= \left(F^{\mathrm{T}} \widehat{R}^{(\mathrm{I})-1} F\right)^{-1} F^{\mathrm{T}} \widehat{R}^{(\mathrm{I})-1}, \\
\widehat{R}^{(\mathrm{II})} &= \left(F^{\mathrm{T}} \widehat{R}^{(\mathrm{I})-1} F\right)^{-1}, \\
\widehat{\overline{\Phi}} &= \Phi - \widehat{J} H^{(\mathrm{I})}.
\end{aligned} \tag{4.1}$$

*Step 2.* From (2.15), solving the following Riccati equation, we get the estimation value $\widehat{\Sigma}^{(\mathrm{II})}$ of $\Sigma^{(\mathrm{II})}$ at the time $t$:

$$\widehat{\Sigma}^{(\mathrm{II})} = \widehat{\overline{\Phi}} \left[\widehat{\Sigma}^{(\mathrm{II})} - \widehat{\Sigma}^{(\mathrm{II})} H^{(\mathrm{II})\mathrm{T}} \left(H^{(\mathrm{II})} \widehat{\Sigma}^{(\mathrm{II})} H^{(\mathrm{II})\mathrm{T}} + \widehat{R}^{(\mathrm{II})}\right)^{-1} H^{(\mathrm{II})} \widehat{\Sigma}^{(\mathrm{II})}\right] \widehat{\overline{\Phi}}^{\mathrm{T}} + \widehat{\overline{Q}}_w. \tag{4.2}$$

*Step 3.* Equations (2.14) are applied, and the self-tuning weighted measurement fusion state estimator is given by

$$\begin{aligned}
\widehat{x}^{(\mathrm{II})s}(t+1 \mid t+1) &= \widehat{x}^{(\mathrm{II})s}(t+1 \mid t) + \widehat{K}_f^{(\mathrm{II})} \widehat{\varepsilon}^{(\mathrm{II})}(t+1), \\
\widehat{x}^{(\mathrm{II})s}(t+1 \mid t) &= \widehat{\Psi}_p^{(\mathrm{II})} \widehat{x}^{(\mathrm{II})s}(t \mid t-1) + \widehat{\overline{K}}_p^{(\mathrm{II})} \widehat{y}^{(\mathrm{II})}(t) + \widehat{\overline{u}}(t), \\
\widehat{x}^{(\mathrm{II})s}(t \mid t+N) &= \widehat{x}^{(\mathrm{II})s}(t \mid t) + \sum_{j=1}^{N} \widehat{K}^{(\mathrm{II})}(j) \widehat{\varepsilon}^{(\mathrm{II})}(t+j), \quad N > 0, \\
\widehat{\varepsilon}^{(\mathrm{II})}(t) &= \widehat{y}^{(\mathrm{II})}(t) - H^{(\mathrm{II})} \widehat{x}^{(\mathrm{II})s}(t \mid t-1), \\
\widehat{K}_f^{(\mathrm{II})} &= \widehat{\Sigma}^{(\mathrm{II})} H^{(\mathrm{II})\mathrm{T}} \left(H^{(\mathrm{II})} \widehat{\Sigma}^{(\mathrm{II})} H^{(\mathrm{II})\mathrm{T}} + \widehat{R}^{(\mathrm{II})}\right)^{-1}, \\
\widehat{\overline{K}}_p^{(\mathrm{II})} &= \widehat{\overline{\Phi}} \widehat{\Sigma}^{(\mathrm{II})} H^{(\mathrm{II})\mathrm{T}} \left(H^{(\mathrm{II})} \widehat{\Sigma}^{(\mathrm{II})} H^{(\mathrm{II})\mathrm{T}} + \widehat{R}^{(\mathrm{II})}\right)^{-1}, \\
\widehat{\Psi}_p^{(\mathrm{II})} &= \widehat{\overline{\Phi}} - \widehat{\overline{K}}_p^{(\mathrm{II})} H^{(\mathrm{II})}, \\
\widehat{K}^{(\mathrm{II})}(j) &= \widehat{\Sigma}^{\mathrm{II}} \left(\left(I_n - \widehat{K}_f^{(\mathrm{II})} H^{(\mathrm{II})}\right)^{\mathrm{T}} \widehat{\overline{\Phi}}^{\mathrm{T}}\right)^{j} H^{(\mathrm{II})\mathrm{T}} \left(H^{(\mathrm{II})} \widehat{\Sigma}^{(\mathrm{II})} H^{(\mathrm{II})\mathrm{T}} + \widehat{R}^{(\mathrm{II})}\right)^{-1}, \\
\widehat{P}^{(\mathrm{II})} &= \left[I_n - \widehat{K}_f^{(\mathrm{II})} H^{(\mathrm{II})}\right] \widehat{\Sigma}^{(\mathrm{II})}.
\end{aligned} \tag{4.3}$$

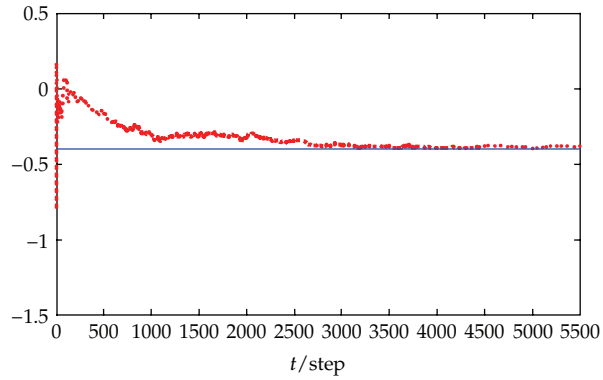


**Figure 1:** $\rho_1$ and the convergence of estimation value $\widehat{\rho}_1(t)$.

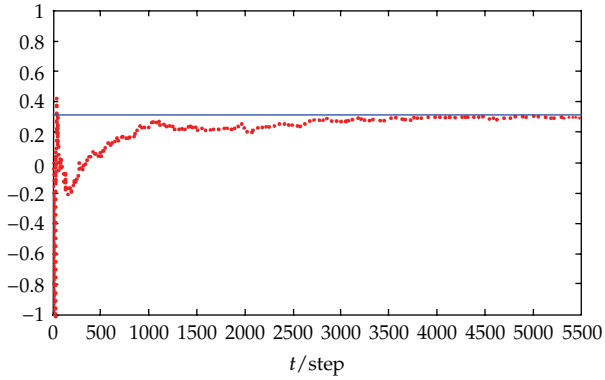


**Figure 2:** $d_{11}$ and the convergence of estimation value $\widehat{d}_{11}(t)$.

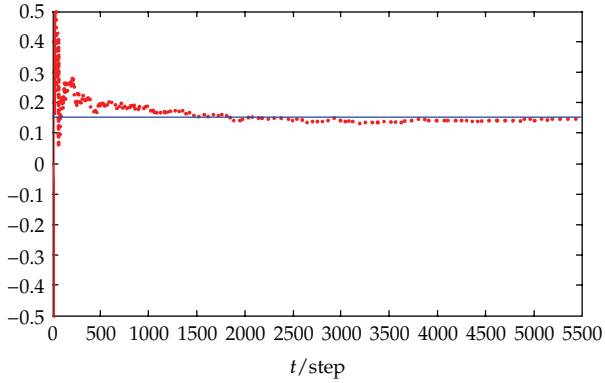


**Figure 3:** $d_{12}$ and the convergence of estimation value $\widehat{d}_{12}(t)$.

*Remark 4.1.* At every moment, the iteration method to solve Riccati equation (4.2) causes comparatively large computation burden, which is not convenient for the real applications. To reduce the computational burden, a computing period (dead band) $T_d$ of (4.2) is set and the estimation value $\widehat{\Sigma}^{(\mathrm{II})}$ keeps invariant in the period $T_d$. So, $\widehat{\Sigma}^{(\mathrm{II})}$ is only computed at the moments of $t = T_d, 2T_d, 3T_d, \ldots$, which can reduce computation burden, and can be called Riccati equation with a dead band [9, 17].

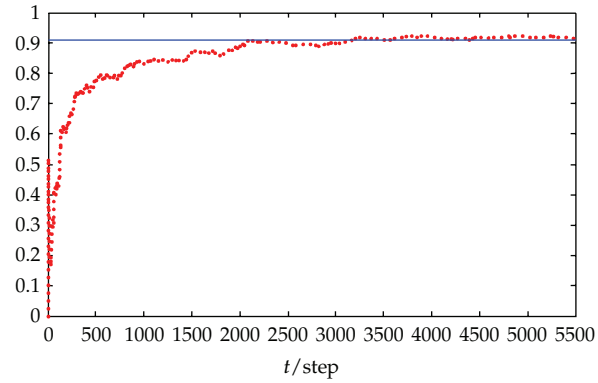


**Figure 4:** $Q_{\varepsilon_1}$ and the convergence of estimation value $\widehat{Q}_{\varepsilon_1}(t)$.

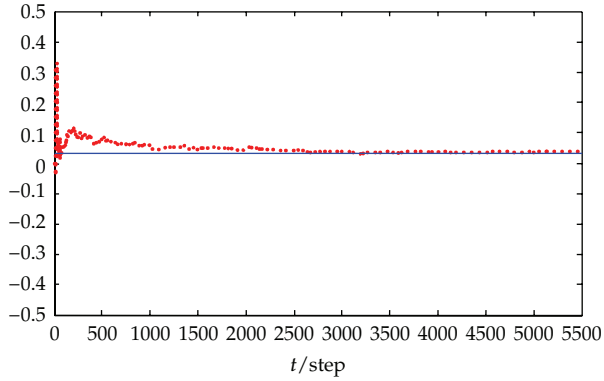


**Figure 5:** $Q_{\xi_1}$ and the convergence of estimation value $\widehat{Q}_{\xi_1}(t)$.

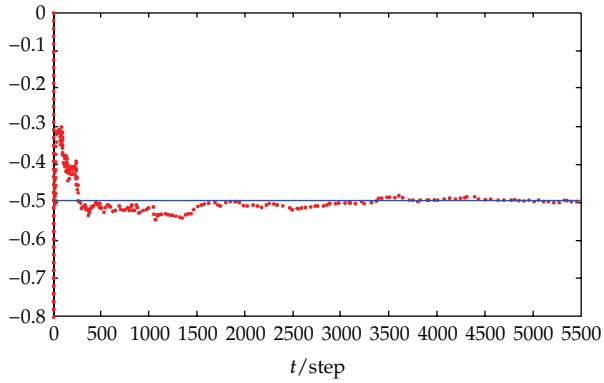


**Figure 6:** $\rho_2$ and the convergence of estimation value $\widehat{\rho}_2(t)$.

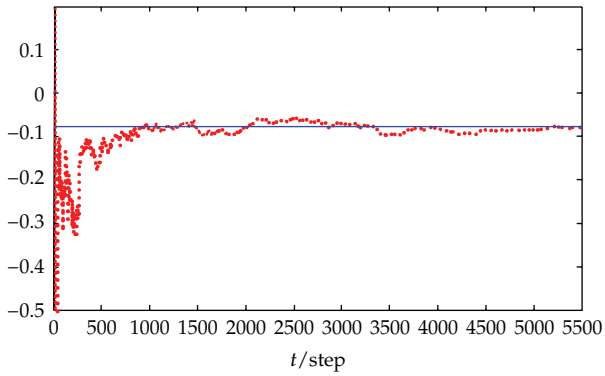


**Figure 7:** $d_{21}$ and the convergence of estimation value $\hat{d}_{21}(t)$.

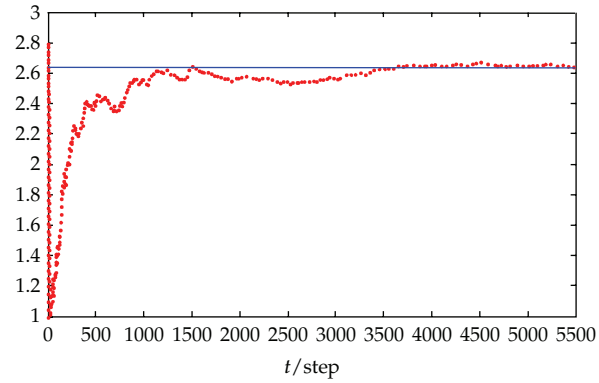


**Figure 8:** $Q_{\varepsilon_2}$ and the convergence of estimation value $\widehat{Q}_{\varepsilon_2}(t)$.

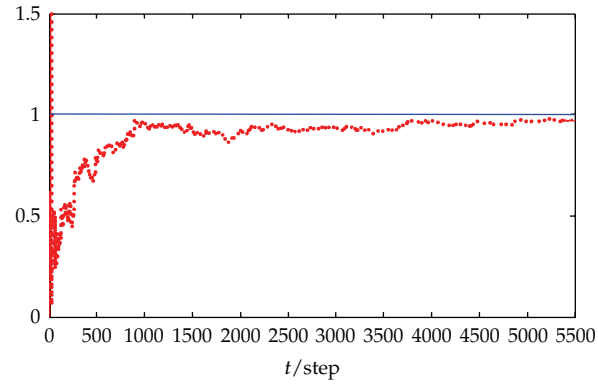


**Figure 9:** $Q_w$ and the convergence of estimation value $\widehat{Q}_w(t)$.

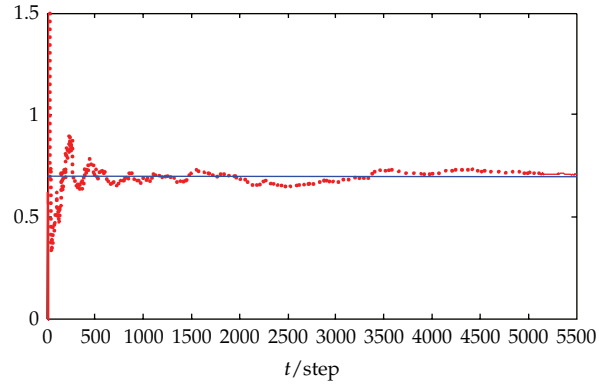


**Figure 10:** $Q_{\xi_2}$ and the convergence of estimation value $\widehat{Q}_{\xi_2}(t)$.

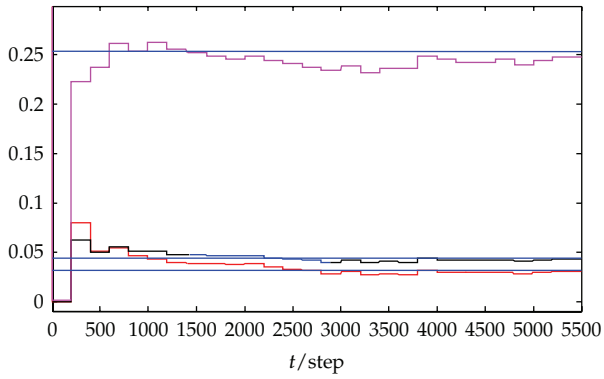


**Figure 11:** $\sum^{(\mathrm{II})}$ and the convergence of estimation value $\widehat{\sum}^{(\mathrm{II})}(t)$.

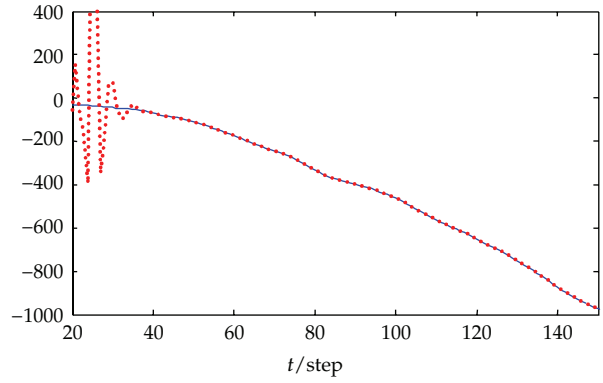


**Figure 12:** Positon $x_1$ and self-tuning WMF Kalman filter $\hat{x}_1^{(\mathrm{II})s}(t \mid t)$.

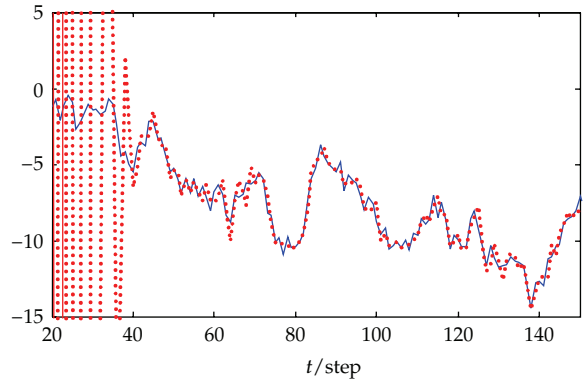


**Figure 13:** Speed $x_2$ and self-tuning WMF Kalman filter $\hat{x}_2^{(\mathrm{II})s}(t \mid t)$.

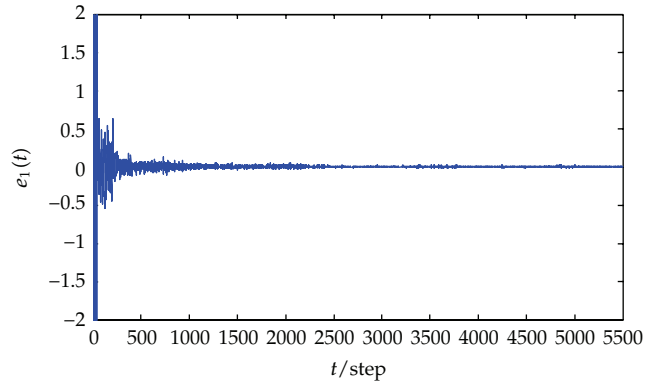


**Figure 14:** The curve of position errors $e_1(t) = \hat{x}_1^{(\mathrm{II})}(t \mid t) - \hat{x}_1^{(\mathrm{II})s}(t \mid t)$ for optimal and self-tuning WMF Kalman filter.

## 5. Simulation Example

The self-tuning $\alpha - \beta$ radar track system with colored measurement noise:

$$\begin{aligned} x(t+1) &= \begin{bmatrix} 1 & T_0 \\ 0 & 1 \end{bmatrix} x(t) + \begin{bmatrix} 0.5T_0^2 \\ T_0 \end{bmatrix} w(t), \\ y_i(t) &= H_{0i}x(t) + v_i(t), \qquad i = 1, 2, \\ v_i(t+1) &= \rho_i v(t) + \xi_i(t), \end{aligned} \tag{5.1}$$

where $w(t)$ and $\xi_i(t)$, $i = 1, 2$, are independent Gaussian white noises with zero means and variances of $Q_w = 1$, $Q_{\xi_1} = 0.04$, and $Q_{\xi_2} = 0.7$, $v_i(t)$ is colored measurement noise, $H_{01} = [1 \quad 0]$ and $H_{02} = [0 \quad 1]$. $T_0 = 1$ is the sampling period, $x(t) = [x_1(t) \; x_2(t)]^{\mathrm{T}}$, $x_1(t)$ and $x_2(t)$, are, respectively, the position and speed of the moving object at $tT_0$, $\rho_1 = -0.4$, $\rho_2 = -0.5$.

When $\rho_i$, $Q_w$ and $Q_{\xi_i}(i = 1, 2)$ are unknown, the problem is to find the self-tuning WMF $\alpha - \beta$ tracking filter $\hat{x}^{(\mathrm{II})s}(t \mid t)$.

The parameter convergence results of subsystem 1 are shown in Figures 1, 2, 3, 4, and 5, and the parameter convergence results of subsystem 2 are shown in Figures 6, 7, 8, 9, and 10,

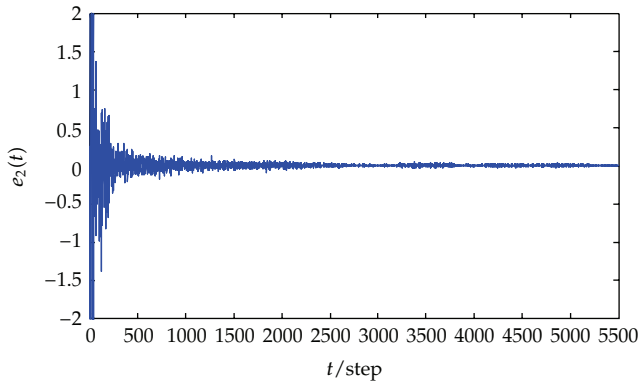


**Figure 15:** The curve of velocity errors $e_2(t) = \hat{x}_2^{(\mathrm{II})}(t \mid t) - \hat{x}_2^{(\mathrm{II})s}(t \mid t)$ for optimal and self-tuning WMF Kalman filter.

where the curved lines denote the estimates and the straight lines denote true values. The self-tuning WMF Kalman filter $\hat{x}^{(\mathrm{II})s}(t \mid t)$ is shown in Figures 11, 12, 13, 14, and 15, where Figure 11 is the convergence of $\widehat{\Sigma}^{(\mathrm{II})}$. Using the iteration algorithm with dead band $T_d = 200$, we can see that the parameter estimates in $\widehat{\Sigma}^{(\mathrm{II})}$ shown in ladder-shape curves converge to the corresponding real values.

The object-tracking curves of self-tuning WMF Kalman filter is shown in Figures 12, 13, 14, and 15. We can see that the system can gradually track the position and speed of the objects as the time increases, where the real lines are real values and the dashed lines are estimates. The error curves between the optimal and self-tuning WMF Kalman filter is shown in Figures 14 and 15. We see that the error curves take on the funnel shape, which demonstrates that the self-tuning filter has better convergence.

## 6. Conclusion

For multisensor linear discrete time-invariant stochastic control system with different measurement matrices and correlated noise, an online identification method is designed when the input noise and measurement noise variance are unknown. It firstly uses Fadeeva formula to construct ARMA innovation model with unknown noise covariance matrices, and then uses the ergodicity of sampling-correlated function in the stationary and inverse ARMA innovation model to identify the noise covariance matrices. Further, a self-tuning WMF Kalman filter has been presented from a steady-state global optimal measurement fusion Kalman filter by matrix full-rank decompostion, weighted least squares method, and measurement feedback. It has asymptotic global optimality. Compared to the centralized fusion algorithm, it can reduce the computational burden.

## Acknowledgments

This work is supported by National Natural Science Foundation of China under Grant NSFC 61174139, Key Project of Chinese Ministry of Education under Grant 209038, Key Laboratory of Electronics Engineering, College of Heilongjiang Province under Grant DZZD 20100038,

Science and Technology Research Foundation of Heilongjiang Province Education Department under Grant 12521420, Open Laboratory Project of Heilongjiang University in China 2012, and High Level Talents Support Project of Heilongjiang University in China under Grant Hdtd2010-03.

## References

[1] Y. B. Shalom, "On the track-to-track correlation problem," *IEEE Transactions on Automatic Control*, vol. 26, no. 2, pp. 571–572, 1981.
[2] Y. B. Shalom and X.-R. Li, *Multigarget-Multisensor Tracking: Principles and Techniques*, Yaakov Bar-Shalom Publishing, Storrs, Conn, USA, 1995.
[3] N. A. Carlson, "Federated square root filter for decentralized parallel processes," *IEEE Transactions on Aerospace and Electronic Systems*, vol. 26, pp. 517–525, 1990.
[4] K. H. Kim, "Development of track to track fusion algotithm," in *Proceeding of the American Control Conference*, pp. 1037–1041, Baltimore, Md, USA, 1994.
[5] X. R. Li, Y. Zhu, J. Wang, and C. Han, "Optimal linear estimation fusion—part I: unified fusion rules," *IEEE Transactions on Information Theory*, vol. 49, no. 9, pp. 2192–2323, 2003.
[6] S.-L. Sun and Z.-L. Deng, "Multi-sensor optimal information fusion Kalman filter," *Automatica*, vol. 40, no. 6, pp. 1017–1023, 2004.
[7] S.-L. Sun, "Multi-sensor information fusion white noise filter weighted by scalars based on Kalman predictor," *Automatica*, vol. 40, no. 8, pp. 1447–1453, 2004.
[8] Q. Gan and J. H. Chris, "Comparison of two measurement fusion methods for Kalman filter based multisensor data fusion," *IEEE Transactions on Aerospace and Electronic Systems*, vol. 37, no. 1, pp. 273–279, 2001.
[9] Y. Gao, W. J. Jia, X. J. Sun, and Z. L. Deng, "Self-tuning multisensor weighted measurement fusion kalman filter," *IEEE Transactions on Aerospace and Electronic Systems*, vol. 45, no. 1, pp. 179–191, 2009.
[10] X. Wang, Q. D. Zhu, and Y. B. Wu, "A measurement fusion fault-tolerating PID control for time-delay system with colored noise disturbance," *Key Engineering Materials*, vol. 419-420, pp. 589–592, 2010.
[11] X. Wang, Q. D. Zhu, and S. L. Sun, "Weighted measurement fusion estimation algorithm with correlated noises and its global optimality," *Systems Engineering and Electronics*, vol. 32, no. 10, pp. 2057–2061, 2010.
[12] X. Wang, Q.-D. Zhu, and S.-L. Sun, "Universal weighted measurement fusion estimation algorithm and its global optimality," *Computer Engineering and Applications*, vol. 46, no. 24, pp. 22–25, 2010.
[13] Z.-L. Deng, *Self-Tuning Filtering Theory with Application*, Harbin institute of Technology Press, Harbin, China, 2003.
[14] S. Sun, "Optimal and self-tuning information fusion Kalman multi-step predictor," *IEEE Transactions on Aerospace and Electronic Systems*, vol. 43, no. 2, pp. 418–427, 2007.
[15] Z.-L. Deng, Y. Gao, C.-B. Li, and G. Hao, "Self-tuning decoupled information fusion Wiener state component filters and their convergence," *Automatica*, vol. 44, no. 3, pp. 685–695, 2008.
[16] Y. Gao, C.-J. Ran, and Z.-L. Deng, "Weighted measurement fusion Kalman filter with correlated measurement noises and its global optimality," in *Proceedings of the International Colloquium on Information Fusion*, pp. 228–234, 2007.
[17] C. J. Ran and L. Z. Deng, "Self-tuning weighted measurement fusion Kalman filtering algorithm," *Computational Statistics and Data Analysis*, vol. 56, pp. 2112–2128, 2012.
[18] R. A. Horn and C. R. Johnson, *Matrix Analysis*, Cambridge University Press, Cambridge, 1985.
[19] T. A. Kailath, H. Sayed, and B. Hassibi, *Linear Estimation*, Prentice-Hall, Upper Saddle River, NJ, USA, 2000.
[20] Z.-L. Deng and X. Wang, *Modeling and Estimation*, Science Press, Beijing, China, 2007.
[21] Z.-L. Deng, *Information Fusion Filtering Theory with Applications*, Harbin institute of Technology Press, Harbin, China, 2007.

Hindawi Publishing Corporation
Journal of Applied Mathematics
Volume 2012, Article ID 548341, 8 pages
doi:10.1155/2012/548341

*Research Article*

# Optimization of Spoken Term Detection System

**Chuanxu Wang[1] and Pengyuan Zhang[2]**

[1] *Institute of Informatics, Qingdao University of Science and Technology, Qingdao 266061, China*
[2] *Thinkit Speech Laboratory, Institute of Acoustics, Chinese Academy of Sciences, Beijing 100190, China*

Correspondence should be addressed to Chuanxu Wang, wangchuanxu_qd@163.com

Received 31 December 2011; Accepted 24 January 2012

Academic Editor: Baocang Ding



Generally speaking, spoken term detection system will degrade significantly because of mismatch between acoustic model and spontaneous speech. This paper presents an improved spoken term detection strategy, which integrated with a novel phoneme confusion matrix and an improved word-level minimum classification error (MCE) training method. The first technique is presented to improve spoken term detection rate while the second one is adopted to reject false accepts. On mandarin conversational telephone speech (CTS), the proposed methods reduce the equal error rate (EER) by 8.4% in relative.

## 1. Introduction

In recent years, there is an increasing trend towards the use of spoken term detection systems for real-world applications. In such systems, it is desirable to achieve the highest possible spoken term detection rate, while minimizing the number of false spoken term insertions. Unfortunately, most speech recognition systems fail to perform well when speakers have a regional accent. Particulary in China, the diversity of Mandarin accents is great and evolving.

Pronunciation variation has become an important topic. Normally, a confusion matrix is adopted to achieve higher recognition rate in speech recognition system. In [1], confusion matrix is adopted in spoken document retrieval system. Retrieval performance is improved by exploiting phoneme confusion probabilities. The work in [2] introduces an accent adaptation approach in which syllable confusion matrix is adopted. Similar approaches are discussed in [3].

The quality of confusion matrix has an obvious influence on the performance of spoken term detection. Based on traditional approaches, we propose an improved method to generate a phoneme confusion matrix.

MCE is one of the main approaches in discriminative training [4]. In [5], MCE is used to optimize the parameters of confidence function in large vocabulary speech recognition

system (LVCSR). The work in[6] introduces MCE into spoken term detection. In this paper, we present an improved MCE training method for calculating spoken term confidence.

The remainder of the paper is structured as follows: Section 2 introduces our baseline system. In Section 3, we discuss the phoneme confusion matrix based on confusion network. An improved MCE training method is presented in Section 4. In Section 5, the experiments are given and discussed, and finally Section 6 draws some conclusions from the proposed research.

## 2. Baseline System

In our baseline system, search space is generated based on all Chinese syllables, not specifically for spoken terms. Phoneme recognition is performed without any lexical constraints. Given a spoken input, our decoder outputs 1-best phoneme sequence. A phoneme confusion matrix is used to extract spoken terms.

The main steps of generating phoneme confusion matrix are listed as follows [2].

(1) Canonical pin-yin level transcriptions of the accent speech data should be obtained firstly.

(2) A standard Mandarin acoustic recognizer whose output is pin-yin stream is used to transcribe those accent speech data.

(3) With the help of dynamic programming (DP) technique, these pin-yin level transcriptions are aligned to the canonical pin-yin level transcriptions.

(4) Regardless of insertion and deletion errors, substitution errors are considered. Each pin-yin can be divided into two phonemes. Given a canonical phoneme $\mathrm{ph}_m$ and an aligning hypothesis $\mathrm{ph}_n$, we can compute confusion probability:

$$P(\mathrm{ph}_n \mid \mathrm{ph}_m) = \frac{\mathrm{count}(\mathrm{ph}_n \mid \mathrm{ph}_m)}{\sum_{i=1}^{N} \mathrm{count}(\mathrm{ph}_i \mid \mathrm{ph}_m)}, \tag{2.1}$$

where $\mathrm{count}(\mathrm{ph}_n \mid \mathrm{ph}_m)$ is the number of $\mathrm{ph}_n$ which is aligned to $\mathrm{ph}_m$. $N$ is the total phoneme number in dictionary.

With 1-best phoneme sequence and confusion matrix, similarities between phonemes are computed. For each spoken term, corresponding phonemes will be searched from pronunciation dictionary firstly. Then, sliding window is used to align phonemes of spoken term and 1-best phoneme sequence. The step of sliding window is set to two because there are two phonemes in each syllable in Chinese. An example of searching "gu zhe" is given in Figure 1.

Given a term $\varphi_1$, $\varphi_2$ is the aligning 1-best phoneme sequence. Then, similarity between them is denoted as $\mathrm{Sim}(\varphi_1, \varphi_2)$:

$$\mathrm{Sim}(\varphi_1, \varphi_2) = \frac{1}{N} \log\left( \prod_{i=1}^{N} P(\beta_i \mid \alpha_i) \right), \tag{2.2}$$

where $\alpha_i$ and $\beta_i$ are the $i_{\mathrm{th}}$ phoneme of $\varphi_1$ and $\varphi_2$, respectively, $N$ is the number of phonemes of $\varphi_1$.

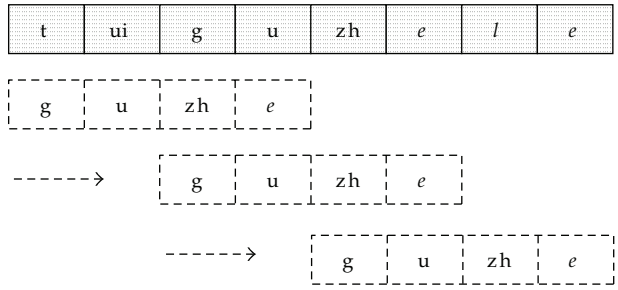


**Figure 1:** Extraction of "gu zhe."

Spoken term rate gets a significant improvement with the help of confusion matrix. But at the same time, false accepts have been increased too. Effective confidence measure should be adopted to reject false hypotheses. In this paper, word confidence is calculated with catch-all model [5]. A confidence score for a hypothesized phoneme $\mathrm{ph}_i$ is estimated by

$$\mathrm{CM}(\mathrm{ph}_i) = \frac{1}{e[i]-b[i]+1}\sum_{n=b[i]}^{e[i]} \log p\left(q^{(n)}\middle| o^{(n)}\right) = \frac{1}{e[i]-b[i]+1}\sum_{n=b[i]}^{e[i]} \log \frac{P\left(o^{(n)}\middle| q^{(n)}\right)P\left(q^{(n)}\right)}{P\left(o^{(n)}\right)}, \tag{2.3}$$

where $b[i]$ is the start time of $\mathrm{ph}_i$ and $e[i]$ is the end time. $q^{(n)}$ represents Viterbi state sequence.

Deriving word level scores from phoneme scores is a natural extension of the recognition process. We adopted the arithmetic mean in logarithmic scale. Spoken term confidence $\mathrm{CM}_{\mathrm{pos}}$ is defined as

$$\mathrm{CM}_{\mathrm{pos}}(w) = \frac{1}{m}\sum_{i=1}^{m}\mathrm{CM}(\mathrm{ph}_i), \tag{2.4}$$

where $m$ is the number of phonemes in $w$.

## 3. Confusion Matrix Based on Confusion Network

Just as the above description, confusion matrix is generated from 1-best hypothesis. However, there is a conceptual mismatch between decoding criterion and confusion probability evaluation. Given an input utterance, a Viterbi decoder is used to find the best sentence. But it does not ensure that each phoneme is the optimal one. In this paper, we propose an improved method of generating confusion matrix. Instead of 1-best phoneme hypothesis, we get hypotheses from confusion network (CN) [7].

Just as Figure 2 describes, CN is composed of several branches. For schematic description, we give top 4 hypotheses in each branch. Corresponding canonical pin-yin stream is also presented in Figure 2.

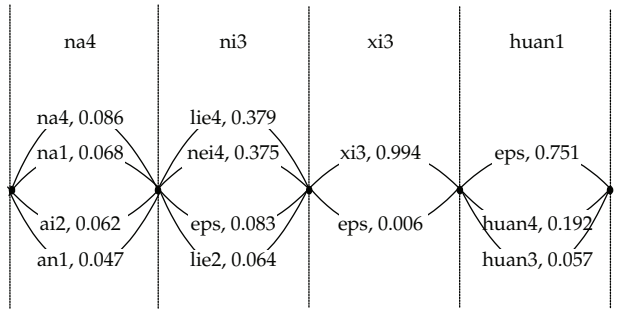


**Figure 2:** An example of confusion network.

Experimental show that syllable error rate (SER) of CN is far lower than that of 1-best sequence. Base on this point, we believe that CN provides us more useful information. In this paper, we attempt to use n-best hypotheses of each branch. Firstly, canonical pin-yin level transcriptions are formatted into a simple CN. Then, recognizer output voting error reduction (ROVER) technology is adopted to align two CNs. At last, we select special branches to generate confusion matrix. Given a canonical phoneme $\mathrm{ph}_m$, only branches including $\mathrm{ph}_m$ are considered. A sequence of class labels $\alpha(k)$ is defined as

$$\alpha(k) = \begin{cases} 1 & \text{if } \mathrm{ph}_m \in \text{the } k\text{th Branch}, \\ 0 & \text{if } \mathrm{ph}_m \notin \text{the } k\text{th Branch}. \end{cases} \tag{3.1}$$

Then, (2.1) can be rewritten as

$$P(\mathrm{ph}_n \mid \mathrm{ph}_m) = \frac{\sum_{k=1}^{C} \alpha(k)\mathrm{count}(\mathrm{ph}_n \mid \mathrm{ph}_m)}{\sum_{i=1}^{N}\sum_{k=1}^{C} \alpha(k)\mathrm{count}(\mathrm{ph}_i \mid \mathrm{ph}_m)}, \tag{3.2}$$

where $C$ is the number of branches in CNs of training data, $N$ is the number of phonemes in dictionary.

Another optional method is also attempted in this paper. Max probability rule can be applied in calculating confusion probability. The branches with maximum probability $\mathrm{ph}_m$ are considered. We define

$$\beta(k) = \begin{cases} 1 & \text{if } \mathrm{ph}_m \text{ is a phoneme with maximum probability in the } k\text{th Branch}, \\ 0 & \text{others.} \end{cases} \tag{3.3}$$

Then, (3.2) can be rewritten as

$$(\mathrm{ph}_n \mid \mathrm{ph}_m) = \frac{\sum_{k=1}^{C} \beta(k)\mathrm{count}(\mathrm{ph}_n \mid \mathrm{ph}_m)}{\sum_{i=1}^{N}\sum_{k=1}^{C} \beta(k)\mathrm{count}(\mathrm{ph}_i \mid \mathrm{ph}_m)}. \tag{3.4}$$

## 4. MCE with Block Training

The work in [5] proposed a word-level MCE training technique in optimizing the parameters of the confidence function. In [6], a revised scheme is implemented under spoken term scenario. In this paper, we attempt to improve the MCE training methods proposed in [6].

According to the update equations in [6], sequential training is used to update parameters. That is to say, the parameters of triphones are modified with each training sample. It is not matched well with optimization method of MCE. We adopt block training method instead. The parameters are modified with all averaged samples at once. The weighted mean confidence measure of $W$ is defined as

$$\mathrm{CM}(W) = \frac{1}{N_w}\sum_{i=1}^{N_w}\left(a_{\mathrm{ph}_i}\mathrm{CM}\left(\mathrm{ph}_i\right) + b_{\mathrm{ph}_i}\right). \tag{4.1}$$

Procedures of block training are listed as follows.

(1) Misclassification measure is defined as

$$d(W) = \left(\mathrm{CM}(W) - C\right) \times \mathrm{Sign}(W), \tag{4.2}$$

where $C$ is confidence threshold, $\mathrm{Sign}(W)$ is defined as

$$\mathrm{Sign}(W) = \begin{cases} 1 & \text{if } W \text{ is incorrect,} \\ -1 & \text{if } W \text{ is correct.} \end{cases} \tag{4.3}$$

(2) A smooth zero-one loss function is given by

$$l(W) = \frac{1}{1 + \exp\left(-\gamma d(W)\right)}. \tag{4.4}$$

(3) The parameter estimation is based on the minimization of the expected loss which, for a training sample of size $M$, is defined as

$$l\left(\overline{W}\right) = E(l(W)) = \frac{1}{M}\sum_{j=1}^{M} l(W_j). \tag{4.5}$$

Generalized probabilistic descent (GPD) algorithm is used to minimize the loss function $l(\overline{W})$ [8]:

$$\frac{\partial l\left(\overline{W}\right)}{\partial a_{\mathrm{ph}_i}} = \frac{1}{M}\sum_{j=1}^{M}\frac{\partial l(W_j)}{\partial a_{\mathrm{ph}_i}} = \frac{\gamma}{M_{\mathrm{ph}_i}}\sum_{j=1}^{M_{\mathrm{ph}_i}}\frac{1}{N_j}K(W_j)\mathrm{CM}_j(\mathrm{ph}_i),$$

$$\frac{\partial l\left(\overline{W}\right)}{\partial b_{\mathrm{ph}_i}} = \frac{1}{M}\sum_{j=1}^{M}\frac{\partial l(W_j)}{\partial b_{\mathrm{ph}_i}} = \frac{\gamma}{M_{\mathrm{ph}_i}}\sum_{j=1}^{M_{\mathrm{ph}_i}}\frac{K(W_j)}{N_j}, \tag{4.6}$$

$$\frac{\partial l\left(\overline{W}\right)}{\partial C} = \frac{1}{M}\sum_{j=1}^{M}\frac{\partial l(W_j)}{\partial C} = \frac{-\gamma}{M}\sum_{j=1}^{M}K(W_j),$$

where $M_{\mathrm{ph}_i}$ is the number of samples that contain the phoneme $\mathrm{ph}_i$, $N_j$ is the number of phonemes of $W_j$, $\mathrm{CM}_j(\mathrm{ph}_i)$ is the confidence of $\mathrm{ph}_i$ in $W_j$. However $k(W_j)$ is defined as

$$k(W_j) = l(W_j)(1 - l(W_j))\mathrm{Sign}(W_j). \tag{4.7}$$

At last, we get the revised update equations as

$$\widetilde{a}_{\mathrm{ph}_i}(n+1) = \widetilde{a}_{\mathrm{ph}_i}(n) - \varepsilon_n\frac{\partial l\left(\overline{W}\right)}{\partial a_{\mathrm{ph}_i}}\exp\left(\widetilde{a}_{\mathrm{ph}_i}(n)\right),$$

$$b_{\mathrm{ph}_i}(n+1) = b_{\mathrm{ph}_i}(n) - \varepsilon_n\frac{\partial l\left(\overline{W}\right)}{\partial b_{\mathrm{ph}_i}}, \tag{4.8}$$

$$C(n+1) = C(n) - \varepsilon_n\frac{\partial l\left(\overline{W}\right)}{\partial C}.$$

## 5. Experiments

We conducted experiments using our real-time spoken term system. Acoustic model is trained using train04, which is collected by Hong Kong University of Science and Technology (HKUST).

### 5.1. Experimental Data Description

The test data is a subset of development data (dev04), which is also collected by HKUST. Total 20 conversations are used for our evaluation. 100 words are selected as the spoken term list, including 75 two-syllable words and 25 three-syllable words.

Confusion matrixes adopted in this paper are generated using 100-hour mandarin CTS corpus. The word-level MCE training set is a subset of train04 corpus. 865667 terms are extracted for the training, including 675998 false accepts and 189669 correct hits.

**Table 1:** SER of CN and 1-best pin-yin sequence.

| | SER | Pruning beam |
|---|---|---|
| 1-best pin-yin | 75.0% | — |
| CN | 71.0% | 0.5 |
| CN | 51.9% | 0.2 |
| CN | 35.3% | 0 |

**Table 2:** Recognition rates of different phoneme confusion matrixes.

| Confusion matrix | Recognition rates |
|---|---|
| 1-best recognition result | 77.3% |
| CN | 80.9% |
| CN + maximum probability | 82.0% |

### *5.2. Experiment Results*

The detection error tradeoff (DET) is used in this paper to evaluate the performance of spoken term. The false acceptation (FA) rate fits the case in which an incorrect word is accepted, and the false reject (FR) fits the case of rejecting the correct word:

$$\begin{aligned} \text{FA} &= \frac{\text{num. of incorrect words labelled as accepted}}{\text{num. of incorrect words}}, \\ \text{FR} &= \frac{\text{num. of correct words labelled as rejected}}{\text{num. of keywords} * \text{hours of testset} * C}, \end{aligned} \tag{5.1}$$

where $C$ is a factor which scales the dynamic range of FA and FR on the same level. In this paper, $C$ is set to 10. Recognition rates (RA) are also computed. It can be obtained as:

$$\text{RA} = \frac{\text{num. of correct words labelled as accepted}}{\text{total num. of recognized words}}. \tag{5.2}$$

In order to assess how CN gives more information than 1-best pin-yin sequence, the syllable error rates (SERs) of both CN and pin-yin sequence are given in Table 1. SER of CN drops significantly with the reduction of pruning beam.

Table 2 summarizes recognition rates of different confusion matrixes. With the $n$-best hypotheses of CN, recognition rates are improved obviously. Then maximum probability rule is applied, and the recognition rate arrives 82.0%.

To evaluate the performance of methods proposed in this paper, EERs of different methods are listed in Table 3.

As we can see from Table 3, the improved confusion matrixes provide obviously EER reduction of up to 3.9% in relative. MCE with block training is superior to sequential training, relative 1.7% EER reduction is achieved. When two methods are used at the same time, we get a further improvement, 8.4% relative reduction compared with the baseline system.

**Table 3:** EER of different methods.

| Methods | EER |
|---|---|
| Baseline | 48.8% |
| CN | 47.5% |
| CN + maximum probability | 46.9% |
| MCE with sequential training | 46.2% |
| MCE with block training | 45.4% |
| CN + maximum probability + MCE with block training | 44.7% |

## 6. Conclusions

In order to describe how the accent-specific pronunciation differs from those assumed by the standard Mandarin recognition system, the phoneme confusion matrix is adopted. Different from traditional algorithm, confusion network is applied in generating confusion matrix. It improves the recognition rate of spoken term system. Moreover, a revised MCE training method is presented in this paper. Experiments prove that it performs obviously better than the sequential training.

## References

[1] N. Moreau, H.-G. Kim, and T. Sikora, "Phonetic confusion based document expansion for spoken document retrieval," in *Proceedings of the 8th International Conference on Spoken Language Processing (ICSLP '04)*, Jeju Island, Korea, October 2004.

[2] M. Liu, B. Xu, T. Huang, Y. Deng, and C. Li, "Mandarin accent adaptation based on context-independent/context-dependent pronunciation modeling," in *Proceedings of the the IEEE Interntional Conference on Acoustics, Speech, and Signal Processing (ICASSP '00)*, pp. 1025–1028, June 2000.

[3] J. Gao, Q. Zhao, Y. Yan, and J. Shao, "Efficient system combination for syllable-confusion-network-based Chinese spoken term detection," in *Proceedings of the 6th International Symposium on Chinese Spoken Language Processing (ISCSLP '08)*, pp. 366–369, December 2008.

[4] B. H. Juang and S. Katagiri, "Discriminative learning for minimum error classification," *IEEE Transactions on Signal Processing*, vol. 40, no. 12, pp. 3043–3054, 1992.

[5] S. Abdou and M. S. Scordilis, "Beam search pruning in speech recognition using a posterior probability-based confidence measure," *Speech Communication*, vol. 42, no. 3-4, pp. 409–428, 2004.

[6] J. Liang, M. Meng, X. Wang, P. Ding, and B. Xu, "An improved mandarin keyword spotting system using MCE training and context-enhanced verification," in *Proceedings of the IEEE International Conference on Acoustics, Speech and Signal Processing (ICASSP '06)*, pp. I1145–I1148, May 2006.

[7] T. Hori, I. L. Hetherington, T. J. Hazen, and J. R. Glass, "Open-vocabulary spoken utterance retrieval using confusion networks," in *Proceedings of the IEEE International Conference on Acoustics, Speech and Signal Processing (ICASSP '07)*, vol. 4, pp. IV73–IV76, April 2007.

[8] D. Povey, *Discriminative Training for Large Vocabulary Speech Recognition*, Cambridge University, Cambridge, UK, 2004.